Department of Mechanical Engineering
National Institute of Technology,
Rourkela –769 008
India

CERTIFICATE

This is to certify that the thesis entitled "**Experimental Studies on a DI Diesel Engine Fueled with Jatropha Methyl Ester-Wood Pyrolysis Oil Emulsions**" being submitted by **Mr. R. Prakash** for the award of Ph.D. degree is a record of bonafide research carried out by him in the Mechanical Engineering Department, National Institute of Technology, Rourkela, under our guidance and supervision. To the best of our knowledge, the results presented in this thesis have not been submitted to any other University or Institute for the award of any degree or diploma.

Co-Supervisor

Prof. R.K.Singh
Professor and Head
Department of Chemical Engineering
National Institute of Technology
Rourkela- 769008.

Supervisor

Prof.S.Murugan
Associate Professor
Department of Mechanical Engineering
National Institute of Technology
Rourkela- 769008.

ACKNOWLEDGEMENT

One of the joys of completion is to look over the journey past and remember all the faculty, friends and family who have helped and supported me along this long but fulfilling road.

At the outset, I would like to express my heartfelt gratitude to **Prof. S. Murugan** for his advice during my doctoral research endeavor for the past three and half years. As my supervisor, he constantly forced me to remain focused on achieving my goal. His observations and comments helped me to establish the overall direction of the research and to move forward with investigation in depth. I thank him for providing me with the opportunity to work with him. I could not have asked for better role models, each inspirational, supportive, and patient. I could not be prouder of my academic roots and hope that I can in turn pass on the research values and the dreams that he has given to me.

I would like to thank **Prof. R.K.Singh** for his unflagging encouragement and supportive guidance throughout my research career. As my co-supervisor, his guidance has helped me well and I owe my heartfelt appreciation. He has also provided insightful discussions about the research whenever required.

I am happy to acknowledge **Prof. Sunil Kumar Sarangi**, Director, NIT Rourkela for providing required infrastructural facilities and financial assistance in the form of Junior Research Fellowship and Research Assistance ship, which buttressed me to perform my work comfortably and I will forever be grateful to him. I warmly thank **Prof. K.P.Maity**, Professor and Head, Department of Mechanical Engineering and **Prof. R.K. Sahoo**, Group Head, for their valuable advice, and support to my work.

I would like to express my sincere thanks to DST, Government of India for sponsoring this research project and Dean, Assistant Registrar and other staff members of SRICCEE for their timely help in all financial matters connected with the project and also for extending their support in all official corresponding.

I take this opportunity to sincerely acknowledge and thank my Doctoral Scrutiny Committee members, **Prof. Japes Bera**, Ceramic Engineering Department, **Prof. Mithilesh Kumar**, Metallurgical and Materials Engineering Department and **Prof. Alok Satapathy**, Mechanical Engineering Department, who have provided encouraging and constructive feedback and suggestions whenever required. To the many anonymous reviewers from various journals and

conferences, thank you for helping to shape and guide the direction of work with your careful and instructive comments.

I would like to thank our technical staff members Mr.N.P.Barik, Mr. Bisoyi, Mr. Ramkrishna Mandal, Mr. Laxman Kumar Mohanta and specially Mr.Harihar Barkey and other administrative staff who have been kind enough to help in their respective roles. I also thank my all research colleagues for providing support and friendship that I needed.

I would like to thank my parents, brothers, sister, in-laws, especially, to my wife Mrs. C.Hema, as well as my children Hariharan and Kavya for their great support, patience and unconditional love during my good and bad times. Above all, I owe it all to Almighty God for granting me the wisdom, health and strength to undertake this research task and enabling me to its completion.

(R.Prakash)

ABSTRACT

The major technical problems associated with the use of biodiesel in large proportions are (i) more prone to oxidation which can cause the fuel to become acidic and to form insoluble gums and sediments that can plug fuel filters, (ii) cold flow properties and (iii) higher NO_x emissions compared to diesel fueled engines. It is reported that addition of antioxidants, emulsifying water with biodiesel, addition of fuel with high latent heat of vaporization, and low cetane fuel can reduce the NO_x emissions in biodiesel fueled engines. Addition of antioxidants to biodiesel can improve both the cold flow properties and oxidation stability, and reduce the NO_x emission, the reason being that, the antioxidants contain phenolic compounds. Also, in economic point of view, the cost of biodiesel is higher at this moment because, the availability of seeds is limited. This motivates less use of biodiesel in many countries. The use of alternative hydrocarbon sources other than petroleum fuels, as extenders for biodiesel can solve this problem. Many literatures report that pyrolysis oil obtained from biomass sources contain hindered phenols in them. Therefore, bio oil can be used as an extender to biodiesel. The bio oil not only contains phenolic compounds, it also contains small percentage of water which is inseparable.

In this research work, an attempt was made to study the effects of using bio oil as an extender to biodiesel on engine combustion, performance, emission and durability issues. For this purpose, wood pyrolysis oil (WPO) - bio oil obtained from pyrolysis of wood was used in low percentages (i.e., 5%, 10% and 15%). Waste wood from the packing container boxes was used as feedstock for the production of WPO, while the JME was collected from a commercial pilot plant in India. The JME-WPO emulsions were obtained using six different surfactant combinations viz. 2% and 4% of Span 20 (Sorbitan monolaurate), 2% and 4% of Span 80 (Sorbitan monooleate), and 2 and 4% of (Span 80 + Tween 80 (Polysorbate 80) mixed). Three different percentages of emulsions containing 5, 10 and 15% of WPO were prepared using six different surfactants and tested as fuels in a single cylinder, four stroke, air cooled direct injection (DI) diesel engine developing a power of 4.4 kW at a constant speed of 1500 rpm. After evaluating the combustion, performance and emission parameters of the engine fueled with different emulsions, an optimum emulsion (Z2JOE15) was chosen, which contains 15% WPO, 81% JME and 4% of a mixed surfactant; Span 80-Tween 80. The highest thermal efficiency was noticed with the Z2JOE15 emulsion compared to all other

emulsions tested in this study. The thermal efficiency for the Z2JOE15 was found to be higher by 11.3% compared to that of diesel at full load. Lower HC, CO and smoke emissions are noticed with the Z2JOE15 emulsion compared to that of diesel operation at full load. The NO emissions for all the emulsions were found to be lower than that of JME operation, but higher than that of diesel operation at full load. A maximum reduction in the NO emission of 16.8% was observed with the Z2JOE15 emulsion compared to that of JME operation.

Further, this Z2JOE15 emulsion was upgraded for its quality by an acid treatment process. The acid treated emulsion (ATJOE15) was tested in the same engine to evaluate the engine behaviour in terms of the combustion, performance and emission and compared with that of diesel operation. In the performance aspect, the brake thermal efficiency of ATJOE15 emulsion was higher by about 8.2% and 8.5% than those of diesel and JME at full load. The HC emissions were lower by about 73% for the ATJOE15 emulsion at full load compared to that of diesel. The CO emissions of ATJOE15 emulsion were found to be higher by about 46% than that of diesel at full load. An increase of about 2% in the NO emission was noticed with the ATJOE15 emulsion at full load compared to that of diesel. A two zone mathematical model, using a MATLAB software program was developed to validate the experimental results obtained from the same engine fueled with the ATJOE15 emulsion. The validation of experimental results with the theoretical model indicated that the combustion characteristics such as cylinder pressure and heat release were in good agreement, and were within the deviation of 2-6%.

Further the engine was run with the ATJOE15 emulsion to evaluate the combined effects of different compression ratio (CR), injection timing (IT) and nozzle opening pressure (IP) on the combustion, performance and emission parameters of the engine. Engine experiments were conducted with the ATJOE15 emulsion only at three different compression ratios (16.5, 17.5 and 18.5), and for each compression ratio, three nozzle opening pressures (200, 220, and 240 bar) and three injection timings (21.5, 23 and 24.5 ^{o}CA bTDC) were selected and conducted as per the full factorial design (3^3 = 27). With the ATJOE15 emulsion, about 25.81% higher brake thermal efficiency was obtained at 18.5 compression ratio with the standard injection timing and nozzle opening pressure compared to that of diesel. The HC and smoke emissions were found to be lower by 45% and 9.6% respectively at full load with the same operating condition. The CO and NO emissions were found to be higher by about 10% and 4.88% in comparison with diesel at full load. The NO emissions were found to be

lower with a lower compression ratio (16.5) and retarded injection timing (21.5 ^{o}CA bTDC) conditions.

A short term endurance test was conducted with the ATJOE15 emulsion as per IS 10000 Part V-1980 method for 100 hrs. After the endurance test, carbon deposits were noticed in the cylinder head, combustion chamber and nozzle tip. About 26 g of carbon deposits were found in the cylinder head and combustion chamber. A marginal wear was observed in the plunger of the fuel injection pump. The fuel filter was found to be clogged with some sediments of WPO. The engine lubrication oil, used in the test engine fueled with the ATJOE15 emulsion for the endurance test was analyzed by the atomic absorption spectroscopy (AAS). In this investigation, the variation in the concentration of the wear metal debris, including Fe, Cu, Zn, Al, Cr, Pb and CO in the used lubricating oil with the engine operation time, was obtained using the AAS. Out of all, Fe was the most abundant wear metal found in the lubrication oil. The viscosity of the lubrication oil after 100 hrs of operation, was found to be increased by about 10% compared to that of reference one. The ash content present in the used lubrication oil was found to be about 0.087 (wt %).

Keywords: Diesel engine, biodiesel, transesterification, Jatropha methyl ester (JME), pyrolysis, bio oil, wood pyrolysis oil (WPO), emulsion, performance, combustion, emission, durability, modeling.

CONTENTS

LIST OF FIGURES

LIST OF TABLES

NOMENCLATURE

$\frac{d(mu)}{d\theta}$	rate of change of internal energy of the system of mass m.
$\frac{dQ_r}{d\theta}$	rate of heat release during combustion period
$\frac{dQ_h}{d\theta}$	rate of heat transfer from gases to walls
$\frac{dW}{d\theta}$	rate of mechanical work done by the system on the boundary
p	Pressure
v	instantaneous cylinder volume
m	Mass
R	gas constant
T	Temperature
$\frac{dV}{d\theta}$	change of volume with crank angle
h	heat transfer coefficient
A	heat transfer area
T_w	wall temperature
V_{cl}	cylinder clearance volume
λ	crank radius to piston length ratio
$\frac{dQ}{dt}$	rate of heat release
K	thermal conductivity of the cylinder gas
d	cylinder bore
Re	Reynolds number
T_g	cylinder bulk gas temperature
Cmodel	model constant=1000 kJ/kg degree
f_1, f_2	functions
q	heat losses
m_f	cumulative mass of fuel injected
Q	cumulative heat release rate
LCV	lower calorific value of fuel
C_{rate}	constant for mixing rate=0.002 s
k	density of turbulent kinetic energy

$Eu/d\theta$	total turbulent energy of the fuel jet at a given crank angle instant, θ
$E_{diss}/d\theta$	rate of energy dissipation across the control surface
$dEi/d\theta$	rate of generation of kinetic energy of fuel jet in to the cylinder
C_{turb}	efficiency of conversion of kinetic energy to turbulent energy in the free jet=0.2
n	engine speed
ρ_f	density of fuel
C_d	coefficient of discharge of nozzle
A_n	area of nozzle holes
$\frac{dmf/d\theta}{\rho f}$	volumetric injection rate of the fuel
Eu	total turbulent energy of the fuel jet at a given crank angle instant
C_{diss}	dissipation constant
λ_{diff}	excess air ratio for diffusion burning=1.4
Φ	Crank angle
Φ_{inj}	Fuel injection crank angle
Φ_{exh}	Crank angle at exhaust valve opens
CHR	Cumulative Heat Release
WPO	Wood Pyrolysis Oil
JME	Jatropha Methyl Ester
ATJOE15	Acid treated Jatropha oil Emulsion with 15% WPO
TDC	Top Dead Centre
BDC	Bottom Dead Centre
DI	Direct Injection
O	Oxygen
N	Nitrogen
NO	Nitric Oxide

Annexure -1

Cost analysis of ATJOE15 emulsion

I. Generally, the cost for making one litre of ATJOE15 emulsion is described as follows:

(a) Cost of one litre of biodiesel (JME) = INR 80

(b) Cost for producing one litre of WPO = INR 27

(c) Cost of one litre surfactant Span 80 = INR 624

(d) Cost of one litre surfactant Tween 80 = INR 530

II. For making 1litre of ATJOE15, 810 ml of JME, 150 ml of WPO and 40 ml of surfactant (20 ml of Span 80 + 20 ml of Tween 80) has been used.

(a) Cost of 810 ml of JME = 0.810 x 80 = INR 64.8

(b) Cost of 150 ml of WPO = 0.150 x 27 = INR 4.05

(c) Cost of 40 ml surfactant = (0.02 x 624) + (0.02 x 530) = INR 23.08

III. The mechanical stirrer used for emulsification, was connected to a small AC motor, whose capacity was 1/20 HP (37.3W). Hence, the electrical energy consumed for the preparation of each sample was about 0.01865 kWh.

(a) Cost involved in emulsification process = 0.01865 x 3 = INR 0.05595

(b) Amount of KOH used to neutralize 1 litre of ATJOE15 emulsion = 17.6 g

(c) Cost of 500 g of KOH = INR 400

(d) Cost of 17.6 g of KOH = INR 14.08

IV. From the above details, the cost of producing one litre of ATJOE15 will be around INR 106 or 1.69 USD approximately. In larger production, the cost may reduce considerably.

Annexure -2

Technical specifications of the engine

Make	**Kirloskar**
Model	TAF 1
Bore x Stroke, mm	87.5 x 110
Compression ratio	17.5:1
Piston type	Bowl-in-piston
Number of valves	2
Rated power, kW	4.4
Rated speed, rpm	1500
Type of fuel injection	Pump-line-nozzle injection system
Nozzle type	Multi hole
No. of holes	3
Needle lift, mm	0.25
Spray-hole diameter, mm	0.25
Cone angle, deg	110
Start of injection, ^{o}CA bTDC	23
Nozzle opening pressure, bar	200
Inlet valve opening, ^{o}CA bTDC	4.5
Inlet valve closing, ^{o}CA aBDC	35.5
Exhaust valve opening, ^{o}CA bBDC	35.5
Exhaust valve closing, ^{o}CA bBDC	4.5
Method of cooling	Air cooled with radial fan
Connecting rod length, mm	220
Weight, kg	163

Annexure -3

Specification of the pressure transducer

Description	Data
Model	KISTLER, Switzerland
	601 A, air cooled
Range	0-100 bar
Sensitivity	25 mV/bar
Linearity	0.1 <+ % FSO
Acceleration sensitivity	< 0.001 bar / g
Operating temperature range	-196 to 200 ^{o}C
Capacitance	5 PF
Weight	1.7 g
Connector, Teflon insulator	M4 x 0.35

Annexure-4

Specification of the charge amplifier

Description	Data
Make	KISLTER instruments, Switzerland
Measuring ranges	12 stages graded pC 10-50000
	1:2:5 and stepless 1 to 10
Accuracy of two most sensitive ranges	<± 3 %
Accuracy of other range stages	<± 1%
Linearity, of Transducer sensitivity	<±0.5%
Calibration capacitor	1000 ± 0.5 pF
Operating temperature range	-196 to 200 ^{o}C
Calibration input sensitivity	1±0.5 pC/mV
Input voltage, maximum with pulses	+ 12 V
Connector, Teflon insulator	M4 x 0.35

Annexure-5

Technical specification of AVL DiGAS 444 analyzer

Measured quantity	Measuring range	Accuracy
CO	0-10%	< 0.6% vol: ±0.03% vol
		≥ 0.6% vol: ± 5% of initial value
CO_2	0-20%	< 10% vol: ±0.05% vol
		≥ 10% vol: ± 5% of vol
HC	0-20000 ppm vol	< 200 ppm vol: ± 10 ppm vol
		≥ 200 ppm vol: ± 5% of initial value
O_2	0-22% vol	< 2% vol: ±0.01% vol
		≥ 2% vol: ± 5% of vol
NO	0-5000 ppm vol	< 500 ppm vol: ± 50 ppm vol
		≥ 500 ppm vol: ± 10% of initial value
Voltage	11-22 V DC	
Power consumption	≈25W	
Warm up time	≈ 7 min	
Operating temperature	5-45 ^{o}C	
Dimensions (WxDxH)	270x320x85	
Weight	4.5 kg net weight without accessories.	

Annexure-6

Technical specification of AVL 437C Diesel smoke meter

Description	Data
Measuring chamber	0-100% opacity
Accuracy and repeatability	±1 % of full scale
Alarming signal temperature	Lights up when temperature of measuring chamber is below 70 ^{o}C
Linearity check	48.4% - 53.1% or 1.54 m^{-1} - 1.54 m^{-1} of measurement range
Measuring chamber length	430 ± 5 mm
Light source	Halogen lamp, 12V
Sensor	Selenium Photocell
Weight	24 kg

Annexure 7

Calculation of uncertainty for crank angle encoder

X_1 CA	X_2 CA	X_3 CA	X_4 CA	X_5 CA	$\dot{x}$ CA	$(X_1-\dot{x})^2$	$(X_2-\dot{x})^2$	$(X_3-\dot{x})^2$	$(X_4-\dot{x})^2$	$(X_5-\dot{x})^2$	σ	U (Y)	5% Sig.level	% U(Y)
0.574162	0.566037	0.568721	0.567376	0.564264	0.568112	3.66E-05	4.3E-06	3.7E-07	5.42E-07	1.48E-05	0.003762	0.001682	0.003298	0.3298
0.574163	0.566038	0.56872	0.567376	0.564263	0.568112	3.66E-05	4.3E-06	3.7E-07	5.42E-07	1.48E-05	0.003763	0.001682	0.003298	0.3298
0.574163	0.566038	0.568721	0.567376	0.564263	0.568112	3.66E-05	4.3E-06	3.71E-07	5.42E-07	1.48E-05	0.003763	0.001682	0.003298	0.3298
0.574162	0.566038	0.56872	0.567375	0.564264	0.568112	3.66E-05	4.3E-06	3.7E-07	5.43E-07	1.48E-05	0.003762	0.001682	0.003297	0.3297
0.574163	0.566037	0.56872	0.567376	0.564263	0.568112	3.66E-05	4.3E-06	3.7E-07	5.41E-07	1.48E-05	0.003763	0.001682	0.003298	0.3298
0.574163	0.566038	0.568721	0.567376	0.564263	0.568112	3.66E-05	4.3E-06	3.71E-07	5.42E-07	1.48E-05	0.003763	0.001682	0.003298	0.3298
0.574162	0.566038	0.56872	0.567376	0.564264	0.568112	3.66E-05	4.3E-06	3.7E-07	5.42E-07	1.48E-05	0.003762	0.001682	0.003297	0.3297
0.574163	0.566038	0.56872	0.567376	0.564263	0.568112	3.66E-05	4.3E-06	3.7E-07	5.42E-07	1.48E-05	0.003763	0.001682	0.003298	0.3298
0.574163	0.566037	0.568721	0.567376	0.564263	0.568112	3.66E-05	4.31E-06	3.71E-07	5.42E-07	1.48E-05	0.003763	0.001682	0.003298	0.3298
0.574162	0.566038	0.56872	0.567376	0.564264	0.568112	3.66E-05	4.3E-06	3.7E-07	5.42E-07	1.48E-05	0.003762	0.001682	0.003297	0.3297
0.574163	0.566038	0.568721	0.567376	0.564263	0.568112	3.66E-05	4.3E-06	3.71E-07	5.42E-07	1.48E-05	0.003763	0.001682	0.003298	0.3298
0.574163	0.566038	0.56872	0.567376	0.564263	0.568112	3.66E-05	4.3E-06	3.7E-07	5.42E-07	1.48E-05	0.003763	0.001682	0.003298	0.3298
0.574163	0.566037	0.56872	0.567375	0.564264	0.568112	3.66E-05	4.3E-06	3.7E-07	5.43E-07	1.48E-05	0.003762	0.001682	0.003298	0.3298
0.574162	0.566038	0.568721	0.567376	0.564263	0.568112	3.66E-05	4.3E-06	3.71E-07	5.42E-07	1.48E-05	0.003762	0.001682	0.003298	0.3298
0.574163	0.566038	0.56872	0.567376	0.564263	0.568112	3.66E-05	4.3E-06	3.7E-07	5.42E-07	1.48E-05	0.003763	0.001682	0.003298	0.3298
0.574163	0.566038	0.56872	0.567376	0.564263	0.568112	3.66E-05	4.3E-06	3.7E-07	5.42E-07	1.48E-05	0.003763	0.001682	0.003298	0.3298
0.574164	0.566038	0.568724	0.56738	0.564264	0.568114	3.66E-05	4.31E-06	3.72E-07	5.39E-07	1.48E-05	0.003763	0.001682	0.003298	0.3298
0.57416	0.56604	0.56872	0.56737	0.56426	0.56811	3.66E-05	4.28E-06	3.72E-07	5.48E-07	1.48E-05	0.003762	0.0016827	0.003298	0.3298
0.57416	0.56603	0.56872	0.56738	0.56427	0.568112	3.66E-05	4.33E-06	3.7E-07	5.36E-07	1.48E-05	0.003760	0.001681	0.003296	0.3296
											0.003762	0.001682	0.003298	0.3298

Where, X_1, X_2, X_3, X_4 and X_5 are difference in the crank angle (CA) degree values for 20 consecutive readings
Uncertainty with 5% significance level = 1.96 $\sigma/\sqrt{n}$
The calculated uncertainty of crank angle encoder with 5 % significance/confidence level = ± 0.3298 %.

Annexure 8

MATLAB program

```
% Two Zone model: Performance combustion and emission analysis: RUN
clear all
close all
clc
s=0.11;d=0.0875;kkk=0;theta=0;mf=0;mfinjr=0;q=0;pr=2e7;
pphi=0;m11=0;mfj=0;tt=0;tbr=0 ;yty1=0;yty2=0;msn=0;dmsn=0;dnox=0;noxx=0;
mfb=0;
n=1500;                      % Rpm
bp=4.38282;             % brake power in kw
M=48.27;                       % fuel molecular Weight
mfrt=1.615886*(0.028e-3); mfkg=1.615886;          % mass flow rate of fuel in
kg/cycle
dtheta=40;                   % total duration of fuel injection
roa=1.29;                    % density of air in kg/m^3
ro=926.7;                    % density of fuel in kg/m^3
afrs=7.26;                     % stoichiometric air/fuel
afr=14.72876181;                      % afr
mainj=afr*mfrt;            % mass of air present inside cylinder in kg/cycle
LCV=36320;                   % lower calorific value of fuel in kJ/kg
a=12; b=22; g=0; delta=0;
epss=0.210/(a+0.25*b-0.5*g);
er=afrs/afr;     % alpha, beta gamma, delta ,epsilon, equivalence ratio
phi=zeros(1,290);
p=zeros(1,290);
t=zeros(1,290);tu=zeros(1,290); tb=zeros(1,290);
v=zeros(1,290); vu=zeros(1,290);vb=zeros(1,290);
ht=zeros(1,290);
chr=zeros(1,290);Qf=zeros(1,290);x=zeros(1,290);
qq=zeros(1,2);
qg=zeros(1,290);mf=zeros(1,290);mfinjr=zeros(1,290);qh=zeros(1,290);
K=zeros(1,6); c=zeros(1,6); d=zeros(1,3);A=zeros(4,5);
f=zeros(1,4);y=zeros(1,10);
yco2=zeros(1,290); yh2o=zeros(1,290); yn2=zeros(1,290); yo2=zeros(1,290);
yco=zeros(1,290);    yh2=zeros(1,290);    yh=zeros(1,290);    yo=zeros(1,290);
yoh=zeros(1,290); yno=zeros(1,290);
sot=zeros(1,290);noxf=zeros(1,290);N=0.000001;mloss=0;molu=0;molb=0;fp=0;effm
=0;BTE=0;idx=0;idd1=0;ccvv=0;mmf=0;

id=10;       % ignition delay in degree
phis=339+id; % start of combustion
phid=40;     % duration of combustion
aa=6.908;
m=2;         % combustion exponent
Qchr=2200;   % cumm heat release in kJ


phi(1)=-145;
t(1)=360;
p(1)=1.516163e5;
v(1)=0.0000401+0.0003305*(1+4-cos(phi(1)*0.017453)-sqrt(16-
sin(phi(1)*0.017453)*sin(phi(1)*0.017453)));
```

```
 mftot=mfrt/M;          %mass of fuel in kmol
 matot=mainj/29;        %mass of air in kmol

 E(1)=ienergy(t(1))*matot*1000;   %internal energy in J/mol

 for j1=1:122
    phi(j1+1)=phi(j1)+1;
    theta=theta+1;
    v(j1+1)=0.0000401+0.0003305*(1+4-cos(phi(j1+1)*0.017453)-sqrt(16-
sin(phi(j1+1)*0.017453)*sin(phi(j1+1)*0.017453)));
    t(j1+1)=t(j1)*(v(j1)/v(j1+1))^0.4;           % gamma=1.4
    p(j1+1)=(p(j1)*v(j1)*t(j1+1))/(t(j1)*v(j1+1));

    for j2=1:10
        [fe fed dq]=ebalance24(p(j1),p(j1+1),t(j1),t(j1+1),v(j1),v(j1+1));
        t(j1+1)=t(j1+1)-fe/fed;                  %newton raphson method
        ffe(j1)=fe;
        dqqq=dq;
        ddd(j1+1)=dq;
     end
     ht(j1+1)=-dqqq;

 end

          % combustion and expansion
          y(3)=0.1; y(4)=0.1; y(5)=1e-6; y(6)=1e-6;
          vu(123)=v(123);vb(123)=0;tu(123)=t(123);tb(123)=t(123);
 for k11=123:289
    phi(k11+1)=phi(k11)+1;
    pphi=pphi+1;
    v(k11+1)=0.0000401+0.0003305*(1+4-cos(phi(k11+1)*0.017453)-sqrt(16-
sin(phi(k11+1)*0.017453)*sin(phi(k11+1)*0.017453)));
    t(k11+1)=t(k11)*(v(k11)/v(k11+1))^0.4;           % gamma=1.4
    p(k11+1)=(p(k11)*v(k11)*t(k11+1))/(t(k11)*v(k11+1));

    phiii=phi(k11+1)+id+360;

    if phi(k11+1)<(phi(123)+id)
    x(k11+1)=0;
    dmf=0;

    else
 x(k11+1)=1-exp(-((phiii-phis)/phid)^(m+1)); % cumulative mass fraction burn
dmf=mfrt*(x(k11+1)-x(k11));  % mass of fuel to be burn in the time step in kg
mmf=dmf*mfrt*1000/M;
%Qf(k11+1)=(6.908*(m+1)/(phid*0.017453))*(((phiii-phis)/phid)^m)*exp(-
6.908*((phiii-phis)/phid)^(m+1)); % cumm fraction heat release
          %q=Qf*dmf*LCV*1000;   % heat release rate in j/deg
          q=0.446*aa*(m+1)*(Qchr/phid)*(((phiii-phis)/phid)^m)*exp(-
aa*((phiii-phis)/phid)^(m+1));
          ht(k11+1)=q;
          end
     %ccvv=cvmol(t(k11));
     %t(k11+1)=mftot*1000*x(k11)*Qchr/ccvv;t(k11+1)
```

```
     %t(k11+1)=t(123)+t(k11+1);
     %p(k11+1)=p(k11)*(t(k11)/t(k11+1))^3.857;     % cp/cv=1.35

     for kk2=1:10          % energy balance for burning zone
[fe fed dqb dw]=
ebalancec24(p(k11),p(k11+1),tb(k11),t(k11+1),v(k11),v(k11+1),q,mloss,mmf);
        if fed<eps
           t(k11+1)=t(k11);
        else
        t(k11+1)=t(k11+1)-fe(1)/fed(1);        %newton raphson method
        ffe(k11)=fe(1);
        end
        dqqq=dqb;

    end

K(1)=10^(0.432168*log(t(k11+1)/1000)+(-0.112464e5)/t(k11+1)+0.267269e1+(-
0.745744e-4)*t(k11+1)+(0.242484e-8)*(t(k11+1)^2));
K(2)=10^(0.310805*log(t(k11+1)/1000)+(-0.129540e5)/t(k11+1)+0.321779e1+(-
0.738336e-4)*t(k11+1)+(0.344645e-8)*(t(k11+1)^2));
K(3)=10^(-0.141784*log(t(k11+1)/1000)-
0.213308e4/t(k11+1)+0.853461+(0.355015e-4)*t(k11+1)+(-0.310227e-
8)*(t(k11+1)^2));
K(4)=10^(0.0150879*log(t(k11+1)/1000)-
0.470959e4/t(k11+1)+0.646096+(0.272805e-5)*t(k11+1)+(-0.154444e-
8)*(t(k11+1)^2));
K(5)=10^((-0.752364*log(t(k11+1)/1000)+0.124210e5/t(k11+1)-
2.60286+(0.259556e-3)*t(k11+1)+(-0.162687e-7)*(t(k11+1)^2))/100);
K(6)=(10^(((-0.415303e-2)*log(t(k11+1)/1000)+0.148627e5/t(k11+1)-
0.475746e1+(0.124699e-3)*t(k11+1)+(-0.900227e-8)*(t(k11+1)^2))/1e5));

       %K(1)=1;K(2)=1;K(3)=1;K(4)=1;K(5)=4.7;K(6)=12.18;
        c(1)=K(1)/sqrt(p(k11+1)/1e5);
        c(2)=K(2)/sqrt(p(k11+1)/1e5);
        c(3)=K(3);
        c(4)=K(4);
        c(5)=K(5)*sqrt(p(k11+1)/1e5);
        c(6)=K(6)*sqrt(p(k11+1)/1e5);

        d(1)=b/a;
        d(2)=g/a+0.42/(epss*er*a);
        d(3)=delta/a+1.58/(epss*er*a);

                    for fk=1:10
                       yty1=yty1+y(fk);
                    end
     % newton-Raphson method
     for fi=1:10
        D76=0.5*c(1)/sqrt(y(6));
        D103=0.5*c(4)*sqrt(y(4))/sqrt(y(3));
        D84=0.5*c(2)/sqrt(y(4));
        D26=c(5)*sqrt(y(4));
        D94=0.5*c(3)*sqrt(y(6))/sqrt(y(5));
        D24=0.5*c(5)*y(6)/sqrt(y(4));
        D96=0.5*c(3)*sqrt(y(4)/y(6));
        D14=0.5*c(6)*y(5)/sqrt(y(4));
```

```
D104=0.5*c(4)*sqrt(y(3))/sqrt(y(4));
D15=c(6)*sqrt(y(4));

A(1,1)=1+D103;
A(1,2)=D14+D24+1+D84+D104+D94;
A(1,3)=D15+1;
A(1,4)=D26+1+D76+D96;
A(2,1)=0;
A(2,2)=2*D24+D94-d(1)*D14;
A(2,3)=-d(1)*D15-d(1);
A(2,4)=2*D26+2+D76+D96;
A(3,1)=D103;
A(3,2)=2*D14+D24+2+D84+D94+D104-d(2)*D14;
A(3,3)=2*D15+1-d(2)*D15-d(2);
A(3,4)=D26+D96;
A(4,1)=2+D103;
A(4,2)=D104-d(3)*D14;
A(4,3)=-d(3)*D15-d(3);
A(4,4)=0;

  y(7)=c(1)*sqrt(y(6));
  y(8)=c(2)*sqrt(y(4));
  y(9)=c(3)*sqrt(y(4)*y(6));
  y(10)=c(4)*sqrt(y(4)*y(3));
  y(2)=c(5)*sqrt(y(4))*y(6);
  y(1)=c(6)*sqrt(y(4))*y(5);

  f(1)=y(1)+y(2)+y(3)+y(4)+y(5)+y(6)+y(7)+y(8)+y(9)+y(10)-1;
  f(2)=2*y(2)+2*y(6)+y(7)+y(9)-d(1)*y(1)-d(1)*y(5);
  f(3)=2*y(1)+y(2)+2*y(4)+y(5)+y(8)+y(9)+y(10)-d(2)*y(1)-d(2)*y(5);
  f(4)=2*y(3)+y(10)-d(3)*y(1)-d(3)*y(5);

  A(1,5)=-f(1);
  A(2,5)=-f(2);
  A(3,5)=-f(3);
  A(4,5)=-f(4);

   % gauss elimination

  A=rref(A);              % reduced to echelon form
   dy(4)=A(4,5);
   dy(3)=A(3,5);
   dy(2)=A(2,5);
   dy(1)=A(1,5);

y(3)=y(3)+dy(1);
y(4)=y(4)+dy(2);
y(5)=y(5)+dy(3);
y(6)=y(6)+dy(4);
y(7)=c(1)*sqrt(y(6));
y(8)=c(2)*sqrt(y(4));
y(9)=c(3)*sqrt(y(4)*y(6));
y(10)=c(4)*sqrt(y(4)*y(3));
y(2)=c(5)*y(6)*sqrt(y(4));
y(1)=c(6)*y(5)*sqrt(y(4));
```

```
        for fk=1:10
            yty2=yty2+y(fk);
        end

            yco2(k11+1)=y(1);
            yh2o(k11+1)=y(2);
            yn2(k11+1)=y(3);
            yo2(k11+1)=y(4);
            yco(k11+1)=y(5)*0.44;
            yh2(k11+1)=y(6);
            yh(k11+1)=y(7);
            yo(k11+1)=y(8);
            yoh(k11+1)=y(9);
            yno(k11+1)=y(10)*(504e11);

   N=(y(1)+y(5))/(epss*er*a);   % total no of kmol of product per kmol of air

         mloss=(yn2*N*28+yo2*N*32)*1000/29;        % mloss in mol
         matott=matot*1000-mloss;
         vb(k11+1)=N*matot*mftot*8314*tb(k11+1)/p(k11+1);
         vu(k11+1)=v(k11+1)-vb(k11+1);

%t(k11+1)=(N*matot*mftot*tb(k11+1)+matott*tu(k11+1))/(N*matot*mftot+matott);
% mean temp

    end
    ddd(k11+1)=-dqqq;
    p(k11+1)=(p(k11)*v(k11)*t(k11+1))/(t(k11)*v(k11+1));
   %ht(k11+1)=ht(k11+1);

         % soot formation model
         po21=(y(4)/yty1)*p(k11);
         po22=(y(4)/yty2)*p(k11+1);
          ka1= soot(msn,dmf,p(k11),t(k11),po21);    % change mfinjr with dmf
          ka2=ka1+soot(msn,dmf,p(k11+1),t(k11+1),po22);
          dmsn=dmsn+0.5*(ka1+ka2);
         % msn=msn+dmsn;
          sot(k11+1)=dmsn*19.3e8;
         % nox model
                  %yyy=sqrt(1/100*(y(3)));
                  yyy=y(3);
         kaa1=nox(noxx,t(k11),yyy,y(4),y(9),y(10));
         kaa2=0.5*kaa1+nox(noxx,t(k11),yyy,y(4),y(9),y(10));
         kaa3=0.5*kaa2+nox(noxx,t(k11),yyy,y(4),y(9),y(10));
         kaa4=kaa3+nox(noxx,t(k11+1),yyy,y(4),y(9),y(10));
          dnox=dnox+(1/6)*(kaa1+2*kaa2+2*kaa3+kaa4);
         %noxx=noxx+dnox;

          noxf(k11+1)=dnox*(65.37e5);

 end
 chr(1)=ht(1);
 for n11=1:289
     chr(n11+1)=chr(n11)+ht(n11);
```

```
 end
p=p/1e5; ht=ht+1;ddd=-ddd;chr=2.05*chr;

    bmep=75+0.045*n+0.4*(2*n*s/60);   % brake mean eff pressure in kpa
    fp=(5.512e-6)*bmep*n;     % brake mean eff pressure in kw
    effm=bp*100/(bp+fp);      % mechanical efficiency
    BTE=bp*100*3600/(mfkg*LCV);          % brake thermal efficiency


AAA=[phi' p' t' ht' x' noxf' sot'];
xlswrite('2zonSIM.xlsx',AAA,10);

subplot(4,4,1)
plot(phi,p)
xlabel('Crank angle(Degree)')
ylabel('Pressure(bar)')
subplot(4,4,2)
plot(phi,t)
xlabel('Crank angle(Degree)')
ylabel('Temperature(k)')
subplot(4,4,3)
plot(phi,ht)
xlabel('Crank angle(Degree)')
ylabel('Heat Release Rate(J/K)')
subplot(4,4,4)
plot(phi,chr)
xlabel('Crank angle(Degree)')
ylabel('cumm Heat Release Rate(J/K)')
subplot(4,4,5)
plot(phi,yco2)
xlabel('Crank angle(Degree)')
ylabel('co2')
subplot(4,4,6)
plot(phi,yh2o)
xlabel('Crank angle(Degree)')
ylabel('H2O')
subplot(4,4,7)
plot(phi,yn2)
xlabel('Crank angle(Degree)')
ylabel('N2')
subplot(4,4,8)
plot(phi,yo2)
xlabel('Crank angle(Degree)')
ylabel('O2')
subplot(4,4,9)
plot(phi,yco)
xlabel('Crank angle(Degree)')
ylabel('CO')
subplot(4,4,10)
plot(phi,yh2)
xlabel('Crank angle(Degree)')
ylabel('H2')
subplot(4,4,11)
plot(phi,yh)
xlabel('Crank angle(Degree)')
ylabel('H')
```

```
subplot(4,4,12)
plot(phi,yo)
xlabel('Crank angle(Degree)')
ylabel('O')
subplot(4,4,13)
plot(phi,yoh)
xlabel('Crank angle(Degree)')
ylabel('OH')
subplot(4,4,14)
plot(phi,x)
xlabel('Crank angle(Degree)')
ylabel('mfb')
subplot(4,4,15)
plot(phi,noxf)
xlabel('Crank angle(Degree)')
ylabel('NOx')
subplot(4,4,16)
plot(phi,sot)
xlabel('Crank angle(Degree)')
ylabel('soot')

%%%%%%%%%%%%%%%%%%%%%%%%%%%%%%%%%%%%%%%%%%%%%%%%%%%%%%%%%%%%%%%%%%%%%%%%%%%%%%%
function [fe fed dq dw]=ebalancec24(p1,p2,t1,t2,v1,v2,q,mloss,mf)
M=170;
afr=40;
mfrt=1.18;  % in kg/hr
n=1500;
matot=afr*mfrt*2.8e-3/M ;
mat=afr*mfrt;    % total mass of air in kg
s=0.11;d=0.0875;
 E1=iienergy24(t1)*matot*1000;
 E2=iienergy24(t2)*matot*1000;
      dw=0.5*(p1+p2)*(v2-v1);
        tg=0.5*(t1+t2);    ha=ientalpy24(tg);
        mua=3.3*1e-7*(tg^0.7);
        mua=mua/(1+0.027*0.94);
        re=(0.0387*n*s*d)/mua;
        lg=1005*mua/0.7 ;                       % thermal conductivity
        dq=((0.2626/d)*lg*(re^0.6)*(450-tg)+5.67*(1e-8)*(450^4-tg^4))/(6*n);
% annand formula from rajendraprasad paper
          fe=E2-E1+dw-dq-q-mloss*ha-ha*mf;                  %energy balance
          dqd=((0.2626/d)*lg*(re^0.6)*(-1)+5.67*(1e-8)*(-4*tg^3))/(6*n);
          fed=mat*cvmol(t2)*t2;
%%%%%%%%%%%%%%%%%%%%%%%%%%%%%%%%%%%%%%%%%%%%%%%%%%%%%%%%%%%%%%%%%%%%%%%%%%%%%%%
function [fe fed dq dw]=ebalance24(p1,p2,t1,t2,v1,v2)
M=170;
afrs=15;
afr=40;
mfrt=0.5*0.028e-3;        % total mass of fuel kg/cycle
n=1500;
matot=afr*mfrt/29; % total mass of fuel kmol/cycle
mat=afr*mfrt;      % total mass of air in kg
s=0.11;d=0.0875;
 E1=ienergy24(t1)*matot*1000;
 E2=ienergy24(t2)*matot*1000;
      dw=0.5*(p1+p2)*(v2-v1);
```

```
          tg=0.5*(t1+t2);
          mua=3.3*1e-7*(tg^0.7);
          mua=mua/(1+0.027*afr/afrs);
          re=(0.0387*n*s*d)/mua;
          lg=1005*mua/0.7 ;                      % thermal conductivity
          dq=((0.2626/d)*lg*(re^0.6)*(450-tg)+5.67*(1e-8)*(450^4-
tg^4))/(6*n);  % annand formula from rajendraprasad paper
          fe=E2-E1+dw-dq;                 %energy balance
          %dqd=((0.2626/d)*lg*(re^0.6)*(-1)+5.67*(1e-8)*(-4*tg^3))/(6*n);
          fed=matot*1000*cvmol(t2)*t2;

%%%%%%%%%%%%%%%%%%%%%%%%%%%%%%%%%%%%%%%%%%%%%%%%%%%%%%%%%%%%%%%%%%%%%%%%%%%
function [u h]=ienergy24(t)
hn2=8.314*(3.34*t+2.94e-4*t^2+1.95e-9*t^3-6.57e-12*t^4);
ho2=8.314*(3.25*t+6.52e-4*t^2-1.50e-7*t^3+1.54e-11*t^4);
h=0.79*hn2+0.21*ho2;
u=h-8.314*t;        % internal energy in j/mol
%un2=8.314*(3.34*t+2.94e-4*t^2+1.95e-9*t^3-6.57e-12*t^4)-8.314*t;
%uo2=8.314*(3.25*t+6.52e-4*t^2-1.5e-7*t^3+1.54e-11*t^4)-8.314*t;
%u=0.79*un2+0.21*uo2;    %internal energy in j/mol

%%%%%%%%%%%%%%%%%%%%%%%%%%%%%%%%%%%%%%%%%%%%%%%%%%%%%%%%%%%%%%%%%%%%%%%%%%%
function y=soot(msn,dmf,p,t,po2)
n=1500;
dmsf=0.8*dmf^0.8*p^0.5*exp(-3000/(8314*t))*6*n;
dmsc=0.8*msn*(po2/p)*p^2.5*exp(-50000/(8314*t))*6*n;
y=(dmsf-dmsc)/1e12;
```

CHAPTER-1

INTRODUCTION

1.1 Need for Biofuels

Energy sustainability is one of the major tasks of any country, because any country's economic development depends mainly on electrical energy generation and the energy sources available. The gap between the energy demand and supply increases unpredictably every year, as a result of continuous growth in industrialization and improvement in life style. The electrical energy is consumed heavily in all the sectors including industries, households, transportation, commerce and agriculture. During the last two decades, almost all the houses in the developed and developing countries have been provided with electricity for lighting, domestic appliances, refrigeration and air conditioning. In order to increase the supply of domestic appliances and utilities, many industries and manufacturing units have come up, which also consume huge electricity. The consumption of electrical energy in commercial buildings for lighting, air conditioning, recreation purposes and other utilities has also increased enormously. In the transportation sector, electricity is used in electromotive and service units, while the agricultural sector uses electricity primarily for irrigation, mills and processing units. The global energy consumption in the year 2010 by the different sectors (IEO report 2011) is shown in Fig.1.1. [1]

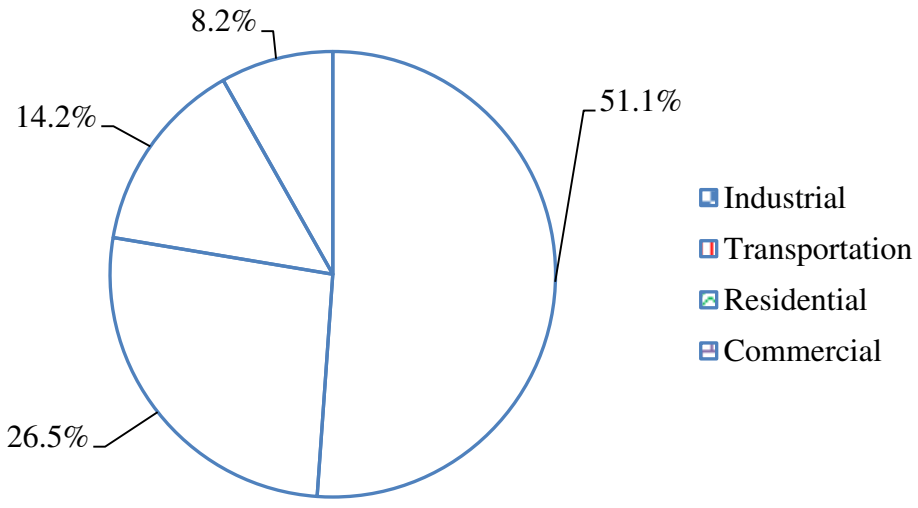

Fig.1.1 Global energy consumption by different sectors in the year 2010

Although electricity is mainly used in all the sectors, the source for the generation of electricity is mainly the combustion of fossil fuels in thermal and nuclear power plants. Over the last two centuries, the consumption of fossil fuels has increased heavily, in particular the consumption of crude oil increased largely. Consequently, the depletion of fossil fuels and the cost of crude oil have increased exponentially. The transportation sector consumes large quantities of petroleum fuels in internal combustion engines and gas turbines.

The US Department of Energy states that the world's oil supply will reach its maximum production and midpoint of depletion sometime around the year 2020. The depleting reserves and environmental issues, in addition to global warming and the ozone depletion concerns have pushed the countries towards searching for alternative energy sources, with particular emphasis on those renewable from nature [2]. While increasing the energy supply for meeting the energy demand in all the sectors, there is also a negative effect on the environment. The various pollutants from the power plants, industries and transport vehicles are the reasons for increasing the global warming potential (GWP) and ozone depletion potential (ODP). The major countries which emit CO_2 emissions from the combustion of fossil fuels and some industrial processes in the year 2010, are given in Fig.1.2. (Courtesy-IEA)[3].

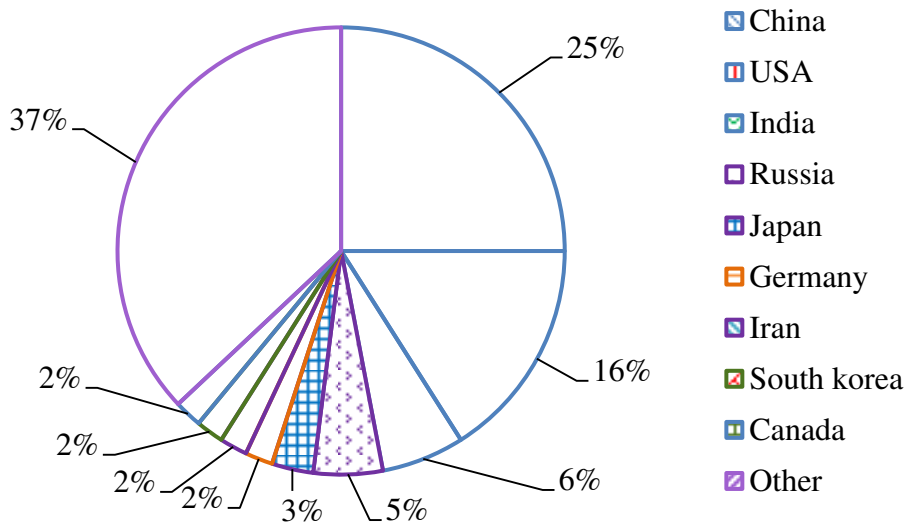

Fig.1.2 Major Countries emit higher CO_2 emissions in the year 2010

Though the depletion of fossil fuels began long back, the realization came only after the two wars associated with oil crisis in the late 1970s and 1980s. Since then, the world research community has been striving hard to find various alternative fuels that are long lasting and eco-friendly, to substitute the petroleum fuels. They also tried to reduce the pollutants from

the combustion devices by introducing emission control devices. In this context, the alternative fuels can be divided into two types; (i) renewable energy sources, and ii) non-conventional energy sources. Renewable energy sources offer distinct advantages that they are abundantly available, derivable from nature, eco-friendly, have a low carbon credit, and are cheaper. There has been a focus on trapping the energy from various renewable sources, such as solar, wind, tide, ocean and biomass. Among these sources, biomass is considered as a potential source in developing and agrarian countries.

The biofuels derived from biomass are considered as good alternative fuels for petroleum fuels. Biofuels are mainly categorized into (i) First generation biofuels,and (ii) Second generation biofuels. The classification of the first and second generation biofuels is given in a block diagram which is shown in Fig.1.3 in the next page, and they are discussed briefly in the subsequent sections.

1.2 First generation biofuels

Bioethanol and biodiesel are referred to as the first generation biofuels.

1.2.1 Bioethanol

The feedstocks used in the production of bioethanol are sugar cane, sugar beet, wheat, molasses, cassava, sweet potato, corn, maize, switchgrass, grass, miscanthus, corn stover and cereals etc. [4-7]. Hydrolysis and fermentation are the common methods for producing bioethanol from the feedstocks. Bioethanol produced by the fermentation of sugar and starch based feedstock was earlier called as ethanol only. Ethanol is produced mainly from sugar cane in developing countries with warm climates. It is much cheaper to produce ethanol from grain or sugar beet in IEA countries. Brazil and India are the top ranking sugar cane producers in the world, where, sugar cane based bioethanol is found to be economically feasible [8]. Ethanol has a high octane value, which makes it an attractive blending component; it has generally good performance characteristics, though its energy content by volume is only two-thirds that of gasoline. Efforts were made to introduce ethanol as an alternative fuel for spark-ignition (SI) engines. A low percentage of ethanol blended with gasoline, for example, 10% ethanol with 90% gasoline (E10) has been used as gasohol in Brazil for over 20 years. These blends are already available as gasoline vehicle fuel, in the fuel filling stations of many countries; they do not require any engine modifications and can be used in the same way as gasoline. Higher-percentage blends, with more than 30% ethanol, or pure ethanol can only be used with some modifications in the vehicle engine [9].

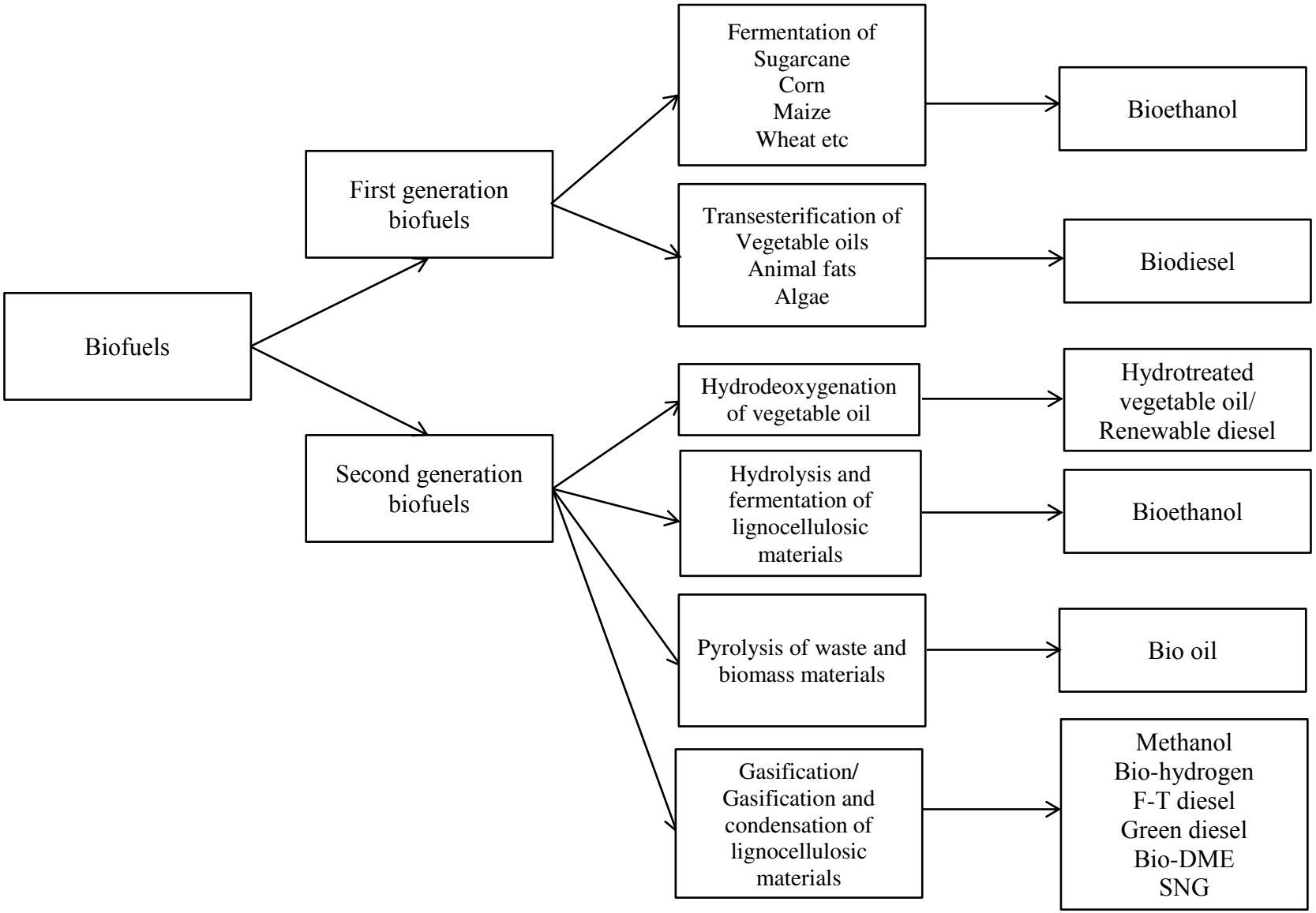

Fig.1.3 Block diagram of first and second generation biofuels

In the case of CI engine vehicles, upto 20% by volume of bioethanol (E20) has been used with diesel in the form of solution/emulsion [10]. Higher percentages by volume of ethanol can be used in CI engines, but it requires some engine modifications. The nitric oxide (NO) and smoke emissions from CI engines operated with bioethanol-diesel emulsions are reported to be lower, compared to that of diesel fuel operation. It is reported that, poor lubrication properties, poor miscibility with diesel fuel in the presence of water, corrosion and chemical degradation of engine materials, were the problems associated with ethanol diesel mixtures [11].

1.2.2 Biodiesel

Vegetable oil has been the primary candidate as a substitute for diesel fuel since the early 1900s, and this interest continued in various parts of the world during the Second World War due to insufficient supply and logistic difficulties of fossil fuel. Even the inventor of the diesel engine Rudolph Diesel demonstrated his engine with peanut oil only. Later during the 1970s, the control of oil production by the Organization of Petroleum Exporting Countries (OPEC), and the subsequent rise in fuel prices rekindled the interest in alternative fuels, including vegetable oils as fuels for diesel engines.

The name biodiesel was introduced in the USA in 1992, by the National Soy Diesel Development Board (presently National Bio-diesel Board), which has commercialized biodiesel in the USA. Biodiesel is a simplified version of fatty acids those are available in vegetable oils, animal fats, algae and other materials. It is derived from these sources by the transesterification process. The triglycerides present in these feedstocks are converted into mono esters by reacting them with alcohol in the presence of chemical catalysts. Commonly, the methyl or, ethyl or butyl esters of these feed stocks are known as biodiesel. However, the methyl esters of these feedstocks are mainly focused on, because methanol has a few advantages compared to ethanol and butanol. They are its high reactivity [12], lesser cost and easier methanol recovery, as it does not form azeotrope [13]. Various sources used for biodiesel production and the problems associated with its production are shown in Fig.1.4. In general, biodiesel feedstocks can be categorized into four groups: a) vegetable oils (edible or nonedible oil), b) animal fats, c) algae and d) other materials, as shown in the figure. The various sources of biodiesel production, oil yield and biodiesel yield are given in Table 1.1.

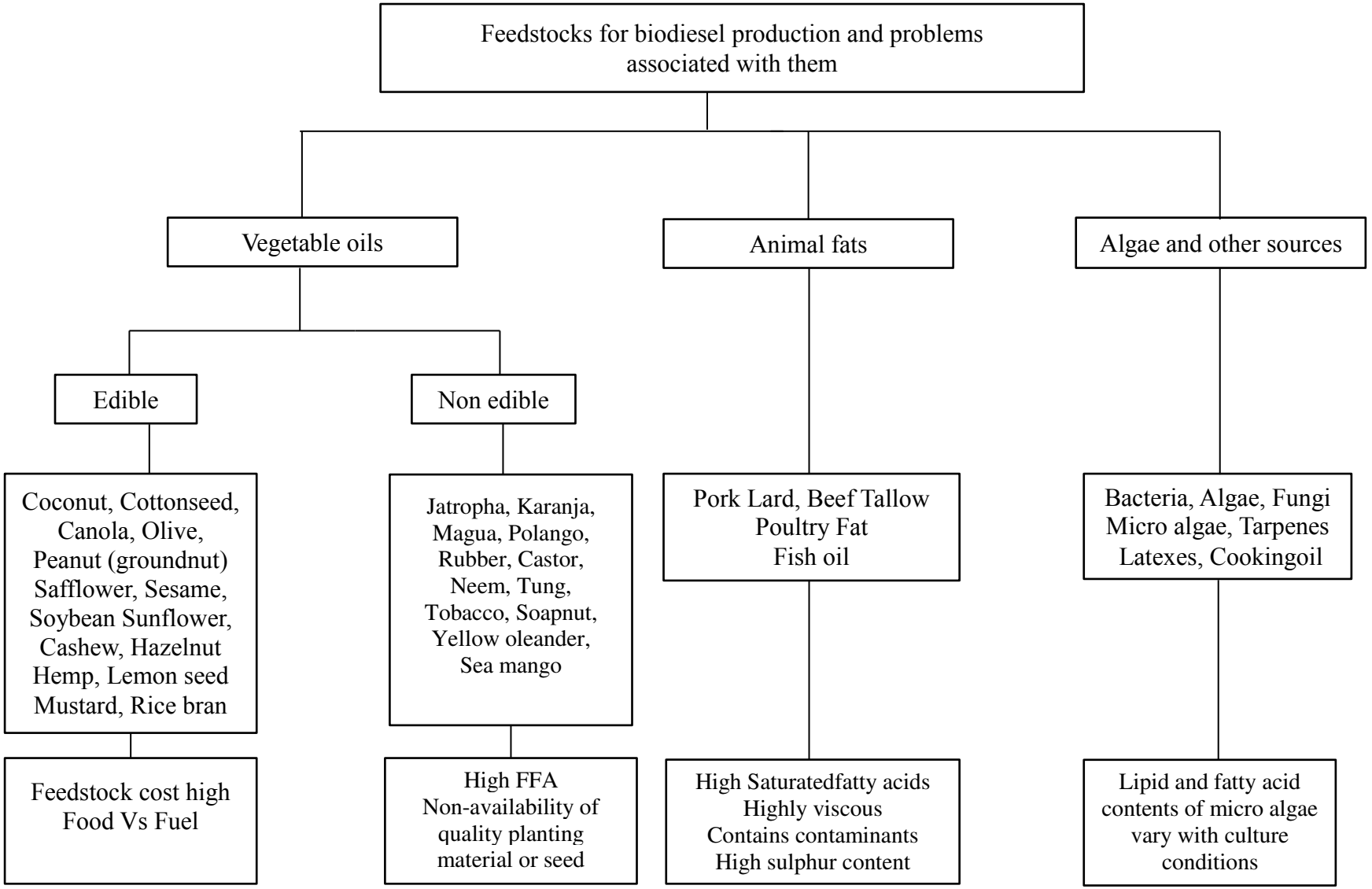

Fig.1.4 Sources of biodiesel production and problems

Table 1.1 Oil content and the biodiesel yield of different oil sources

Nature	Oil Source	Oil content (%)	Biodiesel yield (%)
Edible	Soybean	15-20	>95
	Sunflower	25-35	97.1
	Palm	30-60	89.2
	Peanut	45-55	89
	Corn	48	85-96
	Camelina	29.9-38.3	97.9
	Canola	43	80-95
	Pumpkin	50	97.5
	Rice bran	15-23	< 96
	Coconut	63-65	98
	Olive	45-70	92
Non-Edible	Jatropha (Jatropha curcas)	20–60	98
	Karanja/ Honge (Pongamiapinnata)	25–50	97-98
	Mahua (Madhucaindica)	35–50	98
	Cottonseed	17–25	96.9
	Rapeseed	38-46	95-96
	Neem (Azadirachtaindica)	20–30	88-94
	Putranjiva (Putranjivaroxburghii)	42	91
	Tobacco (Nicotianatabacum)	36-41	88
	Polanga (Calophylluminophyllum)	65	85
	Cardoon (Cynaracardunculus)	25-26	92
	Castor (Ricinuscommunis)	45-50	90
	Jojoba (Simmondsiachinensis)	45-55	93
	Moringa (Moringaoleifera)	45–50	82
	Poon (Sterculiafoetida)	50–55	88
	Sea mango (Cerberaodollam)	54	83.8
Animal Fat	Tallow	41	98.28
	Poultry	-	99.7
Others	Used cooking oil	-	94.6
	Micro algae	20-50	60

Biodiesels play an important role in meeting the world's future fuel requirements, in view of their nature (less toxic), and they have an edge over conventional diesel fuel as they are obtained from renewable sources.

Fig.1.5 shows the general chemical reaction involved in the production of methyl ester from the vegetable oils.

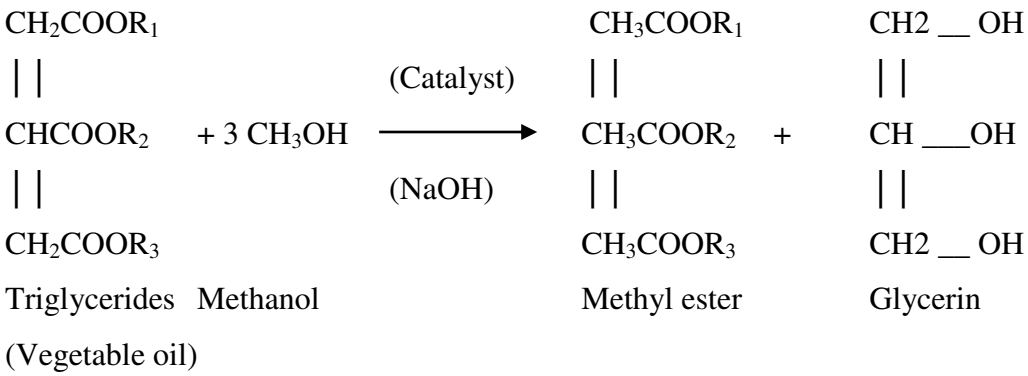

Fig. 1.5 Production of methyl ester by transesterification process

Table 1.2 gives various factors involved in transesterification process of biodiesel production.

Table 1.2 Factors involved in biodiesel production [8]

Feed stock	**Catalyst used**	**Alcohol**	**Temperature /Time**	**Alcohol to oil ratio**	**Biodiesel yield (%)**
Peanut oil	NaOH	Methanol	65°C (60 min)	6:1	90
Soybean	Absence of catalyst	Supercritical methanol, CO_2 co-solvent	280°C	24 and CO_2/methanol = 0.1	98
Soybean	Solid super acid catalysts of sulfatedtin and zirconium oxides tungstated zirconia, Noctanoic acid	Methanol	200-300°C (120min) 175-200°C	6:1	90 for both
Sunflower	Supercritical fluids, Enzyme in supercritical CO_2	Supercritical methanol and ethanol	200-400°C	40:1	800-100
Canola oil	Two-stage process, KOH	Methanol	25°C (90 min)	6:1	87
Karanja	KOH,Solid acid catalysts viz.Hb; K-10 and ZnO	Methanol Tetrahydrofuran (THF), cosolvent	60°C (90 min)	10:1	92 95
Jatropha	Two stage, NaOH	Methanol	60-65°C(90min)	5:1	98
Polanga	Sulphuric acid, KOH	Methanol	65°C (120 min)	6:1	85
Magua oil	Sulphuric acid, KOH	Methanol	70°C (90 min)	6:1	98
Micro algae	Sulfuric acid	Methanol	30°C	56:1	60
Animal fat/Tallow	NaOH	Methanol	60°C (180 min)	6:1	98
Fish oil	KOH	Ethanol	25°C (60 min)	6:1	92
Waste cooking oil	KOH	Methanol	25°C (30 min)	6:1	90

The ASTM test method for diesel and biodiesel are given in Table 1.3.

Table 1.3 Standards and limits for diesel and biodiesel fuels [8]

Property	**ASTM Test method**	**ASTM D975 (diesel) Limits**	**ASTM D6751 (biodiesel, B100) Limits**
Flash point (K)	D 93	325	130 min
Water and sediment (% vol)	D 2709	0.05 max	0.05 max
Kinematic viscosity at 313 K (mm^2/s)	D 445	1.3-4.1	1.9–6.0
Sulfated ash (% wt)	D 874	–	0.02
Ash (% wt)	D 482	0.01	–
Sulfur (% wt)	D 5453	0.05	–
Sulfur (% wt)	D 2622	–	0.05
Copper strip corrosion	D 130	No. 3 max	No. 3 max
Cetane number	D 613	40 min	47 min
Aromaticity (% vol)	D 1319	35	–
Carbon residue (% mass)	D 4530	–	0.05
Carbon residue (% mass)	D 524	0.35	–
Distillation temperature (90% volume) (K)	D 1160	555 min-611 max	–

The first generation biofuels can offer some CO_2 benefits and help to improve domestic energy security. But, attention must be given on the concerns about the sources of feedstock, impact on biodiversity, land use and competition with food crops. Also, there are concerns about environmental impacts and carbon balances, which set limits in increasing the production of biofuels of the first generation category.

1.3 Second generation biofuels

Second generation biofuels are made from lignocellulosic biomass, woody crops, agricultural residues, animal waste, and non-edible vegetable oils.

1.3.1 HVO – Hydrotreated Vegetable Oils

Hydrotreating of vegetable oils is a novel way to produce very high quality and bio based diesel fuels without compromising the fuel properties. The HVO fuel is also referred to as “renewable diesel” instead of “biodiesel” which the name is given to the fatty acid methyl esters. In the HVO production process, hydrogen is used to remove the oxygen from the triglyceride (vegetable oil). This process is described as hydrodeoxygenation.

1.3.2. Processing of lignocellulosic/plant biomass

Plant based biomass is one of the most abundant and unutilized biological resources, and is seen as a promising source of material for fuels and raw materials. A plant biomass can simply be burnt in order to produce heat and electricity. There are two principal methods available for generating heat and electricity from biomass; they are (i) biological conversion, and (ii) thermochemical conversion [14].

1.3.2.1 Biological conversion

Biological conversion technologies involve microbial and enzymatic processes for producing sugar from biomass such as lignocellulosic, starch and cellulosic materials. These sugars can be converted into alcohol and other solvents of interest for fuels and chemicals [15]. Agricultural residue, forest residue, post-harvest processing of industrial food crops and waste wood are examples of feedstocks of lignocellulosic biomass. The conversion of lignocellulosic biomass into bioethanol involves a three step process; i.e. (i) pretreatment of biomass, (ii) acid or enzymatic hydrolysis and (iii) fermentation/distillation; it is shown in Fig.1.6.

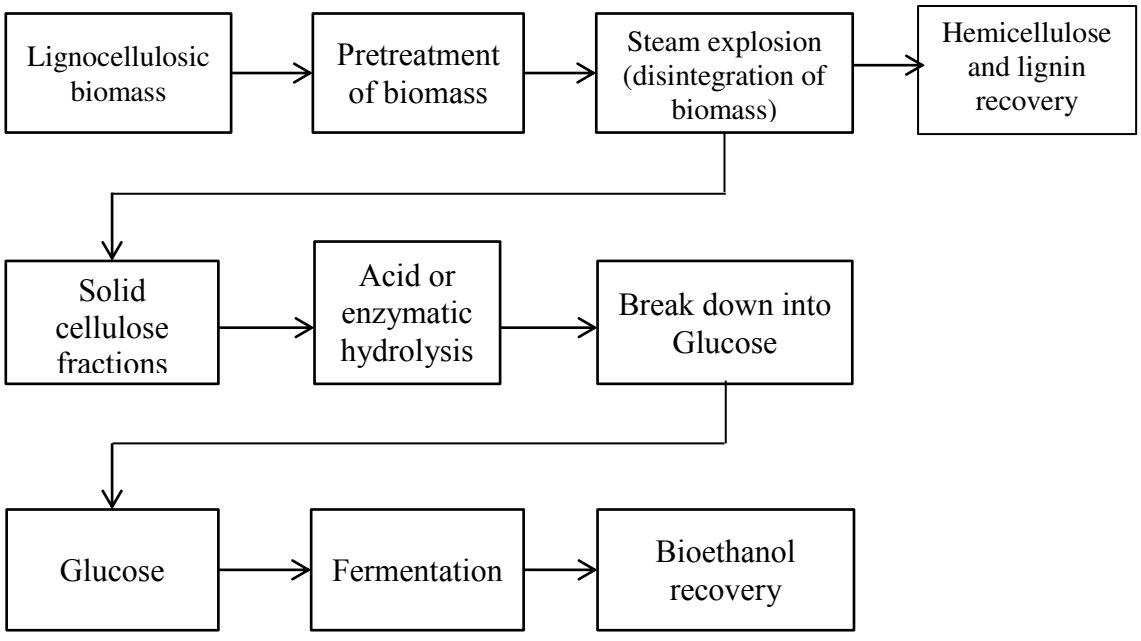

Fig.1.6 Bioethanol production from lignocellulosic biomass

1.3.2.2 Thermochemical conversion

The thermochemical conversion of biomass materials includes, direct combustion, gasification, liquefaction, and pyrolysis process.

(a) Direct combustion

The direct combustion is the chemical reaction between a fuel and oxygen which is usually air, and is more commonly known as burning. The principal products of direct combustion are carbon dioxide, water vapour and some amount of heat release. The biomass can be directly combusted to produce heat in chulas, furnaces and boilers.

(b) Gasification

The gasification method involves reacting biomass with air/oxygen,or steam to produce a gaseous mixture of CO, CO_2, H_2, CH_4, and N_2, known as producer gas or syngas, depending on the relative compositions of the constituents. Producer gas is one of the primary fuels used in stationary power generation applications, whereas syngas can be used to make a range of fuels and chemicals. Bio-hydrogen can be produced from syngas by the water-gas-shifting process, while Fischer-Tropsch (F-T) diesel or synthetic diesel can be produced by the Fischer-Tropsch (F-T) synthesis process. These fuels are also named as BTL (Biomass-to-Liquids) and GTL (Gas-to-Liquids). The F-T synthesis has been used since 1930, to produce hydrocarbon fuels from syngas. The production of methanol from syngas has been practiced since the year 1920 [15].

(c) Liquefaction

Biomass materials can be converted directly into a liquid similar to heavy oils, by reacting them with synthesis gas in the presence of a suitable catalyst in the liquefaction process. This process usually requires solvents, reacting gases such as CO or H_2 and/or catalysts in addition to the biomass. Water insoluble oils of high viscosity are produced in this process.

(d) Pyrolysis

It is a thermal degradation of biomass in the absence of oxygen or with very little presence of oxygen. In this process, the biomass-particularly solid or liquid is fed into a reactor which is indirectly heated up. During heating, the vapours evolved from the reactor are condensed in a condenser preferably water cooled. Three principal products are obtained from the biomass pyrolysis process, namely, (i) bio oil (liquid), (ii) pyro gas (gas), and (iii) char (solid). This

method has been studied, mainly to obtain a liquid product having a medium calorific value. Depending on the operating conditions, the pyrolysis process can be divided into three types: (i) Conventional pyrolysis, or slow pyrolysis (ii) Fast pyrolysis, and (iii) Flash pyrolysis.

(i) Conventional pyrolysis or slow pyrolysis

This process has been applied for thousands of years, and used mainly for the production of charcoal. In this method, the biomass is heated to a temperature about 300-500 °C with a slow heating rate of 3 - 5°C/min. The vapor residence time varies from 5 min to 30 min. The slow pyrolysis process yields charcoal of around 35–40%, together with 30% liquid (bio oil) [16].

(ii) Fast pyrolysis

It is a high-temperature process, in which biomass is rapidly heated in the absence of oxygen. It occurs in the high temperature range of 850-1250 K with a fast heating rate (10-200 K/s), short solid residence time (0.5-10 s) and fine particle size (<1 mm). The fast pyrolysis process produces 60-75 wt % of liquid bio oil, 15-25 wt % of solid char, and 10-20 wt % of non-condensable gases, depending on the feedstock used. No waste is generated, because the bio oil and solid char can each be used as a fuel and the gas can be recycled back into the process.

(iii) Flash pyrolysis

It is a process that occurs in the temperature range of 1050-1300 K, with a fast heating rate (>1000 K/s), short residence time (<0.5 s) and very fine particle size (<0.2 mm). The bio oil production from flash pyrolysis can be mixed with the char to produce bio-slurry, which can be used as a fuel in the gasifier for efficient conversion into syngas. Upto 70% of bio oil yield can be obtained from the flash pyrolysis process. This bio oil can be used in engines and turbines as a supplementary fuel.

The main advantage of pyrolysis is that, the feedstocks which are not convertible to ethanol or biodiesel can be converted into value added products. The other advantages include low production cost, high thermal efficiency, low fossil fuel input, and CO_2 neutrality. It also offers the flexibility of installation and operation with respect to time, scale and place, handling of the products and more-consistent quality, in comparison with gasification [15].

The pyrolysis process has a few drawbacks over the other processes. The bio oil obtained from this process has a high oxygen content which reduces its calorific value. The bio oil also contains many reactive components that can form higher molecular weight species. These components result in an increase in the viscosity and decrease in volatility, which is unfavourable for fueling diesel engines. The hydroscopic nature of the bio oil weakens its stability during blending with diesel fuel.

1.4 Indian scenario on biofuels

India depends heavily on the import of crude oil, and as a result the oil price shoots up frequently. Therefore, the government of India is very keen to introduce a variety of alternative fuels, mainly in the transportation sector. India imports more than 40% of its edible oil requirement, and hence non-edible oils are used for the development of biodiesel. India is an agrarian nation and has a rich plant biodiversity, which can support the development of biodiesel. India also has a vast geographical area with agricultural lands as well as wastelands in which oil bearing plants can be planted. Common non-edible oil bearing trees include Jatropha, Karanja, Neem,Mahua (madhucaindica), etc. These species are, at present insufficient to meet the demand for raw material in large scale production of biodiesel. Hence, there have been initiatives by the government, and also interest from a few private firms to enhance the production and distribution facilities of biodiesel throughout the country. Azam et al. [17] have studied the profile of 75 indigenous plant species in India, which contain 30% or more oil in their seeds, fruits or nuts. Among these plants, 26 species were found to be most suitable for use as biodiesel based on their saponification number, iodine value, cetane number and fatty acid composition, and they also met the biodiesel standards of USA (ASTM D 6751-02, ASTM PS 121-99), Germany (DIN V 51606) and European Standard Organization (EN 14214). It is also reported that 11 other plant species met the specifications of the US biodiesel standards. Among these species, Jatropha (Jatropha curcas), Karanja (Pongamiapinnata), Neem (Azhardictaindica), Mahua (Madhucaindica) and Polanga (Calophylluminophyllum) have drawn the attention of researchers and biodiesel manufacturers in India, while the feasibility of the rest of the plant species still remains unexplored. There are a few drawbacks with feed stock available in India, that pose a setback in promoting large biodiesel production, which are as follows:

i) Non homogeneity of the oil seeds available

ii) Collection and transportation of oil seeds

iii) Oil expellers are available only for edible oils, which do not allow expelling oil from non-edible oil seeds.

1.5 Biodiesel fueled diesel engines - An overview

The biodiesel produced by the transesterification process is completely miscible with diesel in any proportion. The physicochemical properties of biodiesel produced from different oil sources, such as oxygen content, cetane number, flash point, viscosity, density and heating value, can potentially improve or deteriorate the engine performance and emission characteristics [18]. The viscosity of biodiesel is marginally close to that of diesel, and hence there are no problems in the existing fuel handling system [19]. The flash point of biodiesel gets lowered after transesterification and the cetane number gets improved. Even lower concentrations of biodiesel act as cetane number improvers for the biodiesel blend. The calorific value of biodiesel is also found to be very close to that of diesel. Investigations from an engine fueled with biodiesel or biodiesel blends suggested that the thermal efficiency of the engine is marginally high. The exhaust gas temperature is higher while, smoke opacity is lower for the biodiesel blends. The possible reason is the additional lubricity of the biodiesel, which reduces the frictional losses. The energy saved in this manner will increase the thermal efficiency and reduce the cooling and exhaust losses from the engine. The thermal efficiency starts reducing after a certain concentration of biodiesel. The flash point, density, pour point, cetane number and calorific value of biodiesel are in very close to those of diesel. Twenty percent biodiesel (B2O) is considered to be the optimum ratio of the biodiesel-diesel blend for improved performance in a diesel engine.

The molecular structure of biodiesel is similar to that of diesel fuel, and it contains additional oxygen content in it, which is useful to reduce the CO, UHC and smoke emissions in the engine exhaust. In addition, biodiesel is bio-degradable; it can be mixed with diesel fuel in any ratio, and is sulfur-free. Although, it has many advantages over diesel fuel, there are several problems associated with biodiesel which needs to be addressed, such as its lower heating value, higher viscosity, poor cold flow properties and oxidation stability [20-23]. The NO emission from the biodiesel fueled diesel engines is reported to be higher compared to that of diesel operation. Table 1.4 gives the percentage variation in the average biodiesel emissions compared to that of diesel fuel (*Source:EPA, NREL) [24].

Table 1.4 Average biodiesel emissions compared with conventional diesel

Type of emission	B100	B20
Regulated Emissions		
Total Unburned Hydrocarbons (UBHC)	-67%	-20%
Carbon Monoxide (CO)	-48%	-12%
Particulate Matter (PM)	-47%	-12%
Oxides of nitrogen (NO_x)	10%	-2% to 2%
Non-Regulated Emissions		
Sulphates	-100%	-20%
Polycyclic Aromatic Hydrocarbons (PAH)	-80%	-13%
Nitrated PAHs	-90%	-50%
Ozone Potential	-50%	-10%
Carbon Dioxide (CO_2)	-78%	-15%

1.6. NO_x reduction strategies

Diesel engines emit higher NO_x emissions than gasoline engines, and the research on the control of NO_x emissions has advanced significantly, since Zeldovich first proposed the thermal NO_x formation mechanism in 1943. The methods involved, or those that attempted to reduce the NO_x emission in diesel engines, are as follows:

i. Retardation of injection timing,
ii. Use of low injection pressure,
iii. Exhaust gas recirculation, (EGR)
iv. Multivalving/split injection
v. Modification in the combustion chamber geometry to enhance the swirl and squish
vi. Reducing the combustion temperature by water injection or use of emulsified fuels
vii. Excessive cooling of intake air
viii. Inducting fuels with high latent heat of vaporization like alcohol or DEE along with air in the suction
ix. Addition of cetane improvers like 2-ethyl hexyl nitrate
x. Use of biomass based fuels which contain water content in them

Many researchers have attempted to reduce the NO_x emissions from the biodiesel fueled engines, by adopting any one of the above techniques, and now biodiesel run buses in some countries implement the techniques such as EGR etc.

1.7 Present Investigation

This research work intends to replace the usage of diesel fuel completely, and also a certain percentage of JME. Bio oil contains water and phenols that may be helpful to reduce the NO_x emissions in a biodiesel fueled engine.

The main objectives of the present work are as follows:

i) To prepare the JME-WPO emulsions using different surfactants and characterise them as alternative fuels for CI engines.
ii) To evaluate the combustion, performance and emission behaviour of a single cylinder, four stroke, air cooled, direct injection (DI) diesel engine developing a power of 4.4kW at 1500 rpm with different JME-WPO emulsions.
iii) To find the optimum emulsion and upgrade the emulsion quality by acid treatment.
iv) To validate the experimental results using a mathematical modelling.
v) To study the combined effects of compression ratio, injection timing and nozzle opening pressure on the combustion, performance and emission characteristics of the optimum upgraded fuel emulsion.
vi) To assess the lubrication oil properties and short term durability issues.

1.8 Organization of thesis

Chapter 1 Introduction

This chapter briefs the need for biofuels and their classification, an overview of biodiesel fueled diesel engines, the Indian scenario on biofuels and also states the objectives of the present research work.

Chapter 2 Literature Review

A comprehensive review of research works pertaining to the production and characterization of Jatropha methyl ester (JME) for its suitability as an alternative fuel in CI engines are given. The review work also discusses the up to date literature available on the utilization of JME in CI engines. The various issues related to combustion, performance and emission parameters of the CI engine fueled with the JME are discussed in this chapter. The review also includes the NO_x emission reduction strategies adopted in biodiesel fueled engines. The

literature on the production and utilization of Wood pyrolysis oil (WPO) in diesel engines is also presented in this chapter.

Chapter 3 Production and characterization of test materials

This chapter details the methods and materials involved in the production of JME, WPO and JME-WPO emulsions. The chapter also discusses the characterization of the test fuels considered in this study. The test materials have also been tested by the TGA, CHNS and SEM for determining the important properties that there involved in this study.

Chapter 4 Engine experimental setup, instrumentation and experimental methodology

In this chapter, the necessary engine experimental setup and other accessories are described systematically. The method of determining the uncertainty of the experimentation is also included at the end of this chapter. The details on various methodologies adopted, and the modifications involved in the engine experimental setup are also discussed in this chapter. The methods of calculating the important combustion, performance and emissions parameters are discussed. It also explains the method of study on lubricating oil properties, and a few durability issues on the test engine components.

Chapter 5 Results and discussion

Detailed discussions on the comparative analysis of the combustion, performance and emission results obtained from the experimental investigation from a diesel engine fueled with different JME-WPO emulsions under various operating conditions are given in this chapter. This chapter also discusses the sample validation of the experimental results by a theoretical modeling and MATLAB programming for the prediction of heat release and emissions, viz., the NO and smoke of the diesel engine fueled with JME-WPO emulsions.

Chapter 6 Conclusions

The summary of the findings from the experimental investigation carried out in this study are given in this chapter. It also mentions the important conclusions of the investigation, and the scope for future work.

CHAPTER 2
LITERATURE REVIEW

2.1. General

This chapter presents a review of the various research works related to the production of Jatropha methyl ester (JME) and, a bio oil produced by the pyrolysis of biomass. The chapter also includes a review of the utilization of JME and its blends with diesel and other fuels in diesel engines, with fuel and engine modifications. The efforts that have been proposed worldwide to reduce the higher oxides of nitrogen (NO_x) emissions from the diesel engine fueled with the JME and its blends are also reviewed and presented. Further, the review of the utilization of bio oil/WPO in a diesel engine and the problems associated with the WPO, when it is used in its sole form, are given in this chapter.

2.2 Importance of Jatropha methyl ester

The esters of Jatropha oil were investigated by several researchers for their use in CI engines. Numerous documents are available related to the investigation on the use of the esters of Jatropha in diesel engines. The researcher has tried to collect and review the research works as much as possible, to identify the research problem.

Biodiesel from Jatropha oil can be produced by different transesterification methods. Alkali catalyzed [25-28], acid catalyzed [29], enzyme catalyzed [30-31], non-catalytic supercritical alcohol [32-34] and ultrasound assisted transesterification [35] methods have been adopted to produce biodiesel from Jatropha oil. Many researchers have investigated the operating parameters that affect alkali catalyzed transesterification reactions. The optimum variables for the effective transesterification of Jatropha oil are 20% methanol (by weight of oil), a molar ratio of methanol to oil of 5:1, and 1.0% of NaOH as a catalyst (by weight of oil). A maximum methyl ester yield of 98% was obtained after 90 min with a 60^{o}C reaction temperature, and the biodiesel obtained was found to be within the ASTM specified limits of biodiesel [25-26] obtained similar optimum transesterification conditions in their previous work, except that they did so by using KOH as a catalyst. Sahoo and Das [27] have also developed a method of the preparation of biodiesel from non-edible oils, such as Jatropha, Karanja and Polanga. They found that the conversion efficiency is strongly affected by the amount of alcohol because, an excess of alcohol is required to shift the reaction close to

completion. By concentrating on Jatropha curcas, the volumetric ratio of oil to methanol is 11:1, together with 1.1% of KOH by volume basis, which completed the transesterification process within 120 min at 66^{o}C, with a 93% yield of Jatropha methyl ester.

There are a number of documented research works available to prove the utilization of JME in its sole form, and in the blended form with diesel and other fuels, without any modifications to the diesel engine. Table 2.1 presents the review on the performance, combustion and emission parameters of a diesel engine fueled with the JME and its blends with diesel reported by the researchers. The performance, combustion and emission parameters of JME and its blends with different engine modifications are presented in Table 2.2. A literature review pertaining to different experimental studies on the performance, emission and combustion behavior of the CI engine run on JME and its diesel blends with engine modifications is given in Table 2.3.

2.3 NO_x emissions from JME fueled diesel engine

The common behavior of a compression ignition (CI) engine from the emission point of view is the trade-off between oxides of nitrogen (NO_x) and smoke. Although, the CI engines are well suited for today's transport and power applications, the emissions, particularly, the NO_x and the particulate emissions from these engines are difficult to control, irrespective of the type of fuel used. The increased NO_x levels in the air contribute to global warming and acid rain, affecting the human organs, and causing visual impairment, swelling of throats and other respiratory problems. On the other hand, particulates from a diesel engine affect the respiratory system. It is a major concern for researchers to identify suitable technique or method, to reduce the NO_x emission and particulates from CI engines.

So far, many researchers have proved that the NO_x emission from biodiesel fueled engines is higher compared to diesel operation, while a few researchers have proved that the NO_x emissions from some of the biodiesel fueled engines produce lower NO_x emission. It was also given in the literature that a 10% increase in the biodiesel of the biodiesel-diesel blend will cause 1% increase in NO_x emission [96]. The major reasons for the increased NO_x emissions with biodiesel fuels mentioned by several researchers are listed in Table 2.4.

Table 2.1 Review on the engine performance, combustion and emission results obtained from different diesel engine configurations fueled with JME and its blends

Sl.No.	Percentage of JME	Details of engine tested	Test results	Authors/Reference	Journal/Proceedings name/volume/page
1.	JME blends with diesel	3.5 kW, IDI (Indirect Injection) engine, constant speed 2000 rpm	It was observed that the JME-diesel blends produced superior thermal efficiency and fuel consumption equivalent to diesel. Also, it was reported that there was a marginal reduction in black smoke concentration when operating on the JME and its blends. The CO and HC concentrations from the engine increased at light loads and were equivalent to those of diesel at full load.	Ishii and Takeuchi, 1987.[36]	Transactions of the ASABE. 30 (3): 0605-0609.
2.	100% JME	3.7 kW, four stroke, single cylinder, water cooled, direct injection diesel engine, constant speed 1500 rpm	Higher thermal efficiency was reported with the JME compared to that of raw Jatropha oil but, it was found to be lower than that of diesel. Smoke and particulate levels were found to be higher with Jatropha oil than that of diesel. The HC and CO emissions were marginally higher with both Jatropha oil and its methyl ester than with diesel, whereas the NO levels were found to be lower than those of diesel. The ignition delay and combustion duration were observed to be longer and the peak heat release rates were lower with Jatropha oil and JME than those of diesel.	M.Senthilkumar[a], 2001. M.Senthilkumar[b], 2003. [37-38]	[a]Journal of Energy Institute, vol. 74, pp. 24-28. [b]Biomass and Bioenergy, vol. 25, pp. 309-318.
3.	50% blend with diesel and 100% JME	3.7 kW, four stroke, single cylinder, water cooled, DI (Direct Injection), diesel engine at speed 1500 rpm and IDI engine, constant speed 2000 rpm	It was reported that the JME operation under naturally aspirated condition yielded the best result in the case of an IDI engine, with a specific fuel consumption of 0.354 kg/kWh and exhaust smoke level of 14 HSU. With B50 they observed a comparable SFC in the DI engine. Lower smoke emissions were reported with JME operation in the IDI engine compared to that of DI engine.	G.A.P. Rao, 2005 [39]	Journal of the Institution of Engineers, vol.86, pp. 72-76.

4.	15 and 20 % JME blended with diesel	3.68 kW, single cylinder, four stroke, water cooled, DI engine, constant speed 1500 rpm	Higher brake thermal efficiency, lower HC and CO emissions with B20 were reported in comparison with diesel operation.	P.Mahanta, 2006 [40]	International Energy journal, vol. 7, pp.1-8.
5.	100% JME	5.2 kW, single cylinder, four stroke, water cooled, DI diesel engine, constant speed 1500 rpm	About 7% lower brake thermal efficiency, 26% higher smoke and 65% higher HC, 37% higher CO and 10% lower NO emissions (At advanced injection timing of 27^{o} bTDC) were reported in comparison with diesel operation.	N.R. Banapurmath, 2007 [41]	Renewable Energy, vol. 33, pp. 1982-1988.
6.	20% JME blended with diesel and 100% JME	4.4 kW, single cylinder, DI diesel engine, constant speed 1500 rpm	Lower ignition delay, lower rate of pressure rise, lower brake thermal efficiency, higher NO_x, lower HC, CO and PM were reported in comparison with diesel operation.	G. Lakshmi Narayana Rao, 2007. [42]	International Journal of Green Energy, vol.4, pp. 645-658.
7.	10, 20 40% JME blends with diesel and 100% JME	3.7 kW, single cylinder, four stroke, DI, water cooled diesel engine, constant speed 1500 rpm	The brake thermal efficiency was found to be higher for blends than B100, but less than that of diesel. Lower HC, CO and smoke emissions were reported in comparison with diesel operation.	T. Venkateswara Rao, 2008. [43]	Jordan Journal of Mechanical and Industrial Engineering, vol. 2, pp. 117 - 122.
8.	20, 40, 60,80 and 100	3.68 kW, single cylinder four stroke, water cooled diesel engine, constant speed 1500 rpm	Higher brake thermal efficiency with B20 was reported in comparison with diesel operation.	Kalbande, 2008 [44]	ARPN Journal of Engineering and Applied Sciences, vol.3, pp. 7-13.
9.	25, 50, 75 and 100	3.68 kW, single cylinder, four stroke, water cooled diesel engine, constant speed 1500 rpm	Higher thermal efficiency, higher exhaust gas temperature, lower smoke, and 14% lower CO and CO_2 emissions were observed. Higher NO_x emissions were reported in comparison with diesel operation.	Y.V.H.Rao, 2009 [45]	Thermal Science, vol. 13, pp. 207-217.

10.	20,50 and 100	44.1 kW, 3-cylinder, AVL make CI engine, at variable speeds (1200, 1800 and 2200 rpm)	About 28.57%, 40.9%, 64.28% lower smoke and 35.21%, 14.67%, 5.57%, higher CO emissions for B20, B50 and B100 respectively, were observed. The NO emissions were found to be higher by 20.54%, 15.65%, 18.39% compared to that of diesel operation. About 32.28%, 18.19%, 20.73% lower HC emissions and 16.53%, 26.60%, 42.06% lower particulates respectively, were recorded in comparison with diesel operation.	P.K. Sahoo, 2009 [46]	Fuel, vol. 88, pp. 1698-1707.
11.	100	11.1kW, MS 1100, single cylinder, four stroke, and horizontal type diesel engine, constant speed 2240 rpm.	Lower exhaust gas temperature was reported in comparison with diesel operation.	T.T. Kywe, 2009 [47]	World Academy of Science and Engineering Technology, vol. 38, pp. 481-487.
12.	100	3.5 kW, single cylinder, water cooled, four stroke, diesel engine, constant speed 1500 rpm.	Lower brake thermal efficiency, higher SFC, low EGT, lower rate of pressure rise, shorter ignition delay, and lower heat release rate were observed with JME when compared with diesel. About 56% lower HC and 20% lower smoke, 25% lower NO and 38.4% higher CO were reported in comparison with diesel operation.	Jindal,2010 [48]	Energy and Fuels, vol.24, pp. 1565-1572.
13.	100	3.68 kW, single cylinder, four stroke, water cooled, diesel engine, constant speed 1500 rpm.	Lower brake thermal efficiency, higher EGT, HC, CO and smoke and lower NO emissions were reported. Longer ignition delay, high rate of pressure rise, and longer combustion duration were reported in comparison with diesel operation.	M.Senthil kumar, 2010 [49]	Journal of Engineering for Gas Turbines and Power, vol. 132, pp.1-10.
14.	5,10,15 and 20	2.43 kW, single cylinder, four stroke, DI, diesel engine, constant speed 2600 rpm.	Higher exhaust gas temperature, brake thermal efficiency and lower BSFC were reported in comparison with diesel operation.	Ejilah, 2010 [50]	Australian journal of agricultural engineering, vol. 1, pp. 80-85.

15.	100	4.4 kW, single cylinder, four stroke, air cooled, DI, diesel engine, constant speed 1500 rpm.	Higher BSEC at full load and high brake thermal efficiency at lower loads were observed. Lower HC, CO and smoke emissions were reported in comparison with diesel operation.	S.Puhan, 2010 [51]	Biomass and Bioenergy, vol. 34, pp. 1079-1088.
16.	100	8.2 kW, single cylinder, four stroke, water cooled, DI, diesel engine, at speed 1500 rpm and 2000 rpm.	About 3% higher brake thermal efficiency, 6.3% higher BSFC were reported in this work. Also, it was observed that about 25% lower CO emissions, 23% lower HC emissions, 14.5% lower NO emissions, 35% lower smoke emissions were reported in comparison with diesel operation at full load.	J. Huang, 2010 [52]	Fuel Processing Technology, vol. 91, pp. 1761-1767.
17.	10,20,30 and 40	3.5 kW, single cylinder, four stroke, DI, diesel engine, constant speed 1500 rpm.	Lower brake thermal efficiency with all blends and higher BSFC, lower peak pressures, shorter ignition delay were recorded.	T. K. Gogoi, 2011 [53]	World Renewable Energy Congress, Sweden, pp. 3533-3540.
18.	5,10,15,20,25 and 30	3.68 kW, single cylinder, four stroke, water cooled, DI diesel engine, constant speed 1500 rpm.	B20 revealed high brake thermal efficiency and low SFC, in comparison with other blends.	S. Reddy, 2011 [54]	International Journal of Sustainable Energy, vol. 30, pp. 37-41.
19.	10,20,30,40 and 50	4.4 kW, single cylinder, four stroke, air cooled, DI, diesel engine, constant speed 1500 rpm.	It was reported that the SFC was closer to that of diesel with B20. Longer ignition delay was observed with all blends. Lower HC, CO, CO_2 emissions were observed with B20. Higher NO and smoke emissions were observed.	T. Elango, 2011 [55]	Thermal Science, vol. 15, pp. 1205-1214.
20.	10,20,50,75 and 100	3.75 kW, single cylinder, four stroke, water cooled, diesel engine, constant speed 1500 rpm.	B20 results in lower BSFC, and brake thermal efficiency closer to that of diesel fuel were reported in this paper.	R.Prakash, 2011 [56]	Intl. Journal of Advanced Engineering Technology, vol. 2, pp. 186-191.

21.	15	4.5 kW, single cylinder, four stroke, water cooled, diesel engine, constant speed 1500 rpm.	Lower brake thermal efficiency, higher BSFC, lower HC and smoke emissions were observed with B15. The NO emissions were found to be higher than those of diesel.	L. Prasad, 2011 [57]	Journal of Scientific & Industrial Research, vol. 70, pp. 694-698.
22.	20 and 100	4.4 kW, single cylinder, four stroke, water cooled, diesel engine, constant speed 1500 rpm.	It was observed that the SFC of B100 and B20 was about 4.6% and 3.9% respectively higher than those of diesel. Lower brake thermal efficiency was observed. The CO emissions were found to be decreased by about 30% and 15.5% respectively for B100 and B20. The HC emissions was found to be lower by about 28% and 16% for B100 and B20. The NO_x levels were found to be higher for B100 and B20, by about 14.5 % and 22.1% than that of diesel. The particulate matter of B100 and B20 was higher by about 3.1% and 2.1% respectively than that of diesel.	B.R. Prasath, 2011 [58]	Applied Mechanics and Materials, vol. 110-116, pp. 3–7.
23.	5,10,15 and 20	3.68 kW, single cylinder, DI, four stroke, water cooled, diesel engine, constant speed 1500 rpm.	Brake thermal efficiency of B20 was comparable with that of diesel. Higher BSFC and exhaust gas temperature were reported.	D.Vashist, 2011 [59]	International Journal of Engineering Science and Technology, vol. 3, pp. 4765-4773.
24.	100	5.9 kW, single cylinder, four stroke, DI, diesel engine, constant speed 1500 rpm.	Lower brake thermal efficiency, Higher SFC, lower peak pressure, low heat release rate, longer combustion duration, longer ignition delay, lower peak cylinder temperature were reported. Lower HC, CO and smoke emissions and higher NO emissions were reported in comparison with diesel.	D.Kannan, 2011 [60]	Energy Conversion and Management, vol. 53, pp. 322-331.
25.	5, 20,50,80 and 100	3.7 kW, single cylinder, four stroke, diesel engine, constant speed 1500 rpm.	Higher BSFC, exhaust temperature and lower brake thermal efficiency were observed with the JME blends. Lower HC, CO_2, CO emissions, higher NO_x emissions, lesser noise and vibrations were observed for the B20 compared to diesel operation, and hence, it was concluded that optimum blend was B20.	S. Kumar, 2012 [61]	International Journal of Energy and Environment, vol. 3, pp. 471–484.

26.	100	5.2 kW, single cylinder, four stroke, direct injection, water cooled diesel engine, constant speed 1500 rpm.	Lower brake thermal efficiency, higher SFC, exhaust gas temperature, NO, HC and lower CO and smoke emissions were reported in comparison with diesel operation.	A. Yadav, 2012 [62]	Proc IMechE Part A: Journal of Power and Energy, vol. 226, pp. 674-681.
27.	5,10	20 kW, single cylinder, four stroke, water cooled, diesel engine, variable speeds of 1500 to 2400 rpm at an interval of 100 rpm	Average increase in the BSFC compared to DF was found to be 0.54% for JB5, and 1.0% for JB10. Lower HC, CO and CO_2 and higher NO emissions. Lower noise levels were reported with JB5 and JB10 in comparison with diesel operation.	A.M. Liaquat, 2012 [63]	Energy Procedia, vol. 14, pp. 1124-1133.
28.	2, 5 and 10	4.4 kW, single cylinder, four stroke, air cooled diesel engine, constant speed 1500 rpm.	Lower brake thermal efficiency, higher BSFC. Lower HC, CO and smoke emissions and higher NO emissions were reported.	L. Prasad, 2012 [64]	Applied Energy, vol. 93, pp. 245-250.
29.	5,10,20,30 and 100	7.4 kW, single cylinder, air cooled, DI, DAF8 model, diesel engine, constant speed 1500 rpm.	Lower cylinder pressure and heat release rate were observed for JME. Lower brake thermal efficiency, higher BSFC, and EGT were observed for the JME and its blends. Lower HC, CO and smoke emissions and higher NO, CO_2 emissions were reported.	B.S. Chauhan, 2012 [65]	Energy, vol. 37, pp. 616-622.
30.	10, 20,30 and 40 (Jatropha ethyl ester)	3.73 kW, single cylinder, CI engine, constant speed 1500 rpm.	Higher brake thermal efficiency, BSFC and EGT were reported for the JEE blends. Higher NO and lower CO emissions were reported in comparison with diesel operation at full load condition.	R.Kumar, 2012 [66]	International Journal of Automobile Engineering Research and Development, vol. 2, pp. 34-47.

31.	5, 10,20,50 and 100	79 kW, four cylinder, four stroke, turbocharged diesel engine, constant speed 2000 rpm.	The NO emissions were found to be higher for B5, B10, B20, B50, and B100 fuels by about 1.02%, 2.06%, 4.74%, 5.71%, and 13.9% respectively compared to diesel. About 23.1%, 46.7% and 76.9% lower CO, HC and smoke emissions were reported with B100 at full load compared to those of diesel operation.	P.Q. Tan, 2012 [67]	Energy, vol. 39, pp. 356-362.
32.	20, 40, 80 and 100	5.2 kW, four stroke, single cylinder, water-cooled diesel engine, constant speed 1500 rpm.	It was reported that the B20 blend in the diesel engine resulted in smooth operation. The smoke, CO and HC emissions increased with increased percentage of JME blends while the NO_x values were found to be decreased.	G. Shirsath, 2012 [68]	International Journal of Sustainable Engineering vol. 5, No. 3, pp. 252-264.
33.	10,20, 30 and 50	4.5 kW, single cylinder, four-stroke, direct injection, variable compression ratio diesel engine, at variable engine speeds ranging from 1000 to 2000 rpm, at an interval of 250 rpm	Lower brake thermal efficiencies were observed with the JME blends. The peak pressure of B50 was observed to be higher at low and high engine speeds, while those of B10 and B20 are optimum at medium speed. A higher percentage of NO_x was observed in the case of JME compared to that of diesel.	M.EL. Kasaby, 2013 [69]	Alexandria Engineering Journal vol. 52, 2013, pp. 141-149.

Table 2.2 Performance, combustion and emission results of JME and its blends with different engine modifications

Sl.No	JME (%)	Engine tested	Test results compared with diesel	Authors/Reference	Journal/Proceedings name/volume/page
1.	100	3.7 kW, single cylinder, four stroke, water cooled direct injection diesel engine at constant speed 1500 rpm (Hot EGR at 5%, 10%, 15%, 20% and 25%).	The brake thermal efficiency of the JME was found to be comparable with diesel, at all loads with and without EGR. The hot EGR of 15% effectively reduced the NO emission without any adverse effects on the performance, smoke and other emissions. The higher EGR percentages of 20 and 25% resulted in inferior performance and heavy smoke.	V. Pradeep, 2007 [70]	Renewable Energy vol. 32, pp. 1136-1154.
2.	100	3.5 kW, single cylinder, water cooled, four stroke, VCR diesel engine, constant speed 1500 rpm (Compression ratio and injection pressure variation).	About 8.2% higher brake thermal efficiency was observed with a compression ratio (CR) of 18 and injection pressure of 250 bar. The HC emissions were found to be lower at lower injection pressure and at all compression ratios. For high CR, the CO and smoke emissions were found to be lower. Lower CO emissions were observed at CR 18 and injection pressure of 150 bar. High NO at high CR and low injection pressure. Low NO emissions were reported at CR 17 and injection pressure 250 bar.	Jindal, 2010 [20]	Applied Thermal Engineering, vol. 30, pp. 442-448.
3.	20 and 100	5.2 kW, single cylinder, four stroke, NA, open chamber, water cooled, DI diesel engine, constant speed 1500 rpm (Injection timing and injection pressure variation).	Advanced injection timing of 26° bTDC and injection pressure of 220 bar results in on improved engine performance and emissions. High brake thermal efficiency, low HC, smoke and NO_x were reported in this work.	Dhananjaya, 2010 [71]	Thermal Science, vol. 14, pp. 965-977.

4.	100	5 kW, single cylinder, four stroke, air cooled, diesel engine, constant speed 1500 rpm (Compression ratio and injection timing/variation).	Optimum brake thermal efficiency was obtained at 27^{o} bTDC (Advanced) and CR of 17.	T. Ganapathy, 2009 [72]	Thermal Science, vol. 13, pp. 69-82.
5.	20	5.2 kW, single cylinder, four stroke, open chamber, water cooled, diesel engine, constant speed 1500 rpm (Injection timing and injection pressure variation).	Injection pressure of 220 bar and injection timing of 26° bTDC resulted in lower cyclic variations in peak pressure and IMEP.	Barboza, 2010 [73]	International Conference on Mechanical and Electrical Technology, pp. 43-46.
6.	20	4.4 kW, single cylinder, four-stroke, air cooled, DI diesel engine, constant speed 1500 rpm (Compression ratio, injection timing and injection pressure variation)	A maximum brake thermal efficiency was found with JME20 at 27^{o} bTDC, 240 bar and CR of 19:1. Combined increase of CR, injection timing and injection pressure increased the brake thermal efficiency and reduced the BSEC with lower emissions.	M .Venkatraman, 2010 [74]	National Journal on Advances in Building Sciences and Mechanics, vol. 1, pp. 34-39.
7.	100	3.7 kW, single cylinder, water cooled, four stroke diesel engine, constant speed 1500 rpm (LHR engine with internal jet piston)	The brake thermal efficiency was found to be increased by 3%, BSEC decreased by 14% for the JME with partially stabilized zirconia (PSZ) coated internal jet piston. The CO and smoke emissions were found to be decreased, and NO_x emissions were found to be increased with the JME at full load. The maximum pressure and heat release rate were increased and the ignition delay and the combustion duration were decreased for the internal jet piston with the JME.	K. Rajan, 2011 [75]	Second International Conference on Sustainable Energy and Intelligent System, pp. 184-189.

8.	100	5.59 kW, single cylinder, four stroke, air cooled, vertical, Greaves Cotton model GL 400 IIA, diesel engine, with variable speeds 1800, 2500 and 3200 rpm (Injection timing)	Advance in the injection timing caused a reduction in the BSFC, CO, HC and smoke levels, and increase in the brake thermal efficiency, maximum pressure (P_{max}), maximum heat release rate (HRR_{max}), and the NO emissions were observed with the JME operation. At 20^{o} bTDC (advance) the percentage reduction in the BSFC, CO, HC and smoke levels were reported to be about 5.1%, 2.5%, 1.2% and 1.5% respectively. The percentage increase in the brake thermal efficiency, Pmax, HRR_{max} and the NO emissions with this injection timing were observed to be about 5.3%, 1.8%, 26% and 20% respectively at full load.	T. Ganapathy, 2011 [76]	Applied Energy, vol. 88, pp. 4376-4386.
9.	100	3.5 kW, single cylinder, water cooled, four stroke diesel engine, constant speed 1500 rpm (Injection timing)	About 8% higher brake thermal efficiency was observed by retarding the injection timing by 3^{o}. With advanced timings, the brake thermal efficiency dropped considerably. About 9% reduction in the SFC was observed at 3^{o} retarded timing.	S. Jindal, 2011 [77]	International Journal of Energy and Environment, vol. 2, pp. 113-122.
10.	5 and 20	69.14 kW, four cylinder, water cooled, turbocharged, IDI diesel engine, constant speed 2000 rpm. (5%, 10 % EGR)	At 5% EGR with JB5, both NO_x and smoke opacity were reduced by 27% and 17% respectively. The JB20 blend along with 10% EGR, reduced both NO_x and smoke emissions by about 36% and 31%, respectively.	M. Gomaa, 2011.[78]	International Journal of Energy and Environment, vol. 2, pp. 477-490.
11.	100	3.7 kW, single cylinder, four stroke, water cooled, diesel engine, constant speed 1500 rpm (7% and 14% cooled EGR)	It was reported that delayed combustion was observed in both the cases of diesel and JME with the EGR application. Peak pressures reduced with an increase in the EGR percentage. Lower NO_x emissions were reported with EGR.	S. Adinarayana, 2011. [79]	International Journal of Applied Research In Mechanical Engineering, vol.1, pp.10-15.

12.	100	19.8 kW, four cylinder, four stroke, naturally aspirated, diesel engine, constant speed 2200 rpm. (EGR 10%)	Average increase of 2.61% BSEC without EGR and 13.3% compared to diesel was noticed. Reduction in the brake thermal efficiency of 2.48% and 11.6% with JME, JME with 10% EGR. JME with EGR operation results in 5.9% increase in CO emission compared to JME, without EGR reduction of 8.2% compared to that of diesel. A reduction of 4.64% in the HC emissions was observed in comparison with diesel operation. The JME showed an average of 19.6% higher NO_x emission compared to diesel. Use of EGR in JME showed an average of 19.85% reduction in NO_x emission compared to JME without EGR and 4.31% compared to that of neat diesel. About 20.8% higher smoke emission was observed with EGR in comparison without EGR operation and 8.41% higher compared to diesel.	N. Shrivastava, 2012 [80]	International Journal of Renewable Energy Research, vol. 2, pp. 504-509.
13.	100	3.68 kW, single cylinder, four stroke, constant speed, DI diesel engine, constant speed 1500 rpm (Injection pressures 200, 210 bar)	Lower HC, CO and NO emissions were reported with the JME compared to that of diesel operation.	Nagarhalli, 2012 [81]	International Journal of Advanced Engineering Technology, vol.III, pp. 51-54.
14.	20	4.4 kW, single cylinder, four stroke, constant speed 1500 rpm, DI diesel engine with multi chambered piston geometry and injection pressures of 175, 200 and 225 bar.	It was observed that the modified piston showed an enhanced performance and lower emissions compared to the standard piston. The SFC reduced with an increase in injection pressure. The optimum injection pressure was observed as 200 bar for the B20 blend. Brake thermal efficiency was improved with an increase in the injection pressure up to 200 bar, and with further increase in injection pressure the brake thermal efficiency was reduced. The UBHC emission was improved with increased injection pressure.	Rajashekhar, 2012 [82]	Transactions of the Canadian Society for Mechanical Engineering, vol. 36, pp.429-438.

15.	20, 30 and 40 (EGR + Ignition improver)	4.4 kW, computerized, single cylinder, four stroke, direct injection, air cooled diesel engine, constant speed 1500 rpm	It was observed that with an increase in the percentage of EGR, the brake thermal efficiency increased while the BSFC and the exhaust gas temperature decreased. The optimum EGR for the maximum brake thermal efficiency and the minimum BSFC were found to be 20%. The CO and HC emissions were found to increase with the increase in the percentage of EGR. But, the CO and HC emission values were decreased with higher blends of JME. The NO_x emissions decreased with an increase in the percentage of EGR, but a reverse trend was observed with the smoke emissions.	K. Venkateswarlu, 2012 [83]	Front. Energy, vol. 6, pp. 304–310
16.	10, 20 and 30	5.2 kW, single cylinder, four stroke, water cooled, diesel engine, constant speed 1500 rpm Compression ratio 16,18)	The 20% blend of JME with diesel showed a higher brake thermal efficiency at both compression ratios.	S. Abinav Viswanath, 2012 [84]	International Journal of Engineering Science and Technology, vol. 4, pp. 3457-3471.
17.	5,10,20,40,60, 80 and 100	3.5 kW, single cylinder, four stroke, water cooled, diesel engine, constant speed 1500 rpm (Variable compression ratio and variable injection pressure)	The increase in the brake thermal efficiency was in the range from 6.76% to 7.40% for different biodiesel blends. A low smoke opacity was observed with a higher compression ratio due to better combustion. The maximum reduction in smoke opacity was 22% at a compression ratio of 19.5. The CO and HC emissions were decreased by about 7 to 10% with CR 19.5 in comparison with CR 17.5 at all biodiesel blend ratios. The smoke opacity was noticed to be lower with increased blends at higher injection pressures of 180, 200 and 220 bar; a reduction in the smoke opacity of 10 to 15% was observed through the load regions compared to that of diesel and 100% JME. Higher NO emissions by about 1.4% were observed at 220 bar in comparison with 180 bar injection pressure.	Amar Pandhare, 2013 [85]	Journal of Renewable Energy, vol. 2013

Table 2.3 Performance, combustion and emission results of JME and its blends with different fuel modifications

Sl.No	JME (%)	Engine tested	Test results compared with diesel	Authors/Reference	Journal/Proceedings name/volume/page
1.	100 (Preheating)	3.72 kW, single cylinder, water cooled, four stroke diesel engine, constant speed 1500 rpm	It was observed that the brake thermal efficiency increased and BSEC decreased with preheating the JME. Shorter ignition delay, lower heat release rate, higher EGT and lower NO_x emissions were observed. Lower HC, CO and smoke emissions were found.	P. V. Rao, 2011 [86]	World Academy of Science, Engineering and Technology, vol.75, pp.855-868.
2.	25, 50, 75 and 100 (Multi-DM32)	3.68 kW, single cylinder, four stroke, water cooled diesel engine, constant speed 1500 rpm	Higher thermal efficiency, higher exhaust gas temperature, and lower smoke, CO and CO_2 emissions were reported in this work.	Y.V.H.Rao, 2009 [87]	Indian Journal of Science and Technology, vol. 2, pp. 25-31.
3.	JME+ cerium oxide nano particles of 20,40 and 80 ppm.	5.5 kW, naturally aspirated, four stroke, single cylinder, water cooled diesel engine, constant speed 1500 rpm	Engine tests were conducted with the modified biodiesel at different dosing levels (20–80 ppm) of the cerium oxide additive which showed an improvement in the efficiency of the engine. Also, it was reported that the emission levels of hydrocarbon and NO_x were reduced with the addition of cerium oxide nanoparticles.	V. Sajith, 2010 [88]	Advances in Mechanical Engineering, vol. 2010
4.	83% JME, 15% water, and 2% of surfactants (Span80 and Tween80) (alumina nano particles 25, 50, and 100 ppm)	4.4 kW, single cylinder four stroke, air-cooled, direct injection diesel engine, constant speed 1500 rpm	The addition of potential nanoparticles to the biodiesel emulsion resulted in reduced peak pressure, heat release rate, and ignition delay compared to that of neat biodiesel emulsion operation. Higher brake thermal efficiency was achieved at 100 ppm with the addition of Alumina nano particles. NO emission was reported to be lower by about 32% and the smoke emissions were reported to be lower by about 26%.	J. Sadhik Basha, 2011 [89]	Journal of Renewable Sustainable Energy, vol. 3, pp. 1-17.

5.	B20 + DEE 5, 10 and 15 B20 + Ethanol 6 and 10	3.68 kW, single cylinder, direct injection four-stroke, water cooled, diesel engine, constant speed 1500 rpm. (Optimization of injection pressure and nozzle hole size)	With a smaller nozzle hole and high injection pressure of 210 bar, a lower BSFC was obtained. Lower BSFC, HC, CO_2 and smoke emissions were observed with 5% DEE addition. With 15% DEE lower NO emissions were observed.	U.Varaprasad, 2011 [90]	Thermal Science, vol. 15, pp. 1175-1184.
6.	100 + Antioxidant additives (L-ascorbic acid (Vitamin C), a tocopherol acetate (Vitamin E), butylated hydroxytoluene (BHT), p-phenylenediamine (PPDA) and ethylenediamine (EDA))	4.4 kW, single cylinder, four stroke, water cooled, DI diesel engine, constant speed 1500 rpm.	Antioxidant addition reduces the NO_x emissions in the exhaust. Among all the tested antioxidants p-phenylenediamine showed the best emission performance compared to biodiesel.	K.Varadharajan, 2011 [91]	Fuel, vol. 90, pp. 2721–2725.
7.	100 % JME+ Cobalt oxide and Magnalium nano particles	4.4 kW, single cylinder, air cooled, direct injection, diesel engine, constant speed 1500 rpm	It was reported that the addition of nano particles resulted in an increased thermal efficiency of JME compared to that without additives. Cobalt oxide showed about 75% reduction in HC at 75% load, and with magnalium, there was a reduction in HC emission of around 70% at 50% load. There was about, 47% reduction in the NO_x emission with cobalt oxide Nano-fuel additive and with Cobalt oxide there was a 50% reduction in the CO emission at 75% load.	D. Ganesh, 2011 [92]	International Conference on Electrical and Control Engineering, China, pp.3453 – 3459.

8.	Ethanol:Diesel:JME of 5:95:0, 5:75:20, 5:55:40, 5:35:60, 5:15:80 and 5:0:95 for the blends of ethanol, commercial diesel and JME	5.9 kW, four stroke, single cylinder, DI diesel engine, constant speed 1500 rpm	Brake thermal efficiency was reported to be higher in the case of diesel-ethanol-JME blend compared to ethanol-diesel and ethanol-JME, while, the BTE of the ethanol-JME blend was found to be lower, compared to that of diesel. Blend of ethanol-diesel-JME compared with blends of ethanol-JME shows slightly extended heat release and enhanced combustion. The CO, HC and smoke emissions from all blends decreased at high load conditions and increased at low load conditions. The NO emissions were reported to be higher at full load condition.	D.Kannan,2012 [93]	Energy Conversion and Management, vol. 53, pp. 322-331.
9.	JME + PY (Antioxidant)	2.6 kW, Kirloskar, single cylinder, vertical, four stroke, high speed diesel engine, constant speed 1500 rpm	The BSFC of JME with and without antioxidants were observed to be more than that of diesel. The BSFC of JME with antioxidants is lesser than that of JME without antioxidants.	S. Jain, 2013 [94]	Fuel, vol.106, pp. 152–156
10.	JME80+Ethanol 20, JME80+ Acetone 20	3.5 kW, single cylinder, four stroke, water cooled diesel engine, constant speed 1500 rpm	Early pressure rise was observed in the case of B100, BD80E20 and BD80AC20 as compared to diesel. The rate of pressure rise for the ethanol and the acetone blends was intermediate between B100 and diesel. Early heat release was observed with B100 and its ethanol and acetone blends. It was observed that the ignition delay for B100, BD80E20 and BD80AC20 was lesser than that of diesel. The ignition delay for B100 was the lowest of all.	T.K. Gogoi, 2013 [95]	International Journal of Emerging Technology and Advanced Engineering, vol. 3, 2013, pp. 51-57

Table 2.4 Reasons for higher NO_x emission from biodiesel fueled engines

Characteristics of biodiesel	Causes for higher NO_x emission	Authors/Reference	Journal/Proceedings Name/volume/page
High isentropic bulk modulus and density	i) Artificial advance of injection timing ii) Less compressible than diesel iii)Increased injection pressures iv) High spray tip penetration v) Decreased spray cone angle and advanced start of injection	Moneyem et al, 2001 Tat and Van Garpen, 2007. Choi and Reitz, 1997 Yuan and Hansen, 2002 [97-100]	Biomass and Bioenergy, vol.20, pp. 317-325. Fuel, vol.85, pp.1004-9. National Biodiesel Board report, 1997. ASAE;50(4):1123-8 ASAE Paper No. 026083
High adiabatic flame temperature	i) Higher heat release rate ii) Stoichiometric burning	Benajes et al, 2008. Muller et al, 2009. Ban-Weiss et al, 2007. [101-103]	Fuel, vol. 87, pp.1849-58. SAE International Journal of Fuels and Lubricants, vol. 2. 2009-01-1792. Fuel Processing Technology, 88, pp. 659-667.
More wide-spread high temperature distribution areas than diesel	i) Higher heat release rates	Yuan et al, 2005 [104]	ASAE, vol.48, pp.933-39.
Increased premixed combustion	It was reported that the higher premixed combustion is due to higher cetane number of biofuel which initiates the combustion early.	Edwin Geo et al, 2012. [105]	Applied Energy, 94, pp. 224–231.
Increased sauter mean diameter	i) Reduced premixed combustion ii) Increased diffusion combustion and NO_x	Allen and Watts, 2000 [106]	ASAE , vol.43, pp.207-11.
Shorter ignition delay	i) Reduced premixed combustion ii) Increased diffusion combustion and NO_x	Canacki, 2007 Tat et al.2007 [107-108]	Bioresource Technology, vol.98, pp.1167-75. ASAE , vol.50, pp.1123-8
Lower vapour pressure	i) Slower evaporation rate ii) Longer ignition delay	Ra et al, 2008 [109]	SAE Transactions-Journal of Fuels and Lubricants, vol. 117, 2008-2101-1379.
Unsaturated fatty acids	i) CH radicals formation followed by acetylene formation	Garner et al, 2009 [110]	Proceedings of the Combustion Institute, vol.32, pp.461-7

High iodine number	i) More degree of unsaturation of the fatty acid	Mccormick, 2001 [111]	Environmental Science and Technology, vol. 35, pp.1742-7.
Low cetane number	i) Longer ignition delay and higher heat release rate	Lapuerta, 2008 McCormick, 2002 [112-113]	Progress in Energy and Combustion Science vol. 34, pp.198-223. SAE 2002-01-1658
High cetane number	i) Shorter ignition delay ii) Low average combustion temperature iii)Decreased residence time leads to low NO_x iv)Higher peak pressure and temperature leads to high NO_x	Wang et al, 2000. [114]	Environmental Science & Technolology 34, 933-939
Fuel bound oxygen	i) Increases combustion efficiency ii)High reaction temperature	Graboski et al, 1998 Song et al, 2004 [115-116]	Progress in Energy and Combustion Science, vol. 24, pp. 125-164, Energy Fuel, 18, pp. 1282–90
High oxygen content	i) Exhibits low compressibility ii) Increase in boiling point iii) Reduces the droplet evaporation iv) Lesser soot v) Low radiation heat transfer	Muller et al, 2003. Ullman et al,1994 Bittle et al.2009 [117-119]	SAE Transactions - Journal of Fuels and Lubricants, vol. 112. 2003-01-1791. SAE Transactions-Journal of Fuels and Lubricants, vol.103, 941020. SAE 2009-01-2782;
High viscosity	i) Increase in fuel line pressure ii) Advance of injection iii) Increased mass of fuel during spray iv) Poor atomization v) Smaller spray cone angles vi) High penetration vii)Larger droplet size	Tat, 2003 Usta eta al Deshmukh et al, 2012. Yuan and Hansen, 2005 Anderson and Olsen [120-124]	PhD Dissertation. Iowa State University. Fuel, vol. 97, pp. 879–883 ASAE, vol.48, pp.933-9
Fuel density	i) Advanced fuel injection timing ii) Higher fuel injection pressure iii) shorter fuel spray penetration iv) shorter fuel spray angle v) Longer ignition delay	Sun et al, 2010. [125]	Progress in Energy and Combustion Science, vol.36, pp. 677-695.
Surface tension	i) High surface tension ii) Larger droplet size	Ahmed et al., 2006. [126]	SAE Paper No. 2006-01-0893

2.4 Biomass pyrolysis

Pyrolysis is a method, by which biomass or any organic substance can be converted into pyrolysis oil, pyrogas and char by the thermal decomposition in the absence of oxygen, or in the presence of very little oxygen [14]. There are two main pyrolytic techniques, namely, slow and fast. Slow pyrolysis has been used for many years for charcoal production, but can also be carried out using modern reactors. Slow pyrolysis is characterized by slow heating rates and relatively long residence times with lower reaction temperature, whereas; the fast pyrolysis process is characterized by high heating rates and short residence times. Other methods include intermediate and flash pyrolysis, of which intermediate pyrolysis deals with controlled heating rates, thus avoiding tar formation. Flash pyrolysis occurs with very fast heating rates and shorter solid residence times, than with the fast pyrolysis process. Different types of reactors have been used for pyrolysis that include the bubbling fluidized bed, circulating fluidized bed, rotating cone, ablative reactor, vacuum pyrolysis reactor, entrained flow reactor, wire mesh reactor, and auger (screw) reactor [127]. The pyrolysis oil obtained from biomass sources has great attraction, but is not used in the proper way. Many attempts have been made in the recent past, to extract fuel called as bio oil or bio-crude oil from the pyrolysis of various biomass sources, like saw dust, waste wood, rice husk, cotton stalk, sugar cane bagasse and olive bagasse, and from the nut shells of jatropha and palm kernel shell, etc [128-135]. Bio oils are mixtures of multi-components of different sized molecules derived from the depolymerization and fragmentation of cellulose, hemi cellulose and lignin [136]. Chir pine (Pinus roxburghii) is widely planted for timber applications, being one of the most important trees in forestry in northern Pakistan, India and Nepal. This pine wood finds application in making packing container boxes.

2.4.1 Wood pyrolysis oil (WPO)

Pyrolysis liquid obtained from biomass sources is referred to in the literature by terms, such as pyrolysis oil, bio oil, bio-crude oil, bio-fuel oil, wood liquid, wood oil, liquid smoke, wood distillates, pyroligneous tar, and pyroligneous acid. The bio oil can be used as a fuel in boilers, diesel engines or gas turbines for heat and electricity generation [137]. The WPO obtained from the pyrolysis of wood, is a free flowing dark-brown organic liquid accompanied by a strong acid smell. The oil comprises of different sized molecules, which are derived from the depolymerization and fragmentation reaction of three biomass building blocks: cellulose, hemicellulose and lignin [138]. It has a high oxygen content and moisture

content, but poor volatility, high viscosity, corrosiveness and cold flow properties, which limit its use as additives in transportation fuel, rather than being used as transportation fuel by itself. The WPO cannot be made to mix directly with diesel due to poor miscibility, different surface tension and hydroscopic characteristics [139].

Water content is commonly seen in the bio oil obtained from any biomass feedstock. The mass fraction of water content in the bio oil lies between 10-35% in most of the cases. This fraction depends on the original moisture content of biomass and also on the pyrolysis conditions. The water content of bio oil is usually measured by the Karl-Fischer titration method. The bio oil becomes unstable, if more than a certain amount of water is added to it; the microstructure of the bio oil will be destroyed, and it will separate into water soluble and oily phases [140]. There are both positive and negative effects of water when considering bio oil combustion. In one way, the water content in the bio oil decreases the combustion reaction rates, adiabatic flame temperature, but increases the ignition delay and heat of evaporation [141]. On the other hand, water can enhance the atomization process by decreasing viscosity and increasing the chance of effective micro-explosions of the fuel droplets. Also, it can reduce the NO_x emissions by decreasing the flame temperatures and accelerate soot oxidation by providing OH radicals [140-142].

Engine experiments were conducted by Yrjo Solantausta et al. [143] with different fuels, such as diesel, ethanol and pyrolysis oil with a certain proportion of an ignition improver addition, by volume to pyrolysis oil and ethanol. Injector nozzle coking and clogging of the bore for the cylinder pressure transducer were observed from the results. Frigo et al. [144] conducted a series of tests like the thermo gravimetric analysis (TGA), single drop reactor tests, corrosion tests, spray analysis, and engine tests to check the feasibility of using wood flash-pyrolysis oil in diesel engines. Problems such as the buildup of carbonaceous deposits, injection system fault and engine seizing were noticed, when WPO was fueled in a diesel engine.

The application of an emulsification technique is considered to be one of the possible approaches to reduce diesel engine pollutants, as well as the rate of fuel consumption. The emulsification of biomass derived bio oil in diesel has been carried out, to avoid the problem of miscibility and stability of bio oil and diesel [145]. Stable emulsions are prepared, using two surfactants, namely, hypermer and CANMET. The reduction in the viscosity and corrosivity of the emulsion has been reported in this work. It was also reported that the

emulsified bio oil showed a better friction reduction performances than that of commercial diesel under selected frictional conditions [145]. Two different fuels like Diethylene glycol dimethyl ether (Diglyme) and the WPO blends in different percentages, and two different emulsions with 30% of WPO in diesel were tested in a Ruggerini RP170 model, diesel engine. Lower NO emissions are reported with increasing percentage of WPO, and lower HC emissions are found up to 30% WPO, but beyond that, the HC emissions increased significantly. The CO emissions are found to be more, due to the poor self-ignition characteristics of the WPO [146]. Two emulsions prepared with 10% and 20% bio-oil, obtained from corn stalk by mass fraction in No. 0 diesel, using an ultrasonic emulsification method, were tested in a direct injection diesel engine. It is reported that the two emulsions display longer ignition delays, exhibit higher peak values of the premixed burning rate and pressure rise rate, lower peak values of the in-cylinder pressure and combustion temperature and have a shorter combustion duration compared to that of No. 0 diesel [147].

Upgrading the bio oil through emulsification with biodiesel explores the possibility of replacing petroleum based fuels completely. A method of emulsifying bio oil with biodiesel has been investigated, using an Octanol surfactant, and an attempt has been made to study the various effects on the mixture stability [148]. It is reported that the process of emulsifying a bio oil with biodiesel is a novel method to extract some of the best fuel fractions present in the bio oil, for use as an additive in transportation fuel. Various properties of the emulsion have shown more desirable values in the acid number, viscosity, and water content compared to the original bio oil. The impact of bio oils on the oxidation stability and cold flow properties of biodiesel containing bio oil fractions is carried out, using Differential Scanning Calorimetric techniques [149]. It is reported that the bio oil can be considered as a good source of anti-oxidants to enhance the biodiesel oxidation stability.

The biodiesel emulsion fuel prepared by the emulsification technique, comprising of 83% of Jatropha biodiesel, 15% of water, and 2% of mixed surfactant, comprising Span 80 and Tween 80 in equal percentages, with the aid of a mechanical agitator, was tested in a single cylinder DI diesel engine. The experimental results revealed that there is a substantial enhancement in the performance and a reduction in the harmful emissions for the biodiesel emulsion fuels, compared to those of biodiesel [150]. Kannan et al. [151] performed experiments on a single cylinder, direct injection, diesel engine using diesel, biodiesel and biodiesel-diesel-ethanol (diestrol) water micro emulsion fuels, to investigate the performance,

emission and combustion characteristics of the engine under different load conditions. The results indicated that the biodiesel and micro emulsion fuels showed a higher brake specific fuel consumption throughout the engine operation. The carbon monoxide, unburnt hydrocarbon, nitric oxide, and smoke emissions were found to be lower than those of diesel in all load conditions. Chen et al. [152] demonstrated that the emulsified bio-solution/palm-biodiesel/diesel blends have the advantage of saving energy and reducing emissions of both polycyclic aromatic hydrocarbons (PAHs) and particulate matter (PM) from diesel engines. Alcala, and Bridgwater [153] prepared homogeneous blends of bio oil and biodiesel in the presence of alcohol, that are extremely stable over time, particularly in comparison with bio oil. The feedstock used for bio oil was pine wood.

2.5 Summary

It is understood that many research works were carried out using JME and its blends by adopting fuel and engine modifications. Most of them reported that higher NO emission in diesel engines, when the JME and its diesel blends were used as fuels. Also, it is understood from the literatures that the use of WPO is limited in its sole form. Problems like poor miscibility with diesel, along with durability related issues are reported in many works. From the literature review, it is observed that no research work was carried out on the utilization of WPO emulsified with the JME in diesel engines, to study the NO_x reduction. Hence, it is proposed to use the WPO with the JME, as an alternative fuel in the form of an emulsion in a DI diesel engine.

CHAPTER 3

MATERIALS AND METHODS

3.1 General

In this research work, two principal biofuels, namely, Jatropha methyl ester (JME) and, Wood pyrolysis oil (WPO) - a bio oil are considered for the preparation of emulsions. The production methods of these two oils are described with the necessary schematic diagrams and photographs shown in this chapter. The production of emulsions from different surfactants, and their characterization are also described in this chapter with the necessary illustrations.

3.2 Production of JME

Vegetable oil is considered as one of the best feedstocks obtained from biomass sources. It can be used in combustion devices after proper treatment. The use of vegetable oils in IC engines particularly in CI engines is not a new, because Rudolph Diesel used peanut oil to demonstrate his patented diesel engine. But, the uses of vegetable oil in CI engines are prone to cause problems such as injector coking, piston wear etc. This is because of the higher viscosity and poor volatility of vegetable oils. The viscosity of vegetable oils can be reduced by blending, preheating transesterification, and thermal or chemical cracking. Transesterification is the best method to reduce the viscosity of vegetable oil. Biodiesel is commonly referred to as methyl or ethyl or butyl esters of vegetable oil or animal fat or algae. Vegetable oil of the edible or non-edible type is used for the production of biodiesel. Jatropha oil, a non-edible oil is considered as a potential feedstock for the production of biodiesel in India. Hence, it was chosen as a feedstock for the production of biodiesel in this study. Methanol is more reactive, because it contains short chain hydrocarbons, and is easily available in the market, and hence it is also considered for the biodiesel production. The JME used in this investigation was obtained from the transesterification of Jatropha oil. The fatty acid composition of Jatropha oil is given in Table 3.1. In the transesterification of vegetable oils, a triglyceride reacts with an alcohol in the presence of a strong acid or base, producing a mixture of fatty acid alkyl esters and glycerol. The block diagram of the production of JME from Jatropha oil is presented in Fig. 3.1.

Table 3.1 Fatty acid composition of Jatropha oil [38]

Fatty acid	Structure	Formula	Composition (% wt)
Palmitic	16:0	$C_{16}H_{32}O_2$	14.1–15.3
Stearic	18:0	$C_{18}H_{36}O_2$	3.7–9.8
Oleic	18:1	$C_{18}H_{34}O_2$	34.3–45.8
Linoleic	18:2	$C_{18}H_{32}O_2$	29–44.2

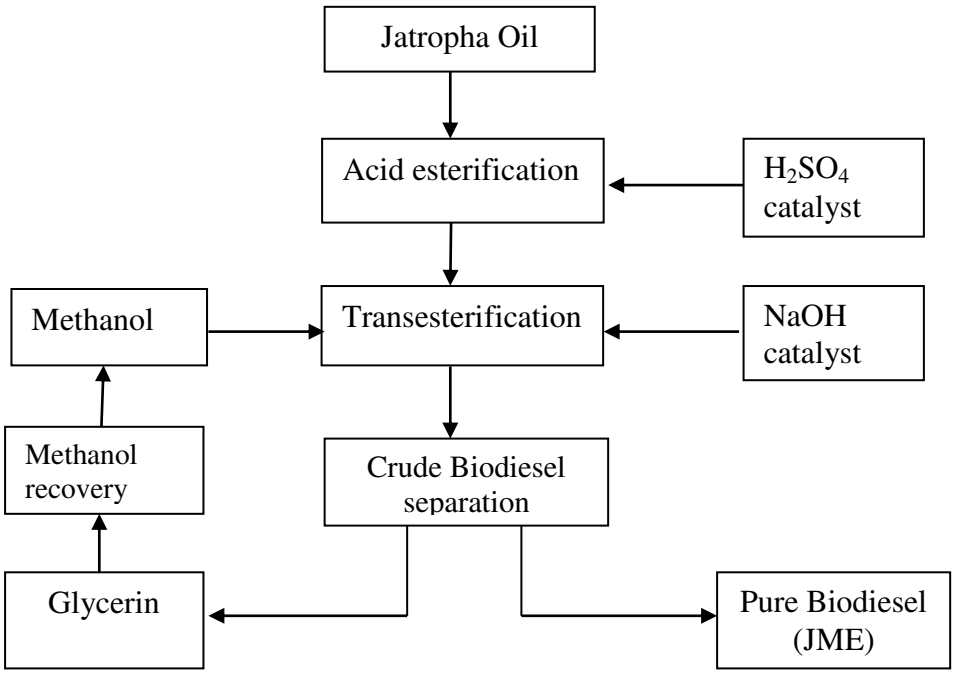

Fig. 3.1 Block diagram of JME production from Jatropha oil

Initially, sodium hydroxide (NaOH) as a catalyst of about 3-4 grams was dissolved in 100 ml of methanol to prepare methoxide, which was required to activate the methanol. Vigorous stirring was done for about 15-20 min in a closed container, until the alkali was dissolved completely. Further, this mixture was transferred to the reactor containing moisture-free Jatropha oil. A continuous stirring of the resulting mixture at temperatures between 60-65°C was carried out for one hour. A mixture comprising a certain quantity of methyl ester, glycerol and methanol was obtained after cooling the mixture for about 24 hours. Then, the mixture was taken out and poured into the separating funnel to separate the glycerol and

methyl ester of Jatropha oil. Water washing was done finally, in order to remove the moisture and impurities from the JME. The photograph of the JME is shown in Fig.3.2.

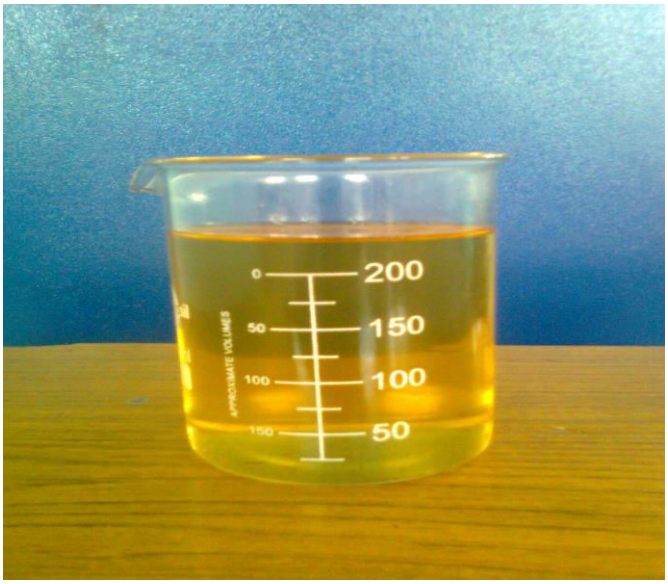

Fig. 3.2 Photograph of JME

3.3 Analysis of raw material for WPO

3.3.1 Ultimate and proximate analysis of pine wood

WPO was obtained from the pyrolysis of waste pine wood obtained from packing boxes. Before extracting pyrolysis oil from pine wood, the proximate and ultimate analyses were performed, to ensure whether it is possible to derive oil out of it.

3.3.1.1 Proximate analysis

The basic method for the proximate analysis is given by the ASTM D3172 standard. It determines the mass percentages of the fixed carbon, volatile matter, moisture, and ash. Fixed carbon is the elemental carbon that exists in the wood. In the proximate analysis, its determination is approximated by assuming it to be the difference between the original sample and the sum of the volatile matter, moisture, and ash. The volatile matter is that portion of wood, other than water vapor, which is driven off when the sample is heated in the absence of oxygen in a standard test (up to 1750°F or 7 min). It consists of hydrocarbon and other gases that result from distillation and decomposition. The moisture is determined by the standard procedure of drying in an oven. This does not account for all the water present, which includes the combined water and the water of hydration. Ash is determined in practice

as the noncombustible residue after the combustion of dried wood in a standard test (at 1380°F).

3.3.1.2 Ultimate analysis

An ultimate analysis is done for the pine wood by the ASTM D 3176 method. The ultimate analysis gives the mass percentages of the chemical elements that constitute the wood. These include carbon, hydrogen, nitrogen, oxygen, and sulfur. The ultimate analysis of pine wood shows that, the pine wood contains about 50% carbon, 5.4% hydrogen, and 44% oxygen on a moisture and ash free basis. The sulfur and nitrogen content of wood is usually less than 0.1%. The proximate analysis of wood shows about 77% volatile matter and 11% fixed carbon. The ultimate and proximate analysis of pine wood are given in Table 3.2.

Table 3.2 Ultimate and proximate analysis of pine wood

Proximate analysis	**wt (%)**	**Ultimate analysis**	**wt (%)**
Water content	3	C	50.15
Volatile matter	77	H	5.41
Fixed carbon	11	N	0.06
Ash content	9	O	44.37

3.3.2 Thermo Gravimetric Analysis (TGA)

Initially, the raw wooden chip was characterized by Thermo gravimetric analysis (TGA) apparatus. The schematic diagram of the experimental TGA apparatus is shown in Fig. 3.3.

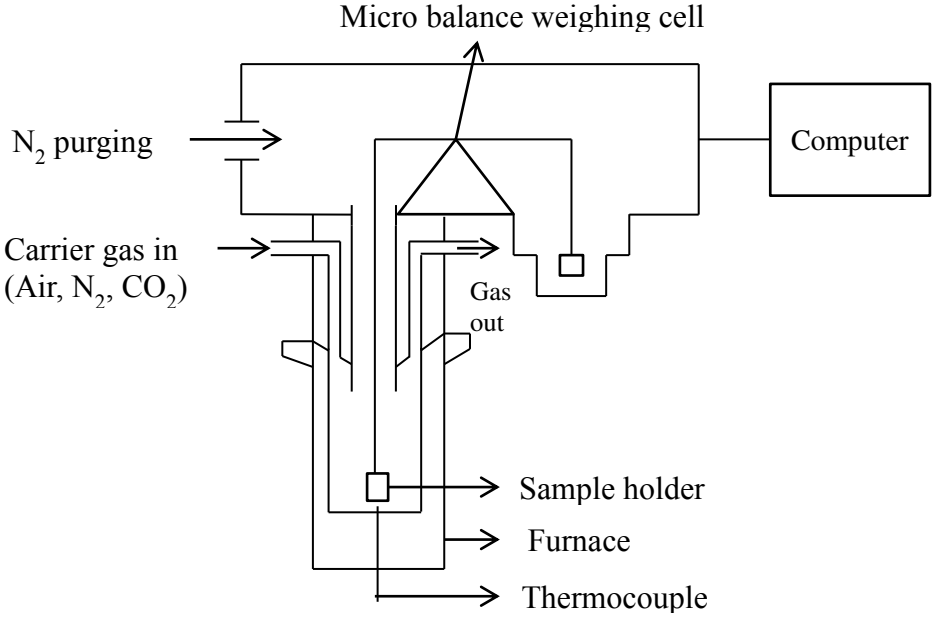

Fig. 3.3 Schematic diagram of the experimental TGA apparatus

The TGA is generally used to determine a material's thermal stability and its fraction of volatile compounds, by monitoring the weight loss that occurs when the specimen is heated. All the experiments with TGA comprise of three main different phases: drying, de-volatilization in an inert atmosphere, and combustion in oxygen [154]. The measurement is normally carried out in air or in an inert atmosphere, such as helium or argon, and the weight is recorded as a function of increasing temperature. In nitrogen, the moisture and volatiles are lost at temperatures up to 900^{o}C, and fixed carbon is burnt in oxygen leaving ash as a residue. The TGA curve of pine wood is depicted in Fig. 3.4.

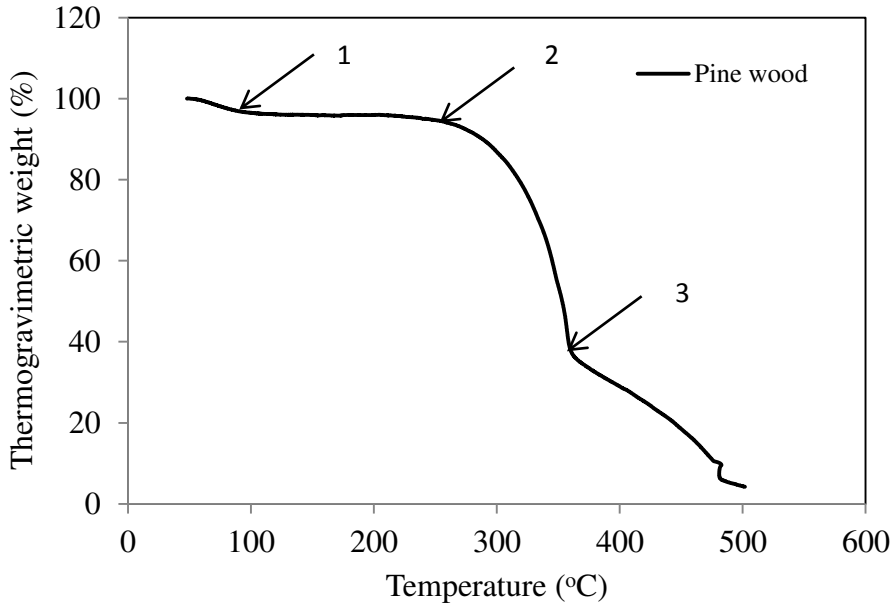

Fig. 3.4 TGA curve of pine wood

The TGA analysis of the pine wood sample was done by using a model SHIMADZU TGA-60H, with nitrogen as a carrier gas at a constant flow rate of 45 ml/min. A sample of 25 mg was heated in a furnace from an initial temperature of 30^{o}C to 600^{o}C, at a heating rate of 25^{o}C/min for a residence time of 5 min. The thermal degradation of the sample showed three weight loss regions. The first weight loss occurred at the temperature range of 70 to 120^{o}C, where the moisture content in the wood was removed. The second weight loss occurred at the temperature range of 120 to 260^{o}C, where the volatilization of hemicelluloses and residual oil occurred. A major weight loss occurred from 260 to 500^{o}C with the deflection point at 350^{o}C, where the maximum rate of weight loss occurred which may be due to the degradation of cellulose and lignin.

3.4 Production of the WPO

Pyrolysis is the breakdown of organic matter into value added products in the absence of oxygen or very little presence of oxygen. The schematic diagram of the pyrolysis process for deriving the WPO is shown in Fig. 3.5.

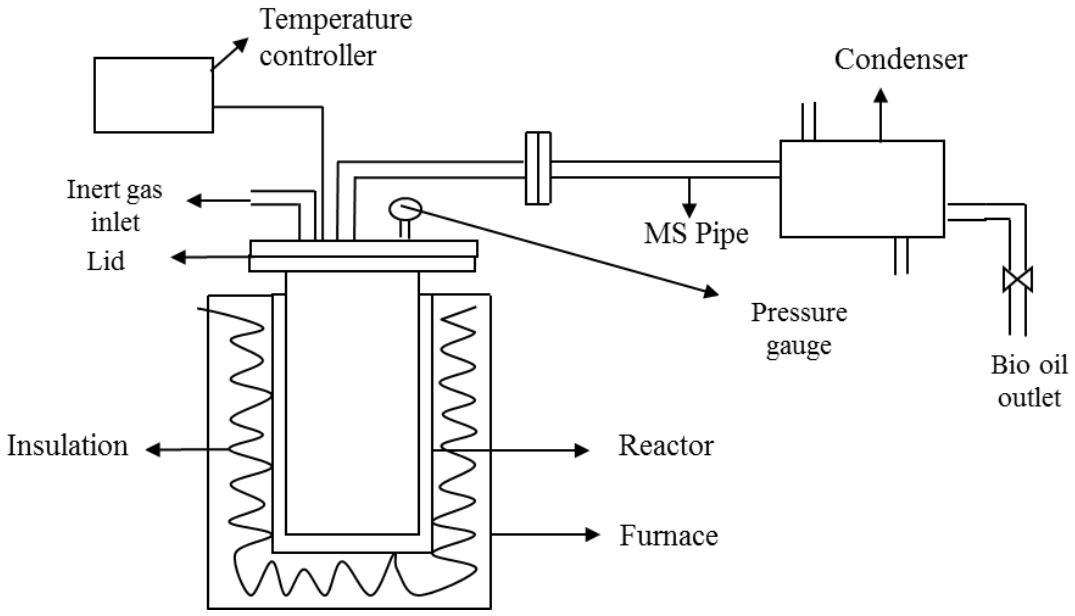

Fig. 3.5 Schematic diagram of pyrolysis setup

In the pyrolysis process, wooden chips obtained from pine wood feed stock were fed into an externally heated mild steel reactor unit. The fed chips were heated in the reactor unit in the absence of oxygen. The temperature of the reactor was maintained with the help of a highly sensitive temperature controller. The temperature was measured by a Cr-Al: K-type thermocouple fixed outside the reactor. Fig. 3.6 shows the sample of wood chips considered for the pyrolysis process. During pyrolysis, the reactions were carried out at different temperature ranges to find the optimum yield temperature, by taking 750 g of the sample in the reactor. The heating rate, at which the pyrolysis process was carried out, was 10^{o}C per minute. The temperature, at which the maximum yield of pyrolytic oil obtained, was in the range of 400^{o}C and 450^{o}C. The volatile matter that evolved in the form of vapour was condensed in a water cooled condenser. Three principal products such as WPO, pyrogas and char were obtained in the process. The optimum yield of the WPO obtained was about 65% and the cost for producing one litre of WPO was (Indian) Rupees 27. The photographic view of the pyrolysis setup used in this study is shown in Fig. 3.7.

Fig. 3.6 Photographic view of the reactor with feed material

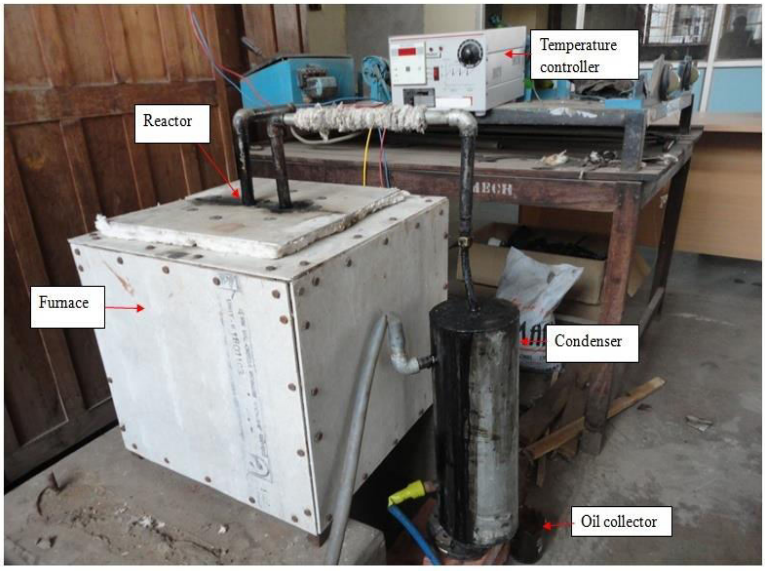

Fig. 3.7 Photographic view of pyrolysis setup

Fig.3.8 and 3.9 show the photographic views of WPO and char respectively.

Fig. 3.8 Photographic view of the WPO

Fig. 3.9 Photographic view of the char

The optimum yield of WPO obtained was calculated as follows:

Individual weight of the pine wood chips = 750 ± 10 g

Weight of the liquid product = 485 ±10 g

Weight of the char = 200 ±10 g

Wood pyrolysis oil yield = 485/750 = 65 ±1.3 % by weight.

Pyrolysis char yield = 200/750 = 26 ±1.3 % by weight.

3.5 Analysis of Wood pyrolysis oil

3.5.1 FTIR analysis of WPO

The functional groups present in the WPO were determined with the help of the Fourier Transform Infrared spectroscopy (FTIR) analysis. On the interaction of an infrared light with oil, a chemical bond will stretch, contract, and absorb infrared radiation in a specific wave length range, regardless of the structure of the rest of the molecules. Fig.3.10 illustrates the working principle of a FTIR spectrometer. A common FTIR spectrometer consists of a source, interferometer, sample compartment, detector, amplifier, A/D convertor, and a computer. The source generates radiation, which passes the sample through the interferometer and reaches the detector. Then the signal is amplified and converted to a digital signal by the amplifier and analog-to-digital converter, respectively.

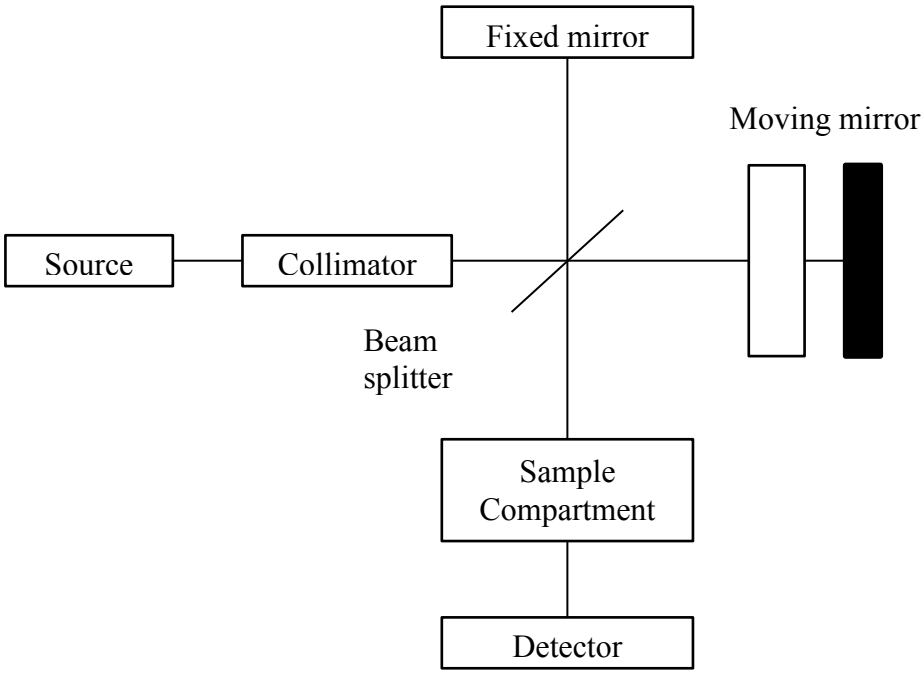

Fig.3.10 Block diagram of an FTIR spectrometer

Based on this principle, the functional groups present in the WPO were identified by using the Perkin Elmer RX. The FTIR spectra were collected in the range of 400-4000 cm^{-1} region with 8 cm^{-1} resolution. The results of the FTIR analysis are in the form of a graph plotted between the wave number and the percentage transmittance, which will give the information about the position of various bond vibrations distinguished by several modes, such as stretching, distortion, bending etc. The graphical result obtained for the WPO is shown in Fig. 3.11.

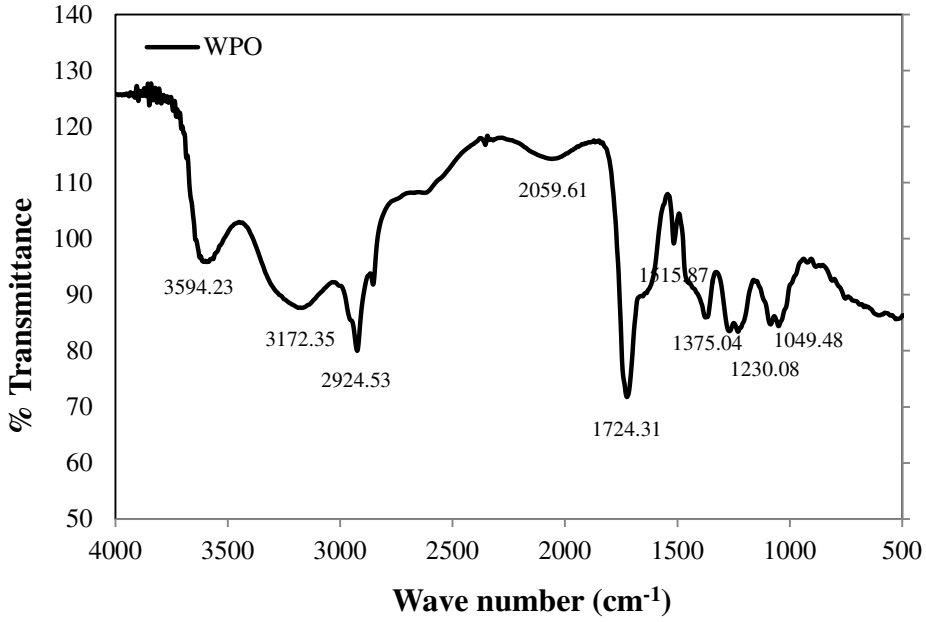

Fig. 3.11 FTIR graph of WPO

The various bonds present in the WPO are given in Table 3.3. From the FTIR graph, it can be observed that the wood derived pyrolysis oil has a few strong bonds of carbon that may result in a high carbon deposit on the piston, combustion chamber etc, when it is used in a CI engine. The stretching vibrations exist in the functional groups leading to an increase or decrease in bond length.

Table 3.3 Various bonds presents in the WPO

Wave number	Wave length	Functional groups	Bond
1049.48	7.7-11.1	Amines, acids, esters, ether and alcohols, Phospates, Silicates	C-F, C-C, C-O, C-N,
1230.08	7.4-10	Alcohols and phenols, acids, esters, ether	C-F, C-N,C-O, C-C, O-H
1375.04	6.9-8.3	Nitrates, alcohols and phenols, alkanes	O-H, C-H, Bend in plane
1515.87	6.1-6.7	Amines	N-H, Stretch
1724.31	5.4-6.1	Acids, esters, ether and alcohols	C=O, Stretch
2059.61	4.2-4.8	Alkenes/aromatics, nitriles	C≡C, C≡N, Stretch
2924.53	3.0-3.7	Alkanes	C-H, Bend in plane
3172.35	2.7-3.3	Amines, alkanes, alcohols and phenols	C-H,O-H,N-H, Bend in plane
3594.23	2.8-3.0	Alcohols, alkanes and phenols, amines	O-H,N-H, C=O, Stretch, Bend

3.5.2 GC-MS analysis of WPO

The Gas Chromatography and Mass Spectrometry (GC-MS) is a method that combines the features of gas-liquid chromatography and the mass spectrometry, to identify different substances present in the WPO. The GC-MS analysis is used both for the qualitative identification and for the quantitative measurement of the volatile and semi volatile organic compounds in complex mixtures. The working principle of the GC-MS instrument is illustrated in Fig. 3.12.

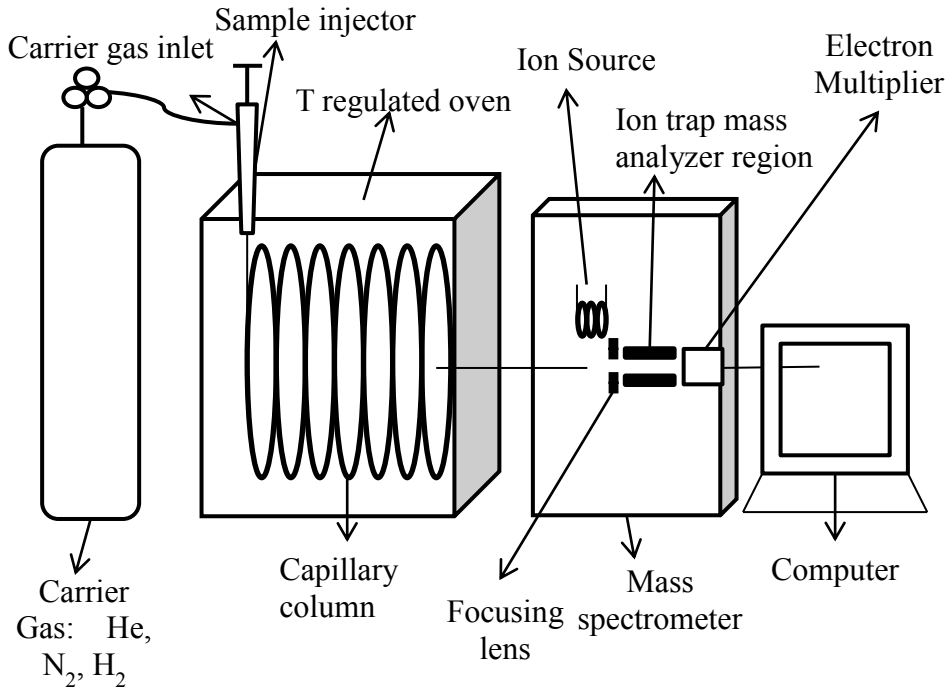

Fig. 3.12 Working principle of GC-MS analyzer

A capillary column coated with a 0.25 µm film of DB-5 with a length of 30 m and diameter 0.25 mm was used. The GC was equipped with a split injector at 200^{o}C with a split ratio of 1:10. The helium gas of 99.995% purity was used as the carrier gas at a flow rate of 1.51 ml/min. The oven's initial temperature was set at 70^{o}C for 2 min and then increased to 300^{o}C at a rate of 10^{o}C/min and maintained for 7 min. All the compounds were identified by means of the software developed by the National Institute of Standards (NIST-USA) library. The mass spectrometer was operated at an interface temperature of 240^{o}C, with an ion source temperature of 200^{o}C in the range of 40-1000 m/z. The WPO obtained was characterized by using GC/MS-QP 2010 SHIMADZU, equipped with flame ionization and mass spectrometry detection (GC-FID-MS). The GC-MS chromatogram of WPO is shown in Fig. 3.13.

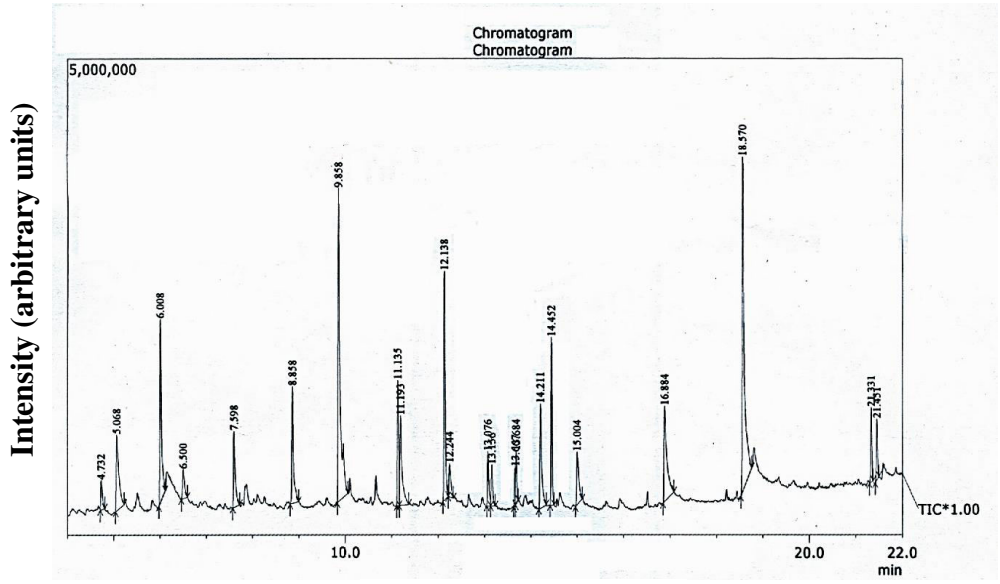

Fig. 3.13 Gas chromatogram of wood pyrolysis oil

The GC-MS report of the WPO is noted in the following Table 3.4.

Table 3.4 Main components obtained from GC-MS analysis

Reaction time	Area %	Compound Name	Molecular formula
4.732	1.20	Tetrahydro-2-furanmethanol	$C_5H_{10}O_2$
5.068	4.86	3-Methlcyclopentane-1,2-dione	$C_6H_8O_2$
6.008	7.24	0-Methoxyphenol	$C_7H_8O_2$
7.598	3.17	1-hydroxy-2-methoxy-4-methylbenzene	$C_8H_{10}O_2$
8.858	4.63	1-hydroxy-2-methoxy-4-ethylbenzene	$C_9H_{12}O_2$
9.858	15.29	1,3-Dimethoxy-2-hydroxybenzene	$C_8H_{10}O_3$
11.135	3.98	1,2,4-Trimethoxybenzene	$C_9H_{12}O_3$
11.193	4.58	(E)-Isoeugenol	$C_{10}H_{12}O_2$
12.138	7.34	1,2,3-Trimethoxy-5-methylbenzene	$C_{10}H_{14}O_3$
12.244	1.50	2-Propanone, 1-(4-Hydroxy-3-Methoxyphenyl)	$C_{10}H_{12}O_3$
13.076	1.90	2,6-Dimethoxy-4-(2-Propenyl)Phenol	$C_{11}H_{14}O_3$
13.156	1.52	2,4-Hexadienedioc acid, 3-Methyl-4-Propyl, Dimethyl ester, (Z,E)	$C_8H_{12}O_2$
13.667	0.88	N-[2-(2-Isopropyl-phenoxy)-ethyl]-2-methylsulfanyl-benzamide	$C_{19}H_{23}NO_2S$
13.684	1.50	1,3-Diphenylpropane	$C_{15}H_{16}$
14.211	4.48	2,6-Dimethoxy-4-(2-Propenyl)Phenol	$C_{11}H_{14}O_3$
14.452	4.59	N-Methylene-1,2-diphenylethanamine	$C_{15}H_{15}N$
15.004	2.78	1-(2,6-Dihydroxy-4-methoxyphenyl)-1-butanone	$C_{11}H_{14}O_4$
16.884	6.65	n-Hexadecanoic acid	$C_{16}H_{32}O_2$
18.57	16.70	Oleic Acid	$C_{18}H_{34}O_2$

The GC-MS of WPO indicates that the WPO contains compounds like Oleic acid, 1, 3-Dimethoxy-2-hydroxybenzene, and Methoxyphenol in a large proportion. Most of the components identified are phenols, with ketones and aldehyde groups attached, and nearly all the functional groups showed the extensive existence of the oxygen. On the other hand, the

analysis proved that the abundant aldehydes and ketones make the pyrolysis oil hydrophilic and hydrated in nature that prevents the separation of water from WPO [139].

3.5.3 Physicochemical properties of WPO, JME and diesel

The proximate analysis indicates the percentages of the moisture, volatile, ash and fixed carbon contents in the raw materials. From the ultimate analysis, one can know the percentage composition of the various elements present in the raw materials such as Carbon, Hydrogen, Nitrogen, Sulphur and Oxygen content. The proximate and ultimate analyses of WPO are compared with that of diesel and given in Table 3.5.

Table 3.5 Proximate and ultimate analysis of WPO compared with diesel

Proximate analysis	**WPO**	**Diesel**
Water content (%)	28.8	0.025
Ash content (%)	0.012	0.13
Fixed carbon (%)	12.85	Nil
Ultimate analysis		
Carbon (%)	49.1	86.5
Hydrogen (%)	6.2	13.2
Nitrogen (%)	3.0	Nil
Sulphur (%)	0.05	0.3
Oxygen by difference (%)	41.65	Nil

The important physico chemical properties of WPO are tested in a standard test facility. All the tests are conducted by following the ASTM standard test procedure. Table 3.6 gives the comparison of the physical properties of WPO with those of JME and diesel.

Table 3.6 Comparison of fuel properties of WPO with diesel and JME

Properties	ASTM method	Diesel	JME	WPO
Specific gravity at 15 °C	D 4052	0.83	0.88	1.15
Net calorific value (MJ/kg)	D 4809	43.8	39.1	20.58
Flash point (°C)	D 93	50	118	98
Fire point (^{o}C)	D 93	56	126	108
Pour point (°C)	D 97	-6	-1	2
Carbon residue (%)	D 4530	0.1	0.01	12.85
Kinematic viscosity at 40 °C (cSt)	D 445	2.58	4.6	25.3
Copper strip corrosion @ 100^{o}C for 3 hrs		-	No.1	No.1
Surface tension (mN/m)	D 971	26.7	29.2	30.7
Cetane number	D 613	50	55	27
Moisture content (wt %)	D 2709	0.025	1	15-30
Final boiling point (^{o}C)	D 86	344	342	250-280
Oxidation stability (mg/l00g)	-	-	0.4	-
Acid value (mg KOH/g)	-	-	0.38	0.45
Carbon (%)	D 3178	86.5	77.1	49.1
Hydrogen (%)	D 3178	13.2	11.81	6.2
Nitrogen (%)	D 3179	Nil	0.119	3.0
Sulphur (%)	D 3177	0.3	0.001	0.05
Oxygen by difference (%)	E 385	Nil	10.97	41.65
Stoichiometric A/F ratio (%)	-	14.5	12.4	3.39
Empirical formula	-	$C_{10}H_{22}$	$C_{7.56}H_{13.89}N_{0.01}O_{0.81}$	$C_{1.13}H_{2.92}N_{0.01}S_{0.01}O_{1.62}$

3.6 Preparation of JME-WPO emulsions

Emulsification is one of the techniques used to mix two liquids of different densities and surface tension. It can also be defined as the mixing of one substance with another, which is hydroscopic in nature. Surfactants are compounds that lower the surface tension of a liquid that decreases the interfacial tension between two liquids. Surfactants may act as detergents, wetting agents, emulsifiers, foaming agents and dispersants. In this investigation, the role of the surfactant is that of an emulsifier. In the emulsification process one of the biggest

challenges is, choosing a suitable surfactant for the two liquids to be emulsified. This depends on the HLB value of the surfactant. HLB, i.e., the Hydrophilic Lipophilic Balance is the measure of degree to which the liquid is hydrophilic or lipophilic. Depending upon the nature of the dispersed phase and dispersing medium, the emulsions are classified into two types:

(i) Oil-in-water emulsions (O/W)

(ii) Water-in-oil emulsions (W/O)

Surfactants with HLB values ranging between 4 and 8 are considered to make water-in-oil type of emulsions and HLB values between 8 and 12 are considered to make oil-in-water emulsions. The accuracy of the HLB values taken into consideration will be around ± 0.5. Depending on the size of the droplets, emulsions are classified into two types:

(a) Macro emulsions: The size of the particles ranges from 0.2 to 50 mm, and they are kinetically stable.

(b) Micro emulsions: The size of the particles ranges from 0.01 to 0.02 mm, and they are thermodynamically stable.

In this investigation, a water-in-oil type emulsion was considered to make the JME-WPO emulsions. The non-ionic surfactants having, HLB values in the range between 4 and 9 were selected for this study. The list of surfactants used in this study and their specifications are given in Table 3.7.

Table 3.7 List of surfactants used in this study and their HLB values

Sl.No	Name of the surfactant	Chemical formula	HLB value
1.	Span 20 (Sorbitan monolaurate)	$C_{18}H_{34}O_6$	8.6
2.	Span 80 (Sorbitan monooleate)	$C_{24}H_{44}O_6$	4.3
3.	Tween 80 (Polysorbate 80)	$C_{64}H_{124}O_{26}$	15
4.	Span 80 + Tween 80 mixed	-	6.45

The JME-WPO emulsions were prepared by adding 5, 10 and 15% of WPO with 95, 90 and 85% JME respectively, with the addition of the different surfactant combinations by volume percentage. Table 3.8 gives the details of the composition of the materials used in the preparation of different JME-WPO emulsions.

Table 3.8 Composition of materials used in JME-WPO emulsions

Sample No.	WPO (vol %)	JME (vol %)	Surfactant (vol %)	Notation
1.	5	93	Span 20 2%	X1JOE5
2.	10	88	Span 20 2%	X1JOE10
3.	15	83	Span 20 2%	X1JOE15
4.	5	91	Span 20 4%	X2JOE5
5.	10	86	Span 20 4%	X2JOE10
6	15	81	Span 20 4%	X2JOE15
7	5	93	Span 80 2%	Y1JOE5
8.	10	88	Span 80 2%	Y1JOE10
9.	15	83	Span 80 2%	Y1JOE15
10.	5	91	Span 80 4%	Y2JOE5
11.	10	86	Span 80 4%	Y2JOE10
12.	15	81	Span 80 4%	Y2JOE15
13.	5	93	2% of (50% of Span 80 + 50% of Tween 80)	Z1JOE5
14.	10	88	2% of (50% of Span 80 + 50% of Tween 80)	Z1JOE10
15.	15	83	2% of (50% of Span 80 + 50% of Tween 80)	Z1JOE15
16.	5	91	4% of (50% of Span 80 + 50% of Tween 80)	Z2JOE5
17.	10	86	4% of (50% of Span 80 + 50% of Tween 80)	Z2JOE10
18.	15	81	4% of (50% of Span 80 + 50% of Tween 80)	Z2JOE15

A mechanical stirrer is used to mix the JME with WPO and the surfactant. The stirrer was connected to a small AC motor whose capacity was 1/20 HP (37.3W). Hence, the electrical energy consumed for the preparation of each sample was about 0.01865 kWh. Fig. 3.14 (a) shows the photographic view of arrangement of mechanical stirrer. Fig. 3.14 (b) shows the photographic view of the stirring action during emulsification process.

Fig. 3.14 (a) Arrangement of mechanical stirrer

Fig.3.14 (b) Stirring action during emulsification process

Fig. 3.15 (a) and Fig. 3.15 (b) show the Y1JOE10 and Y1JOE15 emulsion respectively.

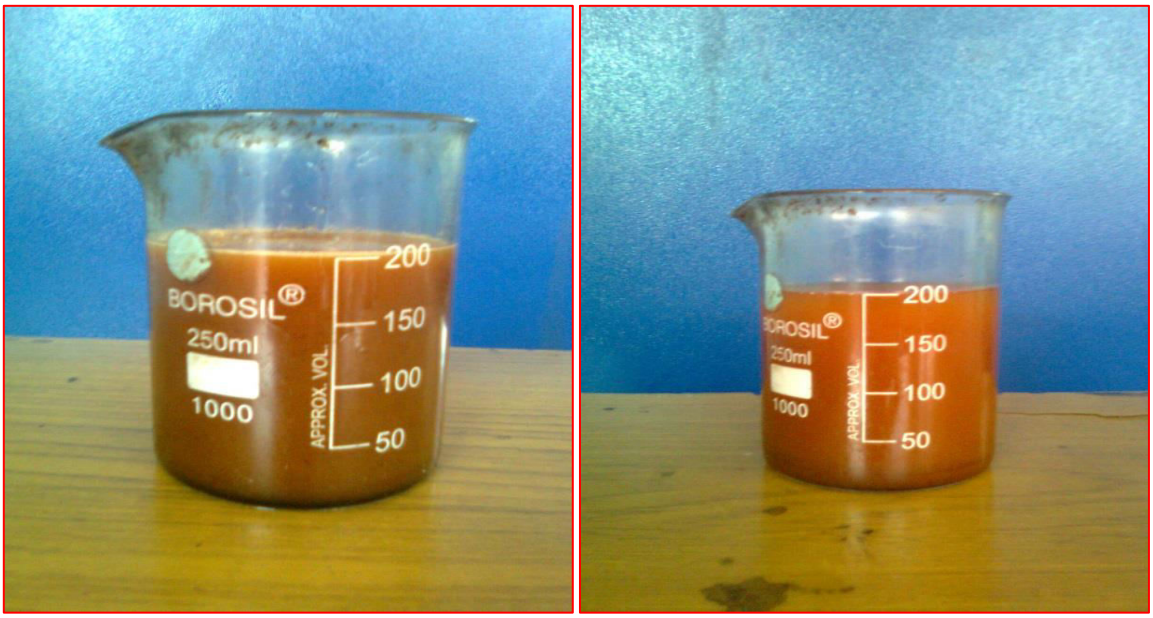

Fig.3.15 (a) Y1JOE10 emulsion **Fig.3.15 (b)** Y1JOE15 emulsion

Fig. 3.16 (a) and Fig. 3.16 (b) show the Y2JOE10 and Y2JOE15 emulsion respectively.

Fig.3.16 (a) Y2JOE10 emulsion **Fig.3.16 (b)** Y2JOE15 emulsion

Fig. 3.17 (a) and Fig. 3.17 (b) show the X1JOE10 and X1JOE15 emulsion respectively.

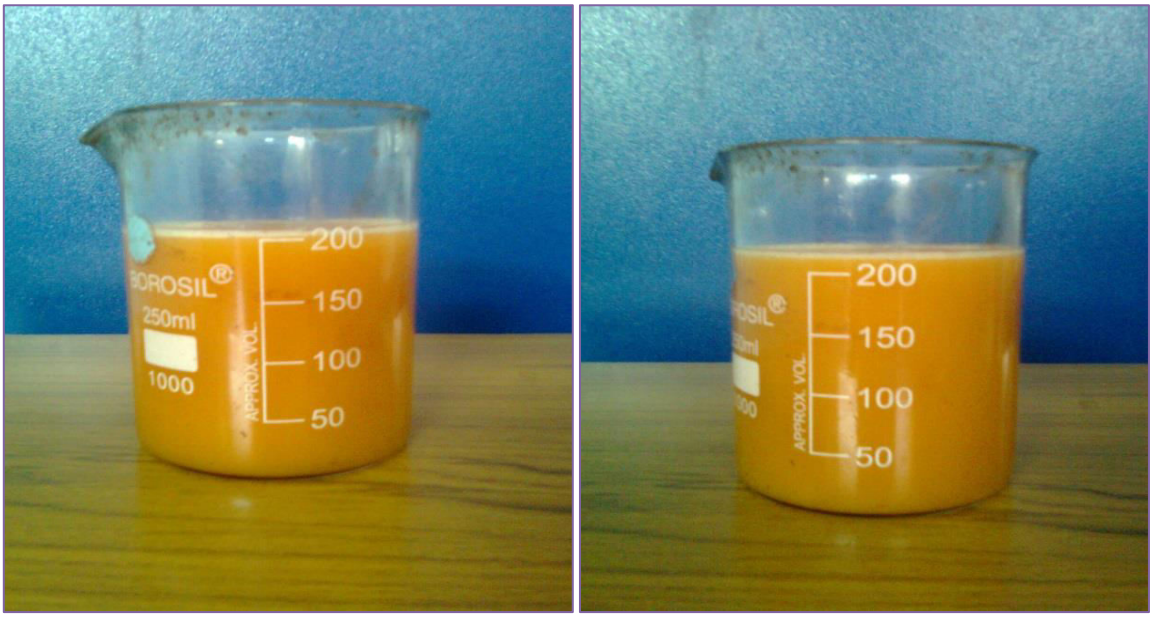

Fig.3.17 (a) X1JOE10 emulsion **Fig.3.17 (b)** X1JOE15 emulsion

Fig. 3.18 (a) and Fig. 3.18 (b) show the X2JOE10 and X2JOE15 emulsion respectively.

Fig.3.18 (a) X2JOE10 emulsion **Fig.3.18 (b)** X2JOE15 emulsion

Fig. 3.19 (a) and Fig. 3.19 (b) show the Z1JOE10 and Z1JOE15 emulsion respectively.

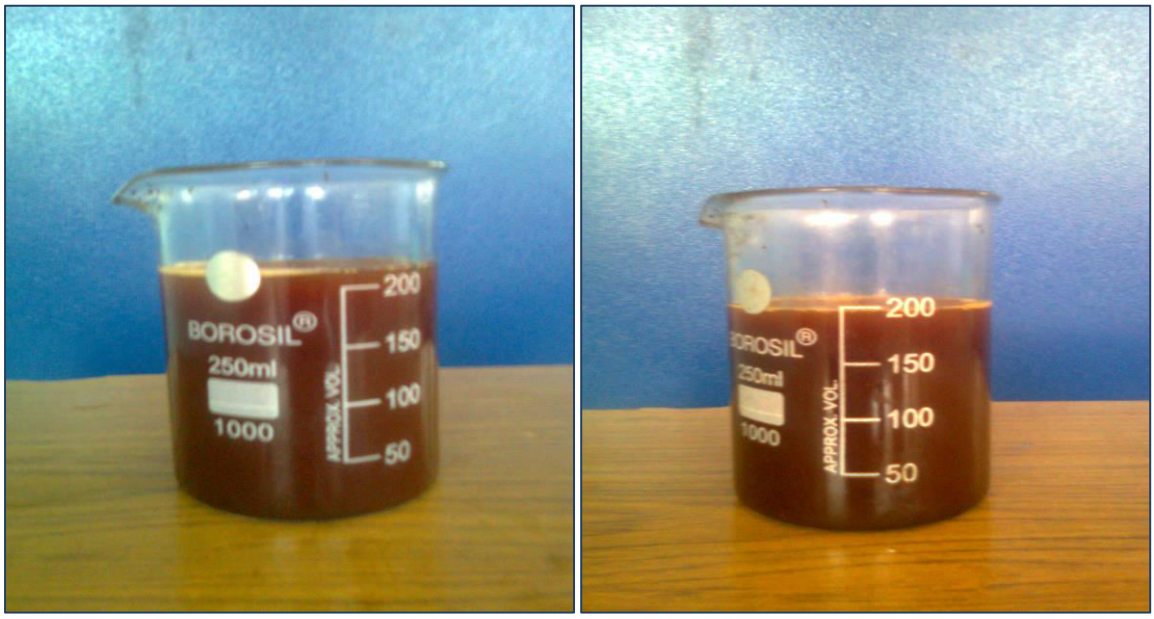

Fig.3.19 (a) Z1JOE10 emulsion **Fig.3.19 (b)** Z1JOE15 emulsion

Fig. 3.20 (a) and Fig. 3.20 (b) show the Z2JOE10 and Z2JOE15 emulsion respectively.

Fig.3.20 (a) Z2JOE10 emulsion **Fig.3.20 (b)** Z2JOE15 emulsion

3.7 Image analysis of emulsions

A microscopic analysis was carried out to check the dispersion of emulsion droplet. The microscopic images of the sample droplet distribution of four different emulsions are shown in Figs. 3.21 to 3.24.

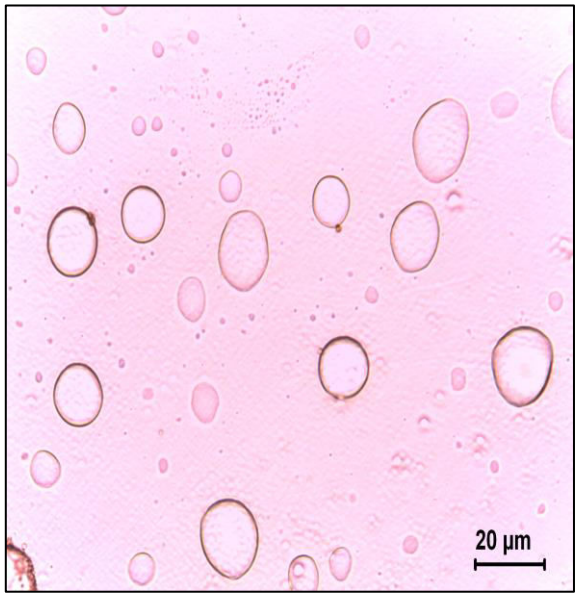

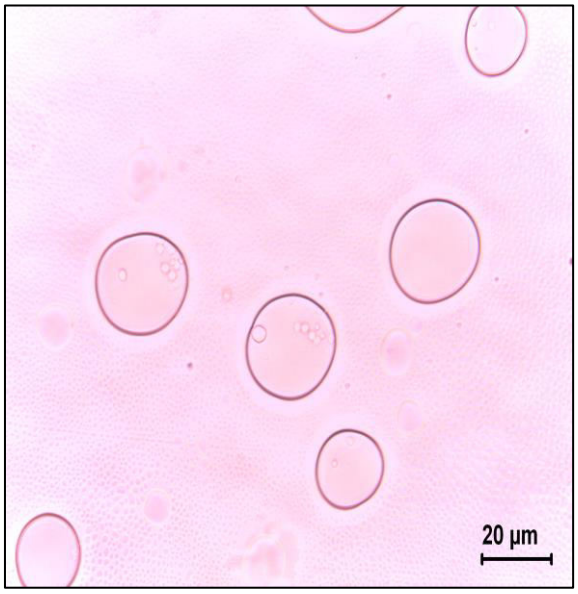

Fig.3.21 X1JOE15 emulsion **Fig.3.22** Y1JOE15 emulsion

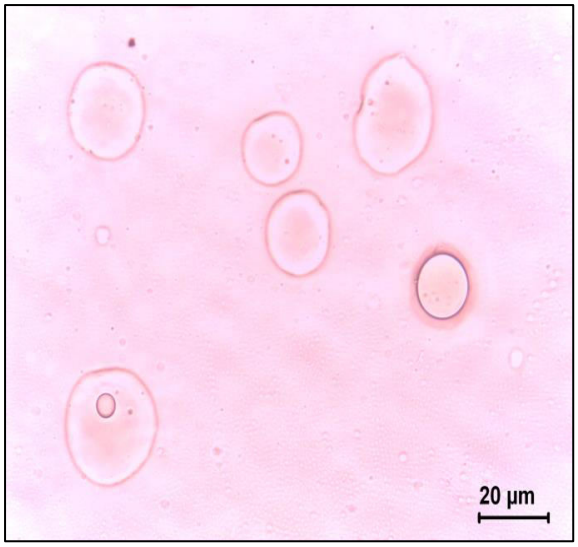

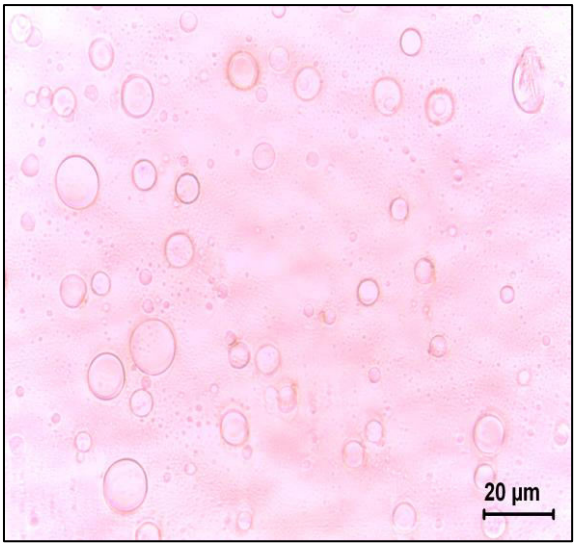

Fig.3.23 Z1JOE15 emulsion **Fig.3.24** Z2JOE15 emulsion

The images were obtained with the help of a digital camera connected to an electron microscope whose magnification index was 500X. It can be observed from the microscopic images that the Z2JOE15 emulsion using a mixed surfactant Span 80 and Tween 80 contains smaller mean droplet diameter compared to those of the other JME-WPO emulsions studied. This indicates that the emulsion stability of Z2JOE15 is considerably larger than that of other emulsions. The physico chemical properties of different JME-WPO emulsions used in this study are given in Table 3.9.

3.8 Acid treatment of JOE15 emulsion

The acidity of pyrolytic liquids is typically determined by the pH value. The acids in the bio oil are produced mainly by the degradation of the hemicelluloses in wood. The pH is a representation of how corrosive the oil may be, but it does not indicate the concentration of the acidic constituents. The pH of the WPO is low (2–3). The total acid number (TAN) can also be used for measuring the acidity of the bio oil. The TAN is the amount of potassium hydroxide (KOH) in milligrams that is needed to neutralize the acids in one gram of liquid. After attempting trials with different emulsions, to evaluate the combustion, performance and emissions of the engine, it was understood that the JOE15 emulsion gave a better results than other emulsions. However, since the emulsion was acidic in nature, the researcher tried to neutralize the emulsion with acid treatment. Therefore, in this study, the TAN value of JOE15 was determined by the potentiometric titration method. In this method, the sample of JOE15 was dissolved in toluene (50%), propanol (49.5%) and water (0.5%). Then, it was titrated with alcoholic potassium hydroxide using a burette at a constant rate.

Table 3.9 Fuel properties of JME-WPO emulsions

Properties	X1JOE10	X1JOE15	X2JOE10	X2JOE15	Y1JOE10	Y1JOE15	Y2JOE10	Y2JOE15	Z1JOE10	Z1JOE15	Z2JOE10	Z2JOE15
Specific gravity at 15 °C	0.906	0.926	0.908	0.9167	0.907	0.9265	0.905	0.9155	0.918	0.9267	0.907	0.9205
Net calorific value (MJ/kg)	37.24	36.32	34.28	32.24	37.24	36.32	37.24	36.32	37.24	36.32	38.17	36.72
Flash point (°C)	158	152	159	152	158	153	162	158	160	156	160	154
Kinematic viscosity at 40 °C (cSt)	6.75	6.97	6.91	7.28	6.62	7.12	6.73	6.97	6.91	7.28	6.43	7.06
Carbon (%)	65.88	77.26	60.82	64.36	61.23	58.50	51.265	46.9	58.6	51.72	56.35	48.79
Hydrogen (%)	8.125	12.27	7.63	8.324	7.265	6.851	7.812	7.556	9.12	8.558	9.57	7.652
Nitrogen (%)	0.09	0.07	0.32	0.18	0.243	0.16	0.23	0.15	0.21	0.29	0.156	0.25
Sulphur (%)	0.312	0.495	0.76	0.25	0.356	0.856	0.24	0.385	0.52	0.736	0.83	1.571
Oxygen by difference (%)	25.593	9.901	30.47	26.886	30.906	33.633	40.45	45.009	31.55	38.696	33.094	41.737
Stoichiometric A/F ratio (%)	-	13.55	-	-	-	-	-	-	8.559	7.26	-	-

A glass electrode and reference electrode were immersed in the sample and connected to a potentiometer. The meter reading (in millivolts) was plotted against the volume of the titrant. Based on the inflection in the curve, the buffer potential was considered to be the acid number of the sample. The TAN value determined by this method for JOE15 was 17.6 (mg of KOH/g). The physical properties of acid treated JOE15 emulsion tested in a standard test facility and the results are given in Table 3.10. The economic analysis to prepare 1 litre of ATJOE15 emulsion is given in Annexure 1.

Table 3.10 Properties of the acid treated JOE15 emulsion compared with JOE15

Properties	JOE15	ATJOE15
Specific gravity at 15 °C	0.9167	0.9176
Net calorific value (MJ/kg)	36.32	30.82
Kinematic viscosity at 40 °C (cSt)	7.28	6.50
Surface tension (mN/m)	30.679	30.179
Flash point (°C)	156	148
pH value	3-4	7
TAN (mg of KOH/g)	17.6	-

CHAPTER 4

EXPERIMENTAL SETUP AND METHODOLOGY

4.1 General

This chapter details the test engine with loading device and complete instrumentation used in this investigation. With the help of instrumentation, the procedure followed to determine the performance parameters such as brake thermal efficiency, brake specific fuel consumption and exhaust gas temperature of the engine for all the emulsions, at different loads are discussed. Further, the working principle and the use of the analysers to measure the exhaust gas emissions such as nitric oxide (NO), carbon monoxide (CO), unburnt hydrocarbon (HC) and smoke opacity are illustrated. The devices used to measure the cylinder pressure and crank angle are also discussed. The description of data acquisition system (DAS) is also given. This chapter also provides information on the accuracies and uncertainties of the instrumentation adopted in this study. The methods followed to conduct the short term and long term endurance tests are also reported in this chapter. Also, the procedure to evaluable the lubrication oil properties after long run is also discussed.

4.2 Engine experimental setup

A detailed layout of experimental setup is shown in Fig. 4.1. A photographic view of the experimental setup is given in Fig.4.2. The engine experiments were conducted as per IS: 10,000 [Part IV, V, VI, VIII, IX and X]:1980 standard test methods. A Kirloskar TAF1 model, single cylinder, four stroke, air cooled, DI diesel engine with a displacement volume of 661.5 cc and developing a rated power of 4.4 kW was used in this study. The engine was run at a constant speed of 1500 rpm. The detailed specification of the test engine is given in Annexure 2. An electrical dynamometer connected to a resistive load bank, was used to load the engine. The fuel measuring system consisted of a burette fitted with two optical sensors, one at a higher level and the other at a lower level. As the fuel passed through the higher level optical sensor, the sensor gave a signal to the data acquisition system (DAS) to start the counter time. Once the fuel reached the lower level sensor, the sensor gave a signal to the DAS to stop the counter time and refill the burette. From this, the time taken for the consumption of fuel for a fixed volume was calculated. A differential pressure sensor fitted in the air box measured the air consumption. The differential pressure sensor was used to measure the pressure difference between the orifice plates. The differential pressure sensor gave a proportional voltage output with respect to the difference in pressure.

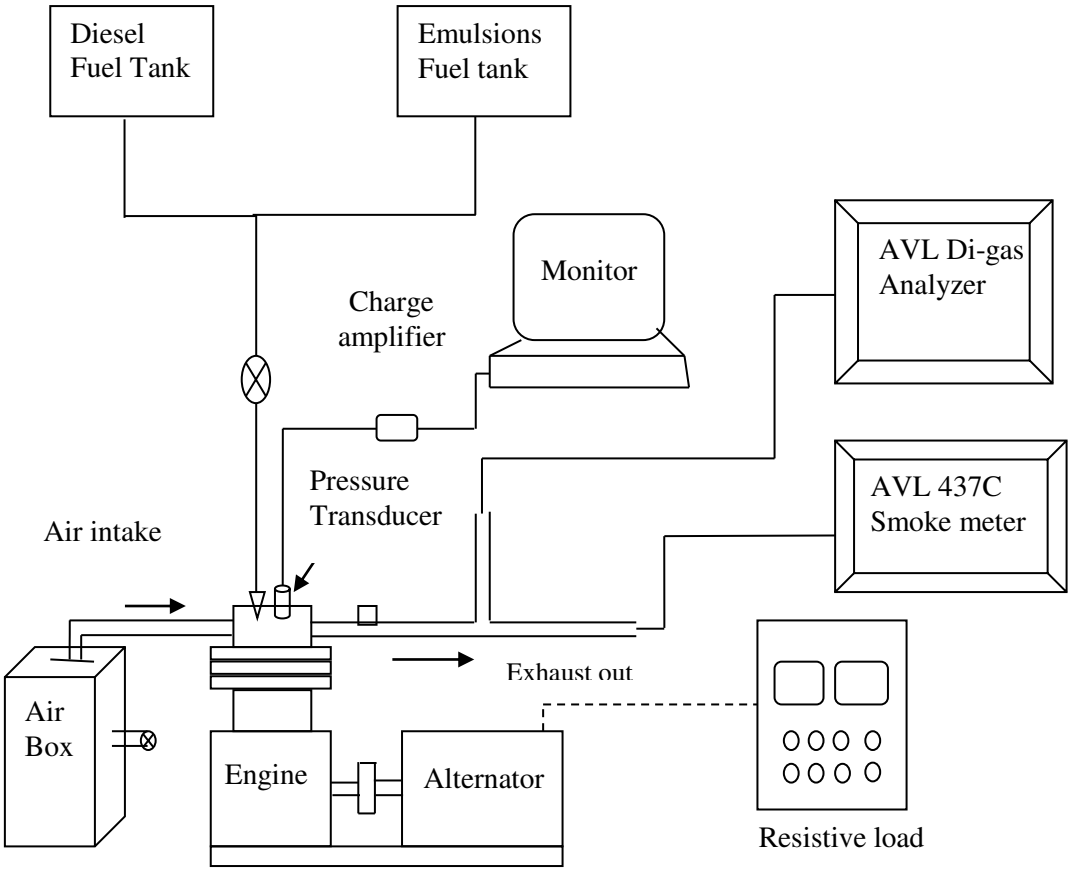

Fig. 4.1 Schematic diagram of experimental setup

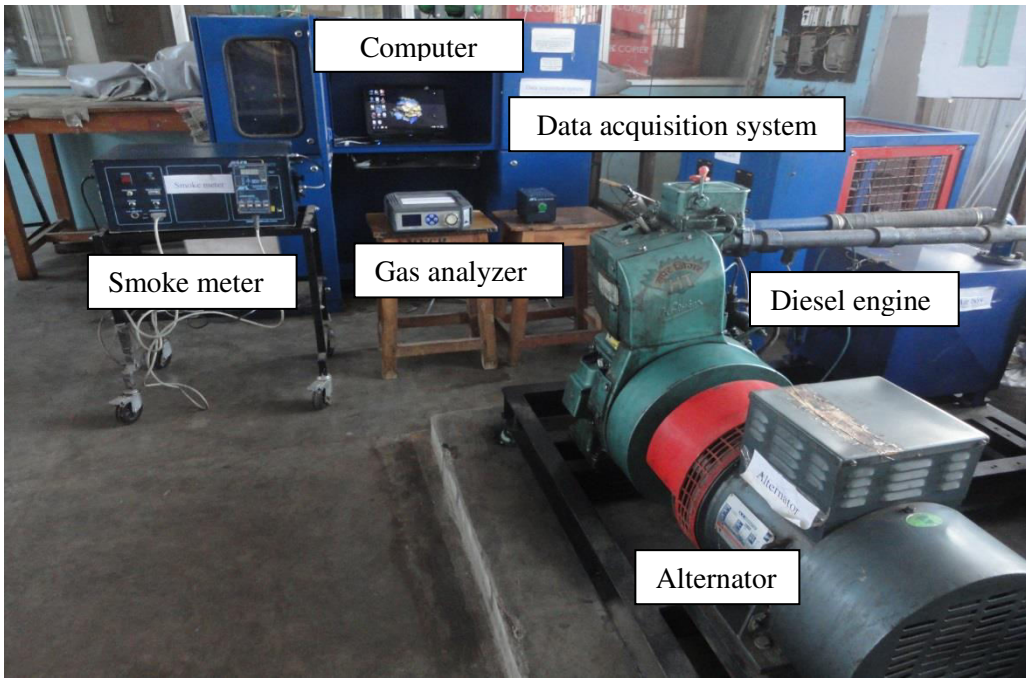

Fig. 4.2 Photographic view of experimental setup

A surge tank was used to damp out the pulsations produced by the engine, for ensuring a steady flow of air through the intake manifold. A K-type thermocouple fitted in exhaust pipe measured the exhaust gas temperature. A non-contact PNP type sensor was connected near the flywheel of the engine to measure the engine speed. The PNP sensor gave the pulse output for each revolution of the crank shaft. The frequency of the pulses was converted into voltage output and connected to the computer. A standalone frequency to voltage converter is used for signal conditioning. The in-cylinder pressure of the diesel engine was obtained by means of a pressure transducer, which was flush mounted on the cylinder head. Initially, the combustion, performance and emission parameters of the diesel engine were studied with diesel at a compression ratio of 17.5 and nozzle opening pressure of 200 bar, which was prescribed by the manufacturer, by maintaining a rated speed of 1500 rpm to get the diesel data.

4.3 Data collection for performance parameters

4.3.1 Brake thermal efficiency (BTE)

In order to determine the brake thermal efficiency of the engine, three important inputs were measured: i) Time taken for 20 cc of fuel consumption ii) Lower heating value of the test fuel and iii) Fuel density. The formula used to calculate the brake thermal efficiency, is given below:

BTE = (brake power x 3600 x 100/ (volumetric fuel flow rate per hour x fuel density x calorific value of fuel)). (4.1)

4.3.2 Brake specific fuel consumption (BSFC)

The formula used to calculate the brake specific fuel consumption is given below:

BSFC = (volumetric fuel flow rate per hour x fuel density/brake power) (4.2)

The BTE and BSFC were displayed in the form of excel sheet generated by the data acquisition system software (Engine test express) using the above mentioned expressions.

4.4 Combustion parameters measurement

4.4.1 Piezo electric transducer

For acquiring important combustion parameters, such as ignition delay, heat release rate, combustion duration etc., the cylinder pressure and crank angle values are necessary. The

cylinder gas pressure was measured using a Kistler piezo-electric transducer (model 5395A) in conjunction with a Kistler charge amplifier.

Fig. 4.3 Photographic view of Kistler pressure transducer

The cylinder gas pressure data was recorded as the average of 20 cycles of data, with a resolution of 0.5°CA using a data acquisition system. From the average data of the pressure and crank angle values, the peak pressure, occurrence of the peak pressure, maximum rate of pressure rise, and heat release rate were calculated and stored in an excel file. A photographic view of the Kistler pressure transducer is shown in Fig. 4.3. The exploded view of the piezoelectric transducer is shown in Fig. 4.4.

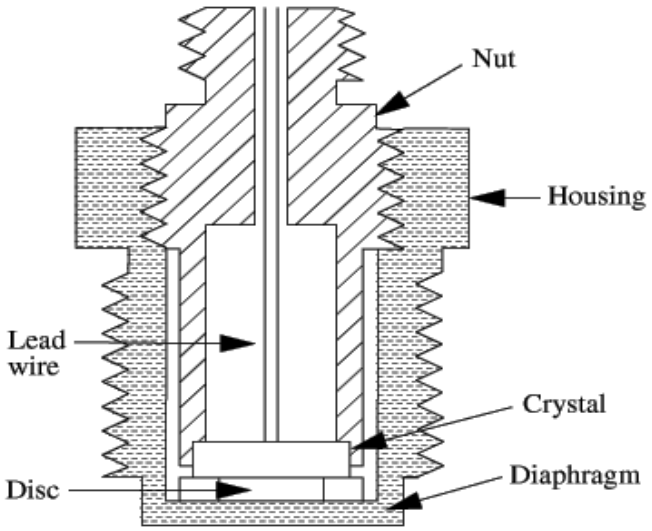

Fig. 4.4 Exploded view of piezoelectric transducer

The quartz sensors can withstand very high pressure varying from 0 to 250 bar. A hole was drilled on the dummy plug and the pressure sensor was placed in it. The drilled hole diameter was 5 mm, and an internal thread of pitch 1 mm is made. The piezo electric sensor was properly sealed so that there is no change in the compression ratio of the cylinder. The pressure produced by the engine cylinder was sensed by the pressure sensor placed on the dummy plug. The measured pressure acts through a diaphragm on the quartz crystal measuring elements, which transforms the pressure into an electrostatic charge Q in pico coulomb. The sensor was mounted on the combustion chamber plug end by a M5 tapping hole, to accommodate the sensor. The complete specification of the Kistler make piezo quartz pressure sensor is given in Annexure 3. Figure 4.5 shows a photographic view of the location at which the pressure transducer is flush mounted.

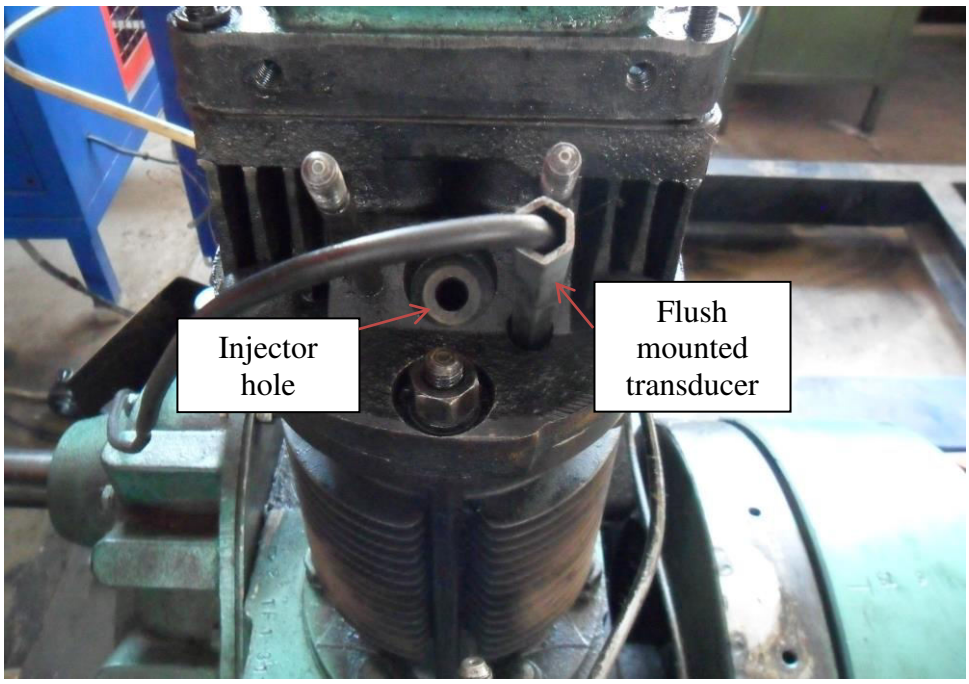

Fig. 4.5 Photographic view of flush mounted transducer in engine cylinder head

The stainless steel diaphragm was welded hermetically to the stainless steel body. The quartz elements were mounted in a highly sensitive arrangement (transversal effect). The quartz element had a high natural frequency. Its connector was welded to the body, but its Teflon insulator was not absolutely tight.

The TDC marker (Kistler model 5015A1000) was placed near the engine flywheel. At the TDC position, a small metallic deflector was fitted. The photographic view of the TDC

marker and metallic deflector is shown in Fig. 4.6. The setup was aligned in such a way that the sensor gives output in the form of a square wave, exactly when the piston is at the TDC.

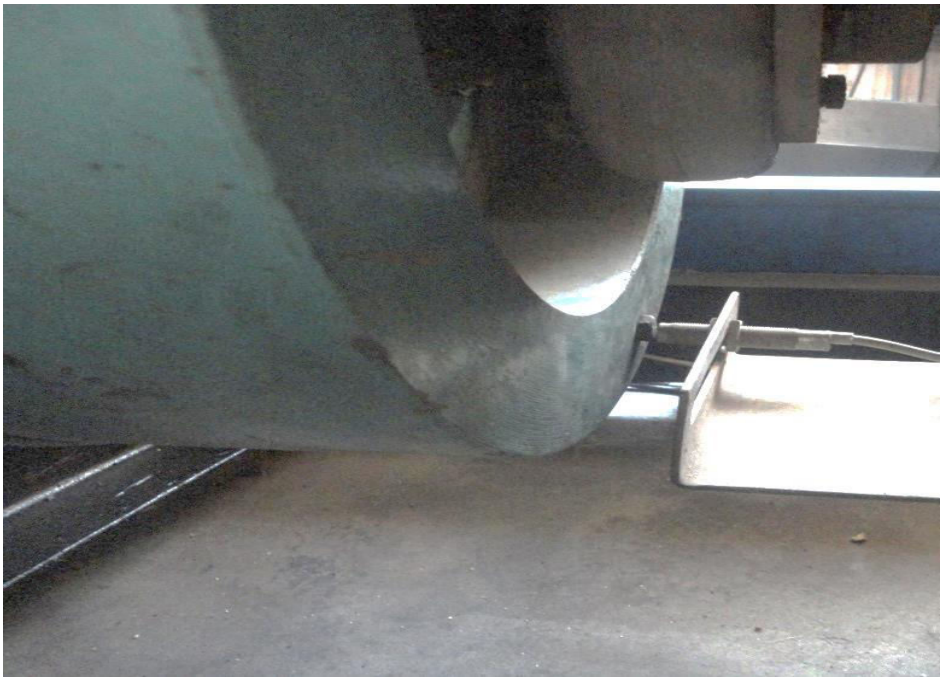

Fig. 4.6 Photographic view of TDC marker and deflector

4.4.1.1 Pressure transducer calibration

The calibration of the pressure transducer was carriedout to measure any differences in the output of the transducer for a known pressure. This was essential to minimize the combustion cylinder-pressure measurement error, and was particularly important for the engine data. The piezo electric transducer signals naturally decay over time, and are therefore only suitable for dynamic measurements, like engine cylinder pressure measurements. Accordingly, they must be calibrated using a dynamic procedure. The Kistler piezo electric transducer of model 5395A was subjected to a dynamic calibration procedure using a standard dead weight tester. The dead weight tester generated the known pressure by hydraulically lifting precise weights with a piston with an accurately known cross-sectional area. The charge output signal of these transducers was used as the input to a charge amplifier via a high impedance cable. The charge amplifier converts the low level charge (which is of the order of several Pico-Coulombs) to a proportional voltage, which can be recorded with standard data acquisition equipment. In this procedure, a known pressure was applied to the transducer. Then, the output was grounded to zero volts, thereby eliminating signal decay. The pressure was then abruptly dropped to the atmospheric level, by rapidly releasing the hydraulic pressure holding up the weights and allowing them to fall. The resulting voltage change was recorded as a

function of time, using a digital oscilloscope programmed to trigger on a voltage drop. The voltage change caused by the pressure change was determined using a peak-to-peak calculation feature on the scope. Dynamic pressures were taken at intervals of 200 psi from 200 to 1000 psi. Ten measurements were taken at each dynamic pressure. These were then averaged, and graphed against the corresponding voltage output. The linearity of the transducer was found to be better than 1%. The repeatability was observed to be about 2 to 3%.

4.4.2 Charge amplifier

A charge amplifier was used to convert the obtained charge into equivalent output voltage. It transferred the input charge to another reference capacitor and produced an output voltage equal to the voltage across the reference capacitor, as shown in Fig. 4.7.

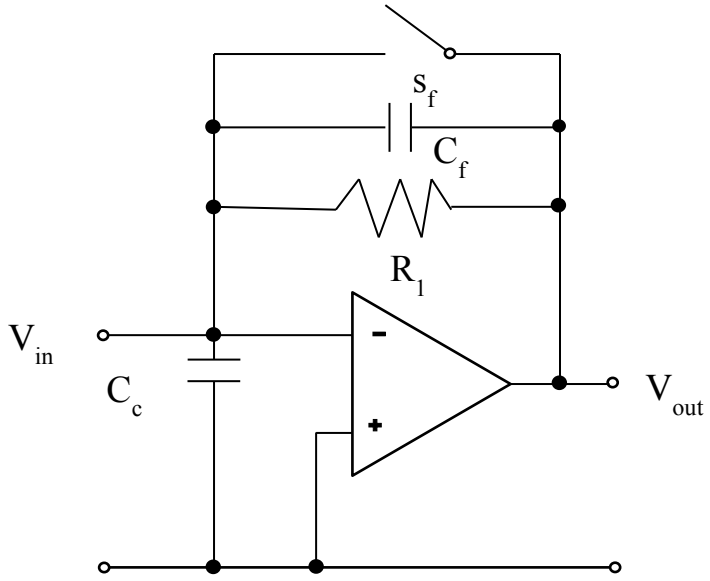

Fig. 4.7 Charge amplifier circuit

Thus, the output voltage was proportional to the charge of the reference capacitor and, respectively to the input charge; hence the circuit acted as a charge to voltage converter. The complete specification of the charge amplifier is given in Annexure 4. The input charge Q_{in} was applied to the summing point (inverting input) of the amplifier. It was distributed to the cable capacitance Cc, the amplifier input capacitance C_{inp} and the feedback capacitor C_f.

The node equation of the input is therefore: $Q_{in} = Q_c + Q_{inp} + Q_f$ (4.3)

Using the electrostatic equation: $Q = U \times C$ (4.4)

and substituting Q_{in}, Q_c, Q_{inp} and Q_f

$Qin = U_{inp} \times (C_c + C_{inp}) + U_f \times C_f$ (4.5)

and solving the output voltage V_O:

$V_O = V_f = Q_{in}/C_f$ which is fed into the data acquisition system. (4.6)

The output of the Kistler charge amplifier lies within ± 10V DC.

4.4.3 Analog to Digital Converter

The analog signals from the sensors were fed into an Analog to Digital Converter (ADC) and then passed to a display unit, through a data acquisition cord and microcontroller. Both the pressure and proximity sensors were interfaced with the engine and the output obtained is an analog signal. Further, the analog signal was converted into digital using the ADC, which was finally fed to a display unit through the data acquisition system. Using the data acquisition system graphical analysis, evaluating the differential equation, computing the mathematical expression, display, control and recording were done for various engine operating parameters, like instantaneous pressure, crank angle, temperature, and the heat release rate. From this, other combustion parameters such as ignition delay, cumulative heat release rate, mass fraction burned and combustion duration were computed. A computer was used to process the data and store during investigation.

4.4.4 Significance of the p-θ diagram

The in-cylinder pressure plotted against the crank angle is called as the P-θ diagram, which is a very useful tool for the combustion analysis. The pressure inside the cylinder depends on the instantaneous cylinder volume, combustion, heat transfer to combustion chamber walls, crevice regions and leakage. The usefulness of the p-θ diagram is given below:

- The p-θ diagram indicates the events occurring near the TDC more clearly than the p-V diagram.
- It gives information about the instantaneous pressure inside the engine cylinder for every crank angle degree.
- It gives the peak cylinder pressure, brake mean effective pressure in the cycle and its position, pressure rise, position and rate of pressure rise and maximum rate of pressure rise.
- It describes quantitative information on the progress of combustion.
- Valve timing, i.e., valve opening and closing can be optimized based on this p-θ diagram.

- The rates of heat release, ignition delay, start of combustion, duration of combustion, mass fractions burned and gas condition for pollutant formation, are also given by the p-θ diagram.

4.4.5 Determination of the combustion parameters

4.4.5.1 Ignition delay

The ignition delay of a compression ignition (CI) engine is defined as the time (or crank angle) interval between the start of injection and start of combustion. This delay is due to physical and chemical processes that takes place before a significant fraction of the chemical energy of the injected liquid fuel is released. The physical processes are: atomization of liquid fuel jet, evaporation of fuel droplets and mixing of fuel vapour with air. The chemical processes are precombustion reactions of fuel, air, residual gas mixture that leads to auto ignition. These processes are affected by engine design, operating variables and fuel characteristics. Ignition delay, in terms of the crank angle, is the difference between the start of injection and the start of ignition (detectable heat release rate). From the heat release rate curve, the start of combustion is determined as the point at which the heat release curve changes from a negative axis to a positive one [155].

Based on the crank angle, ignition delay is determined with the following equation:

$$\text{Ignition delay (CA)} = (\text{CA})_{5\%} - (\text{CA})_{\text{inject}} \tag{4.7}$$

where, $(\text{CA})_{5\%}$ = Crank angle at which 5% heat is released

$(\text{CA})_{\text{inject}}$ = Crank angle at which fuel is injected into the combustion chamber.

4.4.5.2 Heat release rate

The rate of heat release at each crank angle was determined by the following formula derived from the first law of thermodynamics: [155-156]

$$\frac{dU}{dt} = \dot{Q} - \dot{W} \tag{4.8}$$

$$\text{m } C_v \frac{dT}{dt} = \dot{Q} - P \frac{dv}{dt} \tag{4.9}$$

where, $\dot{Q}$= the combination of the heat release rate and the heat transfer rate across the cylinder wall,

$\dot{W}$ = the rate of work done by the system due to the system boundary displacement.

U = Internal energy

To simplify Equation (4.8) the ideal gas assumption can be used.

$$pV = mRT \tag{4.10}$$

Where p = Cylinder pressure in bar.

V= Volume of the cylinder (m^3)

m = mass of gas (kg)

R = Gas constant

T = Absolute temperature

Eqn. (4.9) can be differentiated (assuming constant mass)

$$\frac{dT}{dt} = \frac{1}{mR}\left[P\frac{dV}{dt} + V\frac{dP}{dt}\right] \tag{4.11}$$

After combining eqns. (4.9) and (4.11), the heat release equation becomes

$$\dot{Q} = \left[\frac{Cv}{R} + 1\right] p\frac{dV}{dt} + \frac{Cv}{R} V\frac{dp}{dt} \tag{4.12}$$

After replacing time (t) with the crank angle (θ), the equation becomes

$$\dot{Q} = \frac{\lambda}{\lambda-1} p\frac{dV}{d\theta} + \frac{1}{\lambda-1} V\frac{dp}{d\theta} + Q_w \tag{4.13}$$

where, λ is the ratio of the specific heats (C_p/C_v), p is the cylinder gas pressure, V is the instantaneous volume of the cylinder and Q_w is heat transfer rate across the cylinder wall. The instantaneous cylinder volume can be obtained from the engine geometry and crank angle values.

4.4.5.3 Combustion duration

The crank angle duration from 10% mass fraction burned to 90% mass fractions burned, has been taken as the combustion duration.

4.4.5.4 Rate of pressure rise (ROPR)

The rate of pressure rise defines the load that is imposed by the combustion process on the cylinder head and block, and to a large extent, determines the structural design [157]. Also, the rate of pressure rise is indicative of the noisy operation of the engine. The rate of pressure rise with respect to the crank angle is derived from the following expression: [155].

$$\text{ROPR} = \frac{dp}{d\theta} \tag{4.14}$$

4.4.5.5 Mass fractions burned

Assuming that the pressure rise Δp_c is proportional to the heat added to the in-cylinder medium during the crank angle interval, the mass fraction burned at the end of the considered i-th interval may be calculated as [155].

$$\text{MFB} = \frac{m_b\,(i)}{m_b\,(total)} = \frac{\sum_0^i \Delta p_c}{\sum_0^N \Delta p_c} \tag{4.15}$$

where 0 denotes the start of combustion, N – end of combustion (N is the total number of crank intervals).

4.5 Exhaust emissions measurement methods

4.5.1 NDIR principle for HC, CO and CO_2 emissions measurement

A non-dispersive infrared (IR) measurement was used to determine the concentration of the gaseous pollutants like HC, CO and CO_2 as illustrated in Fig. 4.8. The general working principle of the analyser is discussed in this paragraph. The absorption of IR radiation occurs in narrow-wavelength bands, with each gas exhibiting its own peculiar characteristics. Two infrared sources are provided, as shown, with a chopper to impose an AC signal, which is handled more easily by subsequent electronic detection circuits.

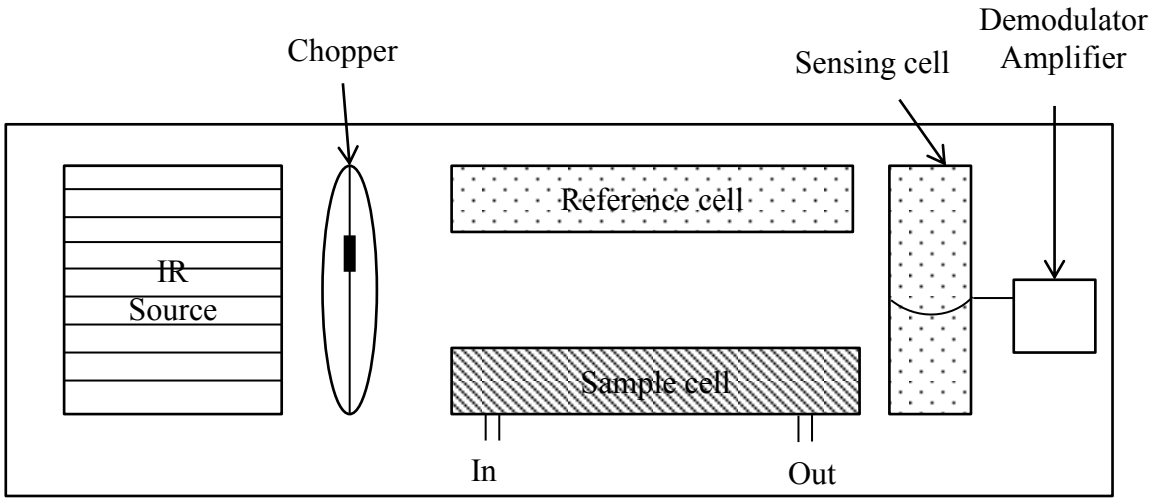

Fig. 4.8 Schematic layout of NDIR principle

Filters may be placed in the path of the sources, so that only the absorption wave length band for the particular gas to be studied is investigated. Two cells are exposed to the IR radiation: (a) a reference cell containing an inert gas (usually nitrogen) and (b) a cell which admits the passage of the sample gas containing the pollutant to be investigated. No IR absorption occurs in the reference cell, while the absorption in the sample cell is proportional to the concentration of the component of interest. Beyond the reference and sample cells there are two detector chambers which absorb the IR radiation transmitted. These chambers are sealed, so that the absorption of the radiation causes the temperature of the gas inside to rise. The two chambers are separated by a thin diaphragm. Because, more radiation is transmitted through the reference cell, there will be a greater temperature rise in the reference detector chamber

than in the sample detector. As a result, a pressure differential is created, which causes the movement of the diaphragm; this can be detected with a capacitance pickup. The resulting signal is amplified and transmitted to an appropriate readout device. The infrared absorption device may be used for continuous monitoring of the combustion products.

4.5.2 Electrochemical principle for the NO measurement

The specific detection of nitric oxide (NO) by the electrochemical sensors is based on a general principle used in electrochemistry. In brief, the NO diffuses across a gas-permeable membrane, and a thin film of electrolyte covering the probe. The NO species is oxidized on the sensor which consists of a working and Ag/AgCl reference electrode pair. A potential (approx 900 mV) is applied to the working/measuring electrode, relative to a reference electrode, and the resulting small redox current due to the oxidation of NO according to the following reaction, is measured by an amplifier system and recorder:

$$NO + 4OH^- \longrightarrow NO_3^- + 2H_2O + 3e^- \quad (4.16)$$

4.5.3 AVL Digas 444 Analyser

The exhaust gas sample was analysed by a 5 Gas analyzer (Make: AVL India, Model: 444) fitted with a DiGas sampler, conforming to ARAI certification: ARAI/TA(4G-RV)/AVL/DiGas 444/0910-12. The principle for measuring the CO, HC, CO_2 emissions was the NDIR, and for the NO and O_2, it was electrochemical. The CO, CO_2, O_2 emissions were measured in volume percentage, while the total unburnt hydrocarbon TUHC was measured in ppm (vol.) of n-hexane equivalent, and the NO emission was measured in ppm (vol.) during each run of the engine operation. The photographic view of the AVL Digas 444 analyzer is shown in Fig. 4.9. The complete technical specification of the AVL Digas 444 analyzer is given in Annexure 5.

The analyzer was interfaced through its RS 232C communication bus to an in-house developed emission data acquisition platform, which recorded the emissions over a span of 120 s in 20 s consecutive intervals, which was greater than the instrument response time of 15 s, for each case of the engine operation. The exhaust gases were tapped from a T joint between the exhaust gas outlet and the smoke meter tapping point. A fine filter to remove the advected particulates and a condensate trap were incorporated, after the main exhaust gas cooler so that the exhaust inlet temperature to the analyzer was maintained $\leq 40^oC$ as per the instruction manual. Stray condensates, if any, were tackled by the condensate separator

inbuilt in the analyzer, which was flushed before every case of data recording. Leak check, HC residue test, zero adjustment and condensate purging of the analyzer, were carried out before each observation. The CO, CO_2 and HC emissions were measured by the Non-Dispersive-Infrared (NDIR) detection principle, while the O_2 and NO emissions were measured by the pre-calibrated electrochemical sensors in the analyzer. It is to be noted that, the analyzer was calibrated with the recommended calibration gas mixture, before the start of the entire range of experimentation.

Fig. 4.9 Photographic view of the AVL Digas 444 analyzer

The detector in the gas analyser was made up of Selenium photocell with a diameter of 45 mm. Its maximum sensitivity in light was within the frequency range of 550-570 nm. Below 430 nm and above 680 nm, the sensitivity of the instrument was less than 4% related to the maximum sensitivity. Emission tests were carried out by inserting a probe into the engine's exhaust tube by opening the ball valve. Before taking the emission test, a leak check was conducted in the digital gas analyser, to discharge the residual gases by closing the probe's nozzle manually.

4.6 Conversion of emission values into g/kWh

It is general practice to express the emission data on a "brake specific" basis, except for the smoke opacity. The brake specific emissions are the mass flow rates of the individual pollutant divided by the engine power. The formulae used to convert the emissions from ppm and % vol into g/kWh are given below:

HC emissions in g/kWh

HC (g/kWh) = [{(mf+ma)/(29*1000)} * HC (in ppm)*13/BP] (4.17)

CO emissions in g/kWh

CO (g/kWh) = [{(mf+ma)/29)*10} * CO (in %vol)*28/BP] (4.18)

NO emissions in g/kWh

NO (g/kWh) = [{(mf+ma)/(29*1000)} * NO (in ppm)*32.4/BP] (4.19)

4.7 Gas analyser calibration procedure

4.7.1 Pre-Test Calibration

The gas analyser is calibrated prior to the emission test with calibration gases certified to ±2% accuracy as per the EPA test methods in 40 CFR 60 and the ISO 3930, 1976 test method. Three calibration gases (zero, mid and high) for CO, NO, and NO_2 may be used. The purified ambient air may be used as the zero gas. The mid-level gas concentration is 40% to 60% of the high range calibration gas. A high-level gas concentration of the high range calibration gas shall not be higher than 125% of the expected concentration nor less than 90% of the expected concentration. The high level gas is equal to the calibration span. The analyser calibration error shall be no more than ±5% of the calibration span value for the mid and high range calibration gases, or 5 ppm, whichever is less restrictive.

The calibration error shall be calculated as follows:

$$\% \text{ Difference} = \frac{\text{Analyzer Response} - \text{Gas Concentration}}{\text{Calibration Span}} \times 100 \quad (4.20)$$

For the zero gas, the calibration error shall be no more than 10 ppm:

Difference in ppm = Analyser response – Zero gas concentration

The steps involved for calibration are as follows:

Step 1: Allow the analyser to purge the calibration gases prior to beginning the emissions test.

Step 2: A test shall consist of three runs, with each run at least 20 minutes in length.

Step 3: Record the readings for HC, CO and NO, at 2 minute intervals during the 20 minute run.

4.7.2 Post-Test calibration

After a maximum of three valid 20-minute emission tests, conduct a post-test calibration as follows for the HC, CO and NO calibration gases:

Step 1: Allow the analyser to purge the gas sample until a stable zero reading is observed. Record the zero reading.

Step 2: Introduce the high range calibration gas to the analyser and allow it to reach a stable reading. Record the analyser reading.

Step 3: Introduce the mid-range calibration gas into the analyser and allow it to reach a stable reading. Record the analyser reading.

Calculate the difference with the pre-test calibration value. If the difference is greater than ±5% or 5 ppm, whichever is less restrictive, the emission test runs are invalid, and must be repeated.

$$\% \text{ Difference} = \frac{(\text{Post}-\text{Test Reading}) - (\text{Pre}-\text{Test Reading})}{\text{Pre}-\text{Test Reading}} \text{ x } 100 \qquad (4.21)$$

For the zero gas, the post-test calibration error shall be no more than 10 ppm.

4.8 Smoke measurement

The smoke emission was measured by a partial-flow sampling AVL (Austria) 437 diesel smoke meter, certified by ARAI, Pune, India, as per ARAI/TA(SM-RV)/AVL/437/1011-02. A photographic view of the AVL 437C diesel smoke meter is shown in Fig. 4.10.

Fig. 4.10 Photographic view of the AVL 437C diesel smoke meter

The operating principle is based on the attenuation of a light beam caused by the exhaust gases in a measuring chamber of defined measuring length, and nonreflecting surface filled homogeneously with the exhaust gas. The loss of light intensity between the light source and a receiver is measured and reported in % opacity, the calculation being based on the Beer-

Lambert law. The absorption coefficient “k” was also reported by the smoke meter, in accordance with the ECE-R24/ISO 3173. Condensation inside the instrument is avoided, as the measuring chamber is thermostatically heat controlled at 70 ± 5 ^{o}C. To ensure accuracy and repeatability observations were recorded, at each case of the engine operation, for a span of 120 s at intervals of 20 s, which was greater than the instrument measurement value resolution time of 10 s. The complete technical specification of the AVL 437C diesel smoke meter is given in Annexure 6.

4.9 Experimental methodology

4.9.1 Engine experimentation with diesel and JME

Initially, the engine was operated with diesel for obtaining the reference data of the combustion, performance and emission parameters. The engine was tested at 25%, 50%, 75% and 100% loads. For each load condition, the engine was run for at least 3 min after which data were recorded. Further, the engine was tested with the JME (100% Jatropha methyl ester).

4.9.2 Engine experimentation with the JME-WPO emulsions

After conducting experiments with diesel and JME to get the relevant data for combustion, performance and emission parameters, the engine was run with the different JME-WPO emulsions. Finally, the engine was allowed to run with diesel to remove the traces of the emulsion in the fuel line and fuel filter. The results were compared with diesel and the JME operations. The exhaust gas analyser and diesel smoke meter were switched on before starting of the experiments in order to stabilize them before starting the measurements. All the instruments were periodically calibrated. Initially the engine was run on diesel, JME and JME-WPO emulsions at a given compression ratio of 17.5 and nozzle opening pressure of 200 bar which is set by the manufacturer by maintaining a rated speed of 1500 rpm.

4.9.3 Investigations with acid treated JOE15 emulsion

Further, from the comparative analysis on the performance, combustion and emission characteristics of all the JME-WPO emulsions, and by consideration of droplet distribution and emulsion stability, an optimum emulsion was selected for further investigation. The optimum emulsion consisted of JME 81%, WPO 15% and a mixed surfactant 4% by volume. This optimum emulsion was treated for removal of its acidity and this acid treated emulsion was used for further study. The process involved in the acid treatment of JOE15 emulsion is described in Chapter 3. The combustion, performance and emission parameters were evaluated in the diesel engine fueled with the acid treated JOE15 emulsion. The results were compared with those of diesel and JME operations.

4.9.4 Design of experiments

Before the start of experimental investigation, it needs a proper planning to obtain adequate, relevant and reliable data so that one can infer the science behind the observed phenomenon.

A Design of Experiment (DOE) is a systematic approach for investigation of a system or process. A series of structured tests are designed in which planned changes are made to the input variables of a process or system. The effects of these changes on a predefined output are then assessed. The DOE is important as a formal way of maximizing information gained, while minimizing the resources required. It allows a judgment on the significance to the output of input variables acting alone, as well input variables acting in combination with one another.

The DOE starts with identifying the input variables and the response (output) that is to be measured. For each input variable, a number of levels are defined that spans over the range for which the effect of that variable is desired to be known. An experimental plan is produced which tells the experimenter where to set each test parameter for each run of the test. The response is then measured for each run. It is very important to get the most information from each experiment performed. Well-designed experiments can produce significantly more information and often require fewer runs than what haphazard or unplanned experiments do require. In addition, a well-designed experiment also ensures significance of the effects that had been identified in the experiment at hand.

Engine experiments were conducted only with the ATJOE15 emulsion, at three different compression ratios (16.5, 17.5 and 18.5), and for each compression ratio, three nozzle opening pressures (200, 220, and 240 bar) and three injection timings (21.5, 23 and 24.5 ^{o}bTDC) were selected and conducted as per the full factorial design ($3^3 = 27$). Table 4.1 gives the full factorial design followed during the conduct of experiments.

Table 4.1 Full factorial design for experiments

Trial No.	Compression ratio	Injection timing	Nozzle opening pressure
1	16.5	21.5	200
2	16.5	21.5	220
3	16.5	21.5	240
4	16.5	23	200
5	16.5	23	220
6	16.5	23	240
7	16.5	24.5	200
8	16.5	24.5	220
9	16.5	24.5	240
10	17.5	21.5	200
11	17.5	21.5	220
12	17.5	21.5	240
13	17.5	23	200
14	17.5	23	220
15	17.5	23	240
16	17.5	24.5	200
17	17.5	24.5	220
18	17.5	24.5	240
19	18.5	21.5	200
20	18.5	21.5	220
21	18.5	21.5	240
22	18.5	23	200
23	18.5	23	220
24	18.5	23	240
25	18.5	24.5	200
26	18.5	24.5	220
27	18.5	24.5	240

4.9.4.1 Variation of compression ratio

The ATJOE15 emulsion was tested as three different compression ratios of diesel engine. There are several methods to change the compression ratio in a CI engine, they are as follows: [158-162]

a) Variation of combustion chamber volume
b) Moving the cylinder head
c) Variation of piston skirt height
d) Modification of the connecting rod geometry (by means of intermediate member)
e) Variation of effective stroke length (by moving the crankpin within the crankshaft)
f) Moving the crankshaft axis

In the present investigation, compression ratio was changed by changing the clearance volume by inserting gaskets of different thicknesses between the cylinder and cylinder head. Figures 4.11(a), 4.11(b) and 4.11(c) show the photographic views of changing the compression ratio and gasket.

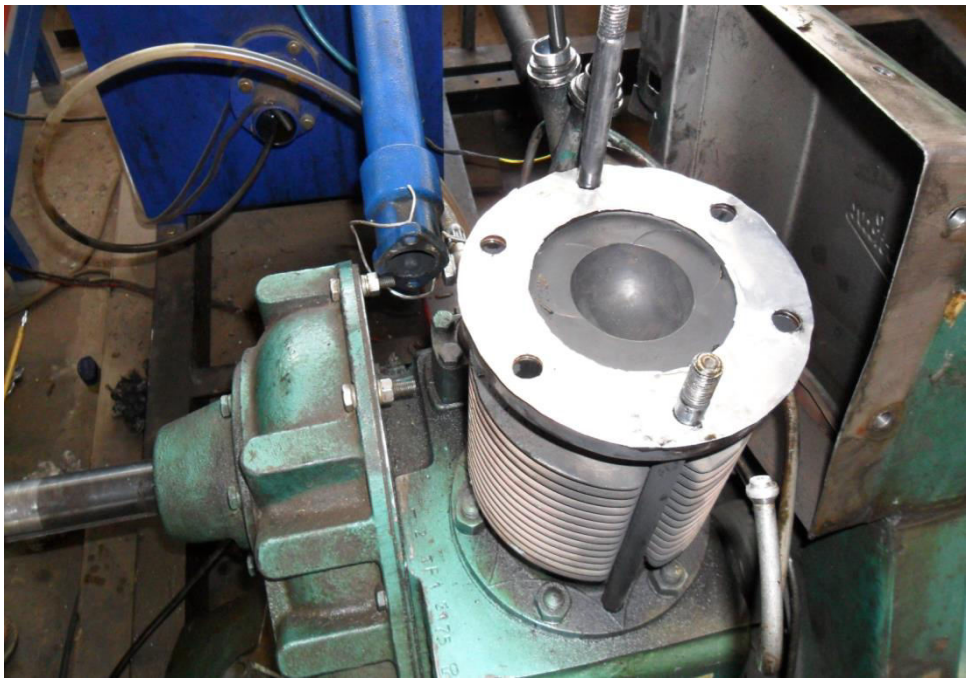

Fig. 4.11(a) Lower thickness gasket fitted with cylinder block

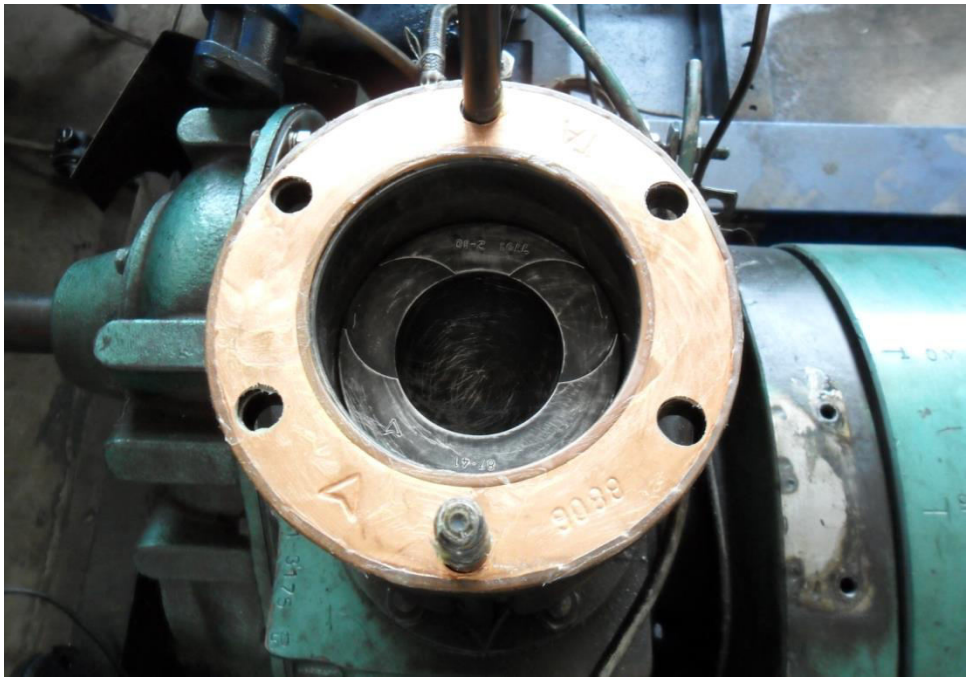

Fig. 4.11(b) Standard gasket fitted with cylinder block

Fig. 4.11(c) Cylinder head gasket

Compression ratios below 16.5 led to a poor power output, and ratios above 18.5 were not possible, due to engine structural constraints. For all settings, the emission values were recorded thrice and the mean of these was taken for comparison.

The steps involved in the compression ratio calculation are as follows:

Compression ratio = $\frac{\text{Maximum cylinder volume } (V_s+V_c)}{\text{Clearance volume } (V_c)}$

Maximum cylinder volume = Swept volume (V_s) + Clearance volume (V_c)

$V_s = \frac{\pi d^2}{4} \times l$

Where, d = bore = 8.75 cm, l = stroke = 11 cm

For standard compression ratio,

$CR = 17.5 = \frac{V_s+V_c}{V_c}$

$17.5 = \frac{V_s}{V_c} + 1$

$17.5 - 1 = \frac{V_s}{V_c}$

$V_c = \frac{V_s}{16.5} = \frac{661.45}{16.5} = 40.08\ cm^3$

Gasket volume = 7.21 cm^3 (d = 8.75 cm, t = 0.12 cm)

For CR = 18.5, $Vc = \frac{Vs}{17.5} = \frac{661.45}{17.5} = 37.79\ cm^3$

Clearance volume excluding gasket volume + Gasket volume = 37.79

32.87 + Gasket volume = 37.79

Gasket volume required for CR = 18.5 = 4.92 cm^3

Gasket thickness required = 0.08 cm

Similarly gasket volume and thickness required for CR = 16.5 was calculated.

The calculated gasket volume and thickness corresponding to the different compression ratios are given in Table 4.2.

Table 4.2 Gasket volume and thickness required for different compression ratios

Compression ratio	Gasket volume (cm^3)	Gasket thickness (cm)
16.5	9.8	0.16
17.5	7.21	0.12
18.5	4.92	0.08

4.9.4.2 Variation of injection timing

In order to change the fuel injection timings, it is required to adjust the fuel injection pump settings. By varying the number of shims under the fuel injection pump fuel injection timing was changed. To advance the fuel injection timing, the shims under the pump were removed and to retard additional shims were introduced under fuel injection pump. At standard injection timing, the number of shims placed under the pump was three. The thickness of the each shim is 0.3 mm. By removing one shim, about 1.5 ^{o}CA injection timing was advanced and by introducing additional shim will retard the timing by 1.5 ^{o}CA. Figure 4.12 shows the photographic view of the fuel pump with shim. Figure 4.13 shows the photographic view of the shim.

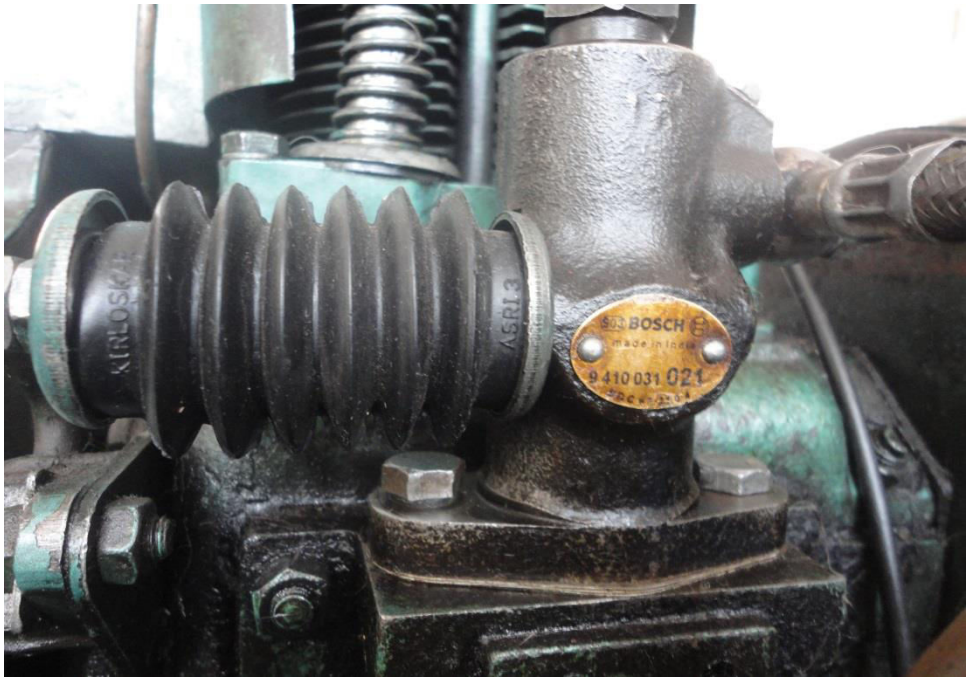

Fig. 4.12 Photographic view of the fuel pump with shim

Fig. 4.13 Photographic view of the shim

The experiments were conducted with one advanced injection timing (24.5 ^{o}CA bTDC) and one retarded injection timing (21.5 ^{o}CA bTDC) along with standard injection timing (23 ^{o}CA bTDC). Since, more retardation will leads to increase the smoke emission and more advancement will leads to increase the NO emission [163], our experiments were limited. The combustion, performance and emission parameters were studied in the diesel engine at all three injection timings, for variable compression ratios (16.5, 17.5 and 18.5) and for variable nozzle opening pressures (200, 220 and 240 bar). The study was conducted for entire load range (from no load to full load). After every set of experiments, engine was operated at standard conditions with diesel to ensure steady conditions.

4.9.4.3 Variation of nozzle opening pressure

The fuel injection strategy is an important parameter in diesel engines to optimize the combustion, performance and tailpipe emissions. An increase of fuel nozzle opening pressure was required to enhance the fuel atomization at the nozzle outlet, resulting in more distributed vapor phase, which improves mixing [164]. The nozzle opening pressure was varied by testing the injector assembly in a nozzle pressure tester, where, the spring tension of the injector needle with setting screw was varied to get different fuel nozzle opening pressures. Figure 4.14 shows a photographic view of the nozzle tester assembly. Figure 4.15 shows the dismantled view of the fuel injector.

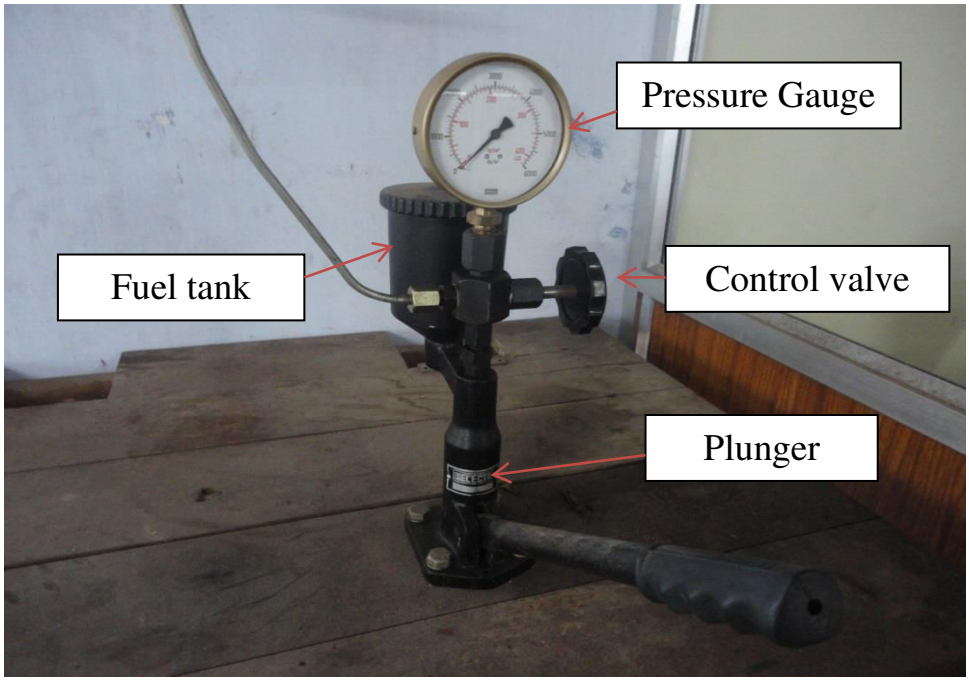

Fig. 4.14 Photographic view of the nozzle pressure tester assembly

Fig. 4.15 Dismantled view of the fuel injector

At standard injection timing (23 ^{o}CA bTDC), the nozzle opening pressure was varied from 200 bar to 220 bar and 240 bar and combustion, performance, and emissions characteristics were recorded from 0% to 100% load in steps of 25% load at a constant speed of 1500 rpm. The experiment was repeated for different injection timings of 21.5 ^{o}CA bTDC, 24.5 ^{o}CA bTDC and different compression ratios of 16.5, 17.5 and 18.5 for ATJOE15 fuel.

4.10 Uncertainty analysis

Uncertainty is a measure of the 'goodness' of a result. Without such a measure, it is impossible to judge the fitness of the value. An uncertainty or error analysis is necessary to establish the bounds on the accuracy of the estimated parameters. The evaluations of some unknown uncertainties from known physical quantities were obtained, using the following general equation [165].

$$\frac{U_Y}{Y} = \left[\sum_{i=1}^{n}\left(\frac{1}{Y}\frac{\partial Y}{\partial xi}\,U_{xi}\right)^2\right]^{1/2} \tag{4.22}$$

In the equation cited, Y is the physical parameter that is dependent on the parameters, xi. The symbol U_Y denotes the uncertainty in Y. As a result, the maximum uncertainty of the experiment obtained was ±2.1%. Table 4.3 gives the instruments used in the present study and their uncertainties. The sample calculations involved in determining the uncertainty of the crank angle encoder are given in Annexure 7.

Table 4.3 Range, accuracy and uncertainty of the instruments

S.No	Instrument	Range	Accuracy	Uncertainty
1.	Load indicator	250-6000W	±10W	0.2
2.	Temperature indicator	0-900	±1 ^{o}C	0.1
3.	Burette	1-30cc	±0.2 cc	1.0
4.	Speed sensor	0-10,000 rpm	±10rpm	0.1
5.	Exhaust gas analyser	NO-0-5000 ppm	±50ppm	1
		HC-0-20000 ppm	±10ppm	0.5
		CO-0-10%	0.03%	1
6.	Smoke meter	0-100%	±1 %	1
7.	Pressure transducer	0-110bar	±0.1bar	0.15
8.	Crank angle encoder	0-720	±1^{o}	0.3298

4.11 Endurance tests

4.11.1 Short term endurance test

The main objective of the endurance test was to evaluate the wear characteristics of engine components and changes in lubrication oil properties of test engine fueled with the ATJOE15 emulsion. Short term endurance test was conducted with the ATJOE15 emulsion as per

IS 10000 Part V – 1980 method for 100 hrs. Before the start of the durability test, the existing fuel injection pump, fuel injector, fuel filter, oil filter were replaced with new one as recommended by the engine manufacturer. Before fitting in the engine, the fuel injector and fuel injection pump were dismantled completely and photographs were taken in order to compare the wear and deposits on them after the durability test. The used lubricating oil was drained completely and fresh lubricating oil of SAE 20-40 grade was filled in the oil sump up to its full capacity. The engine cylinder head was dismantled and the carbon deposits on the cylinder head, piston crown were completely cleaned using methanol. The cylinder head gasket was also changed with new one and the cylinder head was fitted in the engine block. Once the engine was reassembled, it was allowed to run-in for 12 hours in the manner recommended by the manufacturer. This test was carried out to take care of any misalignments occurring during dismantling and re-assembling of the engine.

4.11.1.1 Preliminary run for constant speed engine

The purpose of preliminary run on engine is to ensure that, the engine should run trouble free, by operating both the engines for their running-in period. Under the preliminary run, constant speed engine is subjected to a preliminary run of 49 hours at the rated speed under the operating temperature specified by the manufacturer, in non-stop cycles of seven hours each, given in Table 4.4. During the preliminary run, attention was paid to engine vibration and quietness. It was ensured that the temperature of the lubricating oil reached within 5^{o}C before starting the next cycle.

Table 4.4 Preliminary run pattern of a constant speed engine

Load (Percent of rated load)	Running time (hours)
25	1.5
50	2
75	1.5
100	2

Figure 4.16 shows the photographic view of the dismantled engine before the start of endurance test.

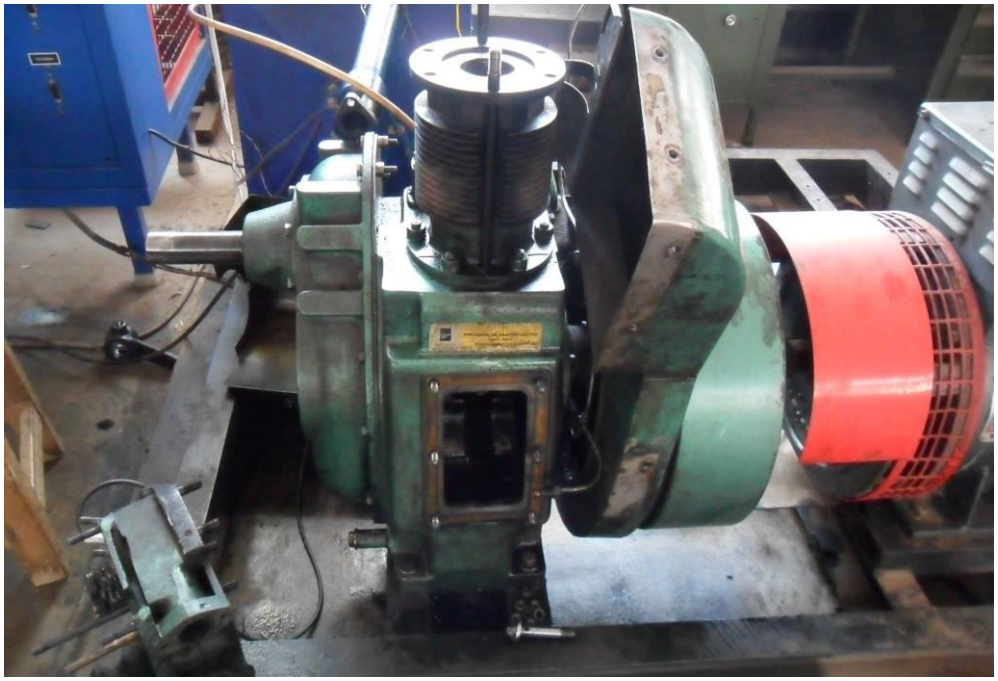

Fig. 4.16 Photographic view of the dismantled engine before endurance test

4.11.1.2 Long term test for constant speed engine

Then the engine is subjected to undergo the long term endurance test (load test) recommended by IS standard 10000 for 32 cycles (each of 16 hours continuous running) at rated speed. But, due to the limited availability of WPO and biodiesel fuels, it was proposed to conduct the short term endurance test comprising 3 cycles only. The test cycle followed is specified in the Table 4.5.

Table 4.5 Test cycle for long-term endurance test

Load (Percent of rated load)	Running time (hours)
100	4
50	4
100	1
No load	0.5
100	3
50	3.5

In this investigation, the short term endurance test was conducted using the ATJOE15 emulsion, and at the end of each 16-hour cycle, the engine was stopped and necessary

servicing, and minor adjustments were carried out in accordance with the manufacturer's schedule. Before starting the next cycle, it was ensured that the temperature of the engine sump oil had reached within 5K of the room temperature. The lubricating oil samples were collected from the engines after every 30 hours (from preliminary run onwards) for conducting various tribological studies. In the entire range of engine operation spread around 100 hours, there was no major breakdown noticed. After completion of the short-term endurance test, the engine was completely disassembled and the deposit formations on cylinder head, piston top, and injector tip were investigated.

4.12 Lubrication oil analysis

The lubrication oil used in the diesel engine picks up the wear debris of various metals depending on the origin. The quantitative evaluation of wear particles present in oil gives the magnitude of engine component deterioration and while qualitative analysis indicates its origin, i.e., wearing component. This ultimately provides adequate information about the components that are deteriorated and the incipient failure of the machine. A careful observation at the literature reveals that, the various contaminant metals present in lube oil might have various possible sources in the engines.

4.12.1 Determination of ash content

The lubricating oil samples were taken in a silicon crucible and kept in the furnace at 450°C for 4 hours and then 600°C for 2 hours to produce ash. The residual ash contains the wear debris of metal primarily. By weighing the crucible before and after the test, the weight percentage of ash was determined.

4.12.2 Atomic Absorption Spectroscopy (AAS) test

The AAS works on the principle of absorption interaction, where atoms in the vapor state absorb radiation at a certain wave length that are well defined and show the characteristics of a particular atomic element. In this process, the source of radiation projects a beam of a specific wavelength through a pure flame (air-acetylene) on to a sensor and the amount of radiation arriving at the photo sensor is recorded. The fluid sample is introduced into the flame and vaporized. The amount of radiation arriving at the photo sensor is reduced in proportion to the quantity of the specific element present in the sample. Hence, various elements such as Fe, Cu, Zn, Cr, Mg, Co, and Pb were analyzed by AAS and the results are discussed in Chapter 5.

This AAS test was conducted to evaluate the concentration of various metals present in the lubricating oil samples from the ATJOE15 emulsion fueled CI engine. This gave a fair idea about the wear of different parts, material compatibility of the new fuel with the existing engines. In the present study, since many sliding components were involved, it was anticipated that the wear debris originating from different metallic parts appeared in the lubricating oil.

The procedure followed is explained in the following steps:

a) Approximately 10 grams of oil sample was weighed in the silica crucible and burnt at 450°C for 4 hours and at 650°C for 2 hours.
b) The ash was dissolved in concentrated HCl acid.
c) The mixture was diluted with distilled water to make 100 ml solution.
d) Standard solutions of various metals (concentrations ranging from 5 ppm to 20 ppm) were prepared.

CHAPTER 5

RESULTS AND DISCUSSION

5.1 Parametric studies on the combustion, performance and emissions with JME-WPO emulsions

5.1.1 General

This chapter presents the results and discussion on the experimental investigations carried out in a 4.4 kW, single cylinder, four stroke, air cooled, direct injection (DI) diesel engine running on different JME-WPO emulsions. The WPO percentage was varied from 5% to 15% at regular intervals of 5% in the emulsions on a volume basis. The notations followed for the emulsions can also be referred to in Table 3.8, which is given in Chapter 3. In this investigation, the results associated with the JME-WPO emulsions containing 5% and 10% WPO in them, did not show much variation. Therefore, only the results associated with all the JME-WPO emulsions which contain 15% WPO in them are discussed in this chapter, for better understanding and clarity. The relevant results are published in reputed journals which are given in Annexure.

Further, from the comparative analysis on the performance, combustion and emission characteristics, consideration of the droplet distribution, emulsion stability and droplet size, an optimum emulsion was selected for further investigation. This optimum emulsion was chosen for the removal of its acidity, and this acid treated emulsion (ATJOE15) was used for further study. A full factorial (L27) design was prepared for conducting the experiments, with engine modifications such as varying compression ratio, injection timing and nozzle opening pressure, which is already given in Chapter 4. Further, the results obtained for the combustion and emission characteristics of an engine fueled with the ATJOE15 emulsion, were validated with the help of two zone modeling. This chapter also presents the results obtained for the short term endurance test, conducted on the same engine with the ATJOE15 emulsion.

5.1.2 Combustion parameters

5.1.2.1 Pressure-crank angle diagram

The pressure crank angle diagram at full load for different emulsions with 15% WPO, obtained with the help of six different surfactants, is depicted in Fig. 5.1.1. In diesel engines, the maximum cylinder pressure depends on the combustion rate in the initial stages, which is influenced by the fuel involved in the uncontrolled combustion phase. This premixed

combustion phase is governed by the delay period, spray envelop, and the air fuel mixture preparation during the delay period [49].

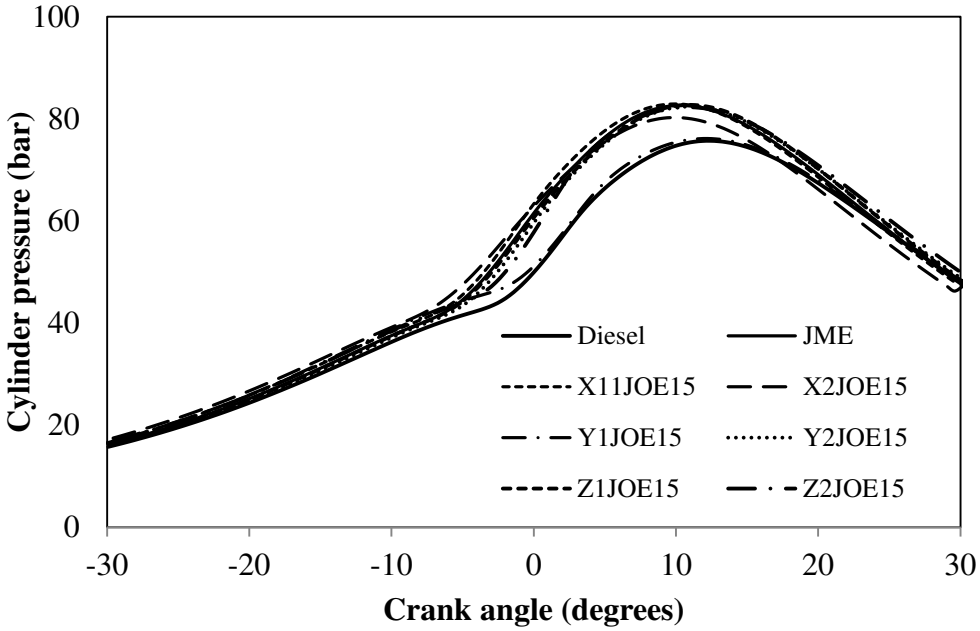

Fig. 5.1.1 Pressure-Crank angle diagram at full load for different emulsions with 15% WPO

The start of fuel injection (SOI) is set at 23 ^{o}CA bTDC. The change in the slope of the pressure-crank angle curve gives the start of combustion approximately [155]. With 15% WPO in the emulsions, the start of ignition for all the emulsions are found to be earlier, which is in the range between 0.5 ^{o}CA and 2.9 ^{o}CA, than that of diesel at full load. It is also found to be earlier by 0.3 ^{o}CA in the case of the X1JOE15 emulsion, whereas other JME-WPO emulsions exhibit a later start of combustion in the range of 0.3 to 2 ^{o}CA, compared to that of JME operation. The JME-WPO emulsions with 15% WPO in them resulted in a higher maximum cylinder pressure in comparison with diesel at full load. This may be due to the higher BSFC, cetane number, boiling point, oxygen content, and advance in the start of the injection (SOI) timing. In this regard, similar reasons have been reported by Ozsezen et al. [23], using biodiesel from waste palm oil methyl ester (WPOME) and canola oil methyl ester (COME).

5.1.2.2 Ignition delay

The variations of ignition delay with different loads for all the emulsions investigated in this study, which contain 15% WPO in them, are shown in Fig. 5.1.2. A group of parameters, such as the fuel type, fuel quality, air-fuel ratio, engine speed, quality of fuel atomization,

intake air temperature, and pressure, influence the ignition delay [166]. It is apparent from the figure that, the ignition delay is found to decrease with an increase in the engine load.

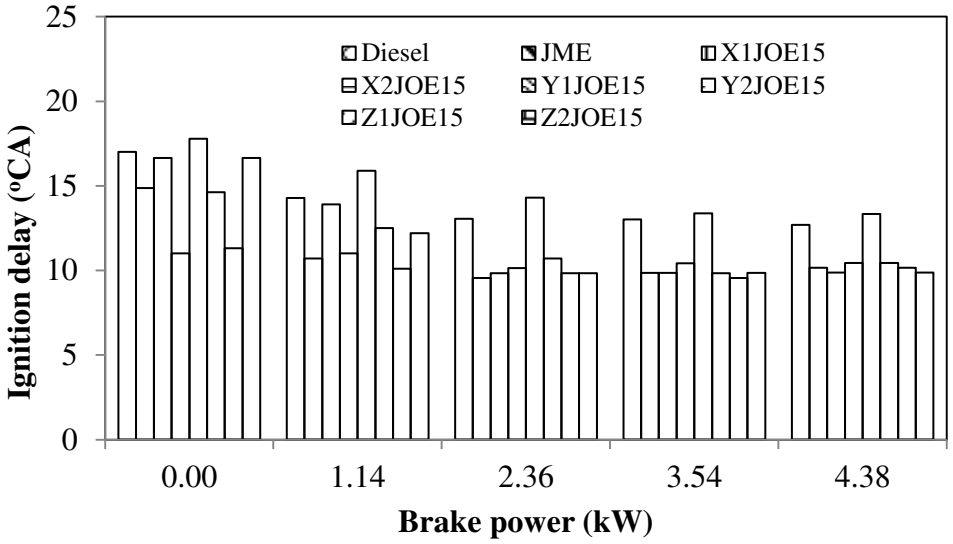

Fig. 5.1.2 Variation of ignition delay with brake power for different emulsions with 15% WPO

This reduction might be the result of higher combustion chamber wall temperature at the time of injection, and reduced exhaust gas dilution. A similar result was reported by Canacki [107], when he carried out experiments with biodiesel fuel in a single cylinder, four stroke, DI diesel engine. It can be observed from the figure that, there is a reduction in the ignition delay for all the emulsions, which contain 15% WPO in them; this is attributed to their quick evaporation rate, improved ignition properties, and enhanced surface area/volume ratio characteristics. A similar result was also obtained by Sadiq basha and Anand [150], in their investigation with nano additive blended biodiesel emulsion fuel in a single cylinder, four stroke, DI diesel engine. For the WPO percentage of 15% in the emulsion, the ignition delay decreases by about 2.3 ^{o}CA to 2.7 ^{o}CA compared to that of diesel, while it is shorter in the range of 0.1 ^{o}CA to 0.3 ^{o}CA for the Z1JOE15, X1JOE15 and Z2JOE15 emulsions, and in the remaining cases, the ignition delay is found to be longer by about 0.1 to 3.1 ^{o}CA, compared to that of the JME operation.

5.1.2.3 Heat release rate

The heat release rate is one of the parameters of a fuel in a CI engine, which is helpful to predict the emission behavior. The maximum heat release depends on the delay period, mixture formation and combustion rate. Figure 5.1.3 illustrates the heat release patterns at full

load, with respect to the crank angle of the engine fueled with different JME-WPO emulsions, which contain 15% WPO in them. The occurrences of maximum heat release rate for the emulsions which contain 15% WPO, are on an average shifted by about 4.4 ^{o}CA at full load. The intensity of the premixed combustion phase for diesel is found to be the highest, whereas, it is lower in the case of JME and the JME-WPO emulsions. The deviation in the maximum heat release rate between the JME operation and all the JME-WPO emulsions is in the range between-2.35 J/^{o}CA to 5.3 J/^{o}CA.

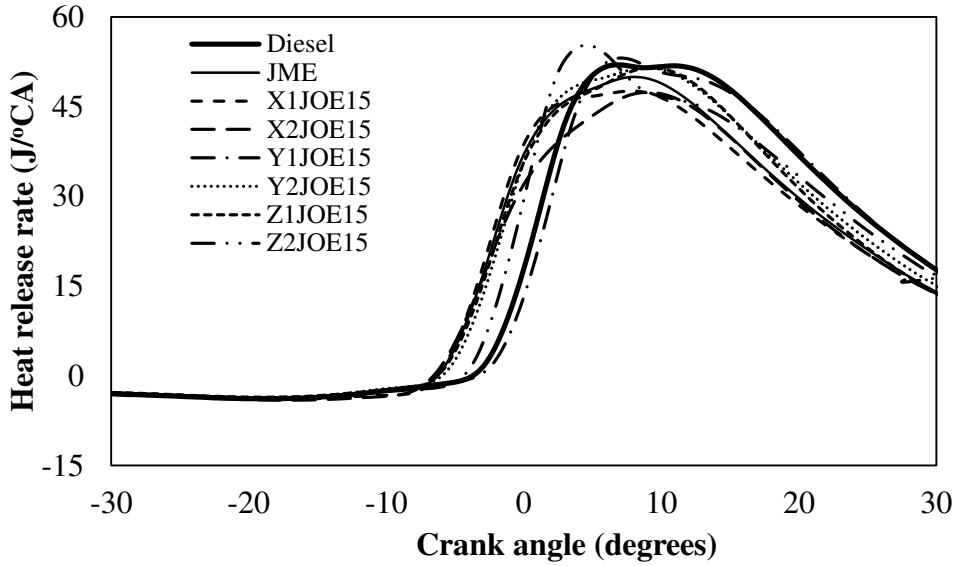

Fig. 5.1.3 Variation of heat release rate with crank angle at full load for 15% WPO emulsions

It is also seen that the quantity of diffusive combustion is found to be shorter for JME and the 15% WPO emulsions in comparison with diesel operation, due to their faster burning characteristics. The oxygen present in JME and the quick evaporating nature of the JME-WPO emulsions are the causes for the faster burning process.

5.1.2.4 Maximum cylinder pressure

Figure 5.1.4 depicts the variation of maximum cylinder pressure with brake power for all the fuels tested in this study. The maximum cylinder pressure depends on the amount of fuel taking part in the uncontrolled phase of combustion. It is seen that the peak cylinder pressure is increased with an increase in the engine load as expected. At no load and 50% load conditions, the peak cylinder pressures of the emulsions with 15% WPO are almost comparable with those of the JME operation.

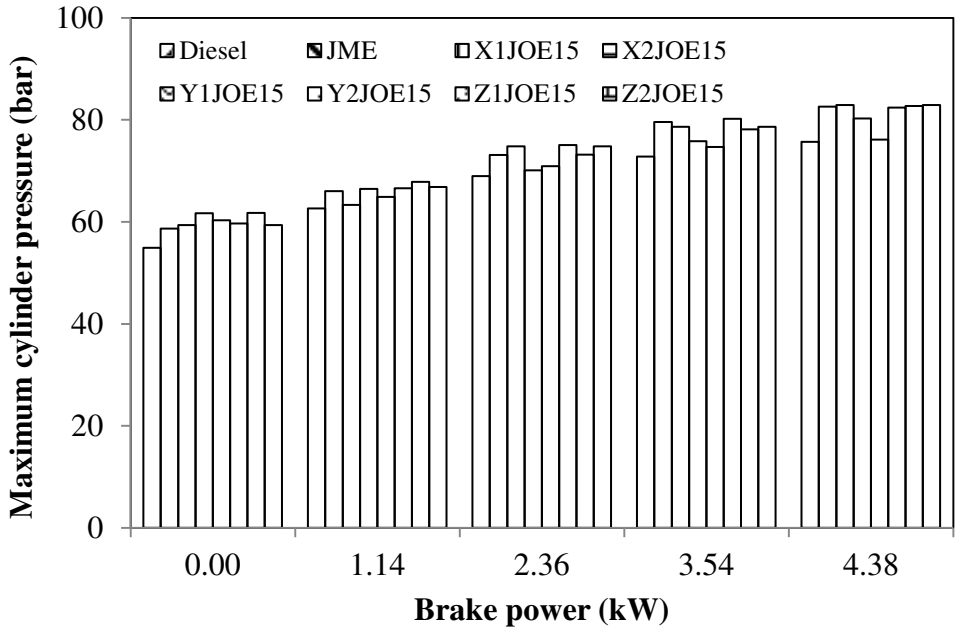

Fig. 5.1.4 Variation of maximum cylinder pressure with brake power for 15% WPO emulsions

All the emulsions with 15% WPO revealed a higher maximum cylinder pressure in comparison with diesel and the JME, at full load. This is due to the advanced combustion process being initiated by the easy flow-ability of biodiesel, and its other relevant physical properties. Similar results have been reported by Tesfa et al. [167] in their work. The deviation in the maximum cylinder pressure values between diesel and all the emulsions is in the range between 0.4 bar to 7.2 bar at full load, while it is in the range between -6.5 bar and 0.3 bar, in comparison with the JME.

5.1.2.5 Mass fraction burned

The variations of mass fraction burned with the crank angle for the diesel, JME and JME-WPO emulsions at full load are given in Fig. 5.1.5. It can be observed from the figure that the 10% and 50% mass fraction burned for all the emulsions which contain 15% WPO in them, seems to be sooner than that of diesel at full load. The 10% and 50% mass fraction burned varies with a minimum difference of 2 ^{o}CA to a maximum of 3 ^{o}CA for the emulsions from that of diesel. The crank angles at which the 90% mass fraction burned, varies with a minimum difference of 1.5 ^{o}CA to a maximum of 4 ^{o}CA, than that of diesel at full load. For the same crank angle values, the mass fraction burned of JME-WPO emulsions which contain 15% WPO in them, is marginally higher than that of diesel at full load. The reason is that,

with addition of the WPO causes reduction in viscosity of the JME-WPO emulsions, and improves the vaporization and atomization, and hence shows better mixing with air.

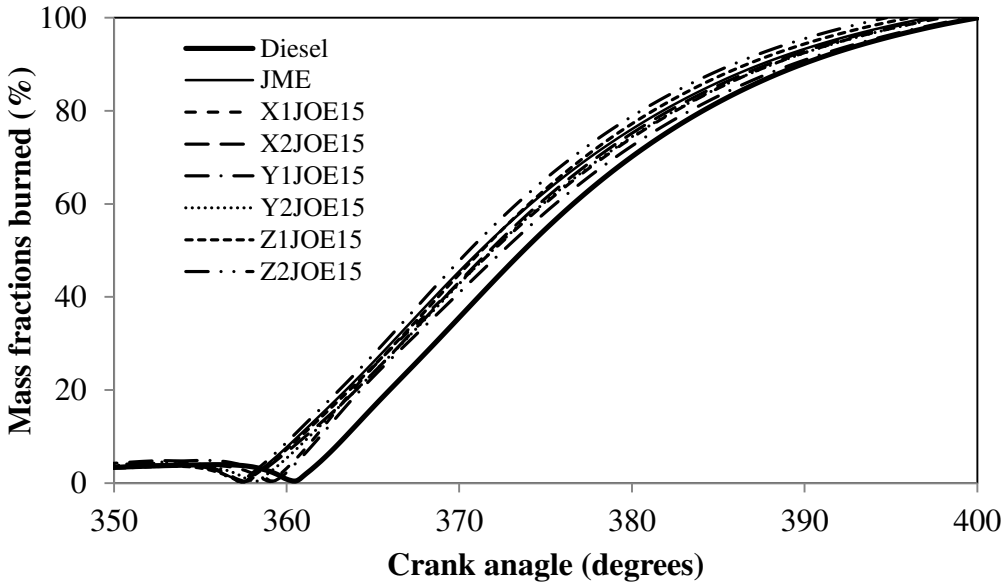

Fig. 5.1.5 Variation of mass fraction burned with crank angle at full load for 15% WPO emulsions

In addition, the presence of water in the WPO may lead to the secondary atomization (microexplosion) of the fuel, and result in more complete combustion and rapid heat release. Similar reasons are mentioned by Sadiq Basha and Anand [150] after their investigation using carbon nanotubes blended water-diesel emulsion as a fuel in a diesel engine.

5.1.2.6 Combustion duration

Figure 5.1.6 depicts the variation in the combustion duration with brake power for diesel, JME and JME-WPO emulsions. The crank angle duration of the 10% mass burned to 90% mass burned, has been taken as the combustion duration. The combustion duration increases with engine load owing to the increase in the fuel quantity. The combustion duration for all the emulsions which contain 15% WPO in them, seems to be lower than that of diesel at low loads. At full load condition, the combustion duration is found to be lower with a minimum of 0.3 ^{o}CA to a maximum of 2.2 ^{o}CA for the emulsions, compared to that of diesel. This may be due to the faster combustion rate in the premixed burning phase and shorter mixing-controlled combustion phase, resulting in a decrease of the total combustion duration of the emulsions at medium and high engine loads. The results are in agreement with those of Qi et al. [168], when they conducted experiments in a DI diesel engine fueled with ethanol-biodiesel-water micro emulsions. The micro explosion phenomenon further accelerates the

diffusion combustion, and decreases the total combustion duration in the case of emulsions. Similar reasons have been reported by Senthil kumar et al. [169], during their experiments in a single cylinder, DI diesel engine fueled with animal fat emulsions.

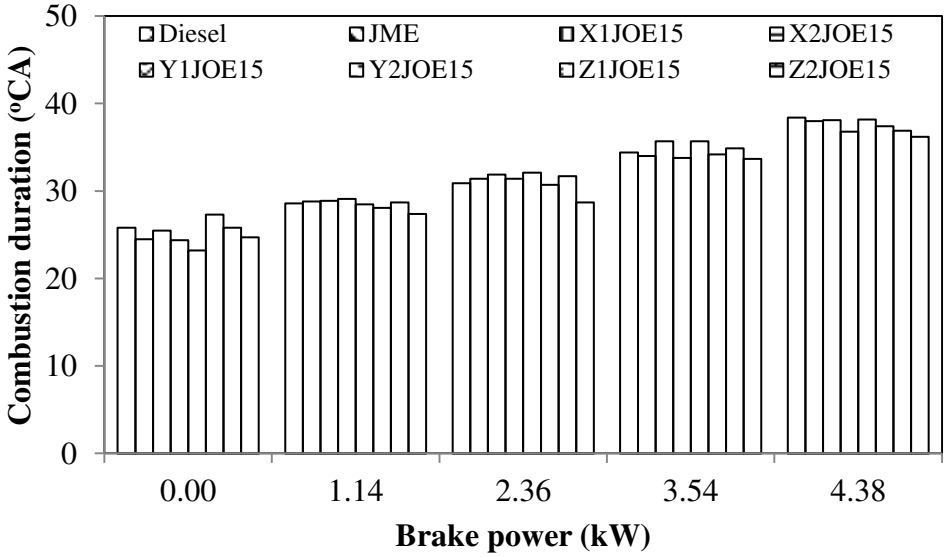

Fig. 5.1.6 Variation of combustion duration with brake power for 15% WPO emulsions

The observed shorter combustion duration may result from 15% WPO emulsions exhibiting a faster diffusion burn rate than that of diesel at full load. This is evidenced in the mass fraction burned curves, where initially the JME-WPO emulsions and diesel may have similar burn rates, but eventually diesel's burn rate slows, as its combustion becomes predominantly diffusive. A similar behavior is also observed by Mueller et al [117].

5.1.3 Performance parameters

5.1.3.1 Brake thermal efficiency

The brake thermal efficiency indicates the effective thermal energy utilization in an engine. The variation of the brake thermal efficiency with load for all the emulsions which contain 15% WPO in them, JME and diesel are depicted in Fig. 5.1.7. The brake thermal efficiency increases with an increase in load, as a result of the increase in the cylinder temperature. The brake thermal efficiency of all the emulsions which contain 15% WPO in them is found to be higher by about 3.9% to 11.3%, compared to that of diesel at full load. The brake thermal efficiency is higher by about 1.6% to 11.8% for all the emulsions in comparison with the JME at full load. The maximum thermal efficiency of 11.3% is noticed with the Z2JOE15 emulsion compared to all other emulsions tested in this study.

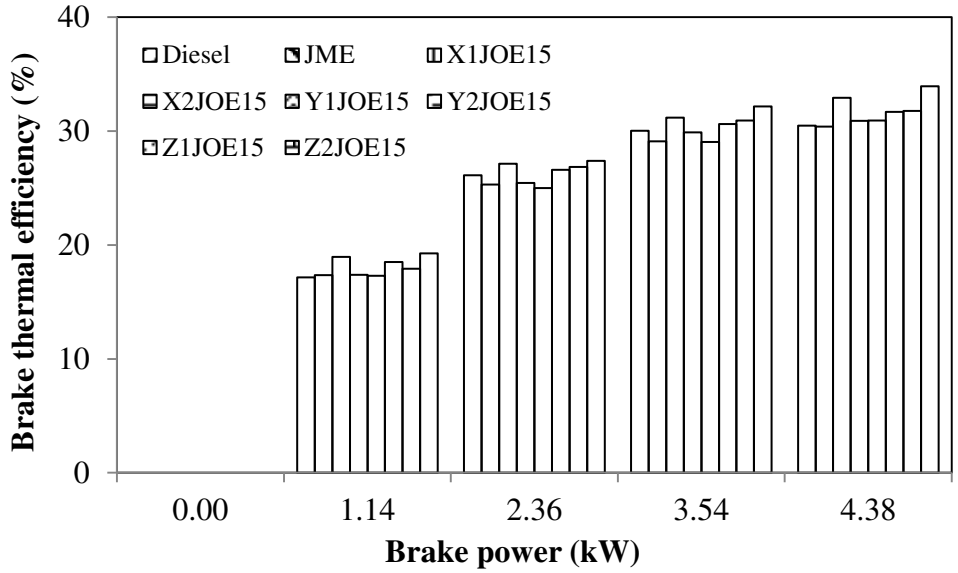

Fig. 5.1.7 Variation of brake thermal efficiency with brake power for 15% WPO emulsions

The higher densities of 15% WPO emulsions yield to earlier injection than that of diesel. Also the JME-WPO emulsions exhibit shorter ignition delay in comparison with diesel, and therefore, the beginning of the heat release is noticed earlier than that of diesel. From this point of view, the combustion itself is faster for the JME-WPO emulsions, which gives increased brake thermal efficiency. Similar reasons are reported by Armas et al. [170] during their experiments with water diesel emulsified fuel in a light duty diesel engine. Another reason may be the additional oxygen molecule available in the 15% WPO emulsions, which takes part in the combustion leading to complete combustion. Similar reasons are reported by Agarwal et al. [171] after their experiments in a diesel engine fueled with vegetable oil.

5.1.3.2 Brake specific fuel consumption

The variation of brake specific fuel consumption with brake power for diesel, JME and JME-WPO emulsions are depicted in Fig. 5.1.8. The brake specific fuel consumption (BSFC) is the ratio between the mass of fuel consumption and the brake power. For the emulsions which contain 15% WPO in them, the differences in the BSFC values are found to be higher by an average of 20% compared to that of diesel at full load. Among all the JME-WPO emulsions, the Z2JOE15 emulsion recorded the lowest specific fuel consumption, which is about 15% higher than that of the diesel consumption.

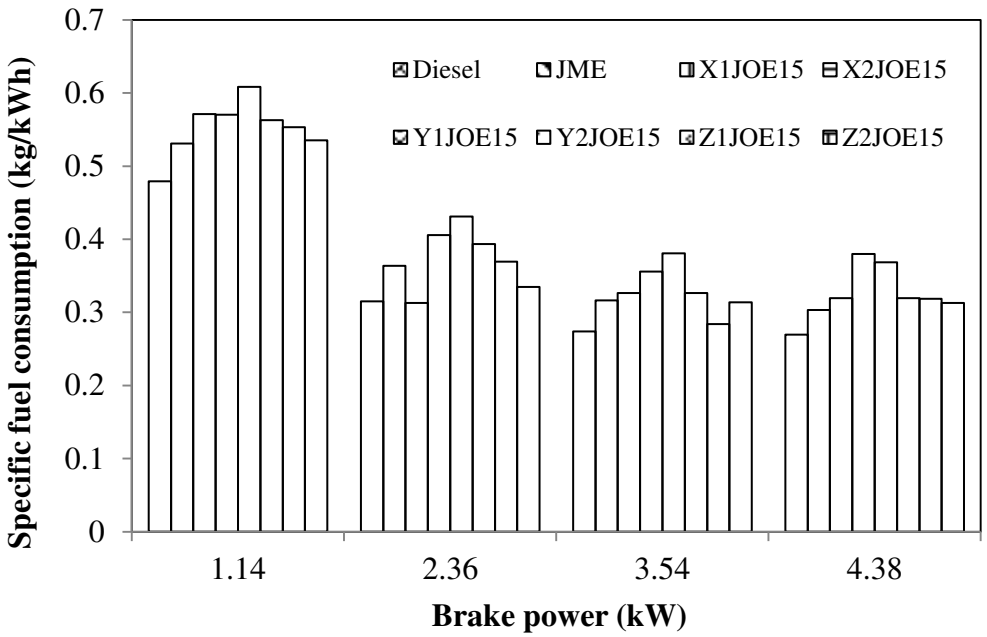

Fig. 5.1.8 Variation of brake specific fuel consumption with brake power for 15% WPO emulsions

The higher BSFC values of JME and its emulsions with WPO are attributed to the fact that more amount of fuel is required by the engine to generate the same power, when the calorific value of the fuel is low.

5.1.3.3 Exhaust gas temperature

The variation of exhaust gas temperature with load for all the emulsions which contain 15%, WPO in them and diesel are depicted in Fig. 5.1.9. It is found that the exhaust gas temperature increases with load for all the fuels. At full load, the exhaust gas temperatures of all the emulsions which contain 15% WPO in them, are found to be higher by an average of 40 ^{o}C compared to that of diesel.

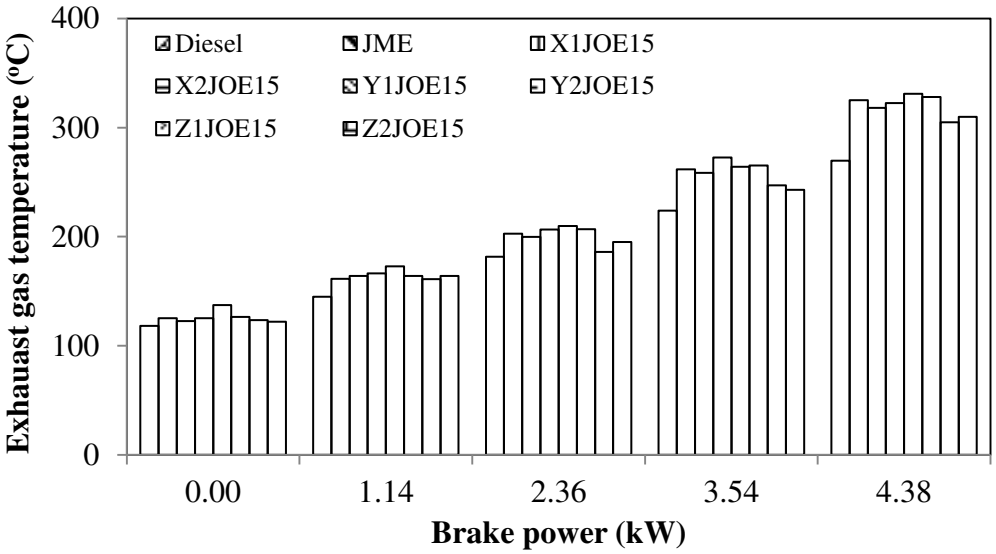

Fig. 5.1.9 Variation of exhaust gas temperature with brake power for 15% WPO emulsions

The water content present in the WPO gets vaporized during the combustion process and absorbs the heat energy which decreases the local adiabatic flame temperature. This result in a reduction in the exhaust gas temperature of 15% WPO emulsions compared to that of JME operation. This is in agreement with the results reported by Bertoli *et al.,*[146] when the WPO blends or emulsions were used as fuels in a diesel engine.

5.1.4 Emission parameters

5.1.4.1 BSHC emissions

The variations of brake specific HC emissions with brake power for different emulsions with 15% WPO are depicted in Fig. 5.1.10. The HC emissions are found to be lower in CI engines, because they always operate with excess air. It is observed from the figure that the BSHC emissions decrease with an increase in the engine load. Compared to diesel operation, the JME and 15% WPO emulsions, exhibit lower BSHC emissions, which may be due to the higher oxygen content of JME that leads to more complete burning than that of diesel operation. Similar reasons are given for lower HC emissions by *Xue et al* [172] in a review article on biodiesel emissions. With 15% WPO in the emulsion, the percentage differences in the HC emissions are noticed from 11.3% to 45.8% compared to that of diesel operation, and 9.6% to 44.8% lower compared to that of the JME operation are noticed.

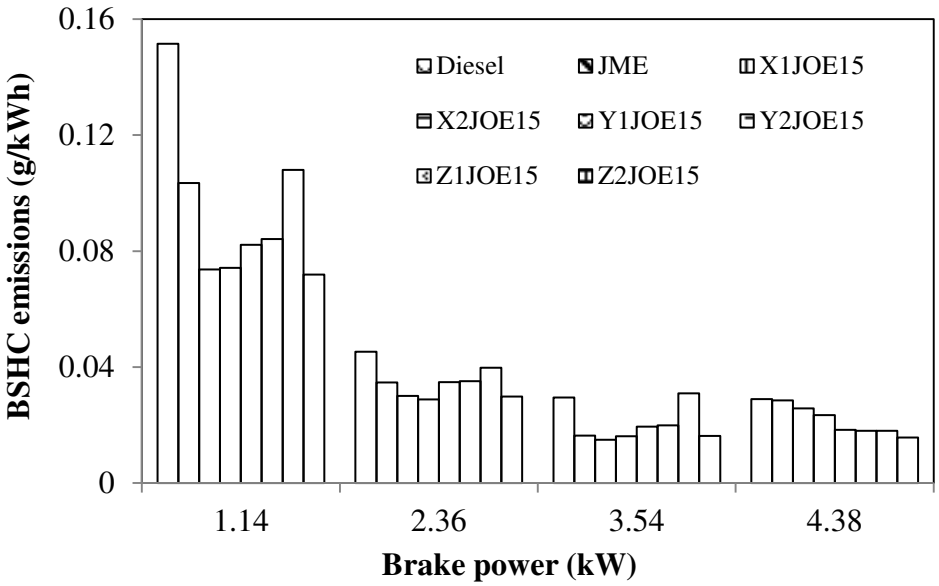

Fig. 5.1.10 Variation of BSHC emission with brake power for 15% WPO emulsions

5.1.4.2 BSCO emissions

Figure 5.1.11 illustrates the variation of brake specific CO emissions with brake power for disel, JME and 15% WPO emulsions, prepared with six different surfactants. Generally, the CO emissions are formed as a result of the incomplete combustion of fuel. However, if the combustion is complete, then the CO will be oxidized into CO_2. Usually, the CO emission of diesel engines is low, because diesel combustion occurs with a lean mixture. Also, the higher combustion temperature accelerates the oxidization rate of CO to form CO_2, and thus results in less CO in the exhaust gases of the engine [173]. The BSCO emissions are found to decrease with an increase in the engine load, due to the increase of the in-cylinder gas temperature. It is reported that the CO emissions are lower with the biodiesel operation, due to the higher oxygen content and lower carbon to hydrogen ratio compared to that of diesel. This reason is supported by Xue *et al.* [172], in their review article on biodiesel emissions. With the WPO percentage of 15% in the emulsion, the differences in the CO emissions are noticed to be from 43.8% to 68.9%, compared to that of diesel at full load.

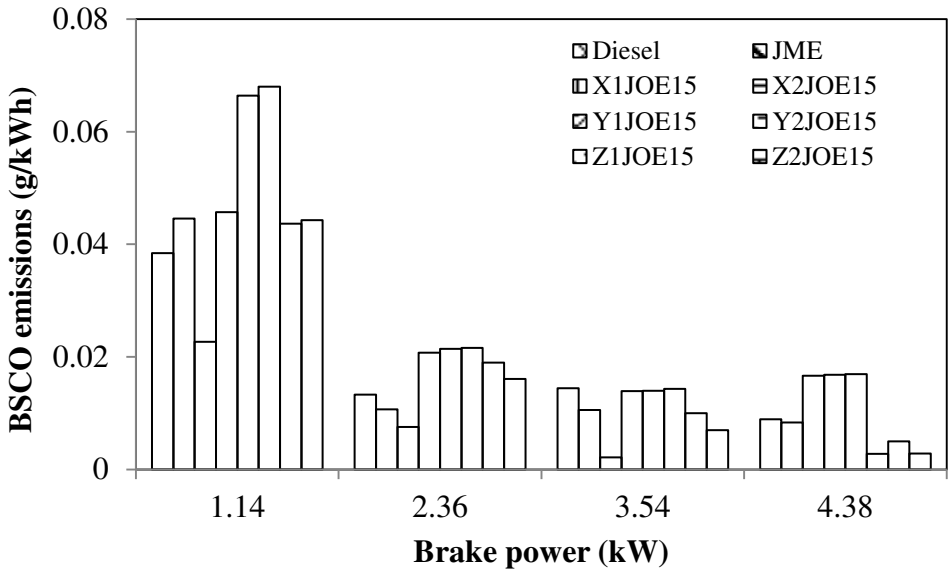

Fig. 5.1.11 Variation of BSCO emission with brake power for 15% WPO emulsions

This may be due to the lower carbon content for the JME-WPO emulsions, compared to that of the JME. Similar observations are reported by Karabektas [174] and Lin and Lin [175], on their experiments with biodiesel. Higher CO emissions are observed with the X1JOE15, X2JOE15 and Y1JOE15 emulsions, which are attributed to poor mixture preparation.

5.1.4.3 BSNO emissions

The variation of brake specific NO emissions with brake power for all the emulsions which contain 15% WPO in them, are shown in Fig. 5.1.12. Two predominant factors affect the formation of NO in CI engines; they are; i) the availability of oxygen and ii) in cylinder temperature. The presence of the oxygen molecule in JME causes an increase in the combustion gas temperature, resulting in a marginal increase in NO emissions. This statement is in agreement with that of Nabi *et al.* [176] during their study on engine emissions, when fueled with karanja biodiesel. At elevated flame temperatures, this oxygen reacts with nitrogen and tends to form NO. The BSNO emissions of the JME operation are higher by 41% compared to that of diesel at full load. The BSNO emissions of JME-WPO emulsions are found to be lower than that of JME, but higher than that of diesel operation. For all the emulsions, the NO emissions are found to be lower in the range between 9.5% and 16.8%, compared to that of JME operation. This may be due to the water content present in the WPO, which will reduce the combustion temperature. Similar reasons were reported by Bertoli *et al.* [146] for lower combustion temperature and NO emissions.

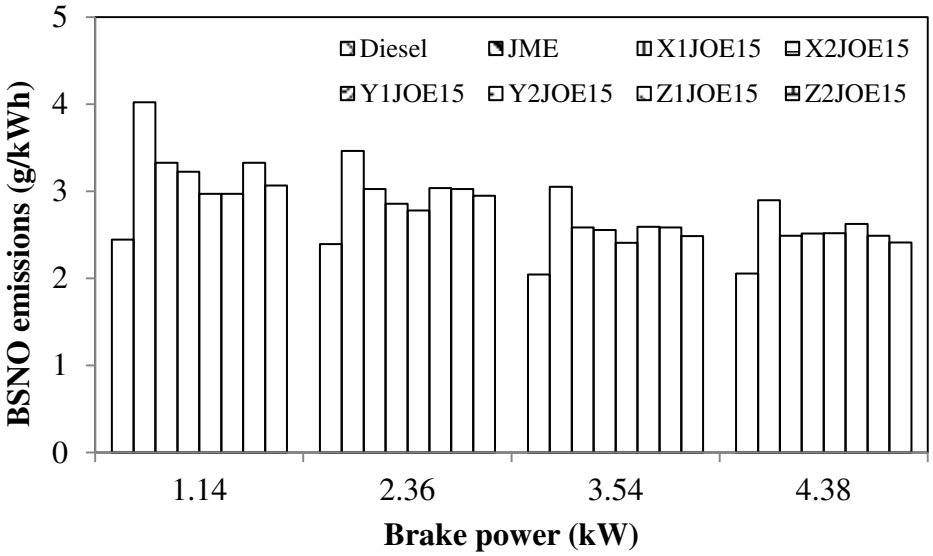

Fig. 5.1.12 Variation of BSNO emission with brake power for 15% WPO emulsions

5.1.4.4 Smoke opacity

Figure 5.1.13 depicts the variation of smoke opacity for diesel, JME and the JME-WPO emulsions at different loads.

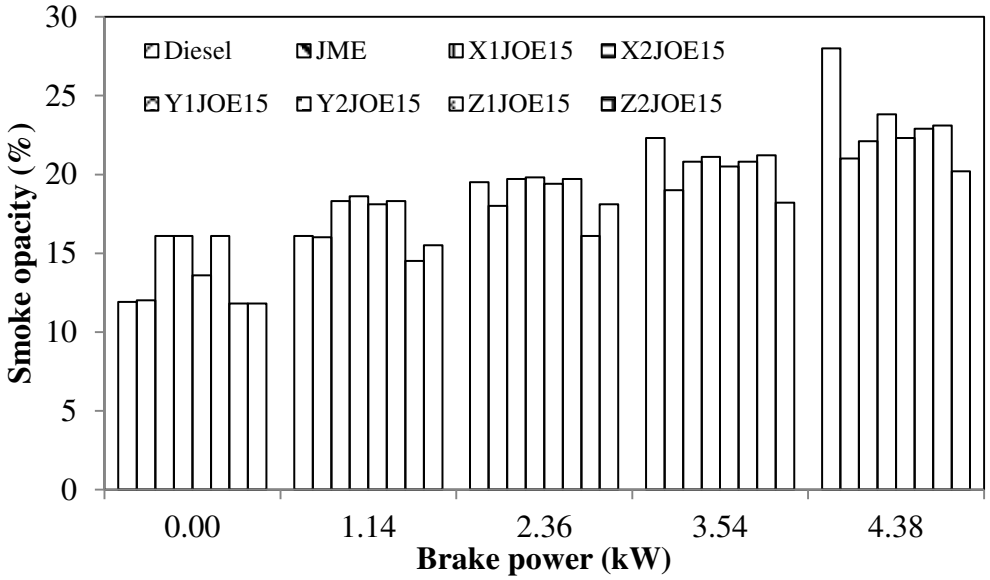

Fig. 5.1.13 Variation of smoke opacity with brake power for 15% WPO emulsions

Soot formation mainly takes place in the fuel-rich zone at high temperature and pressures, specifically within the core region of each fuel spray. The smoke opacity is found to be lower with all the emulsions with 15% WPO, in comparison with that of diesel and JME operations. The reason for the reduction in smoke opacity can be explained by the fact that the oxygenated fuels effectively deliver oxygen to the pyrolysis zone of the burning spray. The same reason is supported by McCormick and Parish [177], and Wang et al. [114], in their

study on biodiesel emissions. The reduction in smoke for all the emulsions investigated in this study is in the range of 15%, to 27.8%, compared to that of diesel at full load.

The summary of the values on the combustion, performance and emission parameters at full load for different emulsions, which contain 5%, 10% and 15% WPO in them, are given in Table 5.1.

5.1.5 Closure

It is summarized that the engine was able to run with a maximum of 15% WPO, in the form of emulsions with the JME. The combustion starts earlier in the case of all the JME-WPO emulsions compared to that of diesel and the JME. The maximum thermal efficiency is noticed with the Z2JOE15 emulsion, compared to all other emulsions tested in this study. The thermal efficiency of Z2JOE15 is found to be higher by about 11.3% compared to that of diesel. Lower HC, CO and smoke emissions are noticed with the Z2JOE15 emulsion, compared to that of diesel operation. The NO emissions for all the emulsions are found to be lower than that of JME operation, but higher than that of diesel operation. The maximum reduction in the nitric oxide emission of 16.8% is observed with the Z2JOE15 emulsion, compared to that of JME operation. Overall, by considering the combustion, performance and emission parameters, it can be concluded that the Z2JOE15 showed a better performance and lower emissions compared to those of diesel and the JME operations.

Table 5.1 Summary of values on combustion, performance and emission parameters at full load for different emulsions which contain 5%, 10% and 15% WPO

Sl.No	Parameter	Diesel	JME	X1JOE5	X2JOE5	Y1JOE5	Y2JOE5	Z1JOE5	Z2JOE5
A.	***Combustion parameters***								
1.	Start of ignition (^{o}CA)	356.6	354	354.8	353.7	357.5	354.2	353.7	354.8
2.	Occurrence of maximum pressure (^{o}CA)	372.4	370.4	370.9	370.7	373.6	370.3	371.3	370.8
3.	Ignition delay (^{o}CA)	12.7	10.2	10.4	9.9	14.1	9.9	9.8	10.4
4.	Occurrence of maximum heat release (^{o} CA aTDC)	6.7	8.2	4	9.1	12.5	4	10.2	4
5.	Maximum heat release (J/^{o}CA)	52.02	49.97	50	49.38	50.65	50.45	53.52	49.86
6.	Maximum cylinder pressure (bar)	75.70	82.61	82.9	80.2	76.1	82.4	82.7	82.9
7.	90% Mass fraction burned (^{o}CA)	389.9	387.5	386.9	387.2	388	387.4	388.5	386.6
8.	Combustion duration (^{o}CA)	38.4	38	38	36.7	37.7	37.8	36.8	37.2
B.	***Performance parameters***								
9.	Brake thermal efficiency (%)	30.4	30.3	30.6	30.0	31.3	31.4	30.9	31.4
10.	Specific fuel consumption (kg/kWh)	0.269	0.302	0.294	0.314	0.299	0.299	0.328	0.266
11	Exhaust gas temperature (^{o}C)	270	325	321	317	319	335	320	320
C.	***Emission parameters***								
12.	BSHC emission (g/kWh)	0.029	0.028	0.027	0.028	0.021	0.023	0.025	0.017
13.	BSCO emission (g/kWh)	0.008	0.008	0.0057	0.0056	0.011	0.008	0.0058	0.0054
14.	BSNO emission (g/kWh)	2.055	2.898	2.695	2.791	2.786	2.819	2.695	2.644
15.	Smoke opacity (%)	28	21	20.5	22.5	20.5	21.5	20.2	18.5

Continued in the next page……

Sl.No	Parameter	Diesel	JME	X1JOE10	X2JOE10	Y1JOE10	Y2JOE10	Z1JOE10	Z2JOE10
D.	***Combustion parameters***								
1.	Start of ignition (^{o}CA)	356.6	354	353.7	353.7	357.7	354.9	354.3	354.2
2.	Occurrence of maximum pressure (^{o}CA)	372.4	370.4	370.1	370.8	372.7	370.7	370.7	370.2
3.	Ignition delay (^{o}CA)	12.7	10.2	9.8	9.9	14.3	10.4	10.4	9.8
4.	Occurrence of maximum heat release (^{o} CA aTDC)	6.7	8.2	8.4	9.1	11.6	9	10.2	8.6
5.	Maximum heat release (J/^{o}CA)	52.02	49.97	49.52	49.25	48.02	50.94	50.7	50.46
6.	Maximum cylinder pressure (bar)	75.70	82.61	83.4	81.8	69.8	81.7	80.9	82.7
7.	90% Mass fraction burned (^{o}CA)	389.9	387.5	387.7	387.9	390.9	388.1	387.8	387.3
8.	Combustion duration (^{o}CA)	38.4	38	38.2	38.5	38.2	38.3	37.5	37.1
E.	***Performance parameters***								
9.	Brake thermal efficiency (%)	30.4	30.3	31.99	31.09	32.0	32.17	31.12	32.4
10.	Specific fuel consumption (kg/kWh)	0.269	0.302	0.315	0.310	0.316	0.317	0.319	0.315
11	Exhaust gas temperature (^{o}C)	270	325	315	321	354	331	313	315
F.	***Emission parameters***								
12.	BSHC emission (g/kWh)	0.029	0.028	0.023	0.0264	0.018	0.023	0.0223	0.0124
13.	BSCO emission (g/kWh)	0.008	0.008	0.0106	0.0056	0.0166	0.0055	0.0053	0.0053
14.	BSNO emission (g/kWh)	2.055	2.898	2.535	2.734	2.59	2.606	2.535	2.498
15.	Smoke opacity (%)	28	21	21.8	23.2	21.6	22.8	19.3	19.1

Continued in the next page……

Sl.No	Parameter	Diesel	JME	X1JOE15	X2JOE15	Y1JOE15	Y2JOE15	Z1JOE15	Z2JOE15
G.	***Combustion parameters***								
1.	Start of ignition (^{o}CA)	356.6	354	354.3	353.7	357.0	354.3	354.0	356.1
2.	Occurrence of maximum pressure (^{o}CA)	372.4	370.4	370.2	370.2	372.2	370.7	371.0	371.0
3.	Ignition delay (^{o}CA)	12.7	10.2	9.9	10.4	13.3	10.4	10.1	9.9
4.	Occurrence of maximum heat release (^{o} CA aTDC)	6.7	8.2	7.9	9.1	6.9	9.1	9.4	4.5
5.	Maximum heat release (J/^{o}CA)	52.02	49.97	47.62	47.42	53.14	51.51	51.52	55.27
6.	Maximum cylinder pressure (bar)	75.70	82.61	82.9	80.2	76.1	82.4	82.7	82.9
7.	90% Mass fraction burned (^{o}CA)	389.9	387.5	388.5	387.8	389.5	387.7	386.9	385.9
8.	Combustion duration (^{o}CA)	38.4	38	38.1	36.8	38.2	37.4	36.9	36.2
H.	***Performance parameters***								
9.	Brake thermal efficiency (%)	30.4	30.3	32.9	30.8	30.9	31.6	31.7	33.9
10.	Specific fuel consumption (kg/kWh)	0.269	0.302	0.319	0.379	0.368	0.319	0.318	0.312
11	Exhaust gas temperature (^{o}C)	270	325	318	322	358	328	305	310
I.	***Emission parameters***								
12.	BSHC emission (g/kWh)	0.029	0.028	0.0257	0.0233	0.0183	0.018	0.018	0.015
13.	BSCO emission (g/kWh)	0.008	0.008	0.0166	0.0167	0.0169	0.0027	0.005	0.0028
14.	BSNO emission (g/kWh)	2.055	2.898	2.489	2.513	2.520	2.624	2.489	2.412
15.	Smoke opacity (%)	28	21	22.1	23.8	22.3	22.9	23.1	20.2

5.2 Experimental studies on the combustion, performance and emission characteristics of acid treated biodiesel bio oil emulsions

5.2.1 General

Preliminary investigations on the utilisation of the emulsion obtained from JME with WPO as an alternative fuel revealed, that up to 15% of WPO can be emulsified with the JME, and used as a fuel in a DI diesel engine. From the experimental results in terms of emulsion stability, combustion, performance and emission parameters, the Z2JOE15 emulsion was selected as an optimum emulsion for further investigation. But, it was found that the Z2JOE15 emulsion was acidic in nature, due to the addition of WPO. This may result in difficulty in storage, handling and utilization of the fuel in transport applications. The acidity of the JOE15 emulsion was reduced by an acid treatment, and this acid treated JOE15 emulsion was denoted as ATJOE15. The acid treatment procedure and properties of the ATJOE15 emulsion are already mentioned in Chapter 3. The acid treated emulsion was tested as a fuel in the same engine. The combustion, performance and emission behaviour of the diesel engine fueled with ATJOE15 in comparison with those of diesel and JME operations are presented in this section.

5.2.2 Combustion parameters

5.2.2.1 Pressure crank angle history

The cylinder pressure for each crank angle rotation for all the test fuels at full load condition is shown in Fig. 5.2.1.

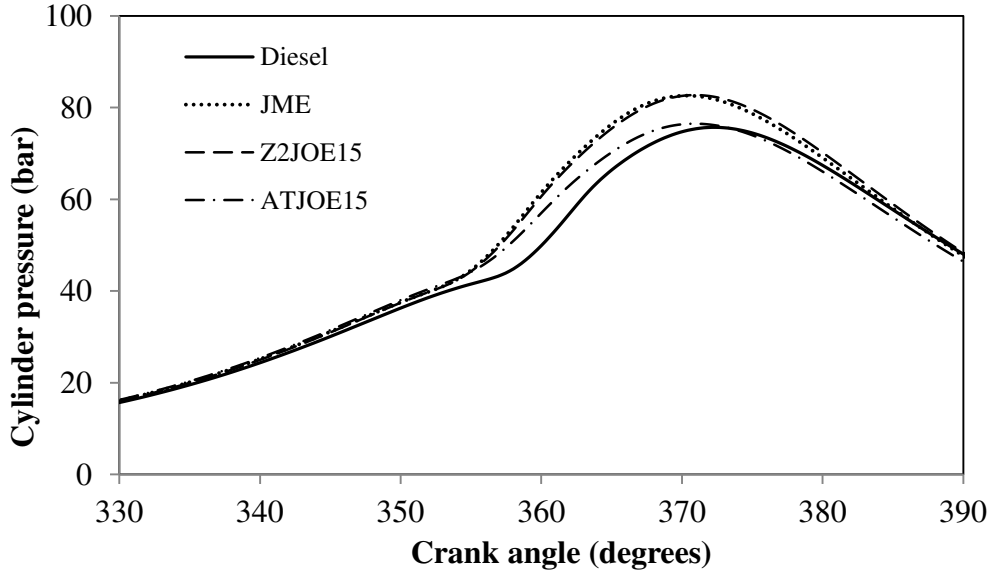

Fig. 5.2.1 Variation of cylinder pressure with crank angle

It is observed from the figure that the combustion commences earlier by 2.6°, 2.8 ° and 2.2 ° CA for JME, Z2JOE15 and ATJOE15 respectively, compared to that of diesel at full load. The combustion starts earlier for the JME and emulsions, due to advanced injection timing as a result of higher bulk modulus and higher density of biodiesel and shorter ignition delay. Similar results are reported by Gumus [178] in his investigation of the combustion and heat release characteristics of a hazelnut kernel oil methyl ester fueled DI diesel engine. The maximum cylinder pressure for diesel occurs at 12.4 °CA aTDC, whereas for the JME, Z2JOE15 and ATJOE15, the peak pressure occurs at about 10.4 °CA aTDC, 10.8 °CA aTDC and 10.2 °CA aTDC respectively at full load, It is ascertained that the peak pressure occurs after the TDC for all the fuels tested in this study.

5.2.2.2 Ignition delay

Figure 5.2.2 depicts the ignition delay for diesel, JME, Z2JOE15 and ATJOE15 at all loads. The ignition delay decreases with an increase in the load for all the fuels as expected in this study. The decrease in ignition delay with the increase in engine load, is due to the influence of the cylinder gas temperature within the ignition delay period [169].

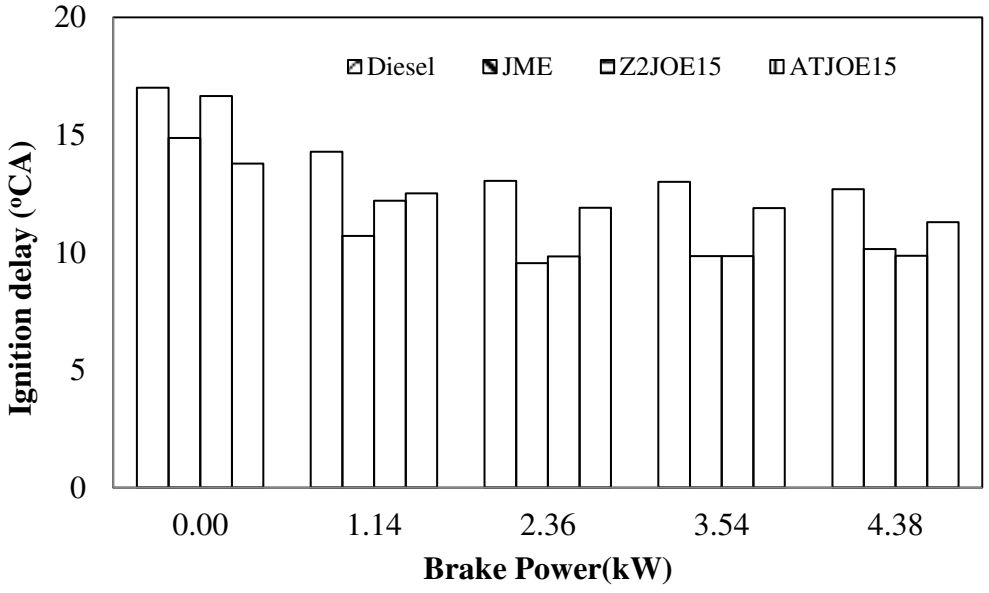

Fig. 5.2.2 Variation of ignition delay with brake power

At full load condition, the values of ignition delay are about 12.7, 10.1, 10.2 and 11.3 °CA, for diesel, JME, Z2JOE15 and ATJOE15 respectively. The delay period is lower by about 2.5°, 2.5° and 1.4° for JME, Z2JOE15 and ATJOE15 respectively, compared to that of diesel.

The advance of the ignition timing is observed with the JME and emulsions, which is attributed to the oxygen present in JME, and the breakdown of the higher molecules of JME into lower molecules of volatile compounds during injection, and this advances the start of ignition resulting in a shorter ignition delay. Similar reasons are given by Rao et al. [179], in their work on the combustion and emission characteristics of diesel engine fueled with rice bran oil methyl ester and its diesel blends. In the case of the Z2JOE15, the ignition delay is found to be the same as JME, and the delay period is longer in the case of ATJOE15, due to inadequate mixing leading to larger droplet size and smaller spray angles.

5.2.2.3 Heat release rate

Figure 5.2.3 depicts the heat release pattern of the various fuels tested in this study.

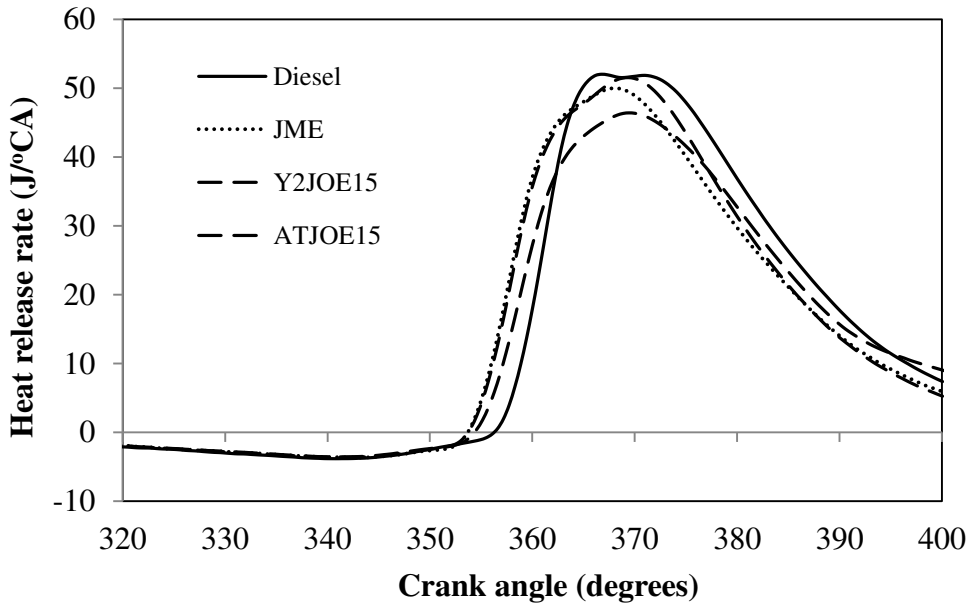

Fig. 5.2.3 Variation of heat release rate with crank angle

The heat release patterns of the JME, Z2JOE15 and ATJOE15 at full load follow the trend of diesel at full load. Because of the heat loss from the cylinder, and the cooling effect of the fuel vaporization, when it is injected into the cylinder, the heat release rate is marginally negative during the ignition delay period. The maximum heat release rate values are about 52, 50, 49.4, 51.5 and 46.4 J/ ^{o}CA for diesel, JME, Z2JOE15 and ATJOE15 respectively, at full load. The maximum heat release rate is found to be higher for diesel, due to more accumulation of fuel during the relatively longer delay period. For the JME and its emulsion with the WPO, less amount of fuel is accumulated during the shorter ignition delay period,

which results in lower heat release rates compared to that of diesel at full load. The reasons are in agreement with those of Qi et al [168], when the diesel engine was fueled with ethanol-biodiesel-water micro emulsions. The maximum heat release rate occurs at about 6.7, 8.2, 9.11 and 9.09 ^{o}CA aTDC for diesel, JME, Z2JOE15 and ATJOE15 respectively, at full load.

5.2.2.4 Maximum cylinder pressure

Figure 5.2.4 illustrates the variation of maximum cylinder pressure with load for the various fuels tested in this study.

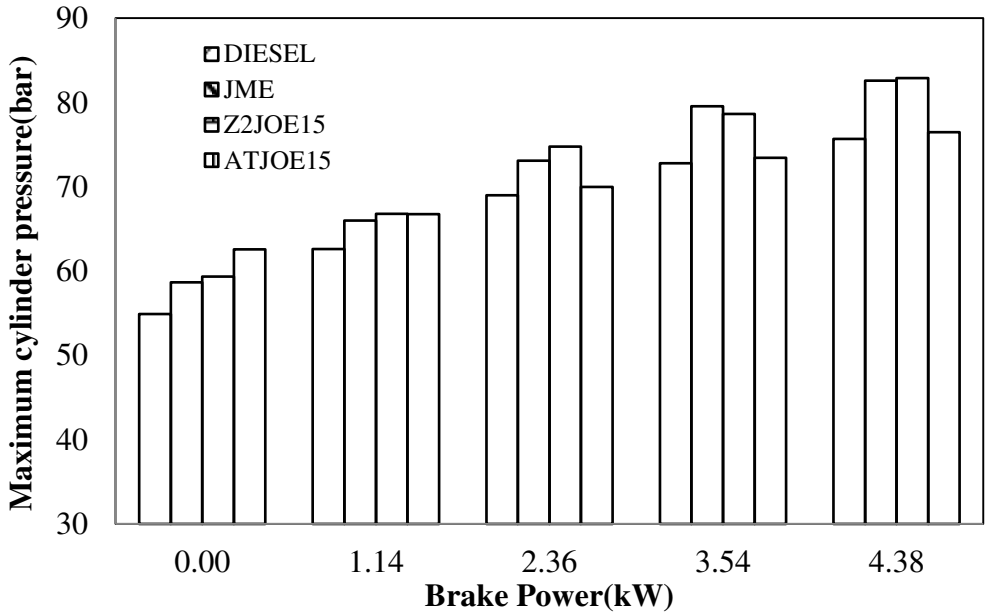

Fig. 5.2.4 Variation of maximum cylinder pressure with brake power

It can be observed from the figure, that at low loads, the maximum cylinder pressure is higher for the JME, Z2JOE15 and ATJOE15 emulsions, compared to those of diesel and the JME. This may be attributed to the shorter ignition delays and rapid combustion of the JME and JME-WPO emulsions, compared to that of diesel. At high loads, the maximum cylinder pressure of the ATJOE15 emulsion is noticed to be higher in comparison with diesel, but lower than that of JME. At full load condition, the maximum cylinder pressure values of diesel, JME, Z2JOE15 and ATJOE15 are 75.7, 82.6, 82.9 and 76.4 bar respectively. In this condition, the ignition delay of the ATJOE15 emulsion is longer, which in turn extends the combustion process, and this may be the reason for the lower peak cylinder pressure of ATJOE15 when compared with the JME.

5.2.2.5 Mass fraction burned

The variations of mass fraction burned with the crank angle for the ATJOE15 emulsion compared with those of diesel, JME and Z2JOE15 at full load, are given in Fig. 5.2.5.

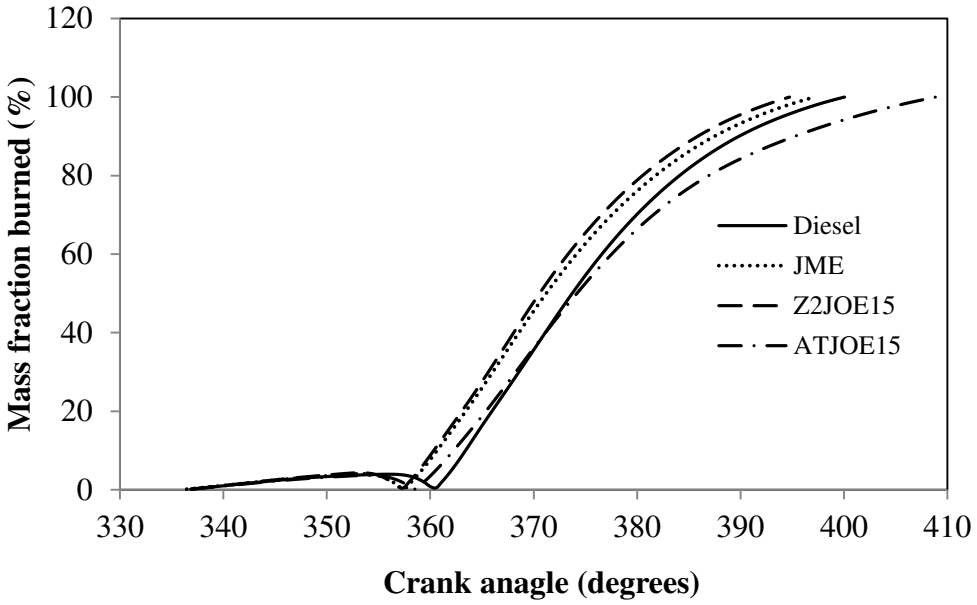

Fig. 5.2.5 Variation of mass fraction burned with crank angle

It is seen from the figure, that the crank angles at which 10% mass fraction burned for the ATJOE15, JME and Z2JOE15 are earlier than that of diesel at full load condition. As a result of longer ignition delay, the 10% mass fraction burned is later than those of JME and Z2JOE15 operations. The crank angles at which 50% mass fraction burned are earlier by about 3 and 4 ^{o}CA for the JME and Z2JOE15 respectively, whereas it is almost the same for the ATJOE15. This indicates that the combustion period upto 50% mass fractions are almost the same as that of diesel for the ATJOE15 emulsion. The 90% mass fraction burned crank angles are earlier for the JME and Z2JOE15 emulsion by 2 and 4 ^{o}CA respectively, whereas it is later by 6 ^{o}CA for the ATJOE15 emulsion. The marginally higher viscosity and density of the ATJOE15 emulsion result in inferior atomization and vaporization, and lead to reduction in the fuel air mixing rates. Hence, more burning occurs in the diffusion phase, in the case of the ATJOE15 emulsion.

5.2.2.6 Combustion duration

Figure 5.2.6 illustrates the variation of combustion duration under different loads of the engine. The crank angle duration from 10% mass burned to 90% mass burned, has been taken

as the combustion duration. The combustion duration increases with engine load, owing to the increase in the fuel quantity. The values of combustion duration at full load are approximately 38.4, 38, 36.9 and 40.6 ^{o}CA for diesel, JME, Z2JOE15 and ATJOE15 respectively. At full load, the combustion duration of the ATJOE15 is longer than those of diesel, JME and Z2JOE15.

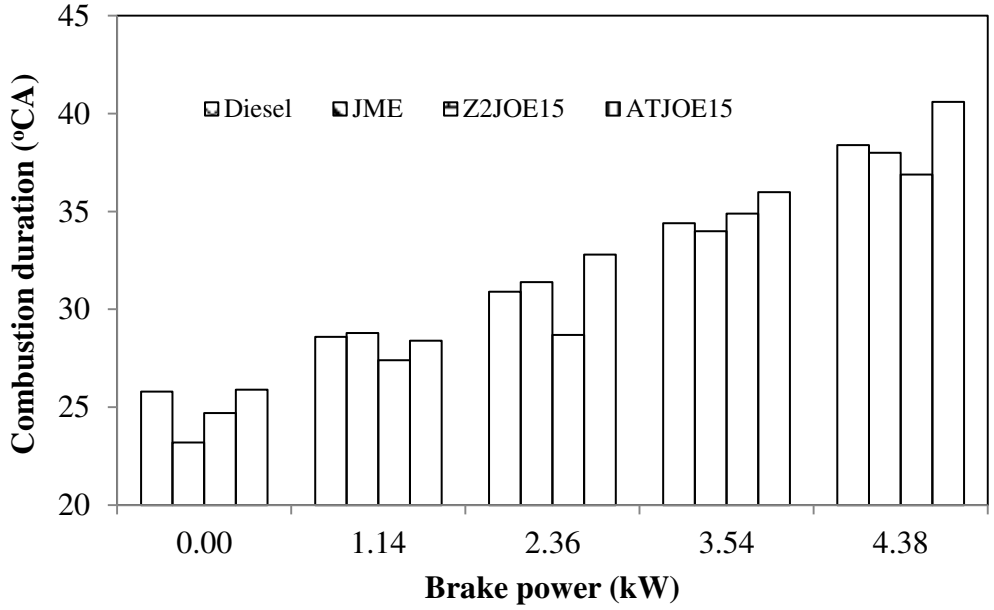

Fig. 5.2.6 Variation of combustion duration with brake power

This may be due to the slower combustion rate in the premixed burning phase, and the longer mixing-controlled combustion phase that increases the total combustion duration of the ATJOE15 emulsion. Similar reasons are reported by Qi et al. [168], when the diesel engine was fueled with ethanol-biodiesel-water micro emulsions. This longer mixing controlled combustion phase depends largely on the fuel injection rate and fuel vapour air mixing rates. Because of the larger droplets and poor breaking of spray, the combustion duration is longer with the ATJOE15.

5.2.3 Performance parameters

5.2.3.1 Brake thermal efficiency

Fig. 5.2.7 shows the variation of brake thermal efficiency with respect to brake power for all the fuels tested in this study. The values of the brake thermal efficiencies at full load are 30.47%, 30.38%, 33.92%, and 32.98% respectively for diesel, JME, Z2JOE15 and ATJOE15 respectively. It is observed that the thermal efficiencies of Z2JOE15 and ATJOE15 emulsions are higher than that of diesel by about 11.3% and 8.2% respectively, at full load. When

compared to JME operation, the thermal efficiencies are higher by 11.6% and 8.5% for the Z2JOE15 and ATJOE15 emulsions respectively, at full load. The increase in the brake thermal efficiency is due to the improvement of the combustion process, on account of the increased oxygen content in the fuels. Similar reasons are reported by Zhu et al [180], in their work on DI diesel engine fueled with ethanol–biodiesel blends. The faster combustion process of the Z2JOE15 and ATJOE15 emulsions may be another contributor to the increase in thermal efficiency. Also, based on the mass fraction burned or heat release analysis, the crank angle at which 50% mass fraction burned is closer to the top dead center, leading to higher positive work done on the piston, and hence, higher brake thermal efficiency is obtained with the Z2JOE15 and ATJOE15 emulsions, compared to that of diesel.

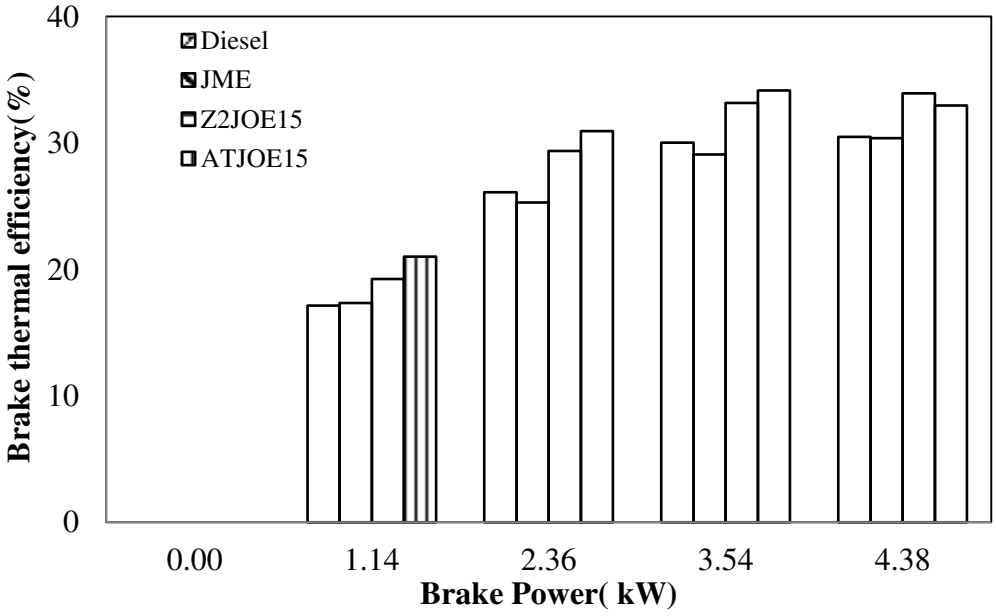

Fig. 5.2.7 Variation of brake thermal efficiency with brake power

A marginally lower thermal efficiency of the ATJOE15 emulsion is noticed at full load, compared to that of Z2JOE15 emulsion, which may be due to longer combustion during the diffusion phase.

5.2.3.2 Brake specific fuel consumption

The variation of brake specific fuel consumption with brake power for the fuels tested in this study, is shown in Fig. 5.2.8. The BSFC of the JME, Z2JOE15 and ATJOE15 follows the trend similar to that of diesel. The BSFC is decreased with the increase in the engine load as expected.

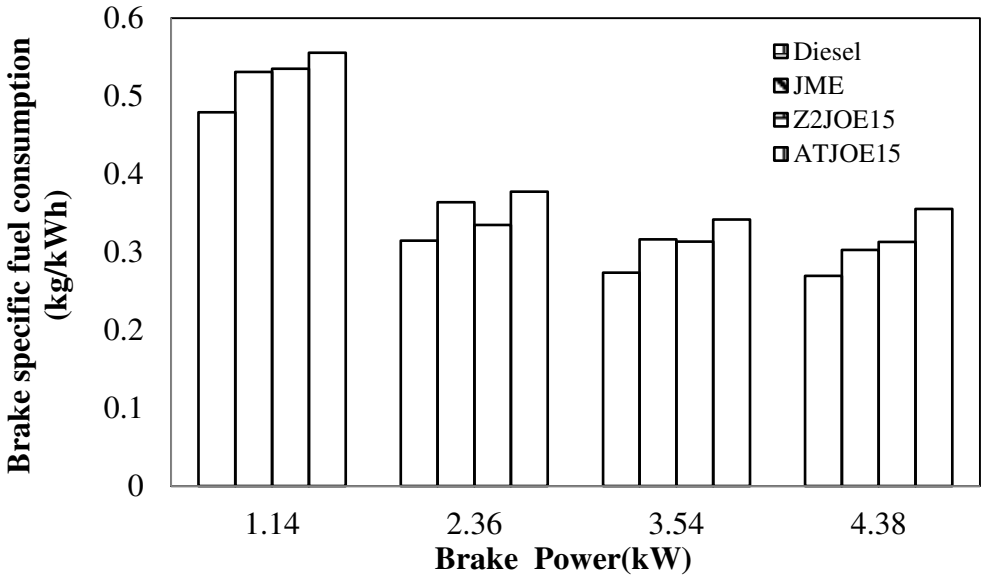

Fig. 5.2.8 Variation of brake specific fuel consumption with brake power

The BSFC values of JME, Z2JOE15 and ATJOE15 are found to be higher by 12.3%, 16% and 31% respectively. This is attributed to the combined effect of viscosity and lower heating values of JME and emulsions, which require larger fuel consumption in order to release the same energy as that of diesel.

5.2.3.3 Exhaust gas temperature

Figure 5.2.9 depicts the trend of the exhaust gas temperature with load for all the fuels tested in this study.

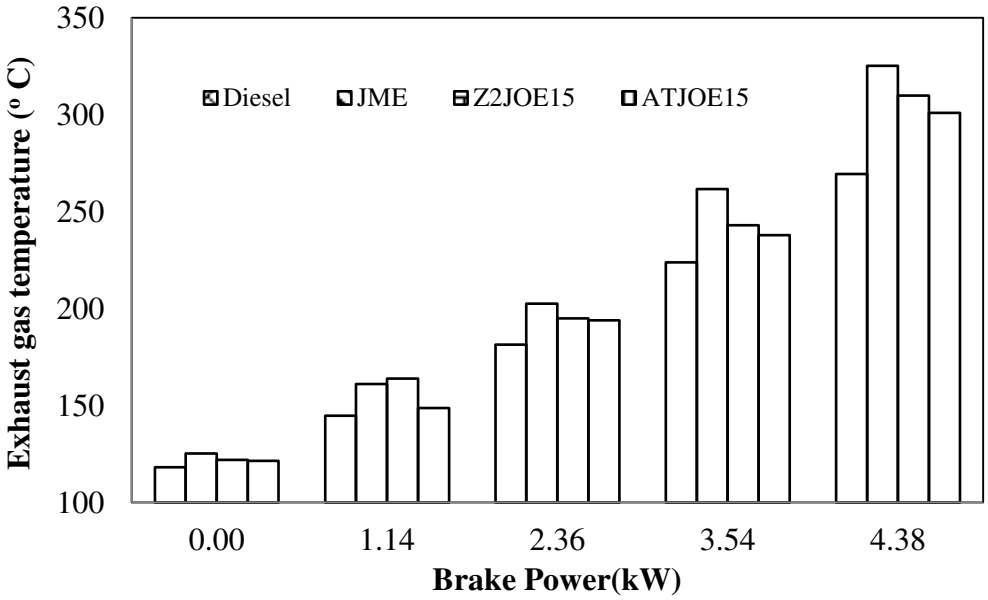

Fig. 5.2.9 Variation of exhaust gas temperature with brake power

The exhaust gas temperatures of diesel, JME, Z2JOE15 and ATJOE15 are 270^{o}C, 325^{o}C, 310^{o}C and 301^{o}C respectively, at full load. It is noted from the figure that at full load, the exhaust gas temperature is the highest for JME and lowest for diesel. The exhaust gas temperatures of Z2JOE15 and ATJOE15 are lower than that of JME operation. The water content present in the WPO gets vaporized during the combustion process, and absorbs the heat energy which decreases the local adiabatic flame temperature. Similar reasons are reported by Bertoli *et al.,* [146] when WPO blends or emulsions are used as the fuel in a diesel engine.

5.2.4 Emission parameters

5.2.4.1 BSHC emissions

Figure 5.2.10 depicts the variation of brake specific hydrocarbon (BSHC) emissions with brake power. All the fuels tested in this study exhibit higher HC emission at low loads, and have a declining trend at higher loads.

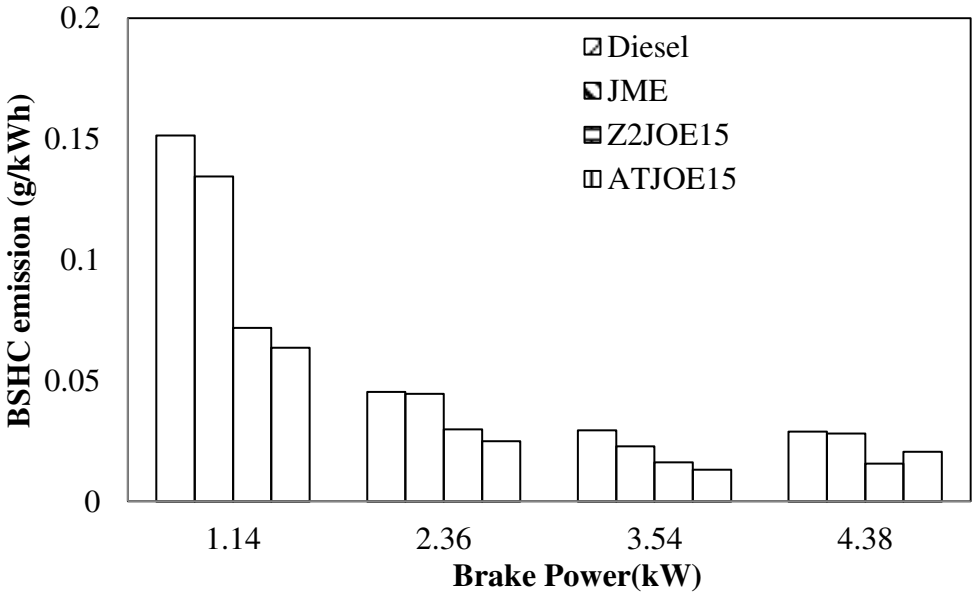

Fig. 5.2.10 Variation of BSHC emissions with brake power

The BSHC emissions are reduced by about 14.2, 45 and 33% for JME, Z2JOE15 and ATJOE15 respectively, at full load compared to that of diesel. The HC emissions of JME are found to be lower than that of diesel since, the higher oxygen content of JME leads to more complete burning than that of diesel. For ATJOE15 emulsion, due to inferior combustion, the HC emissions are found to be higher than that of Z2JOE15 emulsion.

5.2.4.2 BSCO emissions

Figure 5.2.11 describes the comparison of the brake specific carbon monoxide (BSCO) emissions of all the test fuels. Generally, the CO emissions are formed as a result of incomplete combustion of fuel. However, if the combustion is complete, CO will be oxidized into CO_2 [173].

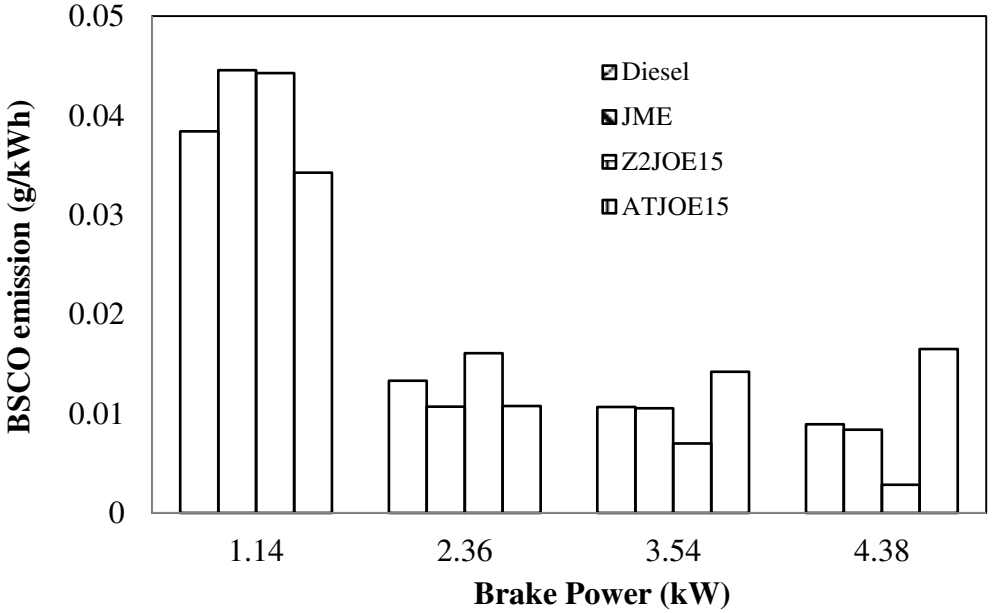

Fig. 5.2.11 Variation of BSCO emissions with brake power

The CO emission is formed when there is a lack of oxygen during combustion, either near full load, or sometimes also at low loads, when there is poor mixing of the fuel with air. It is observed that the BSCO emissions of Z2JOE15 and ATJOE15 are found to be higher by about 17.5%, and 46%, than that diesel at full load. The longer spray penetration and larger fuel droplets may be the factors for higher CO emissions in the case of emulsions. This reason was supported by Zhou [181], in his research work.

5.2.4.3 BSNO emissions

Figure 5.2.12 depicts the variation of brake specific nitric oxide (BSNO) emissions, with respect to brake power. The NO emissions are formed due to high temperature and oxygen availability conditions. This will facilitate the oxidization of nitrogen, which in turn, created higher NO emissions according to the extended Zeldovich mechanism [182]. It is apparent that the BSNO emissions are found to be higher in the JME operation compared to that of diesel. Due to the high temperature environment and availability of about 10% excess

intrinsic oxygen content in biodiesels, the NO emissions are therefore higher in JME operation compared to that of diesel operation.

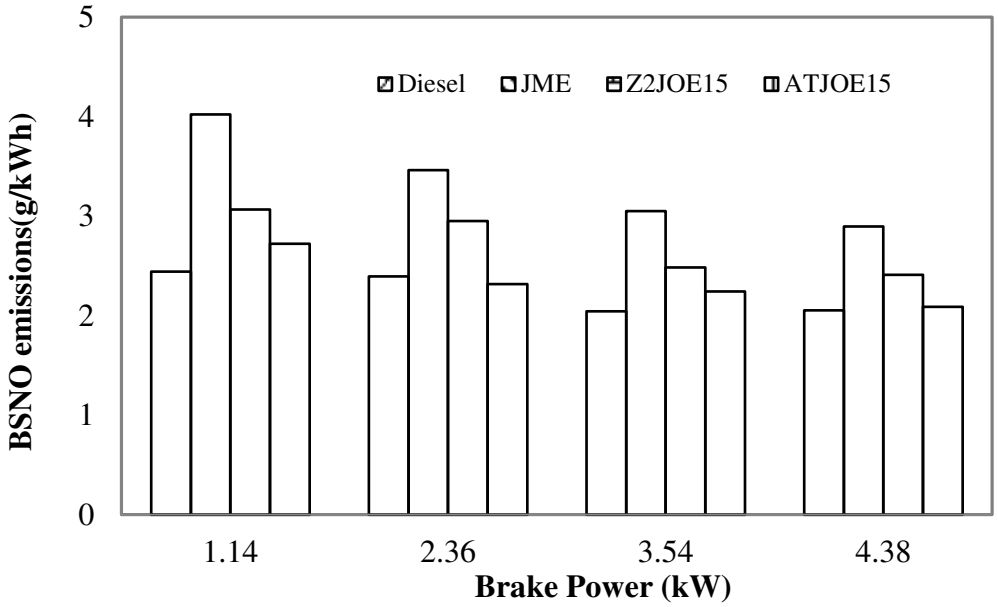

Fig. 5.2.12 Variation of BSNO emissions with brake power

Similar reasons are reported by Szybist et al. [183], in their work on NO_x emissions of alternative diesel fuels: a comparative analysis of biodiesel and FT diesel. It is observed that about 29%, 21.6% and 2% increase in NO emissions is obtained with the JME, Z2JOE15and ATJOE15 respectively, at full load compared to that of diesel. The NO emissions decrease with the addition of WPO in JME, and this may be due to the higher water content in WPO that reduces the combustion temperature. Similar reasons were reported by Bertoli *et al.* [146], for the lower combustion temperature and the NO emissions, when the diesel engine was fueled with the WPO blends or emulsions with diesel.

5.2.4.4 Smoke opacity

Figure 5.2.13 depicts the variation of smoke opacity, with respect to brake power. The smoke opacity of the oxygen enriched fuels with high OH radical concentration, contributes to the reduction of smoke [184]. Good fuel atomisation, better fuel-air mixing and reduction in large droplets, result in a better fuel combustion process; hence, a reduction in smoke opacity. The percentage decrease in the smoke opacity of 19.6% is observed with the JME at full load, in comparison with diesel. When fueled with the Z2JOE15, the smoke opacity is found to be lower by 27.8%, and with the ATJOE15 the smoke opacity increases by about 8%, compared to that of diesel operation.

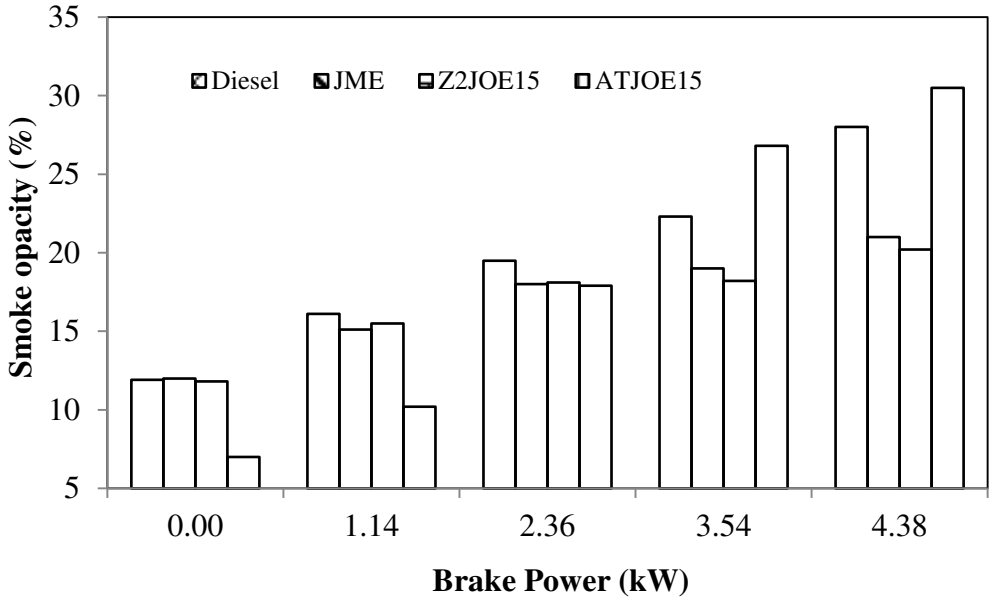

Fig. 5.2.13 Variation of smoke opacity with brake power

When compared to the JME operation, 10% lower smoke is noticed with the Z2JOE15 emulsion, whereas about 30% higher smoke emission is noticed with the ATJOE15 emulsion. The higher smoke opacity may be due to the larger droplets of the ATJOE15 emulsion compared to that of the other tested fuels.

A summary of the combustion, performance and emission parameters at full load for different fuels used in this study is given in Table 5.2.

5.2.5 Closure

The summary of the experimental results on the combustion, performance and emission results in single cylinder diesel engine fueled with ATJOE15 emulsion is as follows:

- The combustion of Z2JOE15 and ATJOE15 emulsions commences earlier than that of diesel at full load. The ignition delay of JME, Z2JOE15 and ATJOE15 is found to be shorter than that of diesel. Lower heat release rates are obtained with the JME and Z2JOE15 and ATJOE15 emulsions compared to that of diesel. A longer combustion duration was observed with ATJOE15 compared to that of diesel, JME and Z2JOE15.
- From the performance aspect, the brake thermal efficiencies of the Z2JOE15 and ATJOE15 emulsions are higher by about 11.3% and 8.2% respectively, than that of diesel, and higher by about 11.6% and 8.5% respectively, than that of JME at full load.

- The BSHC emissions are reduced by about 14.2%, 45% and 33% for JME, Z2JOE15 and ATJOE15 respectively, at full load compared to that of diesel. The BSCO emissions of Z2JOE15 and ATJOE15 are found to be higher by about 17.5%, and 46%, than that of diesel at full load. There is about 29%, 21.6% and 2% increase in the NO emissions, with the JME, Z2JOE15 and ATJOE15 respectively, at full load compared to that of diesel. A percentage decrease in the smoke opacity of 19.6% is observed with the JME at full load, in comparison with diesel. When fueled with the Z2JOE15, the smoke opacity is found to be lower by about 27.8%, and with the ATJOE15 the smoke opacity increases by about 8% compared to that of diesel operation. When compared to JME operation, 10% lower smoke is noticed with the Z2JOE15 emulsion, whereas about 30% higher smoke emission is noticed with the ATJOE15 emulsion.

Table 5.2 Summary of values on combustion, performance and emission parameters at full load for diesel, JME, Z2JOE15 and ATJOE15

Sl.No	Parameter	Diesel	JME	Z2JOE5	ATJOE15
Combustion parameters					
1.	Start of ignition (^{o}CA)	356.6	354	354.0	354.5
2.	Occurrence of maximum pressure (^{o}CA)	372.4	370.4	371.0	371.1
3.	Ignition delay (^{o}CA)	12.7	10.2	10.1	11.2
4.	Occurrence of maximum heat release (^{o} CA aTDC)	6.7	8.2	9.4	9.3
5.	Maximum heat release (J/^{o}CA)	52.02	49.97	51.52	46.4
6.	Maximum cylinder pressure (bar)	75.70	82.61	82.7	76.49
7.	90% Mass fraction burned (^{o}CA)	389.9	387.5	386.9	395.7
8.	Combustion duration (^{o}CA)	38.4	38	36.9	40.6
Performance parameters					
9.	Brake thermal efficiency (%)	30.4	30.3	31.7	32.9
10.	Specific fuel consumption (kg/kWh)	0.269	0.302	0.318	0.3555
11	Exhaust gas temperature (^{o}C)	270	325	305	301
Emission parameters					
12.	BSHC emission (g/kWh)	0.029	0.028	0.018	0.007
13.	BSCO emission (g/kWh)	0.008	0.008	0.005	0.0165
14.	BSNO emission (g/kWh)	2.055	2.898	2.489	2.09
15.	Smoke opacity (%)	28	21	23.1	30.5

5.3 Analysis of the combustion and emission characteristics of a diesel engine fueled with the ATJOE15 emulsion

5.3.1 General

This chapter discusses the development of a mathematical model to validate the experimental results obtained from a single cylinder, four stroke, DI diesel engine fueled with ATJOE15 emulsion. The experimental results were validated with a two zone model, using a MATLAB software program. One zone consisted of pure air called the non-burning zone and the other zone consists of fuel and combustion products called burning zone. The first law of thermodynamics and equations of state were applied in each of the two zones, to get the cylinder temperatures and cylinder pressure histories. Using the two zone combustion model, the combustion parameters and the chemical equilibrium composition were determined theoretically. The extended Zeldovich mechanism was used to predict the NO emissions, while soot density was determined using a semi-empirical model. A comparison of the experimental and theoretical results is also presented in this chapter.

5.3.2 General description of the model

The model deals with a direct injection, bowl-in-piston combustion chamber, into which fuel is injected, in a radial direction, from three holes drilled symmetrically on the injector tip. The model is a two-zone thermodynamic model. The cylinder contents comprise a non-burning zone of air, and another burning zone in which fuel is continuously supplied from the injector holes during injection, and burned with the entrained air from the air zone. The model includes only those processes occurring during the portions of the compression and expansion strokes, when both the inlet and exhaust valves are closed (closed cycle). The compression process in real engines is a polytropic one, which starts from the moment the inlet valve closes, and ends when the injection process starts. The fuels considered are diesel ($C_{12}H_{26}$), JME ($C_{7.56}H_{13.89}N_{0.01}O_{0.81}$) and ATJOE15 ($C_{2.08}H_{4.13}N_{0.01}S_{0.01}O_{1.17}$). The volumetric composition of the ATJOE15 fuel used in this investigation is 15% WPO, 81% JME and 4% of mixed surfactant Span 80 and Tween 80. The main calculation procedure is based on the integration of the first law of thermodynamics, and the perfect gas state equation combined with the various sub-models.

5.3.2.1 Energy equations

During the compression stroke, only one zone (of pure air) exists. Then, the first law of thermodynamics for a closed system is applied, together with the perfect gas state equation [155]. The change in internal energy can be expressed as follows:

$$\frac{d(mu)}{d\theta} = \frac{dQ_r}{d\theta} - \frac{dQ_h}{d\theta} - \frac{dW}{d\theta} \tag{5.1}$$

By replacing the work transfer term $\frac{dW}{d\theta}$ with $P\frac{dV}{d\theta}$ or by the ideal gas law PV = m RT, the above equation (1) can be rearranged as

$$\mathrm{m}\frac{du}{d\theta} = \frac{dQ_r}{d\theta} - \frac{dQ_h}{d\theta} - P\frac{dV}{d\theta} \tag{5.2}$$

where, V is the instantaneous cylinder volume with respect to the crank angle, which is given by,

$$\mathrm{V}=\mathrm{V_{cl}}+\left(\frac{\pi \mathrm{D}^2}{4}\right)\mathrm{r}[1+\lambda^{-1}-cos\phi-\sqrt{\lambda^{-2}-sin^2\phi}] \tag{5.3}$$

In the above equations, the term dQ is given as the fourth order polynomial expressions of the absolute temperature T, including the enthalpy of formation at absolute zero [155].

Internal energy calculation as a function of temperature:

$$\frac{\mathrm{hi}}{\mathrm{RmolT}} = \mathrm{ai1} + \frac{\mathrm{ai2}}{2}\mathrm{T} + \frac{\mathrm{ai3}}{3}\mathrm{T}^2 + \frac{\mathrm{ai4}}{4}\mathrm{T}^3 + \frac{\mathrm{ai5}}{5}\mathrm{T}^4 + \frac{\mathrm{ai6}}{\mathrm{T}} \tag{5.4}$$

$u_i = h_i - RT$

For the surrounding air zone, which only loses mass (air) to the burning zone, the first law of thermodynamics for the unburned zone is written as

$$dE = dQ - pdV - h_a dm_a \tag{5.5}$$

The burning zone not only receives mass from the air zone, but also there is an enthalpy flow from the fuel, which is ready to be burned in the time step. So, the first law of thermodynamics for the burning zone becomes

$$dE = dQ - pdV + h_a dm_a + h_f dm_f \tag{5.6}$$

The first law of thermodynamics for the combustion in time step dt is

$$f(E)=E(T2) - E(T1) - dQ + dW + dm_f\, Qvs = 0 \tag{5.7}$$

If f(E) is greater than the accuracy required the new value of T_2 is calculated using the Newton-Raphson numerical method. The unburned zone temperature is calculated using the equation,

$$T_u = T_{soc}\left(\frac{P}{P_{soc}}\right)^{(\gamma-1)/\gamma} \quad (5.8)$$

5.3.2.2 Heat transfer model

The heat transfer between the cylinder trapped mass and surrounding walls is calculated, using the formula of Anand [185]. The Anand formula to calculate heat loss from the cylinder, is

$$\frac{dQ}{dt} = aK\frac{\mathrm{Re}^b}{d}(T_g - T_w) + c(T_g{}^4 - T_w{}^4) \quad (5.9)$$

In this equation 'Tw' is the cylinder wall temperature which is assumed as 450 K and a, b, c are constants. The constant values are taken as, a=0.2626, b=0.6, c=5.67×10^{-8} W/m^2K^4.

5.3.2.3 Ignition Delay

The time delay between the start of injection and the start of combustion is defined as the ignition delay period. The determination of the start of combustion (SOC) by selecting the proper method is a key issue in ignition delay studies. In the combustion model, the ignition delay is also taken into account. The ignition delay period is calculated by integrating Wolfer's relation, using the trapezoidal rule.

$$\int_{t_{inj}}^{t_{ign}} \frac{dt}{t(p,T)} = \frac{1}{K\ \mathrm{tinj}} \int_{t_{inj}}^{t_{ign}} \frac{dt}{(p(t))^{-q}\exp(E/RT(t))} = 1 \quad (5.10)$$

The values of various constants corresponding to a D.I. diesel engines are K =2272; q =-1:19;

E/R = 4650.t_{inj}.

5.3.2.4 Wiebe's combustion model

The Wiebe function is used to predict the mass fraction burn, and the burn rate in internal combustion engines, operating with different combustion systems and fuels [186]. Wiebe [187] linked the chain chemical reactions with the fuel reaction rate in internal combustion engines, and his approach was based on the premise that a simple one-step rate equation would not be adequate to describe the complex reacting systems, such as those occurring in an internal combustion engine. The Wiebe functions for the non-dimensional burn fraction x and its derivative w (burn rate) as functions of the degrees of crank angle can be written as

$$x=1-e^{-6.908(\phi/\phi d)^{m+1}} \quad (5.11)$$

$$w=\frac{dx}{d\phi}=\frac{6.908(m+1)}{\phi d}\left(\frac{\phi}{\phi d}\right)^{m}e^{-6.908(\phi/\phi d)^{m+1}} \quad (5.12)$$

The non-dimensional burn fraction x and its derivative w (burn rate) as functions of time t can also be written as:

$$x=1-e^{-6.908(t/td)^{m+1}} \quad (5.13)$$

$$w=\frac{dx}{dt}=\frac{6.908(m+1)}{td}\left(\frac{t}{td}\right)^{m}e^{-6.908(t/td)^{m+1}} \quad (5.14)$$

The time it takes to reach the maximum burn rate t_m can be found by the differentiating equation (14) and equating the result to zero

$$t_m=t_d\left(\frac{m}{6.908(m+1)}\right)^{1/(m+1)} \quad (5.15)$$

The corresponding burn fraction is

$$X_m=1-\exp\left(-6.908(t_m/t_d)^{m+1}\right) \quad (5.16)$$

From above equations (13) and (14)

$$X_m=1-\exp\left(-m/(m+1)\right) \quad (5.17)$$

Wiebe suggested the physical meaning of the exponent m which was based on equation (5.15), which shows that, for a given combustion duration, the time it takes for a maximum burn rate to be reached is determined solely by the magnitude of m, which, in turn, determines the magnitude of the maximum burn rate from equation (5.15).When calculating the heat release, prior knowledge of the actual overall equivalence ratio is necessary. The term equivalence ratio is defined as the ratio of the actual air-fuel ratio to the stoichiometric air-fuel ratio. This helps in fixing the mass of fuel to be admitted.

5.3.2.5 Chemistry of combustion

In a combustion process, the fuel and the oxidizer react to produce products of different composition. The theory of combustion is a complex one, and has been the topic of intensive research for many years. Let us represent the chemical formula of a fuel as $C_\alpha H_\beta O_\gamma N_\delta$. In the

present case, it was considered that 10 species were present in the combustion product, and the combustion equation is given by:

$$\epsilon\varphi C_\alpha H_\beta O_\gamma N_\delta + 0.21O_2 + 0.79N_2 \longleftrightarrow \nu_1 CO_2 + \nu_2 H_2O + \nu_3 N_2 + \nu_4 O_2 + \nu_5 CO + \nu_6 H_2 + \nu_7 H + \nu_8 O + \nu_9 OH + \nu_{10} NO \quad (5.18)$$

From the atomic balance of each species C- H- O- N the following 4 equations, are obtained.

$$C \quad \epsilon\varphi\alpha = (y_1+y_5)\ N1 \quad (5.19)$$

$$H \quad \epsilon\varphi\beta = (2y_1+2y_6+y_7+y_9)\ N1 \quad (5.20)$$

$$O \quad \epsilon\varphi\gamma+0.42 = (2y_1+y_2+2y_4+y_5+y_8+y_9+y_{10})\ N1 \quad (5.21)$$

$$N \quad \epsilon\varphi\delta+1.58 = (2y_3+y_{10})\ N1 \quad (5.22)$$

By definition, the total number of mole fraction is unity.

$$\sum_{i=1}^{10} yi - 1 = 0 \quad (5.23)$$

The chemical reactions considered in equilibrium, are as follows:

$$0.5H_2 \longleftrightarrow H \quad (5.24)$$

$$0.5O_2 \longleftrightarrow O \quad (5.25)$$

$$0.5H_2+0.5O_2 \longleftrightarrow OH \quad (5.26)$$

$$0.5O_2+0.5N_2 \longleftrightarrow NO \quad (5.27)$$

$$H_2+0.5O_2 \longleftrightarrow H_2O \quad (5.28)$$

$$CO+0.5O_2 \longleftrightarrow CO_2 \quad (5.29)$$

The use of the equilibrium constant is identical to maximizing the entropy of the gas. This method is similar, when considering a restricted species list such as the present case. The compositions of all the species were found, using the method developed by Olikara and Borman [188]. Once the composition is known, the thermodynamic properties of interest like enthalpy, entropy, specific volume and internal energy, can be computed.

5.3.3 The nitric oxide formation model

The current approach to model the NO_x emissions from diesel engines is, to use the extended Zeldovich thermal NO mechanism, by neglecting other sources of NO_x formation. The extended Zeldovich mechanism consists of the following reactions,

$O + N_2 \longleftrightarrow NO + N$ (5.30)

$N + O_2 \bullet \longleftrightarrow NO + O$ (5.31)

$N + OH \longleftrightarrow NO + H$ (5.32)

This mechanism can be written as an explicit expression for the rate of change of the concentration of NO [10]:

The change of NO concentration is expressed as follows:

$$\frac{d\,(NO)}{dt} = 2\,(1-\alpha^2)\,\frac{R1}{1+\,\alpha R1/(R2+R3)} \tag{5.33}$$

where Ri is the one-way equilibrium rate for reaction i, defined as

$R1 = k_{1f}\,(N)_e(NO)_e,\;\; R2 = k_{2f}\,(N)_e(O_2)_e,$ (5.34)

$R3 = k_{3f}\,(N)_e(OH)_e,\quad \alpha = (NO)/(NO)_e$ (5.35)

5.3.4 The net soot formation model

The exhaust of the CI engines contains solid carbon soot particles that are generated in the fuel rich regions inside the cylinder during combustion. Soot particles are clusters of solid carbon spheres, with the HC and traces of other components absorbed on the surface. They are generated in the combustion chamber in the fuel rich zones, where there is not enough oxygen to convert all the carbon to CO_2. Subsequently, as the turbulence motion continues to mix the components, most of these carbon particles find sufficient oxygen to react and form CO_2.Thus soot particles are formed and consumed simultaneously in the combustion chamber.

The net soot formation rate was calculated, by using the semi-empirical model proposed by Hiroyasu et. al. [189]. According to this model the soot formation rate (index sf) and soot oxidation rate (index so) were given by

$$\frac{dm_{sf}}{\mathrm{dt}} = A_{sf}\,dm_f^{0.8}\,p^{0.5}\exp\left(-\frac{E_{sf}}{R_{mol}T}\right) \tag{5.36}$$

$$\frac{dm_{so}}{dt} = A_{so}\,m_{sn}\left(\frac{p_{o_2}}{p}\right)p^{n}\exp\left(-\frac{E_{so}}{R_{mol}T}\right) \tag{5.37}$$

where, the pressures are expressed in bar, dm_f is the unburned fuel mass in kg to be burned in time step dt. Therefore, the net soot formation rate is expressed as

$$\frac{dm_{sn}}{dt} = \frac{dm_{sf}}{dt} - \frac{dm_{so}}{dt} \tag{5.38}$$

A computer program using the MATLAB software was generated, with all the above mentioned equations, and considering all the values of constants, in order to predict the combustion attributes, like in-cylinder pressure, crank angle, heat release rate, heat losses and the NO emissions. The MATLAB program used for this analysis is given in Annexure 8.

5.3.4 Validation of results

5.3.4.1 Pressure-crank angle diagram

Figure 5.3.1 shows the measured and computed pressure trace and crank angle histories for the fuels tested at full load condition. In a CI engine, the cylinder pressure depends on the burned fuel fraction during the premixed burning phase, which is the initial stage of combustion, and the ability of the fuel to mix well with the air and burn. The high peak pressure and maximum rate of pressure rise correspond to the large amount of fuel burned in the premixed stage.

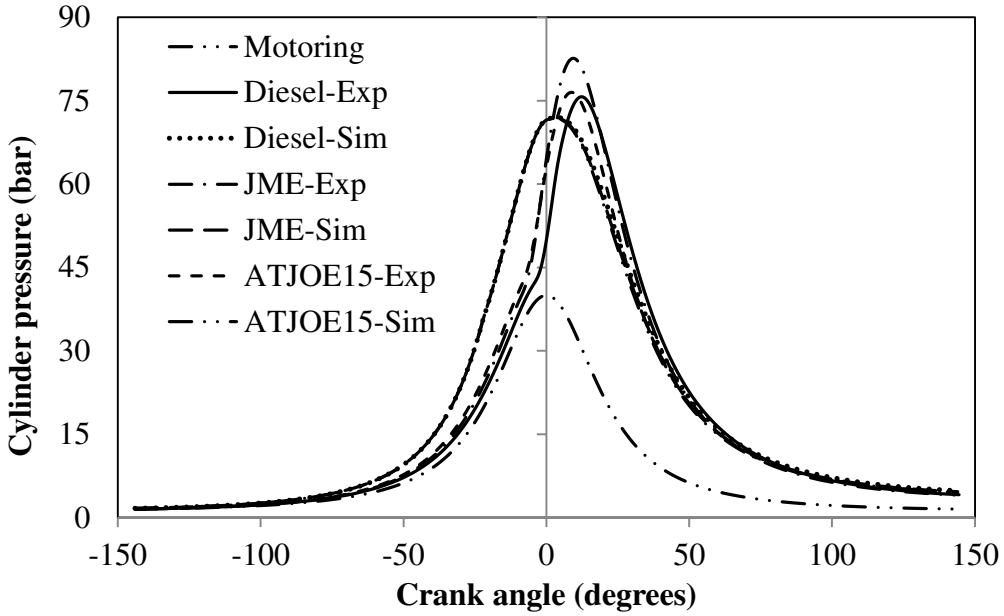

Fig. 5.3.1 Variation of cylinder pressure with crank angle at full load

It is observed from the experimental results that the peak pressures for diesel, JME and ATJOE15 are found to be 75.72, 82.61 and 76.49 bar respectively, at full load. For the simulated conditions, the peak pressure values are noticed to be 71.99, 71.85 and 71.76 bar respectively. It is observed from the figure that the combustion commences earlier by about 2.6^{o}, and 2.2^{o} for the JME, and ATJOE15 respectively, compared to that of diesel at full load. This may be due to the advanced injection timing, as a result of the higher bulk modulus and

higher density of biodiesel and shorter ignition delay. Similar results are reported by Gumus [178] in his investigation, on the combustion and heat release characteristics of a hazelnut kernel oil methyl ester fueled DI diesel engine. Also, the peak cylinder pressures of the JME and ATJOE15 are marginally higher than that of diesel, as a result of high viscosity and low volatility.

5.3.4.2 Apparent or net heat release rate

Figure 5.3.2 depicts the variation in the apparent heat release, with respect to the crank angle for the different fuels tested. The term apparent or net heat release rate is determined by deducting the heat transfer to the cylinder walls, crevice volume, blow-by and the fuel injection effects from the heat energy liberated by burning the fuel. The experimental results of the maximum net heat release rate for diesel, JME and ATJOE15 are found to be about 52.01, 49.97 and 46.4 J/^{o}CA respectively at full load condition. Under simulated conditions, the values are found to be about 54.20, 49.93 and 47.31 J/^{o}CA for diesel, JME and ATJOE15 respectively.

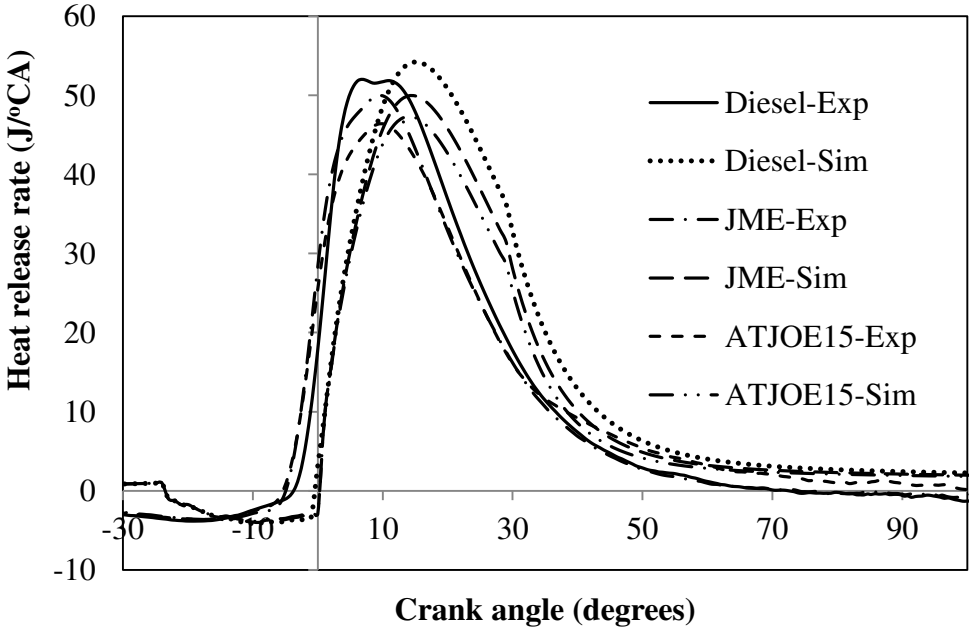

Fig. 5.3.2 Variation of maximum heat release rate with crank angle

For the JME and ATJOE15, less amount of fuel is accumulated during the shorter ignition delay period, which results in lower heat release rates compared to that of diesel at full load. The reasons are in agreement with those of Qi et al [168], when the diesel engine was fueled with ethanol-biodiesel-water micro emulsions. The oxygen present in JME and the quick

evaporation of the emulsified fuel ATJOE15 are the causes for the faster burning process [190].

5.3.4.3 Heat loss

The predicted results of the heat losses are shown in Fig.5.3.3. The difference between the heat energy available in the fuel and the apparent or net heat release gives the heat loss. A part of the released heat is lost to the cooling medium, through the walls of the cylinder and the cylinder head during the combustion and expansion processes.

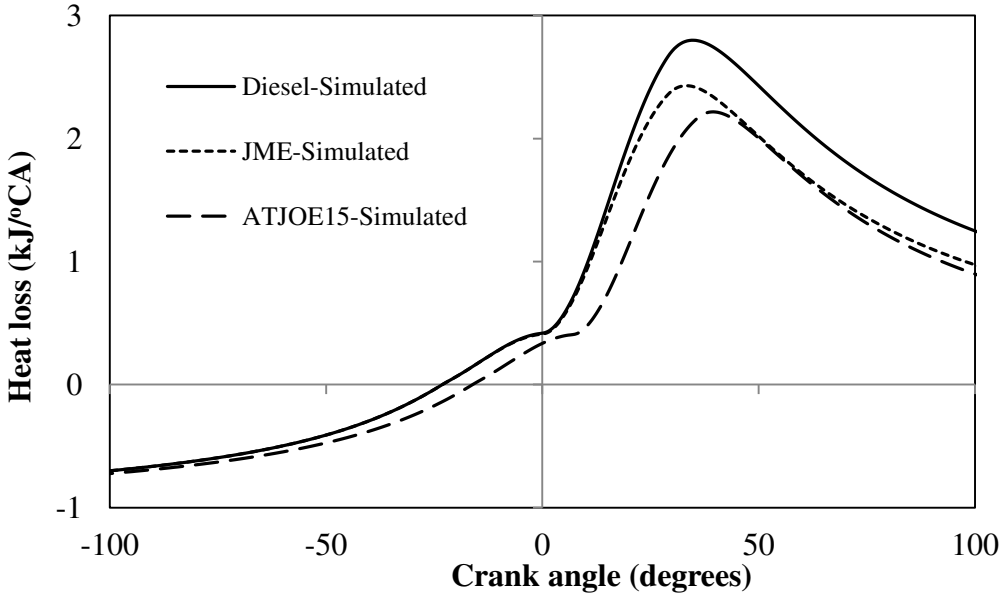

Fig. 5.3.3 Variation of heat losses with crank angle

A small fraction of the heat energy of the fuel is lost, as a result of the dissociation of some combustion products and incomplete chemical reactions. The heat losses due to incomplete combustion, gas leakage and dissociation are usually ignored, and the heat transfer losses by convection and radiation are estimated using empirical correlations [191]. In this case, the radiation component was not taken into consideration.

5.3.4.4 NO emissions

In the diesel engine exhaust, the NO_x emission is predominantly composed of NO, with lesser amounts of NO_2. Other oxides of nitrogen, such as N_2O, N_2O_5, NO_3 are negligible. In general, the NO_x formation mechanisms are described as thermal NO_x, prompt NO_x and fuel NO_x. Under most diesel engine combustion conditions, thermal NO_x is believed to be the predominant contributor to total NO_x. At high temperatures, occurring within the combustion chamber of a diesel engine, N_2 and O_2 can react through a series of chemical steps, known as

the Zeldovich mechanism. The NO_x formation occurs at temperatures above 1500 °C, and the rate of formation increases rapidly with increasing temperature [176]. Figure 5.3.4 depicts the comparison of NO emissions for the tested fuels, in both the experimental and simulated conditions. The experimental results of NO emissions at full load condition for diesel, JME and ATJOE15 are 2.05, 2.89, and 2.09 g/kWh respectively. In the case of simulated conditions, the NO values are found to be about 2.57, 2.822, and 2.112 g/kWh respectively, for the above said fuels.

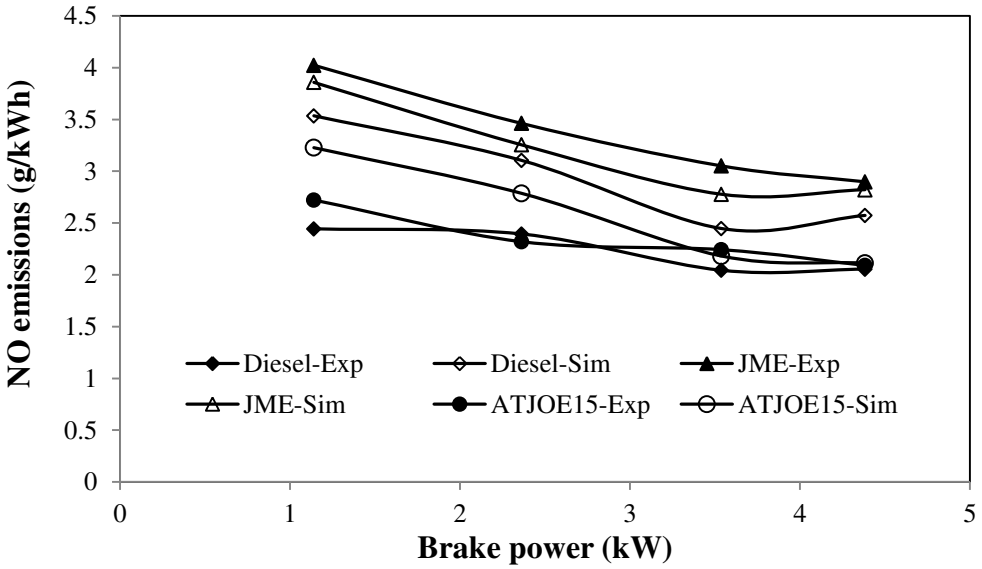

Fig. 5.3.4 Variation of NO emissions with brake power

It can be observed from the figure, that the NO emissions of the JME operation are higher, compared to those of ATJOE15 emulsion as well as diesel operation. The presence of the oxygen molecule in biodiesel causes an increase in the combustion gas temperature resulting in a marginal increase in the NO emissions. Also, it can be observed that the NO emission decreases with the addition of WPO content in the emulsions. This may be due to the water content present in the WPO, which will reduce the combustion temperature [146].

Figure 5.3.5 depicts the NO concentration with respect to the crank angle at full load under simulated conditions. It can be seen that the NO emission increases after the ignition, and reaches the maximum around 27^o aTDC, and then lasts until EVO (exhaust valve opening). The NO concentration is higher in the case of JME operation, and lower in the case of the ATJOE15 operation, in comparison with diesel data. The reduction in the NO concentration of the ATJOE15 may be due to the following two reasons.

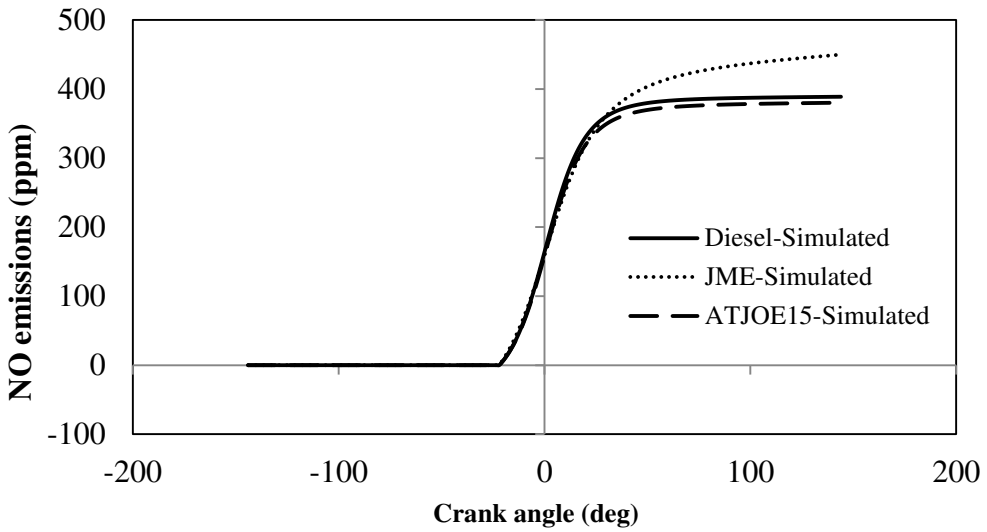

Fig. 5.3.5 Variation of NO concentration with crank angle at full load

First, the in-cylinder temperature decreases, because of the higher specific heat capacity of water available in the WPO. Secondly, the water content in the WPO results in the reduction of N_2 and O_2 concentrations and the improvement of the local rich oxygen [146].

5.3.4.5 Soot density

The variation in the soot density with brake power for both the experimental and simulated conditions is given in Fig. 5.3.6.

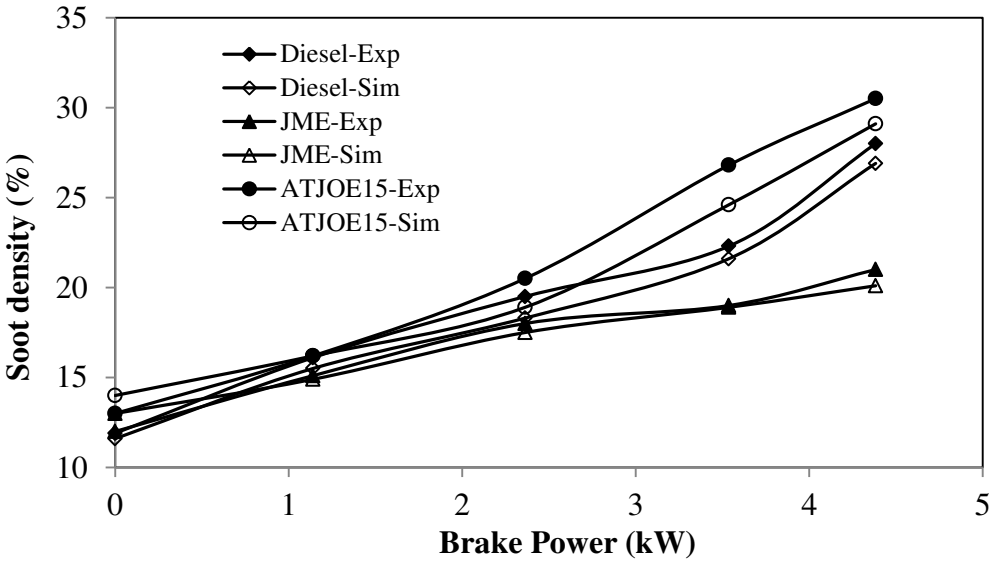

Fig. 5.3.6 Variation of soot density with brake power

Based on the experimental results, the percentage decrease in the soot density of 19.6% is observed with the JME at full load, in comparison with diesel. When fueled with the ATJOE15, the soot density increases by about 8% compared to that of diesel operation.

Under simulated conditions, the soot density is found to be lower for the JME operation by 25.2%, compared to that of diesel, and with the ATJOE15 emulsion, about 8% higher soot density is noticed. The higher soot density may be due to the larger droplets of the ATJOE15 emulsion compared to that of the other tested fuels.

5.3.5 Closure

In the present work, a comprehensive two zone model has been developed for a diesel engine, to validate the experimental results obtained with three different fuels, viz. diesel, JME and ATJOE15. The experimental investigation was conducted on a DI diesel engine. The results reveal that the developed model predicts adequately well, the combustion parameters for the three fuels examined. The conclusions of the results obtained from this study are as follows:

- The experimental and simulated results show that the peak cylinder pressures of the JME and the ATJOE15 are found to be marginally higher than that of diesel, and about 6.1% lower peak cylinder pressures are obtained with the ATJOE15 emulsion at simulated conditions compared to that of experimental conditions.
- The maximum heat release rates of JME and ATJOE15 are found to be lower than that of diesel fuel, in both the experimental and simulated conditions. Compared to experimental conditions, the maximum heat release rate of the ATJOE15 at simulated conditions is found to be lower by 1.96%.
- Compared to diesel operation, the NO concentration is found to be higher in the case of JME operation, and lower in the case of the ATJOE15 operation at both experimental and simulated conditions. With the simulated conditions, the NO emissions of the ATJOE15 emulsion are found to be higher by 1% compared to that of experimental conditions.
- The soot density is found to be lower for the JME operation and it is higher for the ATJOE15 operation compared to that of diesel. The soot density of the ATJOE15 emulsion at simulated condition is found to be lower by about 4.5% than that of experimental condition.

The presented model can predict the combustion characteristics such as cylinder pressure and heat release which are in good agreement with the experimental results.

5.4 Combined effects of the compression ratio and injection timing on the performance and emission parameters of a diesel engine fueled with the ATJOE15 emulsion

5.4.1 General

From the summary of the experimental results of the combustion, performance and emission characteristics of the single cylinder diesel engine fueled with the ATJOE15 emulsion, it is observed that the CO and NO emissions from ATJOE15 fueled engine are higher than that of diesel operation. In order to reduce the diesel engine pollutants, it is proposed to study the combined effects of varying the compression ratio and injection timing. Three different compression ratios (16.5, 17.5 and 18.5) and three injection timings (21.5, 23 and 24.5) are chosen for this study. The nozzle opening pressure is maintained at 200 bar. The results obtained are compared with those of diesel and JME operation, and discussed in this chapter.

5.4.2 Combustion parameters

5.4.2.1 Pressure crank angle history

Figure 5.4.1 depicts the pressure crank angle history of the engine fueled with the ATJOE15 emulsion, running at different compression ratios and injection timings at full load condition. It is observed from the figure, that the combustion starts earlier in the range between 1 and 4 ^{o}CA for the ATJOE15 emulsion, with the compression ratios of 17.5, 18.5 and at all three injection timings, compared to that of diesel at full load. For the same operating conditions, compared to the JME operation, it is found that the combustion starts earlier by about 0.5 to 1.5 ^{o}CA for the ATJOE15 emulsion at injection timings of 23 and 24.5 ^{o}CA. At a lower compression ratio of 16.5, it is found that the commencement of combustion is later by 0.5 to 3.5 ^{o}CA in comparison with diesel operation. The peak cylinder pressure for diesel occurs at 12.4 ^{o}CA aTDC, whereas for the ATJOE15 emulsion, the peak pressure occurs earlier in the range of 0.5 and 3 ^{o}CA, with the compression ratios of 17.5 and 18.5, at injection timings of 23 and 24.5 ^{o}CA bTDC compared to that of diesel. At a lower compression ratio of 16.5 and at retarded injection timing, the peak cylinder pressure is found to be lower in the range of 4 to 13 bar compared to that of diesel operation at full load. Similar results are reported by Kannan and Anand [192] in their investigation of a diesel engine, fueled with biodiesel obtained from waste cooking oil. It is seen from the figure, that among all the tested compression ratios and injection timings, with the compression ratio of 18.5 and advanced injection timing of 24.5 ^{o}bTDC, the ATJOE15 operation produced the highest cylinder pressure value of 85.8 bar at 369.5 ^{o}CA, which is earlier by 2.9 and 1 ^{o}CA than those of diesel

and the JME operations respectively. The early or later occurrences of the ignition are attributed to the increased or decreased cylinder gas temperature respectively.

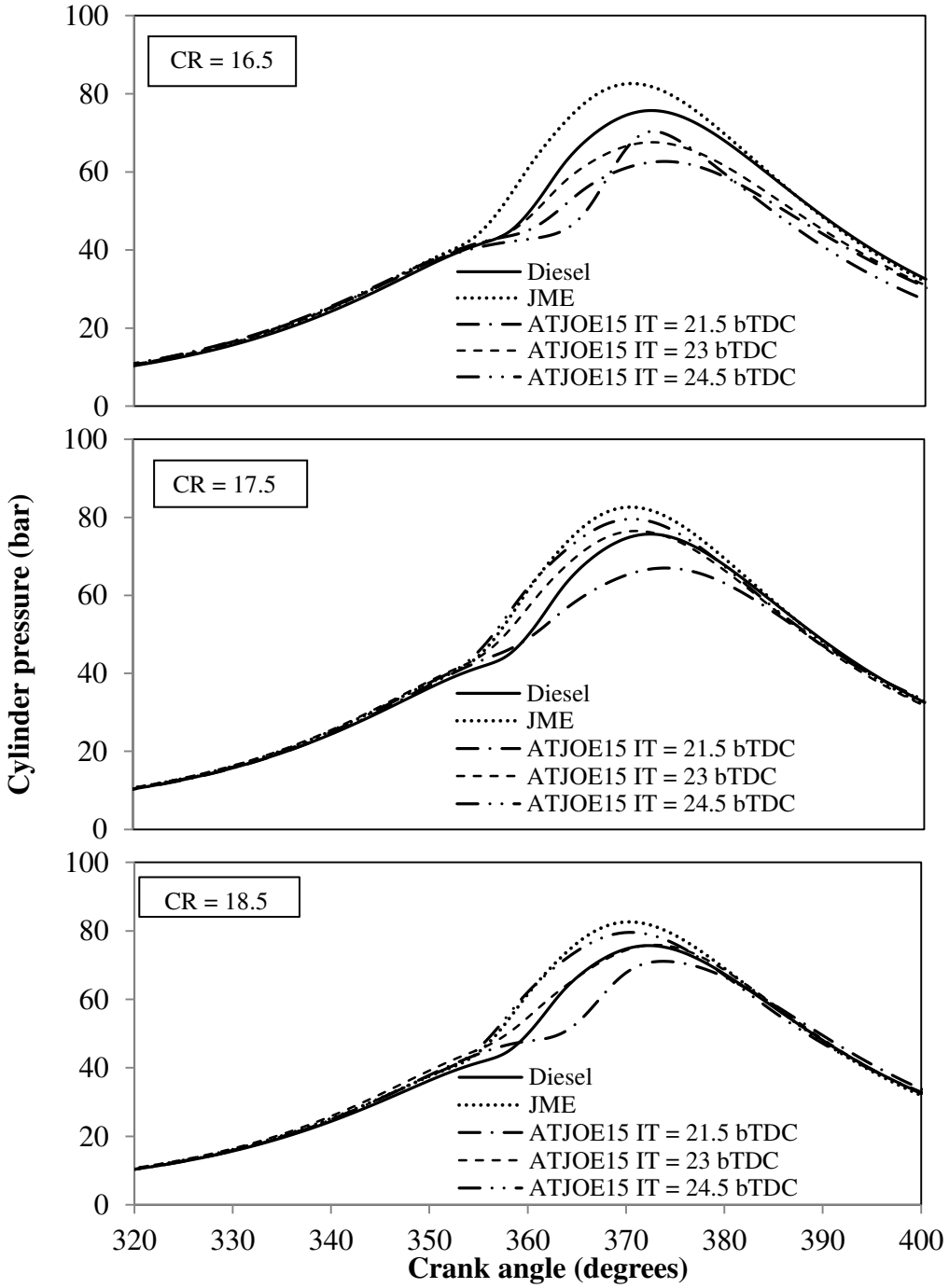

Fig. 5.4.1 Variation of cylinder pressure with crank angle at different compression ratios and injection timings

5.4.2.2 Ignition delay

Figure 5.4.2 depicts the ignition delay for diesel, JME and ATJOE15 for different compression ratios and injection timings at all loads. It is seen from the figure that the

ignition delay is found to be lower with the increase in the engine load, compression ratio and advancement in the injection timing. The reduction in the ignition delay in these conditions might be the result of a higher combustion chamber wall temperature at the time of injection and the reduced exhaust gas dilution [107].

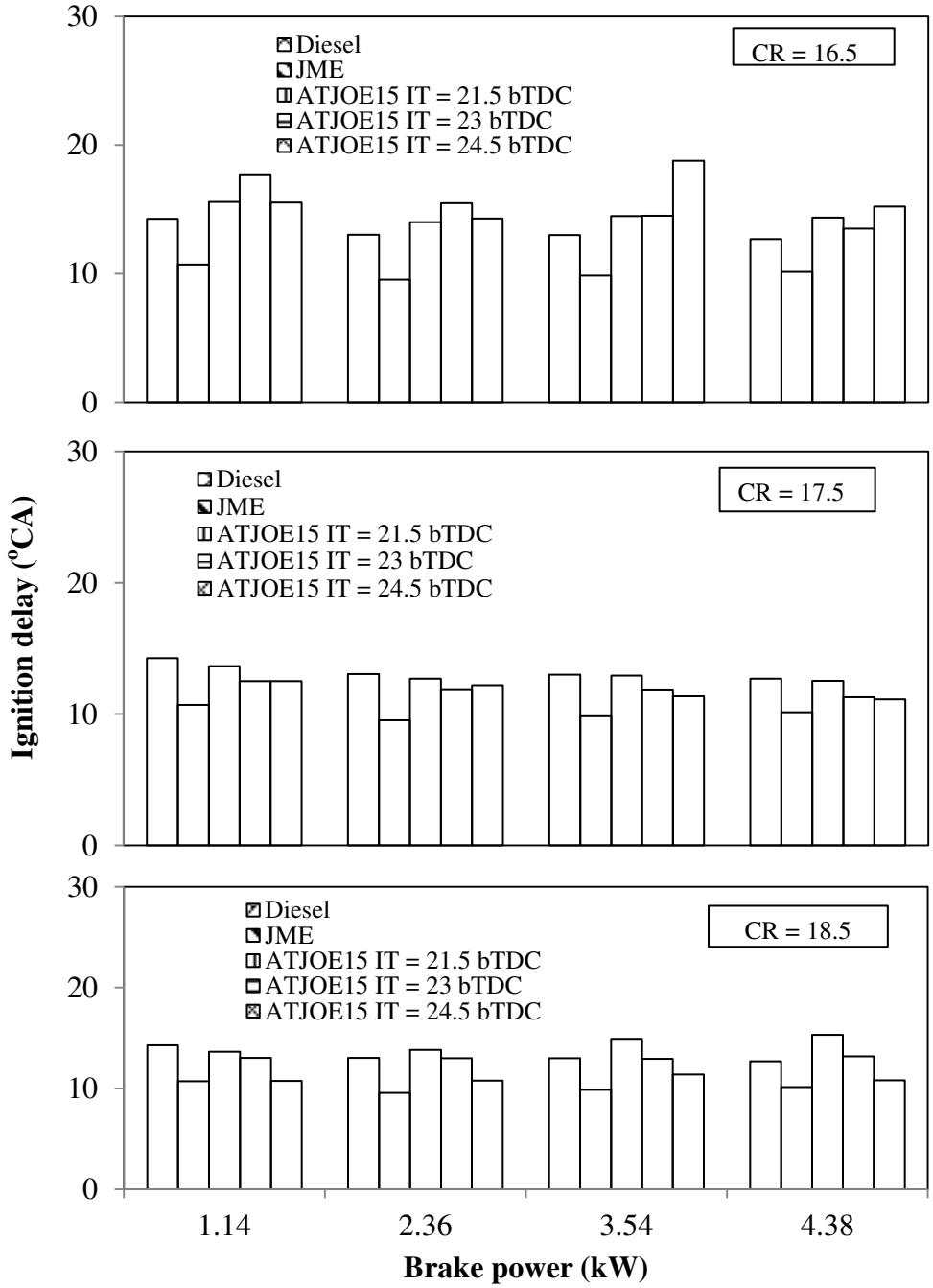

Fig. 5.4.2 Variation of ignition delay with brake power at different compression ratios and injection timings

At the lower compression ratio of 16.5, the ignition delay is found to be higher at an advanced injection timing, also due to the lower cylinder temperature. It is apparent from the figure, that at full load condition, the ignition delay of the ATJOE15 emulsion is found to be

shorter in the range of 0.2 to 1.8 ^{o}CA, with compression ratios of 17.5, 18.5 and the advanced injection timing of 24.5 ^{o}CA bTDC, compared to that of diesel operation. With the lower compression ratio of 16.5 and the retarded injection timing of 21.5 ^{o}CA, the ignition delay values of the ATJOE15 emulsion are found to be longer by about 0.8 to 2.6 ^{o}CA compared to that of diesel operation. In comparison with the JME operation, the engine fueled with the ATJOE15 emulsion exhibits a longer ignition delay at all operating conditions. Among all the tested compression ratios and injection timings, the minimum ignition delay period of 10.81 ^{o}CA is observed for the ATJOE15 operation, with the compression ratio of 18.5 and injection timing of 24.5 ^{o}CA bTDC. The reduction in the ignition delay period is mainly due to the increased cylinder gas temperature, at a higher compression ratio and a higher cetane number of the ATJOE15, compared to that of diesel.

5.4.2.3 Heat release rate

Figure 5.4.3 illustrates the variation of heat release rate, with respect to the crank angle for the ATJOE15 emulsion at full load, for different compression ratios and injection timings. Because of the vaporization of the fuel accumulated during the ignition delay period, at the beginning a negative heat release is observed and after combustion, this behaviour becomes positive. The occurrence of the maximum heat release rate for the ATJOE15 emulsion at different operating conditions on an average, shifted by about 2 to 8 ^{o}CA at full load, compared to that of diesel operation. The intensity of the premixed combustion phase for diesel is found to be the highest, whereas, it is lower in the case of JME and the ATJOE15 emulsion, at compression ratios 17.5, 18.5 and advanced injection timings.

With the lower compression ratio of 16.5, injection timing of 24.5 ^{o}CA bTDC, and compression ratio of 18.5, injection timing of 21.5 ^{o}CA bTDC, the premixed phase of combustion is found to be higher than that of diesel operation. The deviation in the maximum heat release rate between the diesel operation and the ATJOE15 emulsion at different compression ratios and injection timings varies between -14 J/^{o}CA and 15 J/^{o}CA. For the JME and ATJOE15 emulsion, less amount of fuel is accumulated during the shorter ignition delay period, which results in lower heat release rates compared to that of diesel at higher compression ratios.

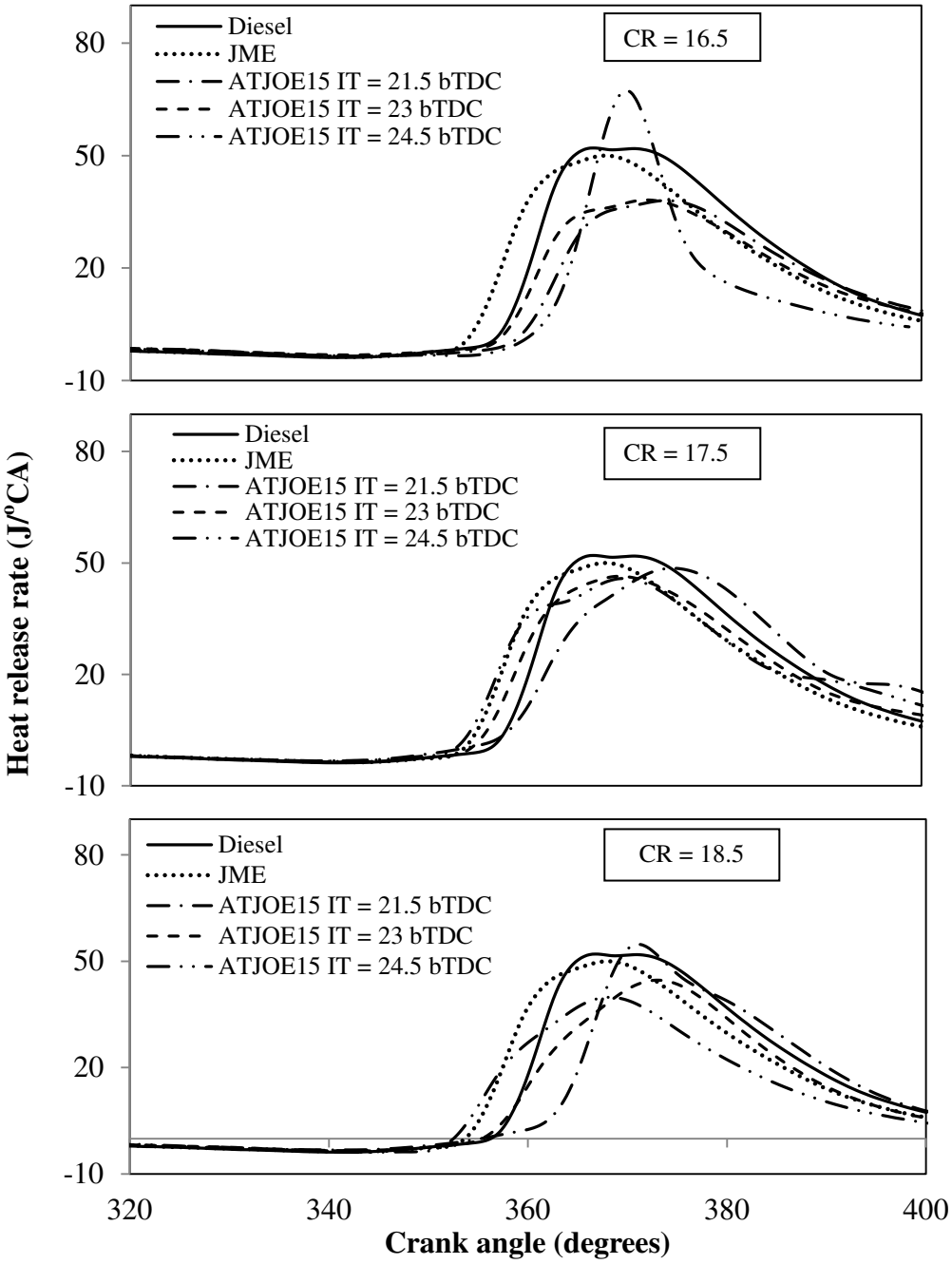

Fig. 5.4.3 Variation of heat release rate with crank angle at different compression ratios and injection timings

5.4.2.4 Maximum cylinder pressure

Figure 5.4.4 depicts the variation of maximum cylinder pressure with brake power for the ATJOE15 emulsion at full load for the different compression ratios and injection timings. It is seen from the figure that the peak cylinder pressure is increased with an increase in the engine load at all operating conditions. With the lower compression ratios, the peak cylinder gas pressure for the JME and diesel is higher than that of the ATJOE15 emulsion at all

injection timings, and at higher compression ratios, the trend is the opposite. This shows that, with higher compression ratios and advanced injection timing, the ATJOE15 emulsion showed faster premixed combustion, which leads to a higher peak cylinder gas pressure.

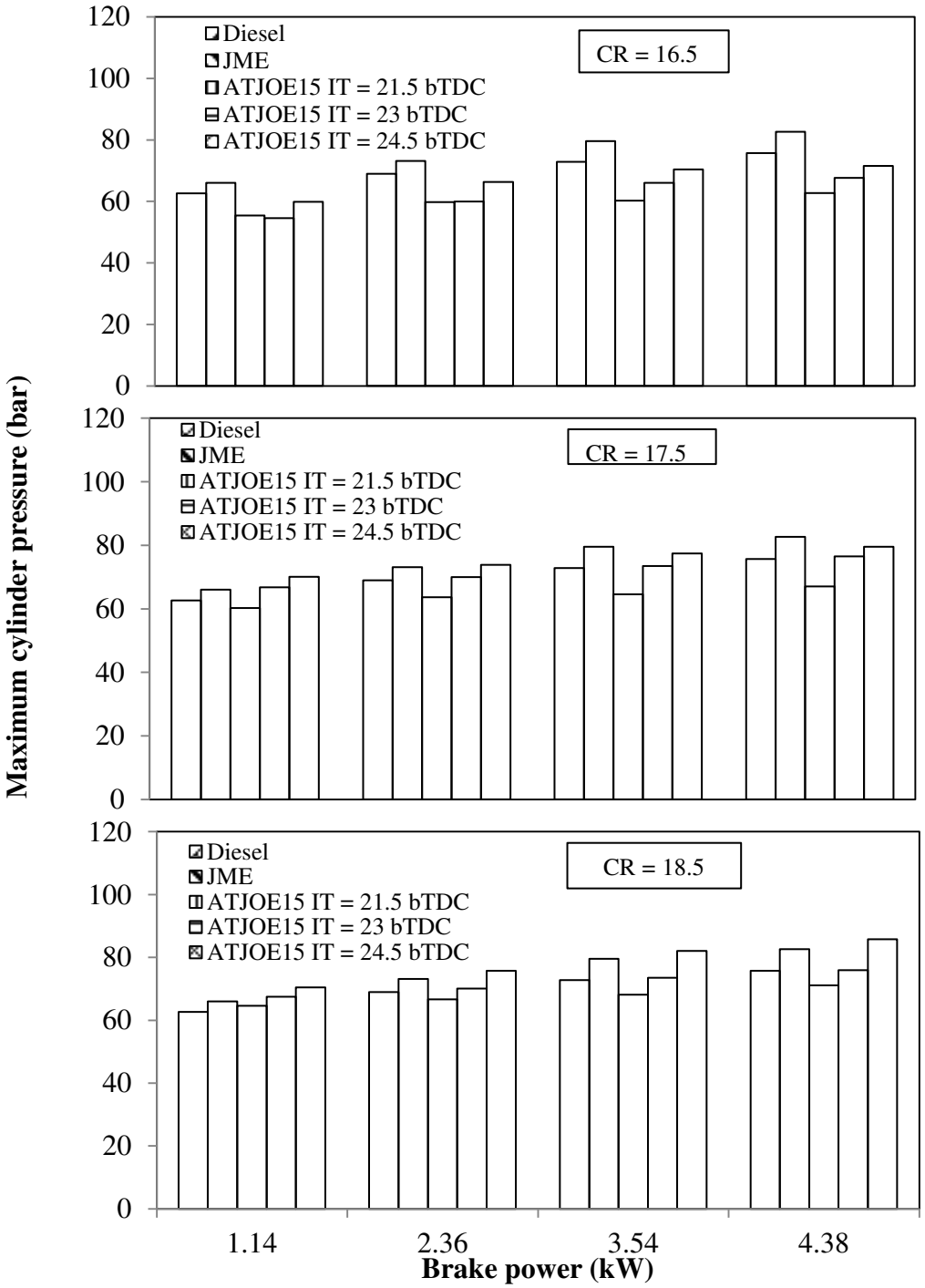

Fig. 5.4.4 Variation of maximum cylinder pressure with brake power at different compression ratios and injection timings

With the compression ratio of 16.5 and all three injection timings, the maximum cylinder pressure of the ATJOE15 emulsion is found to be lower in the range between 4 and 13 bar

compared to that of diesel operation at full load. Also, with the higher compression ratios and retarded injection timing, the maximum cylinder pressure is found to be lower than that of diesel operation. At compression ratios of 17.5, and 18.5, and at standard and advanced injection timings, the maximum cylinder pressure values of the ATJOE15 emulsion are higher in the range of 0.2 to 10 bar compared to that of diesel operation at full load. This may be due to the reduction in the clearance volume, which increases the density of the cylinder gases during the burning process. This increases the peak cylinder pressure and temperature. Except at a compression ratio of 18.5 and advanced injection timing of 24.5 ^{o}CA bTDC, at all other conditions the peak cylinder pressure is found to be lower than that of JME operation.

5.4.2.5 Combustion duration

Figure 5.4.5 illustrates the variation of the combustion duration with the brake power, under different compression ratios and injection timings of the engine fueled with the ATJOE15 emulsion, JME and diesel. The duration between the starting and ending of heat release is called as combustion duration. The combustion duration increases with engine load, owing to the increase of the fuel quantity. It is seen from the figure that the combustion duration decreases with an increase in the compression ratio, which is attributed to the high temperature prevailing inside the cylinder and at lower compression ratios, the trend is the opposite. At a compression ratio 18.5 and at full load, the values of combustion duration are 38.4, 38, 36.08, 37.31 and 37.72 ^{o}CA for diesel, JME and ATJOE15, at injection timings 21.5, 23 and 24.5 ^{o}CA bTDC respectively. The combustion duration of the ATJOE15 is found to be lower between 0.7 and 1.4 ^{o}CA compared to that of diesel at the compression ratio 18.5. At a lower compression ratio of 16.5, the combustion duration of the ATJOE15 emulsion is found to be higher than that of diesel and the JME operation, which is attributed to a longer ignition delay. At 16.5 compression ratio and at different injection timings, the combustion duration of the ATJOE15 emulsion, is found to be higher in the range of 2.83 to 9.06 ^{o}CA and 2.87 to 9.46 ^{o}CA compared to that of diesel and the JME respectively.

At the standard compression ratio of 17.5 and at different injection timings, the combustion duration of the ATJOE15 emulsion is found to be higher between 0.3 and 3.5 ^{o}CA and 0.7 and 3.9 ^{o}CA, compared to that of diesel and the JME respectively. As the calorific value of the ATJOE15 emulsion is lower than that of diesel, a greater quantity of fuel is consumed to maintain the engine speed constant at various loads. Hence, the higher total fuel consumption is the cause for the longer combustion duration of the ATJOE15emulsion than that of diesel.

Similar reasons are reported by Arulmozhi selvan et al. [193] in their work on diesel-biodiesel-ethanol blends.

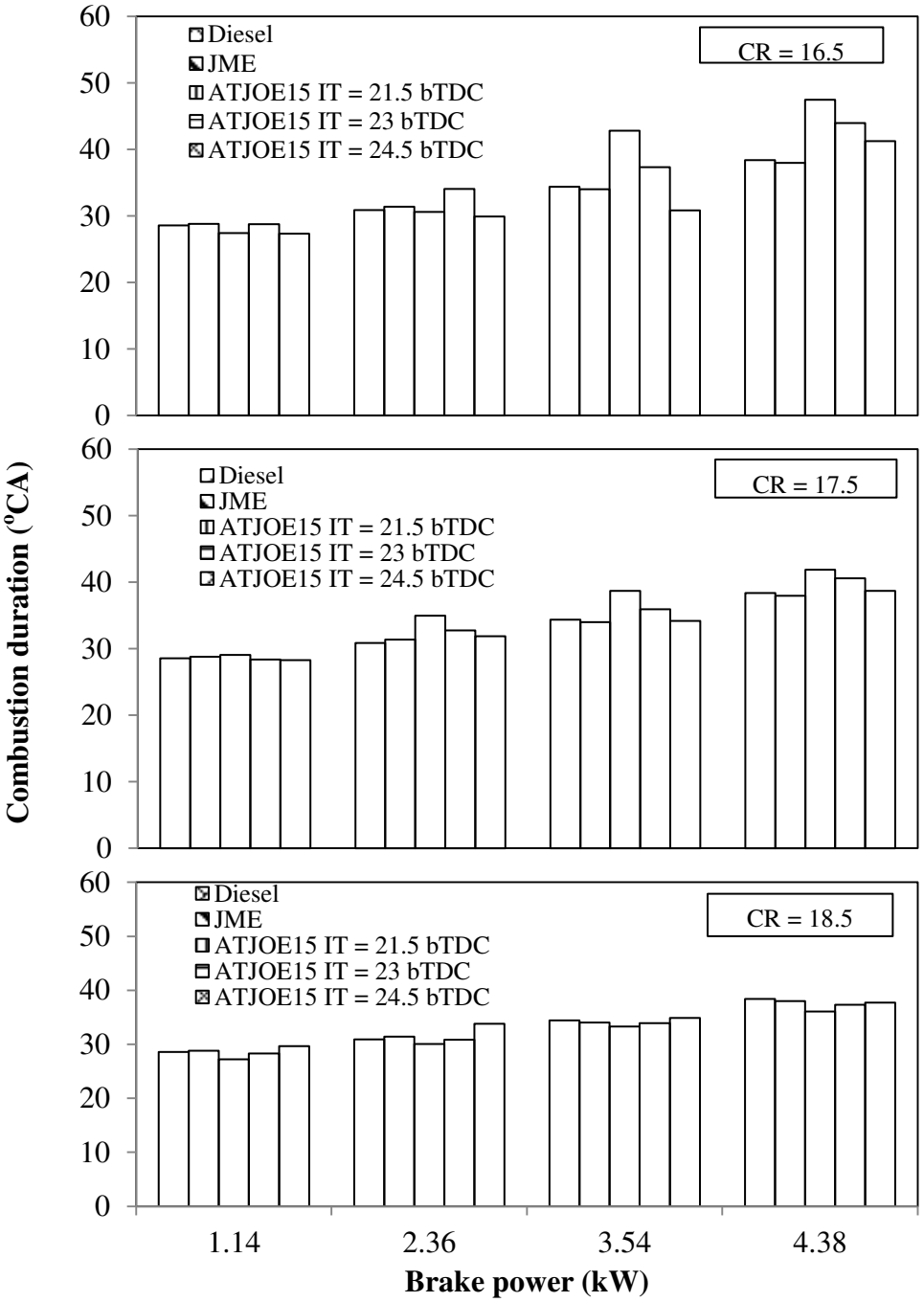

Fig. 5.4.5 Variation of combustion duration with brake power at different compression ratios and injection timings

5.4.3 Performance parameters

5.4.3.1 Brake thermal efficiency

The variation of brake thermal efficiency with brake power for the ATJOE15 at different compression ratios and injection timings, in comparison with the JME and diesel, is shown in

Fig. 5.4.6. It is seen from the figure that, for all the compression ratios and injection timings tested, the brake thermal efficiency of the ATJOE15 emulsion increases with an increase in the load.

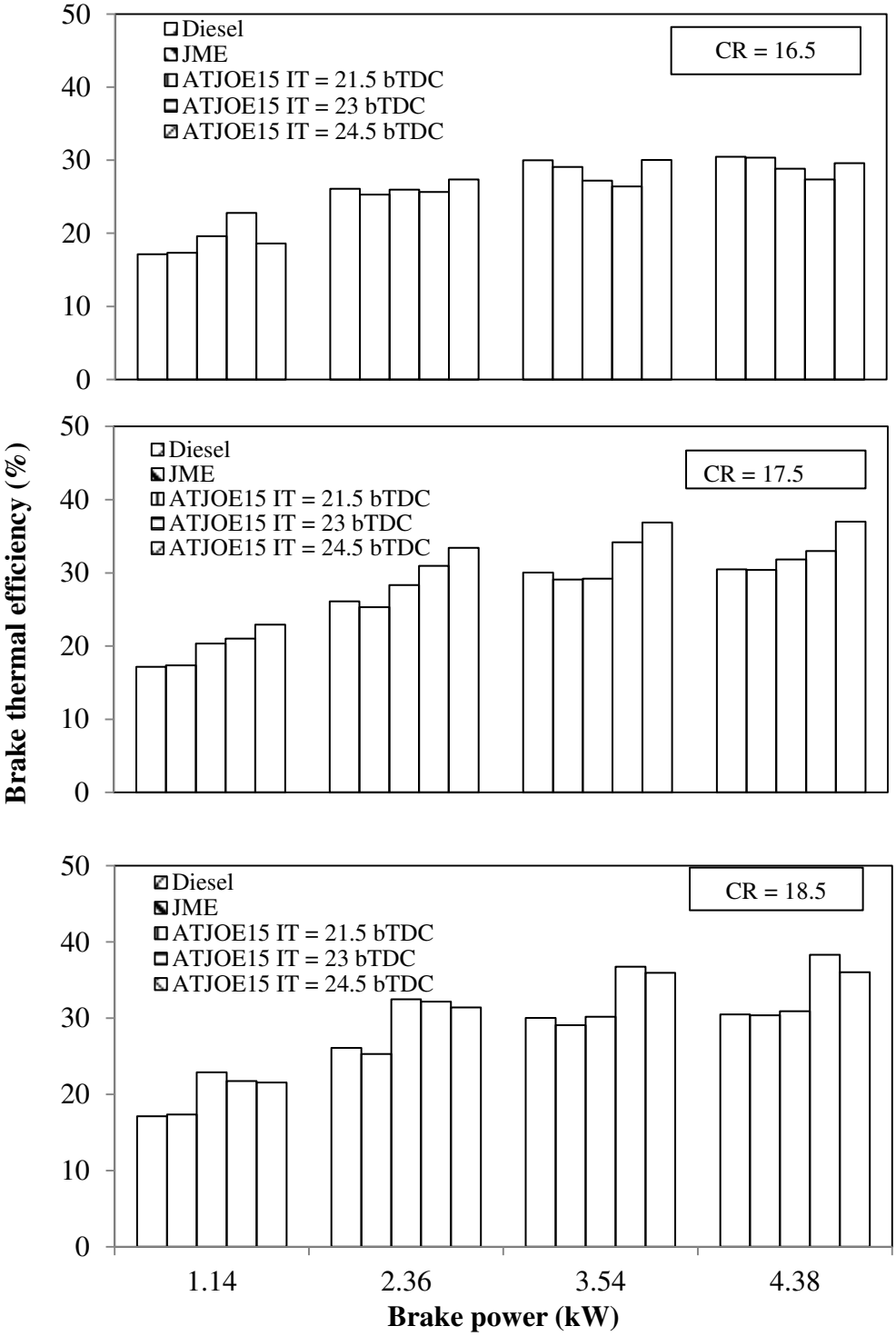

Fig. 5.4.6 Variation of brake thermal efficiency with brake power at different compression ratios and injection timings

At the standard compression ratio and injection timing, the ATJOE15 emulsion produced a maximum thermal efficiency of 32.98% which is higher by about 8.2% compared to that of diesel operation. For the same compression ratio, when the injection timing is retarded by 1.5 ^{o}CA, the brake thermal efficiency of the ATJOE15 emulsion dropped by about 3.5%, but still it is found to be higher than those of diesel and the JME operations, by about 4.4% and 4.7% respectively. When the injection timing is advanced to 24.5 ^{o}CA bTDC, the thermal efficiency of the ATJOE15 emulsion is found to be higher by about 6.5% and 6.8% compared to that of diesel and the JME operations respectively at full load. The advancement in the fuel injection produces a peak pressure closer to TDC, and offers sufficient time to release heat; hence it offers higher thermal efficiency.

When the compression ratio is decreased to 16.5, the brake thermal efficiency of the ATJOE15 emulsion is found to be lower at all the injection timings, which may be due to the poor combustion characteristics caused by the longer ignition delay. The brake thermal efficiency of the ATJOE15 emulsion at this compression ratio is lower, in the order of 2.9% to 5.2% compared to that of diesel operation. With the higher compression ratio of 18.5, the brake thermal efficiency of the ATJOE15 emulsion is found to be higher, in the order of 1.4%, 25% and 18.4% respectively, at injection timings 21.5, 23 and 24.5 ^{o}CA bTDC respectively at full load. This could be due to the fact, that the ATJOE15 emulsion had lower volatility compared to that of diesel, and therefore, the improvement in its combustion characteristics might have been relatively more at higher temperatures resulting from the higher compression ratio.

5.4.3.2 Brake specific fuel consumption

The variation of the brake specific fuel consumption with brake power for diesel, JME and ATJOE15 emulsion, at various compression ratios and injection timings, is depicted in Fig. 5.4.7. It is apparent from the figure, that the BSFC values of the ATJOE15 emulsion are found to be higher than those of diesel and the JME operations, at all compression ratios and injection timings, which is attributed to the lower calorific value of the ATJOE15 emulsion. When comparing the BSFC of the ATJOE15 emulsion at different compression ratios and injection timings, the BSFC values are comparatively higher, with a lower compression ratio and retarded injection timings. The minimum value of the BSFC obtained with 16.5 compression ratio is 0.388 kg/kWh at an advanced injection timing 24.5 ^{o}CA bTDC, which is higher by about 44% compared to that of diesel operation at full load.

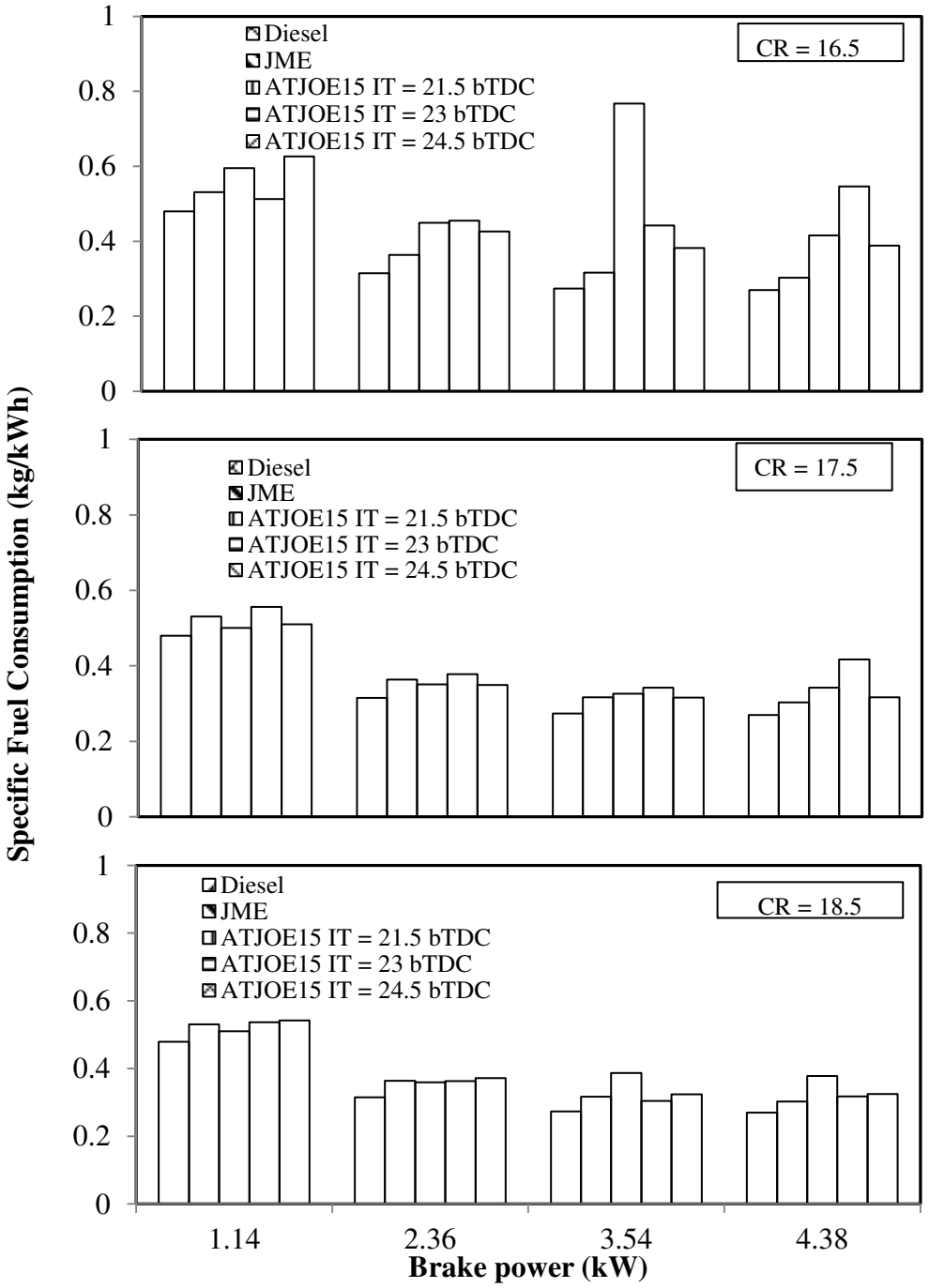

Fig. 5.4.7 Variation of specific fuel consumption with brake power at different compression ratios and injection timings

At the standard compression ratio of 17.5 and advanced injection timing of 24.5 ^{o}CA bTDC, the minimum BSFC obtained is 0.316 kg/kWh, which is higher by about 17.4% compared to that of diesel. The minimum BSFC value of 0.317 kg/kWh is obtained at the compression ratio 18.5 and injection timing 23 ^{o}CA bTDC, which is higher by about 17.8% compared to that of diesel at full load. The BSFC of the ATJOE15 emulsion is found to be lower at a higher compression ratio for all the injection timings. The possible reason for this trend could

be, that with an increase in the compression ratio, the maximum cylinder pressure increases due to the fuel injected in the hotter combustion chamber leading to higher effective power. This will, in turn, decrease the fuel consumption per power output. A similar reason was reported by Ulusoy et al. [194] in their work on biodiesel obtained from used frying oils.

5.4.3.3 Exhaust gas temperature

The variation of the exhaust gas temperature with load for the ATJOE15 emulsion, in comparison with the JME and diesel at different compression ratios and injection timings is depicted in Fig. 5.4.8.

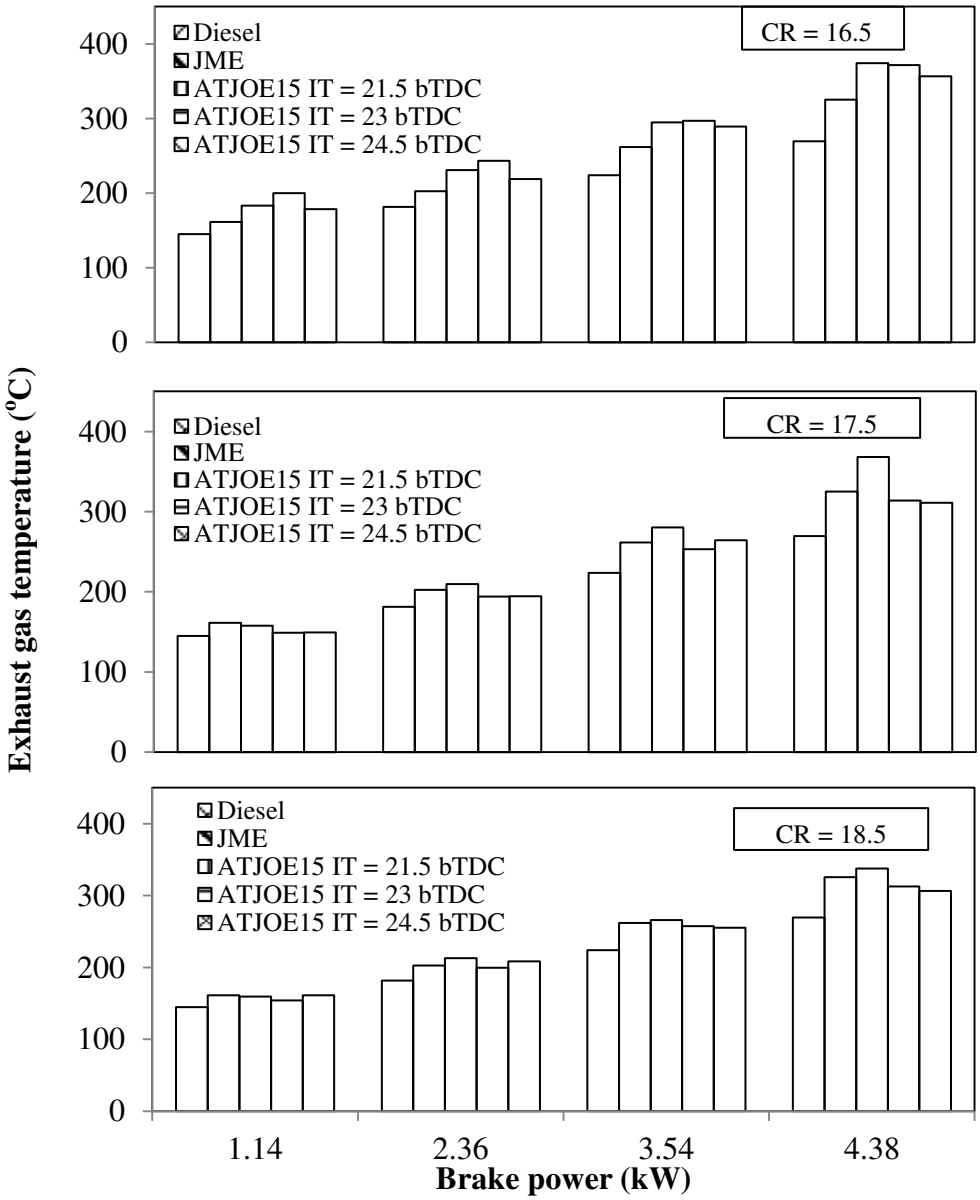

Fig. 5.4.8 Variation of exhaust gas temperature with brake power at different compression ratios and injection timings

It is revealed from the figure, that the exhaust gas temperature of ATJOE15 emulsion increased with an increase in the brake power and decreased with an increase in the compression ratio and advanced injection timings for all the fuels. Also, it can be ascertained from the figure that the engine operating parameters, which resulted with a minimum BSFC and maximum brake thermal efficiency, were the ones which contributed the minimum exhaust gas temperature.

On an average, the exhaust gas temperature of the ATJOE15 emulsion is reduced by about 14.3%, when the compression ratio was increased from 17.5 to 18.5. The possible reason for this trend could be that the increased compression ratio actually increases the air temperature inside the cylinder consequently reducing the ignition delay causing a better and more complete burning of the fuel. Similarly, at advanced injection timings, the exhaust gas temperature of the ATJOE15 emulsion is found to be lower by about 33% than that of retarded injection timings at full load. This might be due to the favourable pressure-temperature profile, which resulted in higher thermal efficiencies at advanced injection timings. The efficiency of the engine cycles increases, when the conversion of chemical energy into heat is concentrated near the TDC. These results are in agreement with those of Rahemen and Ghadge [195], when they conducted experiments with magua biodiesel at variable compression ratios and injection timings.

5.4.4 Emission parameters

5.4.4.1 BSHC emissions

The variations of brake specific HC emissions with the brake power for the ATJOE15 emulsion, JME and diesel at different compression ratios and injection timings are shown in Fig. 5.4.9. The BSHC emissions decreased with increasing engine load. This happened due to higher cylinder gas temperatures at higher engine loads, which led to more efficient combustion of fuel at higher temperatures, producing lower quantities of HC emissions. At advanced injection timings, improved air–fuel mixing is achieved due to the availability of more time for the mixing process; therefore, this led to lower HC emissions.

With the lower compression ratio, the HC emissions are found to be drastically higher, compared to that of diesel and the JME operations. At a lower compression ratio, insufficient heat of compression, delays the ignition, and so, the HC emissions increased. Similar reasons

are reported by Jindal et al [20] in their work, on the effect of the compression ratio and nozzle opening pressure in a DI diesel engine running on Jatropha methyl ester.

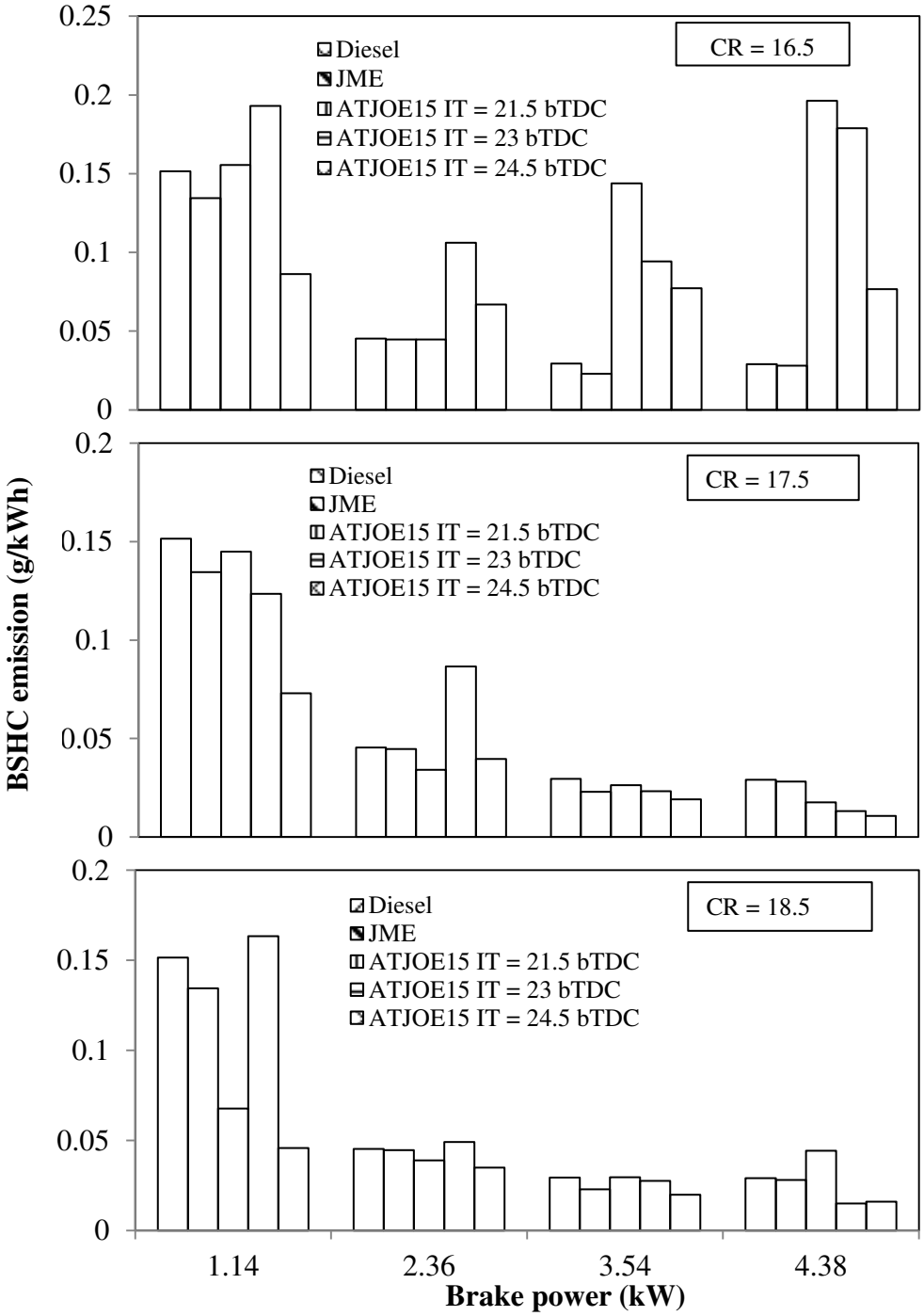

Fig. 5.4.9 Variation of BSHC emission with brake power at different compression ratios and injection timings

At the standard compression ratio, the HC emissions of the ATJOE15 emulsion at different injection timings are found to be lower in the range of 39.5% to 65.5%, compared to that of diesel at full load. At a higher compression ratio, the HC emissions of the ATJOE15 emulsion at standard and advanced injection timings are found to be lower between 45.1%

and 48.2%, compared to those of diesel at full load. At retarded injection timing, the HC emission of ATJOE15 is found to be higher by 52.7%, in comparison with diesel at full load.

5.4.4.2 BSCO emissions

Figure 5.4.10 illustrates the variation of brake specific CO emissions with brake power for the ATJOE15 emulsion, at different compression ratios and injection timings, in comparison with JME and diesel.

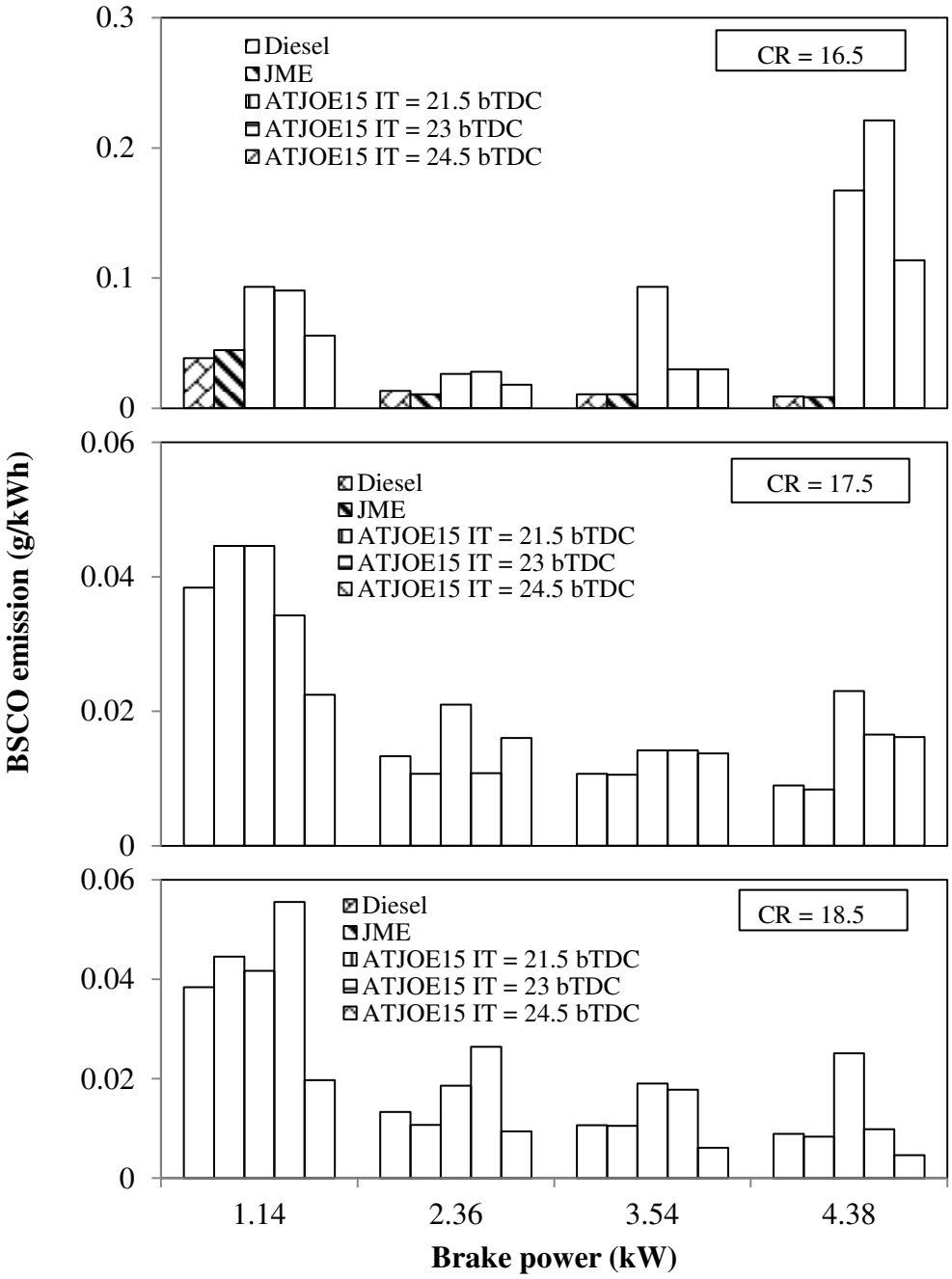

Fig. 5.4.10 Variation of BSCO emission with brake power at different compression ratios and injection timings

With the lower compression ratio of 16.5, the temperature reached is also low, and thus, more CO is exhausted from the engine. The minimum value of CO obtained at this compression ratio is about 0.037 g/kWh, which is higher by about 31.5% compared to that of diesel operation at full load. At the standard compression ratio of 17.5, the CO emissions of ATJOE15 are found to be higher by 61.1%, 45.9% and 44.8% at 21.5 ^{o}CA, 23 ^{o}CA and 24.5 ^{o}CA bTDC injection timings respectively at full load, compared to that of diesel operation. The longer spray penetration, larger fuel droplets and insufficient swirl may be the factors for higher CO emissions in the case of the ATJOE15 emulsion. This reason was supported by Pei Lin Zhou [181], in his research work. It can be observed that the CO emissions are higher at retarded injection timing, and lower with the advancement in the start of ignition. An advancement in the injection timing can also cause a higher cylinder temperature and an increase in the oxidation process between carbon and oxygen molecules, which will lead to a decrease in the CO emissions. This statement is in agreement with Sayin et al [196] in their work on the effect of injection timing on the emissions of a diesel engine fueled with conala methyl ester. At the higher compression ratio of 18.5, the CO emissions of ATJOE15 are found to be higher, at retarded and standard injection timing conditions, by about 64.5% and 9% in comparison with diesel operation. At an advanced injection timing, the CO emissions are found to be lower by about 48% compared to that of diesel. The possible reason for this trend could be, that the increased CR actually increases the air temperature inside the cylinder, reducing the ignition delay, causing a better and more complete burning of the fuel. Similar reasons are reported by Raheman and Ghadge [195], in their work on mahua biodiesel with variable compression ratios.

5.4.4.3 BSNO emissions

Figure 5.4.11 depicts the variation of brake specific nitric oxide (BSNO) emissions with respect to brake power for the ATJOE15, at different compression ratios and injection timings. It is apparent that the BSNO emissions are found to be higher by 29% and 2% in the JME and ATJOE15 operations, compared to that of diesel at full load, standard compression ratio and injection timing. The oxygen content of JME increases the cylinder maximum gas temperature with better combustion, and this tends to increase the NO concentration. With the compression ratio of 17.5, in the ATJOE15 operation, an advancement in the injection timing leads to further increase in NO emissions by about 26.7% and a retardation in the injection timing gives a reduction in the NO emissions of 12.8%, in comparison with diesel at full load. Retarding the injection timing decreases the peak cylinder pressure, because more

fuel burns after TDC. The lower peak cylinder pressures result in lower peak temperatures. As a consequence, the NO concentration starts to diminish. With the advanced injection timings the reason is vice versa. Similar reasons are reported by Sayin et al [197], in their work on the effect of injection timing on a diesel engine fueled with the methanol- diesel blends. In comparison with the JME, the NO emissions from the ATJOE15 emulsion are found to be lower, in the order of 3.2% to 38.2% at the compression ratio of 17.5 and different injection timings at full load.

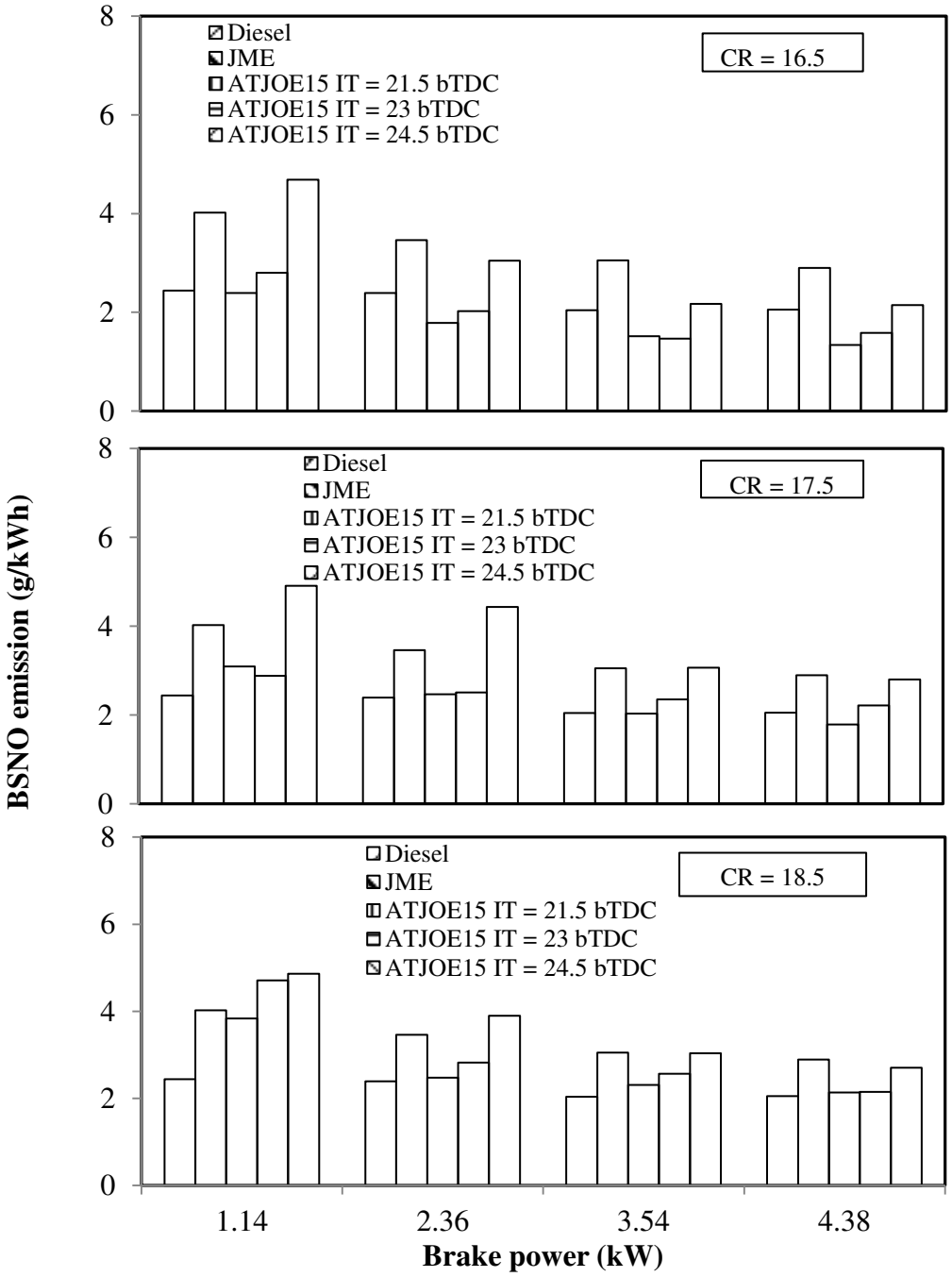

Fig. 5.4.11 Variation of BSNO emission with brake power at different compression ratios and injection timings

When the compression ratio is reduced to 16.5, the NO emissions of the ATJOE15 emulsion are found to be lower by about 34.9% and 23%, compared to that of diesel operation at retarded and standard injection timings. With the advanced injection timing, the NO values are found to be higher by about 4.5% in comparison with diesel operation. When compared to the JME operation, the NO emissions of the ATJOE15 emulsion are found to be lower in the range between 25.8% and 53.8%. A lower compression ratio will reduce the in-cylinder temperatures, and thus, the flame temperatures during combustion, which will suppress the NO emissions. Similar reasons were reported by Raheman and Ghadge [195], in their work on mahua biodiesel with variable compression ratios. With the higher compression ratio of 18.5, the NO emissions from the ATJOE15 emulsion are found to be higher in the range of 4% to 31.8% compared to that of diesel at full load.

5.4.4.4 Smoke opacity

Figure 5.4.12 depicts the variation of smoke opacity, with respect to brake power for the ATJOE15 at different compression ratios and injection timings, the JME and diesel. The percentage decrease in the smoke opacity of 19.6% is observed for the JME at full load in comparison with diesel at the standard compression ratio and injection timing. This may be because, the JME contains oxygen, which reduces locally over the rich region, and the formation of crucial smoke. In the case of ATJOE15 emulsion, the smoke opacity is found to be higher by about 8.9% and 45% at standard and retarded injection timings at full load. When the injection timing is advanced, the smoke opacity value of the ATJOE15 is found to be lower by about 5.3%, compared to that of diesel operation. The values of smoke opacity of the ATJOE15 at different injection timings are higher in the range of 26% to 58% compared to that of JME operation.

At a reduced compression ratio of 16.5, the smoke opacities of the ATJOE15 emulsion at all injection timings were found to be higher in the range between 32% and 52%, compared to that of diesel operation at full load. At a higher compression ratio of 18.5, the smoke opacity of the ATJOE15 emulsion at retarded injection timing is found to be lower by about 4.2% and in the advanced injection timing case, the smoke emission values reduced by about 11.7% compared to that of diesel. As the compression ratio increases, the maximum temperature during the combustion increases, and this, in turn, decreases the smoke opacity, and it is vice versa in the case of a lower compression ratio.

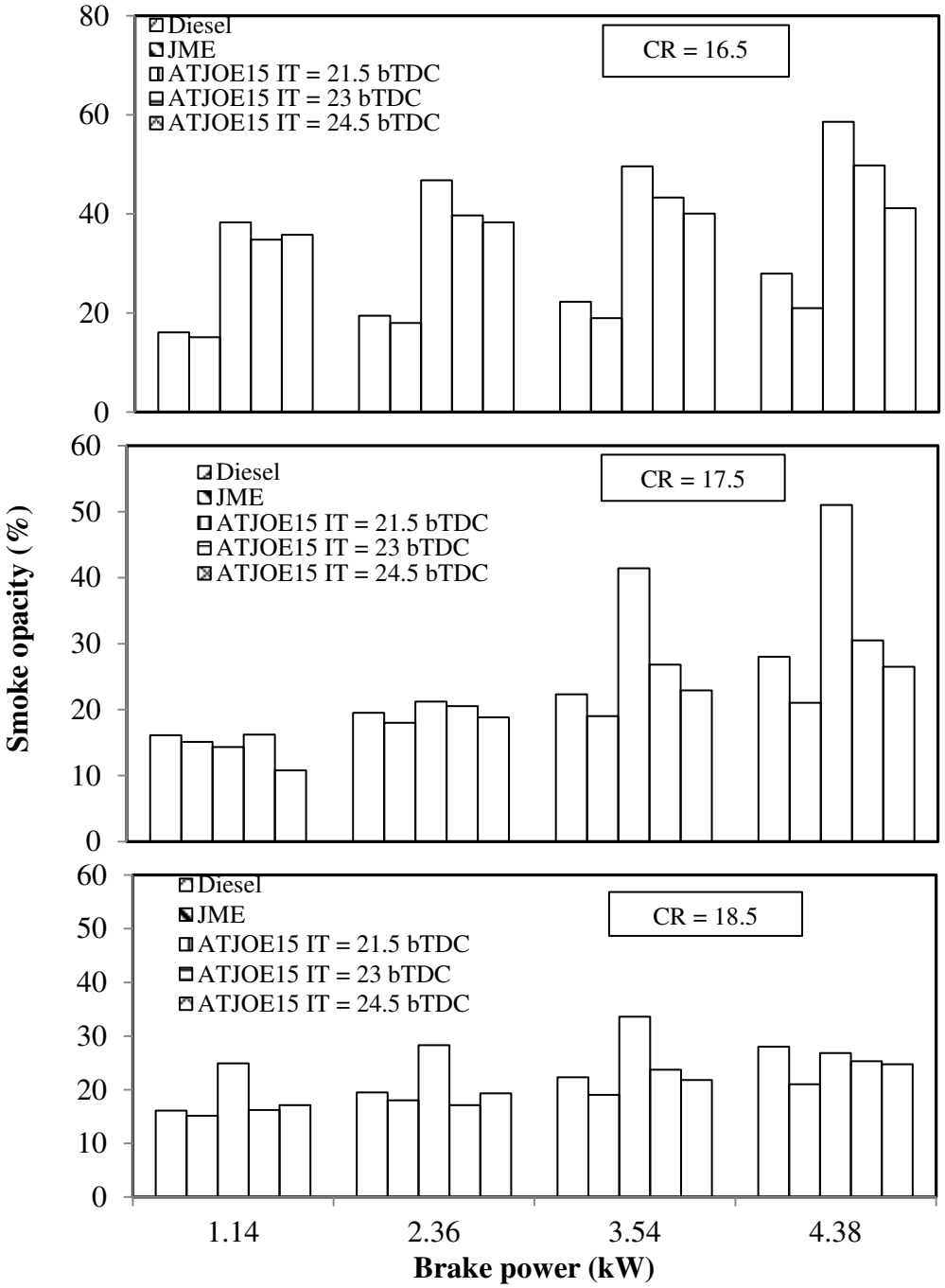

Fig. 5.4.12 Variation of smoke opacity with brake power at different compression ratios and injection timings

5.4.5 Closure

The summary of the experimental results on the effect of the compression ratio and injection timing on the combustion, performance and emission parameters obtained in a single cylinder diesel engine fueled with the ATJOE15 emulsion indicates, that this fuel can be used in a variable compression ratio engine. From the analysis, it is revealed that the ATJOE15 emulsion gives an improved performance and lower emissions, when the engine is operated

with a higher compression ratio of 18.5 and retarded injection timing of 21.5 ^{o}CA bTDC. The NO emission in this condition is still found to be higher by about 31.8% compared to that of diesel operation, at full load. The smoke opacity of the ATJOE15 emulsion with this compression ratio and at retarded injection timing, is found to be lower by about 4.2% compared to that of diesel at full load.

5.5 Combined effects of compression ratio and nozzle opening pressure on the combustion, performance and emission parameters of a diesel engine fueled with ATJOE15 emulsion

5.5.1 General

This chapter discusses the combined effects of the compression ratio and fuel nozzle opening pressure on the combustion, performance and emission characteristics of the diesel engine fueled with the ATJOE15 emulsion. From the summary of the experimental results on the combustion, performance and emission results in the single cylinder diesel engine fueled with the ATJOE15 emulsion, it is observed that the CO and NO emissions from the engine fueled with the ATJOE15 emulsion are higher than those of diesel operation. In this research, it is proposed to study the combined effect of varying the compression ratio and nozzle opening pressure of the engine fueled with the ATJOE15 emulsion, in comparison with diesel and the JME operation. Three different compression ratios, viz., 16.5, 17.5 and 18.5, and three nozzle opening pressures viz. 200, 220 and 240 bar, were chosen for this study. The standard injection timing of 23 ^{o}CA bTDC is maintained for this study.

5.5.2 Combustion parameters

5.5.2.1 Pressure crank angle history

Figure 5.5.1 depicts the pressure crank angle history of the engine fueled with diesel, JME and the ATJOE15 emulsion for different compression ratios and nozzle opening pressures, at full load condition. It is observed from the figure, that the combustion starts earlier in the range between 0.4 and 2.1 ^{o}CA for the ATJOE15 emulsion, with the compression ratios of 17.5, 18.5, and at all three nozzle opening pressures compared to that of diesel. For the same operating conditions, compared to the JME operation, it is found that the combustion starts later by about 0.5 to 2.3 ^{o}CA for the ATJOE15 emulsion at all the nozzle opening pressures. At the lower compression ratio of 16.5, the commencement of combustion is noticed later, which ranges from 0.3 to 2.3 ^{o}CA in comparison with the diesel operation. The peak cylinder pressure for diesel occurs at 12.4 ^{o}CA aTDC, whereas for the ATJOE15, the peak pressure occurs earlier in the range of 0.3 and 1.2 ^{o}CA, with the compression ratios of 17.5 and 18.5, and the nozzle opening pressures of 220 and 240 bar, compared to that of diesel at full load. With the lower compression ratio of 16.5 and at all nozzle opening pressures, the peak cylinder pressure is found to be lower in the range of 8.1 to 11.2 bar, compared to that of diesel operation. Similar results are reported by Kannan and Anand [192], in their investigation on a diesel engine fueled with biodiesel obtained from waste cooking oil. It is

seen from the figure, that among all the tested compression ratios and nozzle opening pressures, with the compression ratio of 18.5 and with the nozzle opening pressure of 220 bar, the ATJOE15 operation produced the highest cylinder pressure value of 77.2 bar at 372.1 ^{o}CA, which is earlier by about 0.3 ^{o}CA and later by about 1.6 ^{o}CA than those of diesel and JME operations respectively. The early or later occurrences of ignition are attributed to the increased or decreased cylinder gas temperature respectively.

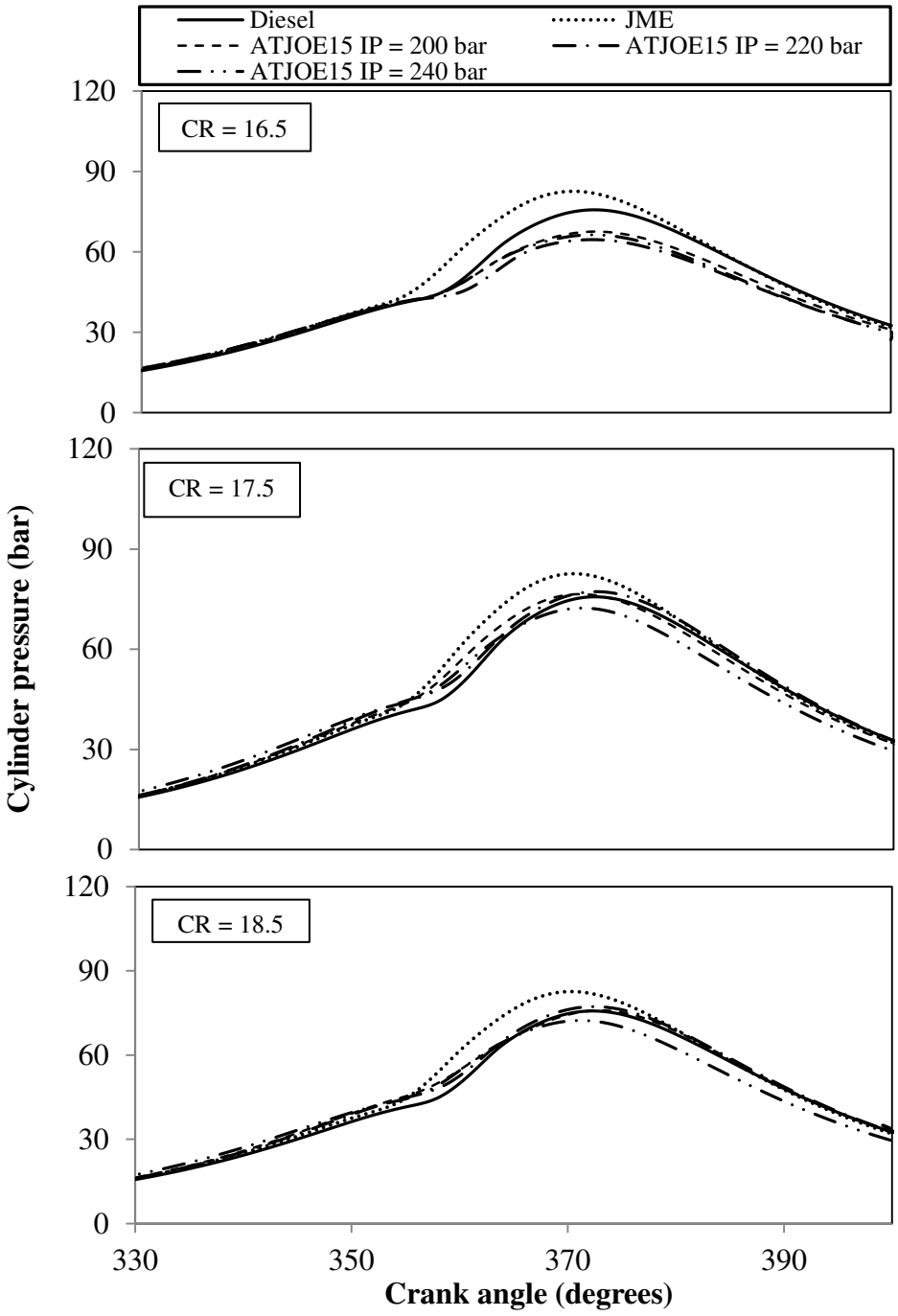

Fig. 5.5.1 Variation of cylinder pressure with crank angle at different compression ratios and nozzle opening pressures

5.5.2.2 Ignition delay

Figure 5.5.2 depicts the ignition delay for diesel, JME and ATJOE15 for the different compression ratios and nozzle opening pressures at all loads. It is seen from the figure, that the ignition delay is found to be lower with the increase in the engine load, compression ratio and nozzle opening pressure. The reduction in the ignition delay in these conditions, might be the result of higher combustion chamber wall temperature at the time of injection and the reduced exhaust gas dilution [107].

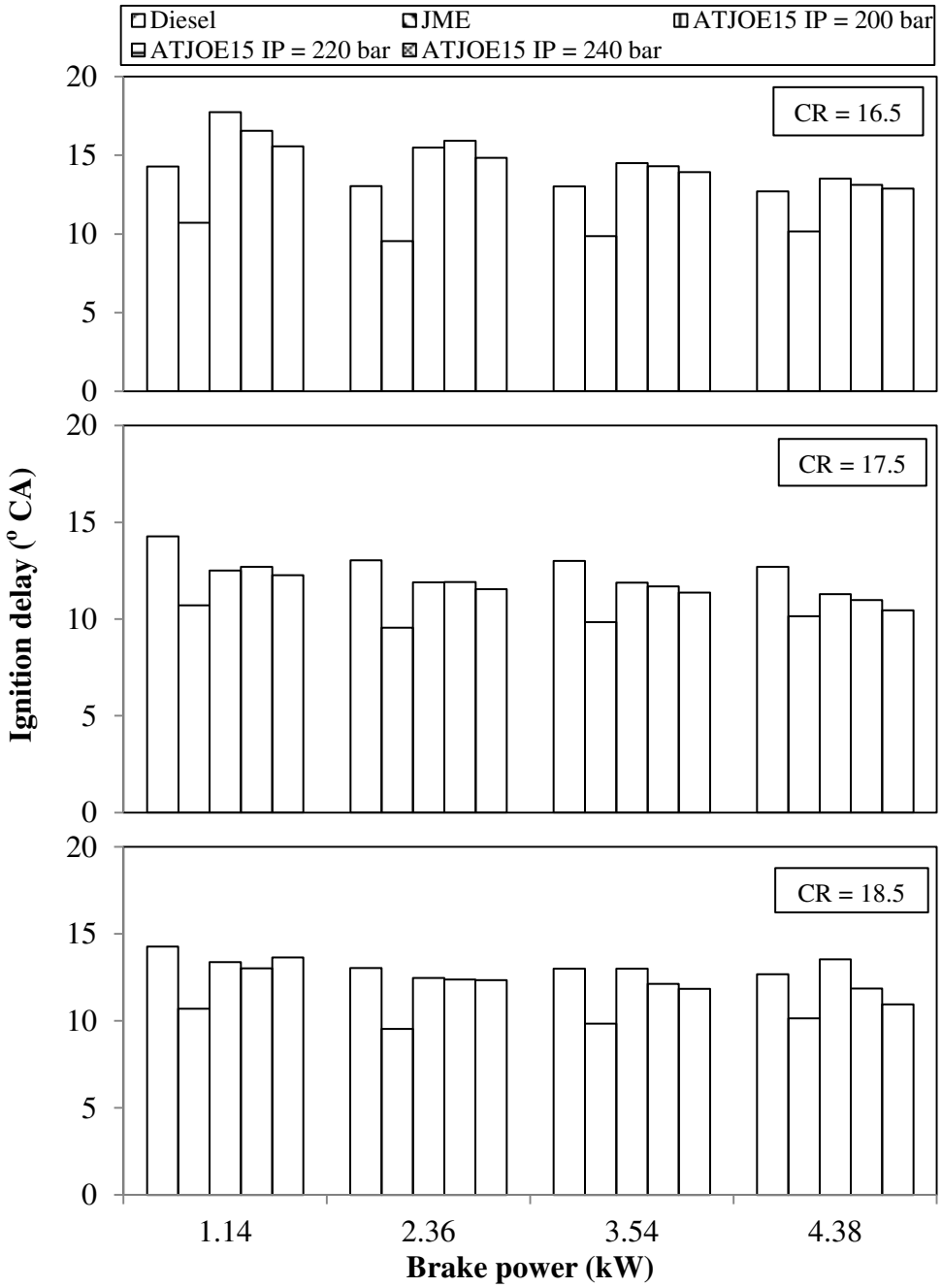

Fig.5.5.2 Variation of ignition delay with brake power at different compression ratios and nozzle opening pressures

With the lower compression ratio of 16.5, the ignition delay of the ATJOE15 emulsion is found to be higher than those of diesel and JME at all nozzle opening pressures, due to the lower cylinder temperature. At this compression ratio and for all the nozzle opening pressures, the ignition delay values of the ATJOE15 emulsion are found to be longer by about 0.2 to 1 ^{o}CA compared to that of diesel operation at full load. It is apparent from the figure, that at full load condition, the ignition delay of the ATJOE15 emulsion is found to be shorter in the range between 0.3 and 2.2 ^{o}CA with the compression ratios of 17.5, 18.5 and the higher nozzle opening pressure of 240 bar compared to that of diesel operation. In comparison with the JME operation, the engine fueled with the ATJOE15 emulsion exhibits a longer ignition delay at all operating conditions. Among all the tested compression ratios and nozzle opening pressures, a minimum ignition delay period of 10.45 ^{o}CA is observed for the ATJOE15 operation with the compression ratio of 17.5 and nozzle opening pressure of 240 bar. The reduction in the ignition delay period is mainly due to the improved atomization at higher nozzle opening pressure and higher cetane number of the ATJOE15 compared to that of diesel, at full load.

5.5.2.3 Heat release rate

Figure 5.5.3 illustrates the variation of the heat release rate with respect to the crank angle, for the ATJOE15 emulsion at full load for the different compression ratios and nozzle opening pressures, and for diesel and JME operations. The occurrence of the maximum heat release rate for the ATJOE15 emulsion at different operating conditions on an average, shifted approximately from 0.4 ^{o}CA to 6.4^{o}CA at full load, compared to that of diesel operation. The intensity of the premixed combustion phase for diesel is found to be the highest, whereas, it is lower in the case of JME and the ATJOE15 emulsion at compression ratios of 17.5, 18.5 and higher nozzle opening pressures.

At a lower compression ratio of 16.5, at all the nozzle opening pressures, the premixed combustion is found to be higher than that of diesel operation, as a result of longer ignition delay. The variation of the maximum heat release rate between diesel, JME operations and the ATJOE15 emulsion at different compression ratios and nozzle opening pressures lies between 7.4 and 15.71 J/^{o}CA. For the JME and the ATJOE15 emulsion, less amount of fuel is accumulated during the shorter ignition delay period, which results in lower heat release rates compared to that of diesel at higher compression ratios.

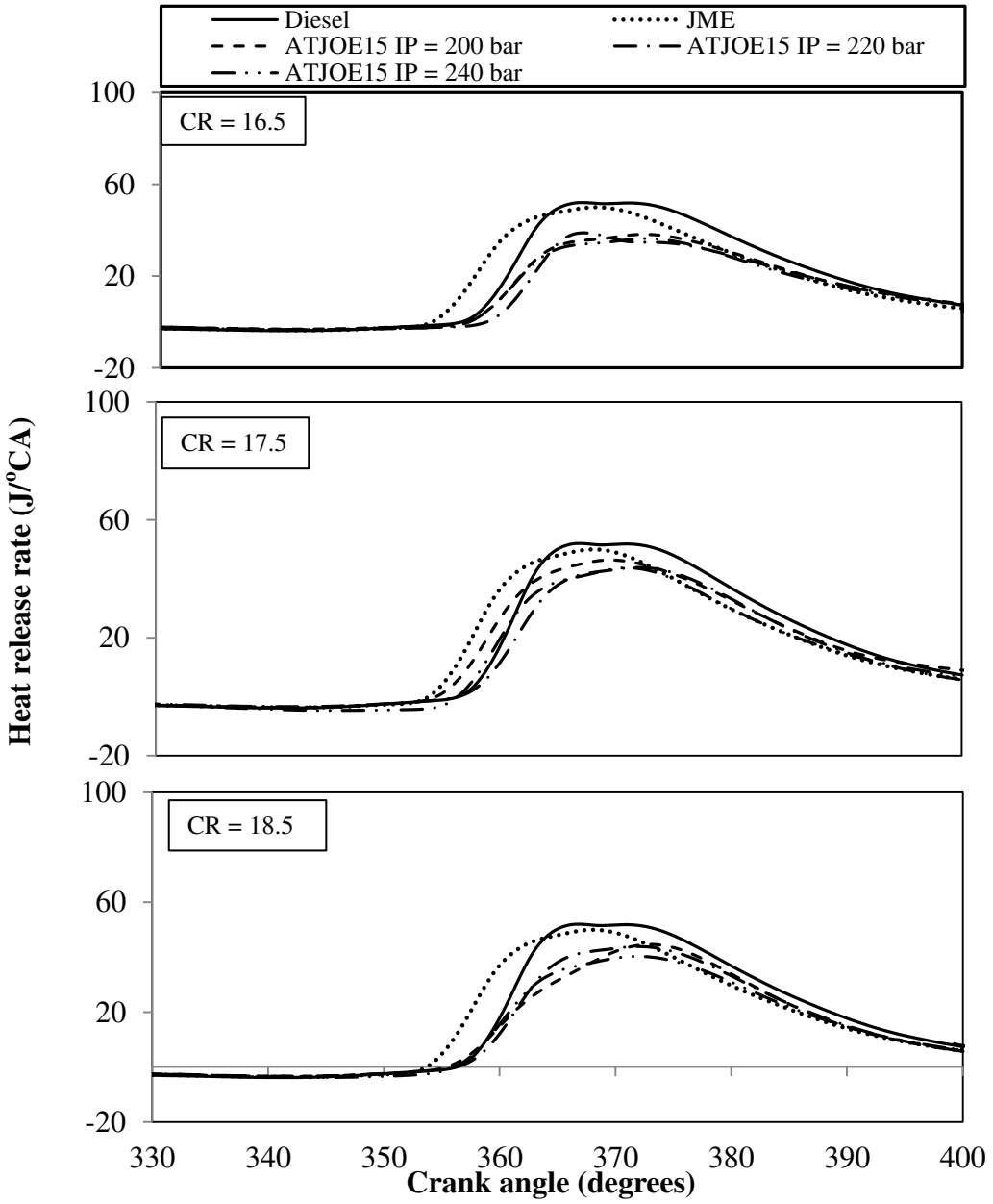

Fig. 5.5.3 Variation of heat release rate with crank angle at different compression ratios and nozzle opening pressures

5.5.2.4 Maximum cylinder pressure

Figure 5.5.4 depicts the variation of the maximum cylinder pressure with brake power for diesel, JME and the ATJOE15 emulsion at full load, for the different compression ratios and nozzle opening pressures. It is seen from the figure that the peak cylinder pressure is increased with an increase in the engine load at all operating conditions. With the lower compression ratio of 16.5, the peak cylinder gas pressures for JME and diesel are found to be higher than that of the ATJOE15 emulsion at all nozzle opening pressures, while the trend is the reverse, at higher compression ratios. This shows that, at higher compression ratios and

all nozzle opening pressures, the ATJOE15 emulsion showed faster premixed combustion, which leads to a higher peak cylinder gas pressure. At the compression ratio of 16.5 and all three nozzle opening pressures, the maximum cylinder pressure of the ATJOE15 emulsion is found to be lower in the range between 9.3 bar and 11.1 bar, compared to that of diesel operation at full load. With the compression ratios of 17.5, 18.5 and at all nozzle opening pressures, the maximum cylinder pressure values of the ATJOE15 emulsion are noticed to be higher in the range of 0.3 to 1.5 bar compared to that of diesel operation.

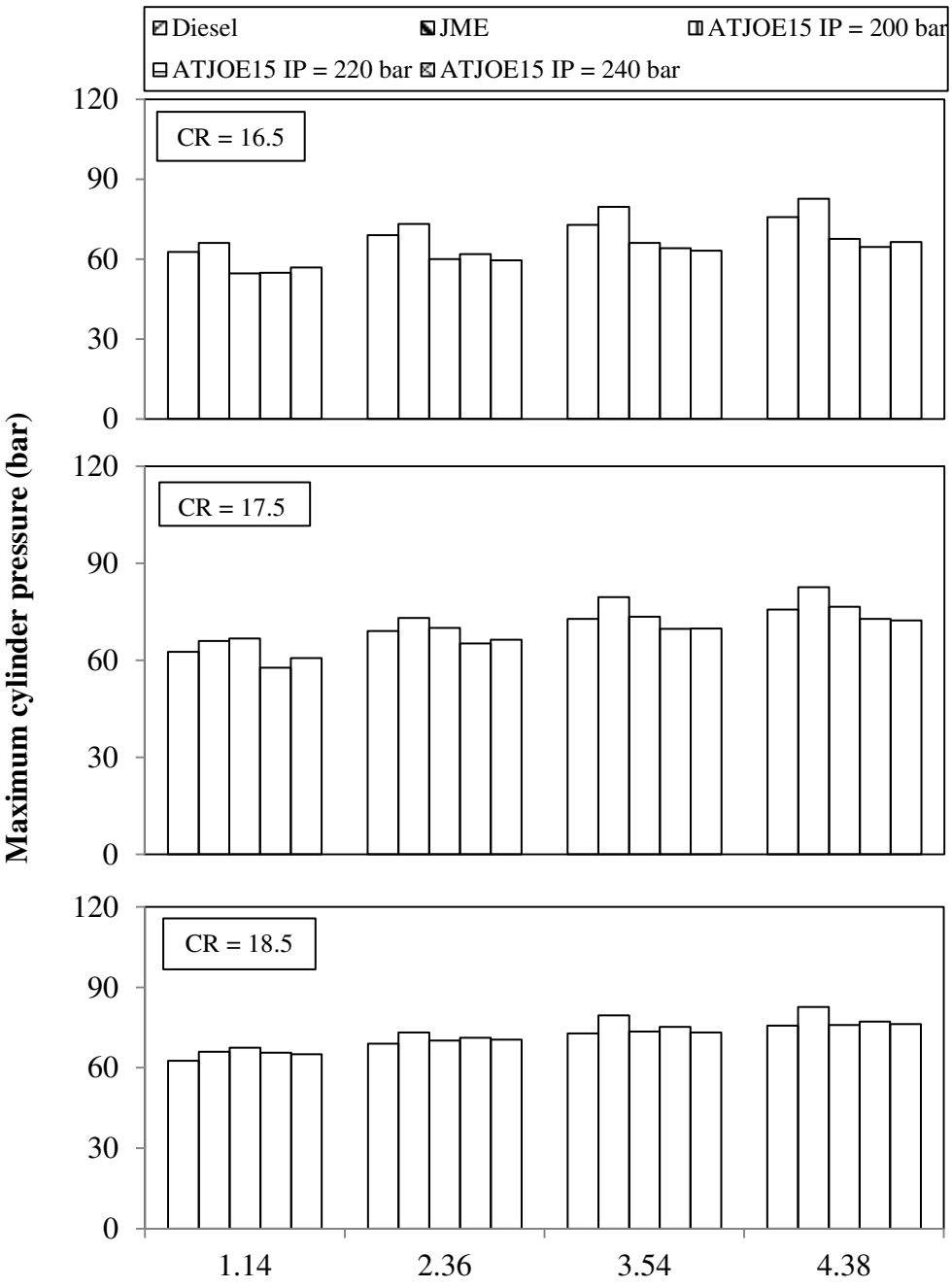

Fig. 5.5.4 Variation of maximum cylinder pressure with brake power at different compression ratios and nozzle opening pressures

This may be due to the reduction in the clearance volume, which increases the density of the cylinder gases during the burning process. This increases the peak cylinder pressure and temperature. In comparison with the JME operation, the peak cylinder pressure of the ATJOE15 emulsion is found to be lower, at all the load conditions.

5.5.2.5 Combustion duration

The variation of the combustion duration with the brake power under different compression ratios and nozzle opening pressures, for the engine fueled with the ATJOE15 emulsion, JME and diesel is illustrated in Fig. 5.5.5.

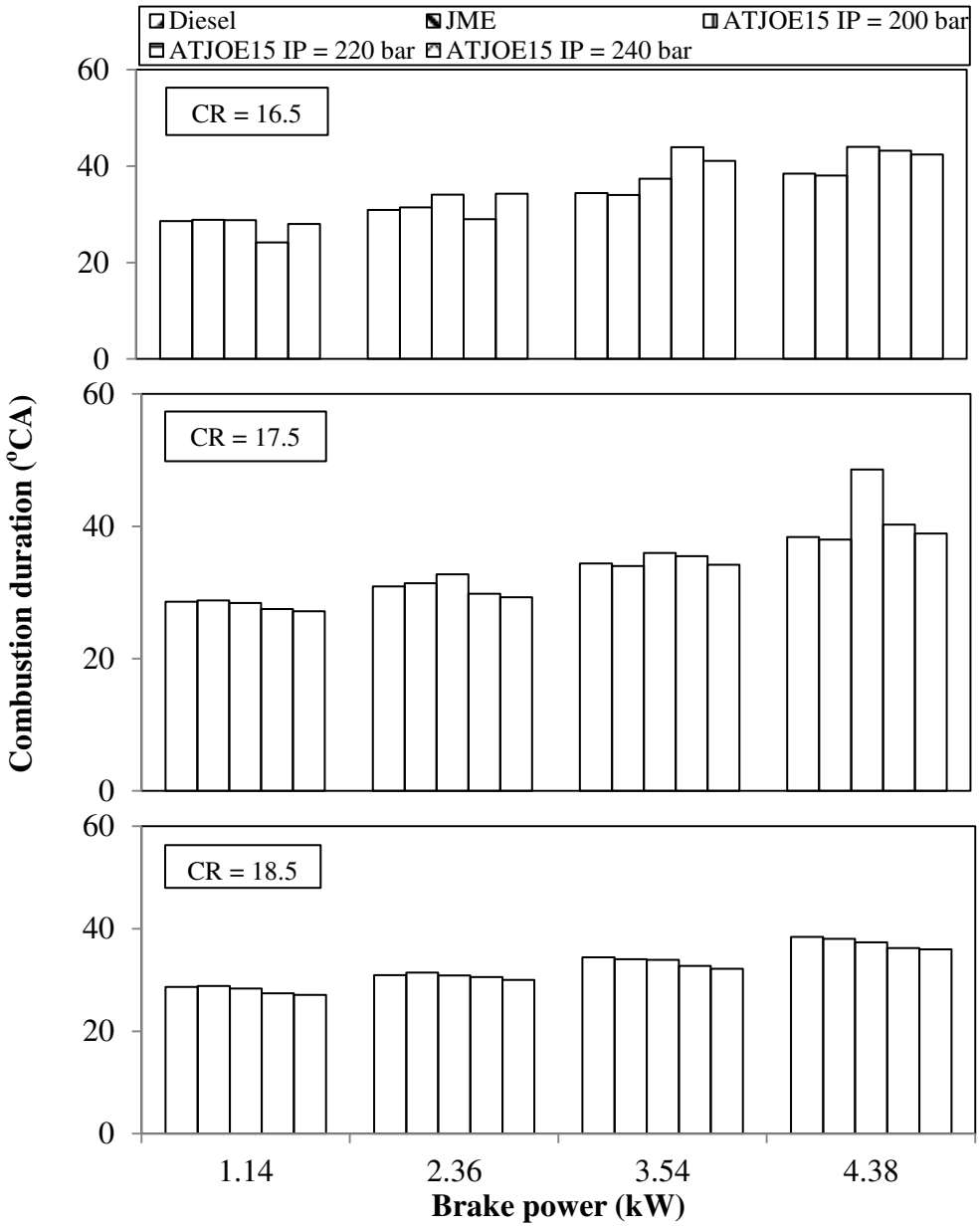

Fig. 5.5.5 Variation of combustion duration with brake power at different compression ratios and nozzle opening pressures

The combustion duration increases with engine load owing to the increase of the fuel quantity. It is seen from the figure that the combustion duration decreases with an increase in the compression ratio and nozzle opening pressure, which is attributed to a high temperature prevailing inside the cylinder, and at a lower compression ratio, the trend is the opposite. With the compression ratio of 18.5 and at full load, the values of the combustion duration are found to be 38.4, 38, 36.3, 36.2 and 35.9 ^{o}CA for diesel, JME and ATJOE15, at nozzle opening pressures of 200, 220 and 240 bar respectively. At a higher compression ratio, the increase in the nozzle opening pressure leads to a lower combustion duration of the ATJOE15 emulsion compared to that of diesel operation. Similar results are reported by Cenk Sayin et al. [198], in their study of the effect of fuel nozzle opening pressure on the combustion and performance characteristics of a DI diesel engine fueled with canola oil methyl esters-diesel fuel blends. The combustion duration of the ATJOE15 is found to be lower, between 2.1 and 2.5 ^{o}CA, compared to that of diesel at the compression ratio of 18.5. With the lower compression ratio of 16.5, the combustion duration of the ATJOE15 emulsion is found to be higher by an average of 4.7 ^{o}CA and 5.1 ^{o}CA, than that of diesel and the JME operation, which is attributed to a longer ignition delay. At the compression ratio of 17.5 at different nozzle opening pressures, the combustion duration of the ATJOE15 emulsion is found to be higher in the range from 0.5 to 10.2 ^{o}CA and 0.9 to 10.6 ^{o}CA, compared to those of diesel and the JME respectively.

5.5.3 Performance parameters

5.5.3.1 Brake thermal efficiency

The variation of brake thermal efficiency with brake power for the ATJOE15 emulsion in comparison with the JME and diesel, at different compression ratios and nozzle opening pressures is depicted in Fig. 5.5.6. It is seen from the figure that, for all the compression ratios and nozzle opening pressures tested, the brake thermal efficiency of the ATJOE15 emulsion increases with the increase in the load. With the standard compression ratio and nozzle opening pressure, the ATJOE15 emulsion produced a maximum thermal efficiency of 32.98% which is higher by about 3.6% compared to that of diesel operation. For the same compression ratio, with the higher nozzle opening pressures of 220 bar and 240 bar, the brake thermal efficiency of ATJOE15 emulsion is found to be higher than that of diesel by about 4.6% and 6.1% respectively, at full load. The increase in the brake thermal efficiency of ATJOE15 emulsion is due to better combustion as a result of the nozzle opening pressure.

This is in agreement with the results reported by Kannan and Anand [192] in their work on waste cooking oil.

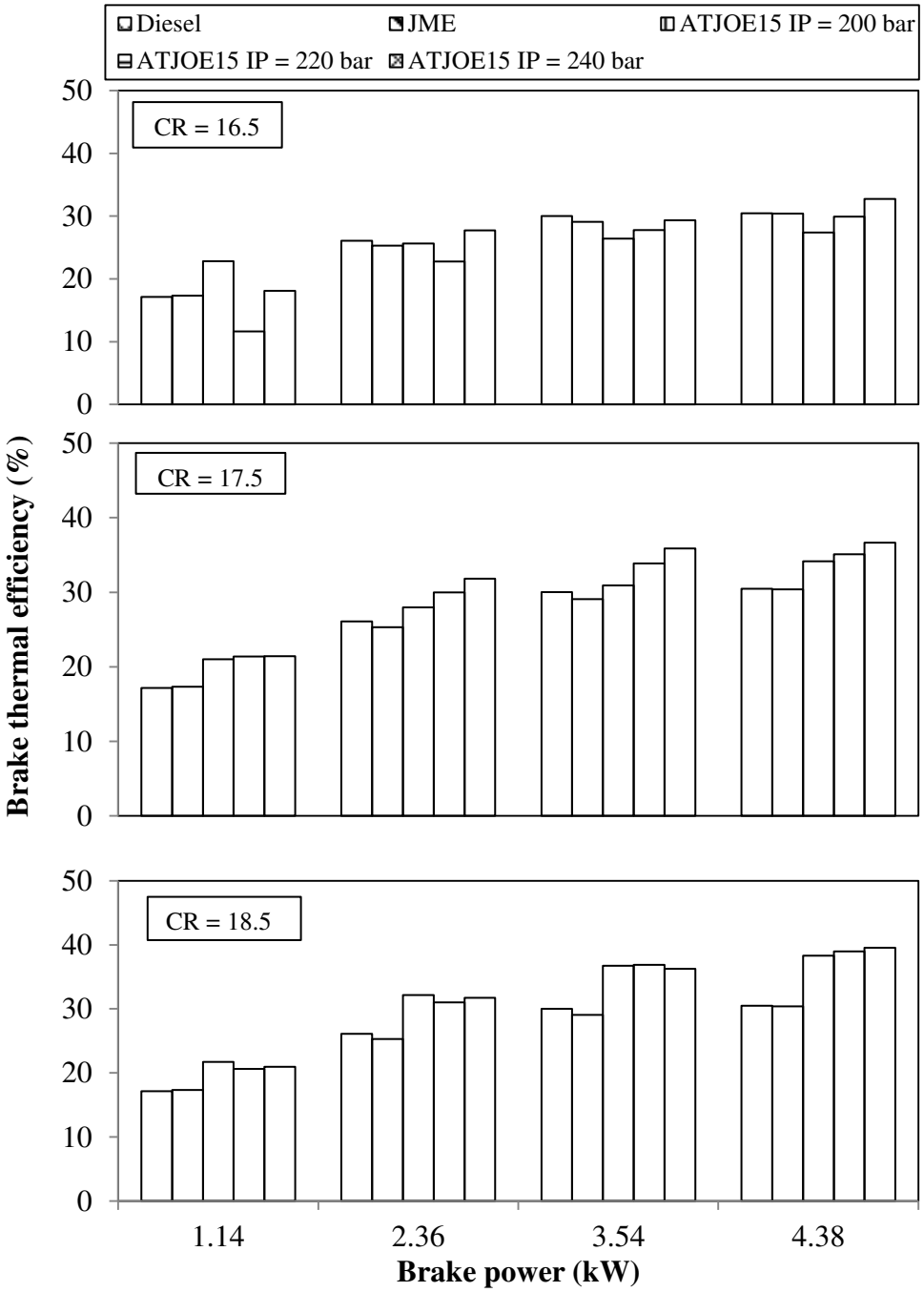

Fig. 5.5.6 Variation of brake thermal efficiency with brake power at different compression ratios and nozzle opening pressures

When the compression ratio is decreased to 16.5, the brake thermal efficiency of the ATJOE15 emulsion is found to be lower by 3.1% and 0.6% at 200 and 220 bar nozzle opening pressures respectively, at full load, which may be due to the poor combustion characteristics caused by the longer ignition delay. At 240 bar nozzle opening pressure, the

brake thermal efficiency of the ATJOE15 emulsion at this compression ratio is found to be higher in the order of 2.3% compared to that of diesel operation. With the higher compression ratio of 18.5, the brake thermal efficiency of the ATJOE15 emulsion is found to be higher in the order of 7.8%, 8.5% and 9% respectively at nozzle opening pressures 200, 220 and 240 bar respectively.

5.5.3.2 Brake specific fuel consumption

The variation of brake specific fuel consumption with brake power for the ATJOE15 emulsion, JME and diesel at various compression ratios and nozzle opening pressures, is depicted in Fig. 5.5.7.

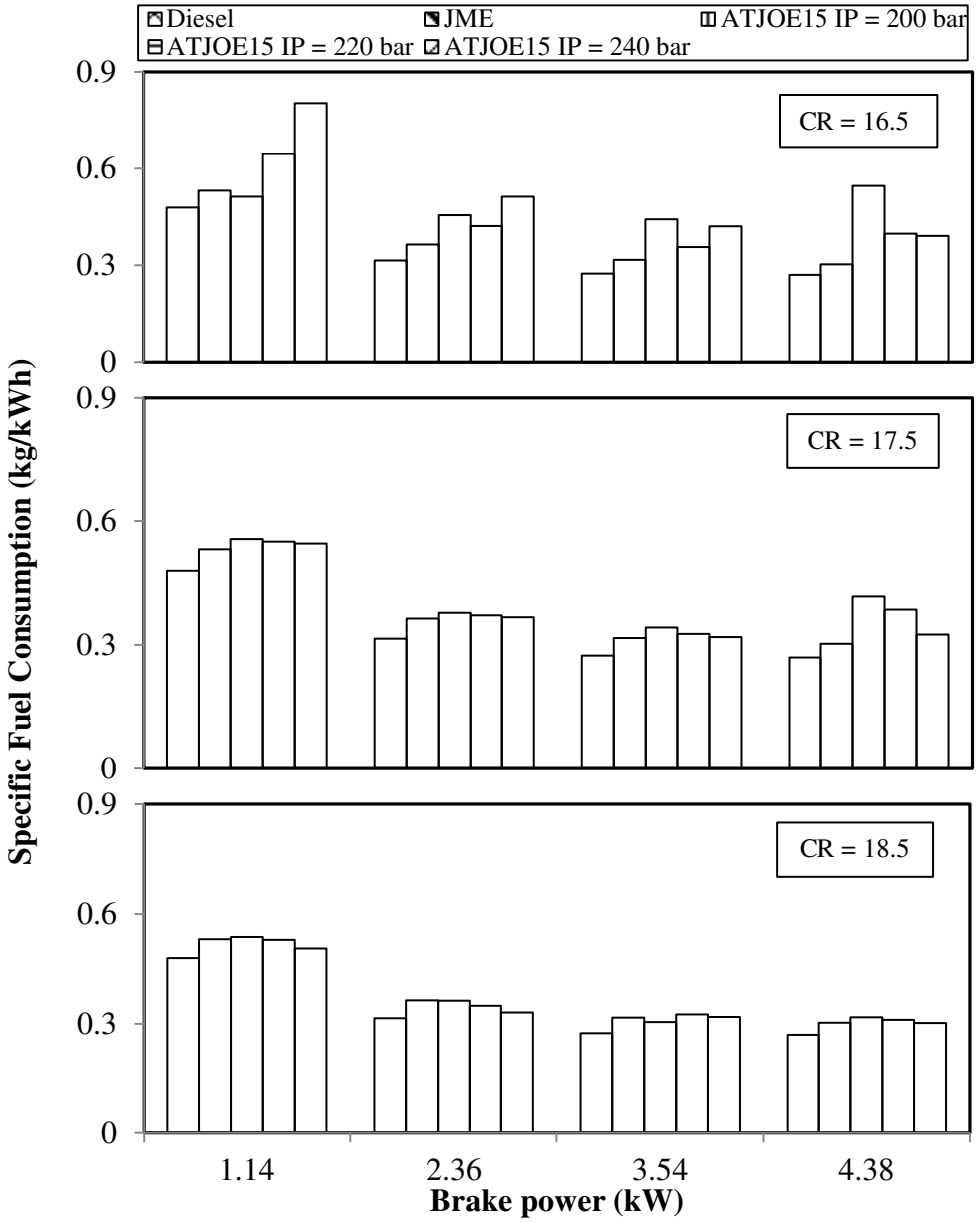

Fig. 5.5.7 Variation of specific fuel consumption with brake power at different compression ratios and nozzle opening pressures

It is apparent from the figure that the BSFC values of ATJOE15 emulsion are found to be higher than those of diesel and the JME operations at all compression ratios and nozzle opening pressures, which is attributed to the lower calorific value of the ATJOE15 emulsion. In comparison, the BSFC values of the ATJOE15 emulsion at different compression ratios and nozzle opening pressures are comparatively higher with the lower compression ratio and at lower nozzle opening pressure. The minimum value of the BSFC obtained for the ATJOE15 emulsion at 16.5 compression ratio is 0.3906 kg/kWh at an nozzle opening pressure of 220 bar, which is higher by about 44.8% compared to that of diesel operation.

At the standard compression ratio of 17.5 and higher nozzle opening pressure of 240 bar, with the ATJOE15 emulsion, a minimum BSFC of 0.316 kg/kWh is obtained, which is higher by about 20.6% compared to that of diesel. The minimum BSFC value of 0.3017 kg/kWh is obtained at the compression ratio of 18.5 and the nozzle opening pressure of 240 bar, which is higher by about 11.9% compared to that of diesel, at full load.

5.5.3.3 Exhaust gas temperature

The variation of exhaust gas temperature with load for the ATJOE15 emulsion at different compression ratios and nozzle opening pressures, in comparison with the JME and diesel is depicted in Fig. 5.5.8. It is apparent from the figure that the exhaust gas temperature of the ATJOE15 emulsion increased with the increase in the brake power, and decreased with the increase in the compression ratio and nozzle opening pressures. Also, it can be ascertained from the figure, that the engine operating parameters which resulted with a minimum BSFC and maximum brake thermal efficiency, were the ones which contributed the minimum exhaust gas temperature.

On an average, the exhaust gas temperature of the ATJOE15 emulsion is reduced by about 10.7%, when the compression ratio was increased from 17.5 to 18.5. The possible reason for this trend could be that, the increased compression ratio actually increases the air temperature inside the cylinder, consequently reducing the ignition delay, causing a better and more complete burning of the fuel. Similarly, at higher nozzle opening pressures, the exhaust gas temperature of the ATJOE15 emulsion is found to be lower by about 5.9% than that of standard nozzle opening pressure. Higher exhaust gas temperatures are found with the ATJOE15 emulsion at a lower nozzle opening pressure.

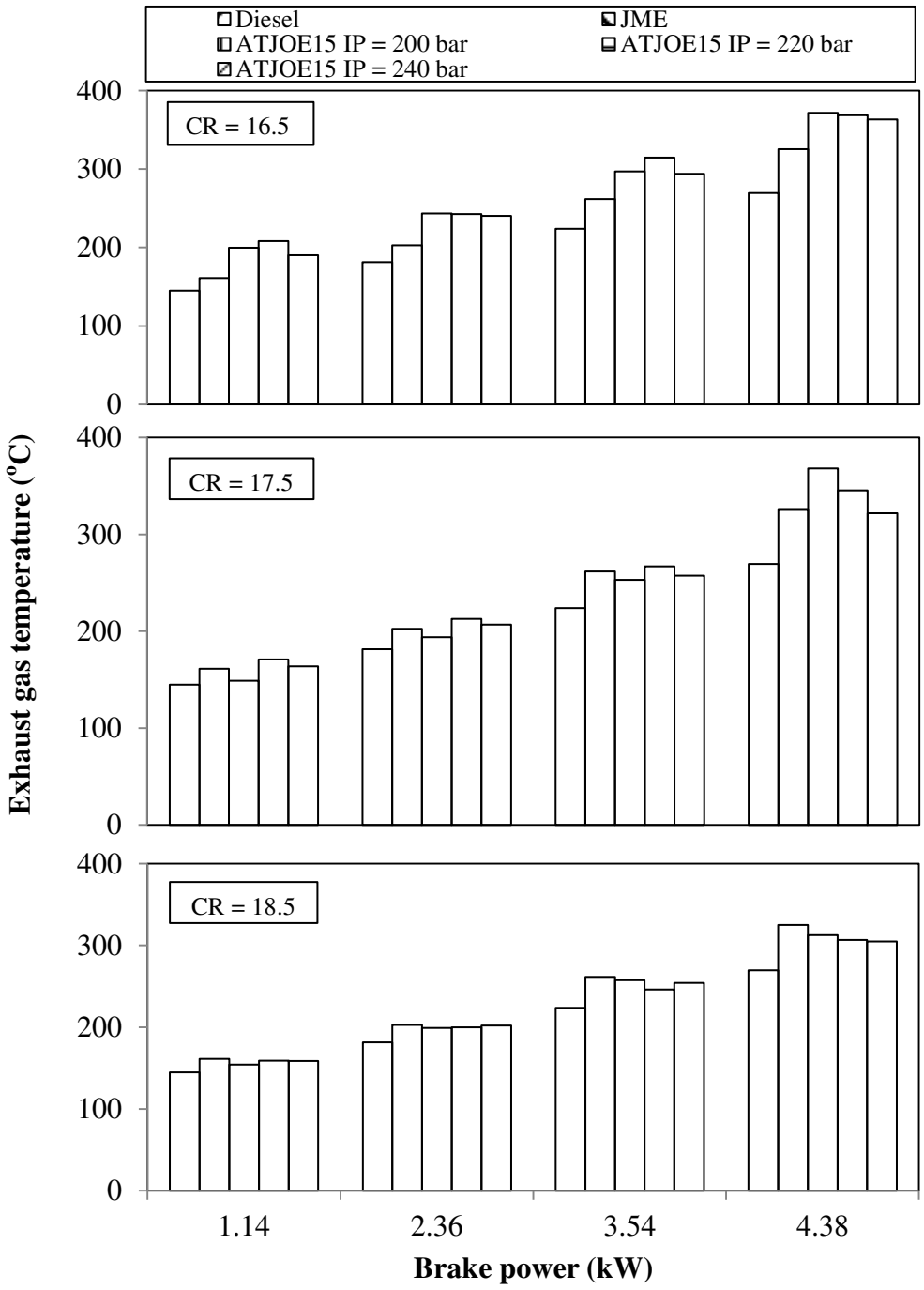

Fig. 5.5.8 Variation of exhaust gas temperature with brake power at different compression ratios and nozzle opening pressures

This happened due to the distribution of larger droplets inside the combustion chamber, which promoted heterogeneous combustion, while a finer droplet size distribution at higher nozzle opening pressures gave a relatively better fuel–air mixing and smoother combustion. Similar reasons are reported by Zhang et al. [199] in their work on the effects of highly dispersed spray nozzle on fuel injection characteristics and emissions of a heavy-duty diesel engine.

5.5.4 Emission parameters

5.5.4.1 BSHC emissions

The variations of the brake specific HC emissions with the brake power for diesel, JME and the ATJOE15 emulsion, at different compression ratios and nozzle opening pressures are shown in Fig. 5.5.9.

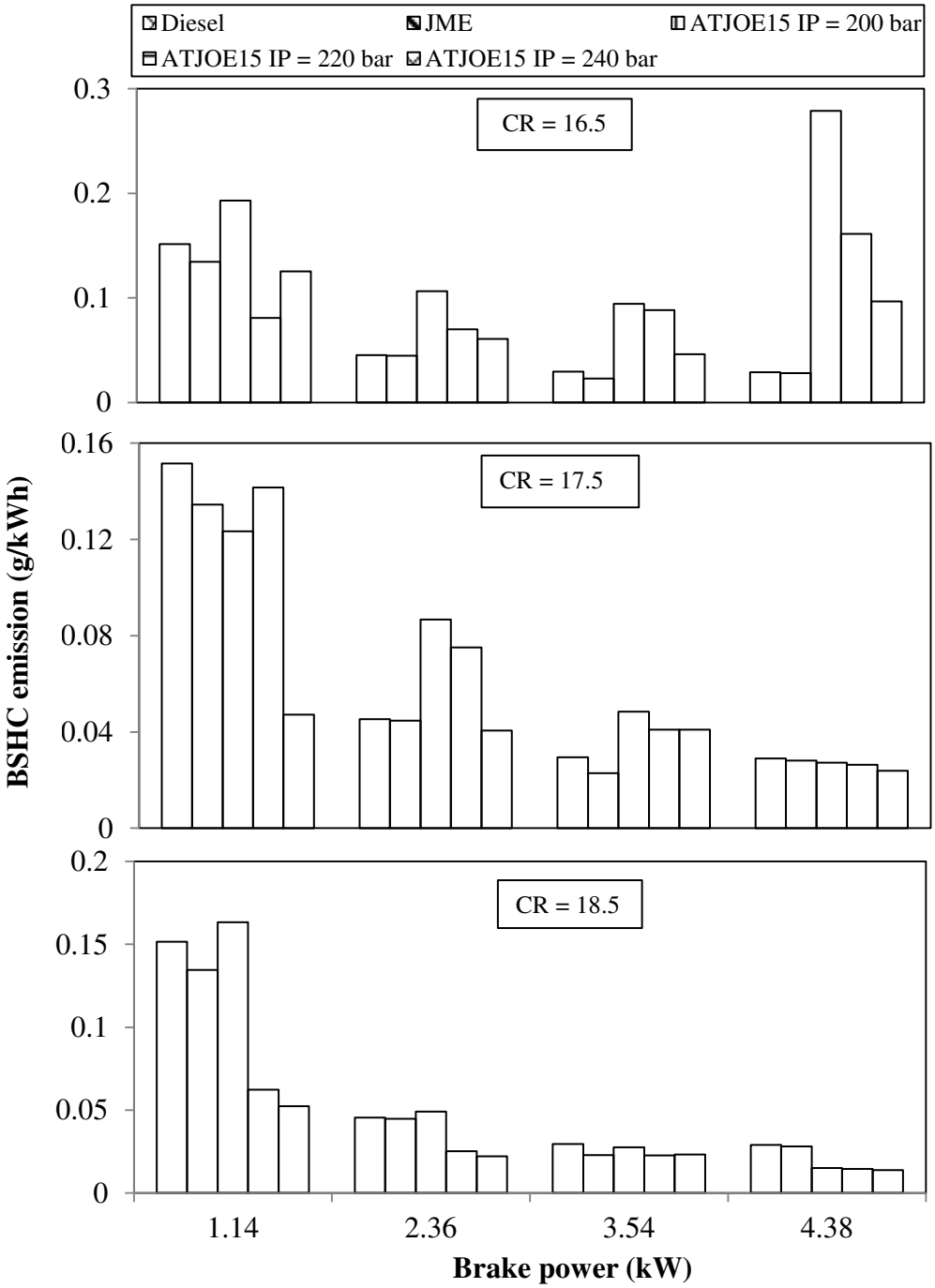

Fig. 5.5.9 Variation of BSHC emission with brake power at different compression ratios and nozzle opening pressures

The BSHC emissions decreased with an increase in the engine load. This is attributed to higher cylinder gas temperatures at higher engine loads, which led to more efficient combustion of fuel at higher temperatures, producing lower quantities of HC emissions. At higher nozzle opening pressures, the HC emissions decreased due to superior fuel-air mixing in the combustion chamber.

With the lower compression ratio, the HC emissions are found to be drastically higher, compared to those of diesel and the JME operations. At a lower compression ratio, insufficient heat of compression, delays the ignition, and therefore, the HC emissions increased. Similar reasons are reported by Jindal et al [20] in their work on the effect of the compression ratio and nozzle opening pressure in a DI diesel engine running on Jatropha methyl ester. At a standard compression ratio, the HC emissions of the ATJOE15 emulsion at different nozzle opening pressures are found to be lower in the range of 5.9% to 17.7% compared to that of diesel at full load. At a higher compression ratio, the HC emissions of the ATJOE15 emulsion at different nozzle opening pressures are found to be lower between 48.2% and 52.8% compared to that of diesel at full load.

5.5.4.2 BSCO emissions

Figure 5.5.10 illustrates the variation of the brake specific CO emissions with brake power for the ATJOE15 emulsion at different compression ratios and nozzle opening pressures, in comparison with the JME and diesel. With the lower compression ratio of 16.5, the temperature reached is also low, and thus more CO is exhausted from the engine. The minimum value of CO obtained at this compression ratio is about 0.1267 g/kWh, which is higher by about 92% compared to that of diesel operation.

At the standard compression ratio of 17.5, the CO emissions of ATJOE15 are found to be higher by about 84.8%, 13.9% and 11.4% at 200, 220 and 240 bar nozzle opening pressures respectively, compared to those of diesel operation. The longer spray penetration and larger fuel droplets may be the factors for the higher CO emissions in the case of the ATJOE15 emulsion. This reason was supported by Pei Lin Zhou [181], in his research work. It can be observed that the CO emissions are higher at lower nozzle opening pressure, and lower at higher nozzle opening pressures. At a higher compression ratio of 18.5, the CO emissions of ATJOE15 are found to be lower by about 48.2%, 50.7% and 55.3% with the 200, 220 and 240 bar nozzle opening pressures respectively, in comparison with diesel operation.

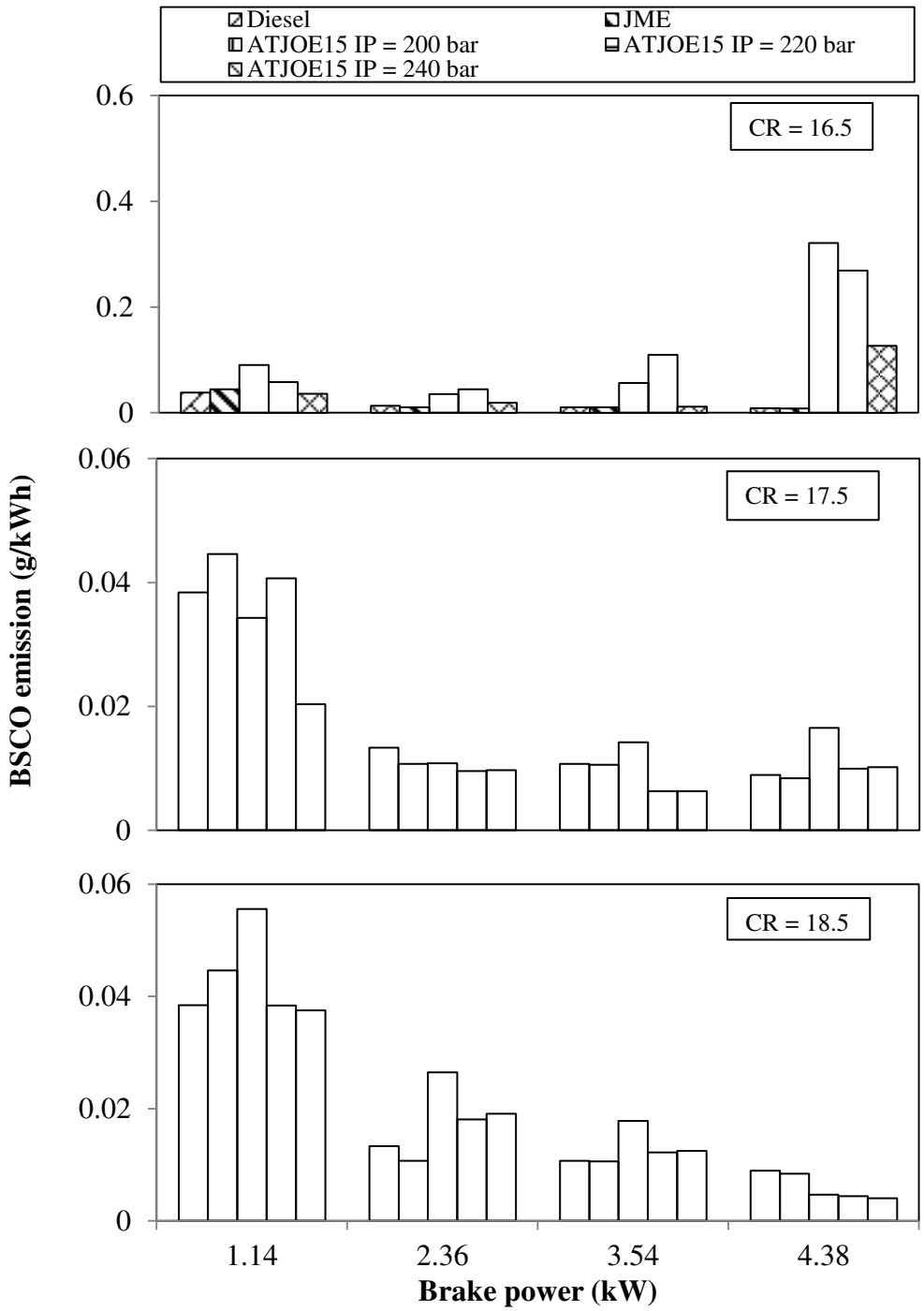

Fig. 5.5.10 Variation of BSCO emission with brake power at different compression ratios and nozzle opening pressures

The possible reason for this trend could be that the increased CR actually increases the air temperature inside the cylinder, reducing the ignition delay, causing a better and more complete burning of the fuel. Similar reasons are reported by Raheman and Ghadge [195], in their work on mahua biodiesel with variable compression ratios.

5.5.4.3 BSNO emissions

Figure 5.5.11 depicts the variation of brake specific nitric oxide (BSNO) emissions, with respect to brake power for the ATJOE15, at different compression ratios and nozzle opening pressures.

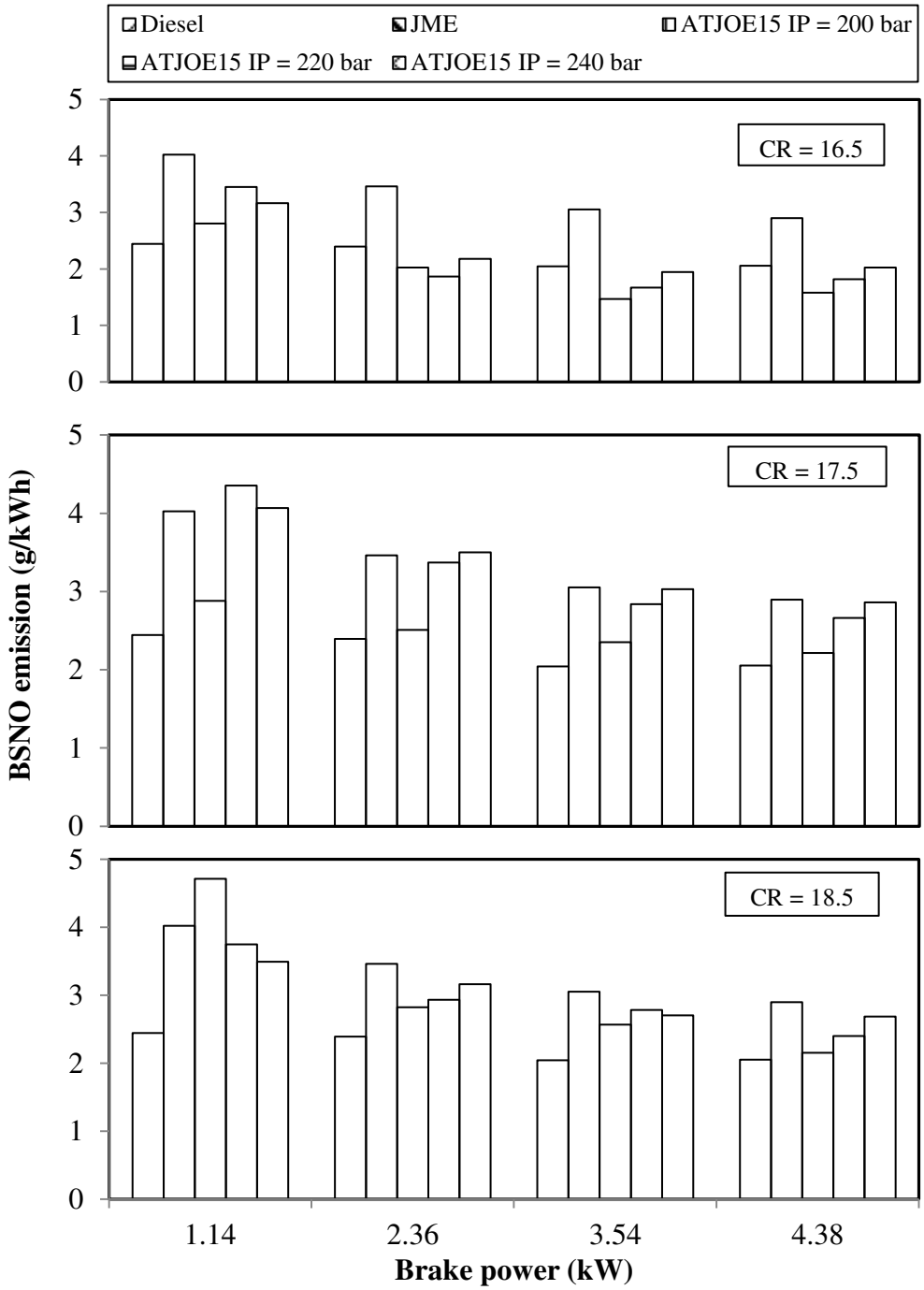

Fig. 5.5.11 Variation of BSNO emission with brake power at different compression ratios and nozzle opening pressures

It is apparent from the figure that the BSNO emissions are found to be higher by about 29% and 2% in the JME and ATJOE15 operations compared to that of diesel at full load, standard

compression ratio and nozzle opening pressure. At the compression ratio of 17.5, in the ATJOE15 operation, the higher nozzle opening pressure leads to further increase in the NO emissions by about 29.6% and 39.1% in comparison with diesel at full load. In comparison with the JME, the NO emissions from the ATJOE15 emulsion are found to be lower in the order of 1.3% to 8.1% at the compression ratio of 17.5 and different nozzle opening pressures. When the nozzle opening pressure is decreased, the NO emissions diminished for all the fuel mixtures. An increase in the nozzle opening pressure decreases the particle diameter and caused the ATJOE15 emulsion fuel spray to vaporize quickly. So, a higher nozzle opening pressure initially generates faster combustion rates, resulting in higher temperatures. As a consequence, the NO concentrations are observed more at higher nozzle opening pressures. Similar results are reported by Gumus [200], in his work on hazelnut kernel oil of Turkish origin as alternative fuel in diesel engines.

When the compression ratio is reduced to 16.5, the NO emissions of the ATJOE15 emulsion are found to be lower by about 23%, 11.6% and 1.6% compared to that of diesel operation at nozzle opening pressures of 200, 220 and 240 bar respectively. When compared to the JME operation, the NO emissions of the ATJOE15 emulsion are found to be lower in the range between 30.2% and 45.4%. A lower compression ratio will reduce the in-cylinder temperatures, and thus the flame temperatures during combustion, which will suppress the NO emissions. Similar reasons are reported by Raheman and Ghadge [195], in their work on mahua biodiesel with variable compression ratios. With the higher compression ratio of 18.5, the NO emissions from the ATJOE15 emulsion are found to be higher in the range of 4.6% to 30.7%, compared to that of diesel.

5.5.4.4 Smoke opacity

Figure 5.5.12 depicts the variation of the smoke opacity, with respect to the brake power for diesel, JME and the ATJOE15 emulsion, at different compression ratios and nozzle opening pressures. The smoke emissions from JME are found to be lower than those of diesel, as a consequence of the oxygen content in the JME that reduces the formation of smoke. In the case of ATJOE15, the smoke opacity is found to be higher by about 8.9% at the standard compression ratio and standard nozzle opening pressure of 200 bar. When the nozzle opening pressure is increased to 220 bar and 240 bar, the smoke opacity of ATJOE15 is found to be reduced by about 3.9% and 26.4% respectively, compared to that of diesel operation.

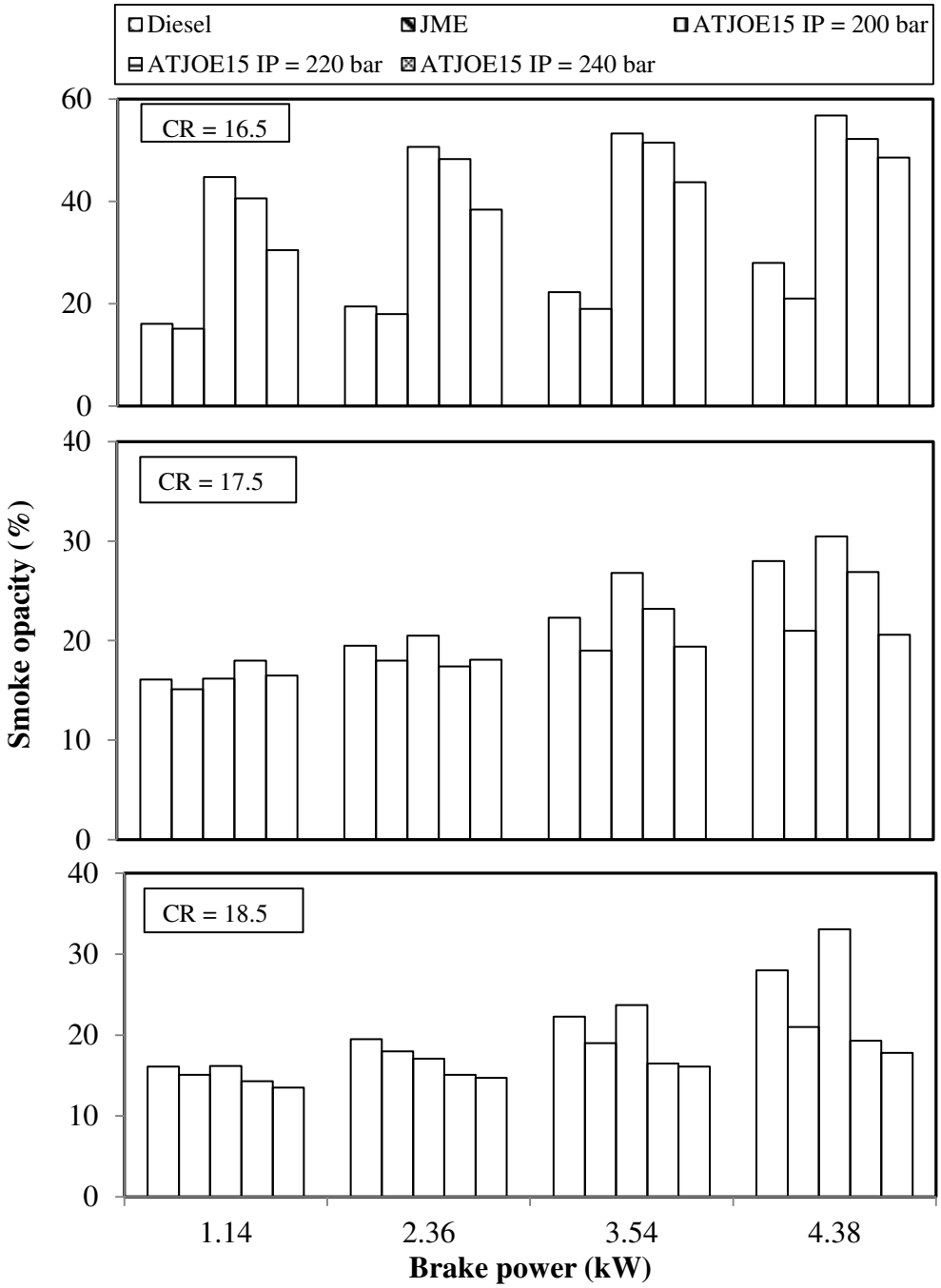

Fig.5.5.12 Variation of smoke opacity with brake power at different compression ratios and nozzle opening pressures

The values of smoke opacity of the ATJOE15 emulsion at nozzle opening pressures of 200, 220 bar are higher in the range of 28% and 45.2% compared to that of JME operation. With 240 bar nozzle opening pressure, the smoke opacity of the ATJOE15 emulsion is found to be lower by 1.9% compared to that of JME.

At a reduced compression ratio of 16.5, the smoke opacities of ATJOE15 emulsion at all the nozzle opening pressures are found to be higher in the range between 42% and 50.6%,

compared to that of diesel operation. At a higher compression ratio of 18.5, the smoke opacity of the ATJOE15 emulsion at nozzle opening pressure 200 bar is found to be higher by about 18.2% and with the higher nozzle opening pressures, the smoke emission values reduced by about 31% and 36.4% compared to that of diesel. As the compression ratio increases, the maximum temperature during combustion increases, and this in turn, decreases the smoke opacity and this is vice versa in the case of a lower compression ratio. When the nozzle opening pressure is increased, the fuel particle diameter will become smaller. Therefore, the fuel-air mixture will become better throughout the combustion period, and hence the smoke opacity will be lower. Similar reasons are reported by Cenk Sayin and Mertin Gumus [201], in their investigation on the impact of the compression ratio and injection parameters on the performance and emissions of a DI diesel engine fueled with biodiesel-blended diesel fuel.

5.5.5 Closure

The summary of the experimental results on the effect of the compression ratio and nozzle opening pressure on the combustion, performance and emission parameters obtained in a single cylinder, diesel engine fueled with the ATJOE15 emulsion shows improved performance and lower emissions, with a higher compression ratio of 18.5 and nozzle opening pressure of 240 bar. The maximum thermal efficiency is noticed at this operating condition. The maximum reduction in the HC, CO and smoke emissions by about 52.8%, 55.3% and 36.4% respectively, is noticed with the ATJOE15 emulsion at the same operating conditions. The NO emission at this condition is still found to be higher, by about 30.7% compared to that of diesel operation, at full load.

5.6 Combined effects of injection timing and nozzle opening pressure on the combustion, performance and emission parameters of a diesel engine fueled with the ATJOE15 emulsion

5.6.1 General

From the summary of the experimental results on the combustion, performance and emissions of a single cylinder diesel engine fueled with the ATJOE15 emulsion, it is observed that the CO and NO emissions from the engine are higher than those of diesel operation. Therefore, it is proposed to study the combined effects of varying the injection timings and nozzle opening pressures of the engine fueled with the ATJOE15 emulsion, in comparison with diesel and JME operation. Three different injection timings viz., 21.5, 23 and 24.5 ^{o}CA bTDC, and three nozzle opening pressures viz. 200, 220 and 240 bar, were chosen for this study. The standard compression ratio of 17.5 is maintained during this study. This chapter details about the combined effects of fuel injection timing and fuel nozzle opening pressure on the combustion, performance and emission characteristics of the diesel engine fueled with the ATJOE15 emulsion.

5.6.2 Combustion parameters

5.6.2.1 Pressure crank angle history

Figure 5.6.1 depicts the pressure crank angle history of the engine fueled with diesel, JME and the ATJOE15 emulsion for different injection timings and nozzle opening pressures, at full load condition. It is observed from the figure, that the combustion starts earlier in the range between 0.3 and 3.4 ^{o}CA for the ATJOE15 emulsion, with the injection timings of 23, 24.5 ^{o}CA bTDC and at all three nozzle opening pressures compared to that of diesel. For the same operating conditions, it is found that the combustion starts later by about 0.5 to 2.1 ^{o}CA for the ATJOE15 emulsion at all the nozzle opening pressures in comparison with the JME operation. At the injection timing of 21.5 ^{o}CA bTDC, it is found that the commencement of combustion is noticed later, which ranges from 1.3 to 2.2 ^{o}CA in comparison with the diesel operation. The peak cylinder pressure for diesel occurs at 12.4 ^{o}CA aTDC, whereas for the ATJOE15, the peak pressure occurs earlier in the range of 0.3 and 2.3 ^{o}CA, with the injection timings of 23 and 24.5 ^{o}CA bTDC, and the nozzle opening pressures of 220 bar and 240 bar compared to that of diesel at full load. With the retarded injection timing of 21.5 ^{o}CA bTDC and at all nozzle opening pressures, the peak cylinder pressure is found to be lower in the range of 8.4 bar to 8.7 bar compared to that of diesel operation. Similar results are reported by Kannan and Anand [202], in their investigation on a diesel engine fueled with diestrol at

varying nozzle opening pressures and injection timings. It is seen from the figure, that among all the tested injection timings and nozzle opening pressures, with the injection timing of 24.5 ^{o}CA bTDC and nozzle opening pressure of 200 bar, the ATJOE15 operation produced the highest cylinder pressure value of 79.5 bar at 370.6 ^{o}CA, which is earlier by about 2.2 ^{o}CA and later by about 0.2 ^{o}CA than those of diesel and the JME operations respectively. The early or later occurrences of the ignition during advancement and retardation in the injection timing are attributed to the increased or decreased cylinder gas temperatures respectively.

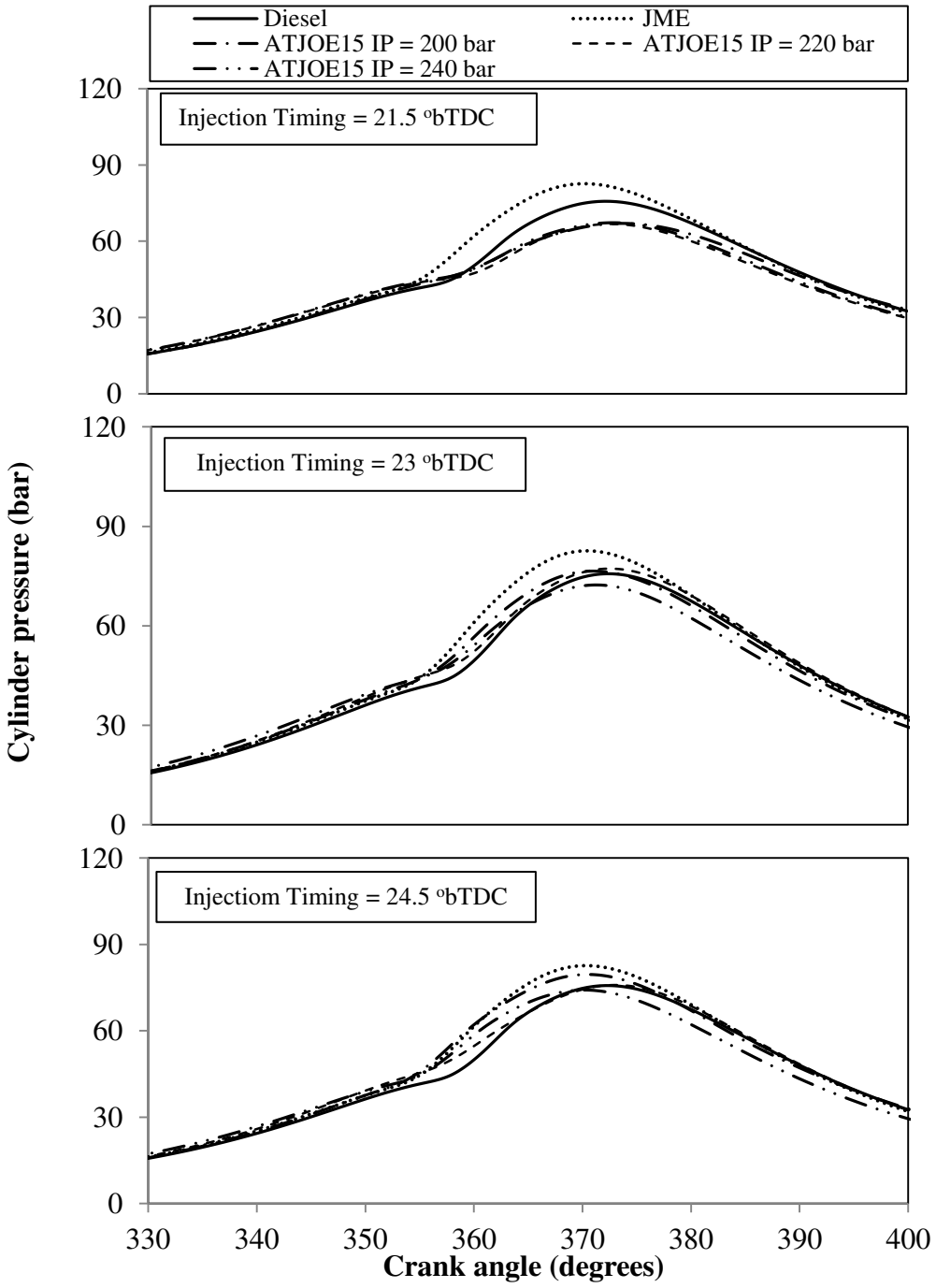

Fig. 5.6.1 Variation of cylinder pressure with crank angle at different injection timings and nozzle opening pressures

5.6.2.2 Ignition delay

Figure 5.6.2 depicts the ignition delay for diesel, JME and ATJOE15, for different injection timings and nozzle opening pressures at all loads. It is seen from the figure, that the ignition delay is found to be lower with the increase in the engine load and advanced injection timing. The reduction in the ignition delay in these conditions might be the result of the higher combustion chamber wall temperature at the time of injection, and reduced exhaust gas dilution [107].

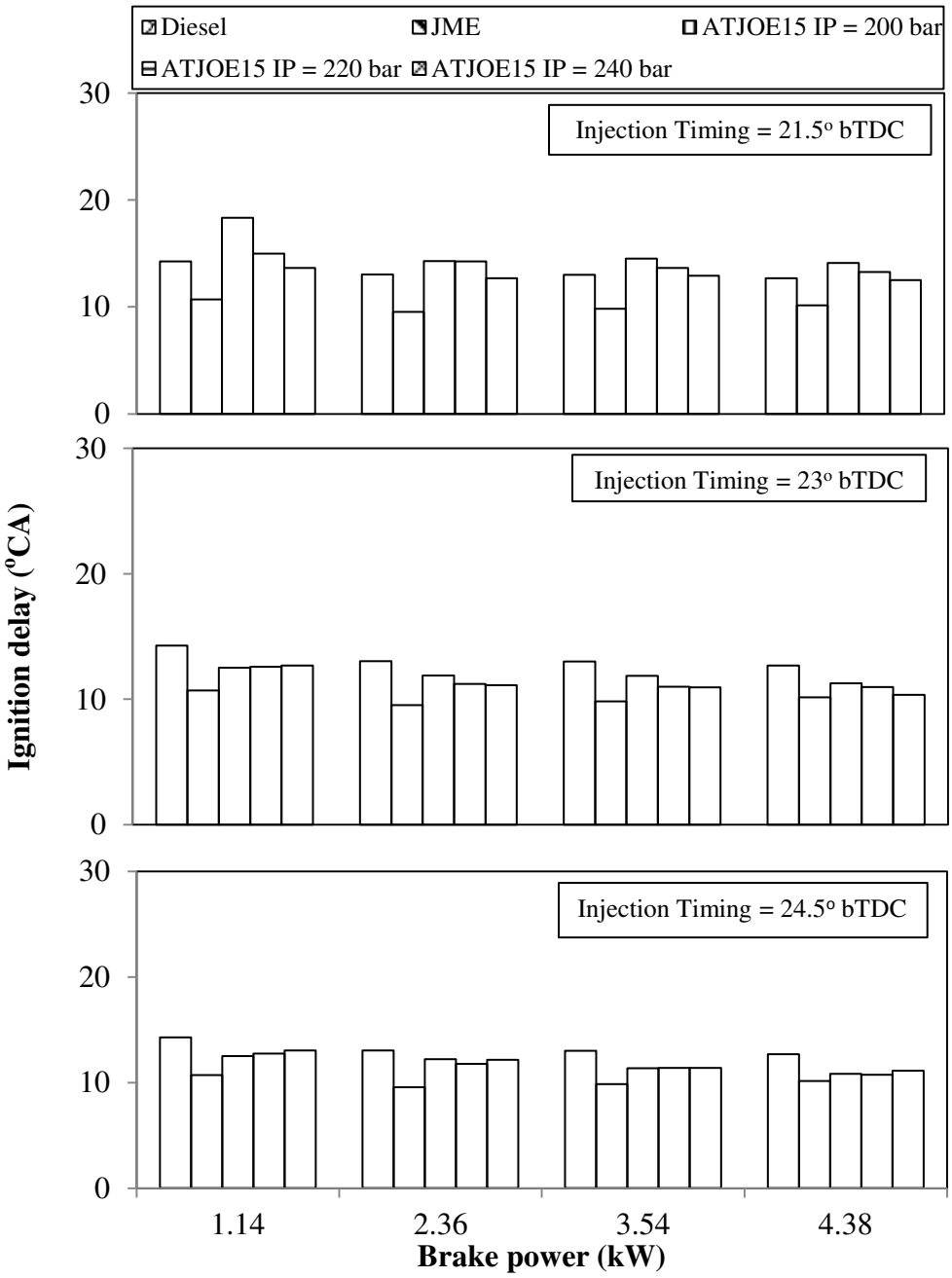

Fig. 5.6.2 Variation of ignition delay with brake power at different injection timings and nozzle opening pressures

With the retarded injection timing of 21.5 ^{o}CA, the ignition delay of the ATJOE15 emulsion is found to be higher than that of diesel and the JME at all nozzle opening pressures. At this injection timing and for all the nozzle opening pressures, the ignition delay values of the ATJOE15 emulsion are found to be longer by about 0.5 ^{o}CA to 1.4 ^{o}CA compared to that of diesel operation at full load. It is apparent from the figure, that at full load condition, the ignition delay of the ATJOE15 emulsion is found to be shorter in the range of 0.3 ^{o}CA to 0.9 ^{o}CA with the injection timings of 23 ^{o}CA and the higher nozzle opening pressures of 220 bar and 240 bar compared to that of diesel operation. In comparison with the JME operation, the engine fueled with the ATJOE15 emulsion exhibits a longer ignition delay under all operating conditions. Among all the tested injection timings and nozzle opening pressures, a shorter ignition delay period of 10.36 ^{o}CA is observed for the ATJOE15 operation, with the injection timing of 23 ^{o}CA bTDC and nozzle opening pressure of 240 bar. The reduction in the ignition delay period is mainly due to the improved atomization at higher nozzle opening pressure and higher cetane number of the ATJOE15 compared to that of diesel, at full load.

5.6.2.3 Heat release rate

Figure 5.6.3 illustrates the variation of heat release rate, with respect to the crank angle for the ATJOE15 emulsion at full load, for different injection timings and nozzle opening pressures, and for diesel and JME operations. The occurrence of the maximum heat release rate for the ATJOE15 emulsion in different operating conditions on an average, shifted approximately from 2.7 to 6.9 ^{o}CA at full load, compared to that of diesel operation. The intensity of the premixed combustion phase for diesel is found to be the highest, whereas, it is lower in the case of JME and the ATJOE15 emulsion at injection timings of 23, 24.5 ^{o}CA and higher nozzle opening pressures.

With the retarded injection timing of 21.5 ^{o}CA, at all the nozzle opening pressures, the premixed combustion is found to be higher than that of diesel operation, as a result of longer ignition delay. The variation of the maximum heat release rate between diesel, JME and the ATJOE15 emulsion operations at different injection timings and nozzle opening pressures lies between 5.4 and 11.19 J/^{o}CA. For the JME and the ATJOE15 emulsion, less amount of fuel is accumulated during the shorter ignition delay period, which results in lower heat release rates, compared to that of diesel at advanced injection timings.

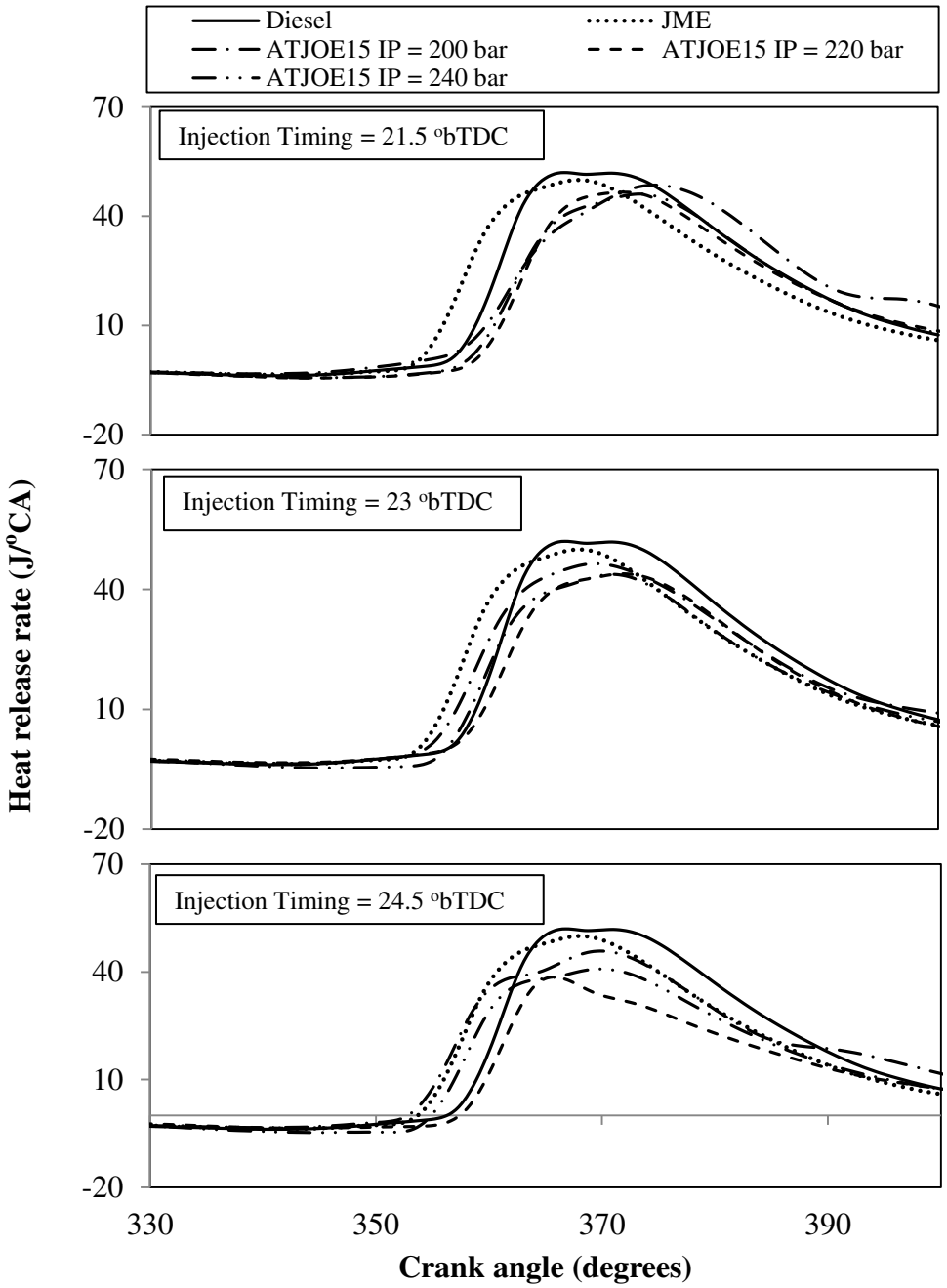

Fig. 5.6.3 Variation of heat release rate with crank angle at different injection timings and nozzle opening pressures

5.6.2.4 Maximum cylinder pressure

Figure 5.6.4 depicts the variation of maximum cylinder pressure with brake power for diesel, JME and the ATJOE15 emulsion at full load, for the different injection timings and nozzle opening pressures. It is seen from the figure that the peak cylinder pressure is increased with an increase in the engine load in all operating conditions. With the retarded injection timing of 21.5 ^{o}CA, the peak cylinder pressure for the JME and diesel are found to be higher than

that of the ATJOE15 emulsion at all nozzle opening pressures, while the trend is the reverse, for the advanced injection timings. This shows that, with the advanced injection timings and all nozzle opening pressures, the ATJOE15 emulsion showed faster premixed combustion, which leads to a higher peak cylinder gas pressure.

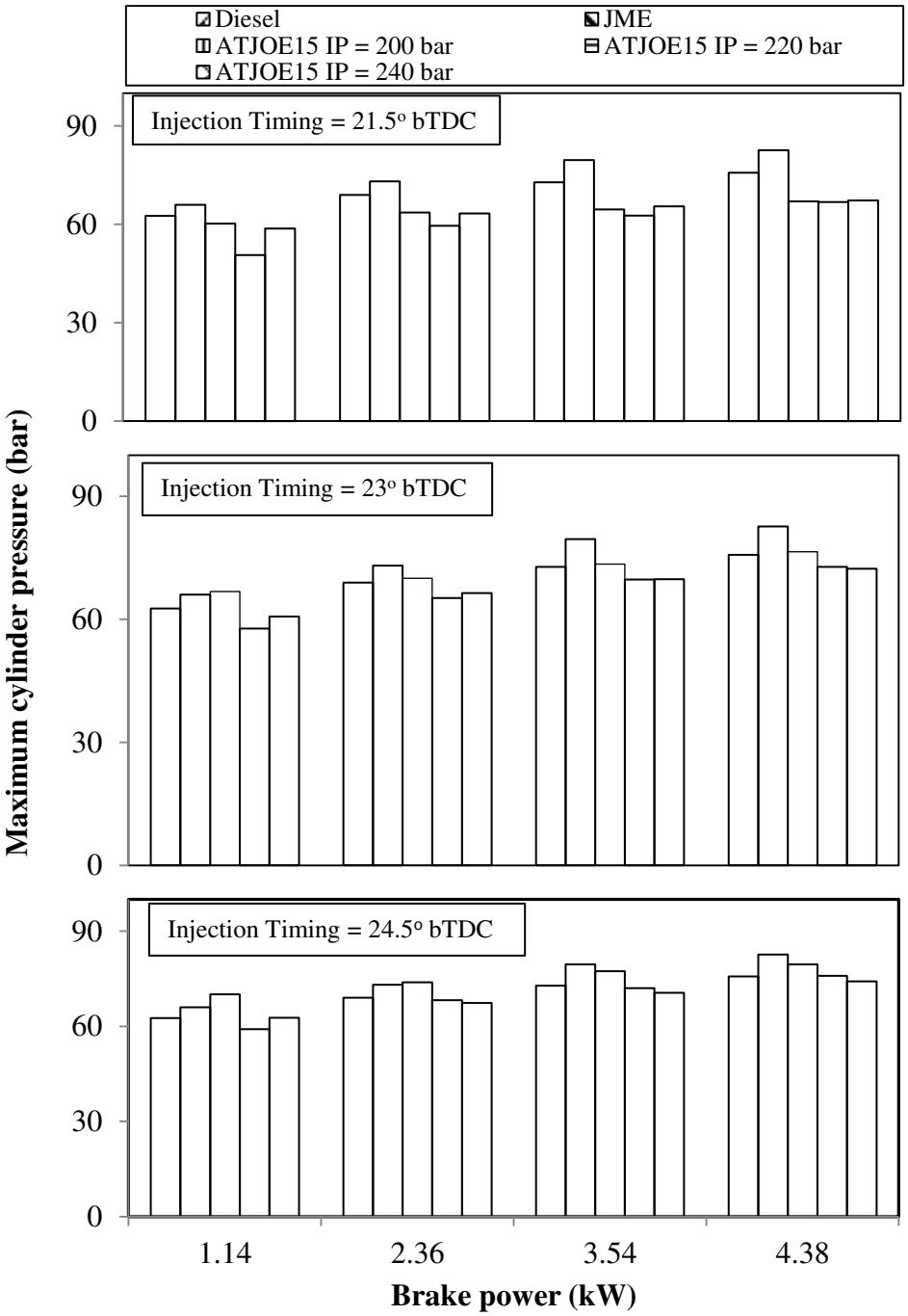

Fig. 5.6.4 Variation of maximum cylinder pressure with brake power at different injection timings and nozzle opening pressures

With the injection timing of 21.5 ^{o}CA and all three nozzle opening pressures, the maximum cylinder pressure of the ATJOE15 emulsion is found to be lower in the range between 8.4

and 8.9 bar, compared to that of diesel operation at full load. With the injection timings of 23, 24.5 ^{o}CA and at all nozzle opening pressures, the maximum cylinder pressure values of the ATJOE15 emulsion are noticed to be higher in the range of 0.2 to 3.8 bar compared to that of diesel operation. In comparison with the JME operation, the peak cylinder pressure of the ATJOE15 emulsion is found to be lower, in all the load conditions.

5.6.2.5 Combustion duration

The variation of combustion duration with the brake power under different injection timings and nozzle opening pressures, for the engine fueled with the ATJOE15 emulsion, JME and diesel is illustrated in Fig. 5.6.5.

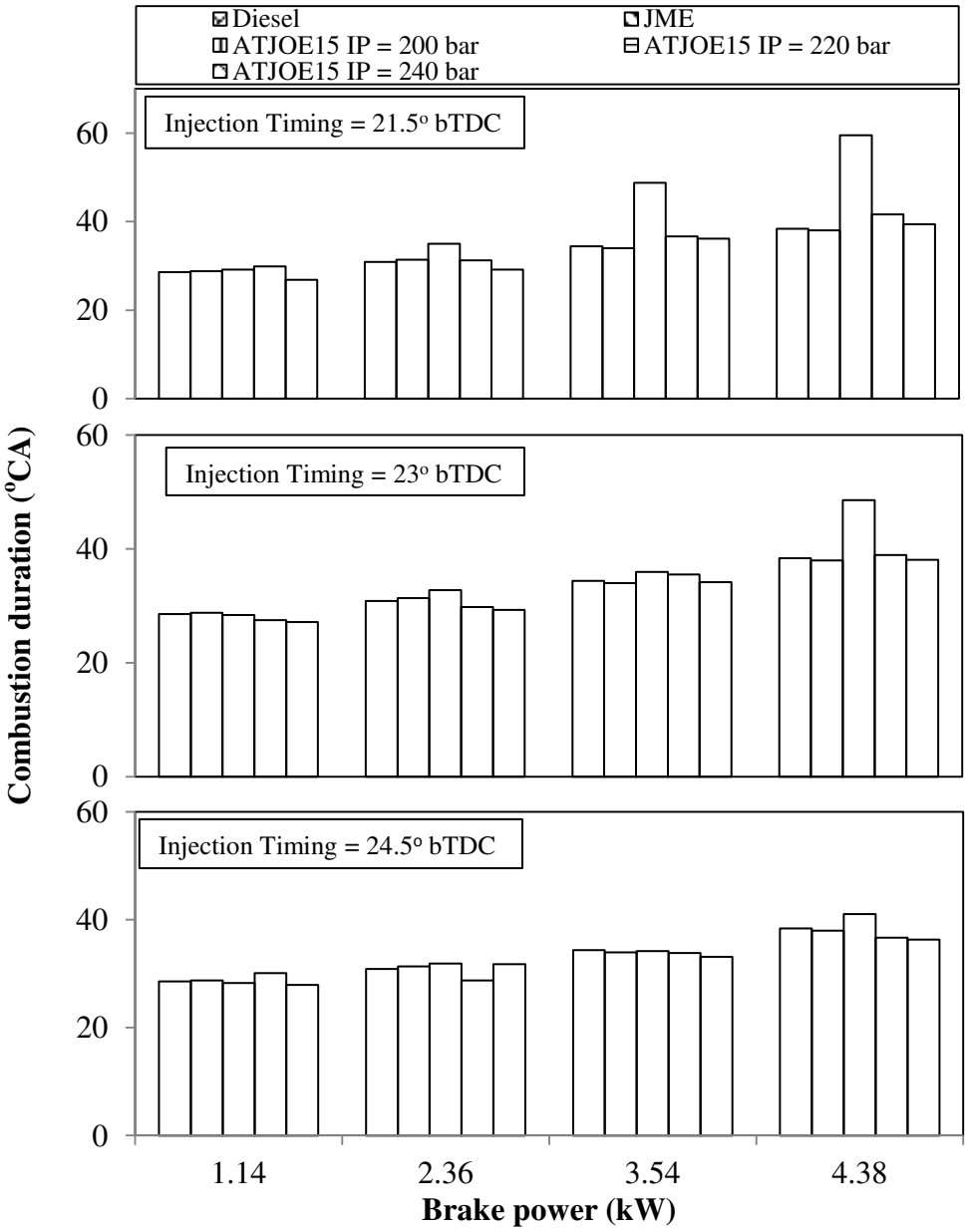

Fig. 5.6.5 Variation of combustion duration with brake power at different injection timings and nozzle opening pressures

With the injection timing of 24.5 ^{o}CA and at full load, the values of the combustion duration are found to be 38.4, 38, 41.1, 36.7 and 36.3 ^{o}CA for the diesel, JME and the ATJOE15 at nozzle opening pressures of 200, 220 and 240 bar respectively. The advancement in the injection timing and increase in the nozzle opening pressure, leads to a lower combustion duration of ATJOE15 emulsion compared to that of diesel operation. The reason was that, the increase in the nozzle opening pressure and advancement in the injection timing, which compensated the slow vaporization of the ATJOE15 emulsion, by proper mixing of the fuel and air that resulted in a better combustion. Further, the faster burning rate in the uncontrolled phase of combustion due to proper mixing of the fuel and air, resulted in the reduction in the combustion duration. Similar results are reported by Kannan et al. [203], in their study on the effect of nozzle opening pressure and timing on the performance of a diesel engine fueled with biodiesel.

The combustion duration of the ATJOE15 is found to be lower between 1.7 and 2.1 ^{o}CA compared to that of diesel at advanced injection timing of 24.5 ^{o}CA bTDC. With the retarded injection timing of 21.5 ^{o}CA bTDC, the combustion duration of the ATJOE15 emulsion is found to be higher by an average of 8.4 and 8.8 ^{o}CA than that of diesel and the JME operation, which is attributed to a longer ignition delay. With the injection timing of 23 ^{o}CA and at different nozzle opening pressures, the combustion duration of the ATJOE15 emulsion is found to be higher in the range from 0.5 to 10.2 ^{o}CA and 0.1 to 10.6 ^{o}CA compared to those of diesel and the JME respectively.

5.6.3 Performance parameters

5.6.3.1 Brake thermal efficiency

The variation of brake thermal efficiency with brake power for the ATJOE15 emulsion in comparison with the JME and diesel, at different injection timings and nozzle opening pressures, is depicted in Fig. 5.6.6. It is seen from the figure that, for all the injection timings and nozzle opening pressures tested, the brake thermal efficiency of the ATJOE15 emulsion increases with an increase in the load. With the standard injection timing and nozzle opening pressure, the ATJOE15 emulsion produced a maximum thermal efficiency of 32.98% which is higher by about 3.6% compared to that of diesel operation. For the same injection timing, with the higher nozzle opening pressures of 220 bar and 240 bar, the brake thermal efficiency of the ATJOE15 emulsion is found to be higher than that of diesel by about 4.6% and 6.1% respectively, at full load. The increase in the brake thermal efficiency of the ATJOE15

emulsion is due to better combustion, caused by the proper atomization and air entrainment, as a result of the nozzle opening pressure. This is in agreement with the results reported by Kannan and Anand [192], in their work on waste cooking oil.

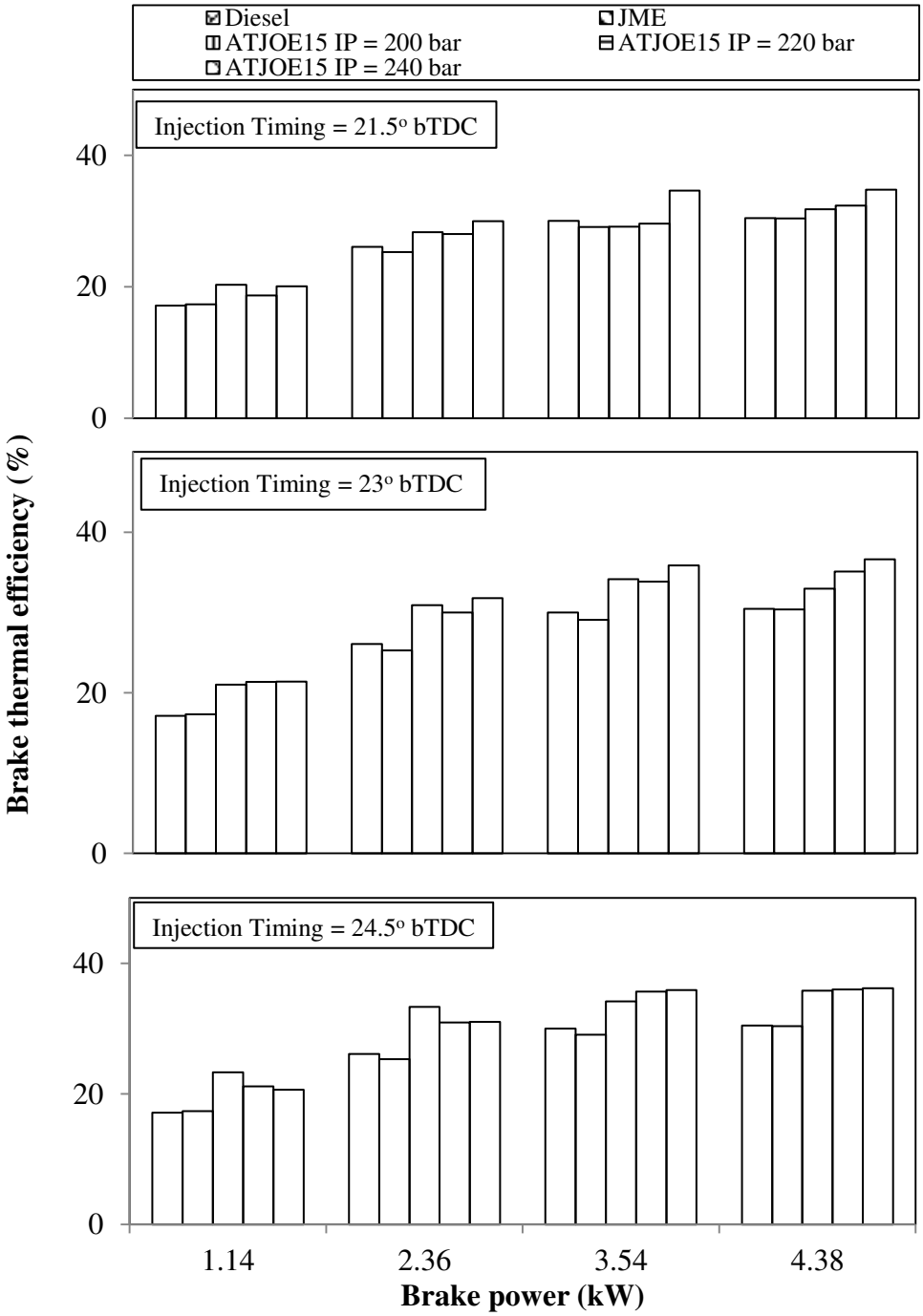

Fig. 5.6.6 Variation of brake thermal efficiency with brake power at different injection timings and nozzle opening pressures

When the injection timing is retarded to 21.5 ^{o}CA bTDC, the brake thermal efficiency of the ATJOE15 emulsion is found to be higher by an average of 2.5% at all nozzle opening pressures, at full load. With the advanced injection timing of 24.5 ^{o}CA bTDC, the brake

thermal efficiency of the ATJOE15 emulsion is found to be higher by an average of 5.5% at all nozzle opening pressures. Overall, the maximum thermal efficiency is noticed with the injection timing of 23 ^{o}CA bTDC and nozzle opening pressure of 240 bar.

5.6.3.2 Brake specific fuel consumption

The variation of brake specific fuel consumption with brake power for the ATJOE15 emulsion, JME and diesel at various injection timings and nozzle opening pressures, is depicted in Fig. 5.6.7.

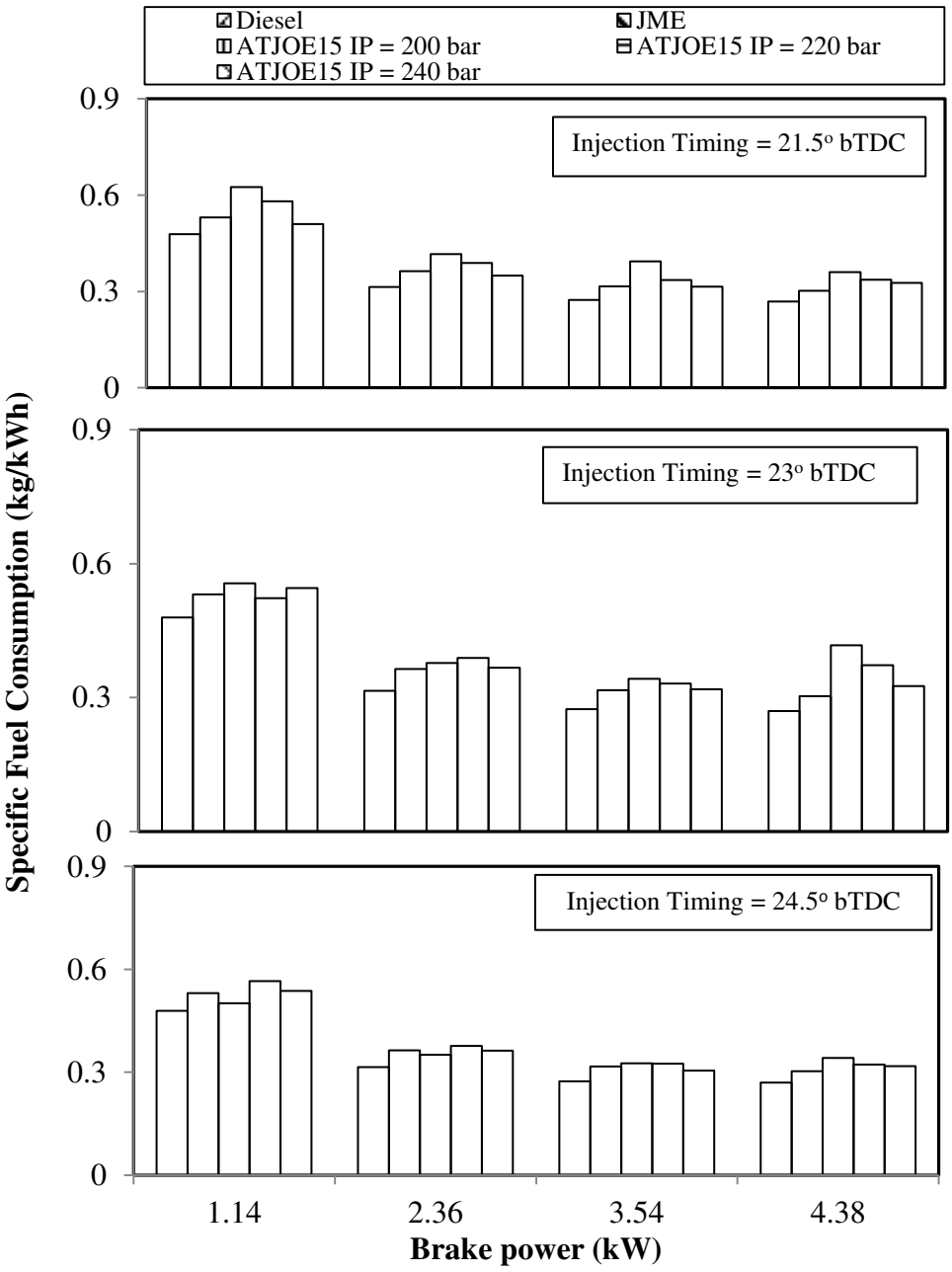

Fig. 5.6.7 Variation of specific fuel consumption with brake power at different injection timings and nozzle opening pressures

It is apparent from the figure, that the BSFC values of the ATJOE15 emulsion are found to be higher than those of diesel and the JME operations at all injection timings and nozzle opening pressures, which is attributed to the lower calorific value of the ATJOE15 emulsion. The BSFC values of the ATJOE15 emulsion are comparatively higher with the retarded injection timings and at lower nozzle opening pressures. The lowest value of the BSFC obtained for the ATJOE15 emulsion at 24.5 ^{o}CA bTDC is 0.3177 kg/kWh at an nozzle opening pressure of 240 bar, which is higher by about 17.8%, compared to that of diesel operation.

At the standard injection timing of 23 ^{o}CA bTDC and higher nozzle opening pressure of 240 bar, with the ATJOE15 emulsion, the minimum BSFC of 0.3254 kg/kWh is obtained, which is higher by about 20.6% compared to that of diesel. The minimum BSFC value of 0.3017 kg/kWh is obtained at the injection timing of 21.5 ^{o}CA bTDC and the nozzle opening pressure of 240 bar, which is higher by about 21.2% compared to that of diesel, at full load. The minimum BSFC values were obtained with increased nozzle opening pressures, because of improved atomization and better mixing process. This is in agreement with the results reported by Jindal et al. [20], in their work on the effect of the compression ratio and nozzle opening pressure in a DI diesel engine running on Jatropha methyl ester. Similarly, at advanced injection timings, the combustion starts earlier and more fuel can burn before the piston reaches the top dead centre, which causes lower BSFC values.

5.6.3.3 Exhaust gas temperature

The variation of exhaust gas temperature with load for the ATJOE15 emulsion at different injection timings and nozzle opening pressures in comparison with the JME and diesel is depicted in Fig. 5.6.8. It is apparent from the figure that the exhaust gas temperature of the ATJOE15 emulsion increased with the increase in the brake power, and decreased with the advanced injection timings and increased nozzle opening pressures. On an average, the exhaust gas temperature of the ATJOE15 emulsion is reduced by about 6.1%, when the injection timing was advanced from 23 to 24.5 ^{o}CA. The possible reason for this trend could be that, with the advancement in injection timing, the efficiency of the engine cycles increases, when the conversion of chemical energy into heat is concentrated near the TDC. These results are in agreement with those of Rahemen and Ghadge [195], when they conducted experiments with magua biodiesel at variable compression ratios and injection timings. Similarly, at higher nozzle opening pressures, the exhaust gas temperature of the

ATJOE15 emulsion is found to be lower by about 11.1% than that of standard nozzle opening pressure.

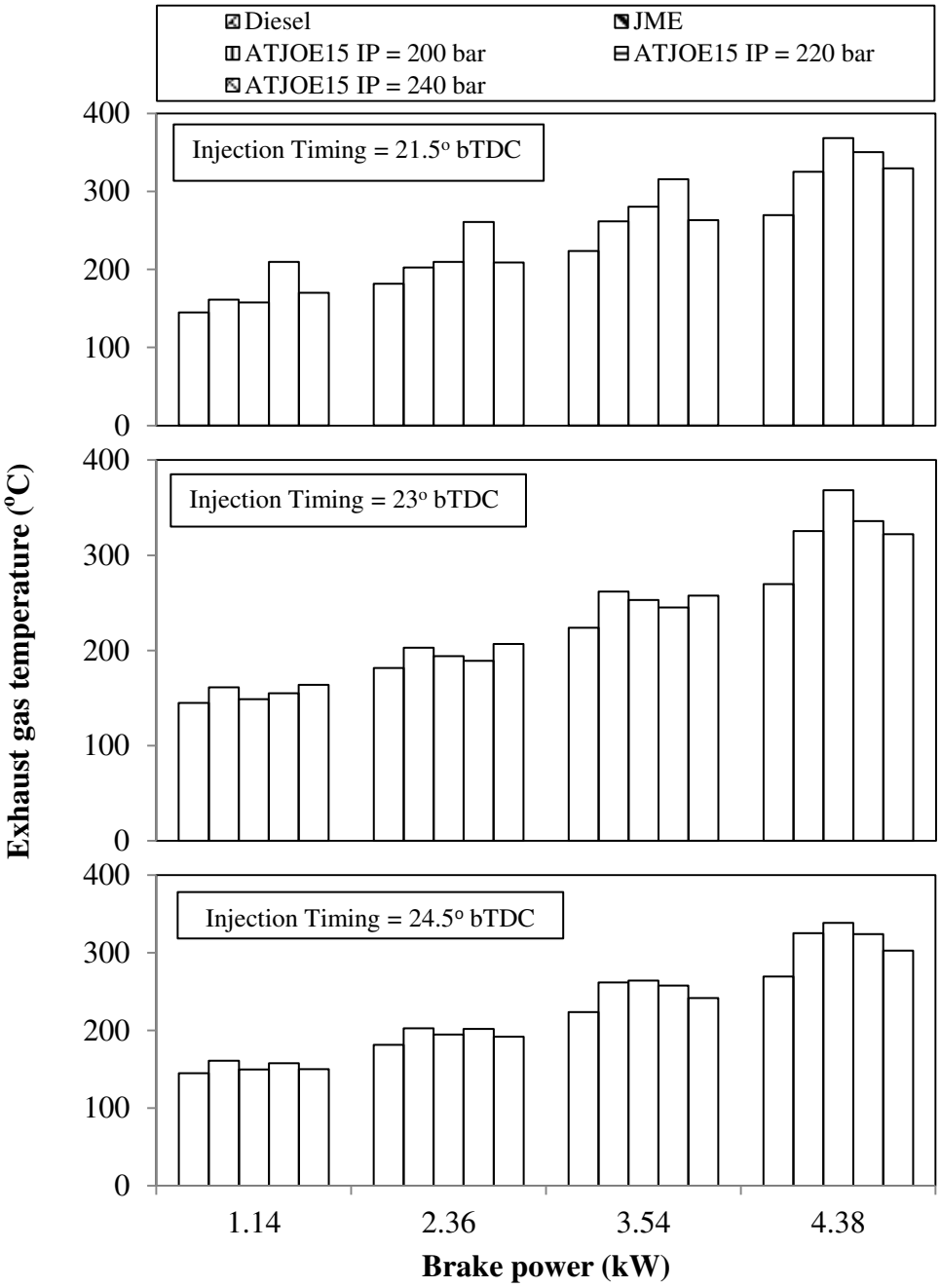

Fig. 5.6.8 Variation of exhaust gas temperature with brake power at different injection timings and nozzle opening pressures

Higher exhaust gas temperatures are found with the ATJOE15 emulsion at a lower nozzle opening pressure, compared to higher nozzle opening pressures. It may be attributed to the distribution of the larger droplets inside the combustion chamber, which promoted heterogeneous combustion, while a finer droplet size distribution at higher nozzle opening pressures gave a relatively better fuel–air mixing and smoother combustion. Similar reasons

are reported by Zhang et al. [199], in their work on the effects of a highly dispersed spray nozzle on the fuel injection characteristics and emissions of a heavy-duty diesel engine. At retarded injection timings, the exhaust gas temperatures of the ATJOE15 emulsion are higher by about 2% compared to that of diesel at full load condition.

5.6.4 Emission parameters

5.6.4.1 BSHC emissions

The variations of brake specific HC emissions with the brake power for diesel, JME and the ATJOE15 emulsion, at different injection timings and nozzle opening pressures are shown in Fig. 5.6.9.

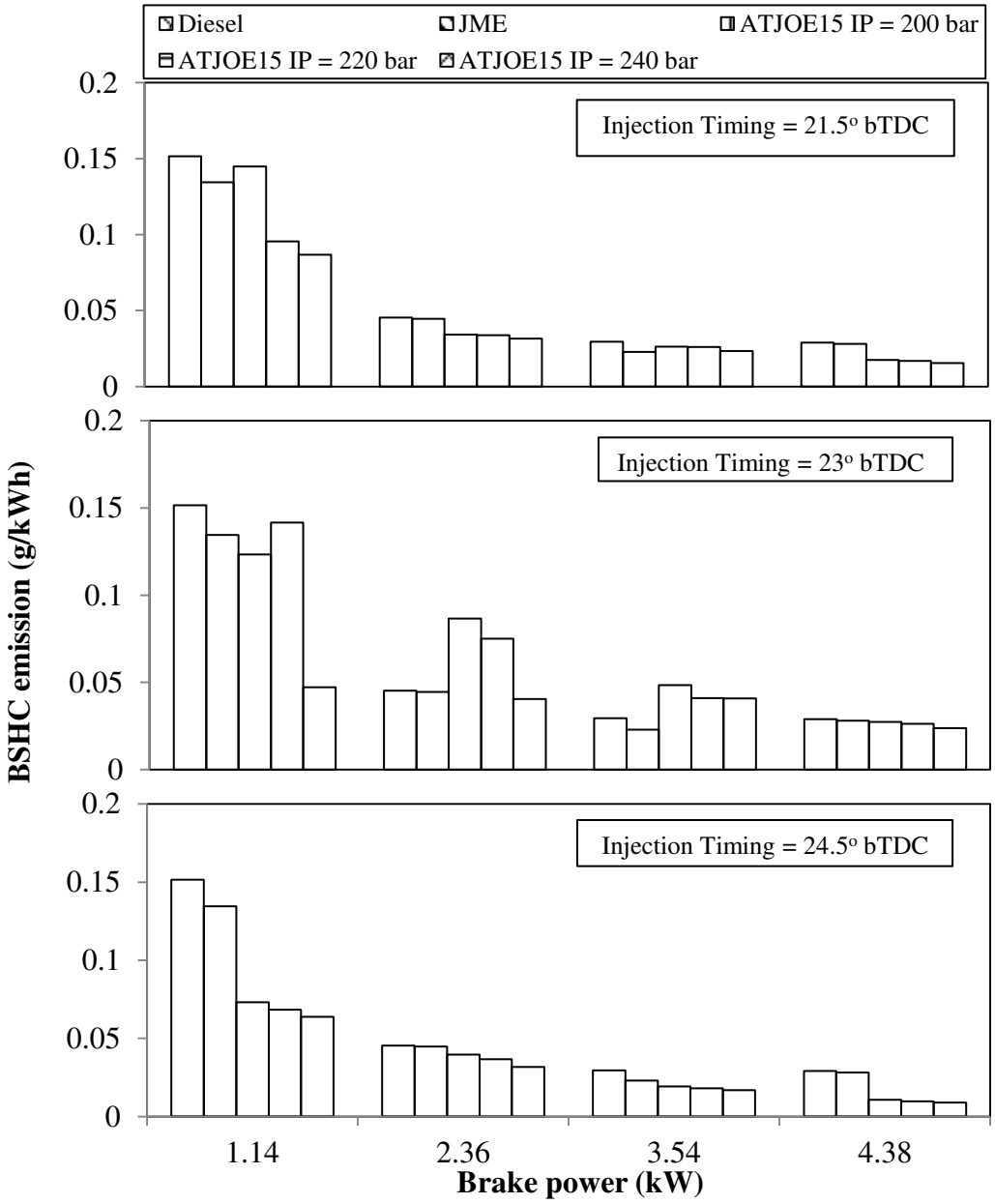

Fig. 5.6.9 Variation of BSHC emission with brake power at different injection timings and nozzle opening pressures

It is apparent from the figure that, with advanced injection timings and higher nozzle opening pressures, the HC emissions are found to be decreased, due to improved fuel-air mixing in the combustion chamber. With the retarded injection timing of 21.5 ^{o}CA, the HC emissions are found to be lesser by an average of 36% and 37%, compared to those of diesel and the JME operations respectively. At the standard injection timing of 23 ^{o}CA, the HC emissions of the ATJOE15 emulsion at different nozzle opening pressures are found to be lower in the range of 6.2% to 17.7% compared to that of diesel at full load. At an advanced injection timing of 24.5 ^{o}CA, the HC emissions of the ATJOE15 emulsion at different nozzle opening pressures are found to be lower between 63.1% and 69.4% compared to that of diesel at full load. At advanced injection timings, the cylinder charge is compressed near the TDC at relatively high temperatures, which diminishes the HC emissions. Similar reasons are also reported by Sayin et al [204] in their study on the performance and emission parameters of DI diesel engine using methanol-blended-diesel fuel.

5.6.4.2 BSCO emissions

Figure 5.6.10 illustrates the variation of brake specific CO emissions with brake power, for the ATJOE15 emulsion at different injection timings and nozzle opening pressures in comparison with the JME and diesel. With the retarded injection timing of 21.5 ^{o}CA, the CO emissions from the ATJOE15 emulsion are higher in the range between 56.2% and 61.2%. The lowest value of CO obtained at this injection timing is about 0.02039 g/kWh, which is higher by about 61.2% compared to that of diesel operation at full load.

At the standard injection timing of 23 ^{o}CA, the CO emissions of ATJOE15 are found to be lower by about 5.9%, 9.1% and 17.7% at 200, 220 and 240 bar nozzle opening pressures respectively, compared to those of diesel operation at full load. The longer spray penetration and larger fuel droplets may be the factors for higher CO emissions in the case of the ATJOE15 emulsion. This reason was supported by Pei Lin Zhou [181], in his research work. It can be observed that the CO emissions are higher at a lower nozzle opening pressure and lower at a high nozzle opening pressure. At the advanced injection timing of 24.5 ^{o}CA, the CO emissions of ATJOE15 are found to be lower by an average of 65% at all nozzle opening pressures, in comparison with diesel operation at full load. The possible reason for this trend could be that, the increased oxidation process between carbon and oxygen molecules happens at higher cylinder temperature.

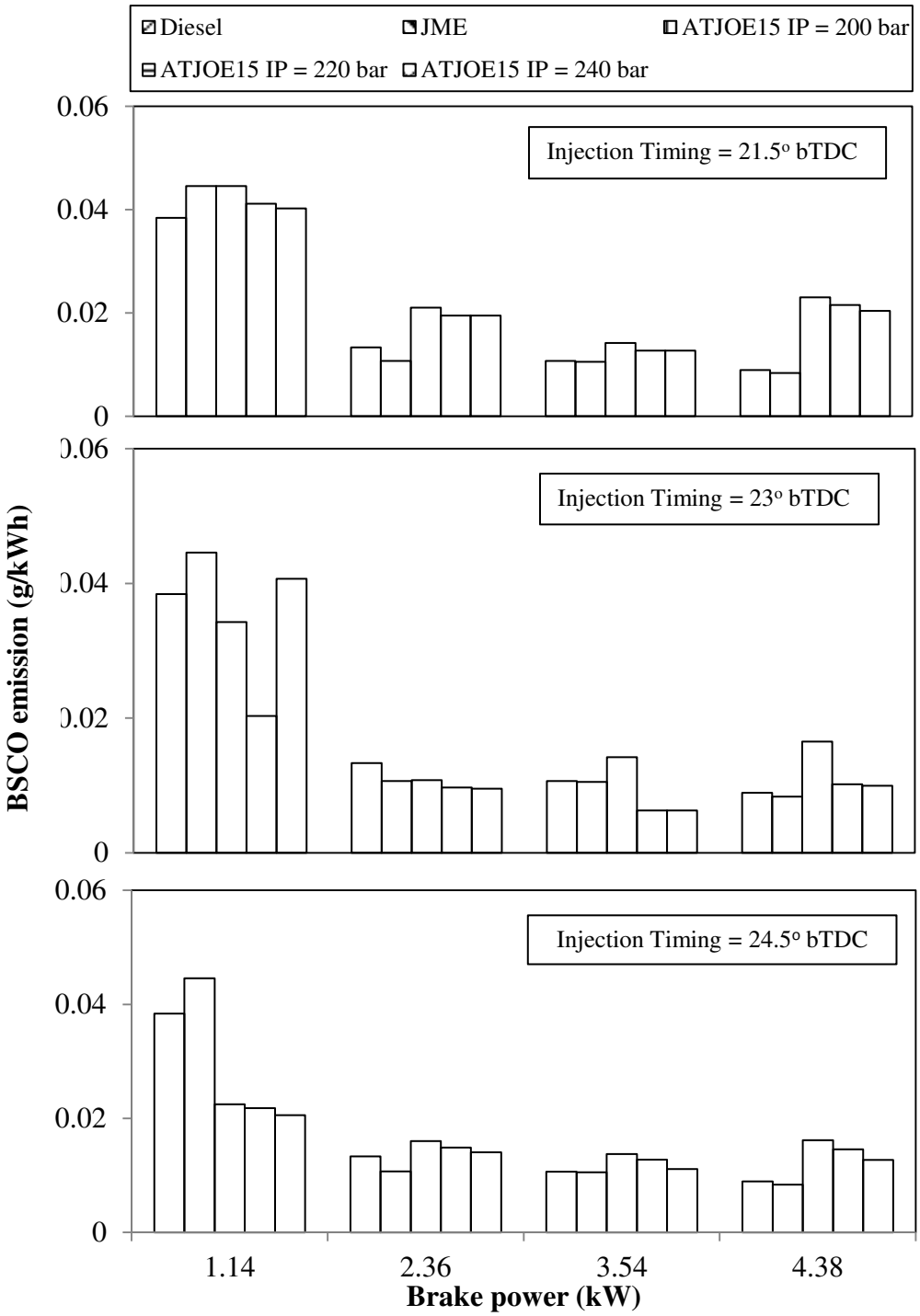

Fig. 5.6.10 Variation of BSCO emission with brake power at different injection timings and nozzle opening pressures

5.6.4.3 BSNO emissions

Figure 5.6.11 depicts the variation of brake specific nitric oxide (BSNO) emissions with respect to the brake power for the ATJOE15 at different injection timings and nozzle opening pressures.

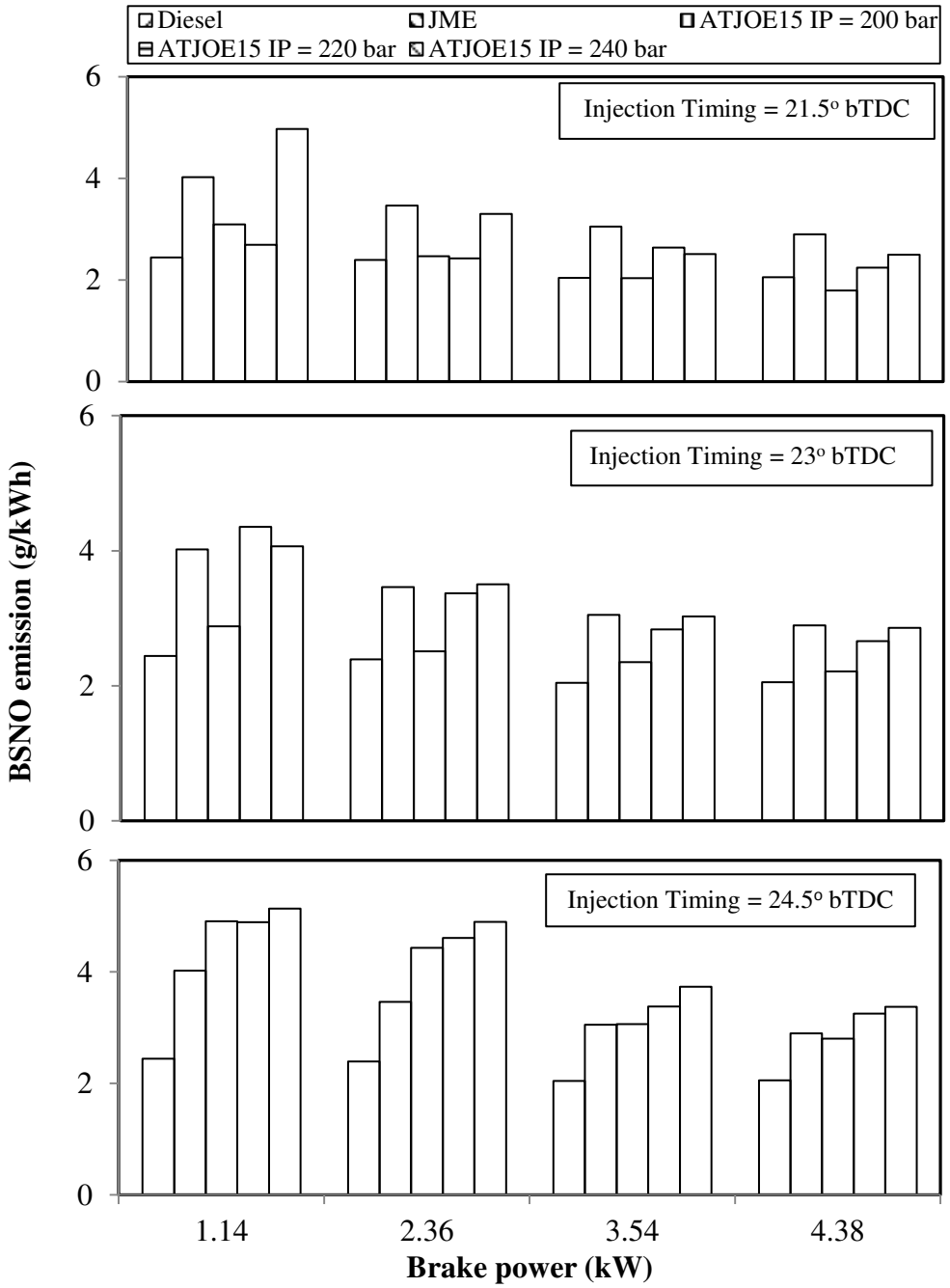

Fig. 5.6.11 Variation of BSNO emission with brake power at different injection timings and nozzle opening pressures

It is apparent from the figure that the BSNO emissions are found to be higher by about 29% and 2% in the JME and ATJOE15 operations, compared to those of diesel at full load, standard injection timing and nozzle opening pressure. Under the same operating condition, a higher nozzle opening pressure leads to further increase in NO emissions by about 29.6% and 39.1% in comparison with diesel at full load. In comparison with the JME, the NO emissions from the ATJOE15 emulsion are found to be lower in the order of 1.3% to 8.1% at an injection timing of 23 ^{o}CA and different nozzle opening pressures. The increase in the nozzle

opening pressure decreases the particle diameter and causes the ATJOE15 emulsion fuel spray to vaporize quickly. So, a higher nozzle opening pressure initially generates faster combustion rates, resulting in higher temperatures. As a consequence, the NO concentrations are observed more at higher nozzle opening pressures. Similar results are reported by Gumus [200], in his work on hazelnut kernel oil of Turkish origin, as an alternative fuel in diesel engines.

With the retarded injection timing of 21.5 ^{o}CA, the NO emissions of the ATJOE15 emulsion are found to be lower by about 12.8%, compared to that of diesel operation at the standard nozzle opening pressure of 200 bar. With the higher nozzle opening pressures of 220 and 240 bar, the NO emissions from the ATJOE15 emulsion are found to be higher by 8.9% and 21.4% respectively in comparison with diesel. In comparison with the JME operation, the NO emissions of the ATJOE15 emulsion are found to be lower in the range between 13.9% and 38.2%. Retarding the injection timing decreases the peak cylinder pressure and peak temperatures. As a consequence, the NO concentration starts to diminish. With the advanced injection timing of 24.5 ^{o}CA, the NO emissions from the ATJOE15 emulsion are found to be higher in the range of 36.4% to 64.3% compared to that of diesel.

5.6.4.4 Smoke opacity

Figure 5.6.12 depicts the variation of smoke opacity with respect to the brake power for the diesel, JME and the ATJOE15 emulsion operations, at different injection timings and nozzle opening pressures. The smoke emissions from JME are found to be lower than those of diesel, as a consequence of the oxygen content in the JME reducing the formation of smoke. In the case of ATJOE15, the smoke opacity is found to be higher by about 8.9% with the standard injection timing and standard nozzle opening pressure of 200 bar. When the nozzle opening pressure is increased to 220 bar and 240 bar, the smoke opacity of the ATJOE15 is found to be reduced by about 3.9% and 26.4% respectively, compared to that of diesel operation. The values of smoke opacity of the ATJOE15 emulsion at nozzle opening pressures of 200 and 220 bar are higher in the range of 28% and 45.2% compared to that of JME operation. With the 240 bar nozzle opening pressure, the smoke opacity of the ATJOE15 emulsion is found to be lower by 1.9% compared to that of JME. With the retarded injection timing of 21.5 ^{o}CA, the smoke opacities of ATJOE15 emulsion at all the nozzle opening pressures is found to be higher in the range between 24.5% and 45.5% compared to

that of diesel operation. With the advanced injection timing of 24.5 ^{o}CA, the smoke opacity of the ATJOE15 emulsion is found to be lower by about 5.3% to 26.7% at all the nozzle opening pressures compared to that of diesel. The smoke opacity decreases with an advancement in the injection timing, due to the existence of a higher combustion temperature which promotes soot oxidation, compared to that of standard injection timing operation, and this is vice versa in case of retarded injection timing.

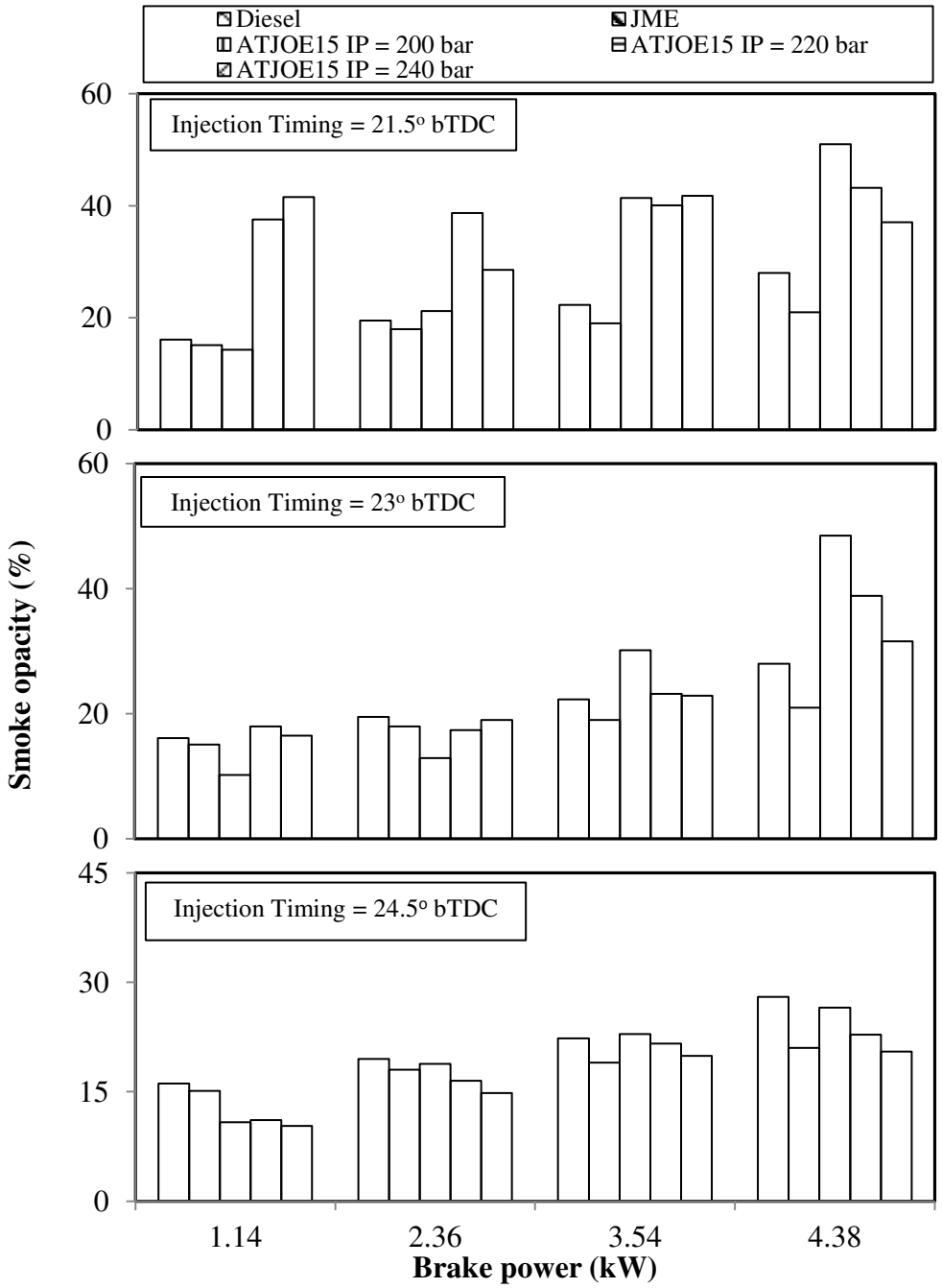

Fig. 5.6.12 Variation of smoke opacity with brake power at different injection timings and nozzle opening pressures

When the nozzle opening pressure is increased, the fuel particle diameter will become smaller. Therefore, the fuel-air mixture will become better throughout the combustion period, and hence, the smoke opacity will be lower. Similar reasons are reported by Sayin and Gumus [201], in their investigation on the impact of the compression ratio and injection parameters on the performance and emissions of a DI diesel engine fueled with biodiesel-blended diesel fuel.

The important findings of the investigation on combined effects of compression ratio, injection timing and nozzle opening pressure, in terms of percentage increase or decrease in different parameters are given in Table 5.3 and best set of parameters for all the tested fuels is given in Table 5.4.

5.6.5 Closure

The summary of the experimental results on the combined effects of injection timing and nozzle opening pressure on the combustion, performance and emission parameters obtained in a single cylinder, diesel engine fueled with the ATJOE15 emulsion, shows that with the retarded injection timing of 21.5 ^{o}CA, the NO emissions are found to be lower by about 12.8%, compared to that of diesel operation at the standard nozzle opening pressure of 200 bar. The brake thermal efficiency of the ATJOE15 emulsion is found to be higher by 4.3% compared to that of diesel in this operating condition. The smoke emissions are noticed to be higher by 23% compared to those of diesel at this condition.

Table 5.3 Percentage increase or decrease in different parameters with respect to diesel at full load

	FULL FACTORIAL DESIGN			Percentage change in the parameter with respect to diesel at full load (%)						
No.	**CR**	**IT**	**IP**	**BTE**	**BSFC**	**EGT**	**UBHC**	**CO**	**NO**	**Smoke**
1	16.5	21.5	200	-5.26	54.15	38.65	>100	>100	-34.97	>100
2	16.5	21.5	220	-1.75	61.98	46.41	>100	>100	-27.31	89.64
3	16.5	21.5	240	-9.06	>100	44.04	>100	>100	**-36.89**	79.64
4	16.5	23	200	-10.17	>100	37.68	>100	>100	-23.05	77.86
5	16.5	23	220	-1.90	44.88	36.53	>100	>100	-31.12	>100
6	16.5	23	240	7.48	47.68	34.59	>100	>100	-1.59	91.43
7	16.5	24.5	200	-2.89	44.09	32.05	>100	>100	4.60	47.14
8	16.5	24.5	220	0.35	48.90	26.03	>100	>100	-0.18	38.21
9	16.5	24.5	240	-2.95	>100	29.10	>100	>100	5.18	39.29
10	17.5	21.5	200	4.40	26.76	36.46	-39.60	>100	-12.87	82.14
11	17.5	21.5	220	6.17	33.91	29.73	94.62	>100	8.98	54.29
12	17.5	21.5	240	14.15	25.02	22.04	63.17	>100	21.41	32.50
13	17.5	23	200	8.24	54.79	16.30	-54.54	84.85	7.82	8.93
14	17.5	23	220	15.21	86.45	14.81	67.13	11.41	29.64	38.93
15	17.5	23	240	20.26	20.71	19.28	79.12	13.98	39.21	84.29
16	17.5	24.5	200	21.33	**17.54**	15.19	**-63.16**	81.21	36.43	-5.36
17	17.5	24.5	220	-12.92	86.45	35.34	>100	>100	24.48	>100
18	17.5	24.5	240	7.06	33.51	29.10	>100	>100	34.49	43.21
19	18.5	21.5	200	1.50	40.08	24.95	52.74	>100	4.07	-4.29
20	18.5	21.5	220	-10.71	59.23	25.41	39.50	72.31	11.43	97.50
21	18.5	21.5	240	0.95	59.07	26.98	86.31	>100	12.00	80.71
22	18.5	23	200	**25.81**	17.85	15.78	-45.00	10.00	4.88	-9.64
23	18.5	23	220	18.79	19.68	13.61	-32.34	5.24	16.89	-31.07
24	18.5	23	240	16.66	22.82	**12.95**	-44.17	11.65	30.75	-4.64
25	18.5	24.5	200	18.28	20.54	13.48	-48.22	**-48.22**	31.86	-11.79
26	18.5	24.5	220	18.12	20.37	18.40	-36.31	11.45	39.48	62.86
27	18.5	24.5	240	19.82	18.66	13.38	-52.24	-44.29	46.17	**-33.57**

Table 5.4 Best set of parameters for different fuel combinations

Sl.No	Parameter	Diesel (Standard conditions)	JME (Standard conditions)	Z2JOE5 (Standard conditions)	ATJOE15 (Standard conditions)	ATJOE15 (Optimum conditions)
Combustion parameters						
1.	Start of ignition (^{o}CA)	356.6	354	354.0	354.5	352.6
2.	Occurrence of maximum pressure (^{o}CA)	372.4	370.4	371.0	371.1	369.5
3.	Ignition delay (^{o}CA)	12.7	10.2	10.1	11.2	11.1
4.	Occurrence of maximum heat release (^{o} CA aTDC)	6.7	8.2	9.4	9.3	7.9
5.	Maximum heat release (J/^{o}CA)	52.02	49.97	51.52	46.4	39.82
6.	Maximum cylinder pressure (bar)	75.70	82.61	82.7	76.49	85.79
7.	90% Mass fraction burned (^{o}CA)	389.9	387.5	386.9	395.7	387
8.	Combustion duration (^{o}CA)	38.4	38	36.9	40.6	37.7
Performance parameters						
9.	Brake thermal efficiency (%)	30.4	30.3	31.7	32.9	36.0
10.	Specific fuel consumption (kg/kWh)	0.269	0.302	0.318	0.3555	0.324
11	Exhaust gas temperature (^{o}C)	270	325	305	301	306
Emission parameters						
12.	BSHC emission (g/kWh)	0.029	0.028	0.018	0.007	0.015
13.	BSCO emission (g/kWh)	0.008	0.008	0.005	0.0165	0.009
14.	BSNO emission (g/kWh)	2.055	2.898	2.489	2.09	2.709
15.	Smoke opacity (%)	28	21	23.1	30.5	24.7

Note: Standard Conditions: Compression Ratio 17.5, Injection Timing 23 ^{o}bTDC, Injection Pressure 200 bar
Optimum Conditions: Compression Ratio 18.5, Injection Timing 24.5 ^{o}bTDC, Injection Pressure 200 bar

5.7 Endurance test on the diesel engine fueled with the ATJOE15 emulsion

5.7.1 General

This chapter discusses the endurance test results obtained from a single cylinder, four stroke, DI diesel engine fueled with the ATJOE15 emulsion. The main objective of the endurance test was to evaluate the wear characteristics of the engine components, and changes in the lubrication oil properties of a test engine fueled with the ATJOE15 emulsion. The photographic views taken before and after the completion of 100 hrs endurance test, and visual inspection of the engine components, wear and carbon deposit results, are discussed in this chapter. The lubricating oil samples collected from the engine were subjected to atomic absorption spectroscopy (AAS) for the measurement of the various wear metal traces present, and the results are discussed in this chapter.

5.7.2 Comparison of carbon deposits on different engine components

5.7.2.1 Cylinder head and piston crown

After running the engine with the ATJOE15 emulsion, black carbon deposits were clearly detected in the combustion chamber, particularly on the engine head and on the piston crown. A comparison of the carbon deposits on the cylinder head and piston crown before and after the endurance test is shown in Figs. 5.7.1 and Fig.5.7.2. About 26 g of carbon deposits were found in the cylinder head and combustion chamber. The formation of deposits is probably due to the properties of WPO in the ATJOE15 emulsion. The ATJOE15 emulsion consists of about unsaturated and saturated fatty acids, which undergoes the chemical reactions at high temperatures inside the combustion chamber. During the chemical reactions, thermal cracking of compounds, particularly at the double bonds, favour combustion through the formation of low molecular weight gases at the fringes of the spray. On the other hand, the polymerisation of the fuel in the liquid core accounts for the contraction at the core of the spray. These polymers can no longer evaporate completely, and will be deposited on the available surfaces. Upon further heating, these deposits form coke-like substances identified as carbon deposits. Similar results are reported by Ziejewski et al. [205], in their investigation on the durability test, with high oleic sunflower and safflower oils in diesel engines.

(a) Before **(b) After**

Fig. 5.7.1 Comparison of cylinder head deposits before and after the endurance test

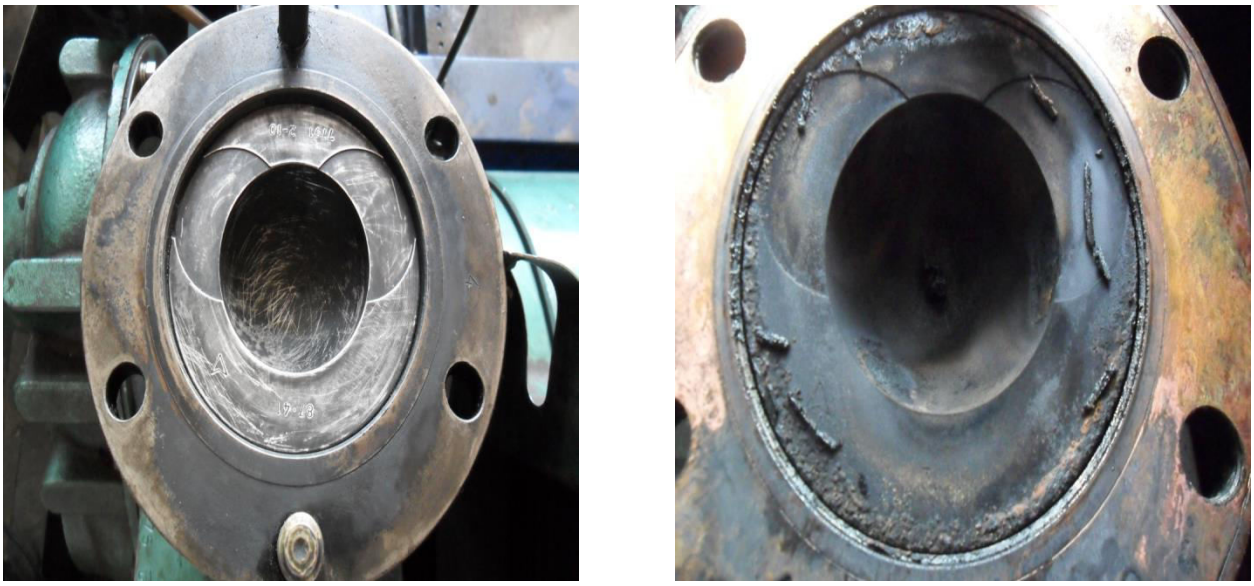

(a) Before **(b) After**

Fig. 5.7.2 Comparison of piston crown deposits before and after the endurance test

5.7.2.3 Fuel injector components

A comparison of the carbon deposits on the injector components, like the needle and nozzle tip, before and after the endurance test, is shown in Figs. 5.7.3 -5.7.5. The deposits were found at the injector nozzle tip and in-between the holes. A spray test was carried out on the nozzle with the

nozzle testing equipment under room conditions. From the visual observation of the spray, a deteriorated quality of the spray or a less misty spray and uneven spray distribution were noticed on the injector.

(a) Before **(b) After**

Fig. 5.7.3 Comparison of fuel injector components before and after the endurance test

(a) Before **(b) After**

Fig. 5.7.4 Comparison of nozzle and needle before and after the endurance test

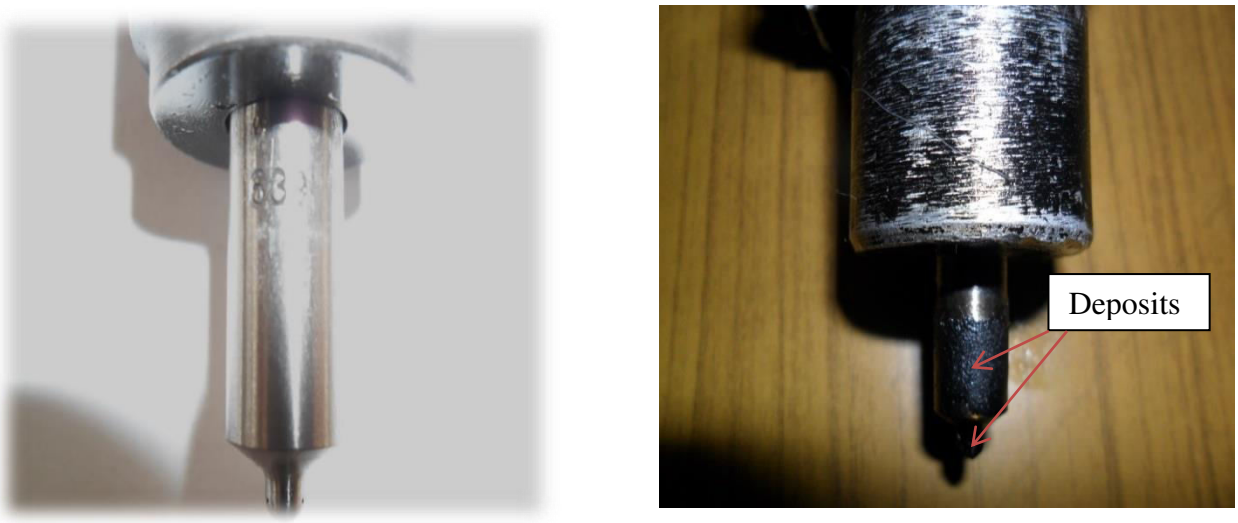

(a) Before **(b) After**

Fig. 5.7.5 Comparison of nozzle tip before and after the endurance test

Usually, a faulty injector tends to produce a distorted spray with a lower atomization of fuel, which in turn, causes less thorough mixing and subsequently unfavourable combustion and engine performance. Similar reasons are reported by Bari et al [206], in their investigation on the durability of the diesel engine fueled with crude palm oil.

5.7.2.6 Fuel injection pump components

The visual inspection of the disassembled fuel injection pump before and after the endurance test, and traces of wear found at the plunger after the endurance test, are shown in Figs. 5.7.6 (a), 5.7.6 (b) and 5.7.7.

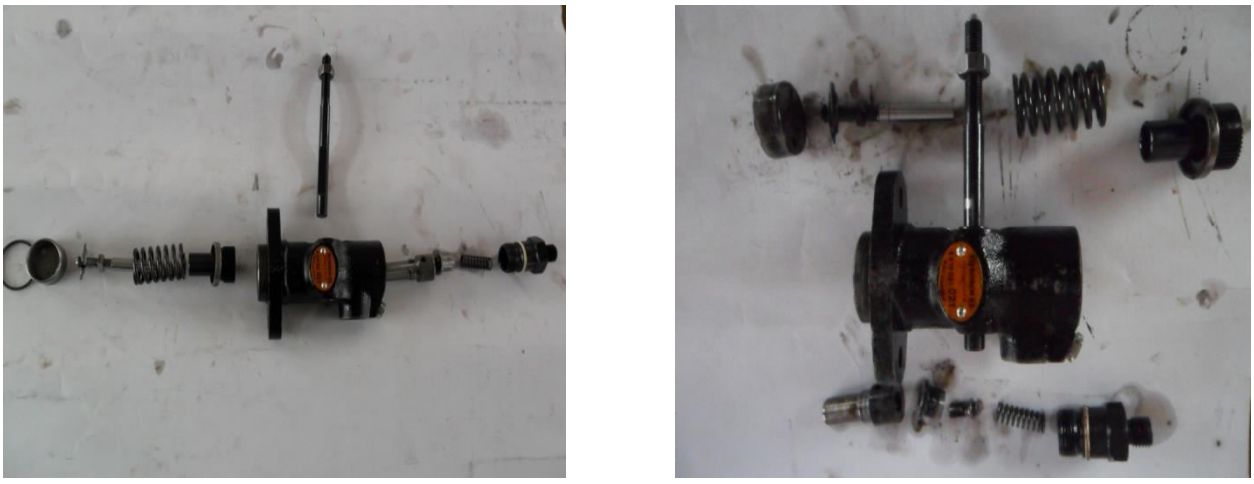

(a) Before **(b) After**

Fig. 5.7.6 (a) & (b) Comparison of fuel injection pump components before and after the endurance test

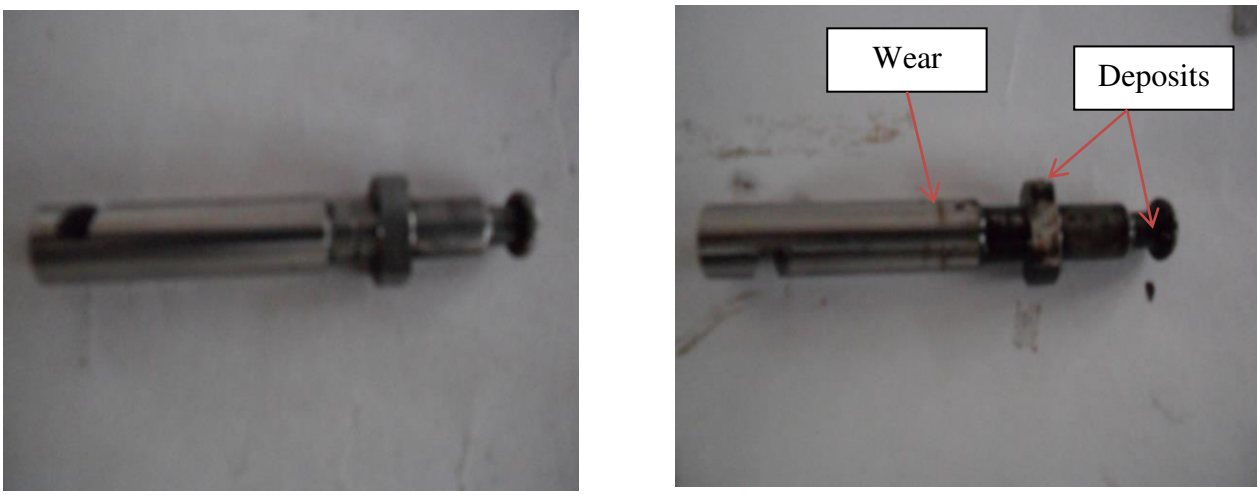

Fig. 5.7.7 Deposits and trace of wear on the plunger after the endurance test

This wear is critical because, under severe conditions, it could affect the sealing between the plunger and the barrel, thereby possibly causing a pressure loss in the injection system, which ultimately affects the injection.

5.7.2.6 Fuel filter

The photographs of the fuel filter before and after the end of the endurance test are shown in Fig.5.7.8.

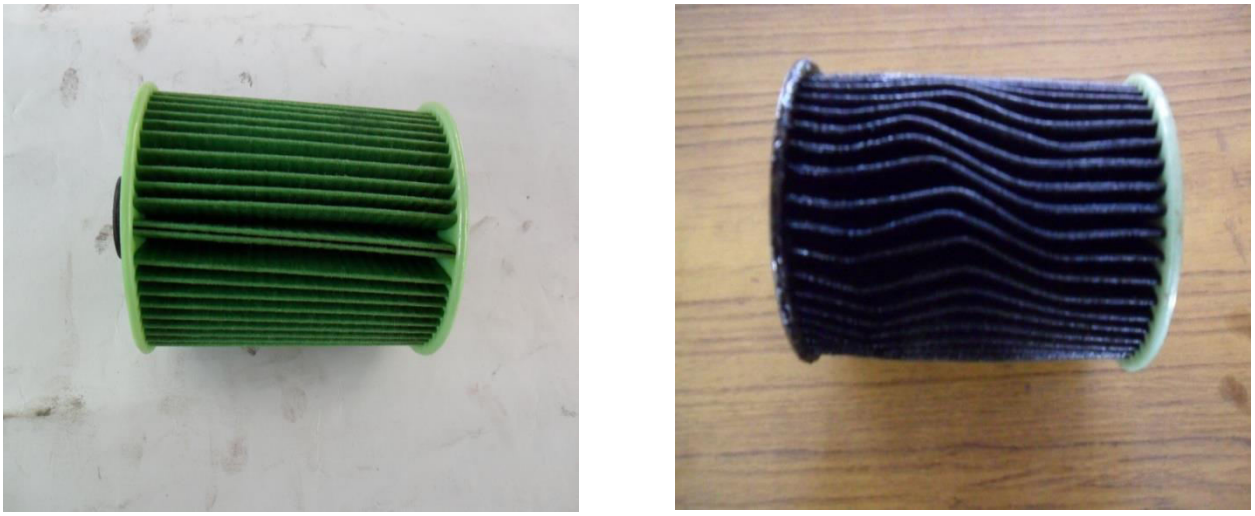

(a) Before **(b) After**

Fig. 5.7.8 Comparison of fuel filter before and after the endurance test

Fig. 5.7.9 Indication of WPO sediments in the ATJOE15 emulsion collected from the fuel filter container after the endurance test

On the visual inspection of fuel filter before and after the endurance test, it is evidenced that the fuel filter is choked after its use for 100 hrs. This may be due to the heavier molecules or sediments present in the WPO. Up to 100 hrs of operation, no problem with the fuel supply system was noticed.

5.7.3 Lubrication oil analysis

5.7.3.1 Determination of the ash content

The lubricating oil samples were kept in the furnace at 450°C for 4 hours and then 600°C for 2 hours to produce ash. The residual ash contains the wear debris of the metal primarily. By weighing the crucible before and after the test, the weight percentage of ash was determined. The calculation procedure of the ash content is as follows:

The weight of the empty crucible No.1 = 20.723 g

The weight of the crucible No.1 (With coke residue of fresh lubrication oil) = 20.781 g

The ash content present in the fresh lubrication oil = 0.058 (wt %)

Similarly, Weight of the empty crucible No.2 = 20.738 g

The weight of the crucible No.2 (With coke residue of used lubrication oil) = 20.825 g

The ash content present in the used lubrication oil = 0.087 (wt %)

More ash content in the lubricating oil after the end of the endurance test is noticed, which may be due to the addition of the metal debris resulting from the wear of the engine components. The viscosity of the lubrication oil after 100 hrs of operation, was found to be increased by about 10% compared to that of reference one.

5.7.3.2 Determination of the metal elements present in the lubrication oil

The engine lubrication oil, used in the test engine fueled with the ATJOE15 emulsion for the endurance test was analyzed by the atomic absorption spectroscopy (AAS). By analyzing a sample of the lubricating oil from the engine after a certain running period, it is possible to collect some information on the operation and condition of the engine. The wear particles generated from the sliding contact of the solid surfaces are suspended in the lubricating oil. In this investigation, the variation in the concentration of the wear metals debris including Fe, Cu, Zn, Al, Cr, Pb and CO in the used lubricating oil with the engine operation time, was obtained using the AAS. The results are presented in part per million (ppm) by weight of the metal to the lubricating oil. A comparison of the metal elements present in the fresh lubricating oil and used lubricating oil, is illustrated in Fig. 5.7.10.

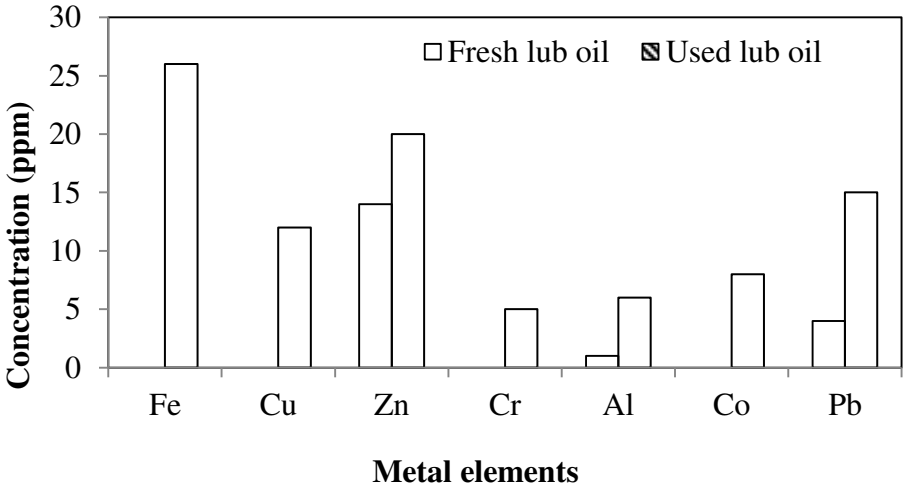

Fig. 5.7.10 Comparison of metal elements present in the fresh lubricating oil and used lubricating oil

In the results obtained, there was a marked increase in Fe concentration in the lubrication oil by about 26 ppm at the end of 100 hours. The iron in the wear debris could be from the cylinder liner, piston, rings, valves, valve guides, gears, shafts, rust and crankshaft. Similar ascending trends of wear metals concentration for Al and Cr were also observed. The aluminum and

chromium in the lubricating oil come from the wear of piston, bearings, cylinder liner, compression rings and crankshaft. With respect to Cu and Pb, the rate of wear is found to be high. The copper and lead in the wear debris may originate from bearings, bushings, paints and grease additives. The Zn elements in the used lubricating oil are found to be higher by 30%, which could be due to the depletion of additives used in bearings and brass components. The Cobalt in the wear debris originates from the wear of bearings. The maximum wear debris present in the used lubricating oil is Fe, but it is far too lower than the condemning level specified for used lubricating oil (50-60 ppm) [207]. Overall, the wear metals did not increase beyond the usual values encountered in the endurance tests.

5.7.4 Comparison of the performance and emission parameters

The percentage change in the performance and emission parameters of the diesel engine fueled with the ATJOE15 emulsion, after the end of the endurance test at full load is presented in Fig. 5.7.11.

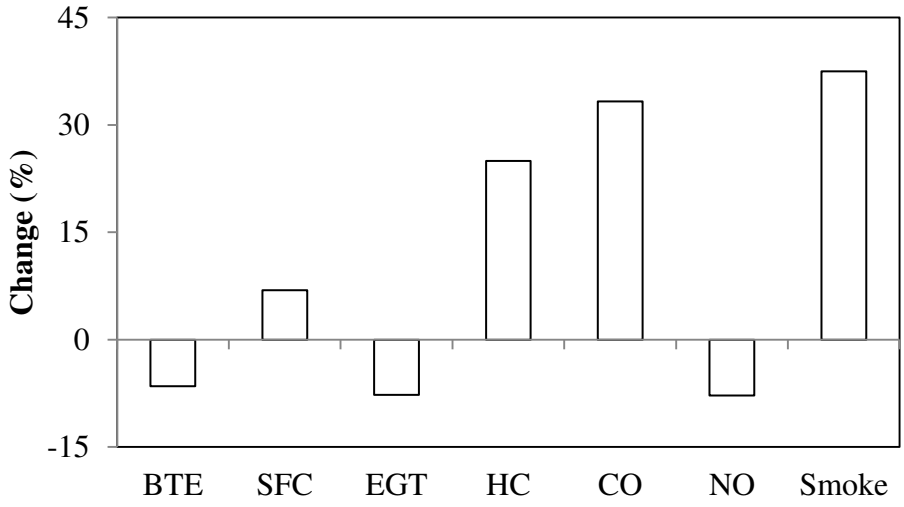

Fig. 5.7.11 Percentage change in the performance and emission parameters of the diesel engine fueled with ATJOE15 emulsion (after endurance test) at full load

It is evidenced from the figure, that the brake thermal efficiency and exhaust gas temperature of the ATJOE15 emulsion is lower by 6.5% and 7.7% respectively, after the end of the endurance test. The specific fuel consumption of the ATJOE15 emulsion is found to be higher by 6.9% after the end of the endurance test. The HC, CO and smoke emissions from the ATJOE15 emulsion after the end of the endurance test are found to be higher by 25%, 33.3% and 37.5% respectively.

The NO emissions are found to be lower by about 7.8%, compared to those of the initial condition (i.e., before the endurance test).

5.7.5 Closure

During the 100 hrs of the endurance test conducted on the diesel engine fueled with the ATJOE15 emulsion, no abnormalities occurred. After the endurance test, on visual inspection of various engine components, carbon deposits were noticed in the cylinder head, combustion chamber and nozzle tip. About 26 g of carbon deposits were found in the cylinder head and combustion chamber. A marginal wear was observed in the plunger of the fuel injection pump. The fuel filter was found to be clogged with the sediments of WPO. From the lubrication oil analysis, an ash content of about 0.087 (wt %) and the existence of various metal debris were noticed. Out of all, Fe was the most abundant wear metal found in the lubrication oil. The viscosity of the lubrication oil after 100 hrs of operation, was found to be increased by about 10% compared to that of reference one. At the end of the endurance test, the engine was able to produce its rated power with a small decrement in the brake thermal efficiency. The specific fuel consumption was found to be higher. The HC, CO and smoke emissions were found to be higher compared to those of the initial condition. The NO emissions alone were found to be lower at the end of the endurance test.

CHAPTER 6

CONCLUSIONS

6.1 General

The combustion, performance and emission characteristics of a single cylinder, four stroke, air cooled, direct injection diesel engine capable of producing 4.4 kW at a constant speed of 1500 rpm, fueled with JME-WPO emulsion with fuel and engine modifications, were analysed, compared with diesel and JME operations of the engine. Also the experimental results were compared with a two zone mathematical model developed. Further, a short term endurance test was also carried out to ensure the technical feasibility of the engine fueled with the JME-WPO emulsion. The conclusions of each technique are given in this section.

6.1.1 Parametric studies on combustion, performance and emissions with the JME-WPO emulsions

- The engine was able to run with a maximum of 15% WPO in the form of emulsions with the JME.
- With 15% WPO in the emulsions, the start of ignition for all the emulsions is found to be earlier than that of diesel at full load.
- The ignition delay of JME-WPO emulsions decreases by about 2.3 ^{o}CA to 2.7 ^{o}CA compared to that of diesel.
- The maximum thermal efficiency is noticed with the Z2JOE15 emulsion compared to all other emulsions tested in this study. The thermal efficiency for Z2JOE15 is found to be higher by 11.3% compared to that of diesel.
- With 15% WPO in the emulsion, the HC emissions are found to be lower from 11.3% to 45.8% compared to that of diesel operation, and 9.6% to 44.8% lower compared to that JME operation are noticed.
- The CO emissions are found to be lower from 43.8% to 68.9%, compared to that of diesel at full load.
- The NO emissions for all the emulsions are found to be lower than that of JME operation, but higher than that of diesel operation. The maximum reduction in the nitric oxide emission by 16.8% is observed with Z2JOE15 emulsion compared to that of JME operation.
- The reduction in smoke for all the emulsions investigated in this study is in the range of 15%, to 27.8%, compared to that of diesel at full load.

- Overall, by considering the combustion, performance and emission parameters, it can be concluded that the Z2JOE15 showed a better performance and lower emissions compared to those of diesel and JME operations.

6.1.2 Experimental studies on combustion, performance and emission characteristics of ATJOE15 emulsion

- The acidity of the Z2JOE15 emulsion was neutralized by acid treatment to avoid the corrosion effect on several engine components.
- The combustion of ATJOE15 emulsion commences earlier than that of diesel at full load. Ignition delay of ATJOE15 is found to be shorter than that of diesel.
- In the performance aspect, the brake thermal efficiency of ATJOE15 emulsion is higher by about 8.2% and 8.5% than those of diesel and JME at full load.
- The BSHC emissions are reduced by about 73% for ATJOE15 emulsion at full load compared to that of diesel. The BSCO emission of ATJOE15 emulsion is found to be higher by about 46% than that of diesel at full load.
- There is about 2% increase in the NO emission is obtained with the ATJOE15 emulsion at full load compared to that of diesel. When fueled with the ATJOE15 the smoke opacity increases by about 8% compared to that of diesel operation.

6.1.3 Analysis of combustion and emission characteristics of a diesel engine fueled with the ATJOE15 emulsion

- The experimental and simulated results show that the peak cylinder pressures of the JME and the ATJOE15 are found to be marginally higher than that of diesel, and about 6.1% lower peak cylinder pressures are obtained with the ATJOE15 emulsion at simulated conditions compared to that of experimental conditions.
- The maximum heat release rates of JME and ATJOE15 are found to be lower than that of diesel fuel, in both the experimental and simulated conditions. Compared to experimental conditions, the maximum heat release rate of the ATJOE15 at simulated conditions is found to be lower by 1.96%.
- Compared to diesel operation, the NO concentration is found to be higher in the case of JME operation, and lower in the case of the ATJOE15 operation at both experimental and simulated conditions. With the simulated conditions, the NO emissions of the ATJOE15 emulsion are found to be higher by 1% compared to that of experimental conditions.

- The soot density is found to be lower for the JME operation and it is higher for the ATJOE15 operation compared to that of diesel. The soot density of the ATJOE15 emulsion at simulated condition is found to be lower by about 4.5% than that of experimental condition.

The presented model can predict the combustion characteristics such as cylinder pressure and heat release which are in good agreement with the experimental results.

6.1.4 Combined effect of compression ratio and injection timing on the performance and emission parameters of diesel engine fueled with the ATJOE15 emulsion

- The peak cylinder pressure is more in the cases of higher compression ratio and advanced injection timing for the ATJOE15 emulsion compared to that of diesel operation. Also the starting of combustion is found to be earlier in such conditions for ATJOE15 emulsion compared to that of diesel.
- The ignition delay of the ATJOE15 emulsion at higher compression ratio is found to be lower compared to that of diesel which results in lower heat release rates at this condition. At lower compression ratio and retarded injection timings this trend is reverse.
- The brake thermal efficiency of the ATJOE15 emulsion at increased compression ratio and advanced injection timings are found to be higher than diesel and JME operations. When the compression ratio is decreased to 16.5, the brake thermal efficiency of ATJOE15 emulsion is found to be lower at all the injection timings.
- The minimum BSFC value of 0.317 kg/kWh is obtained at compression ratio 18.5 and injection timing 23 ^{o}CA bTDC, which is higher by about 17.8% compared to that of diesel.
- At standard compression ratio, the HC emissions of the ATJOE15 emulsion at different injection timings are found to be lower in the range of 39.5% to 65.5% compared to that of diesel at full load.
- The CO emissions of the ATJOE15 emulsion are found to be higher with the lower compression ratio and retarded injection timings. With the advancement in the injection timing, about 48% reduction in the CO emissions are noticed with the ATJOE15 emulsion.
- The NO emissions of the ATJOE15 emulsion are found to be lower with the lower compression ratio and retarded injection timings. With the higher compression ratio of

18.5, the NO emissions from the ATJOE15 emulsion are found to be higher in the range of 4% to 31.8% compared to that of diesel.

- When the injection timing is advanced, the smoke opacity value of the ATJOE15 is found to be lower by about 5.3% compared to that of diesel operation. At reduced compression ratio of 16.5, the smoke opacities of the ATJOE15 emulsion at all the injection timings found to be higher in the range between 32% and 52% compared to that of diesel operation. At higher compression ratio of 18.5, the smoke opacity of the ATJOE15 emulsion at retarded injection timing is found to be lower by about 4.2% and in the advanced injection timing case, the smoke emission values reduced by about 11.7% compared to that of diesel.

6.1.5 Combined effect of compression ratio and nozzle opening pressure on the combustion, performance and emission parameters of diesel engine fueled with the ATJOE15 emulsion

- Among all the tested compression ratios and nozzle opening pressures, the compression ratio of 18.5 and with the nozzle opening pressure of 220 bar, the ATJOE15 operation produced the highest cylinder pressure value of 77.2 bar at 372.1 ^{o}CA, which is earlier by about 0.3 ^{o}CA and later by about 1.6 ^{o}CA than those of diesel and the JME operations respectively.
- The ignition delay of the ATJOE15 emulsion is found to be shorter in the range between 0.3 ^{o}CA and 2.2 ^{o}CA with the compression ratios of 17.5, 18.5 and the higher nozzle opening pressure of 240 bar compared to that of diesel operation. In comparison with the JME operation, the engine fueled with the ATJOE15 emulsion exhibits a longer ignition delay at all operating conditions.
- With a higher compression ratio of 18.5 and nozzle opening pressure of 240 bar, improved performance and lower emissions. The maximum thermal efficiency is noticed at this operating condition.
- A maximum reduction in the HC, CO and smoke emissions by about 52.8%, 55.3% and 36.4% respectively is noticed with ATJOE15 emulsion at the same operating conditions.
- The NO emission at this condition is still found to be higher by about 30.7% compared to that of diesel operation, at full load.
- With the standard compression ratio and standard nozzle opening pressure of 200 bar, the smoke opacity of ATJOE15 is found to be higher by about 8.9%. When the nozzle

opening pressure is increased to 220 bar and 240 bar, the smoke opacity of ATJOE15 is found to be reduced by about 3.9% and 26.4% respectively compared to that of diesel operation.

- When the compression ratio is reduced to 16.5, the NO emissions of the ATJOE15 emulsion are found to be lower by about 23%, 11.6 and 1.6% compared to that of diesel operation at nozzle opening pressures of 200, 220 and 240 bar respectively.
- At reduced compression ratio of 16.5, the smoke opacities of ATJOE15 emulsion at all the nozzle opening pressures found to be higher in the range between 42% and 50.6% compared to that of diesel operation.

6.1.6 Combined effect of injection timing and nozzle opening pressure on the combustion, performance and emission parameters of diesel engine fueled with the ATJOE15 emulsion

- Among all the tested injection timings and nozzle opening pressures, the injection timing of 24.5 ^{o}CA bTDC with the nozzle opening pressure of 200 bar, the ATJOE15 operation produced the highest cylinder pressure value of 79.5 bar at 370.6 ^{o}CA, which is earlier by about 2.2 ^{o}CA and later by about 0.2 ^{o}CA than those of diesel and the JME operations respectively.
- Among all the tested injection timings and nozzle opening pressures, a shorter ignition delay period of 10.36 ^{o}CA is observed for the ATJOE15 operation with the injection timing of 23 ^{o}CA bTDC and nozzle opening pressure of 240 bar.
- For the standard injection timing, with the higher nozzle opening pressures of 220 bar and 240 bar, the brake thermal efficiency of the ATJOE15 emulsion is found to be higher than that of diesel by about 4.6% and 6.1% respectively at full load.
- When the injection timing is retarded to 21.5 ^{o}CA bTDC, the brake thermal efficiency of the ATJOE15 emulsion is found to be higher by an average of 2.5% at nozzle opening pressures at full load.
- With the advanced injection timing of 24.5 ^{o}CA bTDC, the brake thermal efficiency of the ATJOE15 emulsion is found to be higher by an average of 5.5% at all nozzle opening pressures.
- The lowest value of the BSFC obtained for the ATJOE15 emulsion at 24.5 ^{o}CA bTDC is 0.3177 kg/kWh at nozzle opening pressure 240 bar, which is higher by about 17.8% compared to that of diesel operation.

- The HC emissions of the ATJOE15 emulsion are found to be lower with all injection timings and pressures. The CO emissions of the ATJOE15 emulsion are found to be higher with all injection timings and pressures, but it decreases with increase in nozzle opening pressures.
- With the retarded injection timing of 21.5 ^{o}CA, the NO emissions of the ATJOE15 emulsion are found to be lower by about 12.8%, compared to that of diesel operation at standard nozzle opening pressure of 200 bar.
- With the retarded injection timing of 21.5 ^{o}CA, the smoke opacities of ATJOE15 emulsion at all the nozzle opening pressures found to be higher in the range between 24.5% and 45.5% compared to that of diesel operation.

6.1.7 Endurance test on the diesel engine fueled with the ATJOE15 emulsion

- After the end of endurance test, carbon deposits were noticed in the cylinder head, combustion chamber and nozzle tip.
- About 26 g of carbon deposits were found in the cylinder head and combustion chamber.
- A marginal wear was observed in the plunger of the fuel injection pump.
- The fuel filter was found to be clogged with the WPO particles.
- From the lubrication oil analysis, ash content of about 0.087 (wt %) and existence of various metal debris were noticed. Out of all, Fe was the most abundant wear metal found in the lubrication oil.
- The viscosity of the lubrication oil after 100 hrs of operation, was found to be increased by about 10% compared to that of reference one.
- At the end of endurance test, the engine was able to produce its rated power with small decrement in the brake thermal efficiency.
- The specific fuel consumption was found to be higher.
- The HC, CO and smoke emissions from the ATJOE15 emulsion after the end of endurance test are found to be higher by 25%, 33.3% and 37.5% respectively.
- The NO emissions are found to be lower by about7.8% compared to that of initial condition.

6.2 Scope for future work

- The WPO obtained can be upgraded by removal of oxygen content to improve the calorific value of the fuel.
- The water content in the WPO to be removed to avoid corrosion of engine components.
- The chemical stability of the WPO may be increased by esterification process.
- The JME-WPO emulsions can be tested in automotive engines and in gensets.
- Kinetic studies are required for optimization of parameters involved in the production of WPO.

Experimental Studies on a DI Diesel Engine Fueled with Jatropha Methyl Ester-Wood Pyrolysis Oil Emulsions

A Thesis

Submitted by

R.PRAKASH

(Roll No: 510ME607)

In Partial Fulfillment of

the Requirement for the Degree

of

DOCTOR OF PHILOSOPHY

Department of Mechanical Engineering
National Institute of Technology,
Rourkela –769 008
India

September 2013

Department of Mechanical Engineering
National Institute of Technology,
Rourkela –769 008
India

CERTIFICATE

This is to certify that the thesis entitled "**Experimental Studies on a DI Diesel Engine Fueled with Jatropha Methyl Ester-Wood Pyrolysis Oil Emulsions**" being submitted by **Mr. R. Prakash** for the award of Ph.D. degree is a record of bonafide research carried out by him in the Mechanical Engineering Department, National Institute of Technology, Rourkela, under our guidance and supervision. To the best of our knowledge, the results presented in this thesis have not been submitted to any other University or Institute for the award of any degree or diploma.

Co-Supervisor

Prof. R.K.Singh
Professor and Head
Department of Chemical Engineering
National Institute of Technology
Rourkela- 769008.

Supervisor

Prof.S.Murugan
Associate Professor
Department of Mechanical Engineering
National Institute of Technology
Rourkela- 769008.

ACKNOWLEDGEMENT

One of the joys of completion is to look over the journey past and remember all the faculty, friends and family who have helped and supported me along this long but fulfilling road.

At the outset, I would like to express my heartfelt gratitude to **Prof. S. Murugan** for his advice during my doctoral research endeavor for the past three and half years. As my supervisor, he constantly forced me to remain focused on achieving my goal. His observations and comments helped me to establish the overall direction of the research and to move forward with investigation in depth. I thank him for providing me with the opportunity to work with him. I could not have asked for better role models, each inspirational, supportive, and patient. I could not be prouder of my academic roots and hope that I can in turn pass on the research values and the dreams that he has given to me.

I would like to thank **Prof. R.K.Singh** for his unflagging encouragement and supportive guidance throughout my research career. As my co-supervisor, his guidance has helped me well and I owe my heartfelt appreciation. He has also provided insightful discussions about the research whenever required.

I am happy to acknowledge **Prof. Sunil Kumar Sarangi**, Director, NIT Rourkela for providing required infrastructural facilities and financial assistance in the form of Junior Research Fellowship and Research Assistance ship, which buttressed me to perform my work comfortably and I will forever be grateful to him. I warmly thank **Prof. K.P.Maity**, Professor and Head, Department of Mechanical Engineering and **Prof. R.K. Sahoo**, Group Head, for their valuable advice, and support to my work.

I would like to express my sincere thanks to DST, Government of India for sponsoring this research project and Dean, Assistant Registrar and other staff members of SRICCEE for their timely help in all financial matters connected with the project and also for extending their support in all official corresponding.

I take this opportunity to sincerely acknowledge and thank my Doctoral Scrutiny Committee members, **Prof. Japes Bera**, Ceramic Engineering Department, **Prof. Mithilesh Kumar**, Metallurgical and Materials Engineering Department and **Prof. Alok Satapathy**, Mechanical Engineering Department, who have provided encouraging and constructive feedback and suggestions whenever required. To the many anonymous reviewers from various journals and

conferences, thank you for helping to shape and guide the direction of work with your careful and instructive comments.

I would like to thank our technical staff members Mr.N.P.Barik, Mr. Bisoyi, Mr. Ramkrishna Mandal, Mr. Laxman Kumar Mohanta and specially Mr.Harihar Barkey and other administrative staff who have been kind enough to help in their respective roles. I also thank my all research colleagues for providing support and friendship that I needed.

I would like to thank my parents, brothers, sister, in-laws, especially, to my wife Mrs. C.Hema, as well as my children Hariharan and Kavya for their great support, patience and unconditional love during my good and bad times. Above all, I owe it all to Almighty God for granting me the wisdom, health and strength to undertake this research task and enabling me to its completion.

(R.Prakash)

ABSTRACT

The major technical problems associated with the use of biodiesel in large proportions are (i) more prone to oxidation which can cause the fuel to become acidic and to form insoluble gums and sediments that can plug fuel filters, (ii) cold flow properties and (iii) higher NO_x emissions compared to diesel fueled engines. It is reported that addition of antioxidants, emulsifying water with biodiesel, addition of fuel with high latent heat of vaporization, and low cetane fuel can reduce the NO_x emissions in biodiesel fueled engines. Addition of antioxidants to biodiesel can improve both the cold flow properties and oxidation stability, and reduce the NO_x emission, the reason being that, the antioxidants contain phenolic compounds. Also, in economic point of view, the cost of biodiesel is higher at this moment because, the availability of seeds is limited. This motivates less use of biodiesel in many countries. The use of alternative hydrocarbon sources other than petroleum fuels, as extenders for biodiesel can solve this problem. Many literatures report that pyrolysis oil obtained from biomass sources contain hindered phenols in them. Therefore, bio oil can be used as an extender to biodiesel. The bio oil not only contains phenolic compounds, it also contains small percentage of water which is inseparable.

In this research work, an attempt was made to study the effects of using bio oil as an extender to biodiesel on engine combustion, performance, emission and durability issues. For this purpose, wood pyrolysis oil (WPO) - bio oil obtained from pyrolysis of wood was used in low percentages (i.e., 5%, 10% and 15%). Waste wood from the packing container boxes was used as feedstock for the production of WPO, while the JME was collected from a commercial pilot plant in India. The JME-WPO emulsions were obtained using six different surfactant combinations viz. 2% and 4% of Span 20 (Sorbitan monolaurate), 2% and 4% of Span 80 (Sorbitan monooleate), and 2 and 4% of (Span 80 + Tween 80 (Polysorbate 80) mixed). Three different percentages of emulsions containing 5, 10 and 15% of WPO were prepared using six different surfactants and tested as fuels in a single cylinder, four stroke, air cooled direct injection (DI) diesel engine developing a power of 4.4 kW at a constant speed of 1500 rpm. After evaluating the combustion, performance and emission parameters of the engine fueled with different emulsions, an optimum emulsion (Z2JOE15) was chosen, which contains 15% WPO, 81% JME and 4% of a mixed surfactant; Span 80-Tween 80. The highest thermal efficiency was noticed with the Z2JOE15 emulsion compared to all other

emulsions tested in this study. The thermal efficiency for the Z2JOE15 was found to be higher by 11.3% compared to that of diesel at full load. Lower HC, CO and smoke emissions are noticed with the Z2JOE15 emulsion compared to that of diesel operation at full load. The NO emissions for all the emulsions were found to be lower than that of JME operation, but higher than that of diesel operation at full load. A maximum reduction in the NO emission of 16.8% was observed with the Z2JOE15 emulsion compared to that of JME operation.

Further, this Z2JOE15 emulsion was upgraded for its quality by an acid treatment process. The acid treated emulsion (ATJOE15) was tested in the same engine to evaluate the engine behaviour in terms of the combustion, performance and emission and compared with that of diesel operation. In the performance aspect, the brake thermal efficiency of ATJOE15 emulsion was higher by about 8.2% and 8.5% than those of diesel and JME at full load. The HC emissions were lower by about 73% for the ATJOE15 emulsion at full load compared to that of diesel. The CO emissions of ATJOE15 emulsion were found to be higher by about 46% than that of diesel at full load. An increase of about 2% in the NO emission was noticed with the ATJOE15 emulsion at full load compared to that of diesel. A two zone mathematical model, using a MATLAB software program was developed to validate the experimental results obtained from the same engine fueled with the ATJOE15 emulsion. The validation of experimental results with the theoretical model indicated that the combustion characteristics such as cylinder pressure and heat release were in good agreement, and were within the deviation of 2-6%.

Further the engine was run with the ATJOE15 emulsion to evaluate the combined effects of different compression ratio (CR), injection timing (IT) and nozzle opening pressure (IP) on the combustion, performance and emission parameters of the engine. Engine experiments were conducted with the ATJOE15 emulsion only at three different compression ratios (16.5, 17.5 and 18.5), and for each compression ratio, three nozzle opening pressures (200, 220, and 240 bar) and three injection timings (21.5, 23 and 24.5 ^{o}CA bTDC) were selected and conducted as per the full factorial design (3^3 = 27). With the ATJOE15 emulsion, about 25.81% higher brake thermal efficiency was obtained at 18.5 compression ratio with the standard injection timing and nozzle opening pressure compared to that of diesel. The HC and smoke emissions were found to be lower by 45% and 9.6% respectively at full load with the same operating condition. The CO and NO emissions were found to be higher by about 10% and 4.88% in comparison with diesel at full load. The NO emissions were found to be

lower with a lower compression ratio (16.5) and retarded injection timing (21.5 ^{o}CA bTDC) conditions.

A short term endurance test was conducted with the ATJOE15 emulsion as per IS 10000 Part V-1980 method for 100 hrs. After the endurance test, carbon deposits were noticed in the cylinder head, combustion chamber and nozzle tip. About 26 g of carbon deposits were found in the cylinder head and combustion chamber. A marginal wear was observed in the plunger of the fuel injection pump. The fuel filter was found to be clogged with some sediments of WPO. The engine lubrication oil, used in the test engine fueled with the ATJOE15 emulsion for the endurance test was analyzed by the atomic absorption spectroscopy (AAS). In this investigation, the variation in the concentration of the wear metal debris, including Fe, Cu, Zn, Al, Cr, Pb and CO in the used lubricating oil with the engine operation time, was obtained using the AAS. Out of all, Fe was the most abundant wear metal found in the lubrication oil. The viscosity of the lubrication oil after 100 hrs of operation, was found to be increased by about 10% compared to that of reference one. The ash content present in the used lubrication oil was found to be about 0.087 (wt %).

Keywords: Diesel engine, biodiesel, transesterification, Jatropha methyl ester (JME), pyrolysis, bio oil, wood pyrolysis oil (WPO), emulsion, performance, combustion, emission, durability, modeling.

CONTENTS

LIST OF FIGURES

LIST OF TABLES

NOMENCLATURE

$\frac{d(mu)}{d\theta}$	rate of change of internal energy of the system of mass m.
$\frac{dQ_r}{d\theta}$	rate of heat release during combustion period
$\frac{dQ_h}{d\theta}$	rate of heat transfer from gases to walls
$\frac{dW}{d\theta}$	rate of mechanical work done by the system on the boundary
p	Pressure
v	instantaneous cylinder volume
m	Mass
R	gas constant
T	Temperature
$\frac{dV}{d\theta}$	change of volume with crank angle
h	heat transfer coefficient
A	heat transfer area
T_w	wall temperature
V_{cl}	cylinder clearance volume
λ	crank radius to piston length ratio
$\frac{dQ}{dt}$	rate of heat release
K	thermal conductivity of the cylinder gas
d	cylinder bore
Re	Reynolds number
T_g	cylinder bulk gas temperature
Cmodel	model constant=1000 kJ/kg degree
f_1, f_2	functions
q	heat losses
m_f	cumulative mass of fuel injected
Q	cumulative heat release rate
LCV	lower calorific value of fuel
C_{rate}	constant for mixing rate=0.002 s
k	density of turbulent kinetic energy

$Eu/d\theta$	total turbulent energy of the fuel jet at a given crank angle instant, θ
$E_{diss}/d\theta$	rate of energy dissipation across the control surface
$dEi/d\theta$	rate of generation of kinetic energy of fuel jet in to the cylinder
C_{turb}	efficiency of conversion of kinetic energy to turbulent energy in the free jet=0.2
n	engine speed
ρ_f	density of fuel
C_d	coefficient of discharge of nozzle
A_n	area of nozzle holes
$\frac{dmf/d\theta}{\rho f}$	volumetric injection rate of the fuel
Eu	total turbulent energy of the fuel jet at a given crank angle instant
C_{diss}	dissipation constant
λ_{diff}	excess air ratio for diffusion burning=1.4
Φ	Crank angle
Φ_{inj}	Fuel injection crank angle
Φ_{exh}	Crank angle at exhaust valve opens
CHR	Cumulative Heat Release
WPO	Wood Pyrolysis Oil
JME	Jatropha Methyl Ester
ATJOE15	Acid treated Jatropha oil Emulsion with 15% WPO
TDC	Top Dead Centre
BDC	Bottom Dead Centre
DI	Direct Injection
O	Oxygen
N	Nitrogen
NO	Nitric Oxide

CHAPTER-1

INTRODUCTION

1.1 Need for Biofuels

Energy sustainability is one of the major tasks of any country, because any country's economic development depends mainly on electrical energy generation and the energy sources available. The gap between the energy demand and supply increases unpredictably every year, as a result of continuous growth in industrialization and improvement in life style. The electrical energy is consumed heavily in all the sectors including industries, households, transportation, commerce and agriculture. During the last two decades, almost all the houses in the developed and developing countries have been provided with electricity for lighting, domestic appliances, refrigeration and air conditioning. In order to increase the supply of domestic appliances and utilities, many industries and manufacturing units have come up, which also consume huge electricity. The consumption of electrical energy in commercial buildings for lighting, air conditioning, recreation purposes and other utilities has also increased enormously. In the transportation sector, electricity is used in electromotive and service units, while the agricultural sector uses electricity primarily for irrigation, mills and processing units. The global energy consumption in the year 2010 by the different sectors (IEO report 2011) is shown in Fig.1.1. [1]

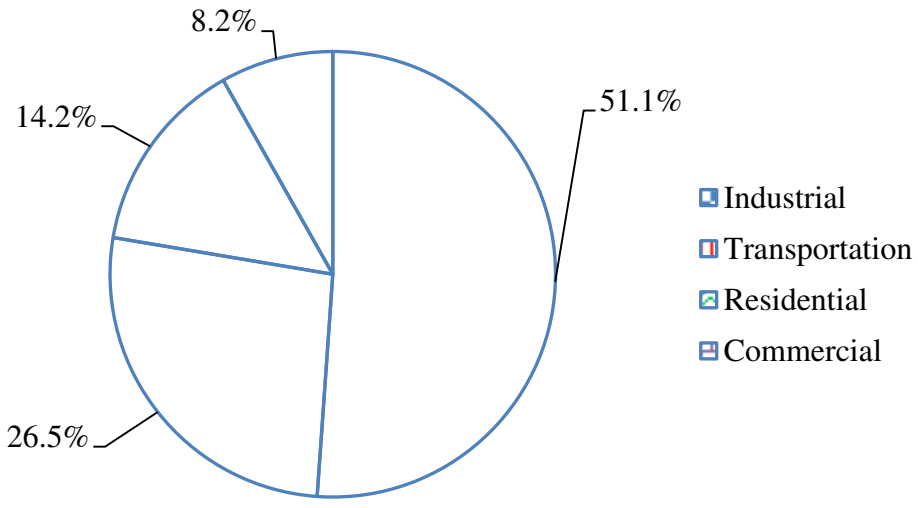

Fig.1.1 Global energy consumption by different sectors in the year 2010

Although electricity is mainly used in all the sectors, the source for the generation of electricity is mainly the combustion of fossil fuels in thermal and nuclear power plants. Over the last two centuries, the consumption of fossil fuels has increased heavily, in particular the consumption of crude oil increased largely. Consequently, the depletion of fossil fuels and the cost of crude oil have increased exponentially. The transportation sector consumes large quantities of petroleum fuels in internal combustion engines and gas turbines.

The US Department of Energy states that the world's oil supply will reach its maximum production and midpoint of depletion sometime around the year 2020. The depleting reserves and environmental issues, in addition to global warming and the ozone depletion concerns have pushed the countries towards searching for alternative energy sources, with particular emphasis on those renewable from nature [2]. While increasing the energy supply for meeting the energy demand in all the sectors, there is also a negative effect on the environment. The various pollutants from the power plants, industries and transport vehicles are the reasons for increasing the global warming potential (GWP) and ozone depletion potential (ODP). The major countries which emit CO_2 emissions from the combustion of fossil fuels and some industrial processes in the year 2010, are given in Fig.1.2. (Courtesy-IEA)[3].

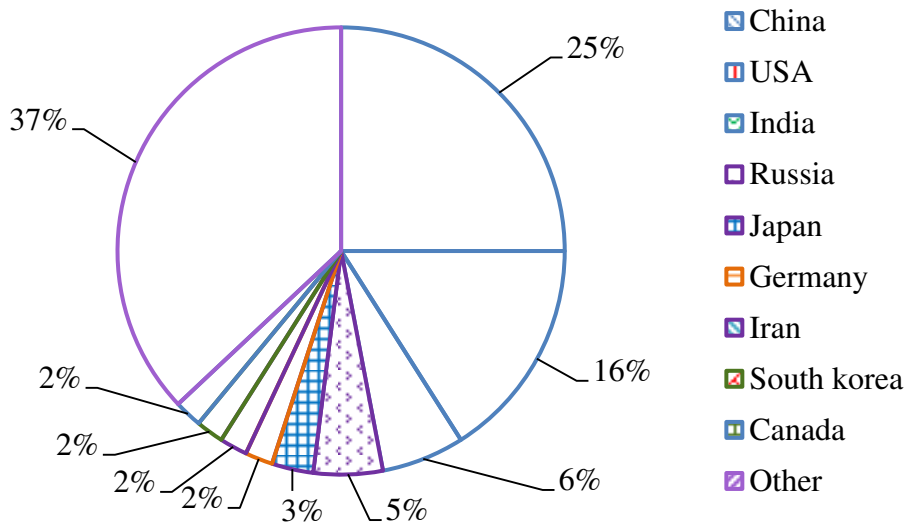

Fig.1.2 Major Countries emit higher CO_2 emissions in the year 2010

Though the depletion of fossil fuels began long back, the realization came only after the two wars associated with oil crisis in the late 1970s and 1980s. Since then, the world research community has been striving hard to find various alternative fuels that are long lasting and eco-friendly, to substitute the petroleum fuels. They also tried to reduce the pollutants from

the combustion devices by introducing emission control devices. In this context, the alternative fuels can be divided into two types; (i) renewable energy sources, and ii) non-conventional energy sources. Renewable energy sources offer distinct advantages that they are abundantly available, derivable from nature, eco-friendly, have a low carbon credit, and are cheaper. There has been a focus on trapping the energy from various renewable sources, such as solar, wind, tide, ocean and biomass. Among these sources, biomass is considered as a potential source in developing and agrarian countries.

The biofuels derived from biomass are considered as good alternative fuels for petroleum fuels. Biofuels are mainly categorized into (i) First generation biofuels,and (ii) Second generation biofuels. The classification of the first and second generation biofuels is given in a block diagram which is shown in Fig.1.3 in the next page, and they are discussed briefly in the subsequent sections.

1.2 First generation biofuels

Bioethanol and biodiesel are referred to as the first generation biofuels.

1.2.1 Bioethanol

The feedstocks used in the production of bioethanol are sugar cane, sugar beet, wheat, molasses, cassava, sweet potato, corn, maize, switchgrass, grass, miscanthus, corn stover and cereals etc. [4-7]. Hydrolysis and fermentation are the common methods for producing bioethanol from the feedstocks. Bioethanol produced by the fermentation of sugar and starch based feedstock was earlier called as ethanol only. Ethanol is produced mainly from sugar cane in developing countries with warm climates. It is much cheaper to produce ethanol from grain or sugar beet in IEA countries. Brazil and India are the top ranking sugar cane producers in the world, where, sugar cane based bioethanol is found to be economically feasible [8]. Ethanol has a high octane value, which makes it an attractive blending component; it has generally good performance characteristics, though its energy content by volume is only two-thirds that of gasoline. Efforts were made to introduce ethanol as an alternative fuel for spark-ignition (SI) engines. A low percentage of ethanol blended with gasoline, for example, 10% ethanol with 90% gasoline (E10) has been used as gasohol in Brazil for over 20 years. These blends are already available as gasoline vehicle fuel, in the fuel filling stations of many countries; they do not require any engine modifications and can be used in the same way as gasoline. Higher-percentage blends, with more than 30% ethanol, or pure ethanol can only be used with some modifications in the vehicle engine [9].

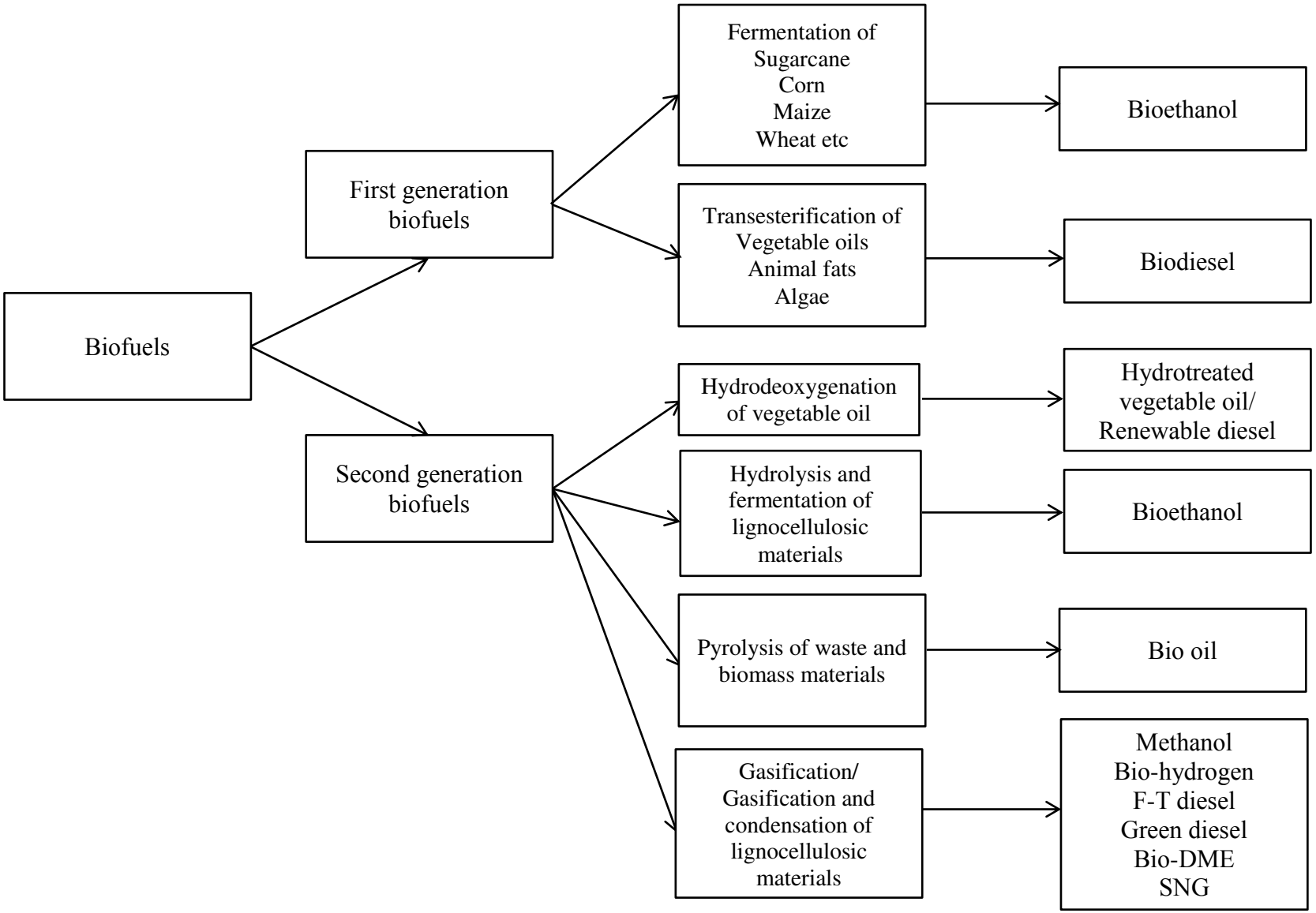

Fig.1.3 Block diagram of first and second generation biofuels

In the case of CI engine vehicles, upto 20% by volume of bioethanol (E20) has been used with diesel in the form of solution/emulsion [10]. Higher percentages by volume of ethanol can be used in CI engines, but it requires some engine modifications. The nitric oxide (NO) and smoke emissions from CI engines operated with bioethanol-diesel emulsions are reported to be lower, compared to that of diesel fuel operation. It is reported that, poor lubrication properties, poor miscibility with diesel fuel in the presence of water, corrosion and chemical degradation of engine materials, were the problems associated with ethanol diesel mixtures [11].

1.2.2 Biodiesel

Vegetable oil has been the primary candidate as a substitute for diesel fuel since the early 1900s, and this interest continued in various parts of the world during the Second World War due to insufficient supply and logistic difficulties of fossil fuel. Even the inventor of the diesel engine Rudolph Diesel demonstrated his engine with peanut oil only. Later during the 1970s, the control of oil production by the Organization of Petroleum Exporting Countries (OPEC), and the subsequent rise in fuel prices rekindled the interest in alternative fuels, including vegetable oils as fuels for diesel engines.

The name biodiesel was introduced in the USA in 1992, by the National Soy Diesel Development Board (presently National Bio-diesel Board), which has commercialized biodiesel in the USA. Biodiesel is a simplified version of fatty acids those are available in vegetable oils, animal fats, algae and other materials. It is derived from these sources by the transesterification process. The triglycerides present in these feedstocks are converted into mono esters by reacting them with alcohol in the presence of chemical catalysts. Commonly, the methyl or, ethyl or butyl esters of these feed stocks are known as biodiesel. However, the methyl esters of these feedstocks are mainly focused on, because methanol has a few advantages compared to ethanol and butanol. They are its high reactivity [12], lesser cost and easier methanol recovery, as it does not form azeotrope [13]. Various sources used for biodiesel production and the problems associated with its production are shown in Fig.1.4. In general, biodiesel feedstocks can be categorized into four groups: a) vegetable oils (edible or nonedible oil), b) animal fats, c) algae and d) other materials, as shown in the figure. The various sources of biodiesel production, oil yield and biodiesel yield are given in Table 1.1.

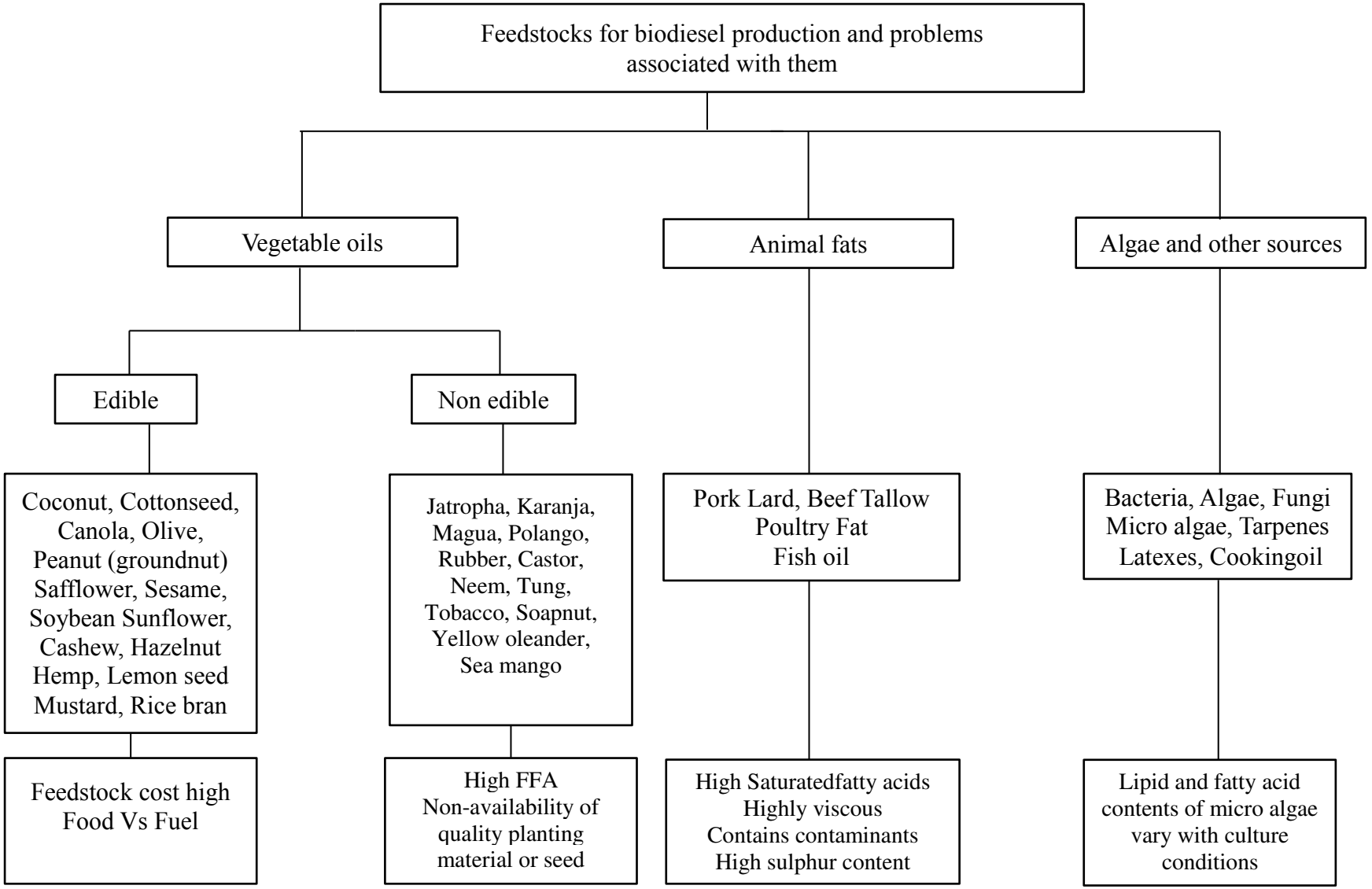

Fig.1.4 Sources of biodiesel production and problems

Table 1.1 Oil content and the biodiesel yield of different oil sources

Nature	Oil Source	Oil content (%)	Biodiesel yield (%)
Edible	Soybean	15-20	>95
	Sunflower	25-35	97.1
	Palm	30-60	89.2
	Peanut	45-55	89
	Corn	48	85-96
	Camelina	29.9-38.3	97.9
	Canola	43	80-95
	Pumpkin	50	97.5
	Rice bran	15-23	< 96
	Coconut	63-65	98
	Olive	45-70	92
Non-Edible	Jatropha (Jatropha curcas)	20–60	98
	Karanja/ Honge (Pongamiapinnata)	25–50	97-98
	Mahua (Madhucaindica)	35–50	98
	Cottonseed	17–25	96.9
	Rapeseed	38-46	95-96
	Neem (Azadirachtaindica)	20–30	88-94
	Putranjiva (Putranjivaroxburghii)	42	91
	Tobacco (Nicotianatabacum)	36-41	88
	Polanga (Calophylluminophyllum)	65	85
	Cardoon (Cynaracardunculus)	25-26	92
	Castor (Ricinuscommunis)	45-50	90
	Jojoba (Simmondsiachinensis)	45-55	93
	Moringa (Moringaoleifera)	45–50	82
	Poon (Sterculiafoetida)	50–55	88
	Sea mango (Cerberaodollam)	54	83.8
Animal Fat	Tallow	41	98.28
	Poultry	-	99.7
Others	Used cooking oil	-	94.6
	Micro algae	20-50	60

Biodiesels play an important role in meeting the world's future fuel requirements, in view of their nature (less toxic), and they have an edge over conventional diesel fuel as they are obtained from renewable sources.

Fig.1.5 shows the general chemical reaction involved in the production of methyl ester from the vegetable oils.

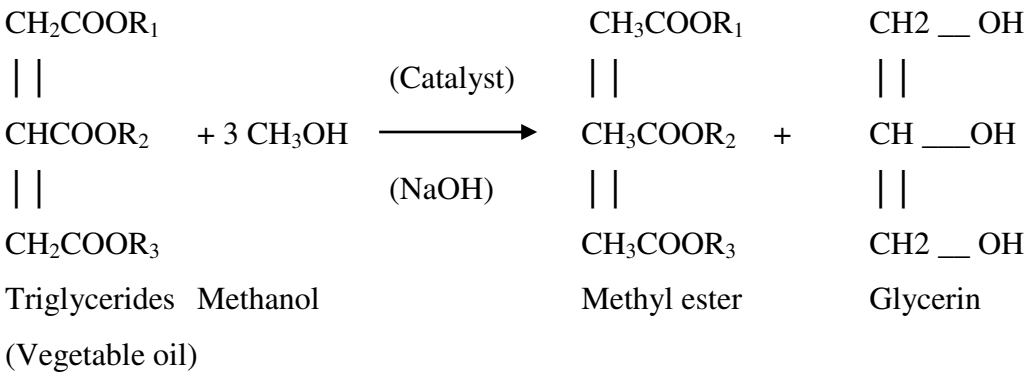

Fig. 1.5 Production of methyl ester by transesterification process

Table 1.2 gives various factors involved in transesterification process of biodiesel production.

Table 1.2 Factors involved in biodiesel production [8]

Feed stock	**Catalyst used**	**Alcohol**	**Temperature /Time**	**Alcohol to oil ratio**	**Biodiesel yield (%)**
Peanut oil	NaOH	Methanol	65°C (60 min)	6:1	90
Soybean	Absence of catalyst	Supercritical methanol, CO_2 co-solvent	280°C	24 and CO_2/methanol = 0.1	98
Soybean	Solid super acid catalysts of sulfatedtin and zirconium oxides tungstated zirconia, Noctanoic acid	Methanol	200-300°C (120min) 175-200°C	6:1	90 for both
Sunflower	Supercritical fluids, Enzyme in supercritical CO_2	Supercritical methanol and ethanol	200-400°C	40:1	800-100
Canola oil	Two-stage process, KOH	Methanol	25°C (90 min)	6:1	87
Karanja	KOH,Solid acid catalysts viz.Hb; K-10 and ZnO	Methanol Tetrahydrofuran (THF), cosolvent	60°C (90 min)	10:1	92 95
Jatropha	Two stage, NaOH	Methanol	60-65°C(90min)	5:1	98
Polanga	Sulphuric acid, KOH	Methanol	65°C (120 min)	6:1	85
Magua oil	Sulphuric acid, KOH	Methanol	70°C (90 min)	6:1	98
Micro algae	Sulfuric acid	Methanol	30°C	56:1	60
Animal fat/Tallow	NaOH	Methanol	60°C (180 min)	6:1	98
Fish oil	KOH	Ethanol	25°C (60 min)	6:1	92
Waste cooking oil	KOH	Methanol	25°C (30 min)	6:1	90

The ASTM test method for diesel and biodiesel are given in Table 1.3.

Table 1.3 Standards and limits for diesel and biodiesel fuels [8]

Property	**ASTM Test method**	**ASTM D975 (diesel) Limits**	**ASTM D6751 (biodiesel, B100) Limits**
Flash point (K)	D 93	325	130 min
Water and sediment (% vol)	D 2709	0.05 max	0.05 max
Kinematic viscosity at 313 K (mm^2/s)	D 445	1.3-4.1	1.9–6.0
Sulfated ash (% wt)	D 874	–	0.02
Ash (% wt)	D 482	0.01	–
Sulfur (% wt)	D 5453	0.05	–
Sulfur (% wt)	D 2622	–	0.05
Copper strip corrosion	D 130	No. 3 max	No. 3 max
Cetane number	D 613	40 min	47 min
Aromaticity (% vol)	D 1319	35	–
Carbon residue (% mass)	D 4530	–	0.05
Carbon residue (% mass)	D 524	0.35	–
Distillation temperature (90% volume) (K)	D 1160	555 min-611 max	–

The first generation biofuels can offer some CO_2 benefits and help to improve domestic energy security. But, attention must be given on the concerns about the sources of feedstock, impact on biodiversity, land use and competition with food crops. Also, there are concerns about environmental impacts and carbon balances, which set limits in increasing the production of biofuels of the first generation category.

1.3 Second generation biofuels

Second generation biofuels are made from lignocellulosic biomass, woody crops, agricultural residues, animal waste, and non-edible vegetable oils.

1.3.1 HVO – Hydrotreated Vegetable Oils

Hydrotreating of vegetable oils is a novel way to produce very high quality and bio based diesel fuels without compromising the fuel properties. The HVO fuel is also referred to as “renewable diesel” instead of “biodiesel” which the name is given to the fatty acid methyl esters. In the HVO production process, hydrogen is used to remove the oxygen from the triglyceride (vegetable oil). This process is described as hydrodeoxygenation.

1.3.2. Processing of lignocellulosic/plant biomass

Plant based biomass is one of the most abundant and unutilized biological resources, and is seen as a promising source of material for fuels and raw materials. A plant biomass can simply be burnt in order to produce heat and electricity. There are two principal methods available for generating heat and electricity from biomass; they are (i) biological conversion, and (ii) thermochemical conversion [14].

1.3.2.1 Biological conversion

Biological conversion technologies involve microbial and enzymatic processes for producing sugar from biomass such as lignocellulosic, starch and cellulosic materials. These sugars can be converted into alcohol and other solvents of interest for fuels and chemicals [15]. Agricultural residue, forest residue, post-harvest processing of industrial food crops and waste wood are examples of feedstocks of lignocellulosic biomass. The conversion of lignocellulosic biomass into bioethanol involves a three step process; i.e. (i) pretreatment of biomass, (ii) acid or enzymatic hydrolysis and (iii) fermentation/distillation; it is shown in Fig.1.6.

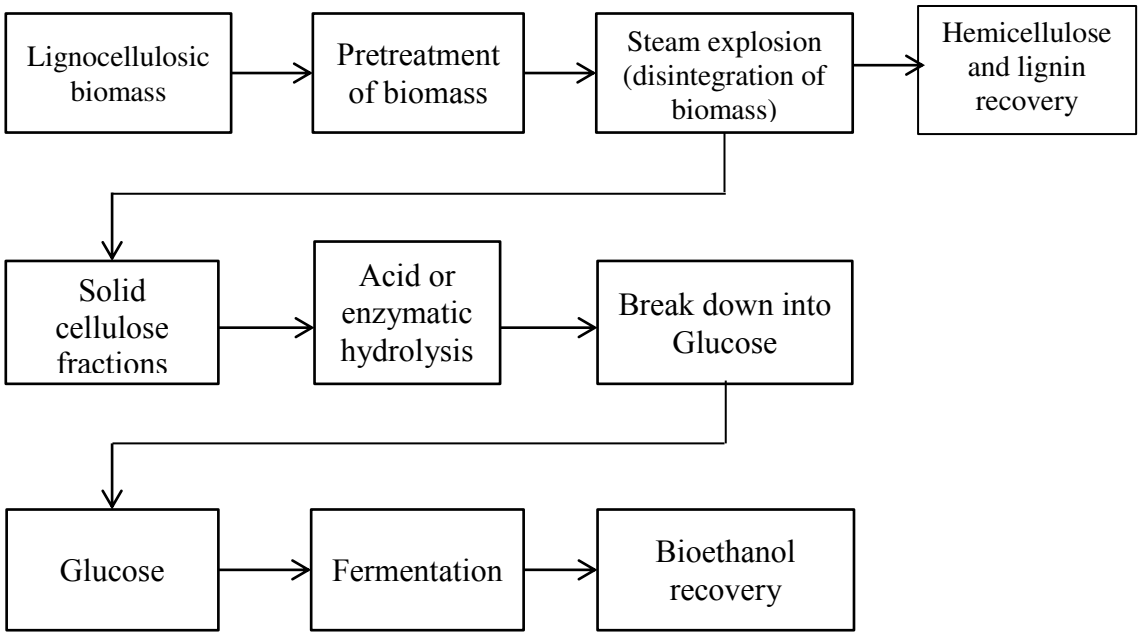

Fig.1.6 Bioethanol production from lignocellulosic biomass

1.3.2.2 Thermochemical conversion

The thermochemical conversion of biomass materials includes, direct combustion, gasification, liquefaction, and pyrolysis process.

(a) Direct combustion

The direct combustion is the chemical reaction between a fuel and oxygen which is usually air, and is more commonly known as burning. The principal products of direct combustion are carbon dioxide, water vapour and some amount of heat release. The biomass can be directly combusted to produce heat in chulas, furnaces and boilers.

(b) Gasification

The gasification method involves reacting biomass with air/oxygen,or steam to produce a gaseous mixture of CO, CO_2, H_2, CH_4, and N_2, known as producer gas or syngas, depending on the relative compositions of the constituents. Producer gas is one of the primary fuels used in stationary power generation applications, whereas syngas can be used to make a range of fuels and chemicals. Bio-hydrogen can be produced from syngas by the water-gas-shifting process, while Fischer-Tropsch (F-T) diesel or synthetic diesel can be produced by the Fischer-Tropsch (F-T) synthesis process. These fuels are also named as BTL (Biomass-to-Liquids) and GTL (Gas-to-Liquids). The F-T synthesis has been used since 1930, to produce hydrocarbon fuels from syngas. The production of methanol from syngas has been practiced since the year 1920 [15].

(c) Liquefaction

Biomass materials can be converted directly into a liquid similar to heavy oils, by reacting them with synthesis gas in the presence of a suitable catalyst in the liquefaction process. This process usually requires solvents, reacting gases such as CO or H_2 and/or catalysts in addition to the biomass. Water insoluble oils of high viscosity are produced in this process.

(d) Pyrolysis

It is a thermal degradation of biomass in the absence of oxygen or with very little presence of oxygen. In this process, the biomass-particularly solid or liquid is fed into a reactor which is indirectly heated up. During heating, the vapours evolved from the reactor are condensed in a condenser preferably water cooled. Three principal products are obtained from the biomass pyrolysis process, namely, (i) bio oil (liquid), (ii) pyro gas (gas), and (iii) char (solid). This

method has been studied, mainly to obtain a liquid product having a medium calorific value. Depending on the operating conditions, the pyrolysis process can be divided into three types: (i) Conventional pyrolysis, or slow pyrolysis (ii) Fast pyrolysis, and (iii) Flash pyrolysis.

(i) Conventional pyrolysis or slow pyrolysis

This process has been applied for thousands of years, and used mainly for the production of charcoal. In this method, the biomass is heated to a temperature about 300-500 °C with a slow heating rate of 3 - 5°C/min. The vapor residence time varies from 5 min to 30 min. The slow pyrolysis process yields charcoal of around 35–40%, together with 30% liquid (bio oil) [16].

(ii) Fast pyrolysis

It is a high-temperature process, in which biomass is rapidly heated in the absence of oxygen. It occurs in the high temperature range of 850-1250 K with a fast heating rate (10-200 K/s), short solid residence time (0.5-10 s) and fine particle size (<1 mm). The fast pyrolysis process produces 60-75 wt % of liquid bio oil, 15-25 wt % of solid char, and 10-20 wt % of non-condensable gases, depending on the feedstock used. No waste is generated, because the bio oil and solid char can each be used as a fuel and the gas can be recycled back into the process.

(iii) Flash pyrolysis

It is a process that occurs in the temperature range of 1050-1300 K, with a fast heating rate (>1000 K/s), short residence time (<0.5 s) and very fine particle size (<0.2 mm). The bio oil production from flash pyrolysis can be mixed with the char to produce bio-slurry, which can be used as a fuel in the gasifier for efficient conversion into syngas. Upto 70% of bio oil yield can be obtained from the flash pyrolysis process. This bio oil can be used in engines and turbines as a supplementary fuel.

The main advantage of pyrolysis is that, the feedstocks which are not convertible to ethanol or biodiesel can be converted into value added products. The other advantages include low production cost, high thermal efficiency, low fossil fuel input, and CO_2 neutrality. It also offers the flexibility of installation and operation with respect to time, scale and place, handling of the products and more-consistent quality, in comparison with gasification [15].

The pyrolysis process has a few drawbacks over the other processes. The bio oil obtained from this process has a high oxygen content which reduces its calorific value. The bio oil also contains many reactive components that can form higher molecular weight species. These components result in an increase in the viscosity and decrease in volatility, which is unfavourable for fueling diesel engines. The hydroscopic nature of the bio oil weakens its stability during blending with diesel fuel.

1.4 Indian scenario on biofuels

India depends heavily on the import of crude oil, and as a result the oil price shoots up frequently. Therefore, the government of India is very keen to introduce a variety of alternative fuels, mainly in the transportation sector. India imports more than 40% of its edible oil requirement, and hence non-edible oils are used for the development of biodiesel. India is an agrarian nation and has a rich plant biodiversity, which can support the development of biodiesel. India also has a vast geographical area with agricultural lands as well as wastelands in which oil bearing plants can be planted. Common non-edible oil bearing trees include Jatropha, Karanja, Neem,Mahua (madhucaindica), etc. These species are, at present insufficient to meet the demand for raw material in large scale production of biodiesel. Hence, there have been initiatives by the government, and also interest from a few private firms to enhance the production and distribution facilities of biodiesel throughout the country. Azam et al. [17] have studied the profile of 75 indigenous plant species in India, which contain 30% or more oil in their seeds, fruits or nuts. Among these plants, 26 species were found to be most suitable for use as biodiesel based on their saponification number, iodine value, cetane number and fatty acid composition, and they also met the biodiesel standards of USA (ASTM D 6751-02, ASTM PS 121-99), Germany (DIN V 51606) and European Standard Organization (EN 14214). It is also reported that 11 other plant species met the specifications of the US biodiesel standards. Among these species, Jatropha (Jatropha curcas), Karanja (Pongamiapinnata), Neem (Azhardictaindica), Mahua (Madhucaindica) and Polanga (Calophylluminophyllum) have drawn the attention of researchers and biodiesel manufacturers in India, while the feasibility of the rest of the plant species still remains unexplored. There are a few drawbacks with feed stock available in India, that pose a setback in promoting large biodiesel production, which are as follows:

i) Non homogeneity of the oil seeds available

ii) Collection and transportation of oil seeds

iii) Oil expellers are available only for edible oils, which do not allow expelling oil from non-edible oil seeds.

1.5 Biodiesel fueled diesel engines - An overview

The biodiesel produced by the transesterification process is completely miscible with diesel in any proportion. The physicochemical properties of biodiesel produced from different oil sources, such as oxygen content, cetane number, flash point, viscosity, density and heating value, can potentially improve or deteriorate the engine performance and emission characteristics [18]. The viscosity of biodiesel is marginally close to that of diesel, and hence there are no problems in the existing fuel handling system [19]. The flash point of biodiesel gets lowered after transesterification and the cetane number gets improved. Even lower concentrations of biodiesel act as cetane number improvers for the biodiesel blend. The calorific value of biodiesel is also found to be very close to that of diesel. Investigations from an engine fueled with biodiesel or biodiesel blends suggested that the thermal efficiency of the engine is marginally high. The exhaust gas temperature is higher while, smoke opacity is lower for the biodiesel blends. The possible reason is the additional lubricity of the biodiesel, which reduces the frictional losses. The energy saved in this manner will increase the thermal efficiency and reduce the cooling and exhaust losses from the engine. The thermal efficiency starts reducing after a certain concentration of biodiesel. The flash point, density, pour point, cetane number and calorific value of biodiesel are in very close to those of diesel. Twenty percent biodiesel (B2O) is considered to be the optimum ratio of the biodiesel-diesel blend for improved performance in a diesel engine.

The molecular structure of biodiesel is similar to that of diesel fuel, and it contains additional oxygen content in it, which is useful to reduce the CO, UHC and smoke emissions in the engine exhaust. In addition, biodiesel is bio-degradable; it can be mixed with diesel fuel in any ratio, and is sulfur-free. Although, it has many advantages over diesel fuel, there are several problems associated with biodiesel which needs to be addressed, such as its lower heating value, higher viscosity, poor cold flow properties and oxidation stability [20-23]. The NO emission from the biodiesel fueled diesel engines is reported to be higher compared to that of diesel operation. Table 1.4 gives the percentage variation in the average biodiesel emissions compared to that of diesel fuel (*Source:EPA, NREL) [24].

Table 1.4 Average biodiesel emissions compared with conventional diesel

Type of emission	B100	B20
Regulated Emissions		
Total Unburned Hydrocarbons (UBHC)	-67%	-20%
Carbon Monoxide (CO)	-48%	-12%
Particulate Matter (PM)	-47%	-12%
Oxides of nitrogen (NO_x)	10%	-2% to 2%
Non-Regulated Emissions		
Sulphates	-100%	-20%
Polycyclic Aromatic Hydrocarbons (PAH)	-80%	-13%
Nitrated PAHs	-90%	-50%
Ozone Potential	-50%	-10%
Carbon Dioxide (CO_2)	-78%	-15%

1.6. NO_x reduction strategies

Diesel engines emit higher NO_x emissions than gasoline engines, and the research on the control of NO_x emissions has advanced significantly, since Zeldovich first proposed the thermal NO_x formation mechanism in 1943. The methods involved, or those that attempted to reduce the NO_x emission in diesel engines, are as follows:

i. Retardation of injection timing,
ii. Use of low injection pressure,
iii. Exhaust gas recirculation, (EGR)
iv. Multivalving/split injection
v. Modification in the combustion chamber geometry to enhance the swirl and squish
vi. Reducing the combustion temperature by water injection or use of emulsified fuels
vii. Excessive cooling of intake air
viii. Inducting fuels with high latent heat of vaporization like alcohol or DEE along with air in the suction
ix. Addition of cetane improvers like 2-ethyl hexyl nitrate
x. Use of biomass based fuels which contain water content in them

Many researchers have attempted to reduce the NO_x emissions from the biodiesel fueled engines, by adopting any one of the above techniques, and now biodiesel run buses in some countries implement the techniques such as EGR etc.

1.7 Present Investigation

This research work intends to replace the usage of diesel fuel completely, and also a certain percentage of JME. Bio oil contains water and phenols that may be helpful to reduce the NO_x emissions in a biodiesel fueled engine.

The main objectives of the present work are as follows:

i) To prepare the JME-WPO emulsions using different surfactants and characterise them as alternative fuels for CI engines.
ii) To evaluate the combustion, performance and emission behaviour of a single cylinder, four stroke, air cooled, direct injection (DI) diesel engine developing a power of 4.4kW at 1500 rpm with different JME-WPO emulsions.
iii) To find the optimum emulsion and upgrade the emulsion quality by acid treatment.
iv) To validate the experimental results using a mathematical modelling.
v) To study the combined effects of compression ratio, injection timing and nozzle opening pressure on the combustion, performance and emission characteristics of the optimum upgraded fuel emulsion.
vi) To assess the lubrication oil properties and short term durability issues.

1.8 Organization of thesis

Chapter 1 Introduction

This chapter briefs the need for biofuels and their classification, an overview of biodiesel fueled diesel engines, the Indian scenario on biofuels and also states the objectives of the present research work.

Chapter 2 Literature Review

A comprehensive review of research works pertaining to the production and characterization of Jatropha methyl ester (JME) for its suitability as an alternative fuel in CI engines are given. The review work also discusses the up to date literature available on the utilization of JME in CI engines. The various issues related to combustion, performance and emission parameters of the CI engine fueled with the JME are discussed in this chapter. The review also includes the NO_x emission reduction strategies adopted in biodiesel fueled engines. The

literature on the production and utilization of Wood pyrolysis oil (WPO) in diesel engines is also presented in this chapter.

Chapter 3 Production and characterization of test materials

This chapter details the methods and materials involved in the production of JME, WPO and JME-WPO emulsions. The chapter also discusses the characterization of the test fuels considered in this study. The test materials have also been tested by the TGA, CHNS and SEM for determining the important properties that there involved in this study.

Chapter 4 Engine experimental setup, instrumentation and experimental methodology

In this chapter, the necessary engine experimental setup and other accessories are described systematically. The method of determining the uncertainty of the experimentation is also included at the end of this chapter. The details on various methodologies adopted, and the modifications involved in the engine experimental setup are also discussed in this chapter. The methods of calculating the important combustion, performance and emissions parameters are discussed. It also explains the method of study on lubricating oil properties, and a few durability issues on the test engine components.

Chapter 5 Results and discussion

Detailed discussions on the comparative analysis of the combustion, performance and emission results obtained from the experimental investigation from a diesel engine fueled with different JME-WPO emulsions under various operating conditions are given in this chapter. This chapter also discusses the sample validation of the experimental results by a theoretical modeling and MATLAB programming for the prediction of heat release and emissions, viz., the NO and smoke of the diesel engine fueled with JME-WPO emulsions.

Chapter 6 Conclusions

The summary of the findings from the experimental investigation carried out in this study are given in this chapter. It also mentions the important conclusions of the investigation, and the scope for future work.

CHAPTER 2
LITERATURE REVIEW

2.1. General

This chapter presents a review of the various research works related to the production of Jatropha methyl ester (JME) and, a bio oil produced by the pyrolysis of biomass. The chapter also includes a review of the utilization of JME and its blends with diesel and other fuels in diesel engines, with fuel and engine modifications. The efforts that have been proposed worldwide to reduce the higher oxides of nitrogen (NO_x) emissions from the diesel engine fueled with the JME and its blends are also reviewed and presented. Further, the review of the utilization of bio oil/WPO in a diesel engine and the problems associated with the WPO, when it is used in its sole form, are given in this chapter.

2.2 Importance of Jatropha methyl ester

The esters of Jatropha oil were investigated by several researchers for their use in CI engines. Numerous documents are available related to the investigation on the use of the esters of Jatropha in diesel engines. The researcher has tried to collect and review the research works as much as possible, to identify the research problem.

Biodiesel from Jatropha oil can be produced by different transesterification methods. Alkali catalyzed [25-28], acid catalyzed [29], enzyme catalyzed [30-31], non-catalytic supercritical alcohol [32-34] and ultrasound assisted transesterification [35] methods have been adopted to produce biodiesel from Jatropha oil. Many researchers have investigated the operating parameters that affect alkali catalyzed transesterification reactions. The optimum variables for the effective transesterification of Jatropha oil are 20% methanol (by weight of oil), a molar ratio of methanol to oil of 5:1, and 1.0% of NaOH as a catalyst (by weight of oil). A maximum methyl ester yield of 98% was obtained after 90 min with a 60^{o}C reaction temperature, and the biodiesel obtained was found to be within the ASTM specified limits of biodiesel [25-26] obtained similar optimum transesterification conditions in their previous work, except that they did so by using KOH as a catalyst. Sahoo and Das [27] have also developed a method of the preparation of biodiesel from non-edible oils, such as Jatropha, Karanja and Polanga. They found that the conversion efficiency is strongly affected by the amount of alcohol because, an excess of alcohol is required to shift the reaction close to

completion. By concentrating on Jatropha curcas, the volumetric ratio of oil to methanol is 11:1, together with 1.1% of KOH by volume basis, which completed the transesterification process within 120 min at 66^{o}C, with a 93% yield of Jatropha methyl ester.

There are a number of documented research works available to prove the utilization of JME in its sole form, and in the blended form with diesel and other fuels, without any modifications to the diesel engine. Table 2.1 presents the review on the performance, combustion and emission parameters of a diesel engine fueled with the JME and its blends with diesel reported by the researchers. The performance, combustion and emission parameters of JME and its blends with different engine modifications are presented in Table 2.2. A literature review pertaining to different experimental studies on the performance, emission and combustion behavior of the CI engine run on JME and its diesel blends with engine modifications is given in Table 2.3.

2.3 NO_x emissions from JME fueled diesel engine

The common behavior of a compression ignition (CI) engine from the emission point of view is the trade-off between oxides of nitrogen (NO_x) and smoke. Although, the CI engines are well suited for today's transport and power applications, the emissions, particularly, the NO_x and the particulate emissions from these engines are difficult to control, irrespective of the type of fuel used. The increased NO_x levels in the air contribute to global warming and acid rain, affecting the human organs, and causing visual impairment, swelling of throats and other respiratory problems. On the other hand, particulates from a diesel engine affect the respiratory system. It is a major concern for researchers to identify suitable technique or method, to reduce the NO_x emission and particulates from CI engines.

So far, many researchers have proved that the NO_x emission from biodiesel fueled engines is higher compared to diesel operation, while a few researchers have proved that the NO_x emissions from some of the biodiesel fueled engines produce lower NO_x emission. It was also given in the literature that a 10% increase in the biodiesel of the biodiesel-diesel blend will cause 1% increase in NO_x emission [96]. The major reasons for the increased NO_x emissions with biodiesel fuels mentioned by several researchers are listed in Table 2.4.

Table 2.1 Review on the engine performance, combustion and emission results obtained from different diesel engine configurations fueled with JME and its blends

Sl.No.	Percentage of JME	Details of engine tested	Test results	Authors/Reference	Journal/Proceedings name/volume/page
1.	JME blends with diesel	3.5 kW, IDI (Indirect Injection) engine, constant speed 2000 rpm	It was observed that the JME-diesel blends produced superior thermal efficiency and fuel consumption equivalent to diesel. Also, it was reported that there was a marginal reduction in black smoke concentration when operating on the JME and its blends. The CO and HC concentrations from the engine increased at light loads and were equivalent to those of diesel at full load.	Ishii and Takeuchi, 1987.[36]	Transactions of the ASABE. 30 (3): 0605-0609.
2.	100% JME	3.7 kW, four stroke, single cylinder, water cooled, direct injection diesel engine, constant speed 1500 rpm	Higher thermal efficiency was reported with the JME compared to that of raw Jatropha oil but, it was found to be lower than that of diesel. Smoke and particulate levels were found to be higher with Jatropha oil than that of diesel. The HC and CO emissions were marginally higher with both Jatropha oil and its methyl ester than with diesel, whereas the NO levels were found to be lower than those of diesel. The ignition delay and combustion duration were observed to be longer and the peak heat release rates were lower with Jatropha oil and JME than those of diesel.	M.Senthilkumar[a], 2001. M.Senthilkumar[b], 2003. [37-38]	[a]Journal of Energy Institute, vol. 74, pp. 24-28. [b]Biomass and Bioenergy, vol. 25, pp. 309-318.
3.	50% blend with diesel and 100% JME	3.7 kW, four stroke, single cylinder, water cooled, DI (Direct Injection), diesel engine at speed 1500 rpm and IDI engine, constant speed 2000 rpm	It was reported that the JME operation under naturally aspirated condition yielded the best result in the case of an IDI engine, with a specific fuel consumption of 0.354 kg/kWh and exhaust smoke level of 14 HSU. With B50 they observed a comparable SFC in the DI engine. Lower smoke emissions were reported with JME operation in the IDI engine compared to that of DI engine.	G.A.P. Rao, 2005 [39]	Journal of the Institution of Engineers, vol.86, pp. 72-76.

4.	15 and 20 % JME blended with diesel	3.68 kW, single cylinder, four stroke, water cooled, DI engine, constant speed 1500 rpm	Higher brake thermal efficiency, lower HC and CO emissions with B20 were reported in comparison with diesel operation.	P.Mahanta, 2006 [40]	International Energy journal, vol. 7, pp.1-8.
5.	100% JME	5.2 kW, single cylinder, four stroke, water cooled, DI diesel engine, constant speed 1500 rpm	About 7% lower brake thermal efficiency, 26% higher smoke and 65% higher HC, 37% higher CO and 10% lower NO emissions (At advanced injection timing of 27^{o} bTDC) were reported in comparison with diesel operation.	N.R. Banapurmath, 2007 [41]	Renewable Energy, vol. 33, pp. 1982-1988.
6.	20% JME blended with diesel and 100% JME	4.4 kW, single cylinder, DI diesel engine, constant speed 1500 rpm	Lower ignition delay, lower rate of pressure rise, lower brake thermal efficiency, higher NO_x, lower HC, CO and PM were reported in comparison with diesel operation.	G. Lakshmi Narayana Rao, 2007. [42]	International Journal of Green Energy, vol.4, pp. 645-658.
7.	10, 20 40% JME blends with diesel and 100% JME	3.7 kW, single cylinder, four stroke, DI, water cooled diesel engine, constant speed 1500 rpm	The brake thermal efficiency was found to be higher for blends than B100, but less than that of diesel. Lower HC, CO and smoke emissions were reported in comparison with diesel operation.	T. Venkateswara Rao, 2008. [43]	Jordan Journal of Mechanical and Industrial Engineering, vol. 2, pp. 117 - 122.
8.	20, 40, 60,80 and 100	3.68 kW, single cylinder four stroke, water cooled diesel engine, constant speed 1500 rpm	Higher brake thermal efficiency with B20 was reported in comparison with diesel operation.	Kalbande, 2008 [44]	ARPN Journal of Engineering and Applied Sciences, vol.3, pp. 7-13.
9.	25, 50, 75 and 100	3.68 kW, single cylinder, four stroke, water cooled diesel engine, constant speed 1500 rpm	Higher thermal efficiency, higher exhaust gas temperature, lower smoke, and 14% lower CO and CO_2 emissions were observed. Higher NO_x emissions were reported in comparison with diesel operation.	Y.V.H.Rao, 2009 [45]	Thermal Science, vol. 13, pp. 207-217.

10.	20,50 and 100	44.1 kW, 3-cylinder, AVL make CI engine, at variable speeds (1200, 1800 and 2200 rpm)	About 28.57%, 40.9%, 64.28% lower smoke and 35.21%, 14.67%, 5.57%, higher CO emissions for B20, B50 and B100 respectively, were observed. The NO emissions were found to be higher by 20.54%, 15.65%, 18.39% compared to that of diesel operation. About 32.28%, 18.19%, 20.73% lower HC emissions and 16.53%, 26.60%, 42.06% lower particulates respectively, were recorded in comparison with diesel operation.	P.K. Sahoo, 2009 [46]	Fuel, vol. 88, pp. 1698-1707.
11.	100	11.1kW, MS 1100, single cylinder, four stroke, and horizontal type diesel engine, constant speed 2240 rpm.	Lower exhaust gas temperature was reported in comparison with diesel operation.	T.T. Kywe, 2009 [47]	World Academy of Science and Engineering Technology, vol. 38, pp. 481-487.
12.	100	3.5 kW, single cylinder, water cooled, four stroke, diesel engine, constant speed 1500 rpm.	Lower brake thermal efficiency, higher SFC, low EGT, lower rate of pressure rise, shorter ignition delay, and lower heat release rate were observed with JME when compared with diesel. About 56% lower HC and 20% lower smoke, 25% lower NO and 38.4% higher CO were reported in comparison with diesel operation.	Jindal,2010 [48]	Energy and Fuels, vol.24, pp. 1565-1572.
13.	100	3.68 kW, single cylinder, four stroke, water cooled, diesel engine, constant speed 1500 rpm.	Lower brake thermal efficiency, higher EGT, HC, CO and smoke and lower NO emissions were reported. Longer ignition delay, high rate of pressure rise, and longer combustion duration were reported in comparison with diesel operation.	M.Senthil kumar, 2010 [49]	Journal of Engineering for Gas Turbines and Power, vol. 132, pp.1-10.
14.	5,10,15 and 20	2.43 kW, single cylinder, four stroke, DI, diesel engine, constant speed 2600 rpm.	Higher exhaust gas temperature, brake thermal efficiency and lower BSFC were reported in comparison with diesel operation.	Ejilah, 2010 [50]	Australian journal of agricultural engineering, vol. 1, pp. 80-85.

15.	100	4.4 kW, single cylinder, four stroke, air cooled, DI, diesel engine, constant speed 1500 rpm.	Higher BSEC at full load and high brake thermal efficiency at lower loads were observed. Lower HC, CO and smoke emissions were reported in comparison with diesel operation.	S.Puhan, 2010 [51]	Biomass and Bioenergy, vol. 34, pp. 1079-1088.
16.	100	8.2 kW, single cylinder, four stroke, water cooled, DI, diesel engine, at speed 1500 rpm and 2000 rpm.	About 3% higher brake thermal efficiency, 6.3% higher BSFC were reported in this work. Also, it was observed that about 25% lower CO emissions, 23% lower HC emissions, 14.5% lower NO emissions, 35% lower smoke emissions were reported in comparison with diesel operation at full load.	J. Huang, 2010 [52]	Fuel Processing Technology, vol. 91, pp. 1761-1767.
17.	10,20,30 and 40	3.5 kW, single cylinder, four stroke, DI, diesel engine, constant speed 1500 rpm.	Lower brake thermal efficiency with all blends and higher BSFC, lower peak pressures, shorter ignition delay were recorded.	T. K. Gogoi, 2011 [53]	World Renewable Energy Congress, Sweden, pp. 3533-3540.
18.	5,10,15,20,25 and 30	3.68 kW, single cylinder, four stroke, water cooled, DI diesel engine, constant speed 1500 rpm.	B20 revealed high brake thermal efficiency and low SFC, in comparison with other blends.	S. Reddy, 2011 [54]	International Journal of Sustainable Energy, vol. 30, pp. 37-41.
19.	10,20,30,40 and 50	4.4 kW, single cylinder, four stroke, air cooled, DI, diesel engine, constant speed 1500 rpm.	It was reported that the SFC was closer to that of diesel with B20. Longer ignition delay was observed with all blends. Lower HC, CO, CO_2 emissions were observed with B20. Higher NO and smoke emissions were observed.	T. Elango, 2011 [55]	Thermal Science, vol. 15, pp. 1205-1214.
20.	10,20,50,75 and 100	3.75 kW, single cylinder, four stroke, water cooled, diesel engine, constant speed 1500 rpm.	B20 results in lower BSFC, and brake thermal efficiency closer to that of diesel fuel were reported in this paper.	R.Prakash, 2011 [56]	Intl. Journal of Advanced Engineering Technology, vol. 2, pp. 186-191.

21.	15	4.5 kW, single cylinder, four stroke, water cooled, diesel engine, constant speed 1500 rpm.	Lower brake thermal efficiency, higher BSFC, lower HC and smoke emissions were observed with B15. The NO emissions were found to be higher than those of diesel.	L. Prasad, 2011 [57]	Journal of Scientific & Industrial Research, vol. 70, pp. 694-698.
22.	20 and 100	4.4 kW, single cylinder, four stroke, water cooled, diesel engine, constant speed 1500 rpm.	It was observed that the SFC of B100 and B20 was about 4.6% and 3.9% respectively higher than those of diesel. Lower brake thermal efficiency was observed. The CO emissions were found to be decreased by about 30% and 15.5% respectively for B100 and B20. The HC emissions was found to be lower by about 28% and 16% for B100 and B20. The NO_x levels were found to be higher for B100 and B20, by about 14.5 % and 22.1% than that of diesel. The particulate matter of B100 and B20 was higher by about 3.1% and 2.1% respectively than that of diesel.	B.R. Prasath, 2011 [58]	Applied Mechanics and Materials, vol. 110-116, pp. 3–7.
23.	5,10,15 and 20	3.68 kW, single cylinder, DI, four stroke, water cooled, diesel engine, constant speed 1500 rpm.	Brake thermal efficiency of B20 was comparable with that of diesel. Higher BSFC and exhaust gas temperature were reported.	D.Vashist, 2011 [59]	International Journal of Engineering Science and Technology, vol. 3, pp. 4765-4773.
24.	100	5.9 kW, single cylinder, four stroke, DI, diesel engine, constant speed 1500 rpm.	Lower brake thermal efficiency, Higher SFC, lower peak pressure, low heat release rate, longer combustion duration, longer ignition delay, lower peak cylinder temperature were reported. Lower HC, CO and smoke emissions and higher NO emissions were reported in comparison with diesel.	D.Kannan, 2011 [60]	Energy Conversion and Management, vol. 53, pp. 322-331.
25.	5, 20,50,80 and 100	3.7 kW, single cylinder, four stroke, diesel engine, constant speed 1500 rpm.	Higher BSFC, exhaust temperature and lower brake thermal efficiency were observed with the JME blends. Lower HC, CO_2, CO emissions, higher NO_x emissions, lesser noise and vibrations were observed for the B20 compared to diesel operation, and hence, it was concluded that optimum blend was B20.	S. Kumar, 2012 [61]	International Journal of Energy and Environment, vol. 3, pp. 471–484.

26.	100	5.2 kW, single cylinder, four stroke, direct injection, water cooled diesel engine, constant speed 1500 rpm.	Lower brake thermal efficiency, higher SFC, exhaust gas temperature, NO, HC and lower CO and smoke emissions were reported in comparison with diesel operation.	A. Yadav, 2012 [62]	Proc IMechE Part A: Journal of Power and Energy, vol. 226, pp. 674-681.
27.	5,10	20 kW, single cylinder, four stroke, water cooled, diesel engine, variable speeds of 1500 to 2400 rpm at an interval of 100 rpm	Average increase in the BSFC compared to DF was found to be 0.54% for JB5, and 1.0% for JB10. Lower HC, CO and CO_2 and higher NO emissions. Lower noise levels were reported with JB5 and JB10 in comparison with diesel operation.	A.M. Liaquat, 2012 [63]	Energy Procedia, vol. 14, pp. 1124-1133.
28.	2, 5 and 10	4.4 kW, single cylinder, four stroke, air cooled diesel engine, constant speed 1500 rpm.	Lower brake thermal efficiency, higher BSFC. Lower HC, CO and smoke emissions and higher NO emissions were reported.	L. Prasad, 2012 [64]	Applied Energy, vol. 93, pp. 245-250.
29.	5,10,20,30 and 100	7.4 kW, single cylinder, air cooled, DI, DAF8 model, diesel engine, constant speed 1500 rpm.	Lower cylinder pressure and heat release rate were observed for JME. Lower brake thermal efficiency, higher BSFC, and EGT were observed for the JME and its blends. Lower HC, CO and smoke emissions and higher NO, CO_2 emissions were reported.	B.S. Chauhan, 2012 [65]	Energy, vol. 37, pp. 616-622.
30.	10, 20,30 and 40 (Jatropha ethyl ester)	3.73 kW, single cylinder, CI engine, constant speed 1500 rpm.	Higher brake thermal efficiency, BSFC and EGT were reported for the JEE blends. Higher NO and lower CO emissions were reported in comparison with diesel operation at full load condition.	R.Kumar, 2012 [66]	International Journal of Automobile Engineering Research and Development, vol. 2, pp. 34-47.

31.	5, 10,20,50 and 100	79 kW, four cylinder, four stroke, turbocharged diesel engine, constant speed 2000 rpm.	The NO emissions were found to be higher for B5, B10, B20, B50, and B100 fuels by about 1.02%, 2.06%, 4.74%, 5.71%, and 13.9% respectively compared to diesel. About 23.1%, 46.7% and 76.9% lower CO, HC and smoke emissions were reported with B100 at full load compared to those of diesel operation.	P.Q. Tan, 2012 [67]	Energy, vol. 39, pp. 356-362.
32.	20, 40, 80 and 100	5.2 kW, four stroke, single cylinder, water-cooled diesel engine, constant speed 1500 rpm.	It was reported that the B20 blend in the diesel engine resulted in smooth operation. The smoke, CO and HC emissions increased with increased percentage of JME blends while the NO_x values were found to be decreased.	G. Shirsath, 2012 [68]	International Journal of Sustainable Engineering vol. 5, No. 3, pp. 252-264.
33.	10,20, 30 and 50	4.5 kW, single cylinder, four-stroke, direct injection, variable compression ratio diesel engine, at variable engine speeds ranging from 1000 to 2000 rpm, at an interval of 250 rpm	Lower brake thermal efficiencies were observed with the JME blends. The peak pressure of B50 was observed to be higher at low and high engine speeds, while those of B10 and B20 are optimum at medium speed. A higher percentage of NO_x was observed in the case of JME compared to that of diesel.	M.EL. Kasaby, 2013 [69]	Alexandria Engineering Journal vol. 52, 2013, pp. 141-149.

Table 2.2 Performance, combustion and emission results of JME and its blends with different engine modifications

Sl.No	JME (%)	Engine tested	Test results compared with diesel	Authors/Reference	Journal/Proceedings name/volume/page
1.	100	3.7 kW, single cylinder, four stroke, water cooled direct injection diesel engine at constant speed 1500 rpm (Hot EGR at 5%, 10%, 15%, 20% and 25%).	The brake thermal efficiency of the JME was found to be comparable with diesel, at all loads with and without EGR. The hot EGR of 15% effectively reduced the NO emission without any adverse effects on the performance, smoke and other emissions. The higher EGR percentages of 20 and 25% resulted in inferior performance and heavy smoke.	V. Pradeep, 2007 [70]	Renewable Energy vol. 32, pp. 1136-1154.
2.	100	3.5 kW, single cylinder, water cooled, four stroke, VCR diesel engine, constant speed 1500 rpm (Compression ratio and injection pressure variation).	About 8.2% higher brake thermal efficiency was observed with a compression ratio (CR) of 18 and injection pressure of 250 bar. The HC emissions were found to be lower at lower injection pressure and at all compression ratios. For high CR, the CO and smoke emissions were found to be lower. Lower CO emissions were observed at CR 18 and injection pressure of 150 bar. High NO at high CR and low injection pressure. Low NO emissions were reported at CR 17 and injection pressure 250 bar.	Jindal, 2010 [20]	Applied Thermal Engineering, vol. 30, pp. 442-448.
3.	20 and 100	5.2 kW, single cylinder, four stroke, NA, open chamber, water cooled, DI diesel engine, constant speed 1500 rpm (Injection timing and injection pressure variation).	Advanced injection timing of 26° bTDC and injection pressure of 220 bar results in on improved engine performance and emissions. High brake thermal efficiency, low HC, smoke and NO_x were reported in this work.	Dhananjaya, 2010 [71]	Thermal Science, vol. 14, pp. 965-977.

4.	100	5 kW, single cylinder, four stroke, air cooled, diesel engine, constant speed 1500 rpm (Compression ratio and injection timing/variation).	Optimum brake thermal efficiency was obtained at 27^{o} bTDC (Advanced) and CR of 17.	T. Ganapathy, 2009 [72]	Thermal Science, vol. 13, pp. 69-82.
5.	20	5.2 kW, single cylinder, four stroke, open chamber, water cooled, diesel engine, constant speed 1500 rpm (Injection timing and injection pressure variation).	Injection pressure of 220 bar and injection timing of 26° bTDC resulted in lower cyclic variations in peak pressure and IMEP.	Barboza, 2010 [73]	International Conference on Mechanical and Electrical Technology, pp. 43-46.
6.	20	4.4 kW, single cylinder, four-stroke, air cooled, DI diesel engine, constant speed 1500 rpm (Compression ratio, injection timing and injection pressure variation)	A maximum brake thermal efficiency was found with JME20 at 27^{o} bTDC, 240 bar and CR of 19:1. Combined increase of CR, injection timing and injection pressure increased the brake thermal efficiency and reduced the BSEC with lower emissions.	M .Venkatraman, 2010 [74]	National Journal on Advances in Building Sciences and Mechanics, vol. 1, pp. 34-39.
7.	100	3.7 kW, single cylinder, water cooled, four stroke diesel engine, constant speed 1500 rpm (LHR engine with internal jet piston)	The brake thermal efficiency was found to be increased by 3%, BSEC decreased by 14% for the JME with partially stabilized zirconia (PSZ) coated internal jet piston. The CO and smoke emissions were found to be decreased, and NO_x emissions were found to be increased with the JME at full load. The maximum pressure and heat release rate were increased and the ignition delay and the combustion duration were decreased for the internal jet piston with the JME.	K. Rajan, 2011 [75]	Second International Conference on Sustainable Energy and Intelligent System, pp. 184-189.

8.	100	5.59 kW, single cylinder, four stroke, air cooled, vertical, Greaves Cotton model GL 400 IIA, diesel engine, with variable speeds 1800, 2500 and 3200 rpm (Injection timing)	Advance in the injection timing caused a reduction in the BSFC, CO, HC and smoke levels, and increase in the brake thermal efficiency, maximum pressure (P_{max}), maximum heat release rate (HRR_{max}), and the NO emissions were observed with the JME operation. At 20^{o} bTDC (advance) the percentage reduction in the BSFC, CO, HC and smoke levels were reported to be about 5.1%, 2.5%, 1.2% and 1.5% respectively. The percentage increase in the brake thermal efficiency, Pmax, HRR_{max} and the NO emissions with this injection timing were observed to be about 5.3%, 1.8%, 26% and 20% respectively at full load.	T. Ganapathy, 2011 [76]	Applied Energy, vol. 88, pp. 4376-4386.
9.	100	3.5 kW, single cylinder, water cooled, four stroke diesel engine, constant speed 1500 rpm (Injection timing)	About 8% higher brake thermal efficiency was observed by retarding the injection timing by 3^{o}. With advanced timings, the brake thermal efficiency dropped considerably. About 9% reduction in the SFC was observed at 3^{o} retarded timing.	S. Jindal, 2011 [77]	International Journal of Energy and Environment, vol. 2, pp. 113-122.
10.	5 and 20	69.14 kW, four cylinder, water cooled, turbocharged, IDI diesel engine, constant speed 2000 rpm. (5%, 10 % EGR)	At 5% EGR with JB5, both NO_x and smoke opacity were reduced by 27% and 17% respectively. The JB20 blend along with 10% EGR, reduced both NO_x and smoke emissions by about 36% and 31%, respectively.	M. Gomaa, 2011.[78]	International Journal of Energy and Environment, vol. 2, pp. 477-490.
11.	100	3.7 kW, single cylinder, four stroke, water cooled, diesel engine, constant speed 1500 rpm (7% and 14% cooled EGR)	It was reported that delayed combustion was observed in both the cases of diesel and JME with the EGR application. Peak pressures reduced with an increase in the EGR percentage. Lower NO_x emissions were reported with EGR.	S. Adinarayana, 2011. [79]	International Journal of Applied Research In Mechanical Engineering, vol.1, pp.10-15.

12.	100	19.8 kW, four cylinder, four stroke, naturally aspirated, diesel engine, constant speed 2200 rpm. (EGR 10%)	Average increase of 2.61% BSEC without EGR and 13.3% compared to diesel was noticed. Reduction in the brake thermal efficiency of 2.48% and 11.6% with JME, JME with 10% EGR. JME with EGR operation results in 5.9% increase in CO emission compared to JME, without EGR reduction of 8.2% compared to that of diesel. A reduction of 4.64% in the HC emissions was observed in comparison with diesel operation. The JME showed an average of 19.6% higher NO_x emission compared to diesel. Use of EGR in JME showed an average of 19.85% reduction in NO_x emission compared to JME without EGR and 4.31% compared to that of neat diesel. About 20.8% higher smoke emission was observed with EGR in comparison without EGR operation and 8.41% higher compared to diesel.	N. Shrivastava, 2012 [80]	International Journal of Renewable Energy Research, vol. 2, pp. 504-509.
13.	100	3.68 kW, single cylinder, four stroke, constant speed, DI diesel engine, constant speed 1500 rpm (Injection pressures 200, 210 bar)	Lower HC, CO and NO emissions were reported with the JME compared to that of diesel operation.	Nagarhalli, 2012 [81]	International Journal of Advanced Engineering Technology, vol.III, pp. 51-54.
14.	20	4.4 kW, single cylinder, four stroke, constant speed 1500 rpm, DI diesel engine with multi chambered piston geometry and injection pressures of 175, 200 and 225 bar.	It was observed that the modified piston showed an enhanced performance and lower emissions compared to the standard piston. The SFC reduced with an increase in injection pressure. The optimum injection pressure was observed as 200 bar for the B20 blend. Brake thermal efficiency was improved with an increase in the injection pressure up to 200 bar, and with further increase in injection pressure the brake thermal efficiency was reduced. The UBHC emission was improved with increased injection pressure.	Rajashekhar, 2012 [82]	Transactions of the Canadian Society for Mechanical Engineering, vol. 36, pp.429-438.

15.	20, 30 and 40 (EGR + Ignition improver)	4.4 kW, computerized, single cylinder, four stroke, direct injection, air cooled diesel engine, constant speed 1500 rpm	It was observed that with an increase in the percentage of EGR, the brake thermal efficiency increased while the BSFC and the exhaust gas temperature decreased. The optimum EGR for the maximum brake thermal efficiency and the minimum BSFC were found to be 20%. The CO and HC emissions were found to increase with the increase in the percentage of EGR. But, the CO and HC emission values were decreased with higher blends of JME. The NO_x emissions decreased with an increase in the percentage of EGR, but a reverse trend was observed with the smoke emissions.	K. Venkateswarlu, 2012 [83]	Front. Energy, vol. 6, pp. 304–310
16.	10, 20 and 30	5.2 kW, single cylinder, four stroke, water cooled, diesel engine, constant speed 1500 rpm Compression ratio 16,18)	The 20% blend of JME with diesel showed a higher brake thermal efficiency at both compression ratios.	S. Abinav Viswanath, 2012 [84]	International Journal of Engineering Science and Technology, vol. 4, pp. 3457-3471.
17.	5,10,20,40,60, 80 and 100	3.5 kW, single cylinder, four stroke, water cooled, diesel engine, constant speed 1500 rpm (Variable compression ratio and variable injection pressure)	The increase in the brake thermal efficiency was in the range from 6.76% to 7.40% for different biodiesel blends. A low smoke opacity was observed with a higher compression ratio due to better combustion. The maximum reduction in smoke opacity was 22% at a compression ratio of 19.5. The CO and HC emissions were decreased by about 7 to 10% with CR 19.5 in comparison with CR 17.5 at all biodiesel blend ratios. The smoke opacity was noticed to be lower with increased blends at higher injection pressures of 180, 200 and 220 bar; a reduction in the smoke opacity of 10 to 15% was observed through the load regions compared to that of diesel and 100% JME. Higher NO emissions by about 1.4% were observed at 220 bar in comparison with 180 bar injection pressure.	Amar Pandhare, 2013 [85]	Journal of Renewable Energy, vol. 2013

Table 2.3 Performance, combustion and emission results of JME and its blends with different fuel modifications

Sl.No	JME (%)	Engine tested	Test results compared with diesel	Authors/Reference	Journal/Proceedings name/volume/page
1.	100 (Preheating)	3.72 kW, single cylinder, water cooled, four stroke diesel engine, constant speed 1500 rpm	It was observed that the brake thermal efficiency increased and BSEC decreased with preheating the JME. Shorter ignition delay, lower heat release rate, higher EGT and lower NO_x emissions were observed. Lower HC, CO and smoke emissions were found.	P. V. Rao, 2011 [86]	World Academy of Science, Engineering and Technology, vol.75, pp.855-868.
2.	25, 50, 75 and 100 (Multi-DM32)	3.68 kW, single cylinder, four stroke, water cooled diesel engine, constant speed 1500 rpm	Higher thermal efficiency, higher exhaust gas temperature, and lower smoke, CO and CO_2 emissions were reported in this work.	Y.V.H.Rao, 2009 [87]	Indian Journal of Science and Technology, vol. 2, pp. 25-31.
3.	JME+ cerium oxide nano particles of 20,40 and 80 ppm.	5.5 kW, naturally aspirated, four stroke, single cylinder, water cooled diesel engine, constant speed 1500 rpm	Engine tests were conducted with the modified biodiesel at different dosing levels (20–80 ppm) of the cerium oxide additive which showed an improvement in the efficiency of the engine. Also, it was reported that the emission levels of hydrocarbon and NO_x were reduced with the addition of cerium oxide nanoparticles.	V. Sajith, 2010 [88]	Advances in Mechanical Engineering, vol. 2010
4.	83% JME, 15% water, and 2% of surfactants (Span80 and Tween80) (alumina nano particles 25, 50, and 100 ppm)	4.4 kW, single cylinder four stroke, air-cooled, direct injection diesel engine, constant speed 1500 rpm	The addition of potential nanoparticles to the biodiesel emulsion resulted in reduced peak pressure, heat release rate, and ignition delay compared to that of neat biodiesel emulsion operation. Higher brake thermal efficiency was achieved at 100 ppm with the addition of Alumina nano particles. NO emission was reported to be lower by about 32% and the smoke emissions were reported to be lower by about 26%.	J. Sadhik Basha, 2011 [89]	Journal of Renewable Sustainable Energy, vol. 3, pp. 1-17.

5.	B20 + DEE 5, 10 and 15 B20 + Ethanol 6 and 10	3.68 kW, single cylinder, direct injection four-stroke, water cooled, diesel engine, constant speed 1500 rpm. (Optimization of injection pressure and nozzle hole size)	With a smaller nozzle hole and high injection pressure of 210 bar, a lower BSFC was obtained. Lower BSFC, HC, CO_2 and smoke emissions were observed with 5% DEE addition. With 15% DEE lower NO emissions were observed.	U.Varaprasad, 2011 [90]	Thermal Science, vol. 15, pp. 1175-1184.
6.	100 + Antioxidant additives (L-ascorbic acid (Vitamin C), a tocopherol acetate (Vitamin E), butylated hydroxytoluene (BHT), p-phenylenediamine (PPDA) and ethylenediamine (EDA))	4.4 kW, single cylinder, four stroke, water cooled, DI diesel engine, constant speed 1500 rpm.	Antioxidant addition reduces the NO_x emissions in the exhaust. Among all the tested antioxidants p-phenylenediamine showed the best emission performance compared to biodiesel.	K.Varadharajan, 2011 [91]	Fuel, vol. 90, pp. 2721–2725.
7.	100 % JME+ Cobalt oxide and Magnalium nano particles	4.4 kW, single cylinder, air cooled, direct injection, diesel engine, constant speed 1500 rpm	It was reported that the addition of nano particles resulted in an increased thermal efficiency of JME compared to that without additives. Cobalt oxide showed about 75% reduction in HC at 75% load, and with magnalium, there was a reduction in HC emission of around 70% at 50% load. There was about, 47% reduction in the NO_x emission with cobalt oxide Nano-fuel additive and with Cobalt oxide there was a 50% reduction in the CO emission at 75% load.	D. Ganesh, 2011 [92]	International Conference on Electrical and Control Engineering, China, pp.3453 – 3459.

8.	Ethanol:Diesel:JME of 5:95:0, 5:75:20, 5:55:40, 5:35:60, 5:15:80 and 5:0:95 for the blends of ethanol, commercial diesel and JME	5.9 kW, four stroke, single cylinder, DI diesel engine, constant speed 1500 rpm	Brake thermal efficiency was reported to be higher in the case of diesel-ethanol-JME blend compared to ethanol-diesel and ethanol-JME, while, the BTE of the ethanol-JME blend was found to be lower, compared to that of diesel. Blend of ethanol-diesel-JME compared with blends of ethanol-JME shows slightly extended heat release and enhanced combustion. The CO, HC and smoke emissions from all blends decreased at high load conditions and increased at low load conditions. The NO emissions were reported to be higher at full load condition.	D.Kannan,2012 [93]	Energy Conversion and Management, vol. 53, pp. 322-331.
9.	JME + PY (Antioxidant)	2.6 kW, Kirloskar, single cylinder, vertical, four stroke, high speed diesel engine, constant speed 1500 rpm	The BSFC of JME with and without antioxidants were observed to be more than that of diesel. The BSFC of JME with antioxidants is lesser than that of JME without antioxidants.	S. Jain, 2013 [94]	Fuel, vol.106, pp. 152–156
10.	JME80+Ethanol 20, JME80+ Acetone 20	3.5 kW, single cylinder, four stroke, water cooled diesel engine, constant speed 1500 rpm	Early pressure rise was observed in the case of B100, BD80E20 and BD80AC20 as compared to diesel. The rate of pressure rise for the ethanol and the acetone blends was intermediate between B100 and diesel. Early heat release was observed with B100 and its ethanol and acetone blends. It was observed that the ignition delay for B100, BD80E20 and BD80AC20 was lesser than that of diesel. The ignition delay for B100 was the lowest of all.	T.K. Gogoi, 2013 [95]	International Journal of Emerging Technology and Advanced Engineering, vol. 3, 2013, pp. 51-57

Table 2.4 Reasons for higher NO_x emission from biodiesel fueled engines

Characteristics of biodiesel	Causes for higher NO_x emission	Authors/Reference	Journal/Proceedings Name/volume/page
High isentropic bulk modulus and density	i) Artificial advance of injection timing ii) Less compressible than diesel iii)Increased injection pressures iv) High spray tip penetration v) Decreased spray cone angle and advanced start of injection	Moneyem et al, 2001 Tat and Van Garpen, 2007. Choi and Reitz, 1997 Yuan and Hansen, 2002 [97-100]	Biomass and Bioenergy, vol.20, pp. 317-325. Fuel, vol.85, pp.1004-9. National Biodiesel Board report, 1997. ASAE;50(4):1123-8 ASAE Paper No. 026083
High adiabatic flame temperature	i) Higher heat release rate ii) Stoichiometric burning	Benajes et al, 2008. Muller et al, 2009. Ban-Weiss et al, 2007. [101-103]	Fuel, vol. 87, pp.1849-58. SAE International Journal of Fuels and Lubricants, vol. 2. 2009-01-1792. Fuel Processing Technology, 88, pp. 659-667.
More wide-spread high temperature distribution areas than diesel	i) Higher heat release rates	Yuan et al, 2005 [104]	ASAE, vol.48, pp.933-39.
Increased premixed combustion	It was reported that the higher premixed combustion is due to higher cetane number of biofuel which initiates the combustion early.	Edwin Geo et al, 2012. [105]	Applied Energy, 94, pp. 224–231.
Increased sauter mean diameter	i) Reduced premixed combustion ii) Increased diffusion combustion and NO_x	Allen and Watts, 2000 [106]	ASAE , vol.43, pp.207-11.
Shorter ignition delay	i) Reduced premixed combustion ii) Increased diffusion combustion and NO_x	Canacki, 2007 Tat et al.2007 [107-108]	Bioresource Technology, vol.98, pp.1167-75. ASAE , vol.50, pp.1123-8
Lower vapour pressure	i) Slower evaporation rate ii) Longer ignition delay	Ra et al, 2008 [109]	SAE Transactions-Journal of Fuels and Lubricants, vol. 117, 2008-2101-1379.
Unsaturated fatty acids	i) CH radicals formation followed by acetylene formation	Garner et al, 2009 [110]	Proceedings of the Combustion Institute, vol.32, pp.461-7

High iodine number	i) More degree of unsaturation of the fatty acid	Mccormick, 2001 [111]	Environmental Science and Technology, vol. 35, pp.1742-7.
Low cetane number	i) Longer ignition delay and higher heat release rate	Lapuerta, 2008 McCormick, 2002 [112-113]	Progress in Energy and Combustion Science vol. 34, pp.198-223. SAE 2002-01-1658
High cetane number	i) Shorter ignition delay ii) Low average combustion temperature iii)Decreased residence time leads to low NO_x iv)Higher peak pressure and temperature leads to high NO_x	Wang et al, 2000. [114]	Environmental Science & Technolology 34, 933-939
Fuel bound oxygen	i) Increases combustion efficiency ii)High reaction temperature	Graboski et al, 1998 Song et al, 2004 [115-116]	Progress in Energy and Combustion Science, vol. 24, pp. 125-164, Energy Fuel, 18, pp. 1282–90
High oxygen content	i) Exhibits low compressibility ii) Increase in boiling point iii) Reduces the droplet evaporation iv) Lesser soot v) Low radiation heat transfer	Muller et al, 2003. Ullman et al,1994 Bittle et al.2009 [117-119]	SAE Transactions - Journal of Fuels and Lubricants, vol. 112. 2003-01-1791. SAE Transactions-Journal of Fuels and Lubricants, vol.103, 941020. SAE 2009-01-2782;
High viscosity	i) Increase in fuel line pressure ii) Advance of injection iii) Increased mass of fuel during spray iv) Poor atomization v) Smaller spray cone angles vi) High penetration vii)Larger droplet size	Tat, 2003 Usta eta al Deshmukh et al, 2012. Yuan and Hansen, 2005 Anderson and Olsen [120-124]	PhD Dissertation. Iowa State University. Fuel, vol. 97, pp. 879–883 ASAE, vol.48, pp.933-9
Fuel density	i) Advanced fuel injection timing ii) Higher fuel injection pressure iii) shorter fuel spray penetration iv) shorter fuel spray angle v) Longer ignition delay	Sun et al, 2010. [125]	Progress in Energy and Combustion Science, vol.36, pp. 677-695.
Surface tension	i) High surface tension ii) Larger droplet size	Ahmed et al., 2006. [126]	SAE Paper No. 2006-01-0893

2.4 Biomass pyrolysis

Pyrolysis is a method, by which biomass or any organic substance can be converted into pyrolysis oil, pyrogas and char by the thermal decomposition in the absence of oxygen, or in the presence of very little oxygen [14]. There are two main pyrolytic techniques, namely, slow and fast. Slow pyrolysis has been used for many years for charcoal production, but can also be carried out using modern reactors. Slow pyrolysis is characterized by slow heating rates and relatively long residence times with lower reaction temperature, whereas; the fast pyrolysis process is characterized by high heating rates and short residence times. Other methods include intermediate and flash pyrolysis, of which intermediate pyrolysis deals with controlled heating rates, thus avoiding tar formation. Flash pyrolysis occurs with very fast heating rates and shorter solid residence times, than with the fast pyrolysis process. Different types of reactors have been used for pyrolysis that include the bubbling fluidized bed, circulating fluidized bed, rotating cone, ablative reactor, vacuum pyrolysis reactor, entrained flow reactor, wire mesh reactor, and auger (screw) reactor [127]. The pyrolysis oil obtained from biomass sources has great attraction, but is not used in the proper way. Many attempts have been made in the recent past, to extract fuel called as bio oil or bio-crude oil from the pyrolysis of various biomass sources, like saw dust, waste wood, rice husk, cotton stalk, sugar cane bagasse and olive bagasse, and from the nut shells of jatropha and palm kernel shell, etc [128-135]. Bio oils are mixtures of multi-components of different sized molecules derived from the depolymerization and fragmentation of cellulose, hemi cellulose and lignin [136]. Chir pine (Pinus roxburghii) is widely planted for timber applications, being one of the most important trees in forestry in northern Pakistan, India and Nepal. This pine wood finds application in making packing container boxes.

2.4.1 Wood pyrolysis oil (WPO)

Pyrolysis liquid obtained from biomass sources is referred to in the literature by terms, such as pyrolysis oil, bio oil, bio-crude oil, bio-fuel oil, wood liquid, wood oil, liquid smoke, wood distillates, pyroligneous tar, and pyroligneous acid. The bio oil can be used as a fuel in boilers, diesel engines or gas turbines for heat and electricity generation [137]. The WPO obtained from the pyrolysis of wood, is a free flowing dark-brown organic liquid accompanied by a strong acid smell. The oil comprises of different sized molecules, which are derived from the depolymerization and fragmentation reaction of three biomass building blocks: cellulose, hemicellulose and lignin [138]. It has a high oxygen content and moisture

content, but poor volatility, high viscosity, corrosiveness and cold flow properties, which limit its use as additives in transportation fuel, rather than being used as transportation fuel by itself. The WPO cannot be made to mix directly with diesel due to poor miscibility, different surface tension and hydroscopic characteristics [139].

Water content is commonly seen in the bio oil obtained from any biomass feedstock. The mass fraction of water content in the bio oil lies between 10-35% in most of the cases. This fraction depends on the original moisture content of biomass and also on the pyrolysis conditions. The water content of bio oil is usually measured by the Karl-Fischer titration method. The bio oil becomes unstable, if more than a certain amount of water is added to it; the microstructure of the bio oil will be destroyed, and it will separate into water soluble and oily phases [140]. There are both positive and negative effects of water when considering bio oil combustion. In one way, the water content in the bio oil decreases the combustion reaction rates, adiabatic flame temperature, but increases the ignition delay and heat of evaporation [141]. On the other hand, water can enhance the atomization process by decreasing viscosity and increasing the chance of effective micro-explosions of the fuel droplets. Also, it can reduce the NO_x emissions by decreasing the flame temperatures and accelerate soot oxidation by providing OH radicals [140-142].

Engine experiments were conducted by Yrjo Solantausta et al. [143] with different fuels, such as diesel, ethanol and pyrolysis oil with a certain proportion of an ignition improver addition, by volume to pyrolysis oil and ethanol. Injector nozzle coking and clogging of the bore for the cylinder pressure transducer were observed from the results. Frigo et al. [144] conducted a series of tests like the thermo gravimetric analysis (TGA), single drop reactor tests, corrosion tests, spray analysis, and engine tests to check the feasibility of using wood flash-pyrolysis oil in diesel engines. Problems such as the buildup of carbonaceous deposits, injection system fault and engine seizing were noticed, when WPO was fueled in a diesel engine.

The application of an emulsification technique is considered to be one of the possible approaches to reduce diesel engine pollutants, as well as the rate of fuel consumption. The emulsification of biomass derived bio oil in diesel has been carried out, to avoid the problem of miscibility and stability of bio oil and diesel [145]. Stable emulsions are prepared, using two surfactants, namely, hypermer and CANMET. The reduction in the viscosity and corrosivity of the emulsion has been reported in this work. It was also reported that the

emulsified bio oil showed a better friction reduction performances than that of commercial diesel under selected frictional conditions [145]. Two different fuels like Diethylene glycol dimethyl ether (Diglyme) and the WPO blends in different percentages, and two different emulsions with 30% of WPO in diesel were tested in a Ruggerini RP170 model, diesel engine. Lower NO emissions are reported with increasing percentage of WPO, and lower HC emissions are found up to 30% WPO, but beyond that, the HC emissions increased significantly. The CO emissions are found to be more, due to the poor self-ignition characteristics of the WPO [146]. Two emulsions prepared with 10% and 20% bio-oil, obtained from corn stalk by mass fraction in No. 0 diesel, using an ultrasonic emulsification method, were tested in a direct injection diesel engine. It is reported that the two emulsions display longer ignition delays, exhibit higher peak values of the premixed burning rate and pressure rise rate, lower peak values of the in-cylinder pressure and combustion temperature and have a shorter combustion duration compared to that of No. 0 diesel [147].

Upgrading the bio oil through emulsification with biodiesel explores the possibility of replacing petroleum based fuels completely. A method of emulsifying bio oil with biodiesel has been investigated, using an Octanol surfactant, and an attempt has been made to study the various effects on the mixture stability [148]. It is reported that the process of emulsifying a bio oil with biodiesel is a novel method to extract some of the best fuel fractions present in the bio oil, for use as an additive in transportation fuel. Various properties of the emulsion have shown more desirable values in the acid number, viscosity, and water content compared to the original bio oil. The impact of bio oils on the oxidation stability and cold flow properties of biodiesel containing bio oil fractions is carried out, using Differential Scanning Calorimetric techniques [149]. It is reported that the bio oil can be considered as a good source of anti-oxidants to enhance the biodiesel oxidation stability.

The biodiesel emulsion fuel prepared by the emulsification technique, comprising of 83% of Jatropha biodiesel, 15% of water, and 2% of mixed surfactant, comprising Span 80 and Tween 80 in equal percentages, with the aid of a mechanical agitator, was tested in a single cylinder DI diesel engine. The experimental results revealed that there is a substantial enhancement in the performance and a reduction in the harmful emissions for the biodiesel emulsion fuels, compared to those of biodiesel [150]. Kannan et al. [151] performed experiments on a single cylinder, direct injection, diesel engine using diesel, biodiesel and biodiesel-diesel-ethanol (diestrol) water micro emulsion fuels, to investigate the performance,

emission and combustion characteristics of the engine under different load conditions. The results indicated that the biodiesel and micro emulsion fuels showed a higher brake specific fuel consumption throughout the engine operation. The carbon monoxide, unburnt hydrocarbon, nitric oxide, and smoke emissions were found to be lower than those of diesel in all load conditions. Chen et al. [152] demonstrated that the emulsified bio-solution/palm-biodiesel/diesel blends have the advantage of saving energy and reducing emissions of both polycyclic aromatic hydrocarbons (PAHs) and particulate matter (PM) from diesel engines. Alcala, and Bridgwater [153] prepared homogeneous blends of bio oil and biodiesel in the presence of alcohol, that are extremely stable over time, particularly in comparison with bio oil. The feedstock used for bio oil was pine wood.

2.5 Summary

It is understood that many research works were carried out using JME and its blends by adopting fuel and engine modifications. Most of them reported that higher NO emission in diesel engines, when the JME and its diesel blends were used as fuels. Also, it is understood from the literatures that the use of WPO is limited in its sole form. Problems like poor miscibility with diesel, along with durability related issues are reported in many works. From the literature review, it is observed that no research work was carried out on the utilization of WPO emulsified with the JME in diesel engines, to study the NO_x reduction. Hence, it is proposed to use the WPO with the JME, as an alternative fuel in the form of an emulsion in a DI diesel engine.

CHAPTER 3

MATERIALS AND METHODS

3.1 General

In this research work, two principal biofuels, namely, Jatropha methyl ester (JME) and, Wood pyrolysis oil (WPO) - a bio oil are considered for the preparation of emulsions. The production methods of these two oils are described with the necessary schematic diagrams and photographs shown in this chapter. The production of emulsions from different surfactants, and their characterization are also described in this chapter with the necessary illustrations.

3.2 Production of JME

Vegetable oil is considered as one of the best feedstocks obtained from biomass sources. It can be used in combustion devices after proper treatment. The use of vegetable oils in IC engines particularly in CI engines is not a new, because Rudolph Diesel used peanut oil to demonstrate his patented diesel engine. But, the uses of vegetable oil in CI engines are prone to cause problems such as injector coking, piston wear etc. This is because of the higher viscosity and poor volatility of vegetable oils. The viscosity of vegetable oils can be reduced by blending, preheating transesterification, and thermal or chemical cracking. Transesterification is the best method to reduce the viscosity of vegetable oil. Biodiesel is commonly referred to as methyl or ethyl or butyl esters of vegetable oil or animal fat or algae. Vegetable oil of the edible or non-edible type is used for the production of biodiesel. Jatropha oil, a non-edible oil is considered as a potential feedstock for the production of biodiesel in India. Hence, it was chosen as a feedstock for the production of biodiesel in this study. Methanol is more reactive, because it contains short chain hydrocarbons, and is easily available in the market, and hence it is also considered for the biodiesel production. The JME used in this investigation was obtained from the transesterification of Jatropha oil. The fatty acid composition of Jatropha oil is given in Table 3.1. In the transesterification of vegetable oils, a triglyceride reacts with an alcohol in the presence of a strong acid or base, producing a mixture of fatty acid alkyl esters and glycerol. The block diagram of the production of JME from Jatropha oil is presented in Fig. 3.1.

Table 3.1 Fatty acid composition of Jatropha oil [38]

Fatty acid	Structure	Formula	Composition (% wt)
Palmitic	16:0	$C_{16}H_{32}O_2$	14.1–15.3
Stearic	18:0	$C_{18}H_{36}O_2$	3.7–9.8
Oleic	18:1	$C_{18}H_{34}O_2$	34.3–45.8
Linoleic	18:2	$C_{18}H_{32}O_2$	29–44.2

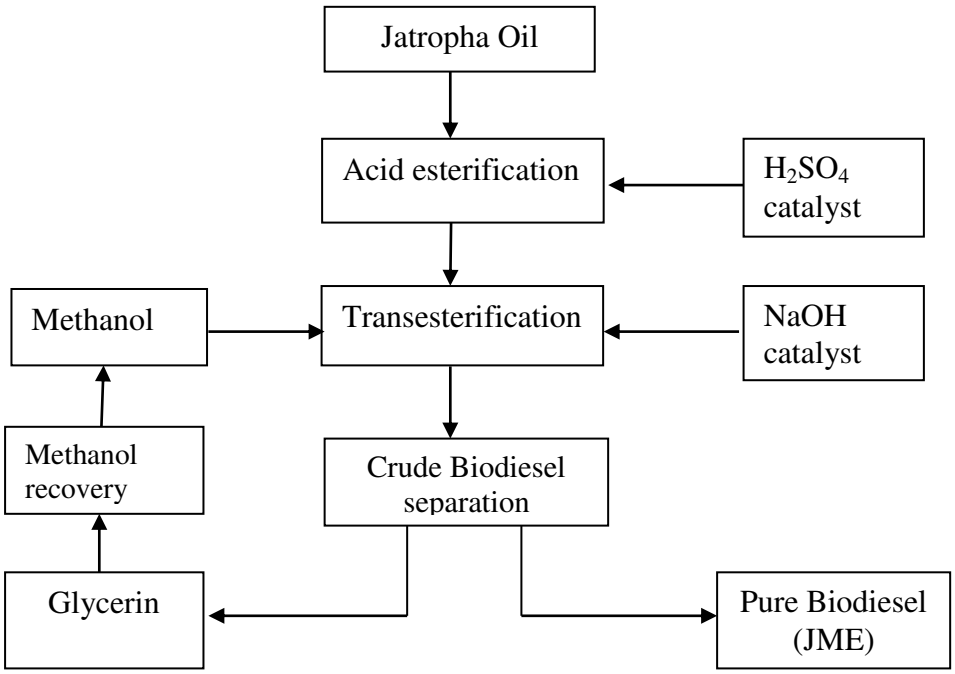

Fig. 3.1 Block diagram of JME production from Jatropha oil

Initially, sodium hydroxide (NaOH) as a catalyst of about 3-4 grams was dissolved in 100 ml of methanol to prepare methoxide, which was required to activate the methanol. Vigorous stirring was done for about 15-20 min in a closed container, until the alkali was dissolved completely. Further, this mixture was transferred to the reactor containing moisture-free Jatropha oil. A continuous stirring of the resulting mixture at temperatures between 60-65°C was carried out for one hour. A mixture comprising a certain quantity of methyl ester, glycerol and methanol was obtained after cooling the mixture for about 24 hours. Then, the mixture was taken out and poured into the separating funnel to separate the glycerol and

methyl ester of Jatropha oil. Water washing was done finally, in order to remove the moisture and impurities from the JME. The photograph of the JME is shown in Fig.3.2.

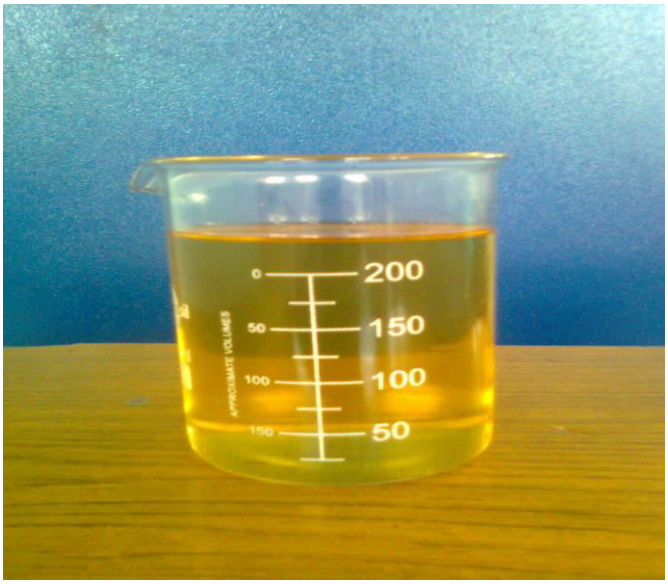

Fig. 3.2 Photograph of JME

3.3 Analysis of raw material for WPO

3.3.1 Ultimate and proximate analysis of pine wood

WPO was obtained from the pyrolysis of waste pine wood obtained from packing boxes. Before extracting pyrolysis oil from pine wood, the proximate and ultimate analyses were performed, to ensure whether it is possible to derive oil out of it.

3.3.1.1 Proximate analysis

The basic method for the proximate analysis is given by the ASTM D3172 standard. It determines the mass percentages of the fixed carbon, volatile matter, moisture, and ash. Fixed carbon is the elemental carbon that exists in the wood. In the proximate analysis, its determination is approximated by assuming it to be the difference between the original sample and the sum of the volatile matter, moisture, and ash. The volatile matter is that portion of wood, other than water vapor, which is driven off when the sample is heated in the absence of oxygen in a standard test (up to 1750°F or 7 min). It consists of hydrocarbon and other gases that result from distillation and decomposition. The moisture is determined by the standard procedure of drying in an oven. This does not account for all the water present, which includes the combined water and the water of hydration. Ash is determined in practice

as the noncombustible residue after the combustion of dried wood in a standard test (at 1380°F).

3.3.1.2 Ultimate analysis

An ultimate analysis is done for the pine wood by the ASTM D 3176 method. The ultimate analysis gives the mass percentages of the chemical elements that constitute the wood. These include carbon, hydrogen, nitrogen, oxygen, and sulfur. The ultimate analysis of pine wood shows that, the pine wood contains about 50% carbon, 5.4% hydrogen, and 44% oxygen on a moisture and ash free basis. The sulfur and nitrogen content of wood is usually less than 0.1%. The proximate analysis of wood shows about 77% volatile matter and 11% fixed carbon. The ultimate and proximate analysis of pine wood are given in Table 3.2.

Table 3.2 Ultimate and proximate analysis of pine wood

Proximate analysis	**wt (%)**	**Ultimate analysis**	**wt (%)**
Water content	3	C	50.15
Volatile matter	77	H	5.41
Fixed carbon	11	N	0.06
Ash content	9	O	44.37

3.3.2 Thermo Gravimetric Analysis (TGA)

Initially, the raw wooden chip was characterized by Thermo gravimetric analysis (TGA) apparatus. The schematic diagram of the experimental TGA apparatus is shown in Fig. 3.3.

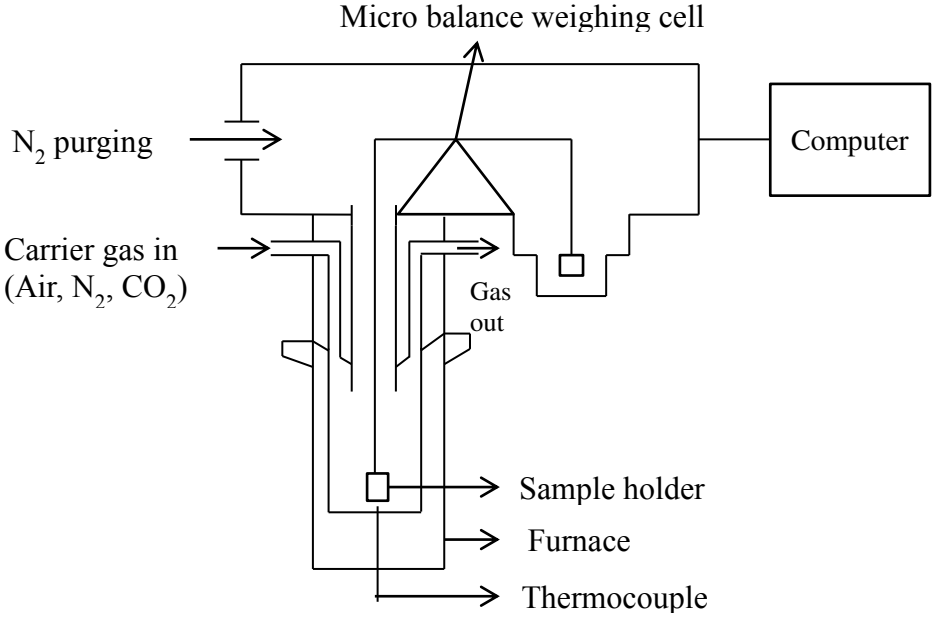

Fig. 3.3 Schematic diagram of the experimental TGA apparatus

The TGA is generally used to determine a material's thermal stability and its fraction of volatile compounds, by monitoring the weight loss that occurs when the specimen is heated. All the experiments with TGA comprise of three main different phases: drying, de-volatilization in an inert atmosphere, and combustion in oxygen [154]. The measurement is normally carried out in air or in an inert atmosphere, such as helium or argon, and the weight is recorded as a function of increasing temperature. In nitrogen, the moisture and volatiles are lost at temperatures up to 900^{o}C, and fixed carbon is burnt in oxygen leaving ash as a residue. The TGA curve of pine wood is depicted in Fig. 3.4.

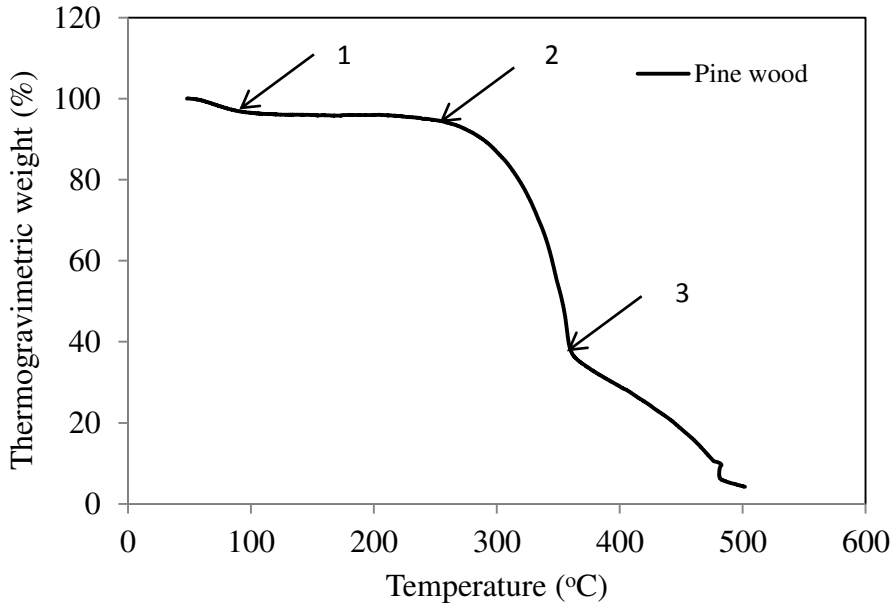

Fig. 3.4 TGA curve of pine wood

The TGA analysis of the pine wood sample was done by using a model SHIMADZU TGA-60H, with nitrogen as a carrier gas at a constant flow rate of 45 ml/min. A sample of 25 mg was heated in a furnace from an initial temperature of 30^{o}C to 600^{o}C, at a heating rate of 25^{o}C/min for a residence time of 5 min. The thermal degradation of the sample showed three weight loss regions. The first weight loss occurred at the temperature range of 70 to 120^{o}C, where the moisture content in the wood was removed. The second weight loss occurred at the temperature range of 120 to 260^{o}C, where the volatilization of hemicelluloses and residual oil occurred. A major weight loss occurred from 260 to 500^{o}C with the deflection point at 350^{o}C, where the maximum rate of weight loss occurred which may be due to the degradation of cellulose and lignin.

3.4 Production of the WPO

Pyrolysis is the breakdown of organic matter into value added products in the absence of oxygen or very little presence of oxygen. The schematic diagram of the pyrolysis process for deriving the WPO is shown in Fig. 3.5.

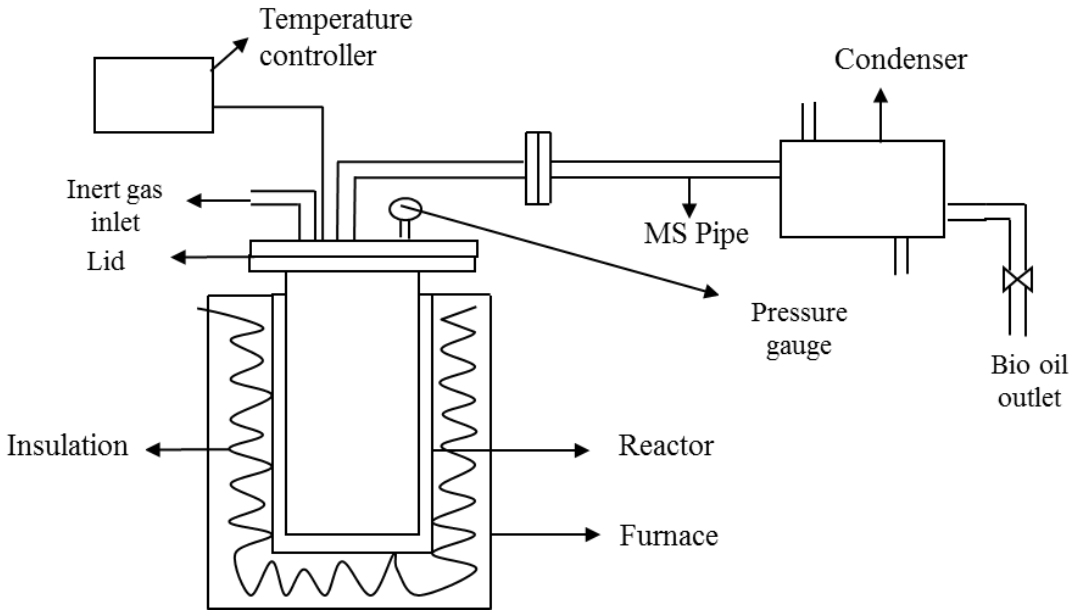

Fig. 3.5 Schematic diagram of pyrolysis setup

In the pyrolysis process, wooden chips obtained from pine wood feed stock were fed into an externally heated mild steel reactor unit. The fed chips were heated in the reactor unit in the absence of oxygen. The temperature of the reactor was maintained with the help of a highly sensitive temperature controller. The temperature was measured by a Cr-Al: K-type thermocouple fixed outside the reactor. Fig. 3.6 shows the sample of wood chips considered for the pyrolysis process. During pyrolysis, the reactions were carried out at different temperature ranges to find the optimum yield temperature, by taking 750 g of the sample in the reactor. The heating rate, at which the pyrolysis process was carried out, was 10^{o}C per minute. The temperature, at which the maximum yield of pyrolytic oil obtained, was in the range of 400^{o}C and 450^{o}C. The volatile matter that evolved in the form of vapour was condensed in a water cooled condenser. Three principal products such as WPO, pyrogas and char were obtained in the process. The optimum yield of the WPO obtained was about 65% and the cost for producing one litre of WPO was (Indian) Rupees 27. The photographic view of the pyrolysis setup used in this study is shown in Fig. 3.7.

Fig. 3.6 Photographic view of the reactor with feed material

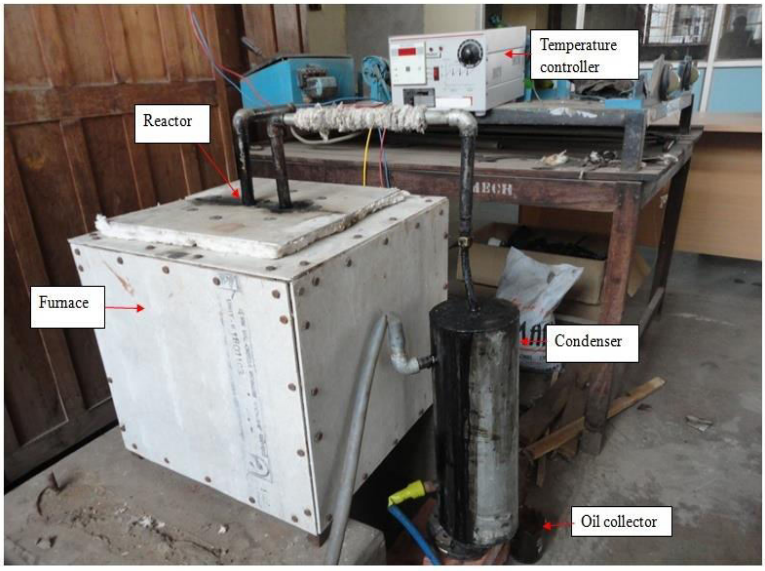

Fig. 3.7 Photographic view of pyrolysis setup

Fig.3.8 and 3.9 show the photographic views of WPO and char respectively.

Fig. 3.8 Photographic view of the WPO

Fig. 3.9 Photographic view of the char

The optimum yield of WPO obtained was calculated as follows:

Individual weight of the pine wood chips = 750 ± 10 g

Weight of the liquid product = 485 ±10 g

Weight of the char = 200 ±10 g

Wood pyrolysis oil yield = 485/750 = 65 ±1.3 % by weight.

Pyrolysis char yield = 200/750 = 26 ±1.3 % by weight.

3.5 Analysis of Wood pyrolysis oil

3.5.1 FTIR analysis of WPO

The functional groups present in the WPO were determined with the help of the Fourier Transform Infrared spectroscopy (FTIR) analysis. On the interaction of an infrared light with oil, a chemical bond will stretch, contract, and absorb infrared radiation in a specific wave length range, regardless of the structure of the rest of the molecules. Fig.3.10 illustrates the working principle of a FTIR spectrometer. A common FTIR spectrometer consists of a source, interferometer, sample compartment, detector, amplifier, A/D convertor, and a computer. The source generates radiation, which passes the sample through the interferometer and reaches the detector. Then the signal is amplified and converted to a digital signal by the amplifier and analog-to-digital converter, respectively.

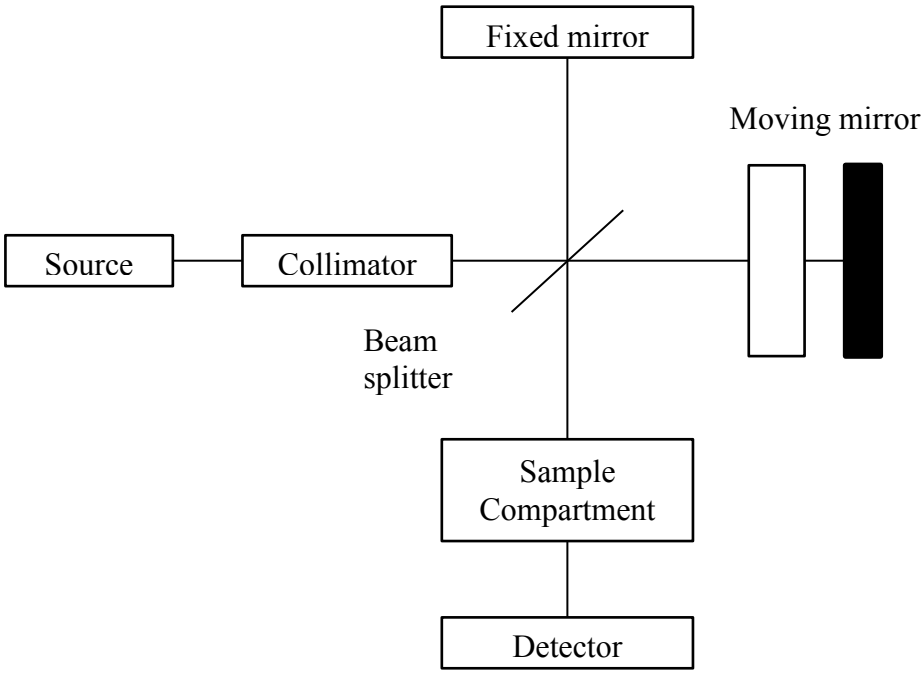

Fig.3.10 Block diagram of an FTIR spectrometer

Based on this principle, the functional groups present in the WPO were identified by using the Perkin Elmer RX. The FTIR spectra were collected in the range of 400-4000 cm^{-1} region with 8 cm^{-1} resolution. The results of the FTIR analysis are in the form of a graph plotted between the wave number and the percentage transmittance, which will give the information about the position of various bond vibrations distinguished by several modes, such as stretching, distortion, bending etc. The graphical result obtained for the WPO is shown in Fig. 3.11.

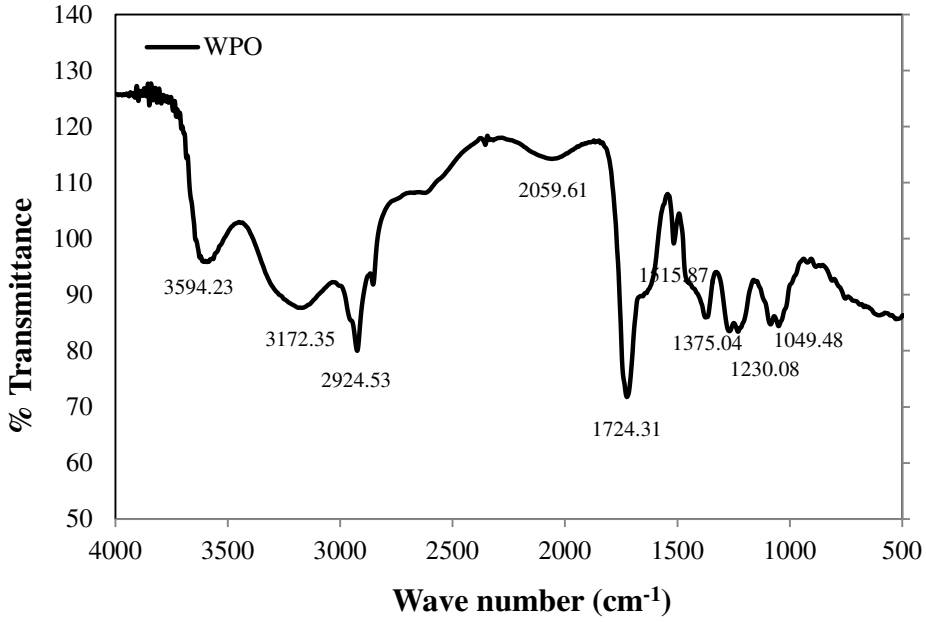

Fig. 3.11 FTIR graph of WPO

The various bonds present in the WPO are given in Table 3.3. From the FTIR graph, it can be observed that the wood derived pyrolysis oil has a few strong bonds of carbon that may result in a high carbon deposit on the piston, combustion chamber etc, when it is used in a CI engine. The stretching vibrations exist in the functional groups leading to an increase or decrease in bond length.

Table 3.3 Various bonds presents in the WPO

Wave number	Wave length	Functional groups	Bond
1049.48	7.7-11.1	Amines, acids, esters, ether and alcohols, Phospates, Silicates	C-F, C-C, C-O, C-N,
1230.08	7.4-10	Alcohols and phenols, acids, esters, ether	C-F, C-N,C-O, C-C, O-H
1375.04	6.9-8.3	Nitrates, alcohols and phenols, alkanes	O-H, C-H, Bend in plane
1515.87	6.1-6.7	Amines	N-H, Stretch
1724.31	5.4-6.1	Acids, esters, ether and alcohols	C=O, Stretch
2059.61	4.2-4.8	Alkenes/aromatics, nitriles	C≡C, C≡N, Stretch
2924.53	3.0-3.7	Alkanes	C-H, Bend in plane
3172.35	2.7-3.3	Amines, alkanes, alcohols and phenols	C-H,O-H,N-H, Bend in plane
3594.23	2.8-3.0	Alcohols, alkanes and phenols, amines	O-H,N-H, C=O, Stretch, Bend

3.5.2 GC-MS analysis of WPO

The Gas Chromatography and Mass Spectrometry (GC-MS) is a method that combines the features of gas-liquid chromatography and the mass spectrometry, to identify different substances present in the WPO. The GC-MS analysis is used both for the qualitative identification and for the quantitative measurement of the volatile and semi volatile organic compounds in complex mixtures. The working principle of the GC-MS instrument is illustrated in Fig. 3.12.

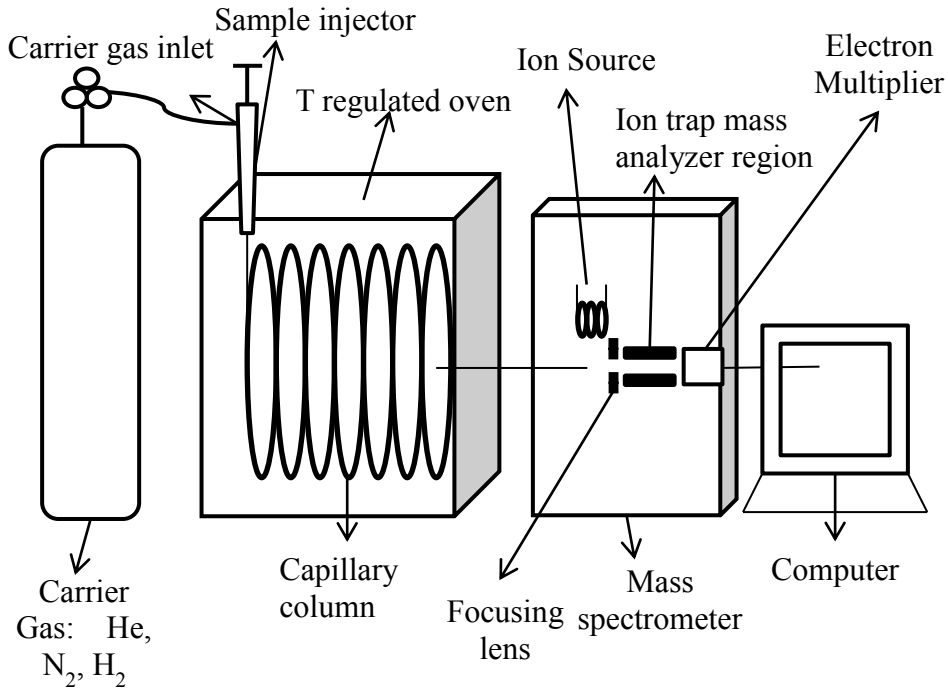

Fig. 3.12 Working principle of GC-MS analyzer

A capillary column coated with a 0.25 µm film of DB-5 with a length of 30 m and diameter 0.25 mm was used. The GC was equipped with a split injector at 200^{o}C with a split ratio of 1:10. The helium gas of 99.995% purity was used as the carrier gas at a flow rate of 1.51 ml/min. The oven's initial temperature was set at 70^{o}C for 2 min and then increased to 300^{o}C at a rate of 10^{o}C/min and maintained for 7 min. All the compounds were identified by means of the software developed by the National Institute of Standards (NIST-USA) library. The mass spectrometer was operated at an interface temperature of 240^{o}C, with an ion source temperature of 200^{o}C in the range of 40-1000 m/z. The WPO obtained was characterized by using GC/MS-QP 2010 SHIMADZU, equipped with flame ionization and mass spectrometry detection (GC-FID-MS). The GC-MS chromatogram of WPO is shown in Fig. 3.13.

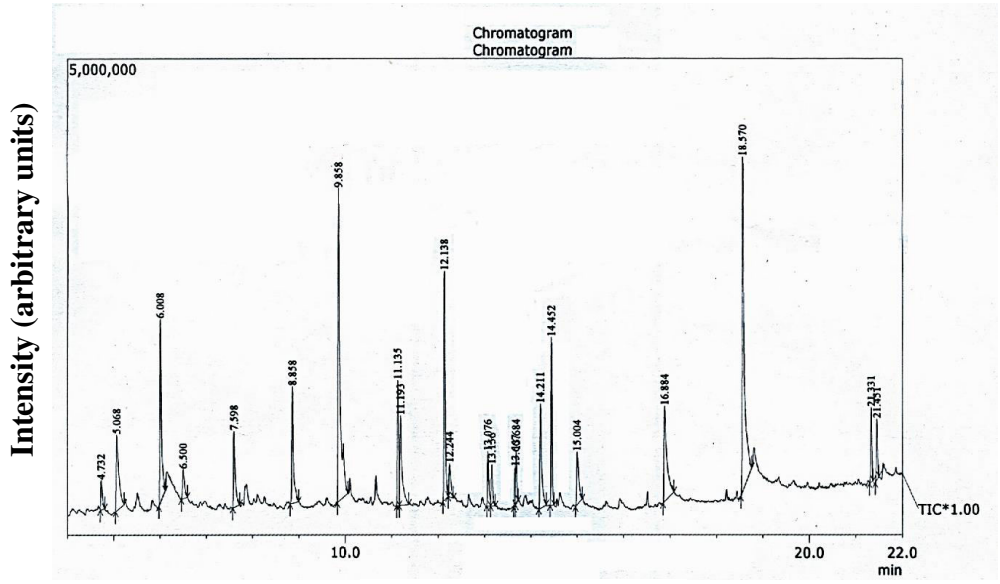

Fig. 3.13 Gas chromatogram of wood pyrolysis oil

The GC-MS report of the WPO is noted in the following Table 3.4.

Table 3.4 Main components obtained from GC-MS analysis

Reaction time	Area %	Compound Name	Molecular formula
4.732	1.20	Tetrahydro-2-furanmethanol	$C_5H_{10}O_2$
5.068	4.86	3-Methlcyclopentane-1,2-dione	$C_6H_8O_2$
6.008	7.24	0-Methoxyphenol	$C_7H_8O_2$
7.598	3.17	1-hydroxy-2-methoxy-4-methylbenzene	$C_8H_{10}O_2$
8.858	4.63	1-hydroxy-2-methoxy-4-ethylbenzene	$C_9H_{12}O_2$
9.858	15.29	1,3-Dimethoxy-2-hydroxybenzene	$C_8H_{10}O_3$
11.135	3.98	1,2,4-Trimethoxybenzene	$C_9H_{12}O_3$
11.193	4.58	(E)-Isoeugenol	$C_{10}H_{12}O_2$
12.138	7.34	1,2,3-Trimethoxy-5-methylbenzene	$C_{10}H_{14}O_3$
12.244	1.50	2-Propanone, 1-(4-Hydroxy-3-Methoxyphenyl)	$C_{10}H_{12}O_3$
13.076	1.90	2,6-Dimethoxy-4-(2-Propenyl)Phenol	$C_{11}H_{14}O_3$
13.156	1.52	2,4-Hexadienedioc acid, 3-Methyl-4-Propyl, Dimethyl ester, (Z,E)	$C_8H_{12}O_2$
13.667	0.88	N-[2-(2-Isopropyl-phenoxy)-ethyl]-2-methylsulfanyl-benzamide	$C_{19}H_{23}NO_2S$
13.684	1.50	1,3-Diphenylpropane	$C_{15}H_{16}$
14.211	4.48	2,6-Dimethoxy-4-(2-Propenyl)Phenol	$C_{11}H_{14}O_3$
14.452	4.59	N-Methylene-1,2-diphenylethanamine	$C_{15}H_{15}N$
15.004	2.78	1-(2,6-Dihydroxy-4-methoxyphenyl)-1-butanone	$C_{11}H_{14}O_4$
16.884	6.65	n-Hexadecanoic acid	$C_{16}H_{32}O_2$
18.57	16.70	Oleic Acid	$C_{18}H_{34}O_2$

The GC-MS of WPO indicates that the WPO contains compounds like Oleic acid, 1, 3-Dimethoxy-2-hydroxybenzene, and Methoxyphenol in a large proportion. Most of the components identified are phenols, with ketones and aldehyde groups attached, and nearly all the functional groups showed the extensive existence of the oxygen. On the other hand, the

analysis proved that the abundant aldehydes and ketones make the pyrolysis oil hydrophilic and hydrated in nature that prevents the separation of water from WPO [139].

3.5.3 Physicochemical properties of WPO, JME and diesel

The proximate analysis indicates the percentages of the moisture, volatile, ash and fixed carbon contents in the raw materials. From the ultimate analysis, one can know the percentage composition of the various elements present in the raw materials such as Carbon, Hydrogen, Nitrogen, Sulphur and Oxygen content. The proximate and ultimate analyses of WPO are compared with that of diesel and given in Table 3.5.

Table 3.5 Proximate and ultimate analysis of WPO compared with diesel

Proximate analysis	**WPO**	**Diesel**
Water content (%)	28.8	0.025
Ash content (%)	0.012	0.13
Fixed carbon (%)	12.85	Nil
Ultimate analysis		
Carbon (%)	49.1	86.5
Hydrogen (%)	6.2	13.2
Nitrogen (%)	3.0	Nil
Sulphur (%)	0.05	0.3
Oxygen by difference (%)	41.65	Nil

The important physico chemical properties of WPO are tested in a standard test facility. All the tests are conducted by following the ASTM standard test procedure. Table 3.6 gives the comparison of the physical properties of WPO with those of JME and diesel.

Table 3.6 Comparison of fuel properties of WPO with diesel and JME

Properties	ASTM method	Diesel	JME	WPO
Specific gravity at 15 °C	D 4052	0.83	0.88	1.15
Net calorific value (MJ/kg)	D 4809	43.8	39.1	20.58
Flash point (°C)	D 93	50	118	98
Fire point (^{o}C)	D 93	56	126	108
Pour point (°C)	D 97	-6	-1	2
Carbon residue (%)	D 4530	0.1	0.01	12.85
Kinematic viscosity at 40 °C (cSt)	D 445	2.58	4.6	25.3
Copper strip corrosion @ 100^{o}C for 3 hrs		-	No.1	No.1
Surface tension (mN/m)	D 971	26.7	29.2	30.7
Cetane number	D 613	50	55	27
Moisture content (wt %)	D 2709	0.025	1	15-30
Final boiling point (^{o}C)	D 86	344	342	250-280
Oxidation stability (mg/l00g)	-	-	0.4	-
Acid value (mg KOH/g)	-	-	0.38	0.45
Carbon (%)	D 3178	86.5	77.1	49.1
Hydrogen (%)	D 3178	13.2	11.81	6.2
Nitrogen (%)	D 3179	Nil	0.119	3.0
Sulphur (%)	D 3177	0.3	0.001	0.05
Oxygen by difference (%)	E 385	Nil	10.97	41.65
Stoichiometric A/F ratio (%)	-	14.5	12.4	3.39
Empirical formula	-	$C_{10}H_{22}$	$C_{7.56}H_{13.89}N_{0.01}O_{0.81}$	$C_{1.13}H_{2.92}N_{0.01}S_{0.01}O_{1.62}$

3.6 Preparation of JME-WPO emulsions

Emulsification is one of the techniques used to mix two liquids of different densities and surface tension. It can also be defined as the mixing of one substance with another, which is hydroscopic in nature. Surfactants are compounds that lower the surface tension of a liquid that decreases the interfacial tension between two liquids. Surfactants may act as detergents, wetting agents, emulsifiers, foaming agents and dispersants. In this investigation, the role of the surfactant is that of an emulsifier. In the emulsification process one of the biggest

challenges is, choosing a suitable surfactant for the two liquids to be emulsified. This depends on the HLB value of the surfactant. HLB, i.e., the Hydrophilic Lipophilic Balance is the measure of degree to which the liquid is hydrophilic or lipophilic. Depending upon the nature of the dispersed phase and dispersing medium, the emulsions are classified into two types:

(i) Oil-in-water emulsions (O/W)

(ii) Water-in-oil emulsions (W/O)

Surfactants with HLB values ranging between 4 and 8 are considered to make water-in-oil type of emulsions and HLB values between 8 and 12 are considered to make oil-in-water emulsions. The accuracy of the HLB values taken into consideration will be around ± 0.5. Depending on the size of the droplets, emulsions are classified into two types:

(a) Macro emulsions: The size of the particles ranges from 0.2 to 50 mm, and they are kinetically stable.

(b) Micro emulsions: The size of the particles ranges from 0.01 to 0.02 mm, and they are thermodynamically stable.

In this investigation, a water-in-oil type emulsion was considered to make the JME-WPO emulsions. The non-ionic surfactants having, HLB values in the range between 4 and 9 were selected for this study. The list of surfactants used in this study and their specifications are given in Table 3.7.

Table 3.7 List of surfactants used in this study and their HLB values

Sl.No	Name of the surfactant	Chemical formula	HLB value
1.	Span 20 (Sorbitan monolaurate)	$C_{18}H_{34}O_6$	8.6
2.	Span 80 (Sorbitan monooleate)	$C_{24}H_{44}O_6$	4.3
3.	Tween 80 (Polysorbate 80)	$C_{64}H_{124}O_{26}$	15
4.	Span 80 + Tween 80 mixed	-	6.45

The JME-WPO emulsions were prepared by adding 5, 10 and 15% of WPO with 95, 90 and 85% JME respectively, with the addition of the different surfactant combinations by volume percentage. Table 3.8 gives the details of the composition of the materials used in the preparation of different JME-WPO emulsions.

Table 3.8 Composition of materials used in JME-WPO emulsions

Sample No.	WPO (vol %)	JME (vol %)	Surfactant (vol %)	Notation
1.	5	93	Span 20 2%	X1JOE5
2.	10	88	Span 20 2%	X1JOE10
3.	15	83	Span 20 2%	X1JOE15
4.	5	91	Span 20 4%	X2JOE5
5.	10	86	Span 20 4%	X2JOE10
6	15	81	Span 20 4%	X2JOE15
7	5	93	Span 80 2%	Y1JOE5
8.	10	88	Span 80 2%	Y1JOE10
9.	15	83	Span 80 2%	Y1JOE15
10.	5	91	Span 80 4%	Y2JOE5
11.	10	86	Span 80 4%	Y2JOE10
12.	15	81	Span 80 4%	Y2JOE15
13.	5	93	2% of (50% of Span 80 + 50% of Tween 80)	Z1JOE5
14.	10	88	2% of (50% of Span 80 + 50% of Tween 80)	Z1JOE10
15.	15	83	2% of (50% of Span 80 + 50% of Tween 80)	Z1JOE15
16.	5	91	4% of (50% of Span 80 + 50% of Tween 80)	Z2JOE5
17.	10	86	4% of (50% of Span 80 + 50% of Tween 80)	Z2JOE10
18.	15	81	4% of (50% of Span 80 + 50% of Tween 80)	Z2JOE15

A mechanical stirrer is used to mix the JME with WPO and the surfactant. The stirrer was connected to a small AC motor whose capacity was 1/20 HP (37.3W). Hence, the electrical energy consumed for the preparation of each sample was about 0.01865 kWh. Fig. 3.14 (a) shows the photographic view of arrangement of mechanical stirrer. Fig. 3.14 (b) shows the photographic view of the stirring action during emulsification process.

Fig. 3.14 (a) Arrangement of mechanical stirrer

Fig.3.14 (b) Stirring action during emulsification process

Fig. 3.15 (a) and Fig. 3.15 (b) show the Y1JOE10 and Y1JOE15 emulsion respectively.

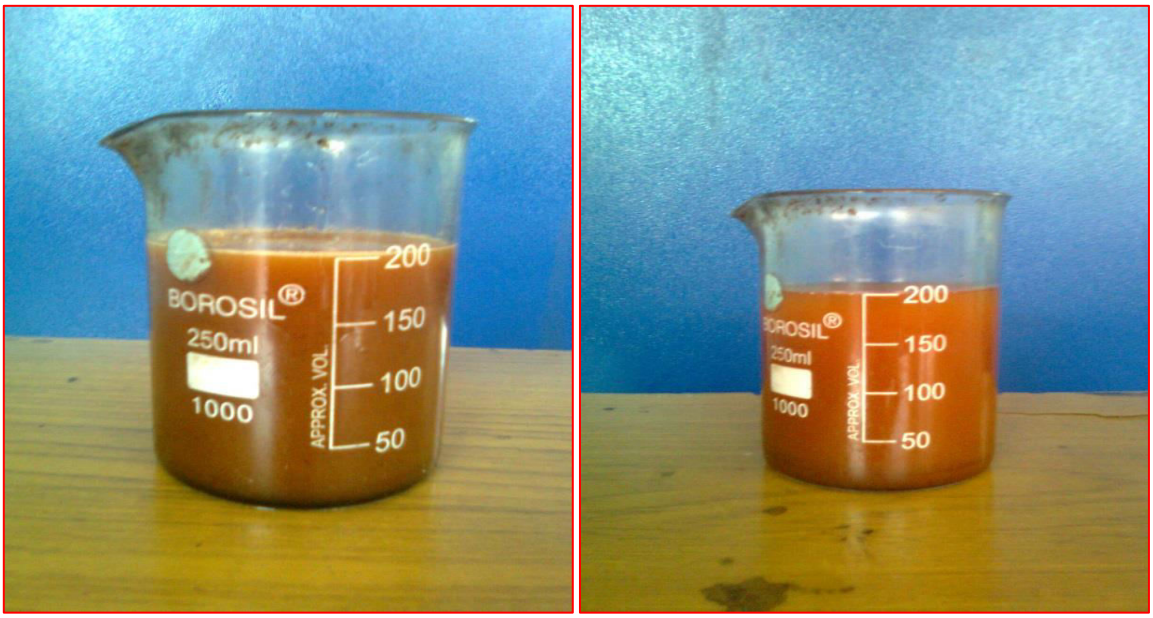

Fig.3.15 (a) Y1JOE10 emulsion **Fig.3.15 (b)** Y1JOE15 emulsion

Fig. 3.16 (a) and Fig. 3.16 (b) show the Y2JOE10 and Y2JOE15 emulsion respectively.

Fig.3.16 (a) Y2JOE10 emulsion **Fig.3.16 (b)** Y2JOE15 emulsion

Fig. 3.17 (a) and Fig. 3.17 (b) show the X1JOE10 and X1JOE15 emulsion respectively.

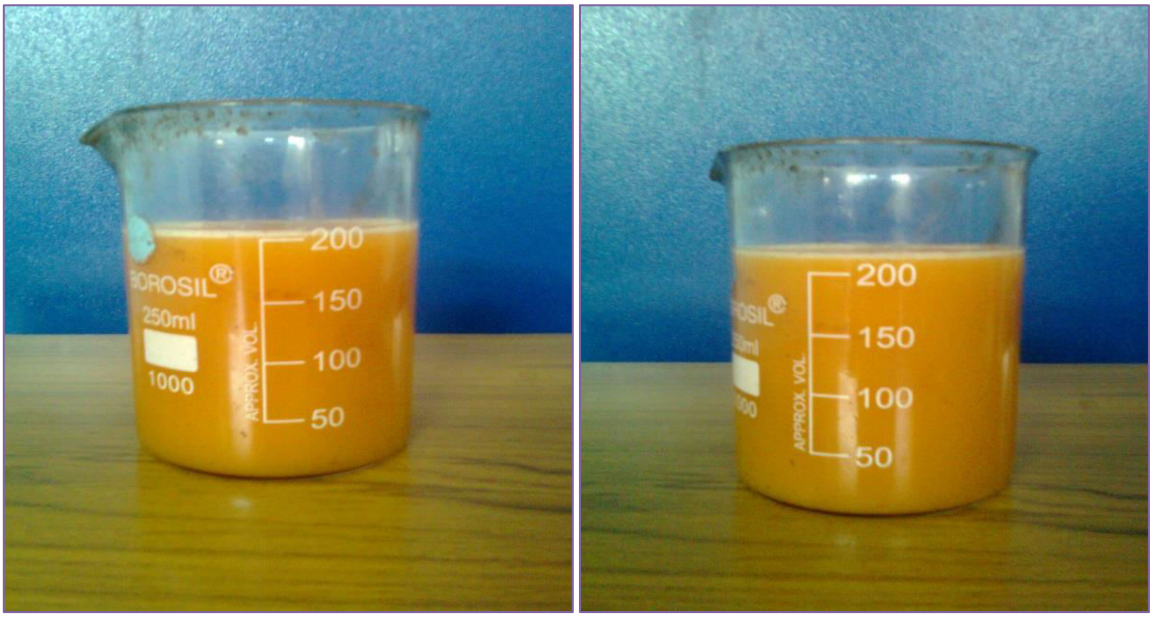

Fig.3.17 (a) X1JOE10 emulsion **Fig.3.17 (b)** X1JOE15 emulsion

Fig. 3.18 (a) and Fig. 3.18 (b) show the X2JOE10 and X2JOE15 emulsion respectively.

Fig.3.18 (a) X2JOE10 emulsion **Fig.3.18 (b)** X2JOE15 emulsion

Fig. 3.19 (a) and Fig. 3.19 (b) show the Z1JOE10 and Z1JOE15 emulsion respectively.

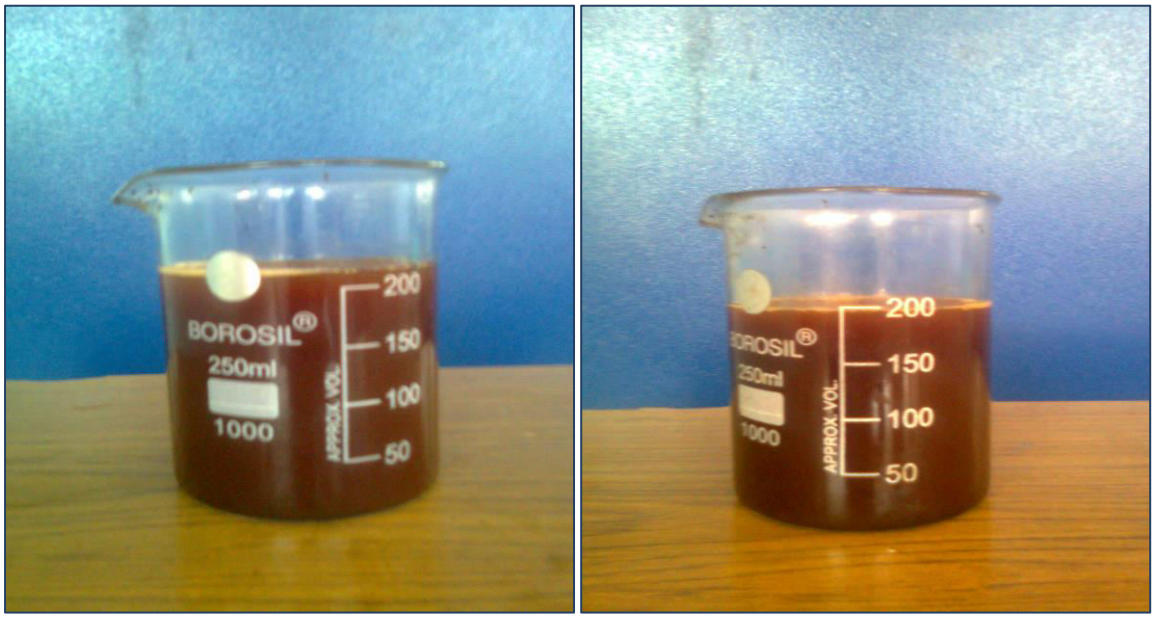

Fig.3.19 (a) Z1JOE10 emulsion **Fig.3.19 (b)** Z1JOE15 emulsion

Fig. 3.20 (a) and Fig. 3.20 (b) show the Z2JOE10 and Z2JOE15 emulsion respectively.

Fig.3.20 (a) Z2JOE10 emulsion **Fig.3.20 (b)** Z2JOE15 emulsion

3.7 Image analysis of emulsions

A microscopic analysis was carried out to check the dispersion of emulsion droplet. The microscopic images of the sample droplet distribution of four different emulsions are shown in Figs. 3.21 to 3.24.

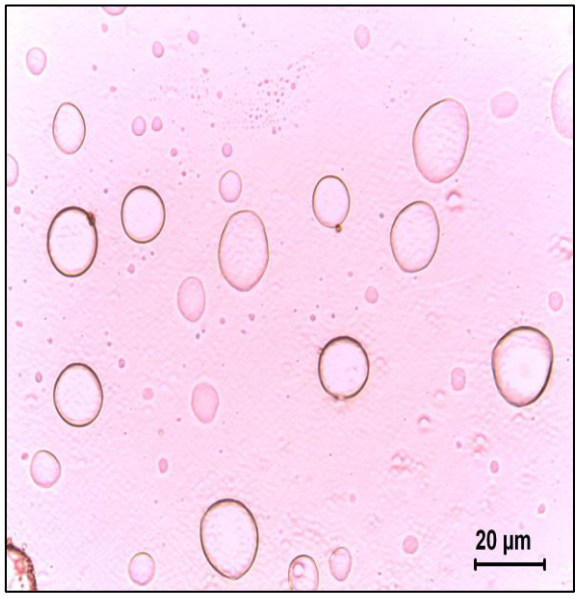

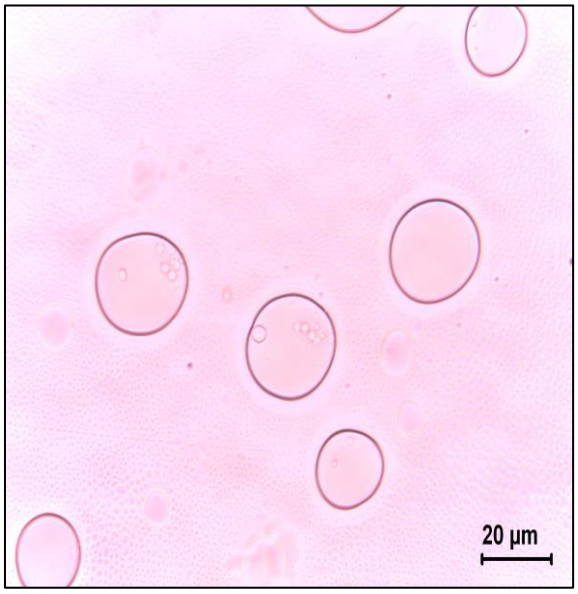

Fig.3.21 X1JOE15 emulsion **Fig.3.22** Y1JOE15 emulsion

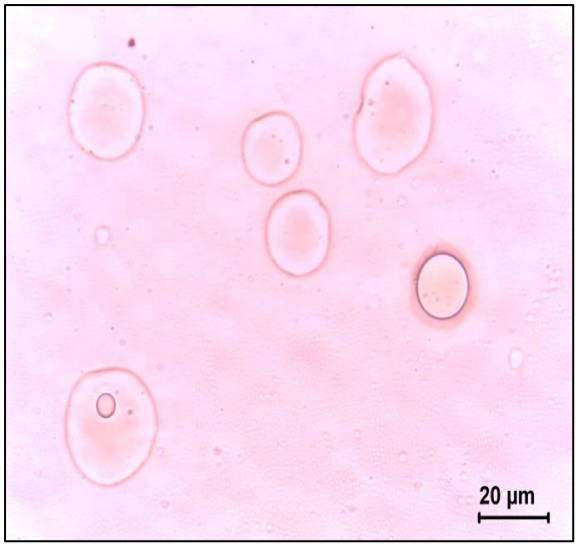

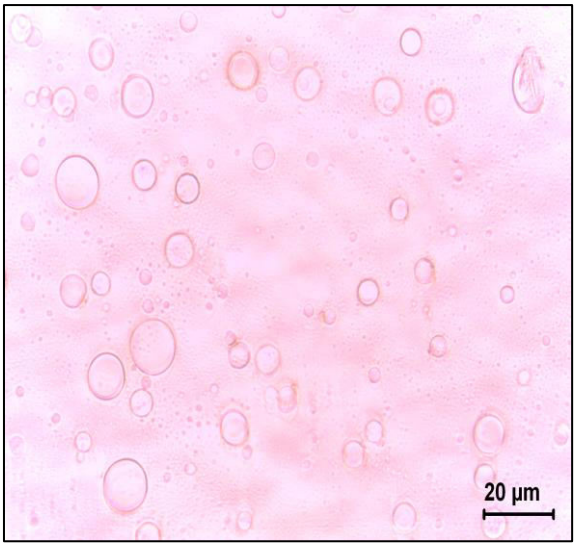

Fig.3.23 Z1JOE15 emulsion **Fig.3.24** Z2JOE15 emulsion

The images were obtained with the help of a digital camera connected to an electron microscope whose magnification index was 500X. It can be observed from the microscopic images that the Z2JOE15 emulsion using a mixed surfactant Span 80 and Tween 80 contains smaller mean droplet diameter compared to those of the other JME-WPO emulsions studied. This indicates that the emulsion stability of Z2JOE15 is considerably larger than that of other emulsions. The physico chemical properties of different JME-WPO emulsions used in this study are given in Table 3.9.

3.8 Acid treatment of JOE15 emulsion

The acidity of pyrolytic liquids is typically determined by the pH value. The acids in the bio oil are produced mainly by the degradation of the hemicelluloses in wood. The pH is a representation of how corrosive the oil may be, but it does not indicate the concentration of the acidic constituents. The pH of the WPO is low (2–3). The total acid number (TAN) can also be used for measuring the acidity of the bio oil. The TAN is the amount of potassium hydroxide (KOH) in milligrams that is needed to neutralize the acids in one gram of liquid. After attempting trials with different emulsions, to evaluate the combustion, performance and emissions of the engine, it was understood that the JOE15 emulsion gave a better results than other emulsions. However, since the emulsion was acidic in nature, the researcher tried to neutralize the emulsion with acid treatment. Therefore, in this study, the TAN value of JOE15 was determined by the potentiometric titration method. In this method, the sample of JOE15 was dissolved in toluene (50%), propanol (49.5%) and water (0.5%). Then, it was titrated with alcoholic potassium hydroxide using a burette at a constant rate.

Table 3.9 Fuel properties of JME-WPO emulsions

Properties	X1JOE10	X1JOE15	X2JOE10	X2JOE15	Y1JOE10	Y1JOE15	Y2JOE10	Y2JOE15	Z1JOE10	Z1JOE15	Z2JOE10	Z2JOE15
Specific gravity at 15 °C	0.906	0.926	0.908	0.9167	0.907	0.9265	0.905	0.9155	0.918	0.9267	0.907	0.9205
Net calorific value (MJ/kg)	37.24	36.32	34.28	32.24	37.24	36.32	37.24	36.32	37.24	36.32	38.17	36.72
Flash point (°C)	158	152	159	152	158	153	162	158	160	156	160	154
Kinematic viscosity at 40 °C (cSt)	6.75	6.97	6.91	7.28	6.62	7.12	6.73	6.97	6.91	7.28	6.43	7.06
Carbon (%)	65.88	77.26	60.82	64.36	61.23	58.50	51.265	46.9	58.6	51.72	56.35	48.79
Hydrogen (%)	8.125	12.27	7.63	8.324	7.265	6.851	7.812	7.556	9.12	8.558	9.57	7.652
Nitrogen (%)	0.09	0.07	0.32	0.18	0.243	0.16	0.23	0.15	0.21	0.29	0.156	0.25
Sulphur (%)	0.312	0.495	0.76	0.25	0.356	0.856	0.24	0.385	0.52	0.736	0.83	1.571
Oxygen by difference (%)	25.593	9.901	30.47	26.886	30.906	33.633	40.45	45.009	31.55	38.696	33.094	41.737
Stoichiometric A/F ratio (%)	-	13.55	-	-	-	-	-	-	8.559	7.26	-	-

A glass electrode and reference electrode were immersed in the sample and connected to a potentiometer. The meter reading (in millivolts) was plotted against the volume of the titrant. Based on the inflection in the curve, the buffer potential was considered to be the acid number of the sample. The TAN value determined by this method for JOE15 was 17.6 (mg of KOH/g). The physical properties of acid treated JOE15 emulsion tested in a standard test facility and the results are given in Table 3.10. The economic analysis to prepare 1 litre of ATJOE15 emulsion is given in Annexure 1.

Table 3.10 Properties of the acid treated JOE15 emulsion compared with JOE15

Properties	JOE15	ATJOE15
Specific gravity at 15 °C	0.9167	0.9176
Net calorific value (MJ/kg)	36.32	30.82
Kinematic viscosity at 40 °C (cSt)	7.28	6.50
Surface tension (mN/m)	30.679	30.179
Flash point (°C)	156	148
pH value	3-4	7
TAN (mg of KOH/g)	17.6	-

CHAPTER 4

EXPERIMENTAL SETUP AND METHODOLOGY

4.1 General

This chapter details the test engine with loading device and complete instrumentation used in this investigation. With the help of instrumentation, the procedure followed to determine the performance parameters such as brake thermal efficiency, brake specific fuel consumption and exhaust gas temperature of the engine for all the emulsions, at different loads are discussed. Further, the working principle and the use of the analysers to measure the exhaust gas emissions such as nitric oxide (NO), carbon monoxide (CO), unburnt hydrocarbon (HC) and smoke opacity are illustrated. The devices used to measure the cylinder pressure and crank angle are also discussed. The description of data acquisition system (DAS) is also given. This chapter also provides information on the accuracies and uncertainties of the instrumentation adopted in this study. The methods followed to conduct the short term and long term endurance tests are also reported in this chapter. Also, the procedure to evaluable the lubrication oil properties after long run is also discussed.

4.2 Engine experimental setup

A detailed layout of experimental setup is shown in Fig. 4.1. A photographic view of the experimental setup is given in Fig.4.2. The engine experiments were conducted as per IS: 10,000 [Part IV, V, VI, VIII, IX and X]:1980 standard test methods. A Kirloskar TAF1 model, single cylinder, four stroke, air cooled, DI diesel engine with a displacement volume of 661.5 cc and developing a rated power of 4.4 kW was used in this study. The engine was run at a constant speed of 1500 rpm. The detailed specification of the test engine is given in Annexure 2. An electrical dynamometer connected to a resistive load bank, was used to load the engine. The fuel measuring system consisted of a burette fitted with two optical sensors, one at a higher level and the other at a lower level. As the fuel passed through the higher level optical sensor, the sensor gave a signal to the data acquisition system (DAS) to start the counter time. Once the fuel reached the lower level sensor, the sensor gave a signal to the DAS to stop the counter time and refill the burette. From this, the time taken for the consumption of fuel for a fixed volume was calculated. A differential pressure sensor fitted in the air box measured the air consumption. The differential pressure sensor was used to measure the pressure difference between the orifice plates. The differential pressure sensor gave a proportional voltage output with respect to the difference in pressure.

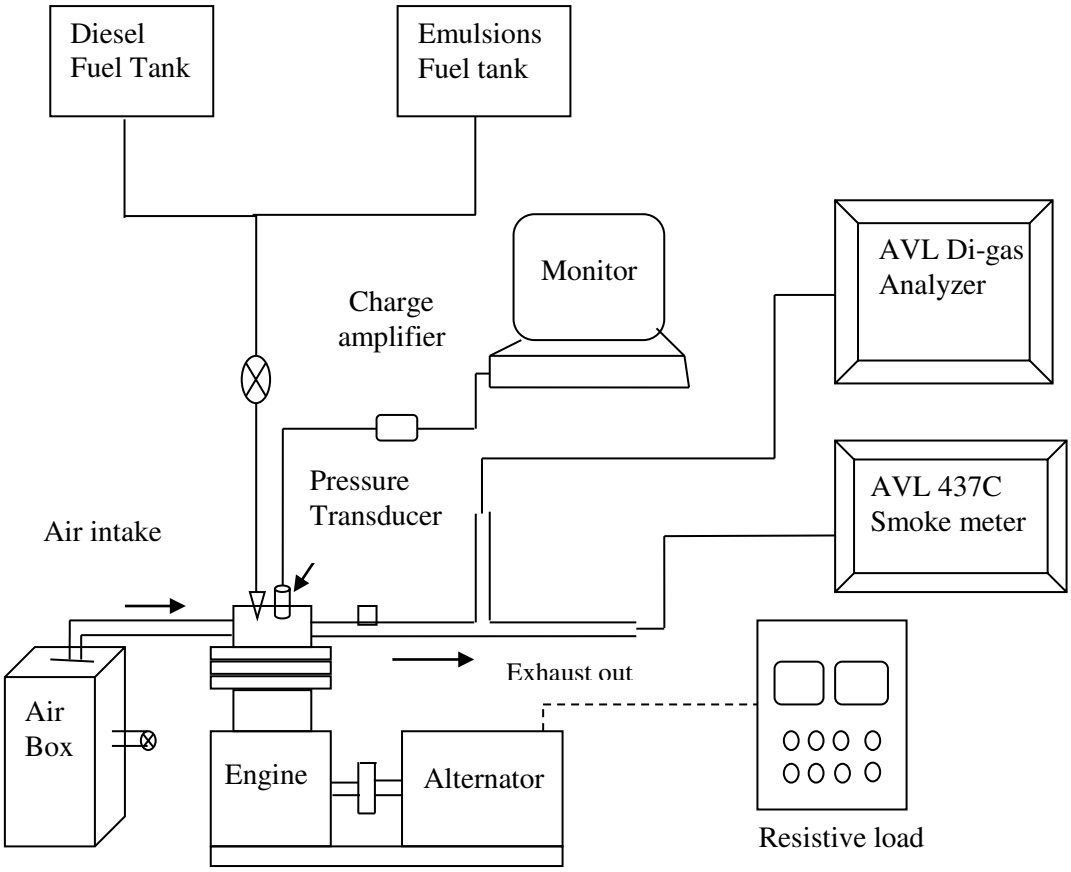

Fig. 4.1 Schematic diagram of experimental setup

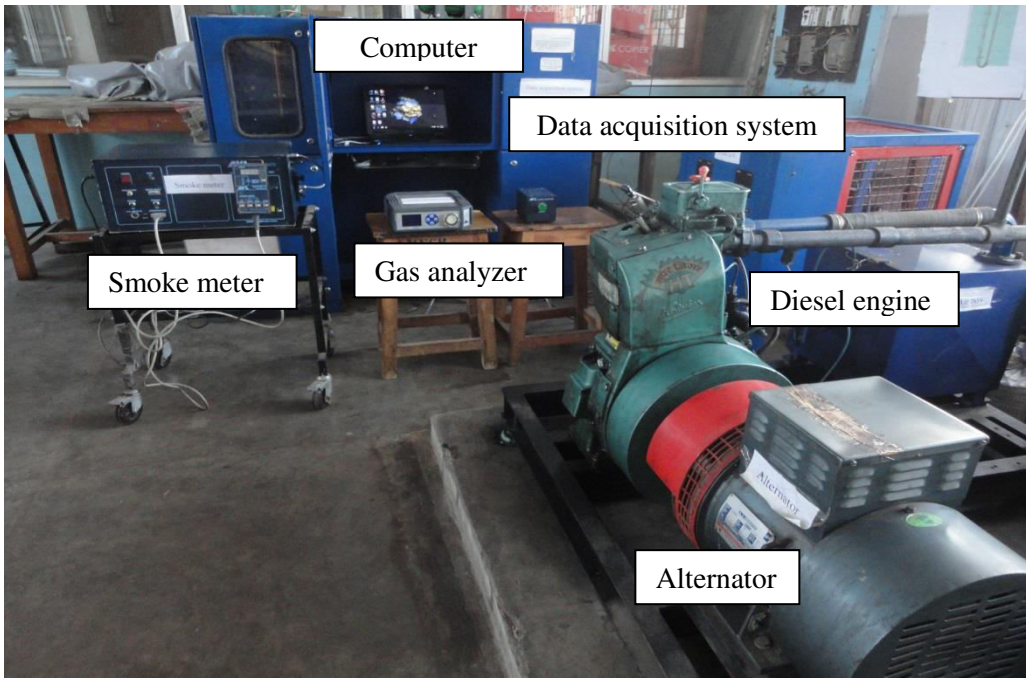

Fig. 4.2 Photographic view of experimental setup

A surge tank was used to damp out the pulsations produced by the engine, for ensuring a steady flow of air through the intake manifold. A K-type thermocouple fitted in exhaust pipe measured the exhaust gas temperature. A non-contact PNP type sensor was connected near the flywheel of the engine to measure the engine speed. The PNP sensor gave the pulse output for each revolution of the crank shaft. The frequency of the pulses was converted into voltage output and connected to the computer. A standalone frequency to voltage converter is used for signal conditioning. The in-cylinder pressure of the diesel engine was obtained by means of a pressure transducer, which was flush mounted on the cylinder head. Initially, the combustion, performance and emission parameters of the diesel engine were studied with diesel at a compression ratio of 17.5 and nozzle opening pressure of 200 bar, which was prescribed by the manufacturer, by maintaining a rated speed of 1500 rpm to get the diesel data.

4.3 Data collection for performance parameters

4.3.1 Brake thermal efficiency (BTE)

In order to determine the brake thermal efficiency of the engine, three important inputs were measured: i) Time taken for 20 cc of fuel consumption ii) Lower heating value of the test fuel and iii) Fuel density. The formula used to calculate the brake thermal efficiency, is given below:

BTE = (brake power x 3600 x 100/ (volumetric fuel flow rate per hour x fuel density x calorific value of fuel)). (4.1)

4.3.2 Brake specific fuel consumption (BSFC)

The formula used to calculate the brake specific fuel consumption is given below:

BSFC = (volumetric fuel flow rate per hour x fuel density/brake power) (4.2)

The BTE and BSFC were displayed in the form of excel sheet generated by the data acquisition system software (Engine test express) using the above mentioned expressions.

4.4 Combustion parameters measurement

4.4.1 Piezo electric transducer

For acquiring important combustion parameters, such as ignition delay, heat release rate, combustion duration etc., the cylinder pressure and crank angle values are necessary. The

cylinder gas pressure was measured using a Kistler piezo-electric transducer (model 5395A) in conjunction with a Kistler charge amplifier.

Fig. 4.3 Photographic view of Kistler pressure transducer

The cylinder gas pressure data was recorded as the average of 20 cycles of data, with a resolution of 0.5°CA using a data acquisition system. From the average data of the pressure and crank angle values, the peak pressure, occurrence of the peak pressure, maximum rate of pressure rise, and heat release rate were calculated and stored in an excel file. A photographic view of the Kistler pressure transducer is shown in Fig. 4.3. The exploded view of the piezoelectric transducer is shown in Fig. 4.4.

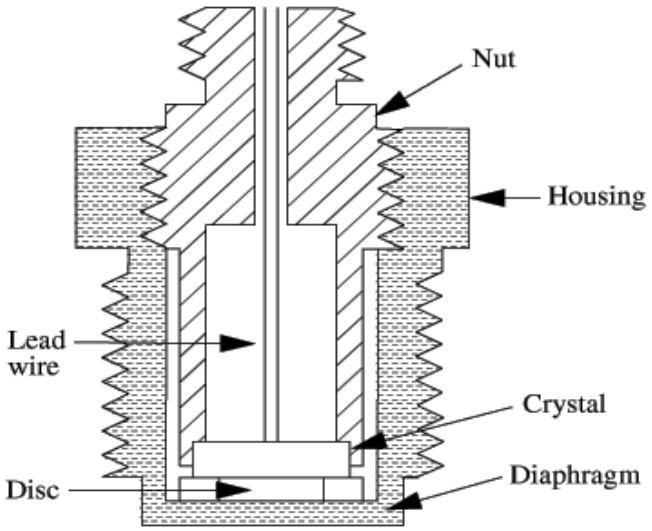

Fig. 4.4 Exploded view of piezoelectric transducer

The quartz sensors can withstand very high pressure varying from 0 to 250 bar. A hole was drilled on the dummy plug and the pressure sensor was placed in it. The drilled hole diameter was 5 mm, and an internal thread of pitch 1 mm is made. The piezo electric sensor was properly sealed so that there is no change in the compression ratio of the cylinder. The pressure produced by the engine cylinder was sensed by the pressure sensor placed on the dummy plug. The measured pressure acts through a diaphragm on the quartz crystal measuring elements, which transforms the pressure into an electrostatic charge Q in pico coulomb. The sensor was mounted on the combustion chamber plug end by a M5 tapping hole, to accommodate the sensor. The complete specification of the Kistler make piezo quartz pressure sensor is given in Annexure 3. Figure 4.5 shows a photographic view of the location at which the pressure transducer is flush mounted.

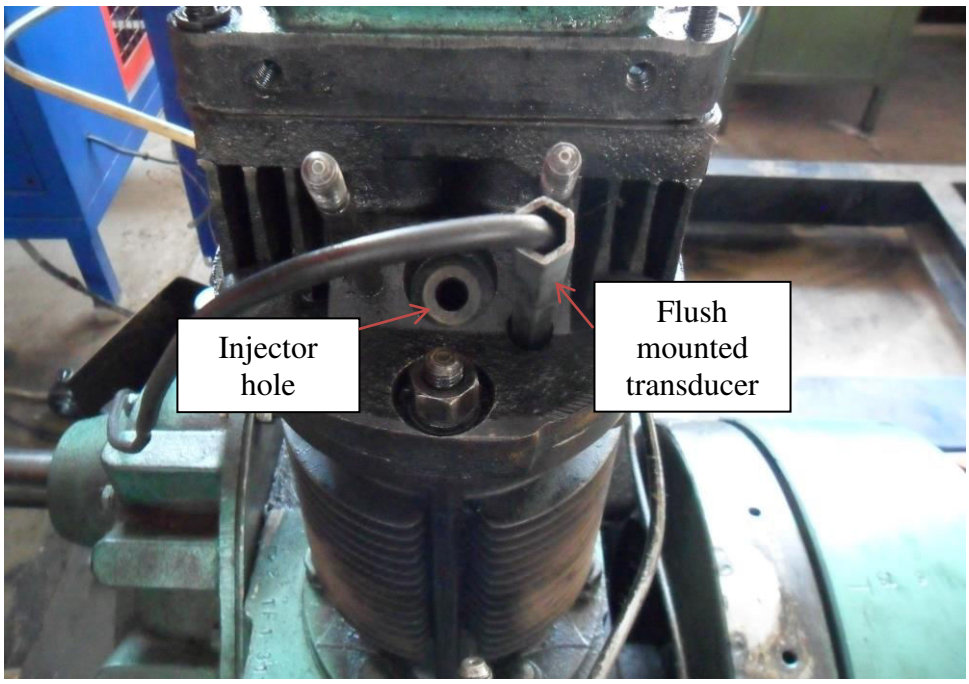

Fig. 4.5 Photographic view of flush mounted transducer in engine cylinder head

The stainless steel diaphragm was welded hermetically to the stainless steel body. The quartz elements were mounted in a highly sensitive arrangement (transversal effect). The quartz element had a high natural frequency. Its connector was welded to the body, but its Teflon insulator was not absolutely tight.

The TDC marker (Kistler model 5015A1000) was placed near the engine flywheel. At the TDC position, a small metallic deflector was fitted. The photographic view of the TDC

marker and metallic deflector is shown in Fig. 4.6. The setup was aligned in such a way that the sensor gives output in the form of a square wave, exactly when the piston is at the TDC.

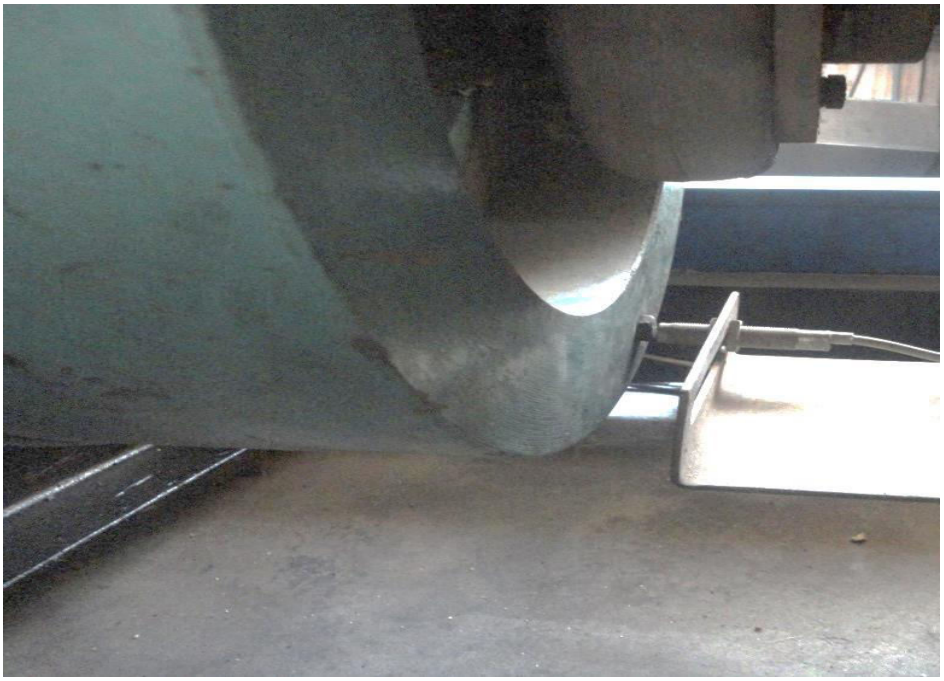

Fig. 4.6 Photographic view of TDC marker and deflector

4.4.1.1 Pressure transducer calibration

The calibration of the pressure transducer was carriedout to measure any differences in the output of the transducer for a known pressure. This was essential to minimize the combustion cylinder-pressure measurement error, and was particularly important for the engine data. The piezo electric transducer signals naturally decay over time, and are therefore only suitable for dynamic measurements, like engine cylinder pressure measurements. Accordingly, they must be calibrated using a dynamic procedure. The Kistler piezo electric transducer of model 5395A was subjected to a dynamic calibration procedure using a standard dead weight tester. The dead weight tester generated the known pressure by hydraulically lifting precise weights with a piston with an accurately known cross-sectional area. The charge output signal of these transducers was used as the input to a charge amplifier via a high impedance cable. The charge amplifier converts the low level charge (which is of the order of several Pico-Coulombs) to a proportional voltage, which can be recorded with standard data acquisition equipment. In this procedure, a known pressure was applied to the transducer. Then, the output was grounded to zero volts, thereby eliminating signal decay. The pressure was then abruptly dropped to the atmospheric level, by rapidly releasing the hydraulic pressure holding up the weights and allowing them to fall. The resulting voltage change was recorded as a

function of time, using a digital oscilloscope programmed to trigger on a voltage drop. The voltage change caused by the pressure change was determined using a peak-to-peak calculation feature on the scope. Dynamic pressures were taken at intervals of 200 psi from 200 to 1000 psi. Ten measurements were taken at each dynamic pressure. These were then averaged, and graphed against the corresponding voltage output. The linearity of the transducer was found to be better than 1%. The repeatability was observed to be about 2 to 3%.

4.4.2 Charge amplifier

A charge amplifier was used to convert the obtained charge into equivalent output voltage. It transferred the input charge to another reference capacitor and produced an output voltage equal to the voltage across the reference capacitor, as shown in Fig. 4.7.

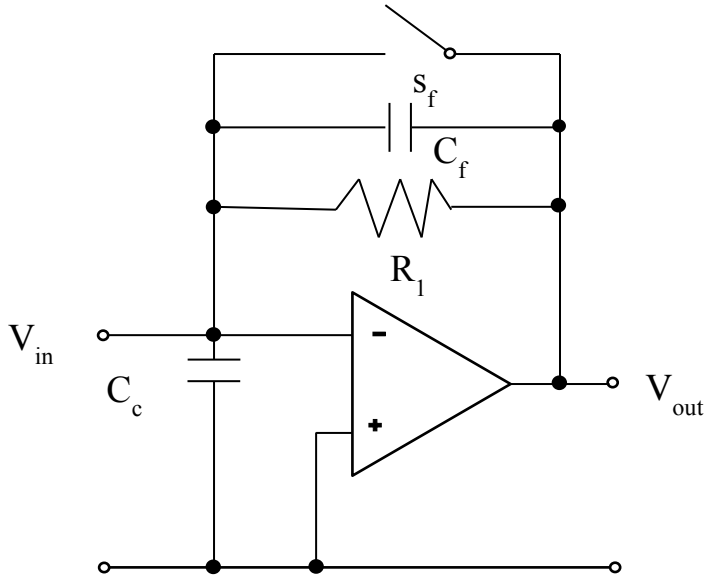

Fig. 4.7 Charge amplifier circuit

Thus, the output voltage was proportional to the charge of the reference capacitor and, respectively to the input charge; hence the circuit acted as a charge to voltage converter. The complete specification of the charge amplifier is given in Annexure 4. The input charge Q_{in} was applied to the summing point (inverting input) of the amplifier. It was distributed to the cable capacitance Cc, the amplifier input capacitance C_{inp} and the feedback capacitor C_f.

The node equation of the input is therefore: $Q_{in} = Q_c + Q_{inp} + Q_f$ (4.3)

Using the electrostatic equation: $Q = U \times C$ (4.4)

and substituting Q_{in}, Q_c, Q_{inp} and Q_f

$Qin = U_{inp} \times (C_c + C_{inp}) + U_f \times C_f$ (4.5)

and solving the output voltage V_O:

$V_O = V_f = Q_{in}/C_f$ which is fed into the data acquisition system. (4.6)

The output of the Kistler charge amplifier lies within ± 10V DC.

4.4.3 Analog to Digital Converter

The analog signals from the sensors were fed into an Analog to Digital Converter (ADC) and then passed to a display unit, through a data acquisition cord and microcontroller. Both the pressure and proximity sensors were interfaced with the engine and the output obtained is an analog signal. Further, the analog signal was converted into digital using the ADC, which was finally fed to a display unit through the data acquisition system. Using the data acquisition system graphical analysis, evaluating the differential equation, computing the mathematical expression, display, control and recording were done for various engine operating parameters, like instantaneous pressure, crank angle, temperature, and the heat release rate. From this, other combustion parameters such as ignition delay, cumulative heat release rate, mass fraction burned and combustion duration were computed. A computer was used to process the data and store during investigation.

4.4.4 Significance of the p-θ diagram

The in-cylinder pressure plotted against the crank angle is called as the P-θ diagram, which is a very useful tool for the combustion analysis. The pressure inside the cylinder depends on the instantaneous cylinder volume, combustion, heat transfer to combustion chamber walls, crevice regions and leakage. The usefulness of the p-θ diagram is given below:

- The p-θ diagram indicates the events occurring near the TDC more clearly than the p-V diagram.
- It gives information about the instantaneous pressure inside the engine cylinder for every crank angle degree.
- It gives the peak cylinder pressure, brake mean effective pressure in the cycle and its position, pressure rise, position and rate of pressure rise and maximum rate of pressure rise.
- It describes quantitative information on the progress of combustion.
- Valve timing, i.e., valve opening and closing can be optimized based on this p-θ diagram.

- The rates of heat release, ignition delay, start of combustion, duration of combustion, mass fractions burned and gas condition for pollutant formation, are also given by the p-θ diagram.

4.4.5 Determination of the combustion parameters

4.4.5.1 Ignition delay

The ignition delay of a compression ignition (CI) engine is defined as the time (or crank angle) interval between the start of injection and start of combustion. This delay is due to physical and chemical processes that takes place before a significant fraction of the chemical energy of the injected liquid fuel is released. The physical processes are: atomization of liquid fuel jet, evaporation of fuel droplets and mixing of fuel vapour with air. The chemical processes are precombustion reactions of fuel, air, residual gas mixture that leads to auto ignition. These processes are affected by engine design, operating variables and fuel characteristics. Ignition delay, in terms of the crank angle, is the difference between the start of injection and the start of ignition (detectable heat release rate). From the heat release rate curve, the start of combustion is determined as the point at which the heat release curve changes from a negative axis to a positive one [155].

Based on the crank angle, ignition delay is determined with the following equation:

$$\text{Ignition delay (CA)} = (\text{CA})_{5\%} - (\text{CA})_{\text{inject}} \tag{4.7}$$

where, $(\text{CA})_{5\%}$ = Crank angle at which 5% heat is released

$(\text{CA})_{\text{inject}}$ = Crank angle at which fuel is injected into the combustion chamber.

4.4.5.2 Heat release rate

The rate of heat release at each crank angle was determined by the following formula derived from the first law of thermodynamics: [155-156]

$$\frac{dU}{dt} = \dot{Q} - \dot{W} \tag{4.8}$$

$$\text{m } C_v \frac{dT}{dt} = \dot{Q} - P \frac{dv}{dt} \tag{4.9}$$

where, $\dot{Q}$= the combination of the heat release rate and the heat transfer rate across the cylinder wall,

$\dot{W}$ = the rate of work done by the system due to the system boundary displacement.

U = Internal energy

To simplify Equation (4.8) the ideal gas assumption can be used.

$$pV = mRT \tag{4.10}$$

Where p = Cylinder pressure in bar.

V= Volume of the cylinder (m^3)

m = mass of gas (kg)

R = Gas constant

T = Absolute temperature

Eqn. (4.9) can be differentiated (assuming constant mass)

$$\frac{dT}{dt} = \frac{1}{mR}\left[P\frac{dV}{dt} + V\frac{dP}{dt}\right] \tag{4.11}$$

After combining eqns. (4.9) and (4.11), the heat release equation becomes

$$\dot{Q} = \left[\frac{Cv}{R} + 1\right] p\frac{dV}{dt} + \frac{Cv}{R} V\frac{dp}{dt} \tag{4.12}$$

After replacing time (t) with the crank angle (θ), the equation becomes

$$\dot{Q} = \frac{\lambda}{\lambda-1} p\frac{dV}{d\theta} + \frac{1}{\lambda-1} V\frac{dp}{d\theta} + Q_w \tag{4.13}$$

where, λ is the ratio of the specific heats (C_p/C_v), p is the cylinder gas pressure, V is the instantaneous volume of the cylinder and Q_w is heat transfer rate across the cylinder wall. The instantaneous cylinder volume can be obtained from the engine geometry and crank angle values.

4.4.5.3 Combustion duration

The crank angle duration from 10% mass fraction burned to 90% mass fractions burned, has been taken as the combustion duration.

4.4.5.4 Rate of pressure rise (ROPR)

The rate of pressure rise defines the load that is imposed by the combustion process on the cylinder head and block, and to a large extent, determines the structural design [157]. Also, the rate of pressure rise is indicative of the noisy operation of the engine. The rate of pressure rise with respect to the crank angle is derived from the following expression: [155].

$$\text{ROPR} = \frac{dp}{d\theta} \tag{4.14}$$

4.4.5.5 Mass fractions burned

Assuming that the pressure rise Δp_c is proportional to the heat added to the in-cylinder medium during the crank angle interval, the mass fraction burned at the end of the considered i-th interval may be calculated as [155].

$$\text{MFB} = \frac{m_b\,(i)}{m_b\,(total)} = \frac{\sum_0^i \Delta p_c}{\sum_0^N \Delta p_c} \tag{4.15}$$

where 0 denotes the start of combustion, N – end of combustion (N is the total number of crank intervals).

4.5 Exhaust emissions measurement methods

4.5.1 NDIR principle for HC, CO and CO_2 emissions measurement

A non-dispersive infrared (IR) measurement was used to determine the concentration of the gaseous pollutants like HC, CO and CO_2 as illustrated in Fig. 4.8. The general working principle of the analyser is discussed in this paragraph. The absorption of IR radiation occurs in narrow-wavelength bands, with each gas exhibiting its own peculiar characteristics. Two infrared sources are provided, as shown, with a chopper to impose an AC signal, which is handled more easily by subsequent electronic detection circuits.

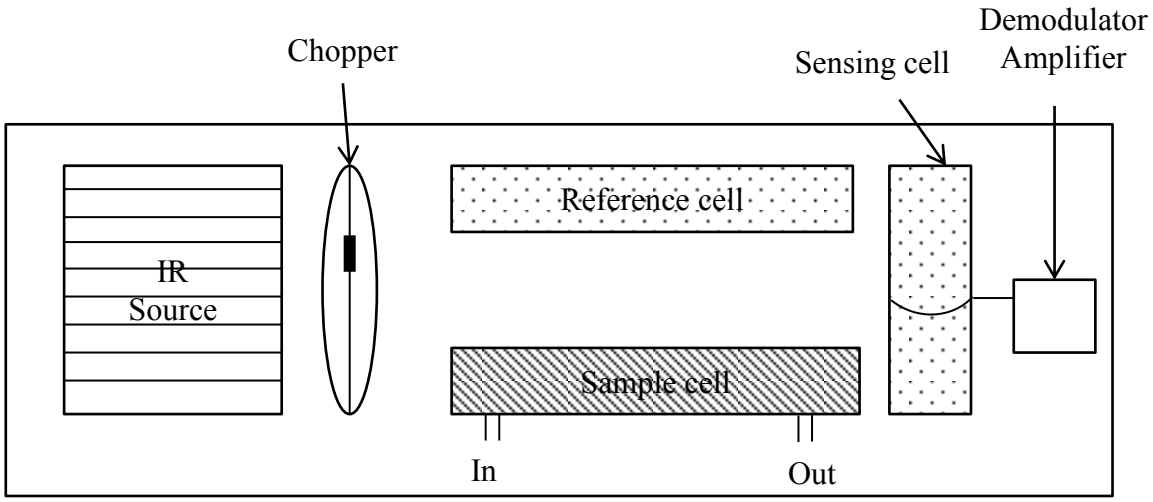

Fig. 4.8 Schematic layout of NDIR principle

Filters may be placed in the path of the sources, so that only the absorption wave length band for the particular gas to be studied is investigated. Two cells are exposed to the IR radiation: (a) a reference cell containing an inert gas (usually nitrogen) and (b) a cell which admits the passage of the sample gas containing the pollutant to be investigated. No IR absorption occurs in the reference cell, while the absorption in the sample cell is proportional to the concentration of the component of interest. Beyond the reference and sample cells there are two detector chambers which absorb the IR radiation transmitted. These chambers are sealed, so that the absorption of the radiation causes the temperature of the gas inside to rise. The two chambers are separated by a thin diaphragm. Because, more radiation is transmitted through the reference cell, there will be a greater temperature rise in the reference detector chamber

than in the sample detector. As a result, a pressure differential is created, which causes the movement of the diaphragm; this can be detected with a capacitance pickup. The resulting signal is amplified and transmitted to an appropriate readout device. The infrared absorption device may be used for continuous monitoring of the combustion products.

4.5.2 Electrochemical principle for the NO measurement

The specific detection of nitric oxide (NO) by the electrochemical sensors is based on a general principle used in electrochemistry. In brief, the NO diffuses across a gas-permeable membrane, and a thin film of electrolyte covering the probe. The NO species is oxidized on the sensor which consists of a working and Ag/AgCl reference electrode pair. A potential (approx 900 mV) is applied to the working/measuring electrode, relative to a reference electrode, and the resulting small redox current due to the oxidation of NO according to the following reaction, is measured by an amplifier system and recorder:

$$NO + 4OH^- \longrightarrow NO_3^- + 2H_2O + 3e^- \quad (4.16)$$

4.5.3 AVL Digas 444 Analyser

The exhaust gas sample was analysed by a 5 Gas analyzer (Make: AVL India, Model: 444) fitted with a DiGas sampler, conforming to ARAI certification: ARAI/TA(4G-RV)/AVL/DiGas 444/0910-12. The principle for measuring the CO, HC, CO_2 emissions was the NDIR, and for the NO and O_2, it was electrochemical. The CO, CO_2, O_2 emissions were measured in volume percentage, while the total unburnt hydrocarbon TUHC was measured in ppm (vol.) of n-hexane equivalent, and the NO emission was measured in ppm (vol.) during each run of the engine operation. The photographic view of the AVL Digas 444 analyzer is shown in Fig. 4.9. The complete technical specification of the AVL Digas 444 analyzer is given in Annexure 5.

The analyzer was interfaced through its RS 232C communication bus to an in-house developed emission data acquisition platform, which recorded the emissions over a span of 120 s in 20 s consecutive intervals, which was greater than the instrument response time of 15 s, for each case of the engine operation. The exhaust gases were tapped from a T joint between the exhaust gas outlet and the smoke meter tapping point. A fine filter to remove the advected particulates and a condensate trap were incorporated, after the main exhaust gas cooler so that the exhaust inlet temperature to the analyzer was maintained $\leq 40^oC$ as per the instruction manual. Stray condensates, if any, were tackled by the condensate separator

inbuilt in the analyzer, which was flushed before every case of data recording. Leak check, HC residue test, zero adjustment and condensate purging of the analyzer, were carried out before each observation. The CO, CO_2 and HC emissions were measured by the Non-Dispersive-Infrared (NDIR) detection principle, while the O_2 and NO emissions were measured by the pre-calibrated electrochemical sensors in the analyzer. It is to be noted that, the analyzer was calibrated with the recommended calibration gas mixture, before the start of the entire range of experimentation.

Fig. 4.9 Photographic view of the AVL Digas 444 analyzer

The detector in the gas analyser was made up of Selenium photocell with a diameter of 45 mm. Its maximum sensitivity in light was within the frequency range of 550-570 nm. Below 430 nm and above 680 nm, the sensitivity of the instrument was less than 4% related to the maximum sensitivity. Emission tests were carried out by inserting a probe into the engine's exhaust tube by opening the ball valve. Before taking the emission test, a leak check was conducted in the digital gas analyser, to discharge the residual gases by closing the probe's nozzle manually.

4.6 Conversion of emission values into g/kWh

It is general practice to express the emission data on a "brake specific" basis, except for the smoke opacity. The brake specific emissions are the mass flow rates of the individual pollutant divided by the engine power. The formulae used to convert the emissions from ppm and % vol into g/kWh are given below:

HC emissions in g/kWh

HC (g/kWh) = [{(mf+ma)/(29*1000)} * HC (in ppm)*13/BP] (4.17)

CO emissions in g/kWh

CO (g/kWh) = [{(mf+ma)/29)*10} * CO (in %vol)*28/BP] (4.18)

NO emissions in g/kWh

NO (g/kWh) = [{(mf+ma)/(29*1000)} * NO (in ppm)*32.4/BP] (4.19)

4.7 Gas analyser calibration procedure

4.7.1 Pre-Test Calibration

The gas analyser is calibrated prior to the emission test with calibration gases certified to ±2% accuracy as per the EPA test methods in 40 CFR 60 and the ISO 3930, 1976 test method. Three calibration gases (zero, mid and high) for CO, NO, and NO_2 may be used. The purified ambient air may be used as the zero gas. The mid-level gas concentration is 40% to 60% of the high range calibration gas. A high-level gas concentration of the high range calibration gas shall not be higher than 125% of the expected concentration nor less than 90% of the expected concentration. The high level gas is equal to the calibration span. The analyser calibration error shall be no more than ±5% of the calibration span value for the mid and high range calibration gases, or 5 ppm, whichever is less restrictive.

The calibration error shall be calculated as follows:

$$\% \text{ Difference} = \frac{\text{Analyzer Response} - \text{Gas Concentration}}{\text{Calibration Span}} \times 100 \quad (4.20)$$

For the zero gas, the calibration error shall be no more than 10 ppm:

Difference in ppm = Analyser response – Zero gas concentration

The steps involved for calibration are as follows:

Step 1: Allow the analyser to purge the calibration gases prior to beginning the emissions test.

Step 2: A test shall consist of three runs, with each run at least 20 minutes in length.

Step 3: Record the readings for HC, CO and NO, at 2 minute intervals during the 20 minute run.

4.7.2 Post-Test calibration

After a maximum of three valid 20-minute emission tests, conduct a post-test calibration as follows for the HC, CO and NO calibration gases:

Step 1: Allow the analyser to purge the gas sample until a stable zero reading is observed. Record the zero reading.

Step 2: Introduce the high range calibration gas to the analyser and allow it to reach a stable reading. Record the analyser reading.

Step 3: Introduce the mid-range calibration gas into the analyser and allow it to reach a stable reading. Record the analyser reading.

Calculate the difference with the pre-test calibration value. If the difference is greater than ±5% or 5 ppm, whichever is less restrictive, the emission test runs are invalid, and must be repeated.

$$\% \text{ Difference} = \frac{(\text{Post}-\text{Test Reading}) - (\text{Pre}-\text{Test Reading})}{\text{Pre}-\text{Test Reading}} \text{ x } 100 \qquad (4.21)$$

For the zero gas, the post-test calibration error shall be no more than 10 ppm.

4.8 Smoke measurement

The smoke emission was measured by a partial-flow sampling AVL (Austria) 437 diesel smoke meter, certified by ARAI, Pune, India, as per ARAI/TA(SM-RV)/AVL/437/1011-02. A photographic view of the AVL 437C diesel smoke meter is shown in Fig. 4.10.

Fig. 4.10 Photographic view of the AVL 437C diesel smoke meter

The operating principle is based on the attenuation of a light beam caused by the exhaust gases in a measuring chamber of defined measuring length, and nonreflecting surface filled homogeneously with the exhaust gas. The loss of light intensity between the light source and a receiver is measured and reported in % opacity, the calculation being based on the Beer-

Lambert law. The absorption coefficient “k” was also reported by the smoke meter, in accordance with the ECE-R24/ISO 3173. Condensation inside the instrument is avoided, as the measuring chamber is thermostatically heat controlled at 70 ± 5 ^{o}C. To ensure accuracy and repeatability observations were recorded, at each case of the engine operation, for a span of 120 s at intervals of 20 s, which was greater than the instrument measurement value resolution time of 10 s. The complete technical specification of the AVL 437C diesel smoke meter is given in Annexure 6.

4.9 Experimental methodology

4.9.1 Engine experimentation with diesel and JME

Initially, the engine was operated with diesel for obtaining the reference data of the combustion, performance and emission parameters. The engine was tested at 25%, 50%, 75% and 100% loads. For each load condition, the engine was run for at least 3 min after which data were recorded. Further, the engine was tested with the JME (100% Jatropha methyl ester).

4.9.2 Engine experimentation with the JME-WPO emulsions

After conducting experiments with diesel and JME to get the relevant data for combustion, performance and emission parameters, the engine was run with the different JME-WPO emulsions. Finally, the engine was allowed to run with diesel to remove the traces of the emulsion in the fuel line and fuel filter. The results were compared with diesel and the JME operations. The exhaust gas analyser and diesel smoke meter were switched on before starting of the experiments in order to stabilize them before starting the measurements. All the instruments were periodically calibrated. Initially the engine was run on diesel, JME and JME-WPO emulsions at a given compression ratio of 17.5 and nozzle opening pressure of 200 bar which is set by the manufacturer by maintaining a rated speed of 1500 rpm.

4.9.3 Investigations with acid treated JOE15 emulsion

Further, from the comparative analysis on the performance, combustion and emission characteristics of all the JME-WPO emulsions, and by consideration of droplet distribution and emulsion stability, an optimum emulsion was selected for further investigation. The optimum emulsion consisted of JME 81%, WPO 15% and a mixed surfactant 4% by volume. This optimum emulsion was treated for removal of its acidity and this acid treated emulsion was used for further study. The process involved in the acid treatment of JOE15 emulsion is described in Chapter 3. The combustion, performance and emission parameters were evaluated in the diesel engine fueled with the acid treated JOE15 emulsion. The results were compared with those of diesel and JME operations.

4.9.4 Design of experiments

Before the start of experimental investigation, it needs a proper planning to obtain adequate, relevant and reliable data so that one can infer the science behind the observed phenomenon.

A Design of Experiment (DOE) is a systematic approach for investigation of a system or process. A series of structured tests are designed in which planned changes are made to the input variables of a process or system. The effects of these changes on a predefined output are then assessed. The DOE is important as a formal way of maximizing information gained, while minimizing the resources required. It allows a judgment on the significance to the output of input variables acting alone, as well input variables acting in combination with one another.

The DOE starts with identifying the input variables and the response (output) that is to be measured. For each input variable, a number of levels are defined that spans over the range for which the effect of that variable is desired to be known. An experimental plan is produced which tells the experimenter where to set each test parameter for each run of the test. The response is then measured for each run. It is very important to get the most information from each experiment performed. Well-designed experiments can produce significantly more information and often require fewer runs than what haphazard or unplanned experiments do require. In addition, a well-designed experiment also ensures significance of the effects that had been identified in the experiment at hand.

Engine experiments were conducted only with the ATJOE15 emulsion, at three different compression ratios (16.5, 17.5 and 18.5), and for each compression ratio, three nozzle opening pressures (200, 220, and 240 bar) and three injection timings (21.5, 23 and 24.5 ^{o}bTDC) were selected and conducted as per the full factorial design ($3^3 = 27$). Table 4.1 gives the full factorial design followed during the conduct of experiments.

Table 4.1 Full factorial design for experiments

Trial No.	Compression ratio	Injection timing	Nozzle opening pressure
1	16.5	21.5	200
2	16.5	21.5	220
3	16.5	21.5	240
4	16.5	23	200
5	16.5	23	220
6	16.5	23	240
7	16.5	24.5	200
8	16.5	24.5	220
9	16.5	24.5	240
10	17.5	21.5	200
11	17.5	21.5	220
12	17.5	21.5	240
13	17.5	23	200
14	17.5	23	220
15	17.5	23	240
16	17.5	24.5	200
17	17.5	24.5	220
18	17.5	24.5	240
19	18.5	21.5	200
20	18.5	21.5	220
21	18.5	21.5	240
22	18.5	23	200
23	18.5	23	220
24	18.5	23	240
25	18.5	24.5	200
26	18.5	24.5	220
27	18.5	24.5	240

4.9.4.1 Variation of compression ratio

The ATJOE15 emulsion was tested as three different compression ratios of diesel engine. There are several methods to change the compression ratio in a CI engine, they are as follows: [158-162]

a) Variation of combustion chamber volume
b) Moving the cylinder head
c) Variation of piston skirt height
d) Modification of the connecting rod geometry (by means of intermediate member)
e) Variation of effective stroke length (by moving the crankpin within the crankshaft)
f) Moving the crankshaft axis

In the present investigation, compression ratio was changed by changing the clearance volume by inserting gaskets of different thicknesses between the cylinder and cylinder head. Figures 4.11(a), 4.11(b) and 4.11(c) show the photographic views of changing the compression ratio and gasket.

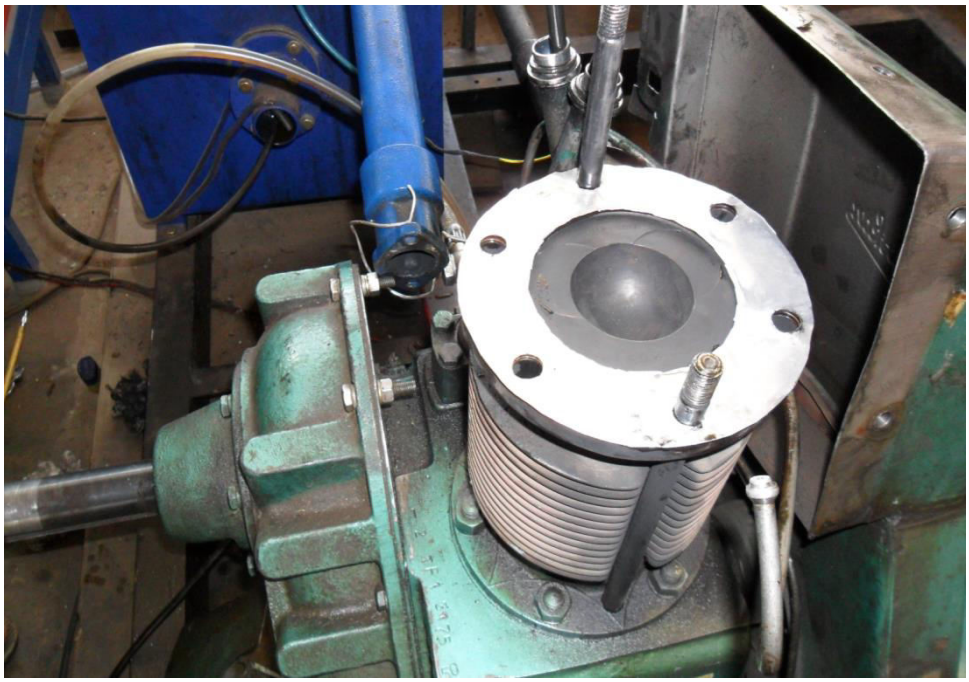

Fig. 4.11(a) Lower thickness gasket fitted with cylinder block

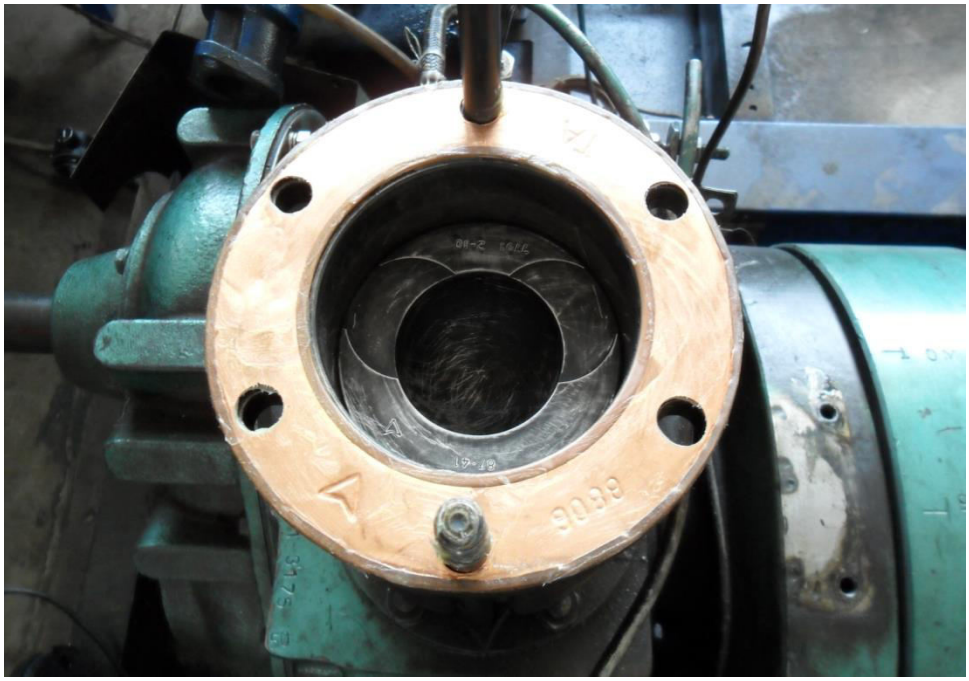

Fig. 4.11(b) Standard gasket fitted with cylinder block

Fig. 4.11(c) Cylinder head gasket

Compression ratios below 16.5 led to a poor power output, and ratios above 18.5 were not possible, due to engine structural constraints. For all settings, the emission values were recorded thrice and the mean of these was taken for comparison.

The steps involved in the compression ratio calculation are as follows:

Compression ratio = $\frac{\text{Maximum cylinder volume } (V_s+V_c)}{\text{Clearance volume } (V_c)}$

Maximum cylinder volume = Swept volume (V_s) + Clearance volume (V_c)

$V_s = \frac{\pi d^2}{4} \times l$

Where, d = bore = 8.75 cm, l = stroke = 11 cm

For standard compression ratio,

$CR = 17.5 = \frac{V_s+V_c}{V_c}$

$17.5 = \frac{V_s}{V_c} + 1$

$17.5 - 1 = \frac{V_s}{V_c}$

$V_c = \frac{V_s}{16.5} = \frac{661.45}{16.5} = 40.08\ cm^3$

Gasket volume = 7.21 cm^3 (d = 8.75 cm, t = 0.12 cm)

For CR = 18.5, $Vc = \frac{Vs}{17.5} = \frac{661.45}{17.5} = 37.79\ cm^3$

Clearance volume excluding gasket volume + Gasket volume = 37.79

32.87 + Gasket volume = 37.79

Gasket volume required for CR = 18.5 = 4.92 cm^3

Gasket thickness required = 0.08 cm

Similarly gasket volume and thickness required for CR = 16.5 was calculated.

The calculated gasket volume and thickness corresponding to the different compression ratios are given in Table 4.2.

Table 4.2 Gasket volume and thickness required for different compression ratios

Compression ratio	Gasket volume (cm^3)	Gasket thickness (cm)
16.5	9.8	0.16
17.5	7.21	0.12
18.5	4.92	0.08

4.9.4.2 Variation of injection timing

In order to change the fuel injection timings, it is required to adjust the fuel injection pump settings. By varying the number of shims under the fuel injection pump fuel injection timing was changed. To advance the fuel injection timing, the shims under the pump were removed and to retard additional shims were introduced under fuel injection pump. At standard injection timing, the number of shims placed under the pump was three. The thickness of the each shim is 0.3 mm. By removing one shim, about 1.5 ^{o}CA injection timing was advanced and by introducing additional shim will retard the timing by 1.5 ^{o}CA. Figure 4.12 shows the photographic view of the fuel pump with shim. Figure 4.13 shows the photographic view of the shim.

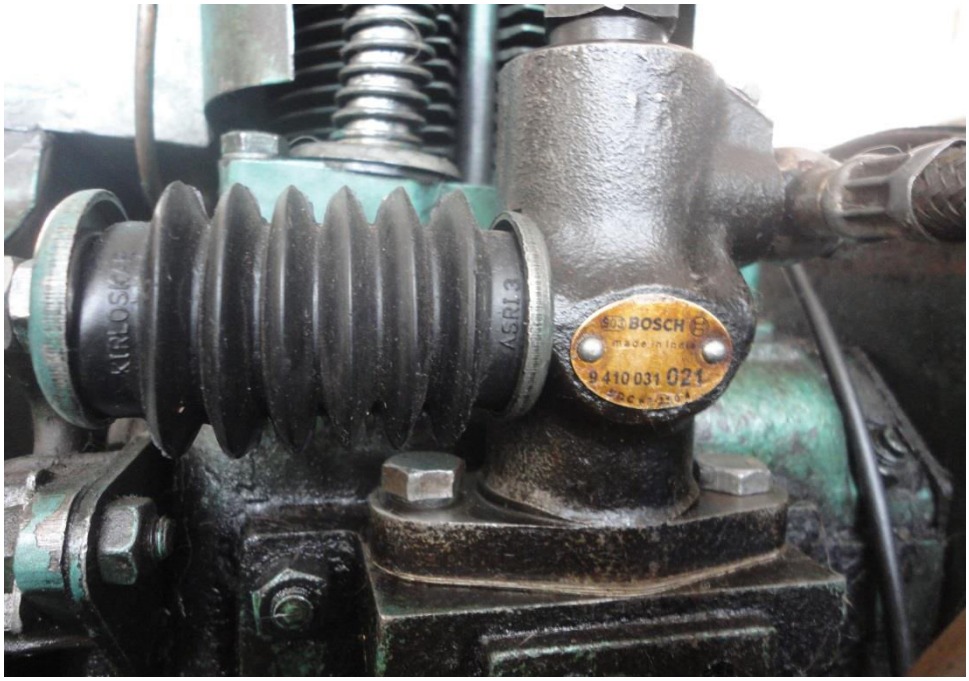

Fig. 4.12 Photographic view of the fuel pump with shim

Fig. 4.13 Photographic view of the shim

The experiments were conducted with one advanced injection timing (24.5 ^{o}CA bTDC) and one retarded injection timing (21.5 ^{o}CA bTDC) along with standard injection timing (23 ^{o}CA bTDC). Since, more retardation will leads to increase the smoke emission and more advancement will leads to increase the NO emission [163], our experiments were limited. The combustion, performance and emission parameters were studied in the diesel engine at all three injection timings, for variable compression ratios (16.5, 17.5 and 18.5) and for variable nozzle opening pressures (200, 220 and 240 bar). The study was conducted for entire load range (from no load to full load). After every set of experiments, engine was operated at standard conditions with diesel to ensure steady conditions.

4.9.4.3 Variation of nozzle opening pressure

The fuel injection strategy is an important parameter in diesel engines to optimize the combustion, performance and tailpipe emissions. An increase of fuel nozzle opening pressure was required to enhance the fuel atomization at the nozzle outlet, resulting in more distributed vapor phase, which improves mixing [164]. The nozzle opening pressure was varied by testing the injector assembly in a nozzle pressure tester, where, the spring tension of the injector needle with setting screw was varied to get different fuel nozzle opening pressures. Figure 4.14 shows a photographic view of the nozzle tester assembly. Figure 4.15 shows the dismantled view of the fuel injector.

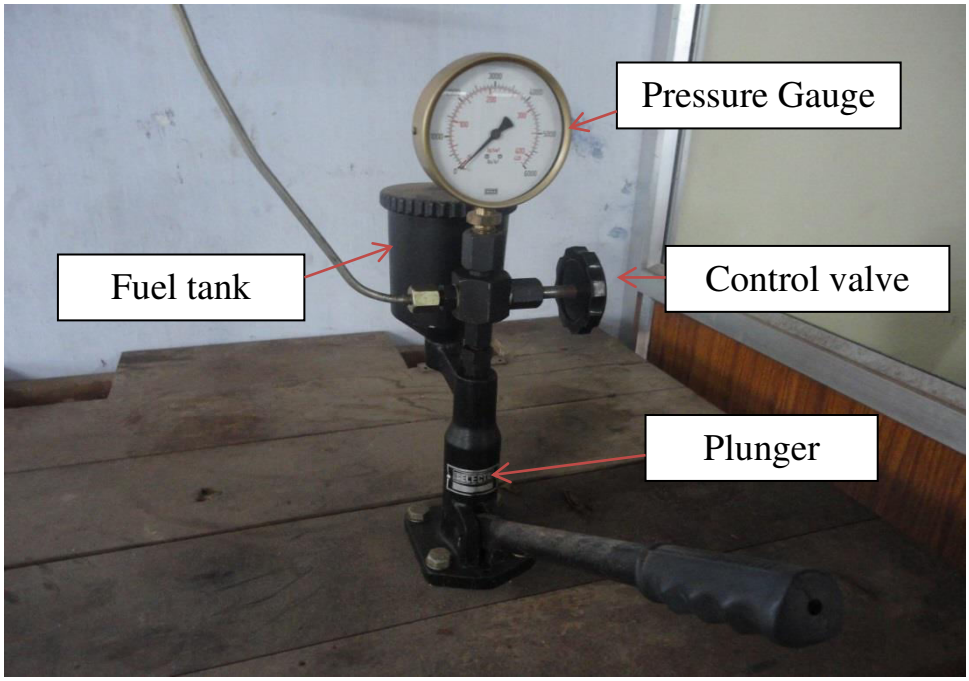

Fig. 4.14 Photographic view of the nozzle pressure tester assembly

Fig. 4.15 Dismantled view of the fuel injector

At standard injection timing (23 ^{o}CA bTDC), the nozzle opening pressure was varied from 200 bar to 220 bar and 240 bar and combustion, performance, and emissions characteristics were recorded from 0% to 100% load in steps of 25% load at a constant speed of 1500 rpm. The experiment was repeated for different injection timings of 21.5 ^{o}CA bTDC, 24.5 ^{o}CA bTDC and different compression ratios of 16.5, 17.5 and 18.5 for ATJOE15 fuel.

4.10 Uncertainty analysis

Uncertainty is a measure of the 'goodness' of a result. Without such a measure, it is impossible to judge the fitness of the value. An uncertainty or error analysis is necessary to establish the bounds on the accuracy of the estimated parameters. The evaluations of some unknown uncertainties from known physical quantities were obtained, using the following general equation [165].

$$\frac{U_Y}{Y} = \left[\sum_{i=1}^{n}\left(\frac{1}{Y}\frac{\partial Y}{\partial xi}\,U_{xi}\right)^2\right]^{1/2} \tag{4.22}$$

In the equation cited, Y is the physical parameter that is dependent on the parameters, xi. The symbol U_Y denotes the uncertainty in Y. As a result, the maximum uncertainty of the experiment obtained was ±2.1%. Table 4.3 gives the instruments used in the present study and their uncertainties. The sample calculations involved in determining the uncertainty of the crank angle encoder are given in Annexure 7.

Table 4.3 Range, accuracy and uncertainty of the instruments

S.No	Instrument	Range	Accuracy	Uncertainty
1.	Load indicator	250-6000W	±10W	0.2
2.	Temperature indicator	0-900	±1 ^{o}C	0.1
3.	Burette	1-30cc	±0.2 cc	1.0
4.	Speed sensor	0-10,000 rpm	±10rpm	0.1
5.	Exhaust gas analyser	NO-0-5000 ppm	±50ppm	1
		HC-0-20000 ppm	±10ppm	0.5
		CO-0-10%	0.03%	1
6.	Smoke meter	0-100%	±1 %	1
7.	Pressure transducer	0-110bar	±0.1bar	0.15
8.	Crank angle encoder	0-720	±1^{o}	0.3298

4.11 Endurance tests

4.11.1 Short term endurance test

The main objective of the endurance test was to evaluate the wear characteristics of engine components and changes in lubrication oil properties of test engine fueled with the ATJOE15 emulsion. Short term endurance test was conducted with the ATJOE15 emulsion as per

IS 10000 Part V – 1980 method for 100 hrs. Before the start of the durability test, the existing fuel injection pump, fuel injector, fuel filter, oil filter were replaced with new one as recommended by the engine manufacturer. Before fitting in the engine, the fuel injector and fuel injection pump were dismantled completely and photographs were taken in order to compare the wear and deposits on them after the durability test. The used lubricating oil was drained completely and fresh lubricating oil of SAE 20-40 grade was filled in the oil sump up to its full capacity. The engine cylinder head was dismantled and the carbon deposits on the cylinder head, piston crown were completely cleaned using methanol. The cylinder head gasket was also changed with new one and the cylinder head was fitted in the engine block. Once the engine was reassembled, it was allowed to run-in for 12 hours in the manner recommended by the manufacturer. This test was carried out to take care of any misalignments occurring during dismantling and re-assembling of the engine.

4.11.1.1 Preliminary run for constant speed engine

The purpose of preliminary run on engine is to ensure that, the engine should run trouble free, by operating both the engines for their running-in period. Under the preliminary run, constant speed engine is subjected to a preliminary run of 49 hours at the rated speed under the operating temperature specified by the manufacturer, in non-stop cycles of seven hours each, given in Table 4.4. During the preliminary run, attention was paid to engine vibration and quietness. It was ensured that the temperature of the lubricating oil reached within 5^{o}C before starting the next cycle.

Table 4.4 Preliminary run pattern of a constant speed engine

Load (Percent of rated load)	Running time (hours)
25	1.5
50	2
75	1.5
100	2

Figure 4.16 shows the photographic view of the dismantled engine before the start of endurance test.

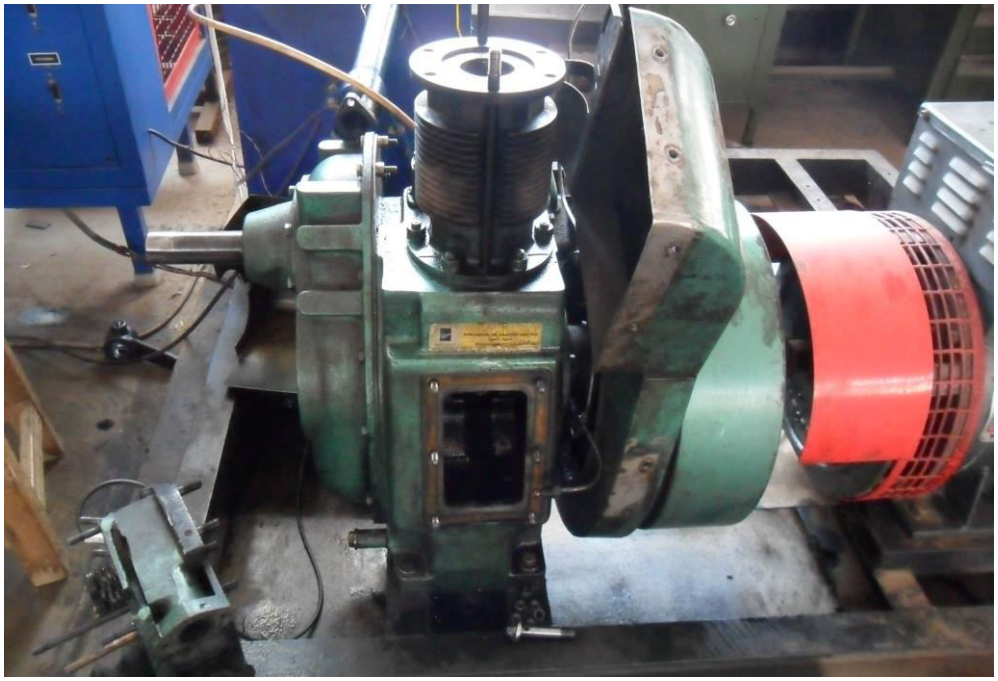

Fig. 4.16 Photographic view of the dismantled engine before endurance test

4.11.1.2 Long term test for constant speed engine

Then the engine is subjected to undergo the long term endurance test (load test) recommended by IS standard 10000 for 32 cycles (each of 16 hours continuous running) at rated speed. But, due to the limited availability of WPO and biodiesel fuels, it was proposed to conduct the short term endurance test comprising 3 cycles only. The test cycle followed is specified in the Table 4.5.

Table 4.5 Test cycle for long-term endurance test

Load (Percent of rated load)	Running time (hours)
100	4
50	4
100	1
No load	0.5
100	3
50	3.5

In this investigation, the short term endurance test was conducted using the ATJOE15 emulsion, and at the end of each 16-hour cycle, the engine was stopped and necessary

servicing, and minor adjustments were carried out in accordance with the manufacturer's schedule. Before starting the next cycle, it was ensured that the temperature of the engine sump oil had reached within 5K of the room temperature. The lubricating oil samples were collected from the engines after every 30 hours (from preliminary run onwards) for conducting various tribological studies. In the entire range of engine operation spread around 100 hours, there was no major breakdown noticed. After completion of the short-term endurance test, the engine was completely disassembled and the deposit formations on cylinder head, piston top, and injector tip were investigated.

4.12 Lubrication oil analysis

The lubrication oil used in the diesel engine picks up the wear debris of various metals depending on the origin. The quantitative evaluation of wear particles present in oil gives the magnitude of engine component deterioration and while qualitative analysis indicates its origin, i.e., wearing component. This ultimately provides adequate information about the components that are deteriorated and the incipient failure of the machine. A careful observation at the literature reveals that, the various contaminant metals present in lube oil might have various possible sources in the engines.

4.12.1 Determination of ash content

The lubricating oil samples were taken in a silicon crucible and kept in the furnace at 450°C for 4 hours and then 600°C for 2 hours to produce ash. The residual ash contains the wear debris of metal primarily. By weighing the crucible before and after the test, the weight percentage of ash was determined.

4.12.2 Atomic Absorption Spectroscopy (AAS) test

The AAS works on the principle of absorption interaction, where atoms in the vapor state absorb radiation at a certain wave length that are well defined and show the characteristics of a particular atomic element. In this process, the source of radiation projects a beam of a specific wavelength through a pure flame (air-acetylene) on to a sensor and the amount of radiation arriving at the photo sensor is recorded. The fluid sample is introduced into the flame and vaporized. The amount of radiation arriving at the photo sensor is reduced in proportion to the quantity of the specific element present in the sample. Hence, various elements such as Fe, Cu, Zn, Cr, Mg, Co, and Pb were analyzed by AAS and the results are discussed in Chapter 5.

This AAS test was conducted to evaluate the concentration of various metals present in the lubricating oil samples from the ATJOE15 emulsion fueled CI engine. This gave a fair idea about the wear of different parts, material compatibility of the new fuel with the existing engines. In the present study, since many sliding components were involved, it was anticipated that the wear debris originating from different metallic parts appeared in the lubricating oil.

The procedure followed is explained in the following steps:

a) Approximately 10 grams of oil sample was weighed in the silica crucible and burnt at 450°C for 4 hours and at 650°C for 2 hours.
b) The ash was dissolved in concentrated HCl acid.
c) The mixture was diluted with distilled water to make 100 ml solution.
d) Standard solutions of various metals (concentrations ranging from 5 ppm to 20 ppm) were prepared.

CHAPTER 5

RESULTS AND DISCUSSION

5.1 Parametric studies on the combustion, performance and emissions with JME-WPO emulsions

5.1.1 General

This chapter presents the results and discussion on the experimental investigations carried out in a 4.4 kW, single cylinder, four stroke, air cooled, direct injection (DI) diesel engine running on different JME-WPO emulsions. The WPO percentage was varied from 5% to 15% at regular intervals of 5% in the emulsions on a volume basis. The notations followed for the emulsions can also be referred to in Table 3.8, which is given in Chapter 3. In this investigation, the results associated with the JME-WPO emulsions containing 5% and 10% WPO in them, did not show much variation. Therefore, only the results associated with all the JME-WPO emulsions which contain 15% WPO in them are discussed in this chapter, for better understanding and clarity. The relevant results are published in reputed journals which are given in Annexure.

Further, from the comparative analysis on the performance, combustion and emission characteristics, consideration of the droplet distribution, emulsion stability and droplet size, an optimum emulsion was selected for further investigation. This optimum emulsion was chosen for the removal of its acidity, and this acid treated emulsion (ATJOE15) was used for further study. A full factorial (L27) design was prepared for conducting the experiments, with engine modifications such as varying compression ratio, injection timing and nozzle opening pressure, which is already given in Chapter 4. Further, the results obtained for the combustion and emission characteristics of an engine fueled with the ATJOE15 emulsion, were validated with the help of two zone modeling. This chapter also presents the results obtained for the short term endurance test, conducted on the same engine with the ATJOE15 emulsion.

5.1.2 Combustion parameters

5.1.2.1 Pressure-crank angle diagram

The pressure crank angle diagram at full load for different emulsions with 15% WPO, obtained with the help of six different surfactants, is depicted in Fig. 5.1.1. In diesel engines, the maximum cylinder pressure depends on the combustion rate in the initial stages, which is influenced by the fuel involved in the uncontrolled combustion phase. This premixed

combustion phase is governed by the delay period, spray envelop, and the air fuel mixture preparation during the delay period [49].

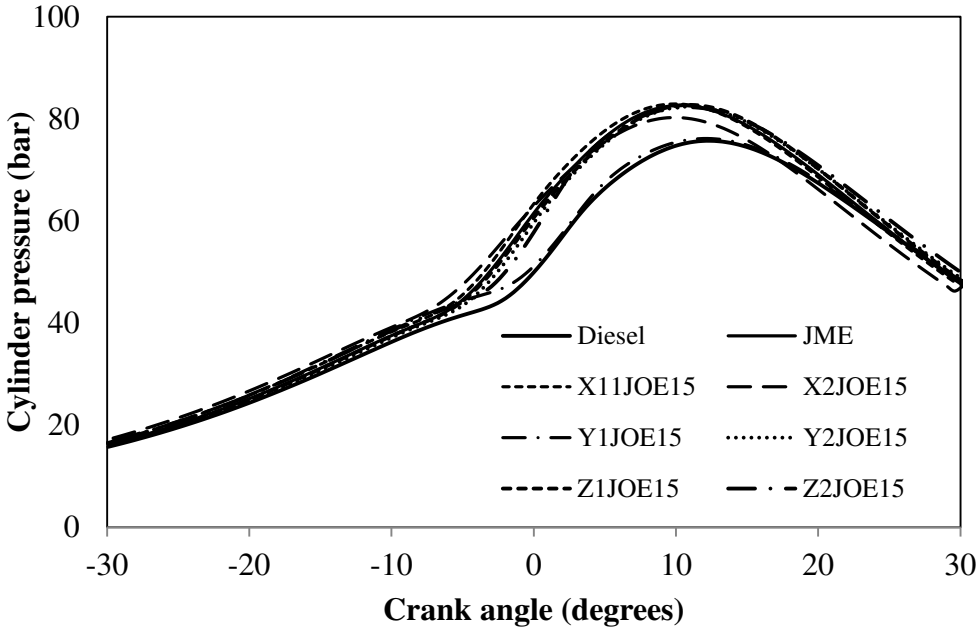

Fig. 5.1.1 Pressure-Crank angle diagram at full load for different emulsions with 15% WPO

The start of fuel injection (SOI) is set at 23 ^{o}CA bTDC. The change in the slope of the pressure-crank angle curve gives the start of combustion approximately [155]. With 15% WPO in the emulsions, the start of ignition for all the emulsions are found to be earlier, which is in the range between 0.5 ^{o}CA and 2.9 ^{o}CA, than that of diesel at full load. It is also found to be earlier by 0.3 ^{o}CA in the case of the X1JOE15 emulsion, whereas other JME-WPO emulsions exhibit a later start of combustion in the range of 0.3 to 2 ^{o}CA, compared to that of JME operation. The JME-WPO emulsions with 15% WPO in them resulted in a higher maximum cylinder pressure in comparison with diesel at full load. This may be due to the higher BSFC, cetane number, boiling point, oxygen content, and advance in the start of the injection (SOI) timing. In this regard, similar reasons have been reported by Ozsezen et al. [23], using biodiesel from waste palm oil methyl ester (WPOME) and canola oil methyl ester (COME).

5.1.2.2 Ignition delay

The variations of ignition delay with different loads for all the emulsions investigated in this study, which contain 15% WPO in them, are shown in Fig. 5.1.2. A group of parameters, such as the fuel type, fuel quality, air-fuel ratio, engine speed, quality of fuel atomization,

intake air temperature, and pressure, influence the ignition delay [166]. It is apparent from the figure that, the ignition delay is found to decrease with an increase in the engine load.

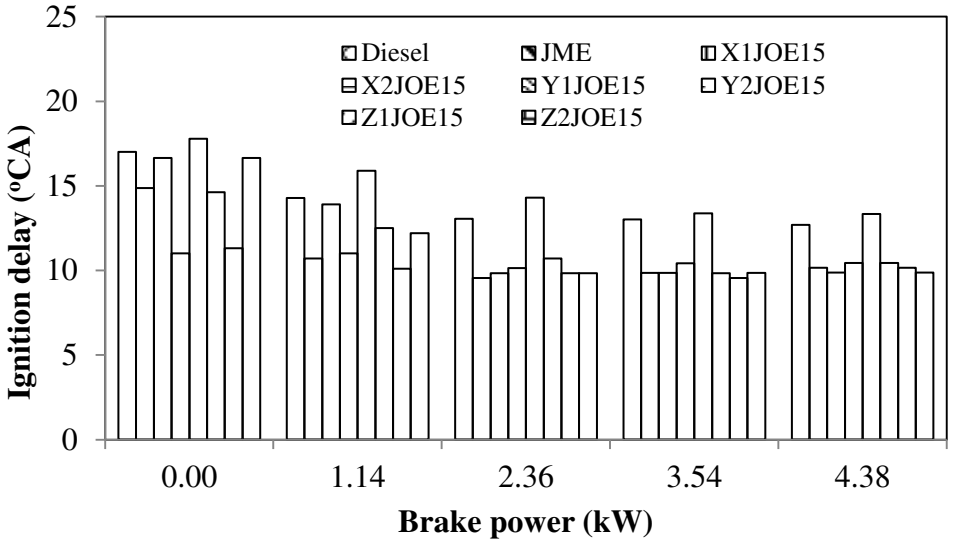

Fig. 5.1.2 Variation of ignition delay with brake power for different emulsions with 15% WPO

This reduction might be the result of higher combustion chamber wall temperature at the time of injection, and reduced exhaust gas dilution. A similar result was reported by Canacki [107], when he carried out experiments with biodiesel fuel in a single cylinder, four stroke, DI diesel engine. It can be observed from the figure that, there is a reduction in the ignition delay for all the emulsions, which contain 15% WPO in them; this is attributed to their quick evaporation rate, improved ignition properties, and enhanced surface area/volume ratio characteristics. A similar result was also obtained by Sadiq basha and Anand [150], in their investigation with nano additive blended biodiesel emulsion fuel in a single cylinder, four stroke, DI diesel engine. For the WPO percentage of 15% in the emulsion, the ignition delay decreases by about 2.3 ^{o}CA to 2.7 ^{o}CA compared to that of diesel, while it is shorter in the range of 0.1 ^{o}CA to 0.3 ^{o}CA for the Z1JOE15, X1JOE15 and Z2JOE15 emulsions, and in the remaining cases, the ignition delay is found to be longer by about 0.1 to 3.1 ^{o}CA, compared to that of the JME operation.

5.1.2.3 Heat release rate

The heat release rate is one of the parameters of a fuel in a CI engine, which is helpful to predict the emission behavior. The maximum heat release depends on the delay period, mixture formation and combustion rate. Figure 5.1.3 illustrates the heat release patterns at full

load, with respect to the crank angle of the engine fueled with different JME-WPO emulsions, which contain 15% WPO in them. The occurrences of maximum heat release rate for the emulsions which contain 15% WPO, are on an average shifted by about 4.4 ^{o}CA at full load. The intensity of the premixed combustion phase for diesel is found to be the highest, whereas, it is lower in the case of JME and the JME-WPO emulsions. The deviation in the maximum heat release rate between the JME operation and all the JME-WPO emulsions is in the range between-2.35 J/^{o}CA to 5.3 J/^{o}CA.

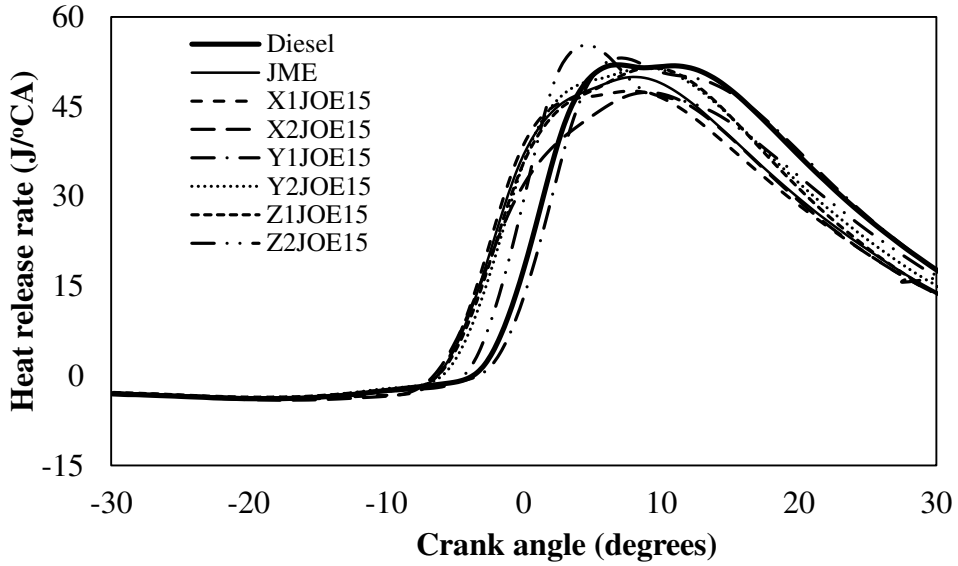

Fig. 5.1.3 Variation of heat release rate with crank angle at full load for 15% WPO emulsions

It is also seen that the quantity of diffusive combustion is found to be shorter for JME and the 15% WPO emulsions in comparison with diesel operation, due to their faster burning characteristics. The oxygen present in JME and the quick evaporating nature of the JME-WPO emulsions are the causes for the faster burning process.

5.1.2.4 Maximum cylinder pressure

Figure 5.1.4 depicts the variation of maximum cylinder pressure with brake power for all the fuels tested in this study. The maximum cylinder pressure depends on the amount of fuel taking part in the uncontrolled phase of combustion. It is seen that the peak cylinder pressure is increased with an increase in the engine load as expected. At no load and 50% load conditions, the peak cylinder pressures of the emulsions with 15% WPO are almost comparable with those of the JME operation.

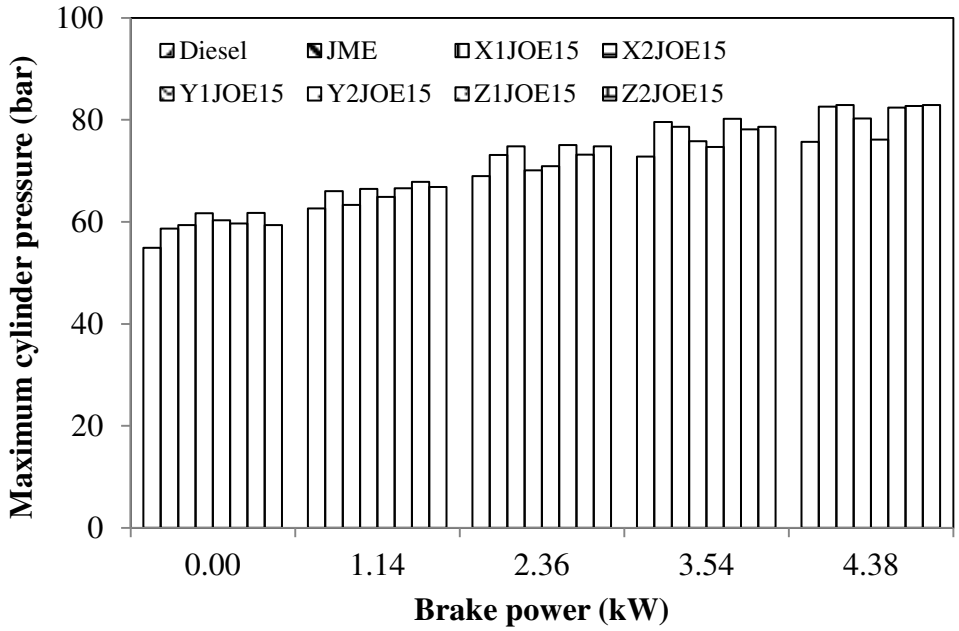

Fig. 5.1.4 Variation of maximum cylinder pressure with brake power for 15% WPO emulsions

All the emulsions with 15% WPO revealed a higher maximum cylinder pressure in comparison with diesel and the JME, at full load. This is due to the advanced combustion process being initiated by the easy flow-ability of biodiesel, and its other relevant physical properties. Similar results have been reported by Tesfa et al. [167] in their work. The deviation in the maximum cylinder pressure values between diesel and all the emulsions is in the range between 0.4 bar to 7.2 bar at full load, while it is in the range between -6.5 bar and 0.3 bar, in comparison with the JME.

5.1.2.5 Mass fraction burned

The variations of mass fraction burned with the crank angle for the diesel, JME and JME-WPO emulsions at full load are given in Fig. 5.1.5. It can be observed from the figure that the 10% and 50% mass fraction burned for all the emulsions which contain 15% WPO in them, seems to be sooner than that of diesel at full load. The 10% and 50% mass fraction burned varies with a minimum difference of 2 ^{o}CA to a maximum of 3 ^{o}CA for the emulsions from that of diesel. The crank angles at which the 90% mass fraction burned, varies with a minimum difference of 1.5 ^{o}CA to a maximum of 4 ^{o}CA, than that of diesel at full load. For the same crank angle values, the mass fraction burned of JME-WPO emulsions which contain 15% WPO in them, is marginally higher than that of diesel at full load. The reason is that,

with addition of the WPO causes reduction in viscosity of the JME-WPO emulsions, and improves the vaporization and atomization, and hence shows better mixing with air.

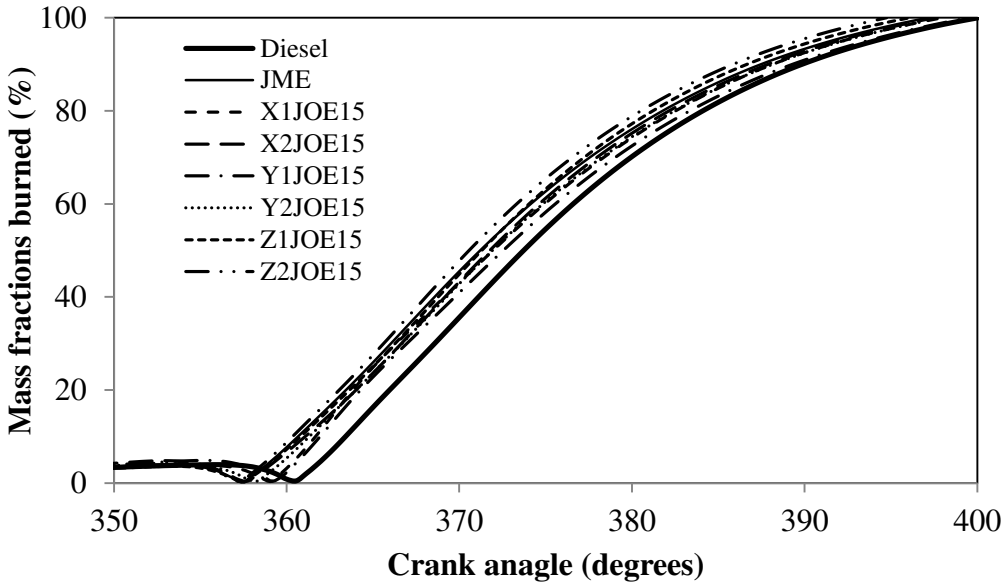

Fig. 5.1.5 Variation of mass fraction burned with crank angle at full load for 15% WPO emulsions

In addition, the presence of water in the WPO may lead to the secondary atomization (microexplosion) of the fuel, and result in more complete combustion and rapid heat release. Similar reasons are mentioned by Sadiq Basha and Anand [150] after their investigation using carbon nanotubes blended water-diesel emulsion as a fuel in a diesel engine.

5.1.2.6 Combustion duration

Figure 5.1.6 depicts the variation in the combustion duration with brake power for diesel, JME and JME-WPO emulsions. The crank angle duration of the 10% mass burned to 90% mass burned, has been taken as the combustion duration. The combustion duration increases with engine load owing to the increase in the fuel quantity. The combustion duration for all the emulsions which contain 15% WPO in them, seems to be lower than that of diesel at low loads. At full load condition, the combustion duration is found to be lower with a minimum of 0.3 ^{o}CA to a maximum of 2.2 ^{o}CA for the emulsions, compared to that of diesel. This may be due to the faster combustion rate in the premixed burning phase and shorter mixing-controlled combustion phase, resulting in a decrease of the total combustion duration of the emulsions at medium and high engine loads. The results are in agreement with those of Qi et al. [168], when they conducted experiments in a DI diesel engine fueled with ethanol-biodiesel-water micro emulsions. The micro explosion phenomenon further accelerates the

diffusion combustion, and decreases the total combustion duration in the case of emulsions. Similar reasons have been reported by Senthil kumar et al. [169], during their experiments in a single cylinder, DI diesel engine fueled with animal fat emulsions.

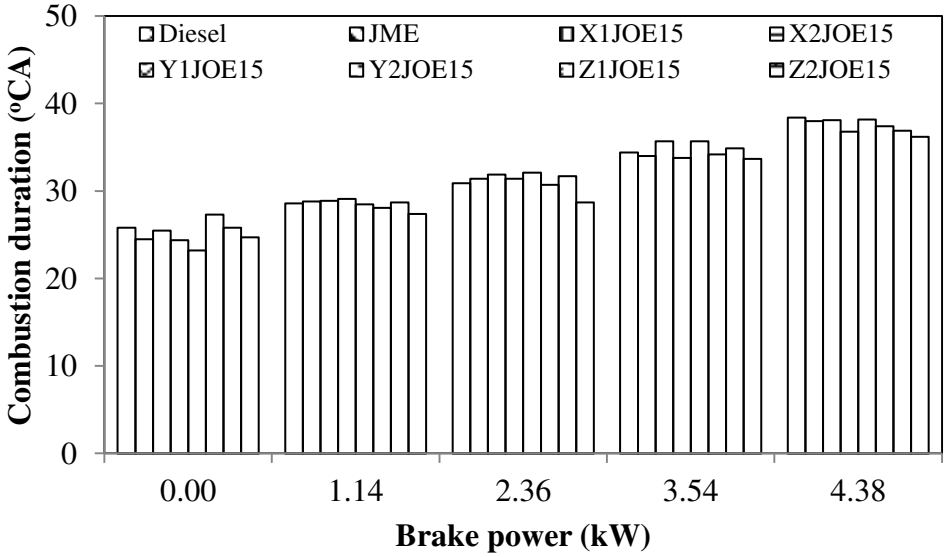

Fig. 5.1.6 Variation of combustion duration with brake power for 15% WPO emulsions

The observed shorter combustion duration may result from 15% WPO emulsions exhibiting a faster diffusion burn rate than that of diesel at full load. This is evidenced in the mass fraction burned curves, where initially the JME-WPO emulsions and diesel may have similar burn rates, but eventually diesel's burn rate slows, as its combustion becomes predominantly diffusive. A similar behavior is also observed by Mueller et al [117].

5.1.3 Performance parameters

5.1.3.1 Brake thermal efficiency

The brake thermal efficiency indicates the effective thermal energy utilization in an engine. The variation of the brake thermal efficiency with load for all the emulsions which contain 15% WPO in them, JME and diesel are depicted in Fig. 5.1.7. The brake thermal efficiency increases with an increase in load, as a result of the increase in the cylinder temperature. The brake thermal efficiency of all the emulsions which contain 15% WPO in them is found to be higher by about 3.9% to 11.3%, compared to that of diesel at full load. The brake thermal efficiency is higher by about 1.6% to 11.8% for all the emulsions in comparison with the JME at full load. The maximum thermal efficiency of 11.3% is noticed with the Z2JOE15 emulsion compared to all other emulsions tested in this study.

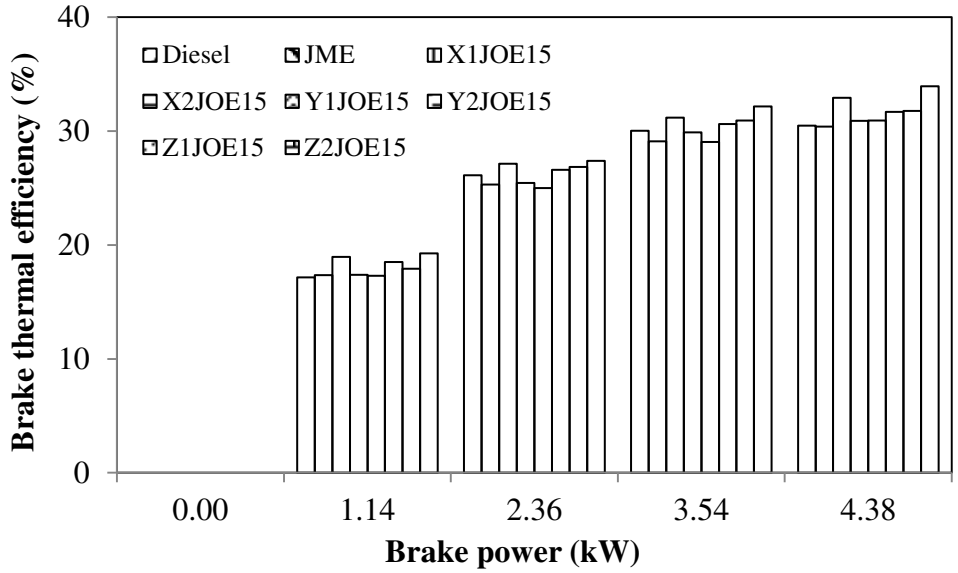

Fig. 5.1.7 Variation of brake thermal efficiency with brake power for 15% WPO emulsions

The higher densities of 15% WPO emulsions yield to earlier injection than that of diesel. Also the JME-WPO emulsions exhibit shorter ignition delay in comparison with diesel, and therefore, the beginning of the heat release is noticed earlier than that of diesel. From this point of view, the combustion itself is faster for the JME-WPO emulsions, which gives increased brake thermal efficiency. Similar reasons are reported by Armas et al. [170] during their experiments with water diesel emulsified fuel in a light duty diesel engine. Another reason may be the additional oxygen molecule available in the 15% WPO emulsions, which takes part in the combustion leading to complete combustion. Similar reasons are reported by Agarwal et al. [171] after their experiments in a diesel engine fueled with vegetable oil.

5.1.3.2 Brake specific fuel consumption

The variation of brake specific fuel consumption with brake power for diesel, JME and JME-WPO emulsions are depicted in Fig. 5.1.8. The brake specific fuel consumption (BSFC) is the ratio between the mass of fuel consumption and the brake power. For the emulsions which contain 15% WPO in them, the differences in the BSFC values are found to be higher by an average of 20% compared to that of diesel at full load. Among all the JME-WPO emulsions, the Z2JOE15 emulsion recorded the lowest specific fuel consumption, which is about 15% higher than that of the diesel consumption.

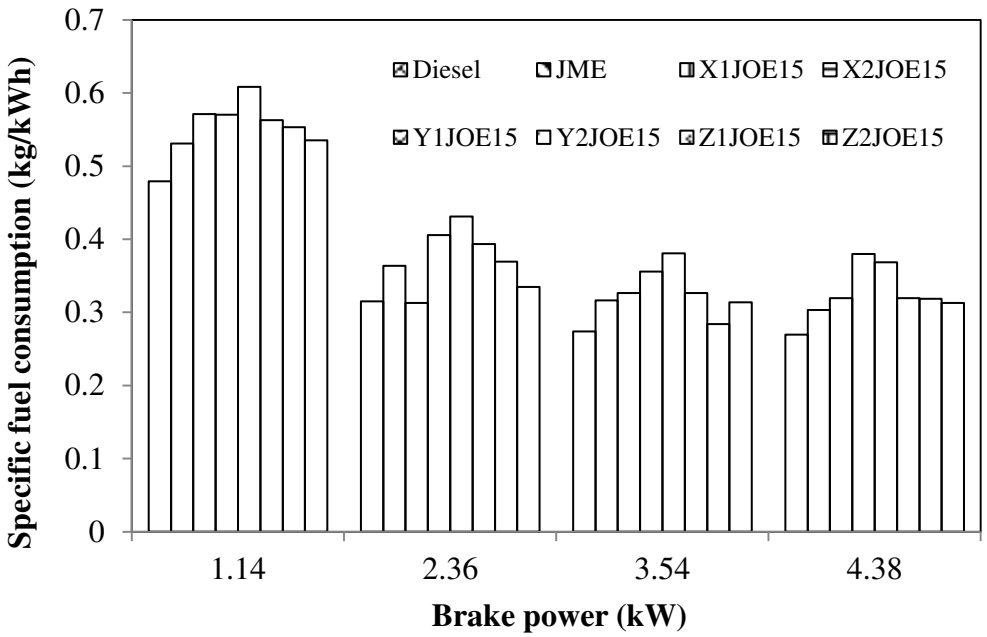

Fig. 5.1.8 Variation of brake specific fuel consumption with brake power for 15% WPO emulsions

The higher BSFC values of JME and its emulsions with WPO are attributed to the fact that more amount of fuel is required by the engine to generate the same power, when the calorific value of the fuel is low.

5.1.3.3 Exhaust gas temperature

The variation of exhaust gas temperature with load for all the emulsions which contain 15%, WPO in them and diesel are depicted in Fig. 5.1.9. It is found that the exhaust gas temperature increases with load for all the fuels. At full load, the exhaust gas temperatures of all the emulsions which contain 15% WPO in them, are found to be higher by an average of 40 ^{o}C compared to that of diesel.

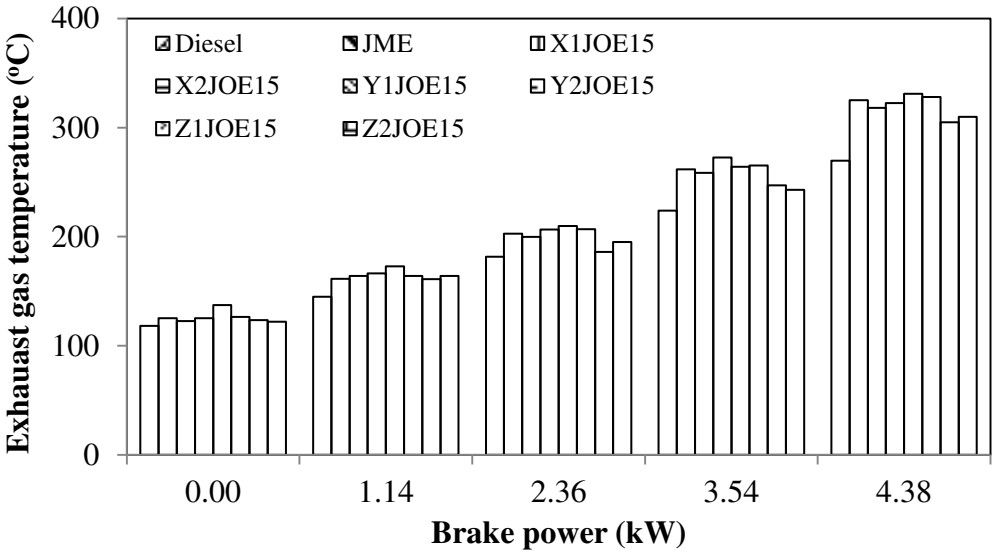

Fig. 5.1.9 Variation of exhaust gas temperature with brake power for 15% WPO emulsions

The water content present in the WPO gets vaporized during the combustion process and absorbs the heat energy which decreases the local adiabatic flame temperature. This result in a reduction in the exhaust gas temperature of 15% WPO emulsions compared to that of JME operation. This is in agreement with the results reported by Bertoli *et al.,*[146] when the WPO blends or emulsions were used as fuels in a diesel engine.

5.1.4 Emission parameters

5.1.4.1 BSHC emissions

The variations of brake specific HC emissions with brake power for different emulsions with 15% WPO are depicted in Fig. 5.1.10. The HC emissions are found to be lower in CI engines, because they always operate with excess air. It is observed from the figure that the BSHC emissions decrease with an increase in the engine load. Compared to diesel operation, the JME and 15% WPO emulsions, exhibit lower BSHC emissions, which may be due to the higher oxygen content of JME that leads to more complete burning than that of diesel operation. Similar reasons are given for lower HC emissions by *Xue et al* [172] in a review article on biodiesel emissions. With 15% WPO in the emulsion, the percentage differences in the HC emissions are noticed from 11.3% to 45.8% compared to that of diesel operation, and 9.6% to 44.8% lower compared to that of the JME operation are noticed.

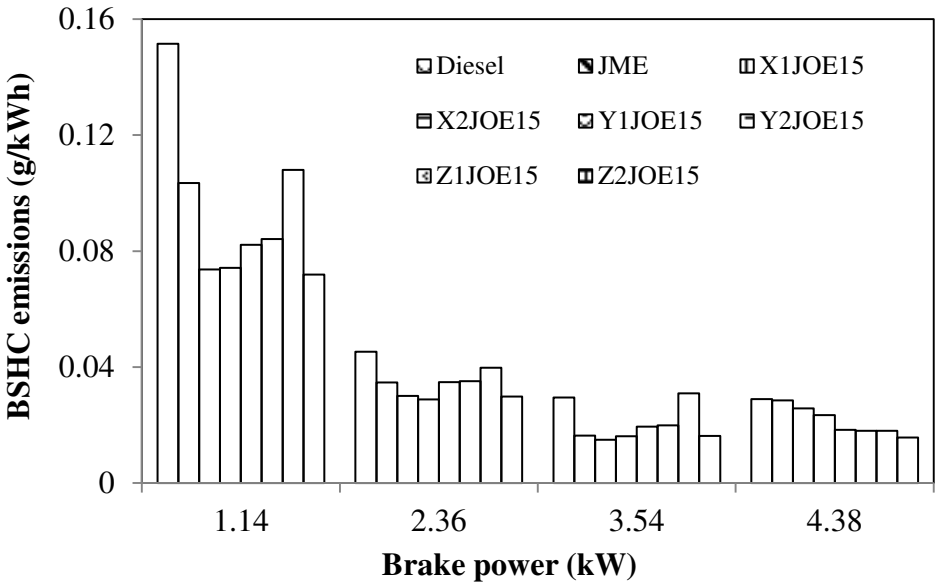

Fig. 5.1.10 Variation of BSHC emission with brake power for 15% WPO emulsions

5.1.4.2 BSCO emissions

Figure 5.1.11 illustrates the variation of brake specific CO emissions with brake power for disel, JME and 15% WPO emulsions, prepared with six different surfactants. Generally, the CO emissions are formed as a result of the incomplete combustion of fuel. However, if the combustion is complete, then the CO will be oxidized into CO_2. Usually, the CO emission of diesel engines is low, because diesel combustion occurs with a lean mixture. Also, the higher combustion temperature accelerates the oxidization rate of CO to form CO_2, and thus results in less CO in the exhaust gases of the engine [173]. The BSCO emissions are found to decrease with an increase in the engine load, due to the increase of the in-cylinder gas temperature. It is reported that the CO emissions are lower with the biodiesel operation, due to the higher oxygen content and lower carbon to hydrogen ratio compared to that of diesel. This reason is supported by Xue *et al.* [172], in their review article on biodiesel emissions. With the WPO percentage of 15% in the emulsion, the differences in the CO emissions are noticed to be from 43.8% to 68.9%, compared to that of diesel at full load.

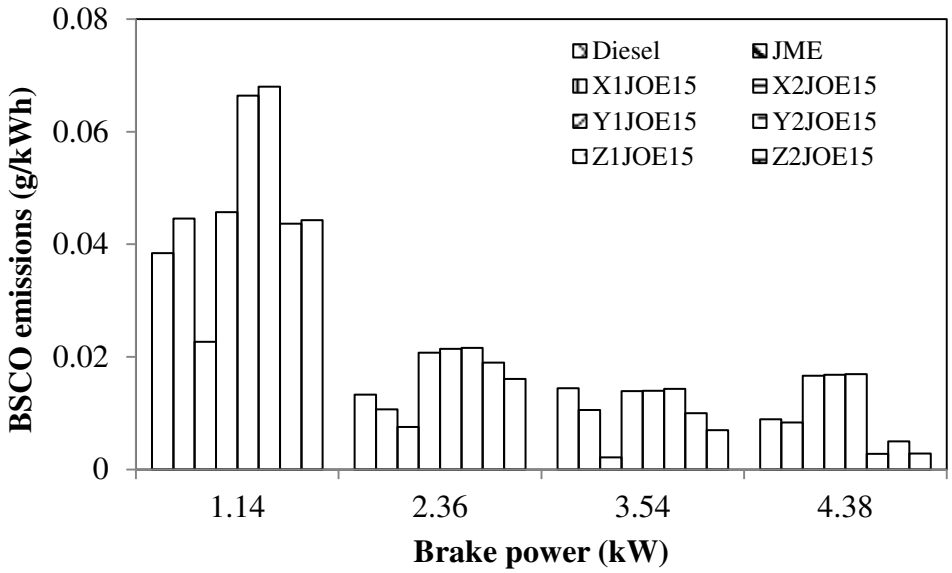

Fig. 5.1.11 Variation of BSCO emission with brake power for 15% WPO emulsions

This may be due to the lower carbon content for the JME-WPO emulsions, compared to that of the JME. Similar observations are reported by Karabektas [174] and Lin and Lin [175], on their experiments with biodiesel. Higher CO emissions are observed with the X1JOE15, X2JOE15 and Y1JOE15 emulsions, which are attributed to poor mixture preparation.

5.1.4.3 BSNO emissions

The variation of brake specific NO emissions with brake power for all the emulsions which contain 15% WPO in them, are shown in Fig. 5.1.12. Two predominant factors affect the formation of NO in CI engines; they are; i) the availability of oxygen and ii) in cylinder temperature. The presence of the oxygen molecule in JME causes an increase in the combustion gas temperature, resulting in a marginal increase in NO emissions. This statement is in agreement with that of Nabi *et al.* [176] during their study on engine emissions, when fueled with karanja biodiesel. At elevated flame temperatures, this oxygen reacts with nitrogen and tends to form NO. The BSNO emissions of the JME operation are higher by 41% compared to that of diesel at full load. The BSNO emissions of JME-WPO emulsions are found to be lower than that of JME, but higher than that of diesel operation. For all the emulsions, the NO emissions are found to be lower in the range between 9.5% and 16.8%, compared to that of JME operation. This may be due to the water content present in the WPO, which will reduce the combustion temperature. Similar reasons were reported by Bertoli *et al.* [146] for lower combustion temperature and NO emissions.

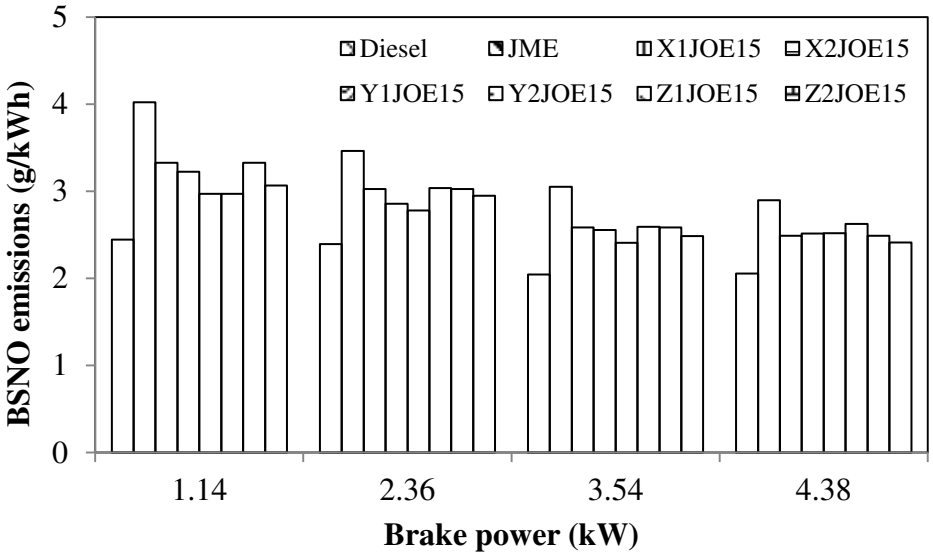

Fig. 5.1.12 Variation of BSNO emission with brake power for 15% WPO emulsions

5.1.4.4 Smoke opacity

Figure 5.1.13 depicts the variation of smoke opacity for diesel, JME and the JME-WPO emulsions at different loads.

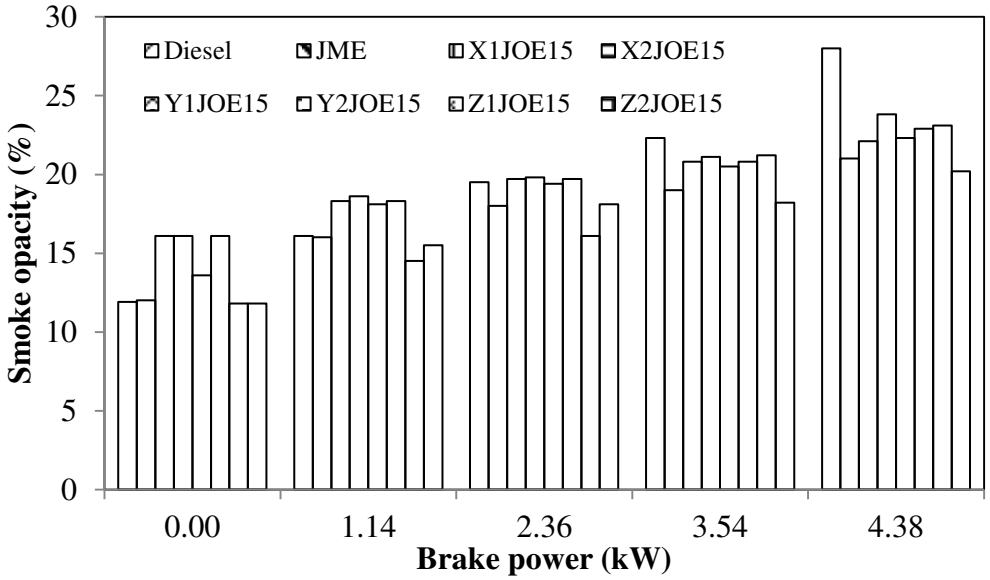

Fig. 5.1.13 Variation of smoke opacity with brake power for 15% WPO emulsions

Soot formation mainly takes place in the fuel-rich zone at high temperature and pressures, specifically within the core region of each fuel spray. The smoke opacity is found to be lower with all the emulsions with 15% WPO, in comparison with that of diesel and JME operations. The reason for the reduction in smoke opacity can be explained by the fact that the oxygenated fuels effectively deliver oxygen to the pyrolysis zone of the burning spray. The same reason is supported by McCormick and Parish [177], and Wang et al. [114], in their

study on biodiesel emissions. The reduction in smoke for all the emulsions investigated in this study is in the range of 15%, to 27.8%, compared to that of diesel at full load.

The summary of the values on the combustion, performance and emission parameters at full load for different emulsions, which contain 5%, 10% and 15% WPO in them, are given in Table 5.1.

5.1.5 Closure

It is summarized that the engine was able to run with a maximum of 15% WPO, in the form of emulsions with the JME. The combustion starts earlier in the case of all the JME-WPO emulsions compared to that of diesel and the JME. The maximum thermal efficiency is noticed with the Z2JOE15 emulsion, compared to all other emulsions tested in this study. The thermal efficiency of Z2JOE15 is found to be higher by about 11.3% compared to that of diesel. Lower HC, CO and smoke emissions are noticed with the Z2JOE15 emulsion, compared to that of diesel operation. The NO emissions for all the emulsions are found to be lower than that of JME operation, but higher than that of diesel operation. The maximum reduction in the nitric oxide emission of 16.8% is observed with the Z2JOE15 emulsion, compared to that of JME operation. Overall, by considering the combustion, performance and emission parameters, it can be concluded that the Z2JOE15 showed a better performance and lower emissions compared to those of diesel and the JME operations.

Table 5.1 Summary of values on combustion, performance and emission parameters at full load for different emulsions which contain 5%, 10% and 15% WPO

Sl.No	Parameter	Diesel	JME	X1JOE5	X2JOE5	Y1JOE5	Y2JOE5	Z1JOE5	Z2JOE5
A.	***Combustion parameters***								
1.	Start of ignition (^{o}CA)	356.6	354	354.8	353.7	357.5	354.2	353.7	354.8
2.	Occurrence of maximum pressure (^{o}CA)	372.4	370.4	370.9	370.7	373.6	370.3	371.3	370.8
3.	Ignition delay (^{o}CA)	12.7	10.2	10.4	9.9	14.1	9.9	9.8	10.4
4.	Occurrence of maximum heat release (^{o} CA aTDC)	6.7	8.2	4	9.1	12.5	4	10.2	4
5.	Maximum heat release (J/^{o}CA)	52.02	49.97	50	49.38	50.65	50.45	53.52	49.86
6.	Maximum cylinder pressure (bar)	75.70	82.61	82.9	80.2	76.1	82.4	82.7	82.9
7.	90% Mass fraction burned (^{o}CA)	389.9	387.5	386.9	387.2	388	387.4	388.5	386.6
8.	Combustion duration (^{o}CA)	38.4	38	38	36.7	37.7	37.8	36.8	37.2
B.	***Performance parameters***								
9.	Brake thermal efficiency (%)	30.4	30.3	30.6	30.0	31.3	31.4	30.9	31.4
10.	Specific fuel consumption (kg/kWh)	0.269	0.302	0.294	0.314	0.299	0.299	0.328	0.266
11	Exhaust gas temperature (^{o}C)	270	325	321	317	319	335	320	320
C.	***Emission parameters***								
12.	BSHC emission (g/kWh)	0.029	0.028	0.027	0.028	0.021	0.023	0.025	0.017
13.	BSCO emission (g/kWh)	0.008	0.008	0.0057	0.0056	0.011	0.008	0.0058	0.0054
14.	BSNO emission (g/kWh)	2.055	2.898	2.695	2.791	2.786	2.819	2.695	2.644
15.	Smoke opacity (%)	28	21	20.5	22.5	20.5	21.5	20.2	18.5

Continued in the next page……

Sl.No	Parameter	Diesel	JME	X1JOE10	X2JOE10	Y1JOE10	Y2JOE10	Z1JOE10	Z2JOE10
D.	***Combustion parameters***								
1.	Start of ignition (^{o}CA)	356.6	354	353.7	353.7	357.7	354.9	354.3	354.2
2.	Occurrence of maximum pressure (^{o}CA)	372.4	370.4	370.1	370.8	372.7	370.7	370.7	370.2
3.	Ignition delay (^{o}CA)	12.7	10.2	9.8	9.9	14.3	10.4	10.4	9.8
4.	Occurrence of maximum heat release (^{o} CA aTDC)	6.7	8.2	8.4	9.1	11.6	9	10.2	8.6
5.	Maximum heat release (J/^{o}CA)	52.02	49.97	49.52	49.25	48.02	50.94	50.7	50.46
6.	Maximum cylinder pressure (bar)	75.70	82.61	83.4	81.8	69.8	81.7	80.9	82.7
7.	90% Mass fraction burned (^{o}CA)	389.9	387.5	387.7	387.9	390.9	388.1	387.8	387.3
8.	Combustion duration (^{o}CA)	38.4	38	38.2	38.5	38.2	38.3	37.5	37.1
E.	***Performance parameters***								
9.	Brake thermal efficiency (%)	30.4	30.3	31.99	31.09	32.0	32.17	31.12	32.4
10.	Specific fuel consumption (kg/kWh)	0.269	0.302	0.315	0.310	0.316	0.317	0.319	0.315
11	Exhaust gas temperature (^{o}C)	270	325	315	321	354	331	313	315
F.	***Emission parameters***								
12.	BSHC emission (g/kWh)	0.029	0.028	0.023	0.0264	0.018	0.023	0.0223	0.0124
13.	BSCO emission (g/kWh)	0.008	0.008	0.0106	0.0056	0.0166	0.0055	0.0053	0.0053
14.	BSNO emission (g/kWh)	2.055	2.898	2.535	2.734	2.59	2.606	2.535	2.498
15.	Smoke opacity (%)	28	21	21.8	23.2	21.6	22.8	19.3	19.1

Continued in the next page……

Sl.No	Parameter	Diesel	JME	X1JOE15	X2JOE15	Y1JOE15	Y2JOE15	Z1JOE15	Z2JOE15
G.	***Combustion parameters***								
1.	Start of ignition (^{o}CA)	356.6	354	354.3	353.7	357.0	354.3	354.0	356.1
2.	Occurrence of maximum pressure (^{o}CA)	372.4	370.4	370.2	370.2	372.2	370.7	371.0	371.0
3.	Ignition delay (^{o}CA)	12.7	10.2	9.9	10.4	13.3	10.4	10.1	9.9
4.	Occurrence of maximum heat release (^{o} CA aTDC)	6.7	8.2	7.9	9.1	6.9	9.1	9.4	4.5
5.	Maximum heat release (J/^{o}CA)	52.02	49.97	47.62	47.42	53.14	51.51	51.52	55.27
6.	Maximum cylinder pressure (bar)	75.70	82.61	82.9	80.2	76.1	82.4	82.7	82.9
7.	90% Mass fraction burned (^{o}CA)	389.9	387.5	388.5	387.8	389.5	387.7	386.9	385.9
8.	Combustion duration (^{o}CA)	38.4	38	38.1	36.8	38.2	37.4	36.9	36.2
H.	***Performance parameters***								
9.	Brake thermal efficiency (%)	30.4	30.3	32.9	30.8	30.9	31.6	31.7	33.9
10.	Specific fuel consumption (kg/kWh)	0.269	0.302	0.319	0.379	0.368	0.319	0.318	0.312
11	Exhaust gas temperature (^{o}C)	270	325	318	322	358	328	305	310
I.	***Emission parameters***								
12.	BSHC emission (g/kWh)	0.029	0.028	0.0257	0.0233	0.0183	0.018	0.018	0.015
13.	BSCO emission (g/kWh)	0.008	0.008	0.0166	0.0167	0.0169	0.0027	0.005	0.0028
14.	BSNO emission (g/kWh)	2.055	2.898	2.489	2.513	2.520	2.624	2.489	2.412
15.	Smoke opacity (%)	28	21	22.1	23.8	22.3	22.9	23.1	20.2

5.2 Experimental studies on the combustion, performance and emission characteristics of acid treated biodiesel bio oil emulsions

5.2.1 General

Preliminary investigations on the utilisation of the emulsion obtained from JME with WPO as an alternative fuel revealed, that up to 15% of WPO can be emulsified with the JME, and used as a fuel in a DI diesel engine. From the experimental results in terms of emulsion stability, combustion, performance and emission parameters, the Z2JOE15 emulsion was selected as an optimum emulsion for further investigation. But, it was found that the Z2JOE15 emulsion was acidic in nature, due to the addition of WPO. This may result in difficulty in storage, handling and utilization of the fuel in transport applications. The acidity of the JOE15 emulsion was reduced by an acid treatment, and this acid treated JOE15 emulsion was denoted as ATJOE15. The acid treatment procedure and properties of the ATJOE15 emulsion are already mentioned in Chapter 3. The acid treated emulsion was tested as a fuel in the same engine. The combustion, performance and emission behaviour of the diesel engine fueled with ATJOE15 in comparison with those of diesel and JME operations are presented in this section.

5.2.2 Combustion parameters

5.2.2.1 Pressure crank angle history

The cylinder pressure for each crank angle rotation for all the test fuels at full load condition is shown in Fig. 5.2.1.

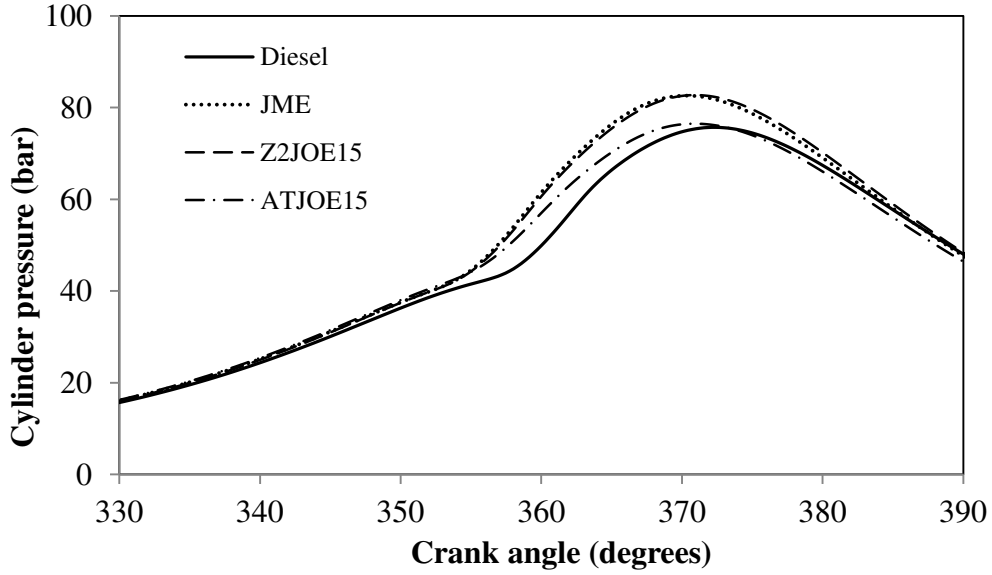

Fig. 5.2.1 Variation of cylinder pressure with crank angle

It is observed from the figure that the combustion commences earlier by 2.6°, 2.8 ° and 2.2 ° CA for JME, Z2JOE15 and ATJOE15 respectively, compared to that of diesel at full load. The combustion starts earlier for the JME and emulsions, due to advanced injection timing as a result of higher bulk modulus and higher density of biodiesel and shorter ignition delay. Similar results are reported by Gumus [178] in his investigation of the combustion and heat release characteristics of a hazelnut kernel oil methyl ester fueled DI diesel engine. The maximum cylinder pressure for diesel occurs at 12.4 °CA aTDC, whereas for the JME, Z2JOE15 and ATJOE15, the peak pressure occurs at about 10.4 °CA aTDC, 10.8 °CA aTDC and 10.2 °CA aTDC respectively at full load, It is ascertained that the peak pressure occurs after the TDC for all the fuels tested in this study.

5.2.2.2 Ignition delay

Figure 5.2.2 depicts the ignition delay for diesel, JME, Z2JOE15 and ATJOE15 at all loads. The ignition delay decreases with an increase in the load for all the fuels as expected in this study. The decrease in ignition delay with the increase in engine load, is due to the influence of the cylinder gas temperature within the ignition delay period [169].

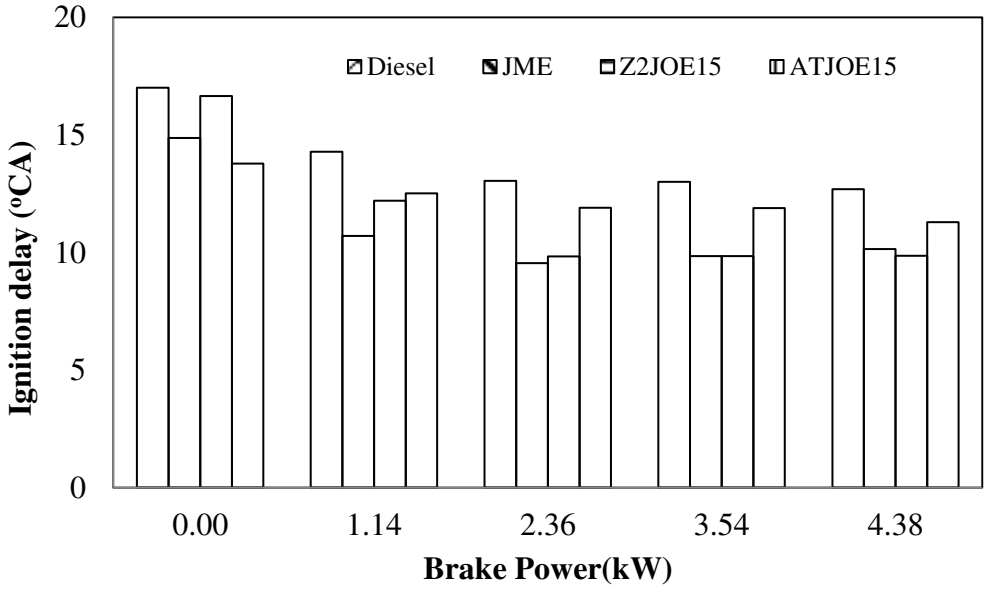

Fig. 5.2.2 Variation of ignition delay with brake power

At full load condition, the values of ignition delay are about 12.7, 10.1, 10.2 and 11.3 °CA, for diesel, JME, Z2JOE15 and ATJOE15 respectively. The delay period is lower by about 2.5°, 2.5° and 1.4° for JME, Z2JOE15 and ATJOE15 respectively, compared to that of diesel.

The advance of the ignition timing is observed with the JME and emulsions, which is attributed to the oxygen present in JME, and the breakdown of the higher molecules of JME into lower molecules of volatile compounds during injection, and this advances the start of ignition resulting in a shorter ignition delay. Similar reasons are given by Rao et al. [179], in their work on the combustion and emission characteristics of diesel engine fueled with rice bran oil methyl ester and its diesel blends. In the case of the Z2JOE15, the ignition delay is found to be the same as JME, and the delay period is longer in the case of ATJOE15, due to inadequate mixing leading to larger droplet size and smaller spray angles.

5.2.2.3 Heat release rate

Figure 5.2.3 depicts the heat release pattern of the various fuels tested in this study.

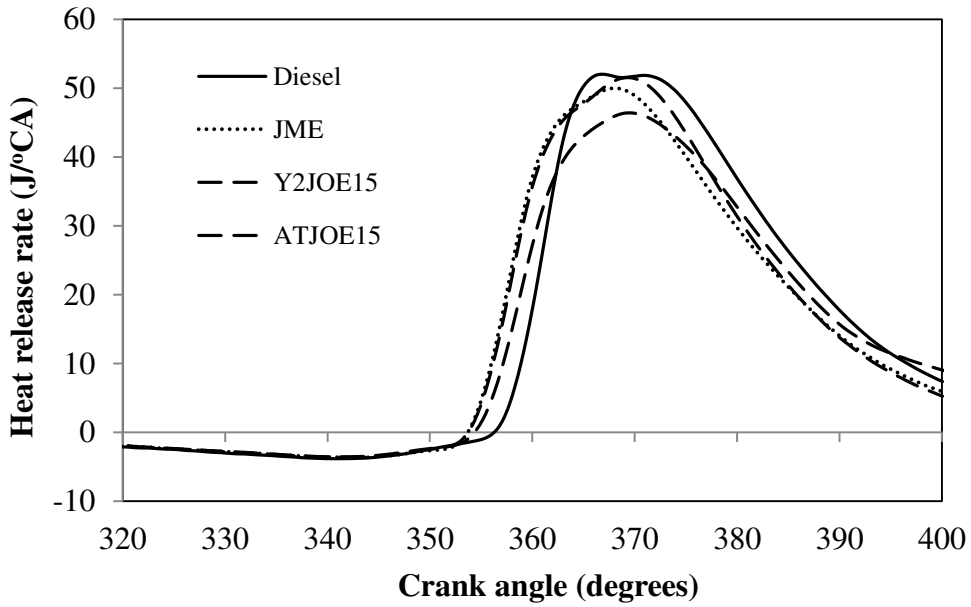

Fig. 5.2.3 Variation of heat release rate with crank angle

The heat release patterns of the JME, Z2JOE15 and ATJOE15 at full load follow the trend of diesel at full load. Because of the heat loss from the cylinder, and the cooling effect of the fuel vaporization, when it is injected into the cylinder, the heat release rate is marginally negative during the ignition delay period. The maximum heat release rate values are about 52, 50, 49.4, 51.5 and 46.4 J/ ^{o}CA for diesel, JME, Z2JOE15 and ATJOE15 respectively, at full load. The maximum heat release rate is found to be higher for diesel, due to more accumulation of fuel during the relatively longer delay period. For the JME and its emulsion with the WPO, less amount of fuel is accumulated during the shorter ignition delay period,

which results in lower heat release rates compared to that of diesel at full load. The reasons are in agreement with those of Qi et al [168], when the diesel engine was fueled with ethanol-biodiesel-water micro emulsions. The maximum heat release rate occurs at about 6.7, 8.2, 9.11 and 9.09 ^{o}CA aTDC for diesel, JME, Z2JOE15 and ATJOE15 respectively, at full load.

5.2.2.4 Maximum cylinder pressure

Figure 5.2.4 illustrates the variation of maximum cylinder pressure with load for the various fuels tested in this study.

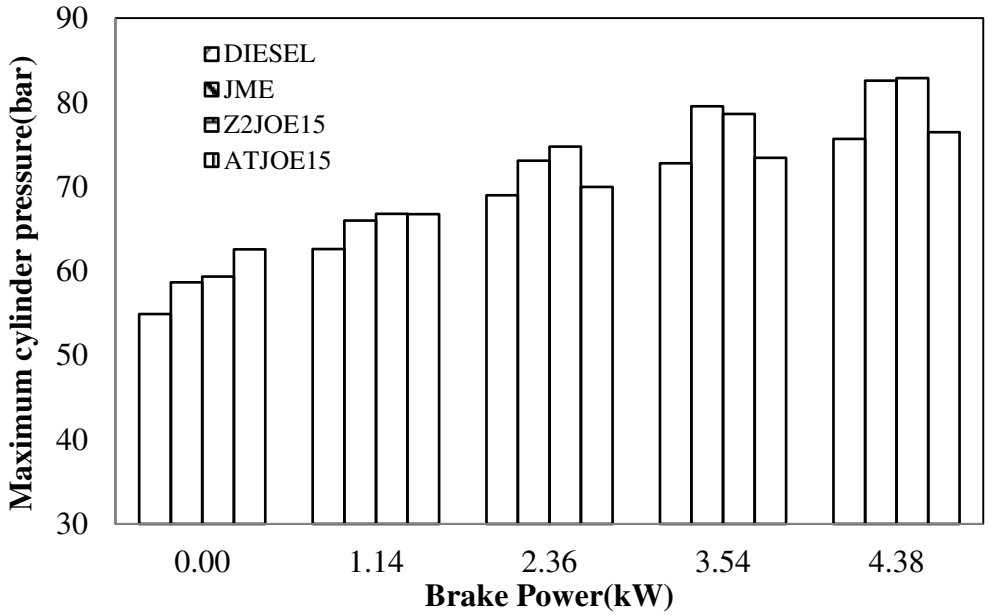

Fig. 5.2.4 Variation of maximum cylinder pressure with brake power

It can be observed from the figure, that at low loads, the maximum cylinder pressure is higher for the JME, Z2JOE15 and ATJOE15 emulsions, compared to those of diesel and the JME. This may be attributed to the shorter ignition delays and rapid combustion of the JME and JME-WPO emulsions, compared to that of diesel. At high loads, the maximum cylinder pressure of the ATJOE15 emulsion is noticed to be higher in comparison with diesel, but lower than that of JME. At full load condition, the maximum cylinder pressure values of diesel, JME, Z2JOE15 and ATJOE15 are 75.7, 82.6, 82.9 and 76.4 bar respectively. In this condition, the ignition delay of the ATJOE15 emulsion is longer, which in turn extends the combustion process, and this may be the reason for the lower peak cylinder pressure of ATJOE15 when compared with the JME.

5.2.2.5 Mass fraction burned

The variations of mass fraction burned with the crank angle for the ATJOE15 emulsion compared with those of diesel, JME and Z2JOE15 at full load, are given in Fig. 5.2.5.

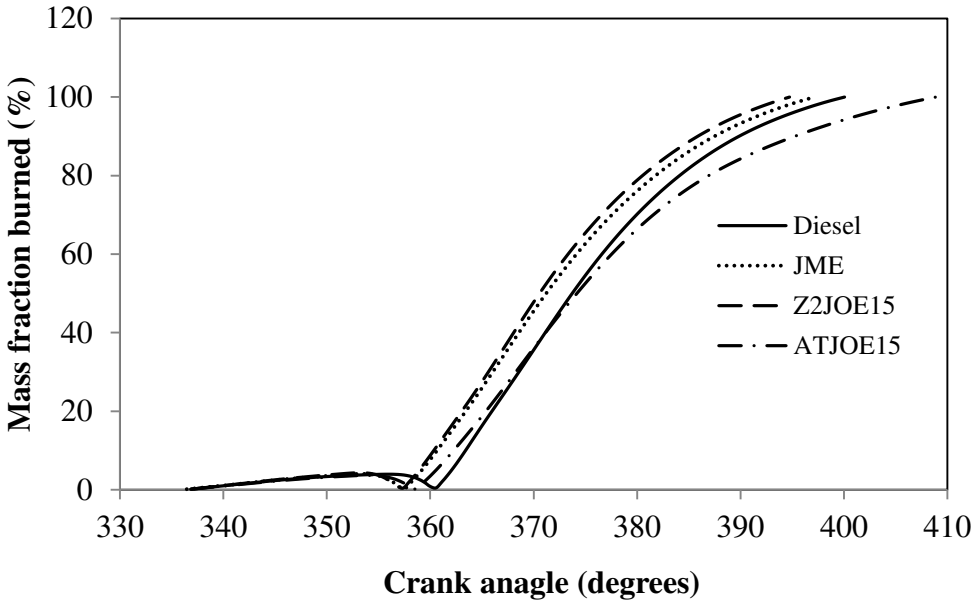

Fig. 5.2.5 Variation of mass fraction burned with crank angle

It is seen from the figure, that the crank angles at which 10% mass fraction burned for the ATJOE15, JME and Z2JOE15 are earlier than that of diesel at full load condition. As a result of longer ignition delay, the 10% mass fraction burned is later than those of JME and Z2JOE15 operations. The crank angles at which 50% mass fraction burned are earlier by about 3 and 4 ^{o}CA for the JME and Z2JOE15 respectively, whereas it is almost the same for the ATJOE15. This indicates that the combustion period upto 50% mass fractions are almost the same as that of diesel for the ATJOE15 emulsion. The 90% mass fraction burned crank angles are earlier for the JME and Z2JOE15 emulsion by 2 and 4 ^{o}CA respectively, whereas it is later by 6 ^{o}CA for the ATJOE15 emulsion. The marginally higher viscosity and density of the ATJOE15 emulsion result in inferior atomization and vaporization, and lead to reduction in the fuel air mixing rates. Hence, more burning occurs in the diffusion phase, in the case of the ATJOE15 emulsion.

5.2.2.6 Combustion duration

Figure 5.2.6 illustrates the variation of combustion duration under different loads of the engine. The crank angle duration from 10% mass burned to 90% mass burned, has been taken

as the combustion duration. The combustion duration increases with engine load, owing to the increase in the fuel quantity. The values of combustion duration at full load are approximately 38.4, 38, 36.9 and 40.6 ^{o}CA for diesel, JME, Z2JOE15 and ATJOE15 respectively. At full load, the combustion duration of the ATJOE15 is longer than those of diesel, JME and Z2JOE15.

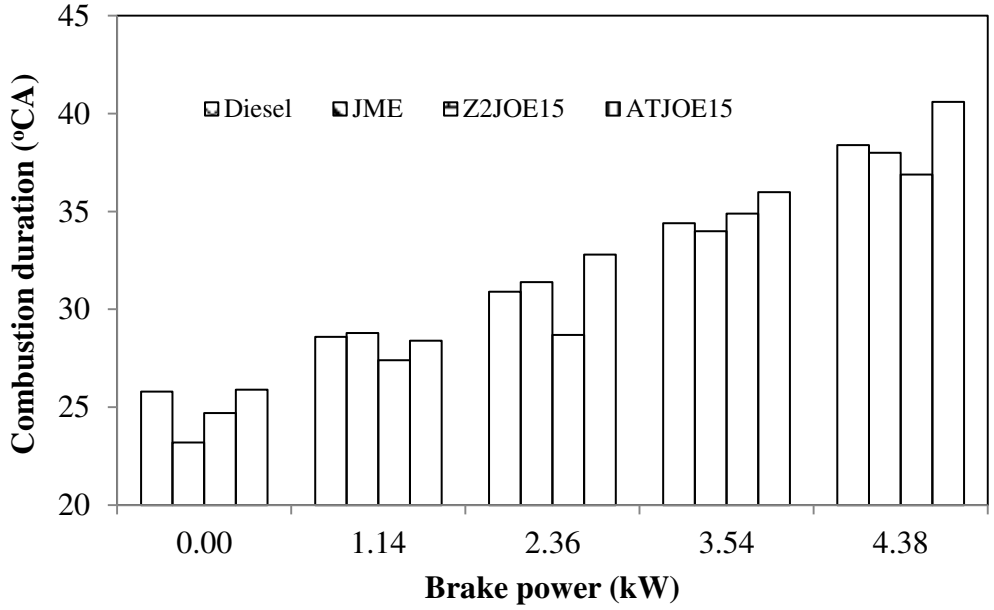

Fig. 5.2.6 Variation of combustion duration with brake power

This may be due to the slower combustion rate in the premixed burning phase, and the longer mixing-controlled combustion phase that increases the total combustion duration of the ATJOE15 emulsion. Similar reasons are reported by Qi et al. [168], when the diesel engine was fueled with ethanol-biodiesel-water micro emulsions. This longer mixing controlled combustion phase depends largely on the fuel injection rate and fuel vapour air mixing rates. Because of the larger droplets and poor breaking of spray, the combustion duration is longer with the ATJOE15.

5.2.3 Performance parameters

5.2.3.1 Brake thermal efficiency

Fig. 5.2.7 shows the variation of brake thermal efficiency with respect to brake power for all the fuels tested in this study. The values of the brake thermal efficiencies at full load are 30.47%, 30.38%, 33.92%, and 32.98% respectively for diesel, JME, Z2JOE15 and ATJOE15 respectively. It is observed that the thermal efficiencies of Z2JOE15 and ATJOE15 emulsions are higher than that of diesel by about 11.3% and 8.2% respectively, at full load. When

compared to JME operation, the thermal efficiencies are higher by 11.6% and 8.5% for the Z2JOE15 and ATJOE15 emulsions respectively, at full load. The increase in the brake thermal efficiency is due to the improvement of the combustion process, on account of the increased oxygen content in the fuels. Similar reasons are reported by Zhu et al [180], in their work on DI diesel engine fueled with ethanol–biodiesel blends. The faster combustion process of the Z2JOE15 and ATJOE15 emulsions may be another contributor to the increase in thermal efficiency. Also, based on the mass fraction burned or heat release analysis, the crank angle at which 50% mass fraction burned is closer to the top dead center, leading to higher positive work done on the piston, and hence, higher brake thermal efficiency is obtained with the Z2JOE15 and ATJOE15 emulsions, compared to that of diesel.

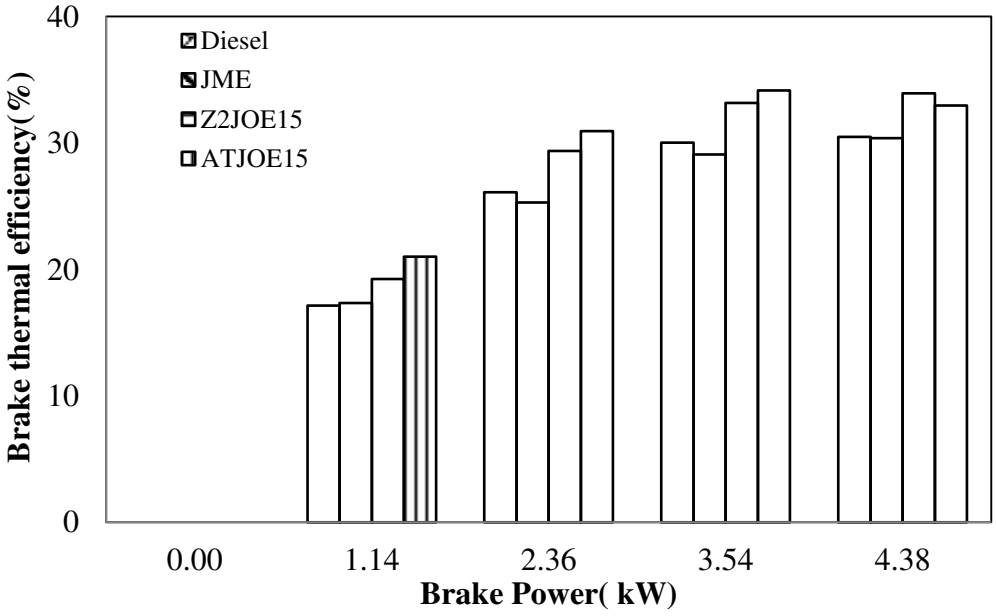

Fig. 5.2.7 Variation of brake thermal efficiency with brake power

A marginally lower thermal efficiency of the ATJOE15 emulsion is noticed at full load, compared to that of Z2JOE15 emulsion, which may be due to longer combustion during the diffusion phase.

5.2.3.2 Brake specific fuel consumption

The variation of brake specific fuel consumption with brake power for the fuels tested in this study, is shown in Fig. 5.2.8. The BSFC of the JME, Z2JOE15 and ATJOE15 follows the trend similar to that of diesel. The BSFC is decreased with the increase in the engine load as expected.

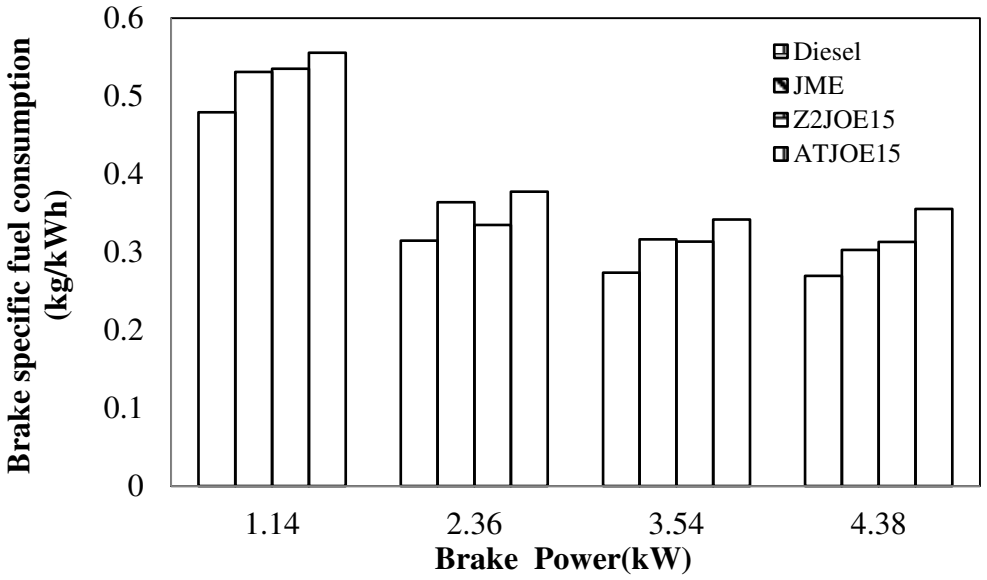

Fig. 5.2.8 Variation of brake specific fuel consumption with brake power

The BSFC values of JME, Z2JOE15 and ATJOE15 are found to be higher by 12.3%, 16% and 31% respectively. This is attributed to the combined effect of viscosity and lower heating values of JME and emulsions, which require larger fuel consumption in order to release the same energy as that of diesel.

5.2.3.3 Exhaust gas temperature

Figure 5.2.9 depicts the trend of the exhaust gas temperature with load for all the fuels tested in this study.

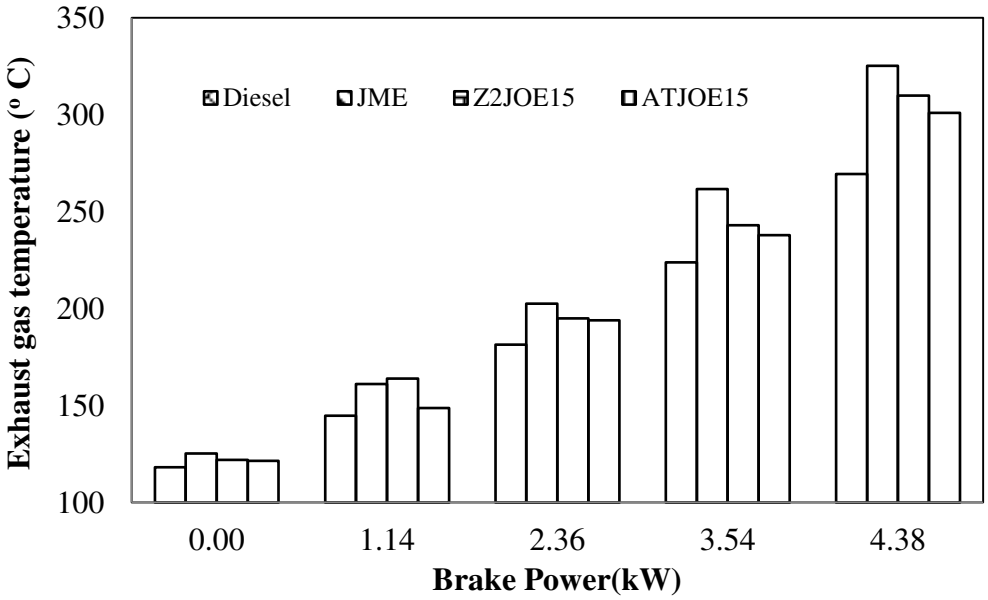

Fig. 5.2.9 Variation of exhaust gas temperature with brake power

The exhaust gas temperatures of diesel, JME, Z2JOE15 and ATJOE15 are 270^{o}C, 325^{o}C, 310^{o}C and 301^{o}C respectively, at full load. It is noted from the figure that at full load, the exhaust gas temperature is the highest for JME and lowest for diesel. The exhaust gas temperatures of Z2JOE15 and ATJOE15 are lower than that of JME operation. The water content present in the WPO gets vaporized during the combustion process, and absorbs the heat energy which decreases the local adiabatic flame temperature. Similar reasons are reported by Bertoli *et al.,* [146] when WPO blends or emulsions are used as the fuel in a diesel engine.

5.2.4 Emission parameters

5.2.4.1 BSHC emissions

Figure 5.2.10 depicts the variation of brake specific hydrocarbon (BSHC) emissions with brake power. All the fuels tested in this study exhibit higher HC emission at low loads, and have a declining trend at higher loads.

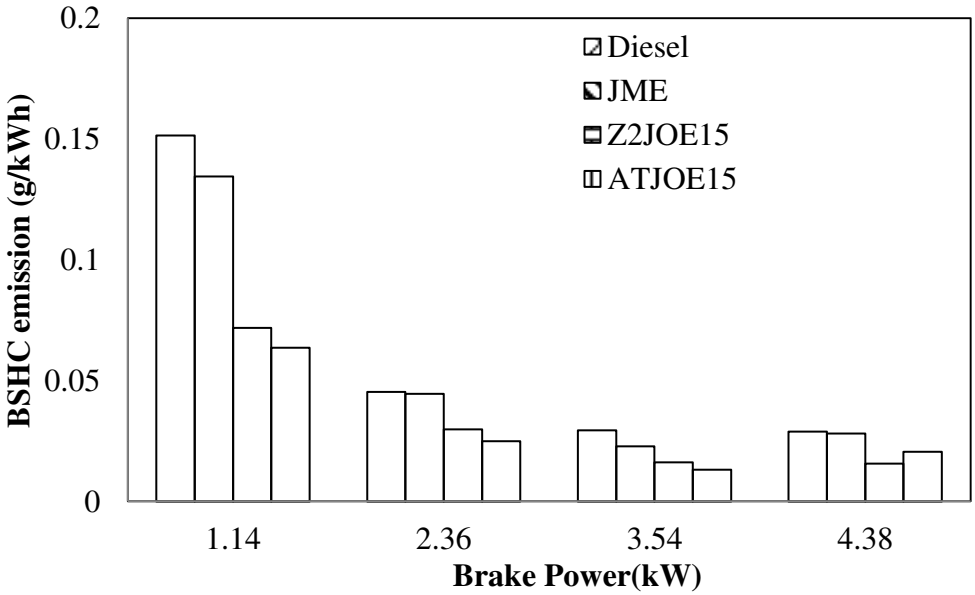

Fig. 5.2.10 Variation of BSHC emissions with brake power

The BSHC emissions are reduced by about 14.2, 45 and 33% for JME, Z2JOE15 and ATJOE15 respectively, at full load compared to that of diesel. The HC emissions of JME are found to be lower than that of diesel since, the higher oxygen content of JME leads to more complete burning than that of diesel. For ATJOE15 emulsion, due to inferior combustion, the HC emissions are found to be higher than that of Z2JOE15 emulsion.

5.2.4.2 BSCO emissions

Figure 5.2.11 describes the comparison of the brake specific carbon monoxide (BSCO) emissions of all the test fuels. Generally, the CO emissions are formed as a result of incomplete combustion of fuel. However, if the combustion is complete, CO will be oxidized into CO_2 [173].

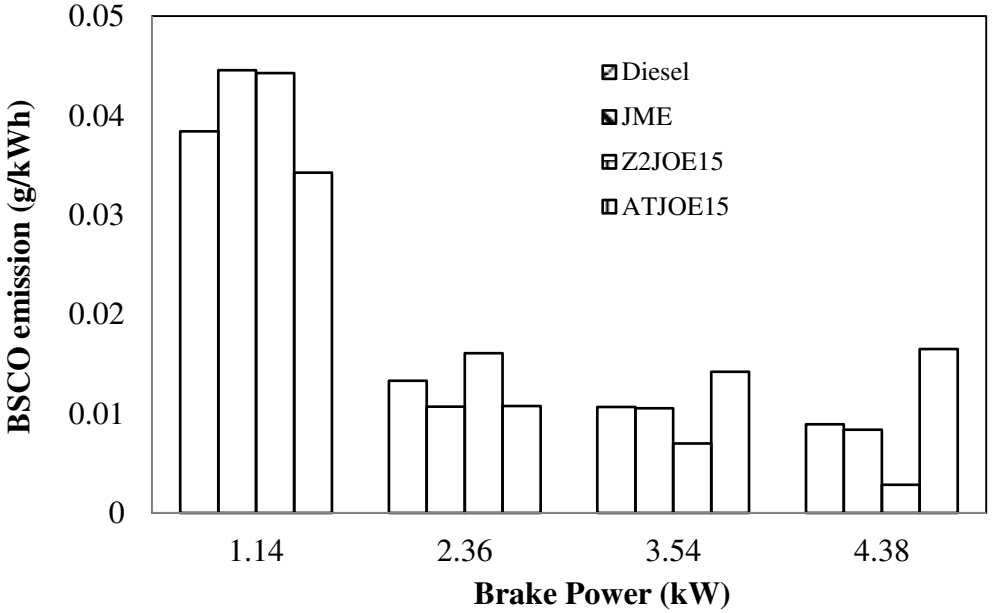

Fig. 5.2.11 Variation of BSCO emissions with brake power

The CO emission is formed when there is a lack of oxygen during combustion, either near full load, or sometimes also at low loads, when there is poor mixing of the fuel with air. It is observed that the BSCO emissions of Z2JOE15 and ATJOE15 are found to be higher by about 17.5%, and 46%, than that diesel at full load. The longer spray penetration and larger fuel droplets may be the factors for higher CO emissions in the case of emulsions. This reason was supported by Zhou [181], in his research work.

5.2.4.3 BSNO emissions

Figure 5.2.12 depicts the variation of brake specific nitric oxide (BSNO) emissions, with respect to brake power. The NO emissions are formed due to high temperature and oxygen availability conditions. This will facilitate the oxidization of nitrogen, which in turn, created higher NO emissions according to the extended Zeldovich mechanism [182]. It is apparent that the BSNO emissions are found to be higher in the JME operation compared to that of diesel. Due to the high temperature environment and availability of about 10% excess

intrinsic oxygen content in biodiesels, the NO emissions are therefore higher in JME operation compared to that of diesel operation.

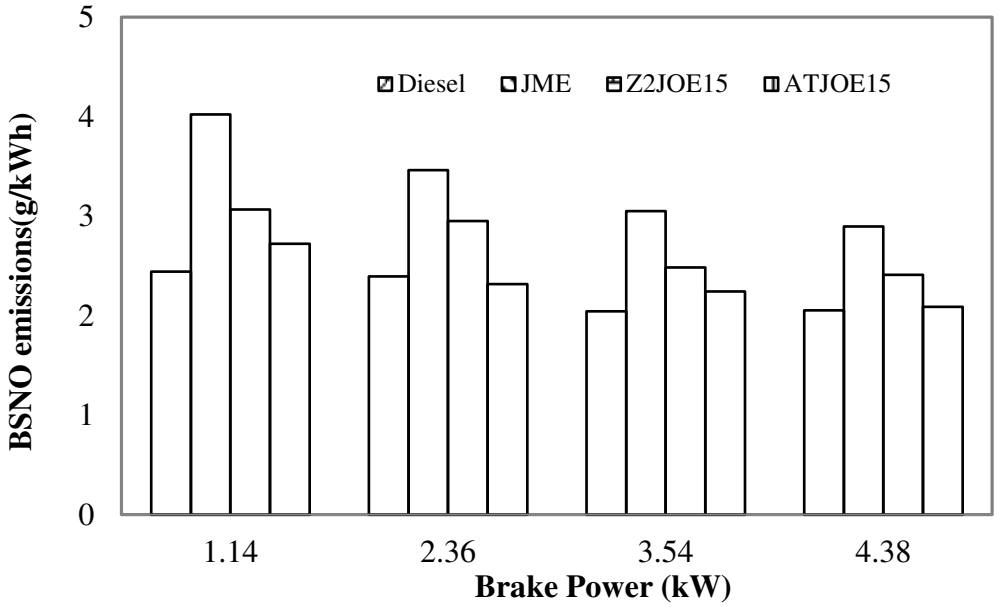

Fig. 5.2.12 Variation of BSNO emissions with brake power

Similar reasons are reported by Szybist et al. [183], in their work on NO_x emissions of alternative diesel fuels: a comparative analysis of biodiesel and FT diesel. It is observed that about 29%, 21.6% and 2% increase in NO emissions is obtained with the JME, Z2JOE15and ATJOE15 respectively, at full load compared to that of diesel. The NO emissions decrease with the addition of WPO in JME, and this may be due to the higher water content in WPO that reduces the combustion temperature. Similar reasons were reported by Bertoli *et al.* [146], for the lower combustion temperature and the NO emissions, when the diesel engine was fueled with the WPO blends or emulsions with diesel.

5.2.4.4 Smoke opacity

Figure 5.2.13 depicts the variation of smoke opacity, with respect to brake power. The smoke opacity of the oxygen enriched fuels with high OH radical concentration, contributes to the reduction of smoke [184]. Good fuel atomisation, better fuel-air mixing and reduction in large droplets, result in a better fuel combustion process; hence, a reduction in smoke opacity. The percentage decrease in the smoke opacity of 19.6% is observed with the JME at full load, in comparison with diesel. When fueled with the Z2JOE15, the smoke opacity is found to be lower by 27.8%, and with the ATJOE15 the smoke opacity increases by about 8%, compared to that of diesel operation.

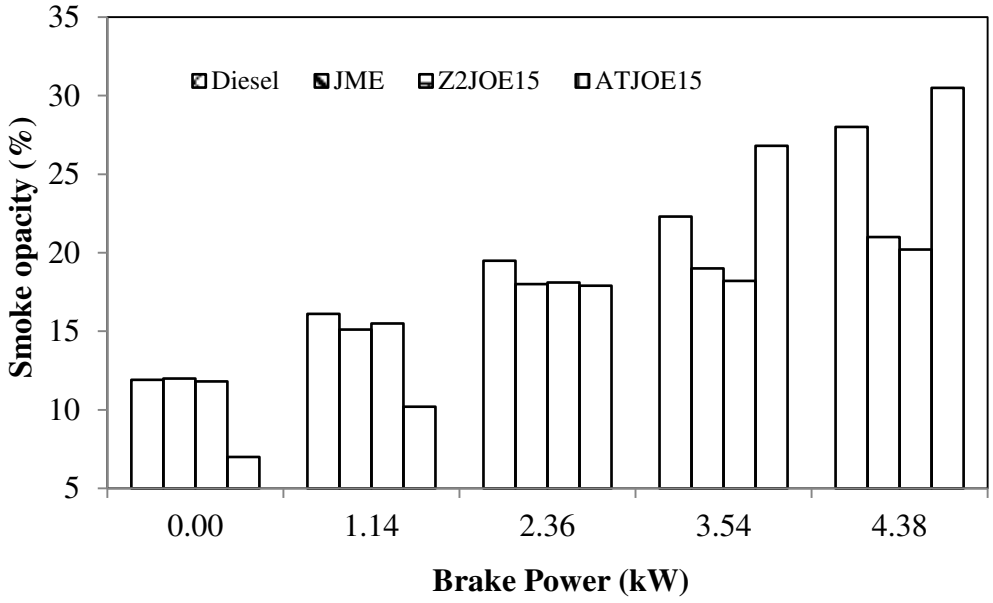

Fig. 5.2.13 Variation of smoke opacity with brake power

When compared to the JME operation, 10% lower smoke is noticed with the Z2JOE15 emulsion, whereas about 30% higher smoke emission is noticed with the ATJOE15 emulsion. The higher smoke opacity may be due to the larger droplets of the ATJOE15 emulsion compared to that of the other tested fuels.

A summary of the combustion, performance and emission parameters at full load for different fuels used in this study is given in Table 5.2.

5.2.5 Closure

The summary of the experimental results on the combustion, performance and emission results in single cylinder diesel engine fueled with ATJOE15 emulsion is as follows:

- The combustion of Z2JOE15 and ATJOE15 emulsions commences earlier than that of diesel at full load. The ignition delay of JME, Z2JOE15 and ATJOE15 is found to be shorter than that of diesel. Lower heat release rates are obtained with the JME and Z2JOE15 and ATJOE15 emulsions compared to that of diesel. A longer combustion duration was observed with ATJOE15 compared to that of diesel, JME and Z2JOE15.
- From the performance aspect, the brake thermal efficiencies of the Z2JOE15 and ATJOE15 emulsions are higher by about 11.3% and 8.2% respectively, than that of diesel, and higher by about 11.6% and 8.5% respectively, than that of JME at full load.

- The BSHC emissions are reduced by about 14.2%, 45% and 33% for JME, Z2JOE15 and ATJOE15 respectively, at full load compared to that of diesel. The BSCO emissions of Z2JOE15 and ATJOE15 are found to be higher by about 17.5%, and 46%, than that of diesel at full load. There is about 29%, 21.6% and 2% increase in the NO emissions, with the JME, Z2JOE15 and ATJOE15 respectively, at full load compared to that of diesel. A percentage decrease in the smoke opacity of 19.6% is observed with the JME at full load, in comparison with diesel. When fueled with the Z2JOE15, the smoke opacity is found to be lower by about 27.8%, and with the ATJOE15 the smoke opacity increases by about 8% compared to that of diesel operation. When compared to JME operation, 10% lower smoke is noticed with the Z2JOE15 emulsion, whereas about 30% higher smoke emission is noticed with the ATJOE15 emulsion.

Table 5.2 Summary of values on combustion, performance and emission parameters at full load for diesel, JME, Z2JOE15 and ATJOE15

Sl.No	Parameter	Diesel	JME	Z2JOE5	ATJOE15
Combustion parameters					
1.	Start of ignition (^{o}CA)	356.6	354	354.0	354.5
2.	Occurrence of maximum pressure (^{o}CA)	372.4	370.4	371.0	371.1
3.	Ignition delay (^{o}CA)	12.7	10.2	10.1	11.2
4.	Occurrence of maximum heat release (^{o} CA aTDC)	6.7	8.2	9.4	9.3
5.	Maximum heat release (J/^{o}CA)	52.02	49.97	51.52	46.4
6.	Maximum cylinder pressure (bar)	75.70	82.61	82.7	76.49
7.	90% Mass fraction burned (^{o}CA)	389.9	387.5	386.9	395.7
8.	Combustion duration (^{o}CA)	38.4	38	36.9	40.6
Performance parameters					
9.	Brake thermal efficiency (%)	30.4	30.3	31.7	32.9
10.	Specific fuel consumption (kg/kWh)	0.269	0.302	0.318	0.3555
11	Exhaust gas temperature (^{o}C)	270	325	305	301
Emission parameters					
12.	BSHC emission (g/kWh)	0.029	0.028	0.018	0.007
13.	BSCO emission (g/kWh)	0.008	0.008	0.005	0.0165
14.	BSNO emission (g/kWh)	2.055	2.898	2.489	2.09
15.	Smoke opacity (%)	28	21	23.1	30.5

5.3 Analysis of the combustion and emission characteristics of a diesel engine fueled with the ATJOE15 emulsion

5.3.1 General

This chapter discusses the development of a mathematical model to validate the experimental results obtained from a single cylinder, four stroke, DI diesel engine fueled with ATJOE15 emulsion. The experimental results were validated with a two zone model, using a MATLAB software program. One zone consisted of pure air called the non-burning zone and the other zone consists of fuel and combustion products called burning zone. The first law of thermodynamics and equations of state were applied in each of the two zones, to get the cylinder temperatures and cylinder pressure histories. Using the two zone combustion model, the combustion parameters and the chemical equilibrium composition were determined theoretically. The extended Zeldovich mechanism was used to predict the NO emissions, while soot density was determined using a semi-empirical model. A comparison of the experimental and theoretical results is also presented in this chapter.

5.3.2 General description of the model

The model deals with a direct injection, bowl-in-piston combustion chamber, into which fuel is injected, in a radial direction, from three holes drilled symmetrically on the injector tip. The model is a two-zone thermodynamic model. The cylinder contents comprise a non-burning zone of air, and another burning zone in which fuel is continuously supplied from the injector holes during injection, and burned with the entrained air from the air zone. The model includes only those processes occurring during the portions of the compression and expansion strokes, when both the inlet and exhaust valves are closed (closed cycle). The compression process in real engines is a polytropic one, which starts from the moment the inlet valve closes, and ends when the injection process starts. The fuels considered are diesel ($C_{12}H_{26}$), JME ($C_{7.56}H_{13.89}N_{0.01}O_{0.81}$) and ATJOE15 ($C_{2.08}H_{4.13}N_{0.01}S_{0.01}O_{1.17}$). The volumetric composition of the ATJOE15 fuel used in this investigation is 15% WPO, 81% JME and 4% of mixed surfactant Span 80 and Tween 80. The main calculation procedure is based on the integration of the first law of thermodynamics, and the perfect gas state equation combined with the various sub-models.

5.3.2.1 Energy equations

During the compression stroke, only one zone (of pure air) exists. Then, the first law of thermodynamics for a closed system is applied, together with the perfect gas state equation [155]. The change in internal energy can be expressed as follows:

$$\frac{d(mu)}{d\theta} = \frac{dQ_r}{d\theta} - \frac{dQ_h}{d\theta} - \frac{dW}{d\theta} \tag{5.1}$$

By replacing the work transfer term $\frac{dW}{d\theta}$ with $P\frac{dV}{d\theta}$ or by the ideal gas law PV = m RT, the above equation (1) can be rearranged as

$$\mathrm{m}\frac{du}{d\theta} = \frac{dQ_r}{d\theta} - \frac{dQ_h}{d\theta} - P\frac{dV}{d\theta} \tag{5.2}$$

where, V is the instantaneous cylinder volume with respect to the crank angle, which is given by,

$$\mathrm{V}=\mathrm{V_{cl}}+\left(\frac{\pi \mathrm{D}^2}{4}\right)\mathrm{r}[1+\lambda^{-1}-cos\phi-\sqrt{\lambda^{-2}-sin^2\phi}] \tag{5.3}$$

In the above equations, the term dQ is given as the fourth order polynomial expressions of the absolute temperature T, including the enthalpy of formation at absolute zero [155].

Internal energy calculation as a function of temperature:

$$\frac{\mathrm{hi}}{\mathrm{RmolT}} = \mathrm{ai1} + \frac{\mathrm{ai2}}{2}\mathrm{T} + \frac{\mathrm{ai3}}{3}\mathrm{T}^2 + \frac{\mathrm{ai4}}{4}\mathrm{T}^3 + \frac{\mathrm{ai5}}{5}\mathrm{T}^4 + \frac{\mathrm{ai6}}{\mathrm{T}} \tag{5.4}$$

$u_i = h_i - RT$

For the surrounding air zone, which only loses mass (air) to the burning zone, the first law of thermodynamics for the unburned zone is written as

$$dE = dQ - pdV - h_a dm_a \tag{5.5}$$

The burning zone not only receives mass from the air zone, but also there is an enthalpy flow from the fuel, which is ready to be burned in the time step. So, the first law of thermodynamics for the burning zone becomes

$$dE = dQ - pdV + h_a dm_a + h_f dm_f \tag{5.6}$$

The first law of thermodynamics for the combustion in time step dt is

$$f(E)=E(T2) - E(T1) - dQ + dW + dm_f\, Qvs = 0 \tag{5.7}$$

If f(E) is greater than the accuracy required the new value of T_2 is calculated using the Newton-Raphson numerical method. The unburned zone temperature is calculated using the equation,

$$T_u = T_{soc}\left(\frac{P}{P_{soc}}\right)^{(\gamma-1)/\gamma} \quad (5.8)$$

5.3.2.2 Heat transfer model

The heat transfer between the cylinder trapped mass and surrounding walls is calculated, using the formula of Anand [185]. The Anand formula to calculate heat loss from the cylinder, is

$$\frac{dQ}{dt} = aK\frac{\mathrm{Re}^b}{d}(T_g - T_w) + c(T_g{}^4 - T_w{}^4) \quad (5.9)$$

In this equation 'Tw' is the cylinder wall temperature which is assumed as 450 K and a, b, c are constants. The constant values are taken as, a=0.2626, b=0.6, c=5.67×10^{-8} W/m^2K^4.

5.3.2.3 Ignition Delay

The time delay between the start of injection and the start of combustion is defined as the ignition delay period. The determination of the start of combustion (SOC) by selecting the proper method is a key issue in ignition delay studies. In the combustion model, the ignition delay is also taken into account. The ignition delay period is calculated by integrating Wolfer's relation, using the trapezoidal rule.

$$\int_{t_{inj}}^{t_{ign}} \frac{dt}{t(p,T)} = \frac{1}{K\ \mathrm{tinj}} \int_{t_{inj}}^{t_{ign}} \frac{dt}{(p(t))^{-q}\exp(E/RT(t))} = 1 \quad (5.10)$$

The values of various constants corresponding to a D.I. diesel engines are K =2272; q =-1:19;

E/R = 4650.t_{inj}.

5.3.2.4 Wiebe's combustion model

The Wiebe function is used to predict the mass fraction burn, and the burn rate in internal combustion engines, operating with different combustion systems and fuels [186]. Wiebe [187] linked the chain chemical reactions with the fuel reaction rate in internal combustion engines, and his approach was based on the premise that a simple one-step rate equation would not be adequate to describe the complex reacting systems, such as those occurring in an internal combustion engine. The Wiebe functions for the non-dimensional burn fraction x and its derivative w (burn rate) as functions of the degrees of crank angle can be written as

$$x=1-e^{-6.908(\phi/\phi d)^{m+1}} \quad (5.11)$$

$$w=\frac{dx}{d\phi}=\frac{6.908(m+1)}{\phi d}\left(\frac{\phi}{\phi d}\right)^{m}e^{-6.908(\phi/\phi d)^{m+1}} \quad (5.12)$$

The non-dimensional burn fraction x and its derivative w (burn rate) as functions of time t can also be written as:

$$x=1-e^{-6.908(t/td)^{m+1}} \quad (5.13)$$

$$w=\frac{dx}{dt}=\frac{6.908(m+1)}{td}\left(\frac{t}{td}\right)^{m}e^{-6.908(t/td)^{m+1}} \quad (5.14)$$

The time it takes to reach the maximum burn rate t_m can be found by the differentiating equation (14) and equating the result to zero

$$t_m=t_d\left(\frac{m}{6.908(m+1)}\right)^{1/(m+1)} \quad (5.15)$$

The corresponding burn fraction is

$$X_m=1-\exp\left(-6.908(t_m/t_d)^{m+1}\right) \quad (5.16)$$

From above equations (13) and (14)

$$X_m=1-\exp\left(-m/(m+1)\right) \quad (5.17)$$

Wiebe suggested the physical meaning of the exponent m which was based on equation (5.15), which shows that, for a given combustion duration, the time it takes for a maximum burn rate to be reached is determined solely by the magnitude of m, which, in turn, determines the magnitude of the maximum burn rate from equation (5.15).When calculating the heat release, prior knowledge of the actual overall equivalence ratio is necessary. The term equivalence ratio is defined as the ratio of the actual air-fuel ratio to the stoichiometric air-fuel ratio. This helps in fixing the mass of fuel to be admitted.

5.3.2.5 Chemistry of combustion

In a combustion process, the fuel and the oxidizer react to produce products of different composition. The theory of combustion is a complex one, and has been the topic of intensive research for many years. Let us represent the chemical formula of a fuel as $C_\alpha H_\beta O_\gamma N_\delta$. In the

present case, it was considered that 10 species were present in the combustion product, and the combustion equation is given by:

$$\epsilon\varphi C_\alpha H_\beta O_\gamma N_\delta + 0.21O_2 + 0.79N_2 \longleftrightarrow \nu_1 CO_2 + \nu_2 H_2O + \nu_3 N_2 + \nu_4 O_2 + \nu_5 CO + \nu_6 H_2 + \nu_7 H + \nu_8 O + \nu_9 OH + \nu_{10} NO \quad (5.18)$$

From the atomic balance of each species C- H- O- N the following 4 equations, are obtained.

$$C \quad \epsilon\varphi\alpha = (y_1+y_5)\ N1 \quad (5.19)$$

$$H \quad \epsilon\varphi\beta = (2y_1+2y_6+y_7+y_9)\ N1 \quad (5.20)$$

$$O \quad \epsilon\varphi\gamma+0.42 = (2y_1+y_2+2y_4+y_5+y_8+y_9+y_{10})\ N1 \quad (5.21)$$

$$N \quad \epsilon\varphi\delta+1.58 = (2y_3+y_{10})\ N1 \quad (5.22)$$

By definition, the total number of mole fraction is unity.

$$\sum_{i=1}^{10} yi - 1 = 0 \quad (5.23)$$

The chemical reactions considered in equilibrium, are as follows:

$$0.5H_2 \longleftrightarrow H \quad (5.24)$$

$$0.5O_2 \longleftrightarrow O \quad (5.25)$$

$$0.5H_2+0.5O_2 \longleftrightarrow OH \quad (5.26)$$

$$0.5O_2+0.5N_2 \longleftrightarrow NO \quad (5.27)$$

$$H_2+0.5O_2 \longleftrightarrow H_2O \quad (5.28)$$

$$CO+0.5O_2 \longleftrightarrow CO_2 \quad (5.29)$$

The use of the equilibrium constant is identical to maximizing the entropy of the gas. This method is similar, when considering a restricted species list such as the present case. The compositions of all the species were found, using the method developed by Olikara and Borman [188]. Once the composition is known, the thermodynamic properties of interest like enthalpy, entropy, specific volume and internal energy, can be computed.

5.3.3 The nitric oxide formation model

The current approach to model the NO_x emissions from diesel engines is, to use the extended Zeldovich thermal NO mechanism, by neglecting other sources of NO_x formation. The extended Zeldovich mechanism consists of the following reactions,

$O + N_2 \longleftrightarrow NO + N$ (5.30)

$N + O_2 \bullet \longleftrightarrow NO + O$ (5.31)

$N + OH \longleftrightarrow NO + H$ (5.32)

This mechanism can be written as an explicit expression for the rate of change of the concentration of NO [10]:

The change of NO concentration is expressed as follows:

$$\frac{d\,(NO)}{dt} = 2\,(1-\alpha^2)\,\frac{R1}{1+\,\alpha R1/(R2+R3)} \tag{5.33}$$

where Ri is the one-way equilibrium rate for reaction i, defined as

$R1 = k_{1f}\,(N)_e(NO)_e,\;\; R2 = k_{2f}\,(N)_e(O_2)_e,$ (5.34)

$R3 = k_{3f}\,(N)_e(OH)_e,\quad \alpha = (NO)/(NO)_e$ (5.35)

5.3.4 The net soot formation model

The exhaust of the CI engines contains solid carbon soot particles that are generated in the fuel rich regions inside the cylinder during combustion. Soot particles are clusters of solid carbon spheres, with the HC and traces of other components absorbed on the surface. They are generated in the combustion chamber in the fuel rich zones, where there is not enough oxygen to convert all the carbon to CO_2. Subsequently, as the turbulence motion continues to mix the components, most of these carbon particles find sufficient oxygen to react and form CO_2.Thus soot particles are formed and consumed simultaneously in the combustion chamber.

The net soot formation rate was calculated, by using the semi-empirical model proposed by Hiroyasu et. al. [189]. According to this model the soot formation rate (index sf) and soot oxidation rate (index so) were given by

$$\frac{dm_{sf}}{\mathrm{dt}} = A_{sf}\,dm_f^{0.8}\,p^{0.5}\exp\left(-\frac{E_{sf}}{R_{mol}T}\right) \tag{5.36}$$

$$\frac{dm_{so}}{dt} = A_{so}\,m_{sn}\left(\frac{p_{o_2}}{p}\right)p^{n}\exp\left(-\frac{E_{so}}{R_{mol}T}\right) \tag{5.37}$$

where, the pressures are expressed in bar, dm_f is the unburned fuel mass in kg to be burned in time step dt. Therefore, the net soot formation rate is expressed as

$$\frac{dm_{sn}}{dt} = \frac{dm_{sf}}{dt} - \frac{dm_{so}}{dt} \tag{5.38}$$

A computer program using the MATLAB software was generated, with all the above mentioned equations, and considering all the values of constants, in order to predict the combustion attributes, like in-cylinder pressure, crank angle, heat release rate, heat losses and the NO emissions. The MATLAB program used for this analysis is given in Annexure 8.

5.3.4 Validation of results

5.3.4.1 Pressure-crank angle diagram

Figure 5.3.1 shows the measured and computed pressure trace and crank angle histories for the fuels tested at full load condition. In a CI engine, the cylinder pressure depends on the burned fuel fraction during the premixed burning phase, which is the initial stage of combustion, and the ability of the fuel to mix well with the air and burn. The high peak pressure and maximum rate of pressure rise correspond to the large amount of fuel burned in the premixed stage.

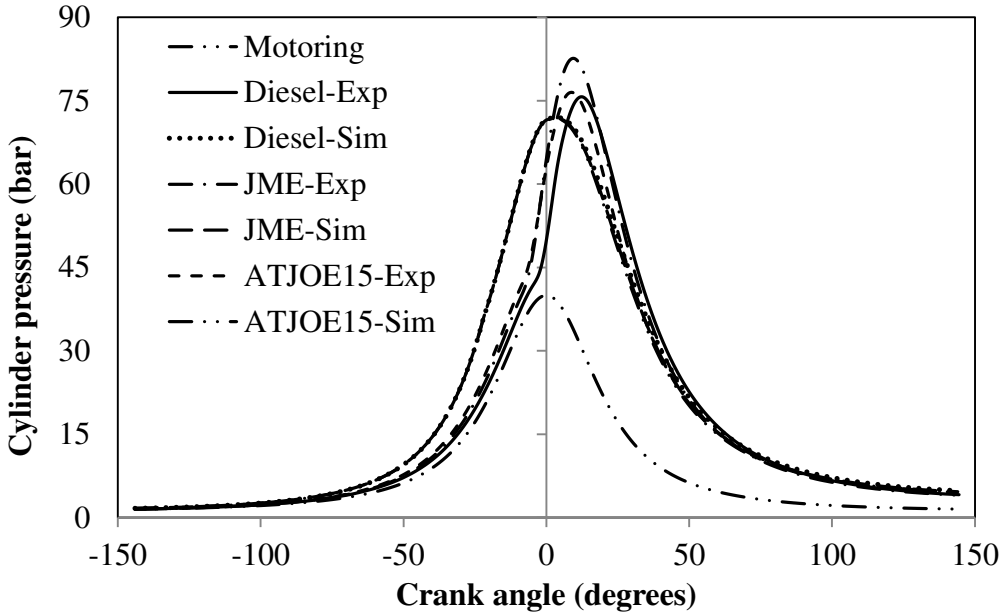

Fig. 5.3.1 Variation of cylinder pressure with crank angle at full load

It is observed from the experimental results that the peak pressures for diesel, JME and ATJOE15 are found to be 75.72, 82.61 and 76.49 bar respectively, at full load. For the simulated conditions, the peak pressure values are noticed to be 71.99, 71.85 and 71.76 bar respectively. It is observed from the figure that the combustion commences earlier by about 2.6^{o}, and 2.2^{o} for the JME, and ATJOE15 respectively, compared to that of diesel at full load. This may be due to the advanced injection timing, as a result of the higher bulk modulus and

higher density of biodiesel and shorter ignition delay. Similar results are reported by Gumus [178] in his investigation, on the combustion and heat release characteristics of a hazelnut kernel oil methyl ester fueled DI diesel engine. Also, the peak cylinder pressures of the JME and ATJOE15 are marginally higher than that of diesel, as a result of high viscosity and low volatility.

5.3.4.2 Apparent or net heat release rate

Figure 5.3.2 depicts the variation in the apparent heat release, with respect to the crank angle for the different fuels tested. The term apparent or net heat release rate is determined by deducting the heat transfer to the cylinder walls, crevice volume, blow-by and the fuel injection effects from the heat energy liberated by burning the fuel. The experimental results of the maximum net heat release rate for diesel, JME and ATJOE15 are found to be about 52.01, 49.97 and 46.4 J/^{o}CA respectively at full load condition. Under simulated conditions, the values are found to be about 54.20, 49.93 and 47.31 J/^{o}CA for diesel, JME and ATJOE15 respectively.

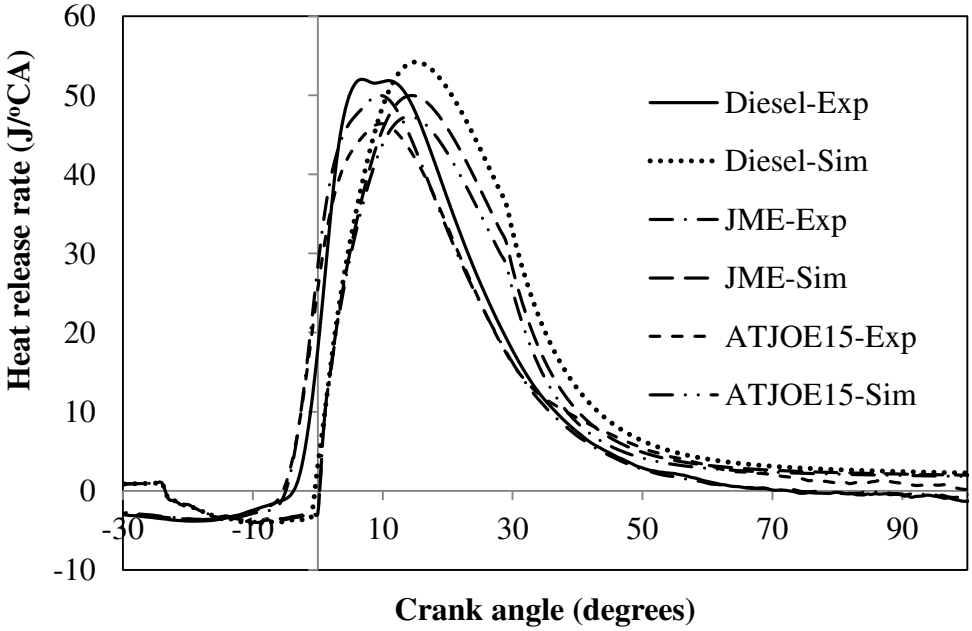

Fig. 5.3.2 Variation of maximum heat release rate with crank angle

For the JME and ATJOE15, less amount of fuel is accumulated during the shorter ignition delay period, which results in lower heat release rates compared to that of diesel at full load. The reasons are in agreement with those of Qi et al [168], when the diesel engine was fueled with ethanol-biodiesel-water micro emulsions. The oxygen present in JME and the quick

evaporation of the emulsified fuel ATJOE15 are the causes for the faster burning process [190].

5.3.4.3 Heat loss

The predicted results of the heat losses are shown in Fig.5.3.3. The difference between the heat energy available in the fuel and the apparent or net heat release gives the heat loss. A part of the released heat is lost to the cooling medium, through the walls of the cylinder and the cylinder head during the combustion and expansion processes.

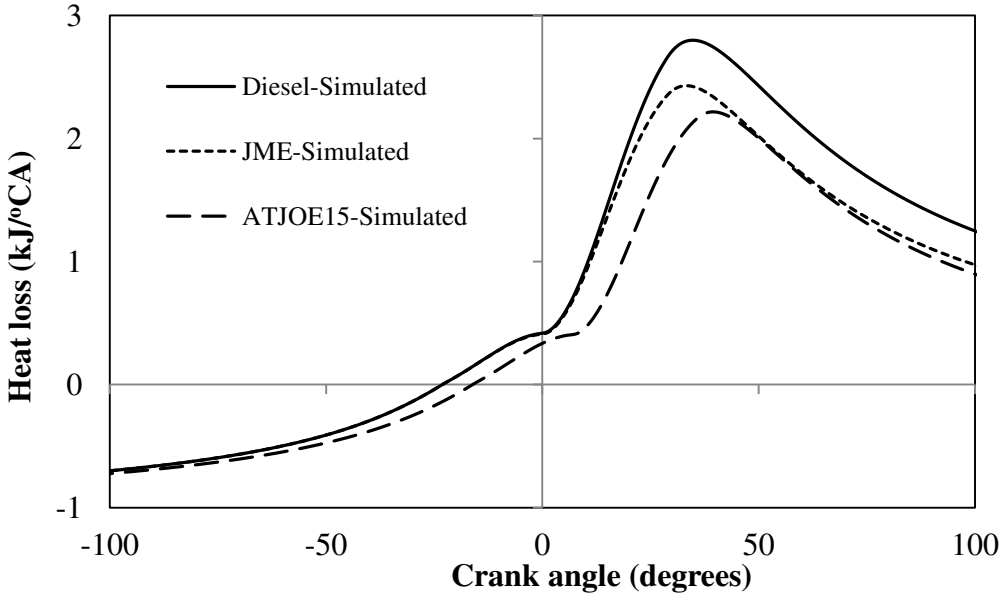

Fig. 5.3.3 Variation of heat losses with crank angle

A small fraction of the heat energy of the fuel is lost, as a result of the dissociation of some combustion products and incomplete chemical reactions. The heat losses due to incomplete combustion, gas leakage and dissociation are usually ignored, and the heat transfer losses by convection and radiation are estimated using empirical correlations [191]. In this case, the radiation component was not taken into consideration.

5.3.4.4 NO emissions

In the diesel engine exhaust, the NO_x emission is predominantly composed of NO, with lesser amounts of NO_2. Other oxides of nitrogen, such as N_2O, N_2O_5, NO_3 are negligible. In general, the NO_x formation mechanisms are described as thermal NO_x, prompt NO_x and fuel NO_x. Under most diesel engine combustion conditions, thermal NO_x is believed to be the predominant contributor to total NO_x. At high temperatures, occurring within the combustion chamber of a diesel engine, N_2 and O_2 can react through a series of chemical steps, known as

the Zeldovich mechanism. The NO_x formation occurs at temperatures above 1500 °C, and the rate of formation increases rapidly with increasing temperature [176]. Figure 5.3.4 depicts the comparison of NO emissions for the tested fuels, in both the experimental and simulated conditions. The experimental results of NO emissions at full load condition for diesel, JME and ATJOE15 are 2.05, 2.89, and 2.09 g/kWh respectively. In the case of simulated conditions, the NO values are found to be about 2.57, 2.822, and 2.112 g/kWh respectively, for the above said fuels.

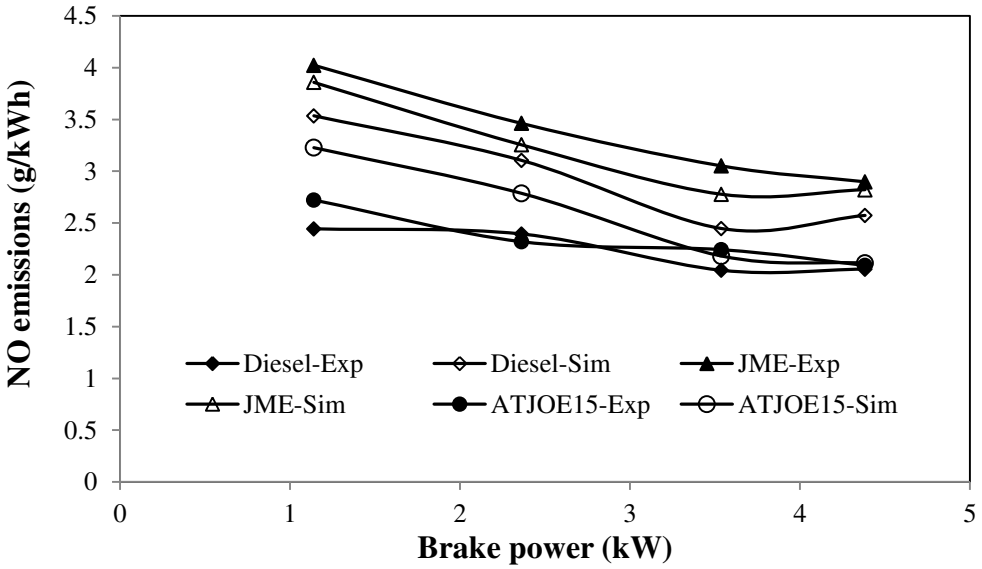

Fig. 5.3.4 Variation of NO emissions with brake power

It can be observed from the figure, that the NO emissions of the JME operation are higher, compared to those of ATJOE15 emulsion as well as diesel operation. The presence of the oxygen molecule in biodiesel causes an increase in the combustion gas temperature resulting in a marginal increase in the NO emissions. Also, it can be observed that the NO emission decreases with the addition of WPO content in the emulsions. This may be due to the water content present in the WPO, which will reduce the combustion temperature [146].

Figure 5.3.5 depicts the NO concentration with respect to the crank angle at full load under simulated conditions. It can be seen that the NO emission increases after the ignition, and reaches the maximum around 27^o aTDC, and then lasts until EVO (exhaust valve opening). The NO concentration is higher in the case of JME operation, and lower in the case of the ATJOE15 operation, in comparison with diesel data. The reduction in the NO concentration of the ATJOE15 may be due to the following two reasons.

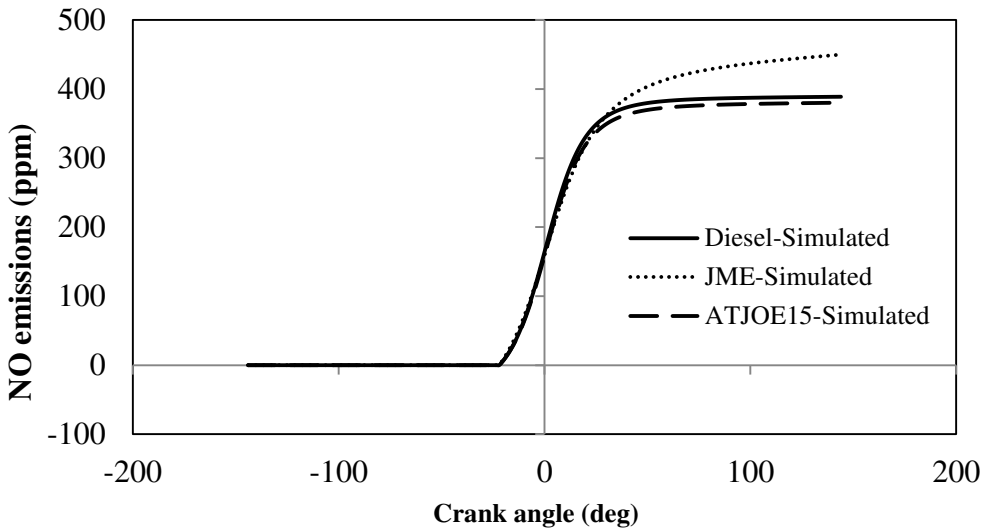

Fig. 5.3.5 Variation of NO concentration with crank angle at full load

First, the in-cylinder temperature decreases, because of the higher specific heat capacity of water available in the WPO. Secondly, the water content in the WPO results in the reduction of N_2 and O_2 concentrations and the improvement of the local rich oxygen [146].

5.3.4.5 Soot density

The variation in the soot density with brake power for both the experimental and simulated conditions is given in Fig. 5.3.6.

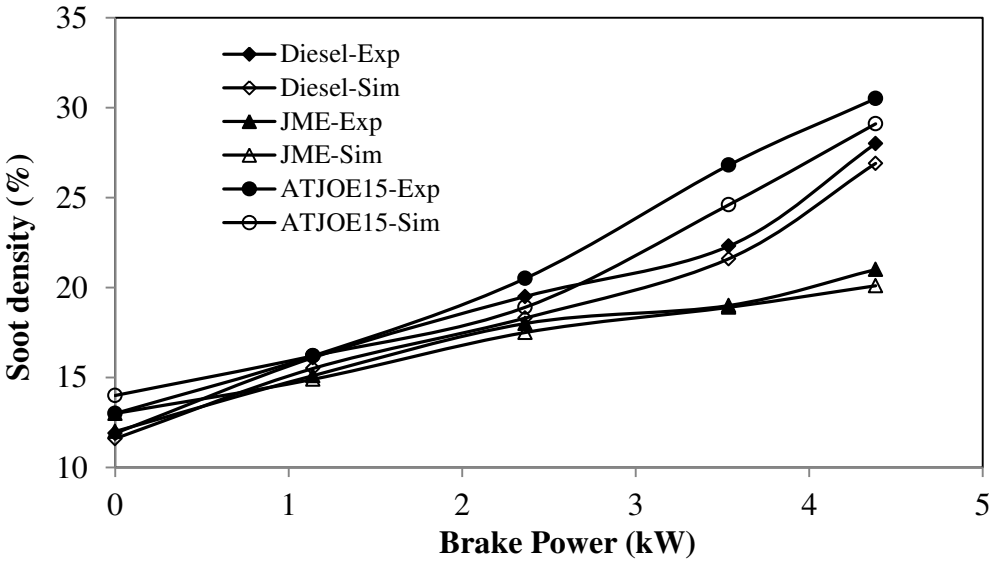

Fig. 5.3.6 Variation of soot density with brake power

Based on the experimental results, the percentage decrease in the soot density of 19.6% is observed with the JME at full load, in comparison with diesel. When fueled with the ATJOE15, the soot density increases by about 8% compared to that of diesel operation.

Under simulated conditions, the soot density is found to be lower for the JME operation by 25.2%, compared to that of diesel, and with the ATJOE15 emulsion, about 8% higher soot density is noticed. The higher soot density may be due to the larger droplets of the ATJOE15 emulsion compared to that of the other tested fuels.

5.3.5 Closure

In the present work, a comprehensive two zone model has been developed for a diesel engine, to validate the experimental results obtained with three different fuels, viz. diesel, JME and ATJOE15. The experimental investigation was conducted on a DI diesel engine. The results reveal that the developed model predicts adequately well, the combustion parameters for the three fuels examined. The conclusions of the results obtained from this study are as follows:

- The experimental and simulated results show that the peak cylinder pressures of the JME and the ATJOE15 are found to be marginally higher than that of diesel, and about 6.1% lower peak cylinder pressures are obtained with the ATJOE15 emulsion at simulated conditions compared to that of experimental conditions.
- The maximum heat release rates of JME and ATJOE15 are found to be lower than that of diesel fuel, in both the experimental and simulated conditions. Compared to experimental conditions, the maximum heat release rate of the ATJOE15 at simulated conditions is found to be lower by 1.96%.
- Compared to diesel operation, the NO concentration is found to be higher in the case of JME operation, and lower in the case of the ATJOE15 operation at both experimental and simulated conditions. With the simulated conditions, the NO emissions of the ATJOE15 emulsion are found to be higher by 1% compared to that of experimental conditions.
- The soot density is found to be lower for the JME operation and it is higher for the ATJOE15 operation compared to that of diesel. The soot density of the ATJOE15 emulsion at simulated condition is found to be lower by about 4.5% than that of experimental condition.

The presented model can predict the combustion characteristics such as cylinder pressure and heat release which are in good agreement with the experimental results.

5.4 Combined effects of the compression ratio and injection timing on the performance and emission parameters of a diesel engine fueled with the ATJOE15 emulsion

5.4.1 General

From the summary of the experimental results of the combustion, performance and emission characteristics of the single cylinder diesel engine fueled with the ATJOE15 emulsion, it is observed that the CO and NO emissions from ATJOE15 fueled engine are higher than that of diesel operation. In order to reduce the diesel engine pollutants, it is proposed to study the combined effects of varying the compression ratio and injection timing. Three different compression ratios (16.5, 17.5 and 18.5) and three injection timings (21.5, 23 and 24.5) are chosen for this study. The nozzle opening pressure is maintained at 200 bar. The results obtained are compared with those of diesel and JME operation, and discussed in this chapter.

5.4.2 Combustion parameters

5.4.2.1 Pressure crank angle history

Figure 5.4.1 depicts the pressure crank angle history of the engine fueled with the ATJOE15 emulsion, running at different compression ratios and injection timings at full load condition. It is observed from the figure, that the combustion starts earlier in the range between 1 and 4 ^{o}CA for the ATJOE15 emulsion, with the compression ratios of 17.5, 18.5 and at all three injection timings, compared to that of diesel at full load. For the same operating conditions, compared to the JME operation, it is found that the combustion starts earlier by about 0.5 to 1.5 ^{o}CA for the ATJOE15 emulsion at injection timings of 23 and 24.5 ^{o}CA. At a lower compression ratio of 16.5, it is found that the commencement of combustion is later by 0.5 to 3.5 ^{o}CA in comparison with diesel operation. The peak cylinder pressure for diesel occurs at 12.4 ^{o}CA aTDC, whereas for the ATJOE15 emulsion, the peak pressure occurs earlier in the range of 0.5 and 3 ^{o}CA, with the compression ratios of 17.5 and 18.5, at injection timings of 23 and 24.5 ^{o}CA bTDC compared to that of diesel. At a lower compression ratio of 16.5 and at retarded injection timing, the peak cylinder pressure is found to be lower in the range of 4 to 13 bar compared to that of diesel operation at full load. Similar results are reported by Kannan and Anand [192] in their investigation of a diesel engine, fueled with biodiesel obtained from waste cooking oil. It is seen from the figure, that among all the tested compression ratios and injection timings, with the compression ratio of 18.5 and advanced injection timing of 24.5 ^{o}bTDC, the ATJOE15 operation produced the highest cylinder pressure value of 85.8 bar at 369.5 ^{o}CA, which is earlier by 2.9 and 1 ^{o}CA than those of diesel

and the JME operations respectively. The early or later occurrences of the ignition are attributed to the increased or decreased cylinder gas temperature respectively.

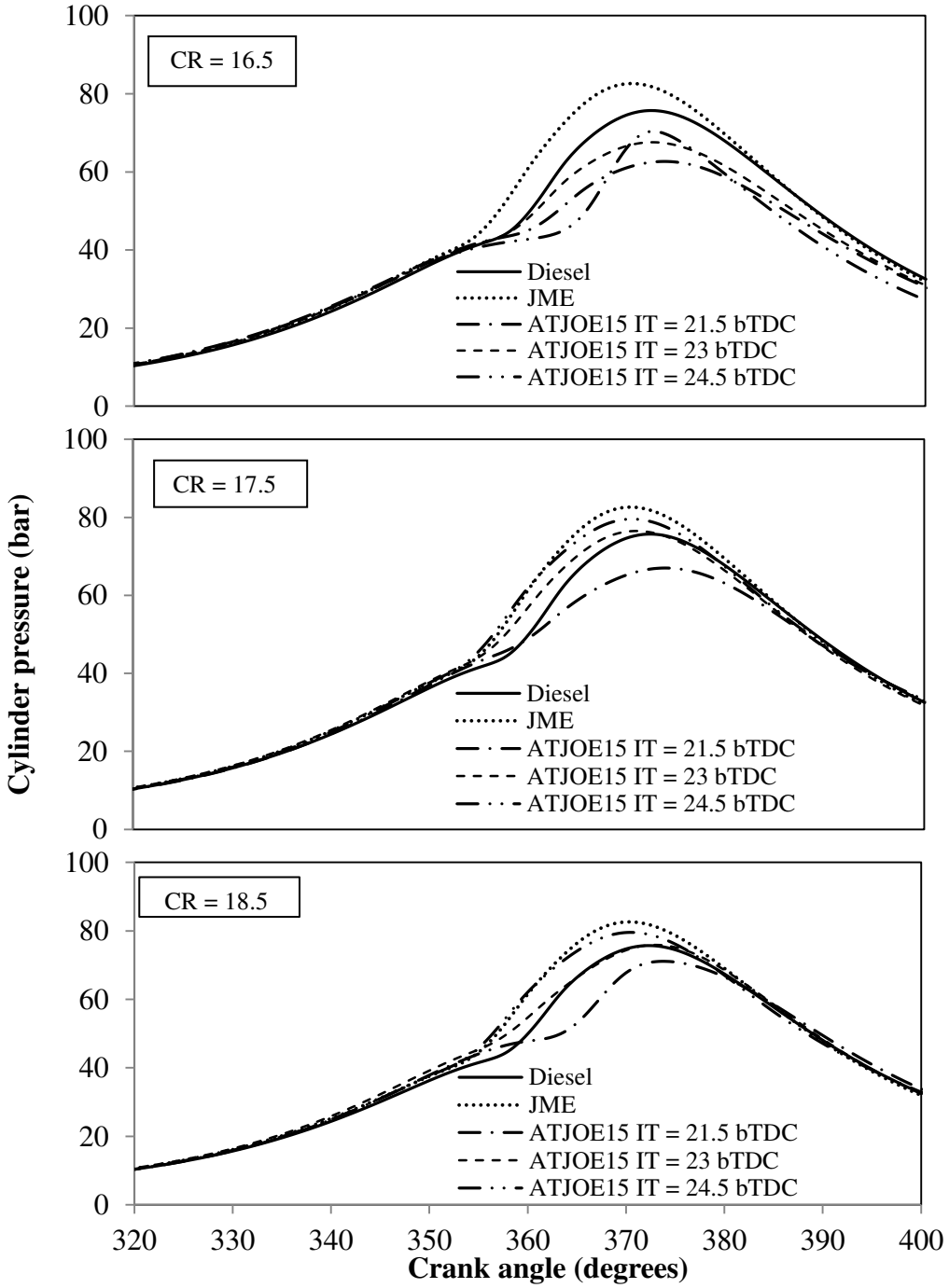

Fig. 5.4.1 Variation of cylinder pressure with crank angle at different compression ratios and injection timings

5.4.2.2 Ignition delay

Figure 5.4.2 depicts the ignition delay for diesel, JME and ATJOE15 for different compression ratios and injection timings at all loads. It is seen from the figure that the

ignition delay is found to be lower with the increase in the engine load, compression ratio and advancement in the injection timing. The reduction in the ignition delay in these conditions might be the result of a higher combustion chamber wall temperature at the time of injection and the reduced exhaust gas dilution [107].

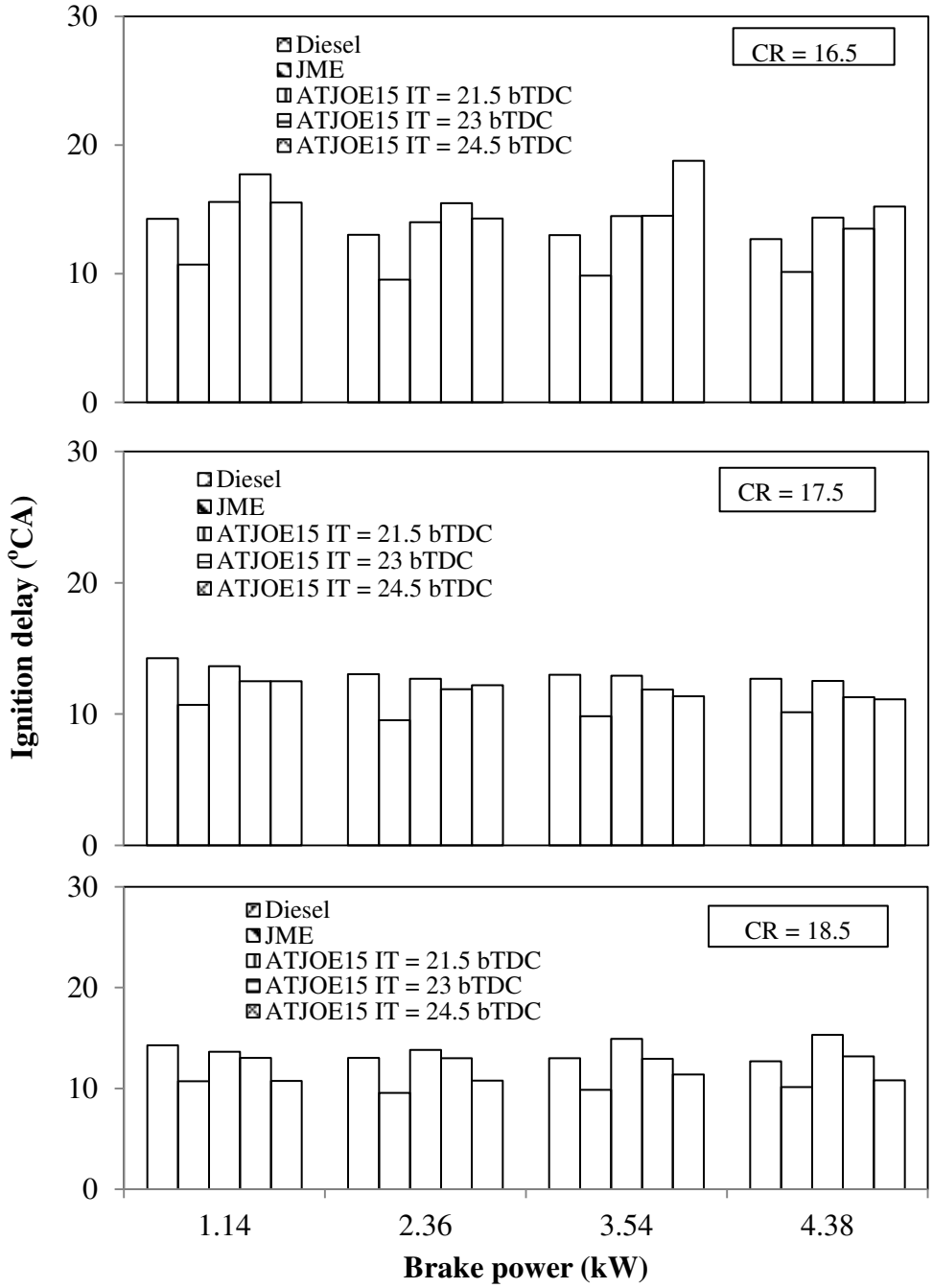

Fig. 5.4.2 Variation of ignition delay with brake power at different compression ratios and injection timings

At the lower compression ratio of 16.5, the ignition delay is found to be higher at an advanced injection timing, also due to the lower cylinder temperature. It is apparent from the figure, that at full load condition, the ignition delay of the ATJOE15 emulsion is found to be

shorter in the range of 0.2 to 1.8 ^{o}CA, with compression ratios of 17.5, 18.5 and the advanced injection timing of 24.5 ^{o}CA bTDC, compared to that of diesel operation. With the lower compression ratio of 16.5 and the retarded injection timing of 21.5 ^{o}CA, the ignition delay values of the ATJOE15 emulsion are found to be longer by about 0.8 to 2.6 ^{o}CA compared to that of diesel operation. In comparison with the JME operation, the engine fueled with the ATJOE15 emulsion exhibits a longer ignition delay at all operating conditions. Among all the tested compression ratios and injection timings, the minimum ignition delay period of 10.81 ^{o}CA is observed for the ATJOE15 operation, with the compression ratio of 18.5 and injection timing of 24.5 ^{o}CA bTDC. The reduction in the ignition delay period is mainly due to the increased cylinder gas temperature, at a higher compression ratio and a higher cetane number of the ATJOE15, compared to that of diesel.

5.4.2.3 Heat release rate

Figure 5.4.3 illustrates the variation of heat release rate, with respect to the crank angle for the ATJOE15 emulsion at full load, for different compression ratios and injection timings. Because of the vaporization of the fuel accumulated during the ignition delay period, at the beginning a negative heat release is observed and after combustion, this behaviour becomes positive. The occurrence of the maximum heat release rate for the ATJOE15 emulsion at different operating conditions on an average, shifted by about 2 to 8 ^{o}CA at full load, compared to that of diesel operation. The intensity of the premixed combustion phase for diesel is found to be the highest, whereas, it is lower in the case of JME and the ATJOE15 emulsion, at compression ratios 17.5, 18.5 and advanced injection timings.

With the lower compression ratio of 16.5, injection timing of 24.5 ^{o}CA bTDC, and compression ratio of 18.5, injection timing of 21.5 ^{o}CA bTDC, the premixed phase of combustion is found to be higher than that of diesel operation. The deviation in the maximum heat release rate between the diesel operation and the ATJOE15 emulsion at different compression ratios and injection timings varies between -14 J/^{o}CA and 15 J/^{o}CA. For the JME and ATJOE15 emulsion, less amount of fuel is accumulated during the shorter ignition delay period, which results in lower heat release rates compared to that of diesel at higher compression ratios.

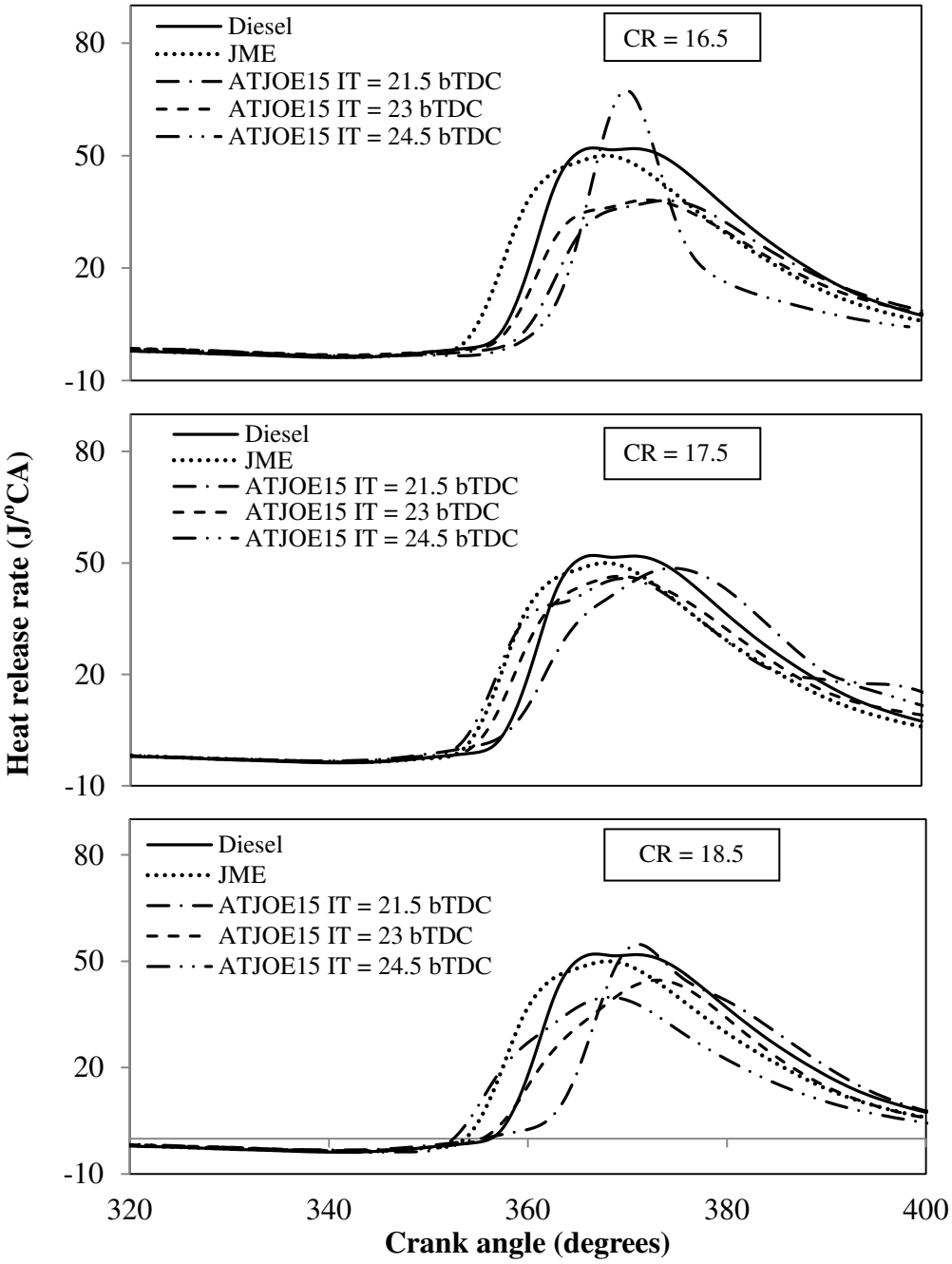

Fig. 5.4.3 Variation of heat release rate with crank angle at different compression ratios and injection timings

5.4.2.4 Maximum cylinder pressure

Figure 5.4.4 depicts the variation of maximum cylinder pressure with brake power for the ATJOE15 emulsion at full load for the different compression ratios and injection timings. It is seen from the figure that the peak cylinder pressure is increased with an increase in the engine load at all operating conditions. With the lower compression ratios, the peak cylinder gas pressure for the JME and diesel is higher than that of the ATJOE15 emulsion at all

injection timings, and at higher compression ratios, the trend is the opposite. This shows that, with higher compression ratios and advanced injection timing, the ATJOE15 emulsion showed faster premixed combustion, which leads to a higher peak cylinder gas pressure.

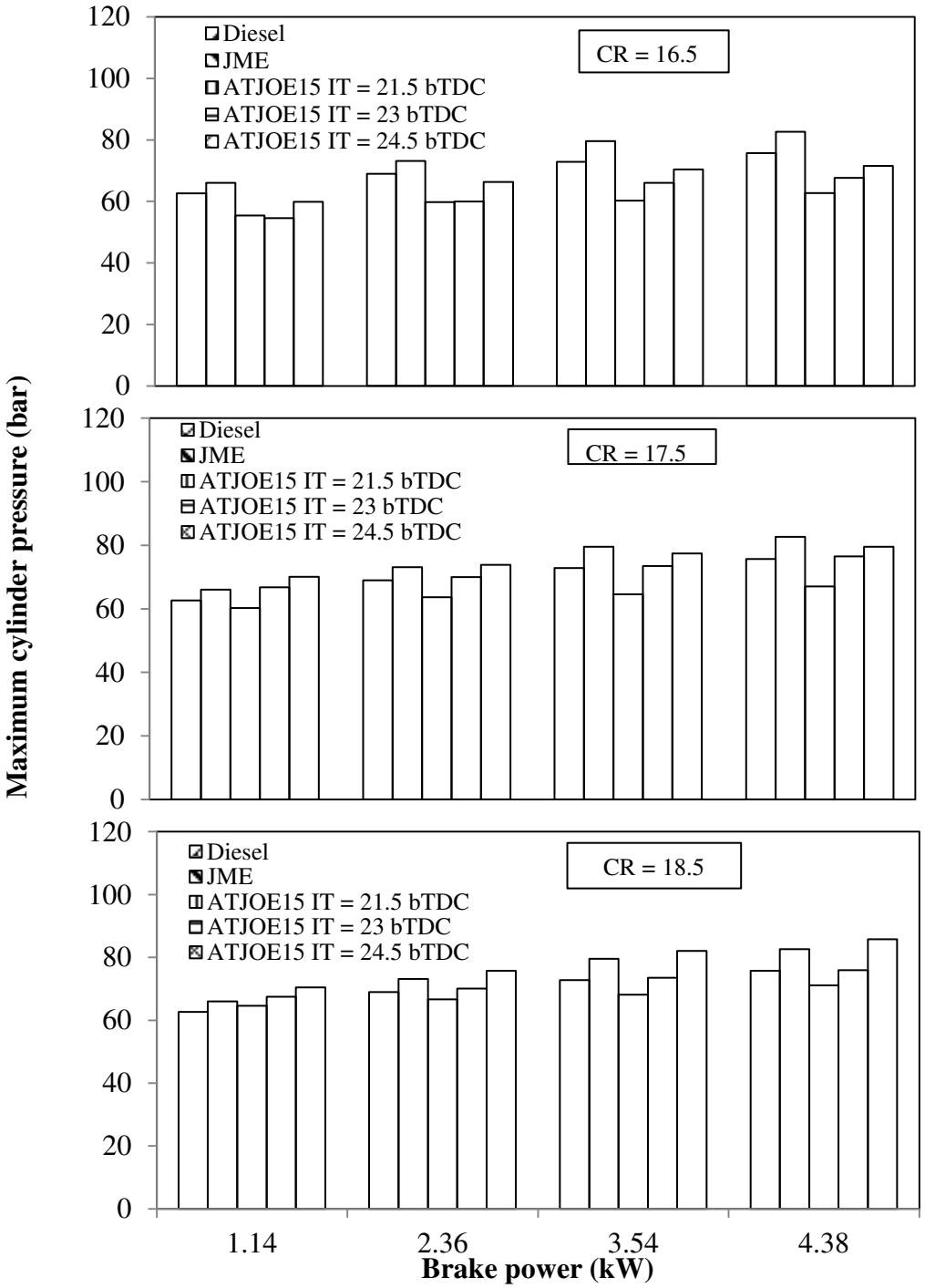

Fig. 5.4.4 Variation of maximum cylinder pressure with brake power at different compression ratios and injection timings

With the compression ratio of 16.5 and all three injection timings, the maximum cylinder pressure of the ATJOE15 emulsion is found to be lower in the range between 4 and 13 bar

compared to that of diesel operation at full load. Also, with the higher compression ratios and retarded injection timing, the maximum cylinder pressure is found to be lower than that of diesel operation. At compression ratios of 17.5, and 18.5, and at standard and advanced injection timings, the maximum cylinder pressure values of the ATJOE15 emulsion are higher in the range of 0.2 to 10 bar compared to that of diesel operation at full load. This may be due to the reduction in the clearance volume, which increases the density of the cylinder gases during the burning process. This increases the peak cylinder pressure and temperature. Except at a compression ratio of 18.5 and advanced injection timing of 24.5 ^{o}CA bTDC, at all other conditions the peak cylinder pressure is found to be lower than that of JME operation.

5.4.2.5 Combustion duration

Figure 5.4.5 illustrates the variation of the combustion duration with the brake power, under different compression ratios and injection timings of the engine fueled with the ATJOE15 emulsion, JME and diesel. The duration between the starting and ending of heat release is called as combustion duration. The combustion duration increases with engine load, owing to the increase of the fuel quantity. It is seen from the figure that the combustion duration decreases with an increase in the compression ratio, which is attributed to the high temperature prevailing inside the cylinder and at lower compression ratios, the trend is the opposite. At a compression ratio 18.5 and at full load, the values of combustion duration are 38.4, 38, 36.08, 37.31 and 37.72 ^{o}CA for diesel, JME and ATJOE15, at injection timings 21.5, 23 and 24.5 ^{o}CA bTDC respectively. The combustion duration of the ATJOE15 is found to be lower between 0.7 and 1.4 ^{o}CA compared to that of diesel at the compression ratio 18.5. At a lower compression ratio of 16.5, the combustion duration of the ATJOE15 emulsion is found to be higher than that of diesel and the JME operation, which is attributed to a longer ignition delay. At 16.5 compression ratio and at different injection timings, the combustion duration of the ATJOE15 emulsion, is found to be higher in the range of 2.83 to 9.06 ^{o}CA and 2.87 to 9.46 ^{o}CA compared to that of diesel and the JME respectively.

At the standard compression ratio of 17.5 and at different injection timings, the combustion duration of the ATJOE15 emulsion is found to be higher between 0.3 and 3.5 ^{o}CA and 0.7 and 3.9 ^{o}CA, compared to that of diesel and the JME respectively. As the calorific value of the ATJOE15 emulsion is lower than that of diesel, a greater quantity of fuel is consumed to maintain the engine speed constant at various loads. Hence, the higher total fuel consumption is the cause for the longer combustion duration of the ATJOE15emulsion than that of diesel.

Similar reasons are reported by Arulmozhi selvan et al. [193] in their work on diesel-biodiesel-ethanol blends.

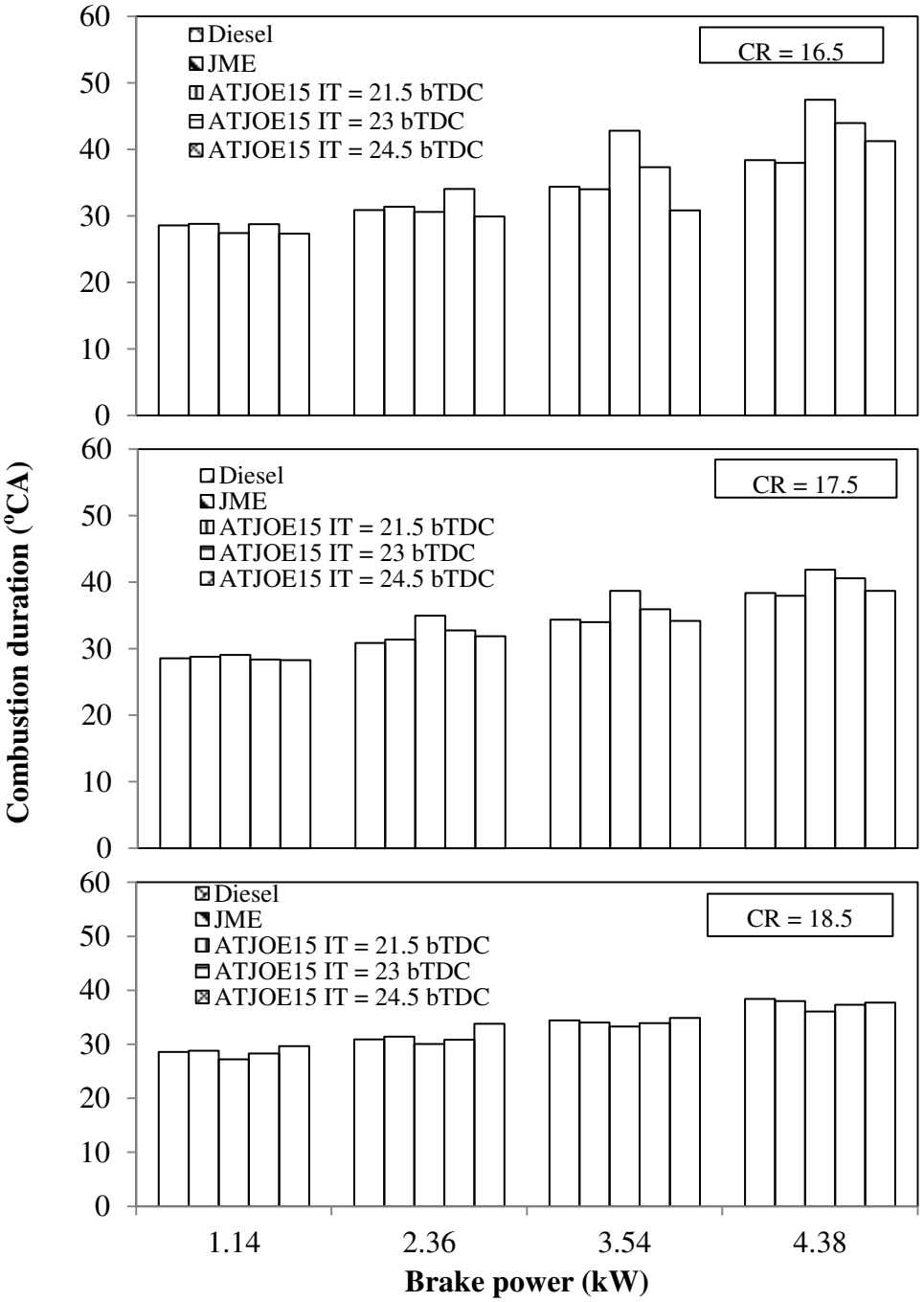

Fig. 5.4.5 Variation of combustion duration with brake power at different compression ratios and injection timings

5.4.3 Performance parameters

5.4.3.1 Brake thermal efficiency

The variation of brake thermal efficiency with brake power for the ATJOE15 at different compression ratios and injection timings, in comparison with the JME and diesel, is shown in

Fig. 5.4.6. It is seen from the figure that, for all the compression ratios and injection timings tested, the brake thermal efficiency of the ATJOE15 emulsion increases with an increase in the load.

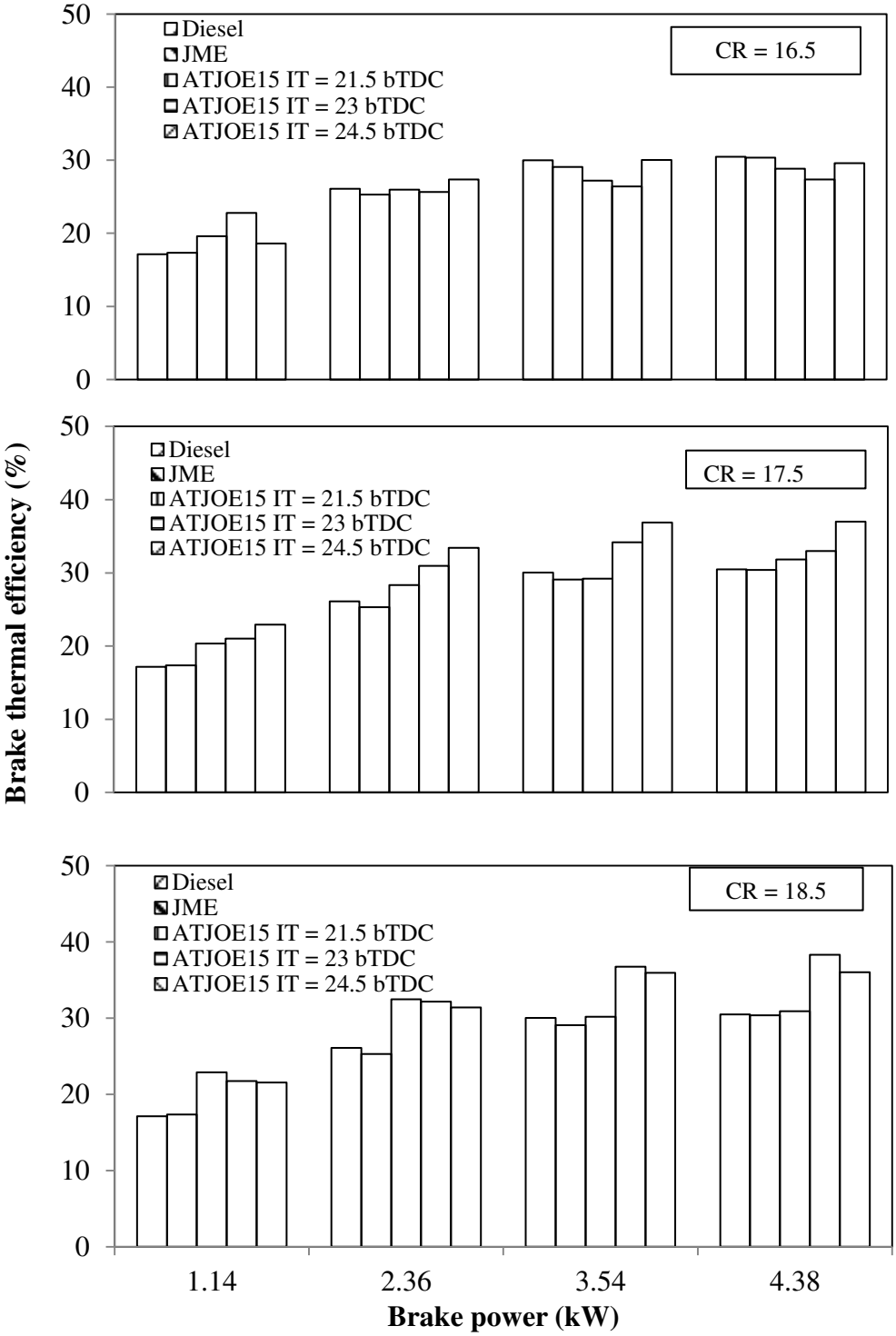

Fig. 5.4.6 Variation of brake thermal efficiency with brake power at different compression ratios and injection timings

At the standard compression ratio and injection timing, the ATJOE15 emulsion produced a maximum thermal efficiency of 32.98% which is higher by about 8.2% compared to that of diesel operation. For the same compression ratio, when the injection timing is retarded by 1.5 ^{o}CA, the brake thermal efficiency of the ATJOE15 emulsion dropped by about 3.5%, but still it is found to be higher than those of diesel and the JME operations, by about 4.4% and 4.7% respectively. When the injection timing is advanced to 24.5 ^{o}CA bTDC, the thermal efficiency of the ATJOE15 emulsion is found to be higher by about 6.5% and 6.8% compared to that of diesel and the JME operations respectively at full load. The advancement in the fuel injection produces a peak pressure closer to TDC, and offers sufficient time to release heat; hence it offers higher thermal efficiency.

When the compression ratio is decreased to 16.5, the brake thermal efficiency of the ATJOE15 emulsion is found to be lower at all the injection timings, which may be due to the poor combustion characteristics caused by the longer ignition delay. The brake thermal efficiency of the ATJOE15 emulsion at this compression ratio is lower, in the order of 2.9% to 5.2% compared to that of diesel operation. With the higher compression ratio of 18.5, the brake thermal efficiency of the ATJOE15 emulsion is found to be higher, in the order of 1.4%, 25% and 18.4% respectively, at injection timings 21.5, 23 and 24.5 ^{o}CA bTDC respectively at full load. This could be due to the fact, that the ATJOE15 emulsion had lower volatility compared to that of diesel, and therefore, the improvement in its combustion characteristics might have been relatively more at higher temperatures resulting from the higher compression ratio.

5.4.3.2 Brake specific fuel consumption

The variation of the brake specific fuel consumption with brake power for diesel, JME and ATJOE15 emulsion, at various compression ratios and injection timings, is depicted in Fig. 5.4.7. It is apparent from the figure, that the BSFC values of the ATJOE15 emulsion are found to be higher than those of diesel and the JME operations, at all compression ratios and injection timings, which is attributed to the lower calorific value of the ATJOE15 emulsion. When comparing the BSFC of the ATJOE15 emulsion at different compression ratios and injection timings, the BSFC values are comparatively higher, with a lower compression ratio and retarded injection timings. The minimum value of the BSFC obtained with 16.5 compression ratio is 0.388 kg/kWh at an advanced injection timing 24.5 ^{o}CA bTDC, which is higher by about 44% compared to that of diesel operation at full load.

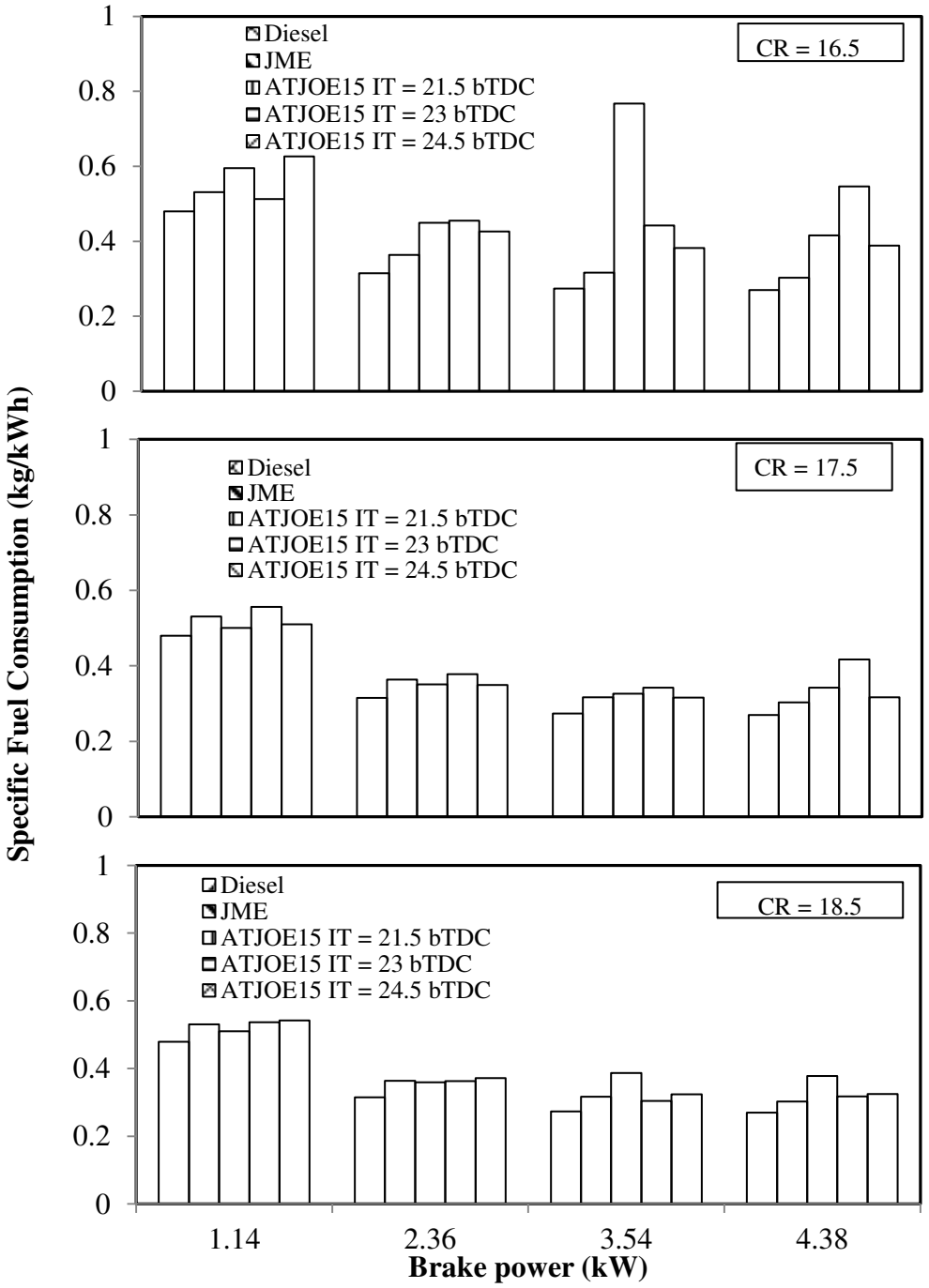

Fig. 5.4.7 Variation of specific fuel consumption with brake power at different compression ratios and injection timings

At the standard compression ratio of 17.5 and advanced injection timing of 24.5 ^{o}CA bTDC, the minimum BSFC obtained is 0.316 kg/kWh, which is higher by about 17.4% compared to that of diesel. The minimum BSFC value of 0.317 kg/kWh is obtained at the compression ratio 18.5 and injection timing 23 ^{o}CA bTDC, which is higher by about 17.8% compared to that of diesel at full load. The BSFC of the ATJOE15 emulsion is found to be lower at a higher compression ratio for all the injection timings. The possible reason for this trend could

be, that with an increase in the compression ratio, the maximum cylinder pressure increases due to the fuel injected in the hotter combustion chamber leading to higher effective power. This will, in turn, decrease the fuel consumption per power output. A similar reason was reported by Ulusoy et al. [194] in their work on biodiesel obtained from used frying oils.

5.4.3.3 Exhaust gas temperature

The variation of the exhaust gas temperature with load for the ATJOE15 emulsion, in comparison with the JME and diesel at different compression ratios and injection timings is depicted in Fig. 5.4.8.

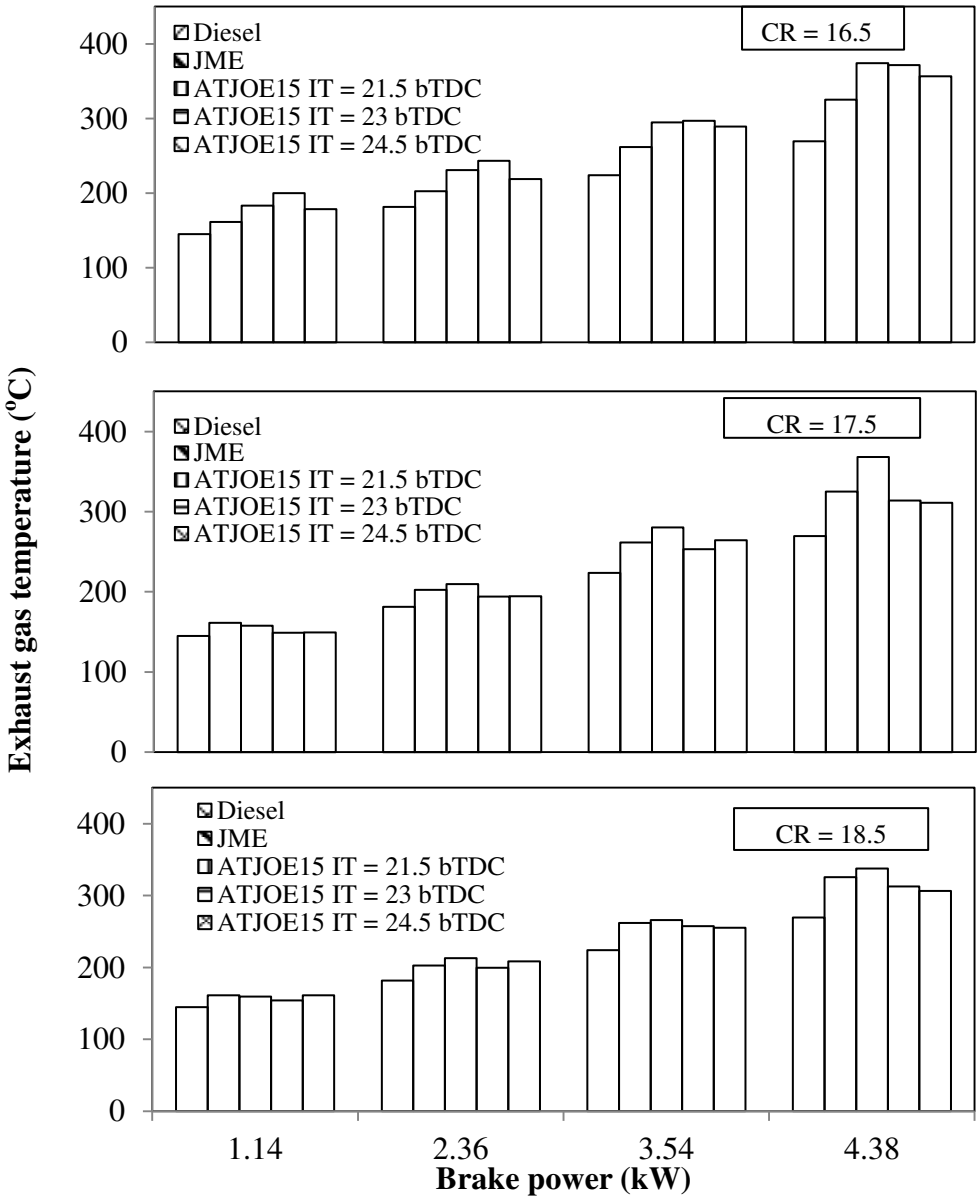

Fig. 5.4.8 Variation of exhaust gas temperature with brake power at different compression ratios and injection timings

It is revealed from the figure, that the exhaust gas temperature of ATJOE15 emulsion increased with an increase in the brake power and decreased with an increase in the compression ratio and advanced injection timings for all the fuels. Also, it can be ascertained from the figure that the engine operating parameters, which resulted with a minimum BSFC and maximum brake thermal efficiency, were the ones which contributed the minimum exhaust gas temperature.

On an average, the exhaust gas temperature of the ATJOE15 emulsion is reduced by about 14.3%, when the compression ratio was increased from 17.5 to 18.5. The possible reason for this trend could be that the increased compression ratio actually increases the air temperature inside the cylinder consequently reducing the ignition delay causing a better and more complete burning of the fuel. Similarly, at advanced injection timings, the exhaust gas temperature of the ATJOE15 emulsion is found to be lower by about 33% than that of retarded injection timings at full load. This might be due to the favourable pressure-temperature profile, which resulted in higher thermal efficiencies at advanced injection timings. The efficiency of the engine cycles increases, when the conversion of chemical energy into heat is concentrated near the TDC. These results are in agreement with those of Rahemen and Ghadge [195], when they conducted experiments with magua biodiesel at variable compression ratios and injection timings.

5.4.4 Emission parameters

5.4.4.1 BSHC emissions

The variations of brake specific HC emissions with the brake power for the ATJOE15 emulsion, JME and diesel at different compression ratios and injection timings are shown in Fig. 5.4.9. The BSHC emissions decreased with increasing engine load. This happened due to higher cylinder gas temperatures at higher engine loads, which led to more efficient combustion of fuel at higher temperatures, producing lower quantities of HC emissions. At advanced injection timings, improved air–fuel mixing is achieved due to the availability of more time for the mixing process; therefore, this led to lower HC emissions.

With the lower compression ratio, the HC emissions are found to be drastically higher, compared to that of diesel and the JME operations. At a lower compression ratio, insufficient heat of compression, delays the ignition, and so, the HC emissions increased. Similar reasons

are reported by Jindal et al [20] in their work, on the effect of the compression ratio and nozzle opening pressure in a DI diesel engine running on Jatropha methyl ester.

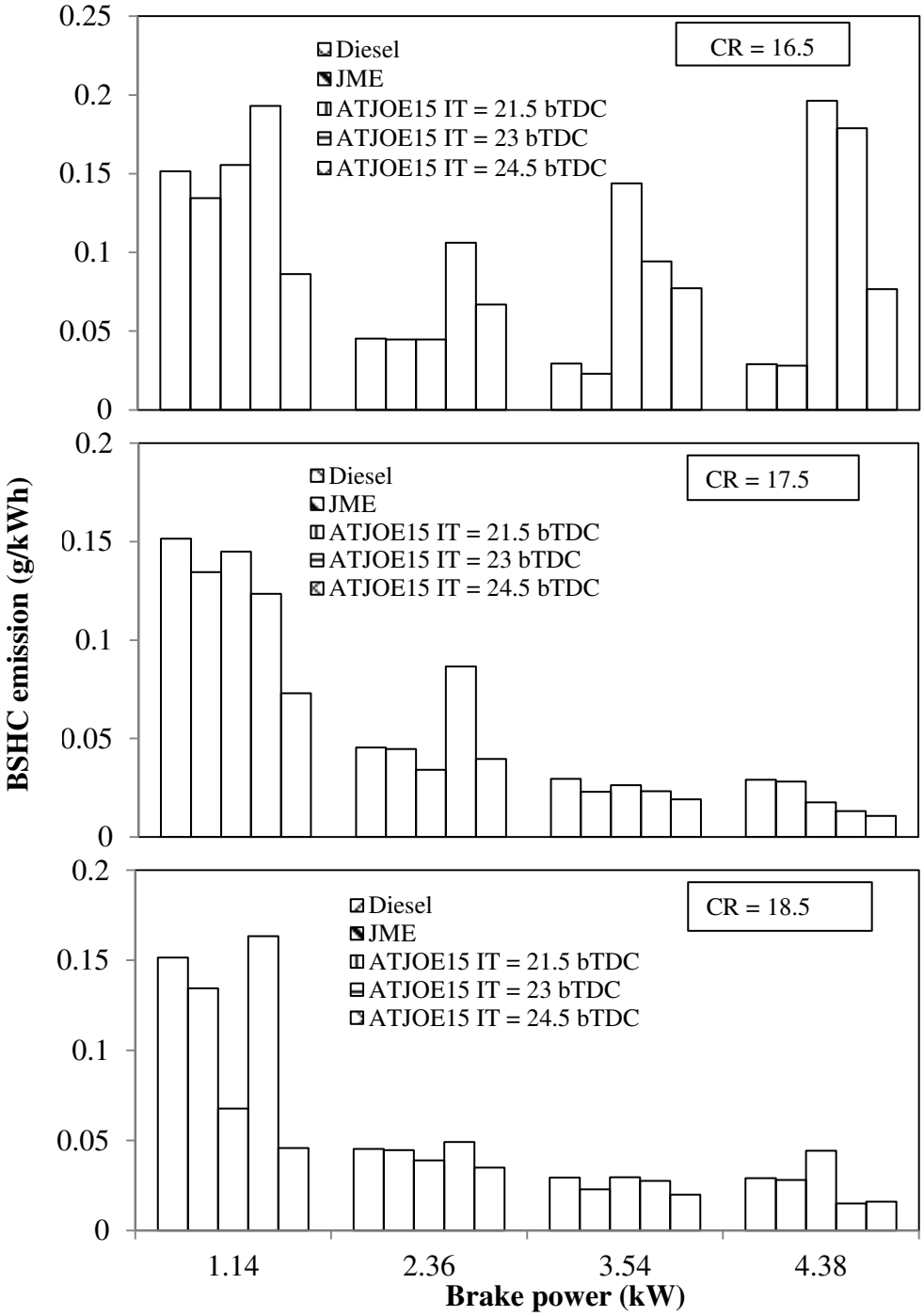

Fig. 5.4.9 Variation of BSHC emission with brake power at different compression ratios and injection timings

At the standard compression ratio, the HC emissions of the ATJOE15 emulsion at different injection timings are found to be lower in the range of 39.5% to 65.5%, compared to that of diesel at full load. At a higher compression ratio, the HC emissions of the ATJOE15 emulsion at standard and advanced injection timings are found to be lower between 45.1%

and 48.2%, compared to those of diesel at full load. At retarded injection timing, the HC emission of ATJOE15 is found to be higher by 52.7%, in comparison with diesel at full load.

5.4.4.2 BSCO emissions

Figure 5.4.10 illustrates the variation of brake specific CO emissions with brake power for the ATJOE15 emulsion, at different compression ratios and injection timings, in comparison with JME and diesel.

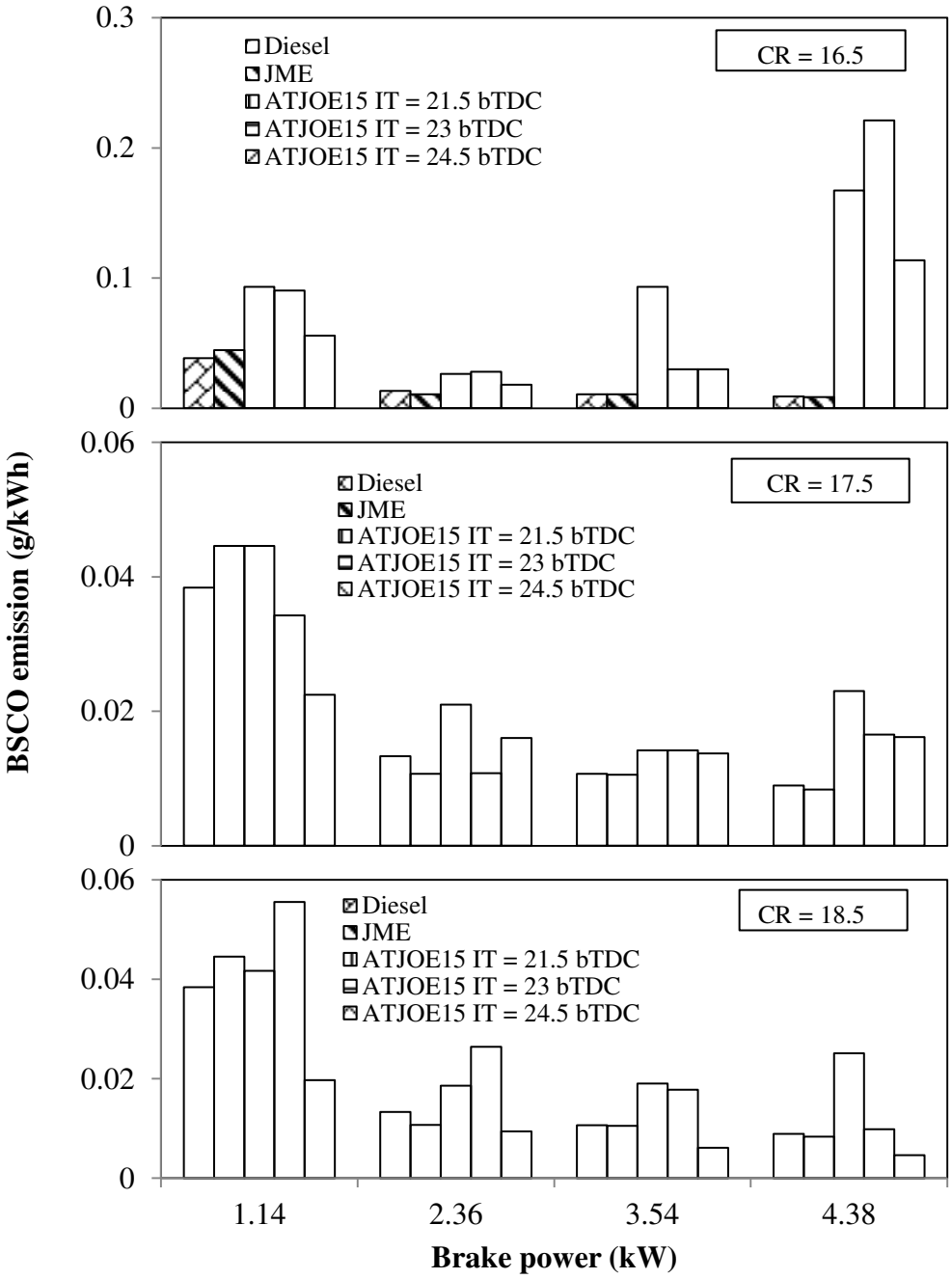

Fig. 5.4.10 Variation of BSCO emission with brake power at different compression ratios and injection timings

With the lower compression ratio of 16.5, the temperature reached is also low, and thus, more CO is exhausted from the engine. The minimum value of CO obtained at this compression ratio is about 0.037 g/kWh, which is higher by about 31.5% compared to that of diesel operation at full load. At the standard compression ratio of 17.5, the CO emissions of ATJOE15 are found to be higher by 61.1%, 45.9% and 44.8% at 21.5 ^{o}CA, 23 ^{o}CA and 24.5 ^{o}CA bTDC injection timings respectively at full load, compared to that of diesel operation. The longer spray penetration, larger fuel droplets and insufficient swirl may be the factors for higher CO emissions in the case of the ATJOE15 emulsion. This reason was supported by Pei Lin Zhou [181], in his research work. It can be observed that the CO emissions are higher at retarded injection timing, and lower with the advancement in the start of ignition. An advancement in the injection timing can also cause a higher cylinder temperature and an increase in the oxidation process between carbon and oxygen molecules, which will lead to a decrease in the CO emissions. This statement is in agreement with Sayin et al [196] in their work on the effect of injection timing on the emissions of a diesel engine fueled with conala methyl ester. At the higher compression ratio of 18.5, the CO emissions of ATJOE15 are found to be higher, at retarded and standard injection timing conditions, by about 64.5% and 9% in comparison with diesel operation. At an advanced injection timing, the CO emissions are found to be lower by about 48% compared to that of diesel. The possible reason for this trend could be, that the increased CR actually increases the air temperature inside the cylinder, reducing the ignition delay, causing a better and more complete burning of the fuel. Similar reasons are reported by Raheman and Ghadge [195], in their work on mahua biodiesel with variable compression ratios.

5.4.4.3 BSNO emissions

Figure 5.4.11 depicts the variation of brake specific nitric oxide (BSNO) emissions with respect to brake power for the ATJOE15, at different compression ratios and injection timings. It is apparent that the BSNO emissions are found to be higher by 29% and 2% in the JME and ATJOE15 operations, compared to that of diesel at full load, standard compression ratio and injection timing. The oxygen content of JME increases the cylinder maximum gas temperature with better combustion, and this tends to increase the NO concentration. With the compression ratio of 17.5, in the ATJOE15 operation, an advancement in the injection timing leads to further increase in NO emissions by about 26.7% and a retardation in the injection timing gives a reduction in the NO emissions of 12.8%, in comparison with diesel at full load. Retarding the injection timing decreases the peak cylinder pressure, because more

fuel burns after TDC. The lower peak cylinder pressures result in lower peak temperatures. As a consequence, the NO concentration starts to diminish. With the advanced injection timings the reason is vice versa. Similar reasons are reported by Sayin et al [197], in their work on the effect of injection timing on a diesel engine fueled with the methanol- diesel blends. In comparison with the JME, the NO emissions from the ATJOE15 emulsion are found to be lower, in the order of 3.2% to 38.2% at the compression ratio of 17.5 and different injection timings at full load.

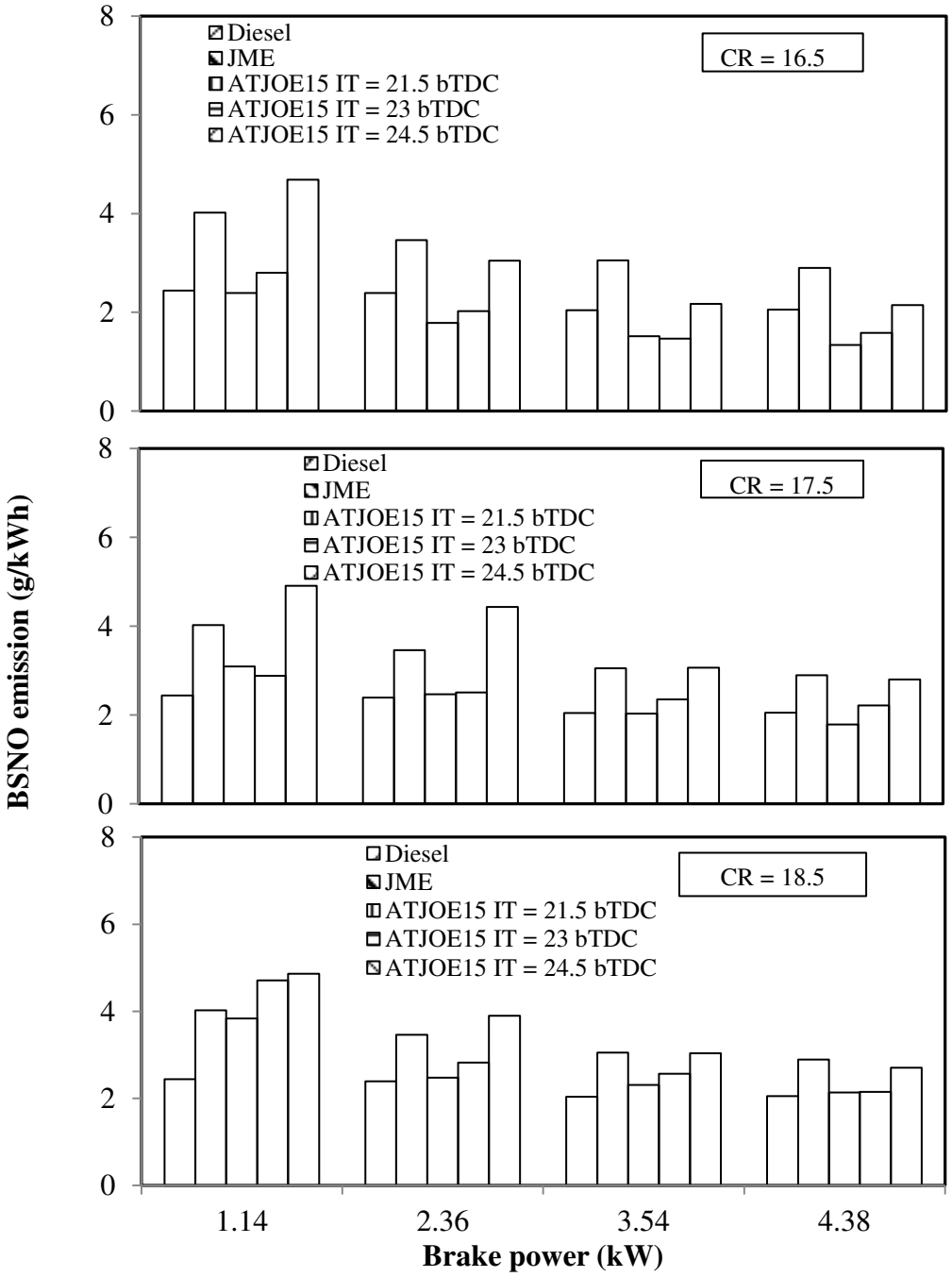

Fig. 5.4.11 Variation of BSNO emission with brake power at different compression ratios and injection timings

When the compression ratio is reduced to 16.5, the NO emissions of the ATJOE15 emulsion are found to be lower by about 34.9% and 23%, compared to that of diesel operation at retarded and standard injection timings. With the advanced injection timing, the NO values are found to be higher by about 4.5% in comparison with diesel operation. When compared to the JME operation, the NO emissions of the ATJOE15 emulsion are found to be lower in the range between 25.8% and 53.8%. A lower compression ratio will reduce the in-cylinder temperatures, and thus, the flame temperatures during combustion, which will suppress the NO emissions. Similar reasons were reported by Raheman and Ghadge [195], in their work on mahua biodiesel with variable compression ratios. With the higher compression ratio of 18.5, the NO emissions from the ATJOE15 emulsion are found to be higher in the range of 4% to 31.8% compared to that of diesel at full load.

5.4.4.4 Smoke opacity

Figure 5.4.12 depicts the variation of smoke opacity, with respect to brake power for the ATJOE15 at different compression ratios and injection timings, the JME and diesel. The percentage decrease in the smoke opacity of 19.6% is observed for the JME at full load in comparison with diesel at the standard compression ratio and injection timing. This may be because, the JME contains oxygen, which reduces locally over the rich region, and the formation of crucial smoke. In the case of ATJOE15 emulsion, the smoke opacity is found to be higher by about 8.9% and 45% at standard and retarded injection timings at full load. When the injection timing is advanced, the smoke opacity value of the ATJOE15 is found to be lower by about 5.3%, compared to that of diesel operation. The values of smoke opacity of the ATJOE15 at different injection timings are higher in the range of 26% to 58% compared to that of JME operation.

At a reduced compression ratio of 16.5, the smoke opacities of the ATJOE15 emulsion at all injection timings were found to be higher in the range between 32% and 52%, compared to that of diesel operation at full load. At a higher compression ratio of 18.5, the smoke opacity of the ATJOE15 emulsion at retarded injection timing is found to be lower by about 4.2% and in the advanced injection timing case, the smoke emission values reduced by about 11.7% compared to that of diesel. As the compression ratio increases, the maximum temperature during the combustion increases, and this, in turn, decreases the smoke opacity, and it is vice versa in the case of a lower compression ratio.

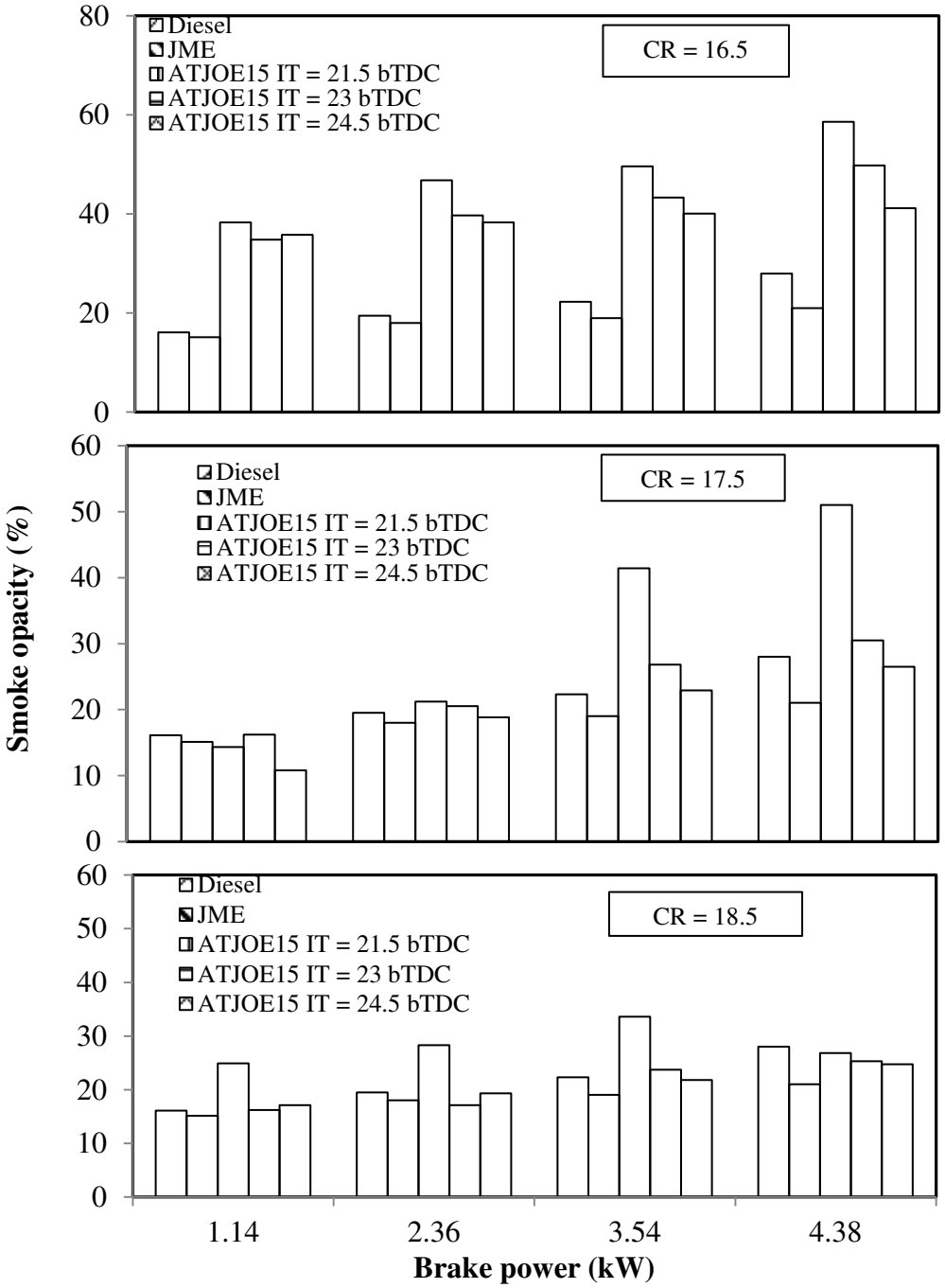

Fig. 5.4.12 Variation of smoke opacity with brake power at different compression ratios and injection timings

5.4.5 Closure

The summary of the experimental results on the effect of the compression ratio and injection timing on the combustion, performance and emission parameters obtained in a single cylinder diesel engine fueled with the ATJOE15 emulsion indicates, that this fuel can be used in a variable compression ratio engine. From the analysis, it is revealed that the ATJOE15 emulsion gives an improved performance and lower emissions, when the engine is operated

with a higher compression ratio of 18.5 and retarded injection timing of 21.5 ^{o}CA bTDC. The NO emission in this condition is still found to be higher by about 31.8% compared to that of diesel operation, at full load. The smoke opacity of the ATJOE15 emulsion with this compression ratio and at retarded injection timing, is found to be lower by about 4.2% compared to that of diesel at full load.

5.5 Combined effects of compression ratio and nozzle opening pressure on the combustion, performance and emission parameters of a diesel engine fueled with ATJOE15 emulsion

5.5.1 General

This chapter discusses the combined effects of the compression ratio and fuel nozzle opening pressure on the combustion, performance and emission characteristics of the diesel engine fueled with the ATJOE15 emulsion. From the summary of the experimental results on the combustion, performance and emission results in the single cylinder diesel engine fueled with the ATJOE15 emulsion, it is observed that the CO and NO emissions from the engine fueled with the ATJOE15 emulsion are higher than those of diesel operation. In this research, it is proposed to study the combined effect of varying the compression ratio and nozzle opening pressure of the engine fueled with the ATJOE15 emulsion, in comparison with diesel and the JME operation. Three different compression ratios, viz., 16.5, 17.5 and 18.5, and three nozzle opening pressures viz. 200, 220 and 240 bar, were chosen for this study. The standard injection timing of 23 ^{o}CA bTDC is maintained for this study.

5.5.2 Combustion parameters

5.5.2.1 Pressure crank angle history

Figure 5.5.1 depicts the pressure crank angle history of the engine fueled with diesel, JME and the ATJOE15 emulsion for different compression ratios and nozzle opening pressures, at full load condition. It is observed from the figure, that the combustion starts earlier in the range between 0.4 and 2.1 ^{o}CA for the ATJOE15 emulsion, with the compression ratios of 17.5, 18.5, and at all three nozzle opening pressures compared to that of diesel. For the same operating conditions, compared to the JME operation, it is found that the combustion starts later by about 0.5 to 2.3 ^{o}CA for the ATJOE15 emulsion at all the nozzle opening pressures. At the lower compression ratio of 16.5, the commencement of combustion is noticed later, which ranges from 0.3 to 2.3 ^{o}CA in comparison with the diesel operation. The peak cylinder pressure for diesel occurs at 12.4 ^{o}CA aTDC, whereas for the ATJOE15, the peak pressure occurs earlier in the range of 0.3 and 1.2 ^{o}CA, with the compression ratios of 17.5 and 18.5, and the nozzle opening pressures of 220 and 240 bar, compared to that of diesel at full load. With the lower compression ratio of 16.5 and at all nozzle opening pressures, the peak cylinder pressure is found to be lower in the range of 8.1 to 11.2 bar, compared to that of diesel operation. Similar results are reported by Kannan and Anand [192], in their investigation on a diesel engine fueled with biodiesel obtained from waste cooking oil. It is

seen from the figure, that among all the tested compression ratios and nozzle opening pressures, with the compression ratio of 18.5 and with the nozzle opening pressure of 220 bar, the ATJOE15 operation produced the highest cylinder pressure value of 77.2 bar at 372.1 ^{o}CA, which is earlier by about 0.3 ^{o}CA and later by about 1.6 ^{o}CA than those of diesel and JME operations respectively. The early or later occurrences of ignition are attributed to the increased or decreased cylinder gas temperature respectively.

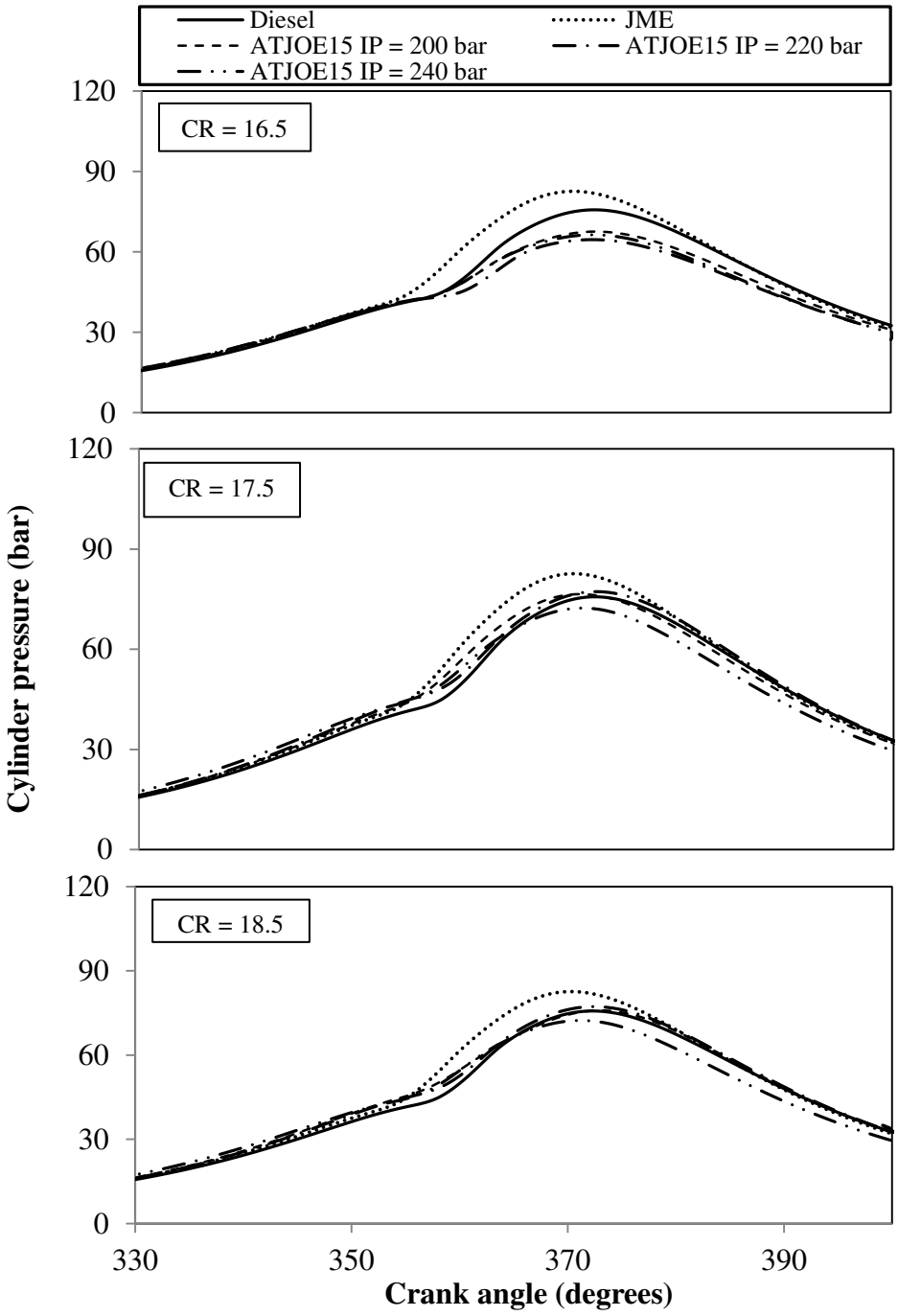

Fig. 5.5.1 Variation of cylinder pressure with crank angle at different compression ratios and nozzle opening pressures

5.5.2.2 Ignition delay

Figure 5.5.2 depicts the ignition delay for diesel, JME and ATJOE15 for the different compression ratios and nozzle opening pressures at all loads. It is seen from the figure, that the ignition delay is found to be lower with the increase in the engine load, compression ratio and nozzle opening pressure. The reduction in the ignition delay in these conditions, might be the result of higher combustion chamber wall temperature at the time of injection and the reduced exhaust gas dilution [107].

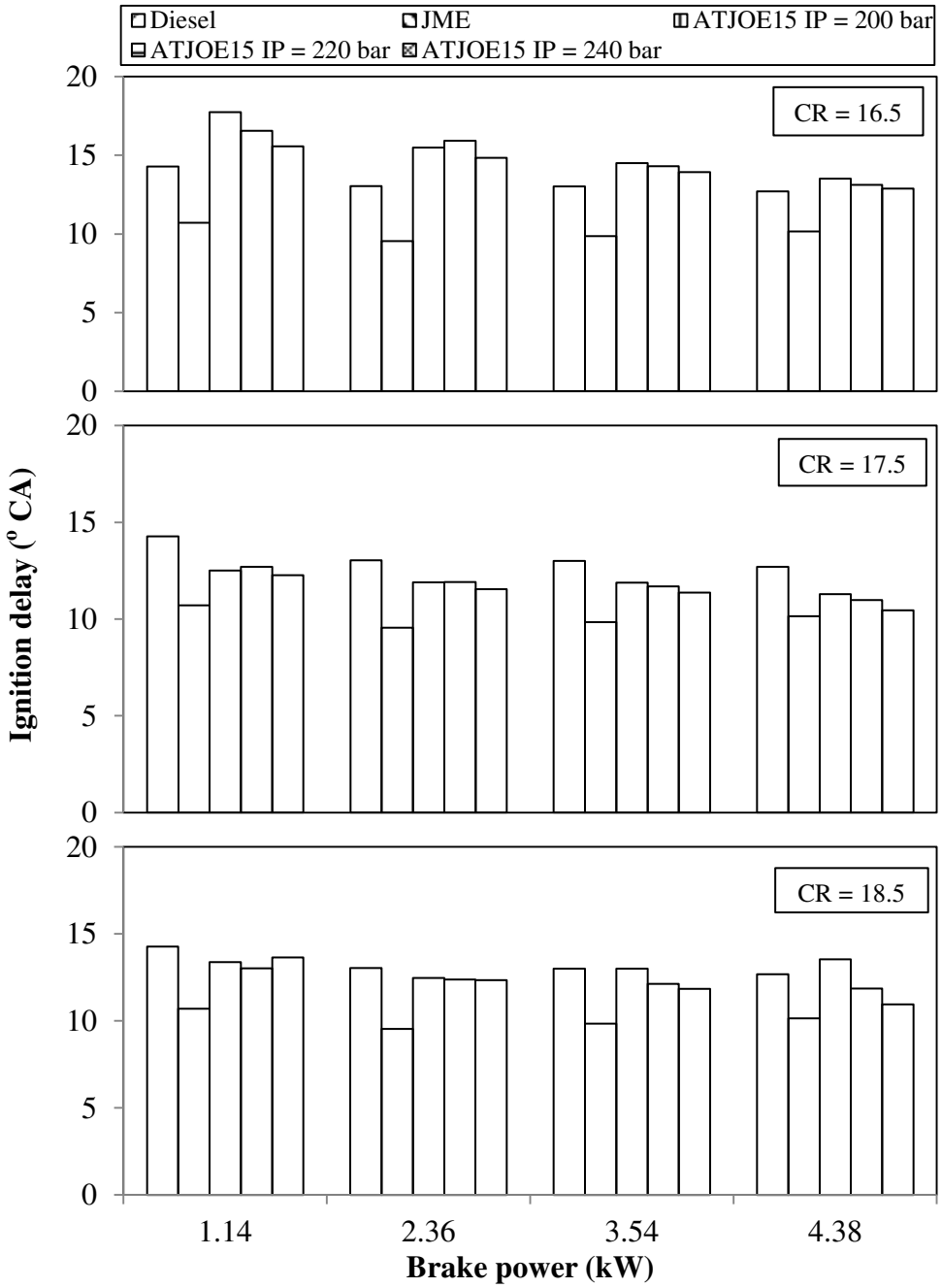

Fig.5.5.2 Variation of ignition delay with brake power at different compression ratios and nozzle opening pressures

With the lower compression ratio of 16.5, the ignition delay of the ATJOE15 emulsion is found to be higher than those of diesel and JME at all nozzle opening pressures, due to the lower cylinder temperature. At this compression ratio and for all the nozzle opening pressures, the ignition delay values of the ATJOE15 emulsion are found to be longer by about 0.2 to 1 ^{o}CA compared to that of diesel operation at full load. It is apparent from the figure, that at full load condition, the ignition delay of the ATJOE15 emulsion is found to be shorter in the range between 0.3 and 2.2 ^{o}CA with the compression ratios of 17.5, 18.5 and the higher nozzle opening pressure of 240 bar compared to that of diesel operation. In comparison with the JME operation, the engine fueled with the ATJOE15 emulsion exhibits a longer ignition delay at all operating conditions. Among all the tested compression ratios and nozzle opening pressures, a minimum ignition delay period of 10.45 ^{o}CA is observed for the ATJOE15 operation with the compression ratio of 17.5 and nozzle opening pressure of 240 bar. The reduction in the ignition delay period is mainly due to the improved atomization at higher nozzle opening pressure and higher cetane number of the ATJOE15 compared to that of diesel, at full load.

5.5.2.3 Heat release rate

Figure 5.5.3 illustrates the variation of the heat release rate with respect to the crank angle, for the ATJOE15 emulsion at full load for the different compression ratios and nozzle opening pressures, and for diesel and JME operations. The occurrence of the maximum heat release rate for the ATJOE15 emulsion at different operating conditions on an average, shifted approximately from 0.4 ^{o}CA to 6.4^{o}CA at full load, compared to that of diesel operation. The intensity of the premixed combustion phase for diesel is found to be the highest, whereas, it is lower in the case of JME and the ATJOE15 emulsion at compression ratios of 17.5, 18.5 and higher nozzle opening pressures.

At a lower compression ratio of 16.5, at all the nozzle opening pressures, the premixed combustion is found to be higher than that of diesel operation, as a result of longer ignition delay. The variation of the maximum heat release rate between diesel, JME operations and the ATJOE15 emulsion at different compression ratios and nozzle opening pressures lies between 7.4 and 15.71 J/^{o}CA. For the JME and the ATJOE15 emulsion, less amount of fuel is accumulated during the shorter ignition delay period, which results in lower heat release rates compared to that of diesel at higher compression ratios.

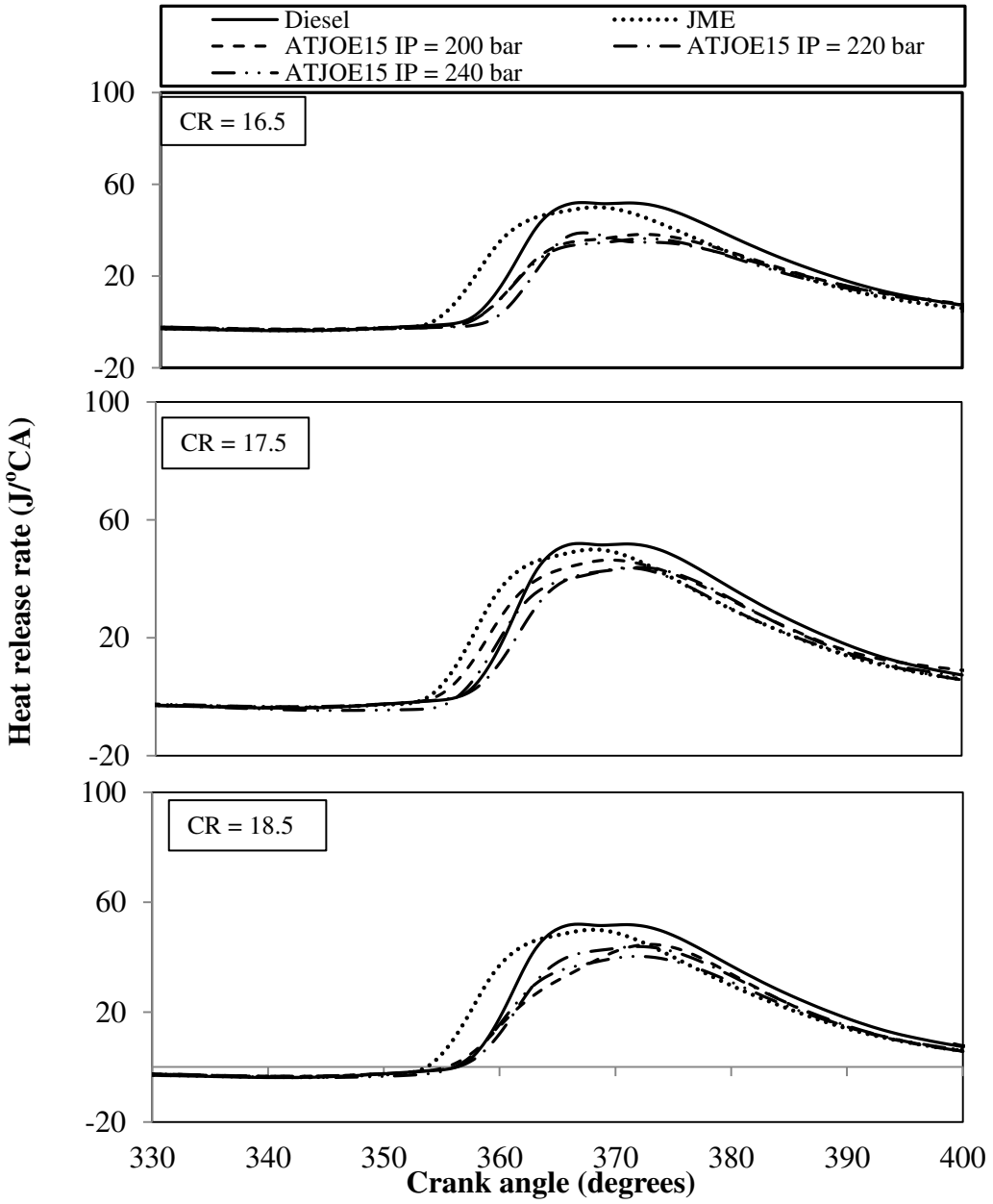

Fig. 5.5.3 Variation of heat release rate with crank angle at different compression ratios and nozzle opening pressures

5.5.2.4 Maximum cylinder pressure

Figure 5.5.4 depicts the variation of the maximum cylinder pressure with brake power for diesel, JME and the ATJOE15 emulsion at full load, for the different compression ratios and nozzle opening pressures. It is seen from the figure that the peak cylinder pressure is increased with an increase in the engine load at all operating conditions. With the lower compression ratio of 16.5, the peak cylinder gas pressures for JME and diesel are found to be higher than that of the ATJOE15 emulsion at all nozzle opening pressures, while the trend is the reverse, at higher compression ratios. This shows that, at higher compression ratios and

all nozzle opening pressures, the ATJOE15 emulsion showed faster premixed combustion, which leads to a higher peak cylinder gas pressure. At the compression ratio of 16.5 and all three nozzle opening pressures, the maximum cylinder pressure of the ATJOE15 emulsion is found to be lower in the range between 9.3 bar and 11.1 bar, compared to that of diesel operation at full load. With the compression ratios of 17.5, 18.5 and at all nozzle opening pressures, the maximum cylinder pressure values of the ATJOE15 emulsion are noticed to be higher in the range of 0.3 to 1.5 bar compared to that of diesel operation.

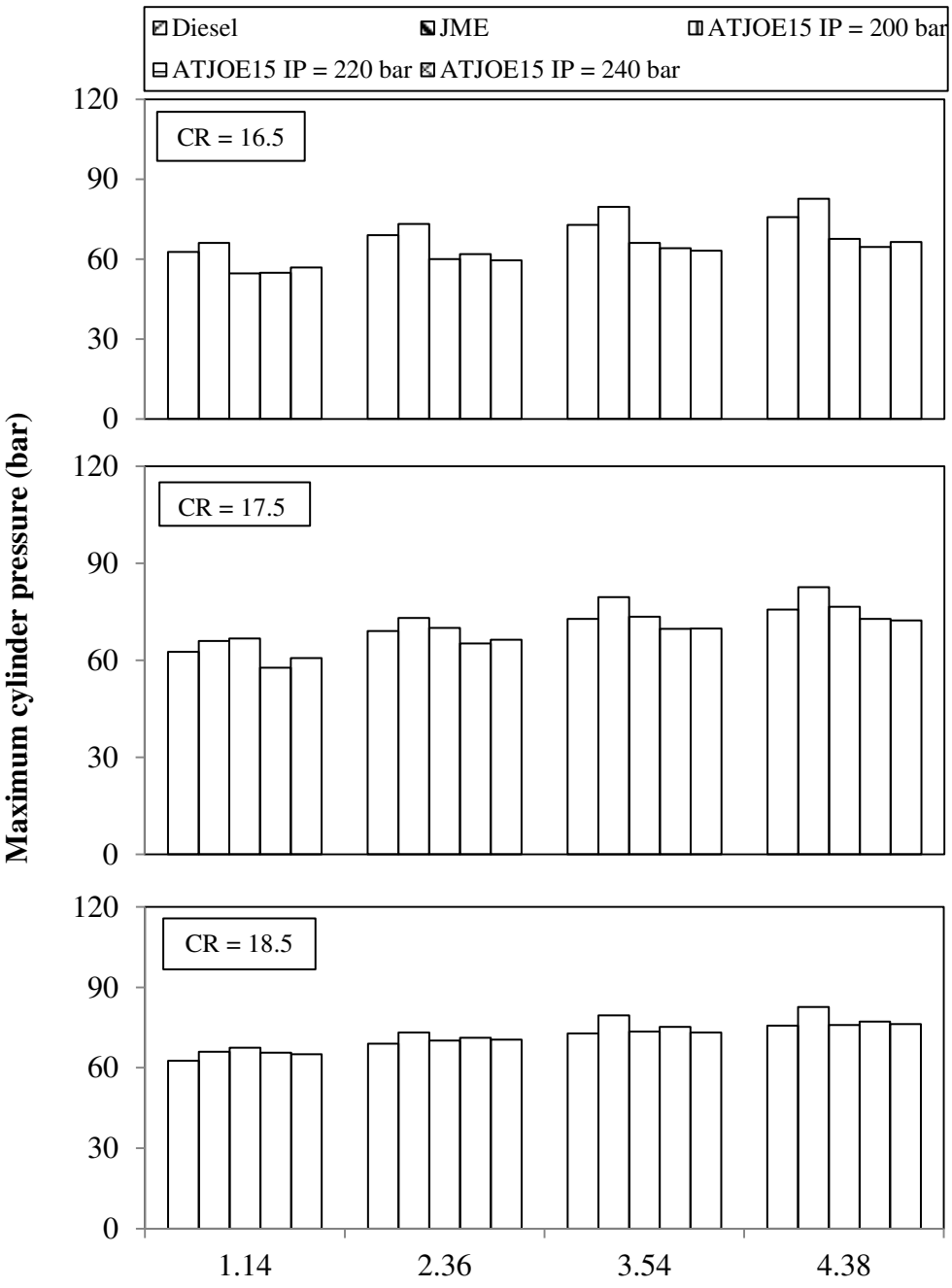

Fig. 5.5.4 Variation of maximum cylinder pressure with brake power at different compression ratios and nozzle opening pressures

This may be due to the reduction in the clearance volume, which increases the density of the cylinder gases during the burning process. This increases the peak cylinder pressure and temperature. In comparison with the JME operation, the peak cylinder pressure of the ATJOE15 emulsion is found to be lower, at all the load conditions.

5.5.2.5 Combustion duration

The variation of the combustion duration with the brake power under different compression ratios and nozzle opening pressures, for the engine fueled with the ATJOE15 emulsion, JME and diesel is illustrated in Fig. 5.5.5.

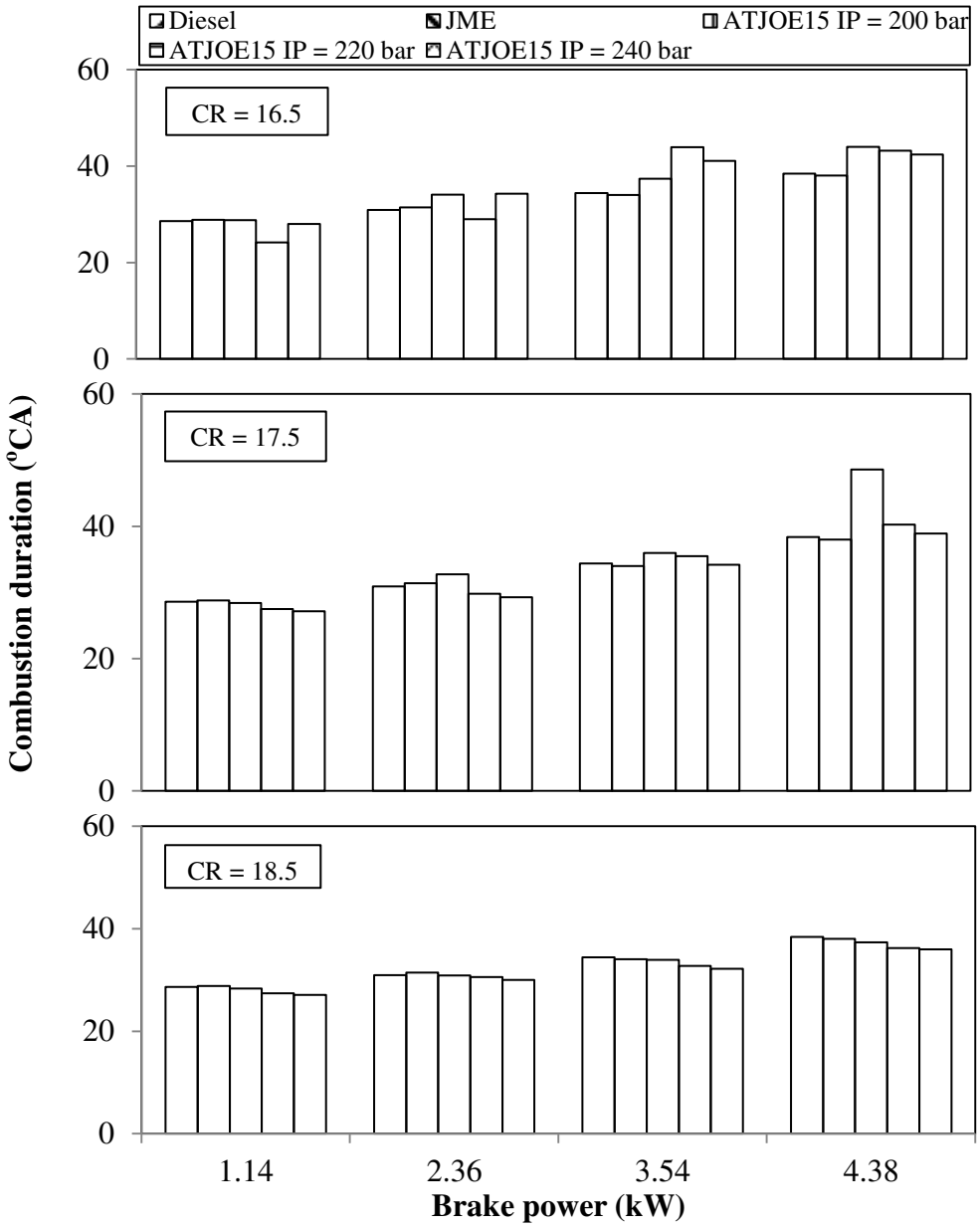

Fig. 5.5.5 Variation of combustion duration with brake power at different compression ratios and nozzle opening pressures

The combustion duration increases with engine load owing to the increase of the fuel quantity. It is seen from the figure that the combustion duration decreases with an increase in the compression ratio and nozzle opening pressure, which is attributed to a high temperature prevailing inside the cylinder, and at a lower compression ratio, the trend is the opposite. With the compression ratio of 18.5 and at full load, the values of the combustion duration are found to be 38.4, 38, 36.3, 36.2 and 35.9 ^{o}CA for diesel, JME and ATJOE15, at nozzle opening pressures of 200, 220 and 240 bar respectively. At a higher compression ratio, the increase in the nozzle opening pressure leads to a lower combustion duration of the ATJOE15 emulsion compared to that of diesel operation. Similar results are reported by Cenk Sayin et al. [198], in their study of the effect of fuel nozzle opening pressure on the combustion and performance characteristics of a DI diesel engine fueled with canola oil methyl esters-diesel fuel blends. The combustion duration of the ATJOE15 is found to be lower, between 2.1 and 2.5 ^{o}CA, compared to that of diesel at the compression ratio of 18.5. With the lower compression ratio of 16.5, the combustion duration of the ATJOE15 emulsion is found to be higher by an average of 4.7 ^{o}CA and 5.1 ^{o}CA, than that of diesel and the JME operation, which is attributed to a longer ignition delay. At the compression ratio of 17.5 at different nozzle opening pressures, the combustion duration of the ATJOE15 emulsion is found to be higher in the range from 0.5 to 10.2 ^{o}CA and 0.9 to 10.6 ^{o}CA, compared to those of diesel and the JME respectively.

5.5.3 Performance parameters

5.5.3.1 Brake thermal efficiency

The variation of brake thermal efficiency with brake power for the ATJOE15 emulsion in comparison with the JME and diesel, at different compression ratios and nozzle opening pressures is depicted in Fig. 5.5.6. It is seen from the figure that, for all the compression ratios and nozzle opening pressures tested, the brake thermal efficiency of the ATJOE15 emulsion increases with the increase in the load. With the standard compression ratio and nozzle opening pressure, the ATJOE15 emulsion produced a maximum thermal efficiency of 32.98% which is higher by about 3.6% compared to that of diesel operation. For the same compression ratio, with the higher nozzle opening pressures of 220 bar and 240 bar, the brake thermal efficiency of ATJOE15 emulsion is found to be higher than that of diesel by about 4.6% and 6.1% respectively, at full load. The increase in the brake thermal efficiency of ATJOE15 emulsion is due to better combustion as a result of the nozzle opening pressure.

This is in agreement with the results reported by Kannan and Anand [192] in their work on waste cooking oil.

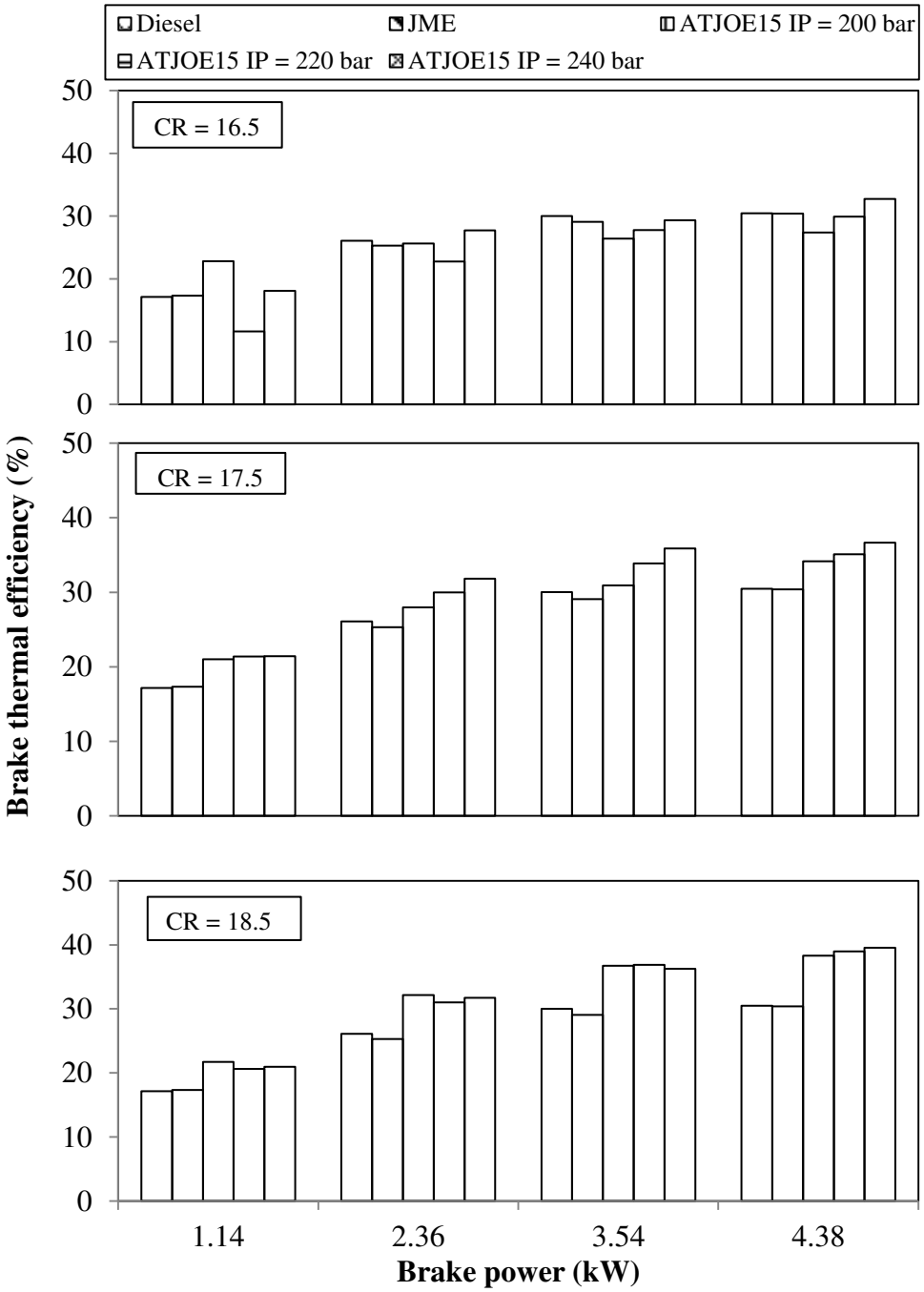

Fig. 5.5.6 Variation of brake thermal efficiency with brake power at different compression ratios and nozzle opening pressures

When the compression ratio is decreased to 16.5, the brake thermal efficiency of the ATJOE15 emulsion is found to be lower by 3.1% and 0.6% at 200 and 220 bar nozzle opening pressures respectively, at full load, which may be due to the poor combustion characteristics caused by the longer ignition delay. At 240 bar nozzle opening pressure, the

brake thermal efficiency of the ATJOE15 emulsion at this compression ratio is found to be higher in the order of 2.3% compared to that of diesel operation. With the higher compression ratio of 18.5, the brake thermal efficiency of the ATJOE15 emulsion is found to be higher in the order of 7.8%, 8.5% and 9% respectively at nozzle opening pressures 200, 220 and 240 bar respectively.

5.5.3.2 Brake specific fuel consumption

The variation of brake specific fuel consumption with brake power for the ATJOE15 emulsion, JME and diesel at various compression ratios and nozzle opening pressures, is depicted in Fig. 5.5.7.

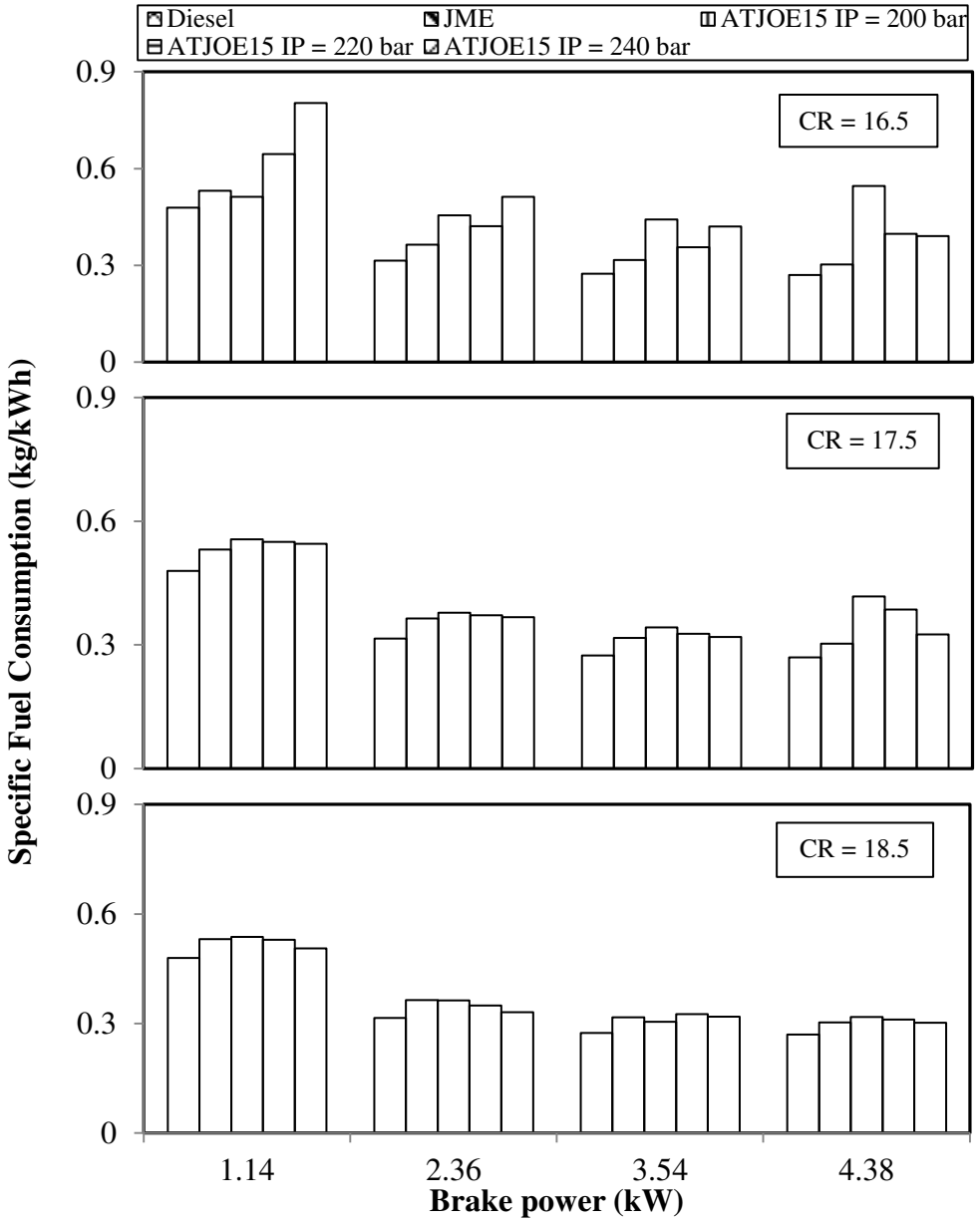

Fig. 5.5.7 Variation of specific fuel consumption with brake power at different compression ratios and nozzle opening pressures

It is apparent from the figure that the BSFC values of ATJOE15 emulsion are found to be higher than those of diesel and the JME operations at all compression ratios and nozzle opening pressures, which is attributed to the lower calorific value of the ATJOE15 emulsion. In comparison, the BSFC values of the ATJOE15 emulsion at different compression ratios and nozzle opening pressures are comparatively higher with the lower compression ratio and at lower nozzle opening pressure. The minimum value of the BSFC obtained for the ATJOE15 emulsion at 16.5 compression ratio is 0.3906 kg/kWh at an nozzle opening pressure of 220 bar, which is higher by about 44.8% compared to that of diesel operation.

At the standard compression ratio of 17.5 and higher nozzle opening pressure of 240 bar, with the ATJOE15 emulsion, a minimum BSFC of 0.316 kg/kWh is obtained, which is higher by about 20.6% compared to that of diesel. The minimum BSFC value of 0.3017 kg/kWh is obtained at the compression ratio of 18.5 and the nozzle opening pressure of 240 bar, which is higher by about 11.9% compared to that of diesel, at full load.

5.5.3.3 Exhaust gas temperature

The variation of exhaust gas temperature with load for the ATJOE15 emulsion at different compression ratios and nozzle opening pressures, in comparison with the JME and diesel is depicted in Fig. 5.5.8. It is apparent from the figure that the exhaust gas temperature of the ATJOE15 emulsion increased with the increase in the brake power, and decreased with the increase in the compression ratio and nozzle opening pressures. Also, it can be ascertained from the figure, that the engine operating parameters which resulted with a minimum BSFC and maximum brake thermal efficiency, were the ones which contributed the minimum exhaust gas temperature.

On an average, the exhaust gas temperature of the ATJOE15 emulsion is reduced by about 10.7%, when the compression ratio was increased from 17.5 to 18.5. The possible reason for this trend could be that, the increased compression ratio actually increases the air temperature inside the cylinder, consequently reducing the ignition delay, causing a better and more complete burning of the fuel. Similarly, at higher nozzle opening pressures, the exhaust gas temperature of the ATJOE15 emulsion is found to be lower by about 5.9% than that of standard nozzle opening pressure. Higher exhaust gas temperatures are found with the ATJOE15 emulsion at a lower nozzle opening pressure.

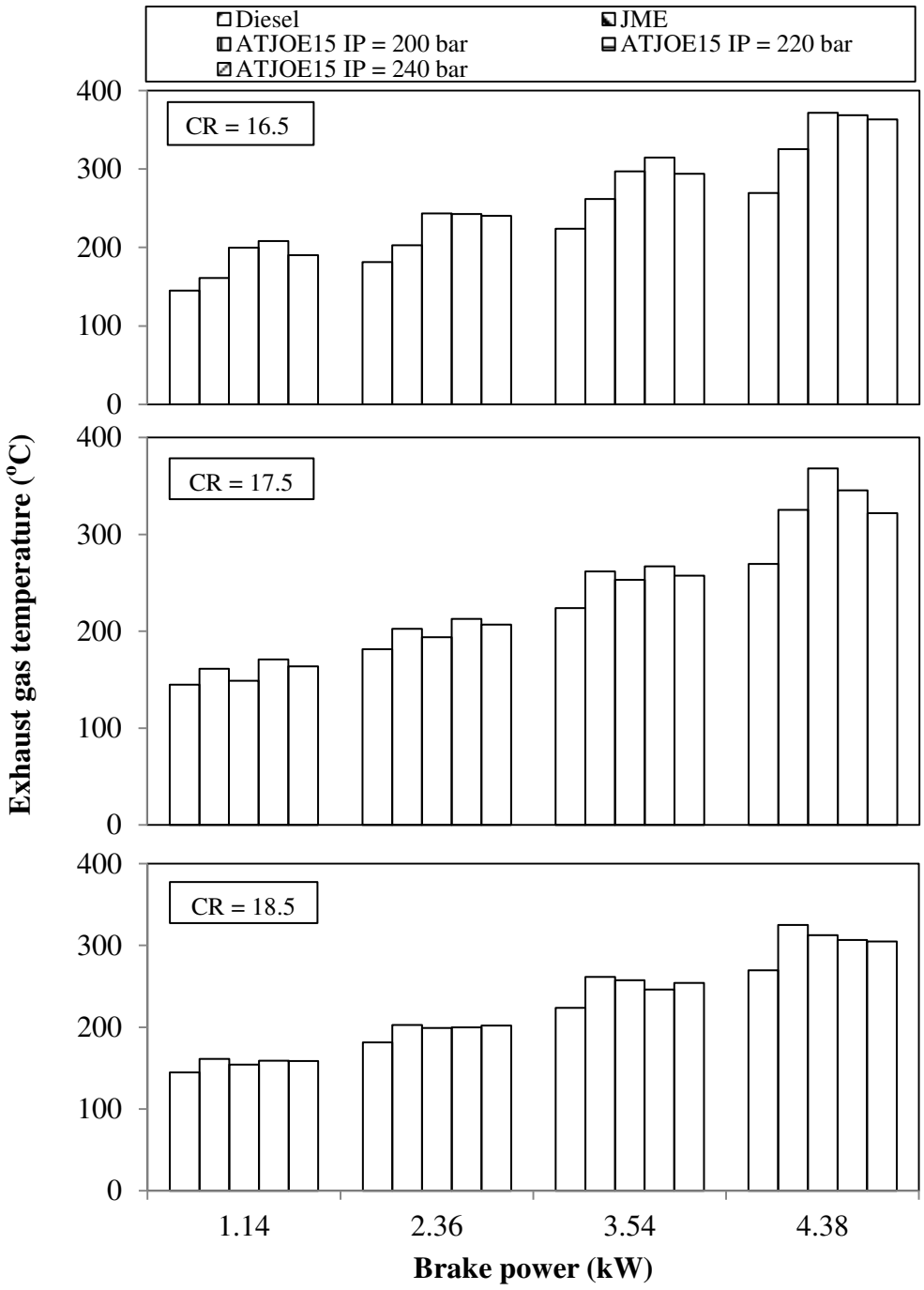

Fig. 5.5.8 Variation of exhaust gas temperature with brake power at different compression ratios and nozzle opening pressures

This happened due to the distribution of larger droplets inside the combustion chamber, which promoted heterogeneous combustion, while a finer droplet size distribution at higher nozzle opening pressures gave a relatively better fuel–air mixing and smoother combustion. Similar reasons are reported by Zhang et al. [199] in their work on the effects of highly dispersed spray nozzle on fuel injection characteristics and emissions of a heavy-duty diesel engine.

5.5.4 Emission parameters

5.5.4.1 BSHC emissions

The variations of the brake specific HC emissions with the brake power for diesel, JME and the ATJOE15 emulsion, at different compression ratios and nozzle opening pressures are shown in Fig. 5.5.9.

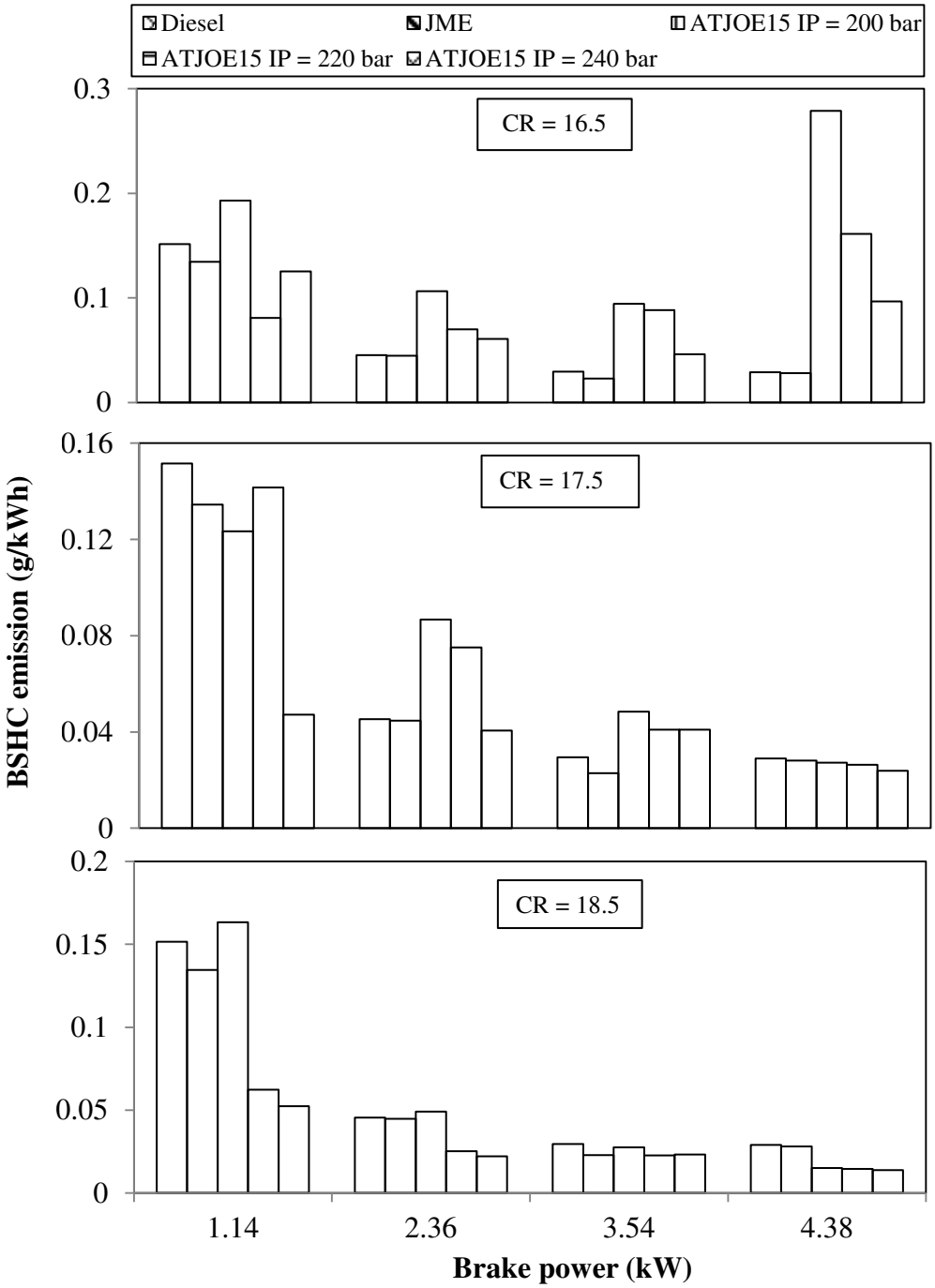

Fig. 5.5.9 Variation of BSHC emission with brake power at different compression ratios and nozzle opening pressures

The BSHC emissions decreased with an increase in the engine load. This is attributed to higher cylinder gas temperatures at higher engine loads, which led to more efficient combustion of fuel at higher temperatures, producing lower quantities of HC emissions. At higher nozzle opening pressures, the HC emissions decreased due to superior fuel-air mixing in the combustion chamber.

With the lower compression ratio, the HC emissions are found to be drastically higher, compared to those of diesel and the JME operations. At a lower compression ratio, insufficient heat of compression, delays the ignition, and therefore, the HC emissions increased. Similar reasons are reported by Jindal et al [20] in their work on the effect of the compression ratio and nozzle opening pressure in a DI diesel engine running on Jatropha methyl ester. At a standard compression ratio, the HC emissions of the ATJOE15 emulsion at different nozzle opening pressures are found to be lower in the range of 5.9% to 17.7% compared to that of diesel at full load. At a higher compression ratio, the HC emissions of the ATJOE15 emulsion at different nozzle opening pressures are found to be lower between 48.2% and 52.8% compared to that of diesel at full load.

5.5.4.2 BSCO emissions

Figure 5.5.10 illustrates the variation of the brake specific CO emissions with brake power for the ATJOE15 emulsion at different compression ratios and nozzle opening pressures, in comparison with the JME and diesel. With the lower compression ratio of 16.5, the temperature reached is also low, and thus more CO is exhausted from the engine. The minimum value of CO obtained at this compression ratio is about 0.1267 g/kWh, which is higher by about 92% compared to that of diesel operation.

At the standard compression ratio of 17.5, the CO emissions of ATJOE15 are found to be higher by about 84.8%, 13.9% and 11.4% at 200, 220 and 240 bar nozzle opening pressures respectively, compared to those of diesel operation. The longer spray penetration and larger fuel droplets may be the factors for the higher CO emissions in the case of the ATJOE15 emulsion. This reason was supported by Pei Lin Zhou [181], in his research work. It can be observed that the CO emissions are higher at lower nozzle opening pressure, and lower at higher nozzle opening pressures. At a higher compression ratio of 18.5, the CO emissions of ATJOE15 are found to be lower by about 48.2%, 50.7% and 55.3% with the 200, 220 and 240 bar nozzle opening pressures respectively, in comparison with diesel operation.

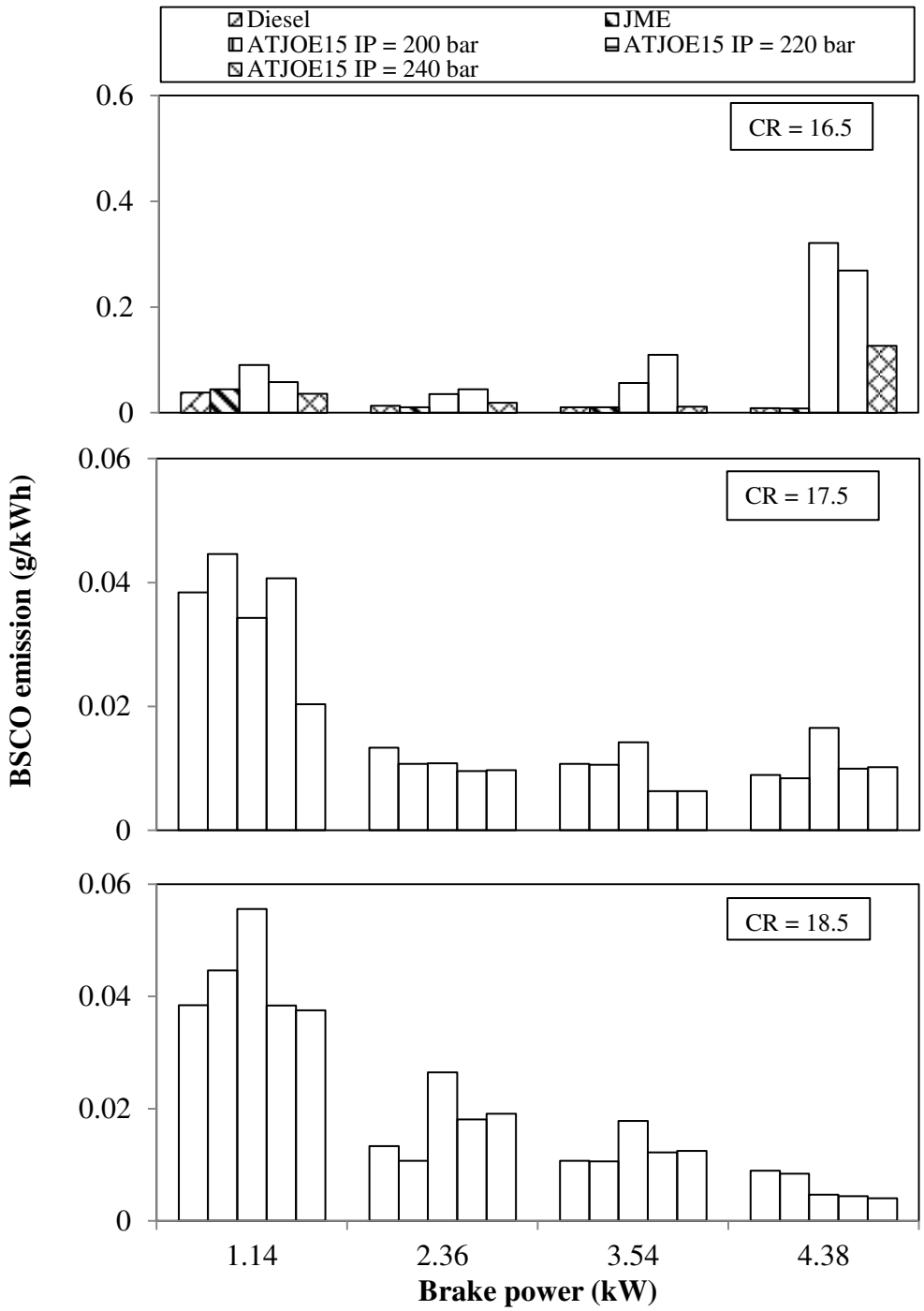

Fig. 5.5.10 Variation of BSCO emission with brake power at different compression ratios and nozzle opening pressures

The possible reason for this trend could be that the increased CR actually increases the air temperature inside the cylinder, reducing the ignition delay, causing a better and more complete burning of the fuel. Similar reasons are reported by Raheman and Ghadge [195], in their work on mahua biodiesel with variable compression ratios.

5.5.4.3 BSNO emissions

Figure 5.5.11 depicts the variation of brake specific nitric oxide (BSNO) emissions, with respect to brake power for the ATJOE15, at different compression ratios and nozzle opening pressures.

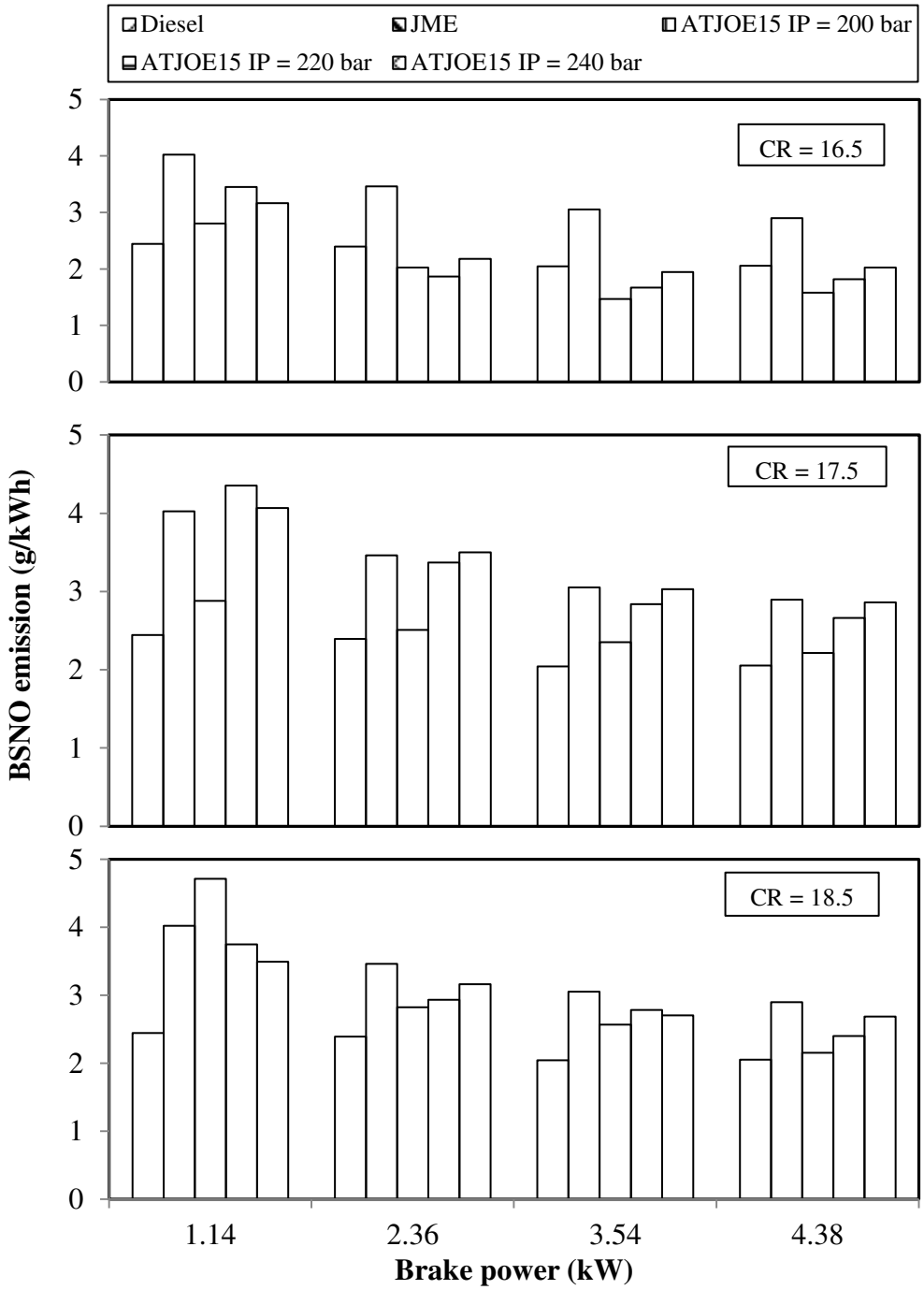

Fig. 5.5.11 Variation of BSNO emission with brake power at different compression ratios and nozzle opening pressures

It is apparent from the figure that the BSNO emissions are found to be higher by about 29% and 2% in the JME and ATJOE15 operations compared to that of diesel at full load, standard

compression ratio and nozzle opening pressure. At the compression ratio of 17.5, in the ATJOE15 operation, the higher nozzle opening pressure leads to further increase in the NO emissions by about 29.6% and 39.1% in comparison with diesel at full load. In comparison with the JME, the NO emissions from the ATJOE15 emulsion are found to be lower in the order of 1.3% to 8.1% at the compression ratio of 17.5 and different nozzle opening pressures. When the nozzle opening pressure is decreased, the NO emissions diminished for all the fuel mixtures. An increase in the nozzle opening pressure decreases the particle diameter and caused the ATJOE15 emulsion fuel spray to vaporize quickly. So, a higher nozzle opening pressure initially generates faster combustion rates, resulting in higher temperatures. As a consequence, the NO concentrations are observed more at higher nozzle opening pressures. Similar results are reported by Gumus [200], in his work on hazelnut kernel oil of Turkish origin as alternative fuel in diesel engines.

When the compression ratio is reduced to 16.5, the NO emissions of the ATJOE15 emulsion are found to be lower by about 23%, 11.6% and 1.6% compared to that of diesel operation at nozzle opening pressures of 200, 220 and 240 bar respectively. When compared to the JME operation, the NO emissions of the ATJOE15 emulsion are found to be lower in the range between 30.2% and 45.4%. A lower compression ratio will reduce the in-cylinder temperatures, and thus the flame temperatures during combustion, which will suppress the NO emissions. Similar reasons are reported by Raheman and Ghadge [195], in their work on mahua biodiesel with variable compression ratios. With the higher compression ratio of 18.5, the NO emissions from the ATJOE15 emulsion are found to be higher in the range of 4.6% to 30.7%, compared to that of diesel.

5.5.4.4 Smoke opacity

Figure 5.5.12 depicts the variation of the smoke opacity, with respect to the brake power for diesel, JME and the ATJOE15 emulsion, at different compression ratios and nozzle opening pressures. The smoke emissions from JME are found to be lower than those of diesel, as a consequence of the oxygen content in the JME that reduces the formation of smoke. In the case of ATJOE15, the smoke opacity is found to be higher by about 8.9% at the standard compression ratio and standard nozzle opening pressure of 200 bar. When the nozzle opening pressure is increased to 220 bar and 240 bar, the smoke opacity of ATJOE15 is found to be reduced by about 3.9% and 26.4% respectively, compared to that of diesel operation.

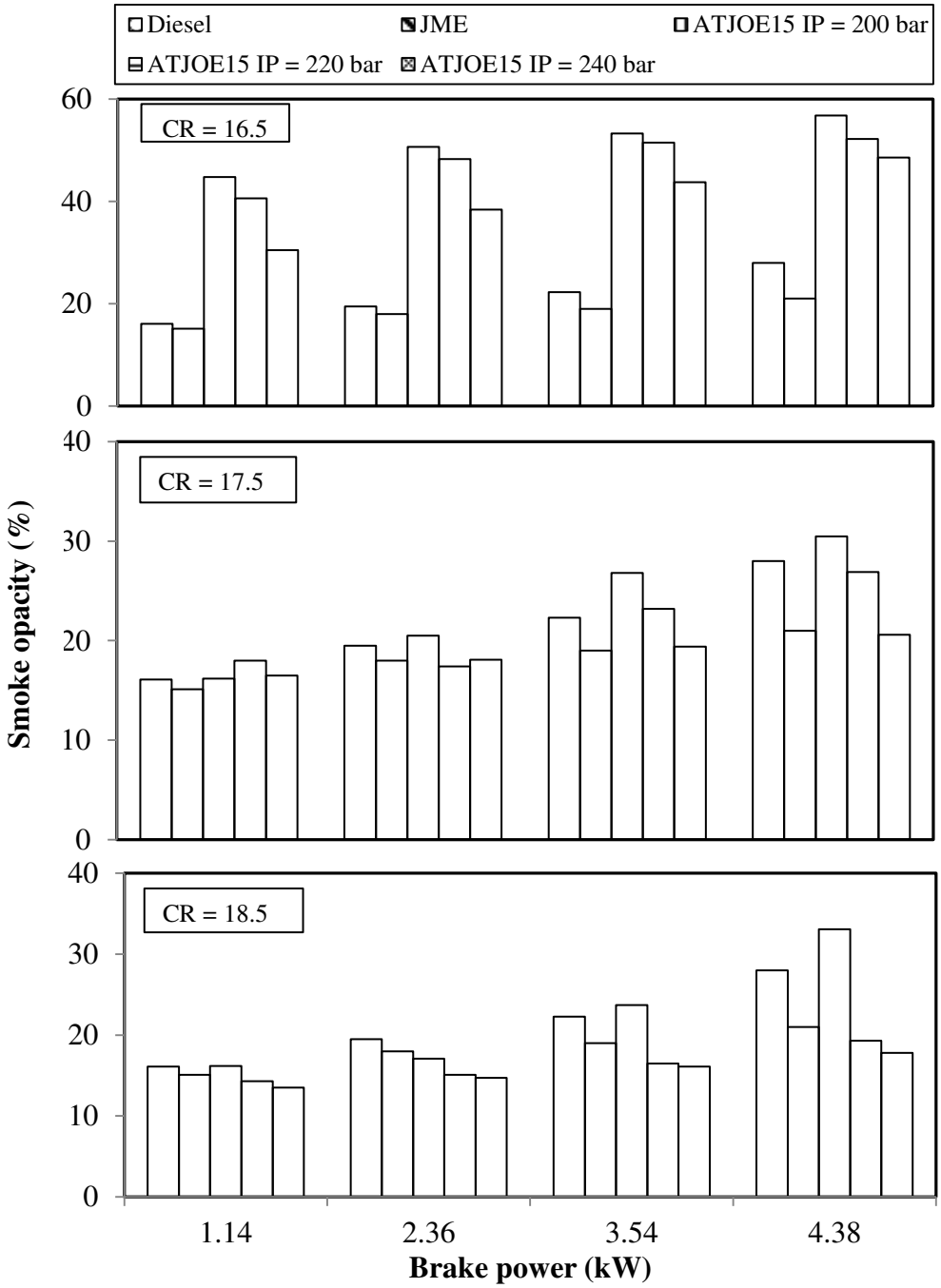

Fig.5.5.12 Variation of smoke opacity with brake power at different compression ratios and nozzle opening pressures

The values of smoke opacity of the ATJOE15 emulsion at nozzle opening pressures of 200, 220 bar are higher in the range of 28% and 45.2% compared to that of JME operation. With 240 bar nozzle opening pressure, the smoke opacity of the ATJOE15 emulsion is found to be lower by 1.9% compared to that of JME.

At a reduced compression ratio of 16.5, the smoke opacities of ATJOE15 emulsion at all the nozzle opening pressures are found to be higher in the range between 42% and 50.6%,

compared to that of diesel operation. At a higher compression ratio of 18.5, the smoke opacity of the ATJOE15 emulsion at nozzle opening pressure 200 bar is found to be higher by about 18.2% and with the higher nozzle opening pressures, the smoke emission values reduced by about 31% and 36.4% compared to that of diesel. As the compression ratio increases, the maximum temperature during combustion increases, and this in turn, decreases the smoke opacity and this is vice versa in the case of a lower compression ratio. When the nozzle opening pressure is increased, the fuel particle diameter will become smaller. Therefore, the fuel-air mixture will become better throughout the combustion period, and hence the smoke opacity will be lower. Similar reasons are reported by Cenk Sayin and Mertin Gumus [201], in their investigation on the impact of the compression ratio and injection parameters on the performance and emissions of a DI diesel engine fueled with biodiesel-blended diesel fuel.

5.5.5 Closure

The summary of the experimental results on the effect of the compression ratio and nozzle opening pressure on the combustion, performance and emission parameters obtained in a single cylinder, diesel engine fueled with the ATJOE15 emulsion shows improved performance and lower emissions, with a higher compression ratio of 18.5 and nozzle opening pressure of 240 bar. The maximum thermal efficiency is noticed at this operating condition. The maximum reduction in the HC, CO and smoke emissions by about 52.8%, 55.3% and 36.4% respectively, is noticed with the ATJOE15 emulsion at the same operating conditions. The NO emission at this condition is still found to be higher, by about 30.7% compared to that of diesel operation, at full load.

5.6 Combined effects of injection timing and nozzle opening pressure on the combustion, performance and emission parameters of a diesel engine fueled with the ATJOE15 emulsion

5.6.1 General

From the summary of the experimental results on the combustion, performance and emissions of a single cylinder diesel engine fueled with the ATJOE15 emulsion, it is observed that the CO and NO emissions from the engine are higher than those of diesel operation. Therefore, it is proposed to study the combined effects of varying the injection timings and nozzle opening pressures of the engine fueled with the ATJOE15 emulsion, in comparison with diesel and JME operation. Three different injection timings viz., 21.5, 23 and 24.5 ^{o}CA bTDC, and three nozzle opening pressures viz. 200, 220 and 240 bar, were chosen for this study. The standard compression ratio of 17.5 is maintained during this study. This chapter details about the combined effects of fuel injection timing and fuel nozzle opening pressure on the combustion, performance and emission characteristics of the diesel engine fueled with the ATJOE15 emulsion.

5.6.2 Combustion parameters

5.6.2.1 Pressure crank angle history

Figure 5.6.1 depicts the pressure crank angle history of the engine fueled with diesel, JME and the ATJOE15 emulsion for different injection timings and nozzle opening pressures, at full load condition. It is observed from the figure, that the combustion starts earlier in the range between 0.3 and 3.4 ^{o}CA for the ATJOE15 emulsion, with the injection timings of 23, 24.5 ^{o}CA bTDC and at all three nozzle opening pressures compared to that of diesel. For the same operating conditions, it is found that the combustion starts later by about 0.5 to 2.1 ^{o}CA for the ATJOE15 emulsion at all the nozzle opening pressures in comparison with the JME operation. At the injection timing of 21.5 ^{o}CA bTDC, it is found that the commencement of combustion is noticed later, which ranges from 1.3 to 2.2 ^{o}CA in comparison with the diesel operation. The peak cylinder pressure for diesel occurs at 12.4 ^{o}CA aTDC, whereas for the ATJOE15, the peak pressure occurs earlier in the range of 0.3 and 2.3 ^{o}CA, with the injection timings of 23 and 24.5 ^{o}CA bTDC, and the nozzle opening pressures of 220 bar and 240 bar compared to that of diesel at full load. With the retarded injection timing of 21.5 ^{o}CA bTDC and at all nozzle opening pressures, the peak cylinder pressure is found to be lower in the range of 8.4 bar to 8.7 bar compared to that of diesel operation. Similar results are reported by Kannan and Anand [202], in their investigation on a diesel engine fueled with diestrol at

varying nozzle opening pressures and injection timings. It is seen from the figure, that among all the tested injection timings and nozzle opening pressures, with the injection timing of 24.5 ^{o}CA bTDC and nozzle opening pressure of 200 bar, the ATJOE15 operation produced the highest cylinder pressure value of 79.5 bar at 370.6 ^{o}CA, which is earlier by about 2.2 ^{o}CA and later by about 0.2 ^{o}CA than those of diesel and the JME operations respectively. The early or later occurrences of the ignition during advancement and retardation in the injection timing are attributed to the increased or decreased cylinder gas temperatures respectively.

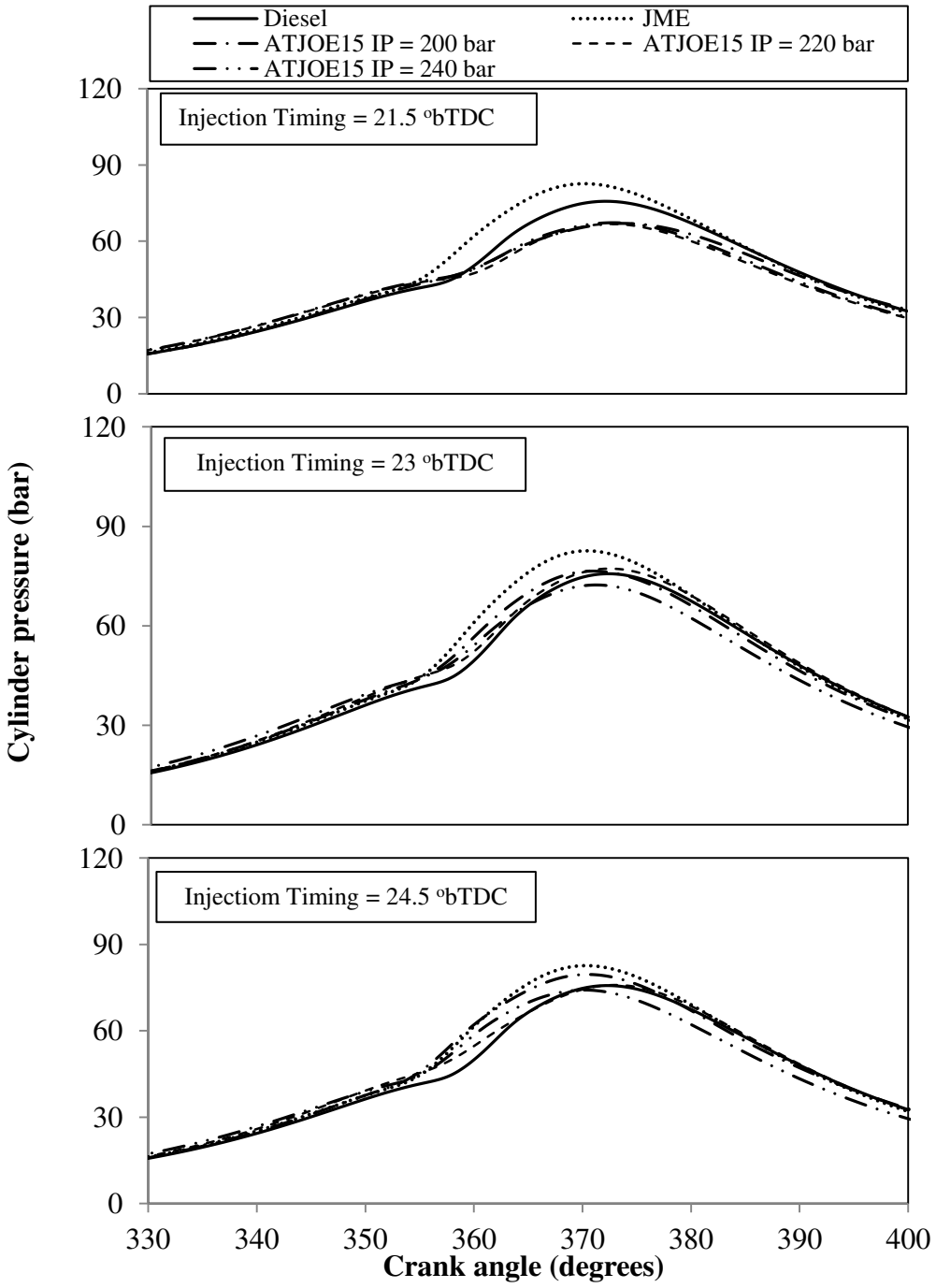

Fig. 5.6.1 Variation of cylinder pressure with crank angle at different injection timings and nozzle opening pressures

5.6.2.2 Ignition delay

Figure 5.6.2 depicts the ignition delay for diesel, JME and ATJOE15, for different injection timings and nozzle opening pressures at all loads. It is seen from the figure, that the ignition delay is found to be lower with the increase in the engine load and advanced injection timing. The reduction in the ignition delay in these conditions might be the result of the higher combustion chamber wall temperature at the time of injection, and reduced exhaust gas dilution [107].

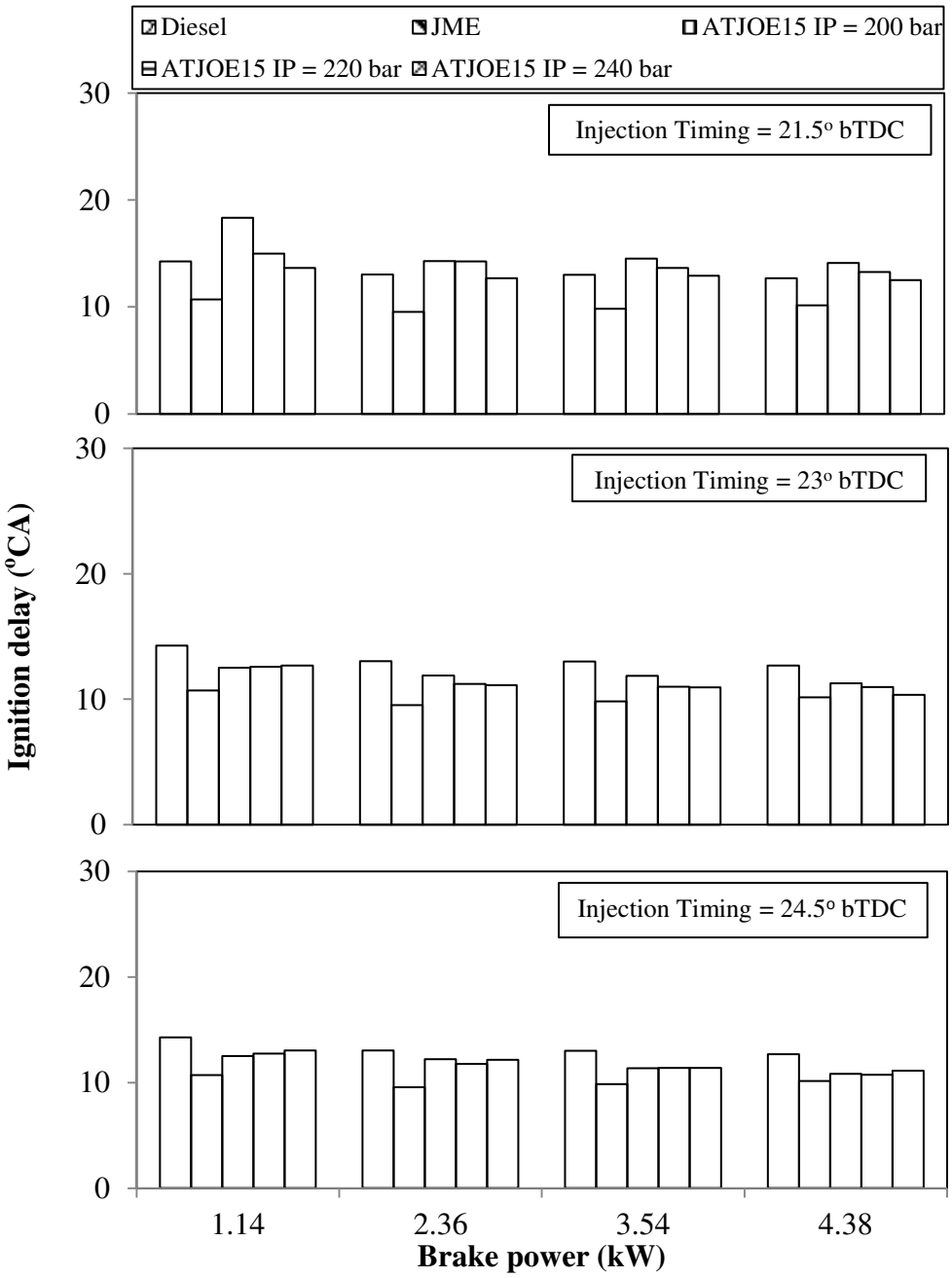

Fig. 5.6.2 Variation of ignition delay with brake power at different injection timings and nozzle opening pressures

With the retarded injection timing of 21.5 ^{o}CA, the ignition delay of the ATJOE15 emulsion is found to be higher than that of diesel and the JME at all nozzle opening pressures. At this injection timing and for all the nozzle opening pressures, the ignition delay values of the ATJOE15 emulsion are found to be longer by about 0.5 ^{o}CA to 1.4 ^{o}CA compared to that of diesel operation at full load. It is apparent from the figure, that at full load condition, the ignition delay of the ATJOE15 emulsion is found to be shorter in the range of 0.3 ^{o}CA to 0.9 ^{o}CA with the injection timings of 23 ^{o}CA and the higher nozzle opening pressures of 220 bar and 240 bar compared to that of diesel operation. In comparison with the JME operation, the engine fueled with the ATJOE15 emulsion exhibits a longer ignition delay under all operating conditions. Among all the tested injection timings and nozzle opening pressures, a shorter ignition delay period of 10.36 ^{o}CA is observed for the ATJOE15 operation, with the injection timing of 23 ^{o}CA bTDC and nozzle opening pressure of 240 bar. The reduction in the ignition delay period is mainly due to the improved atomization at higher nozzle opening pressure and higher cetane number of the ATJOE15 compared to that of diesel, at full load.

5.6.2.3 Heat release rate

Figure 5.6.3 illustrates the variation of heat release rate, with respect to the crank angle for the ATJOE15 emulsion at full load, for different injection timings and nozzle opening pressures, and for diesel and JME operations. The occurrence of the maximum heat release rate for the ATJOE15 emulsion in different operating conditions on an average, shifted approximately from 2.7 to 6.9 ^{o}CA at full load, compared to that of diesel operation. The intensity of the premixed combustion phase for diesel is found to be the highest, whereas, it is lower in the case of JME and the ATJOE15 emulsion at injection timings of 23, 24.5 ^{o}CA and higher nozzle opening pressures.

With the retarded injection timing of 21.5 ^{o}CA, at all the nozzle opening pressures, the premixed combustion is found to be higher than that of diesel operation, as a result of longer ignition delay. The variation of the maximum heat release rate between diesel, JME and the ATJOE15 emulsion operations at different injection timings and nozzle opening pressures lies between 5.4 and 11.19 J/^{o}CA. For the JME and the ATJOE15 emulsion, less amount of fuel is accumulated during the shorter ignition delay period, which results in lower heat release rates, compared to that of diesel at advanced injection timings.

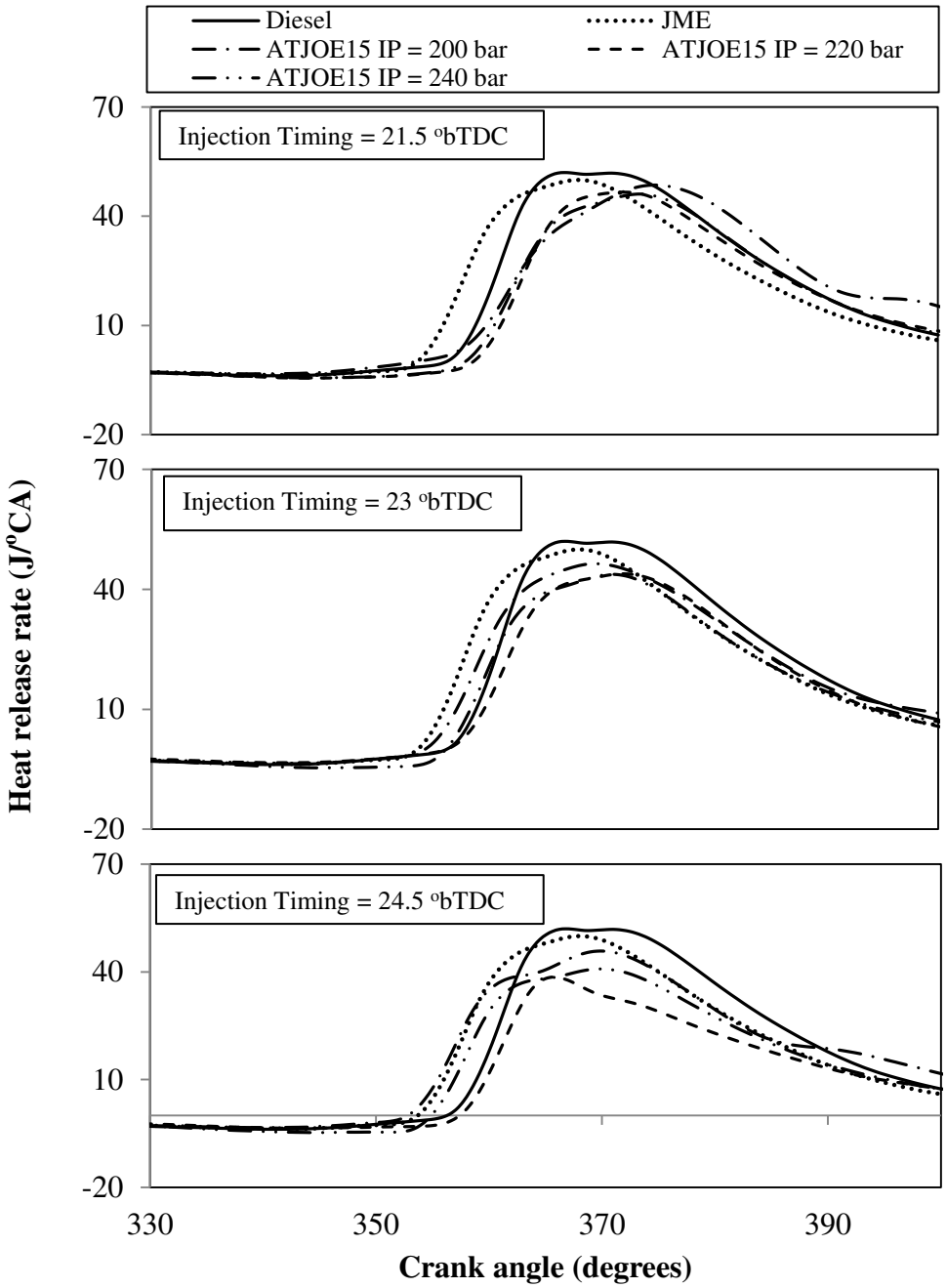

Fig. 5.6.3 Variation of heat release rate with crank angle at different injection timings and nozzle opening pressures

5.6.2.4 Maximum cylinder pressure

Figure 5.6.4 depicts the variation of maximum cylinder pressure with brake power for diesel, JME and the ATJOE15 emulsion at full load, for the different injection timings and nozzle opening pressures. It is seen from the figure that the peak cylinder pressure is increased with an increase in the engine load in all operating conditions. With the retarded injection timing of 21.5 ^{o}CA, the peak cylinder pressure for the JME and diesel are found to be higher than

that of the ATJOE15 emulsion at all nozzle opening pressures, while the trend is the reverse, for the advanced injection timings. This shows that, with the advanced injection timings and all nozzle opening pressures, the ATJOE15 emulsion showed faster premixed combustion, which leads to a higher peak cylinder gas pressure.

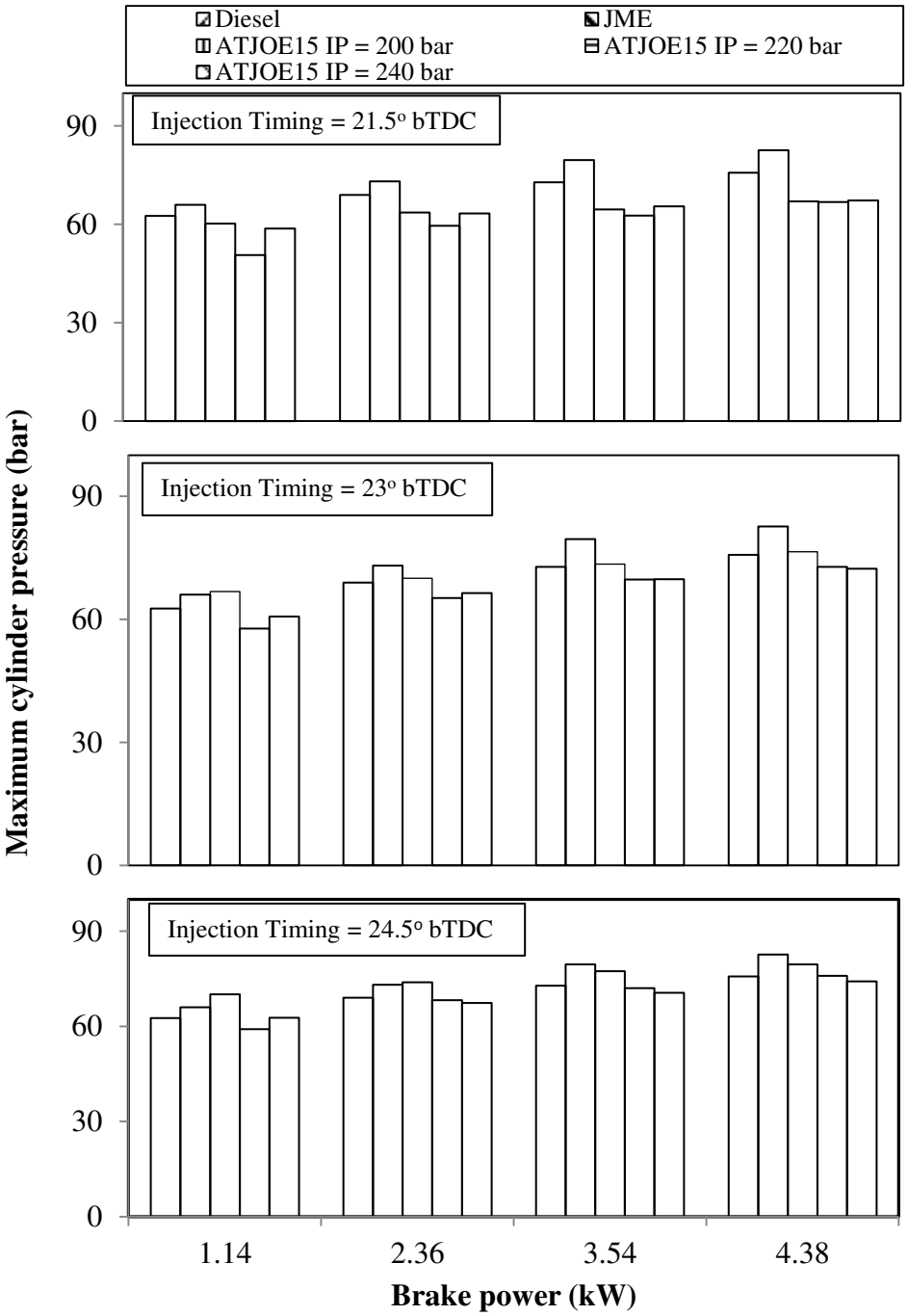

Fig. 5.6.4 Variation of maximum cylinder pressure with brake power at different injection timings and nozzle opening pressures

With the injection timing of 21.5 ^{o}CA and all three nozzle opening pressures, the maximum cylinder pressure of the ATJOE15 emulsion is found to be lower in the range between 8.4

and 8.9 bar, compared to that of diesel operation at full load. With the injection timings of 23, 24.5 ^{o}CA and at all nozzle opening pressures, the maximum cylinder pressure values of the ATJOE15 emulsion are noticed to be higher in the range of 0.2 to 3.8 bar compared to that of diesel operation. In comparison with the JME operation, the peak cylinder pressure of the ATJOE15 emulsion is found to be lower, in all the load conditions.

5.6.2.5 Combustion duration

The variation of combustion duration with the brake power under different injection timings and nozzle opening pressures, for the engine fueled with the ATJOE15 emulsion, JME and diesel is illustrated in Fig. 5.6.5.

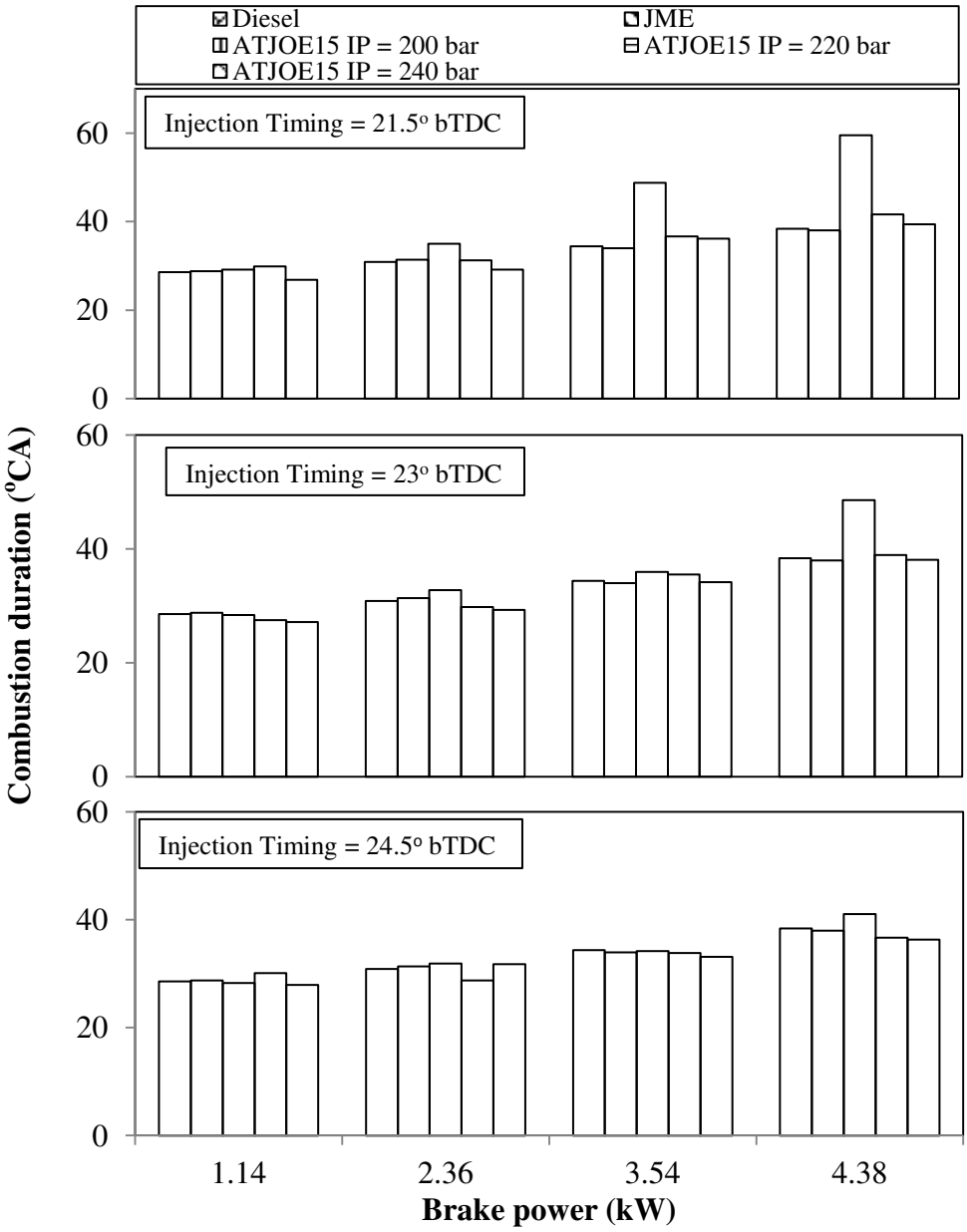

Fig. 5.6.5 Variation of combustion duration with brake power at different injection timings and nozzle opening pressures

With the injection timing of 24.5 ^{o}CA and at full load, the values of the combustion duration are found to be 38.4, 38, 41.1, 36.7 and 36.3 ^{o}CA for the diesel, JME and the ATJOE15 at nozzle opening pressures of 200, 220 and 240 bar respectively. The advancement in the injection timing and increase in the nozzle opening pressure, leads to a lower combustion duration of ATJOE15 emulsion compared to that of diesel operation. The reason was that, the increase in the nozzle opening pressure and advancement in the injection timing, which compensated the slow vaporization of the ATJOE15 emulsion, by proper mixing of the fuel and air that resulted in a better combustion. Further, the faster burning rate in the uncontrolled phase of combustion due to proper mixing of the fuel and air, resulted in the reduction in the combustion duration. Similar results are reported by Kannan et al. [203], in their study on the effect of nozzle opening pressure and timing on the performance of a diesel engine fueled with biodiesel.

The combustion duration of the ATJOE15 is found to be lower between 1.7 and 2.1 ^{o}CA compared to that of diesel at advanced injection timing of 24.5 ^{o}CA bTDC. With the retarded injection timing of 21.5 ^{o}CA bTDC, the combustion duration of the ATJOE15 emulsion is found to be higher by an average of 8.4 and 8.8 ^{o}CA than that of diesel and the JME operation, which is attributed to a longer ignition delay. With the injection timing of 23 ^{o}CA and at different nozzle opening pressures, the combustion duration of the ATJOE15 emulsion is found to be higher in the range from 0.5 to 10.2 ^{o}CA and 0.1 to 10.6 ^{o}CA compared to those of diesel and the JME respectively.

5.6.3 Performance parameters

5.6.3.1 Brake thermal efficiency

The variation of brake thermal efficiency with brake power for the ATJOE15 emulsion in comparison with the JME and diesel, at different injection timings and nozzle opening pressures, is depicted in Fig. 5.6.6. It is seen from the figure that, for all the injection timings and nozzle opening pressures tested, the brake thermal efficiency of the ATJOE15 emulsion increases with an increase in the load. With the standard injection timing and nozzle opening pressure, the ATJOE15 emulsion produced a maximum thermal efficiency of 32.98% which is higher by about 3.6% compared to that of diesel operation. For the same injection timing, with the higher nozzle opening pressures of 220 bar and 240 bar, the brake thermal efficiency of the ATJOE15 emulsion is found to be higher than that of diesel by about 4.6% and 6.1% respectively, at full load. The increase in the brake thermal efficiency of the ATJOE15

emulsion is due to better combustion, caused by the proper atomization and air entrainment, as a result of the nozzle opening pressure. This is in agreement with the results reported by Kannan and Anand [192], in their work on waste cooking oil.

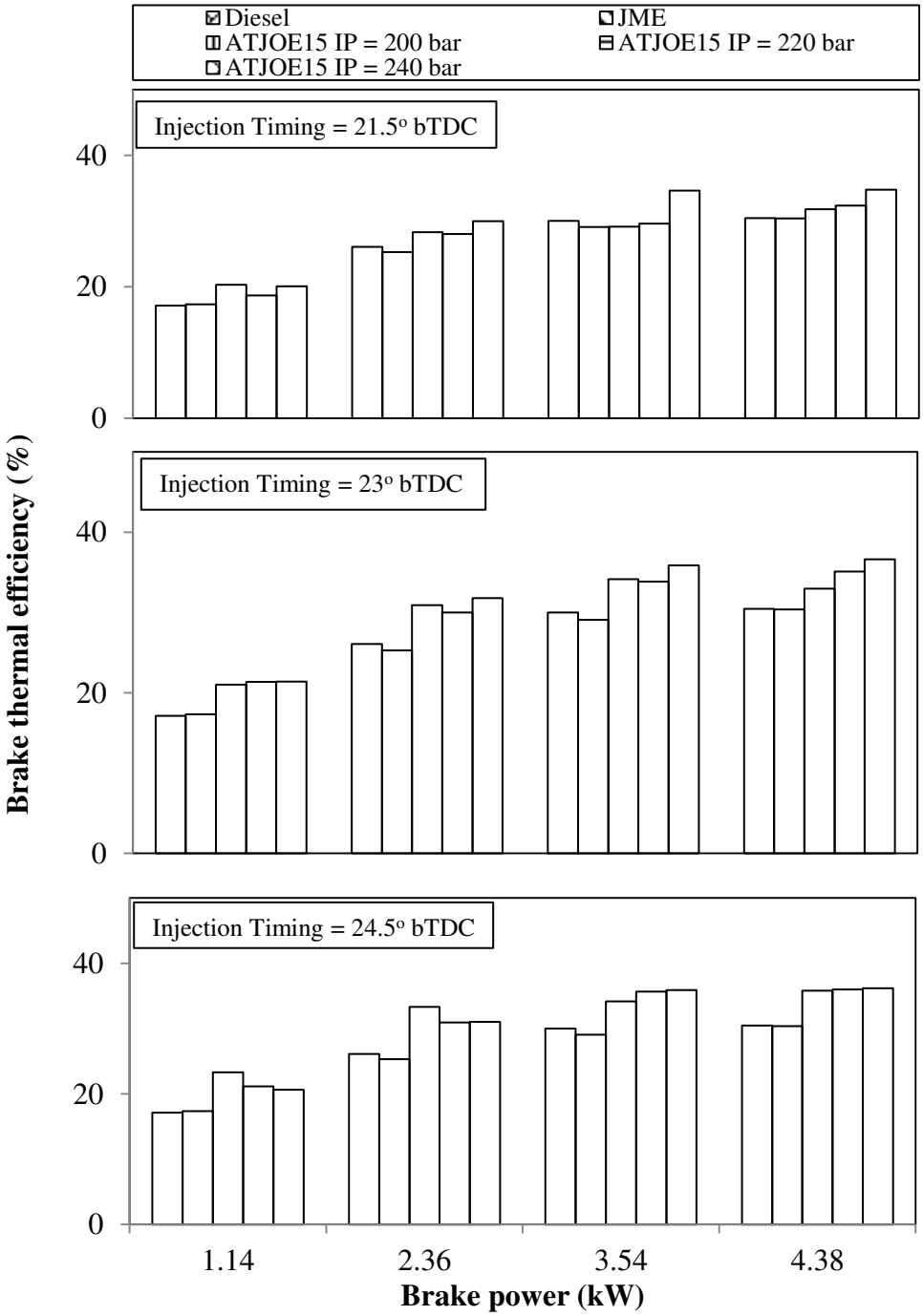

Fig. 5.6.6 Variation of brake thermal efficiency with brake power at different injection timings and nozzle opening pressures

When the injection timing is retarded to 21.5 ^{o}CA bTDC, the brake thermal efficiency of the ATJOE15 emulsion is found to be higher by an average of 2.5% at all nozzle opening pressures, at full load. With the advanced injection timing of 24.5 ^{o}CA bTDC, the brake

thermal efficiency of the ATJOE15 emulsion is found to be higher by an average of 5.5% at all nozzle opening pressures. Overall, the maximum thermal efficiency is noticed with the injection timing of 23 ^{o}CA bTDC and nozzle opening pressure of 240 bar.

5.6.3.2 Brake specific fuel consumption

The variation of brake specific fuel consumption with brake power for the ATJOE15 emulsion, JME and diesel at various injection timings and nozzle opening pressures, is depicted in Fig. 5.6.7.

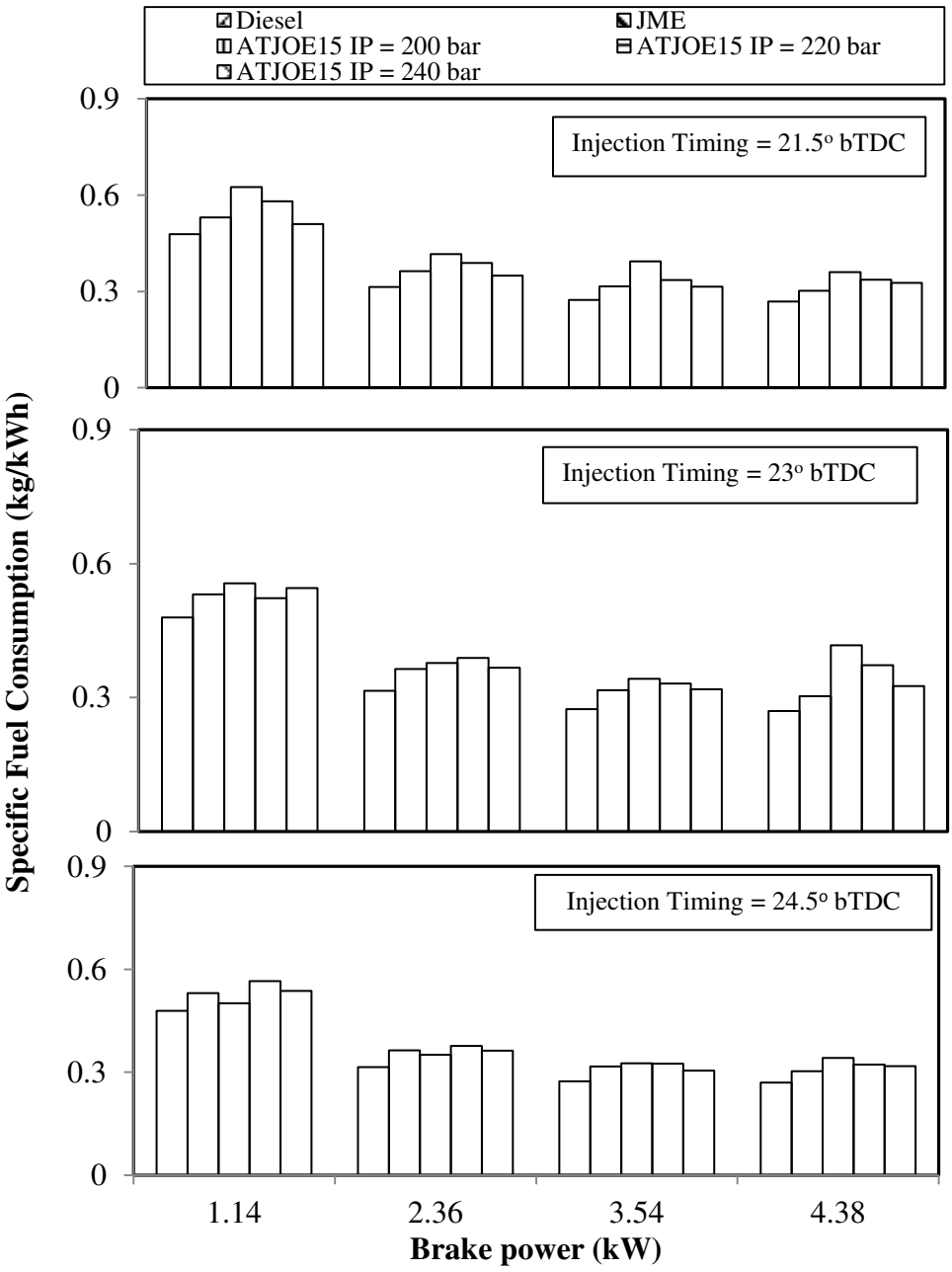

Fig. 5.6.7 Variation of specific fuel consumption with brake power at different injection timings and nozzle opening pressures

It is apparent from the figure, that the BSFC values of the ATJOE15 emulsion are found to be higher than those of diesel and the JME operations at all injection timings and nozzle opening pressures, which is attributed to the lower calorific value of the ATJOE15 emulsion. The BSFC values of the ATJOE15 emulsion are comparatively higher with the retarded injection timings and at lower nozzle opening pressures. The lowest value of the BSFC obtained for the ATJOE15 emulsion at 24.5 ^{o}CA bTDC is 0.3177 kg/kWh at an nozzle opening pressure of 240 bar, which is higher by about 17.8%, compared to that of diesel operation.

At the standard injection timing of 23 ^{o}CA bTDC and higher nozzle opening pressure of 240 bar, with the ATJOE15 emulsion, the minimum BSFC of 0.3254 kg/kWh is obtained, which is higher by about 20.6% compared to that of diesel. The minimum BSFC value of 0.3017 kg/kWh is obtained at the injection timing of 21.5 ^{o}CA bTDC and the nozzle opening pressure of 240 bar, which is higher by about 21.2% compared to that of diesel, at full load. The minimum BSFC values were obtained with increased nozzle opening pressures, because of improved atomization and better mixing process. This is in agreement with the results reported by Jindal et al. [20], in their work on the effect of the compression ratio and nozzle opening pressure in a DI diesel engine running on Jatropha methyl ester. Similarly, at advanced injection timings, the combustion starts earlier and more fuel can burn before the piston reaches the top dead centre, which causes lower BSFC values.

5.6.3.3 Exhaust gas temperature

The variation of exhaust gas temperature with load for the ATJOE15 emulsion at different injection timings and nozzle opening pressures in comparison with the JME and diesel is depicted in Fig. 5.6.8. It is apparent from the figure that the exhaust gas temperature of the ATJOE15 emulsion increased with the increase in the brake power, and decreased with the advanced injection timings and increased nozzle opening pressures. On an average, the exhaust gas temperature of the ATJOE15 emulsion is reduced by about 6.1%, when the injection timing was advanced from 23 to 24.5 ^{o}CA. The possible reason for this trend could be that, with the advancement in injection timing, the efficiency of the engine cycles increases, when the conversion of chemical energy into heat is concentrated near the TDC. These results are in agreement with those of Rahemen and Ghadge [195], when they conducted experiments with magua biodiesel at variable compression ratios and injection timings. Similarly, at higher nozzle opening pressures, the exhaust gas temperature of the

ATJOE15 emulsion is found to be lower by about 11.1% than that of standard nozzle opening pressure.

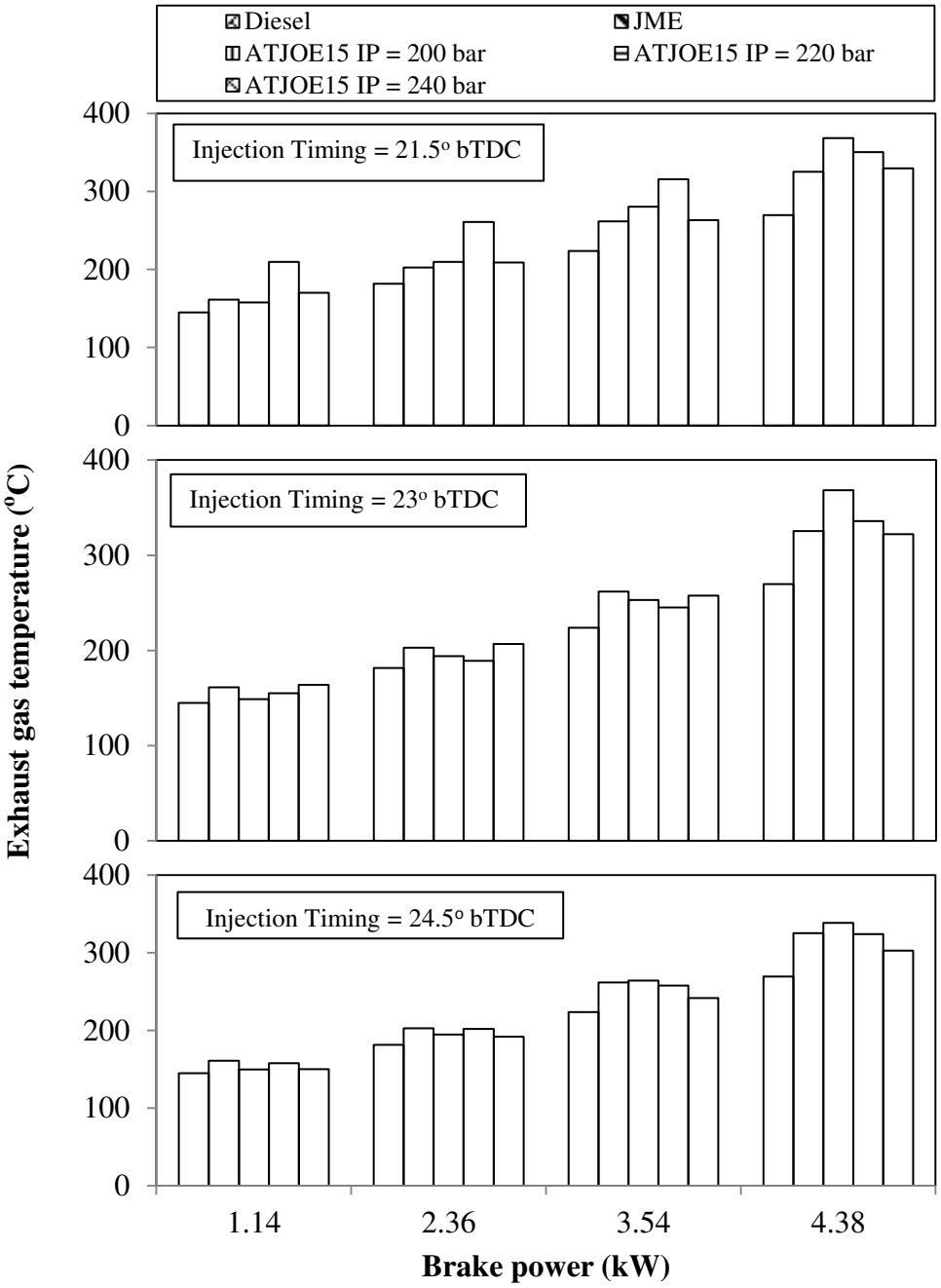

Fig. 5.6.8 Variation of exhaust gas temperature with brake power at different injection timings and nozzle opening pressures

Higher exhaust gas temperatures are found with the ATJOE15 emulsion at a lower nozzle opening pressure, compared to higher nozzle opening pressures. It may be attributed to the distribution of the larger droplets inside the combustion chamber, which promoted heterogeneous combustion, while a finer droplet size distribution at higher nozzle opening pressures gave a relatively better fuel–air mixing and smoother combustion. Similar reasons

are reported by Zhang et al. [199], in their work on the effects of a highly dispersed spray nozzle on the fuel injection characteristics and emissions of a heavy-duty diesel engine. At retarded injection timings, the exhaust gas temperatures of the ATJOE15 emulsion are higher by about 2% compared to that of diesel at full load condition.

5.6.4 Emission parameters

5.6.4.1 BSHC emissions

The variations of brake specific HC emissions with the brake power for diesel, JME and the ATJOE15 emulsion, at different injection timings and nozzle opening pressures are shown in Fig. 5.6.9.

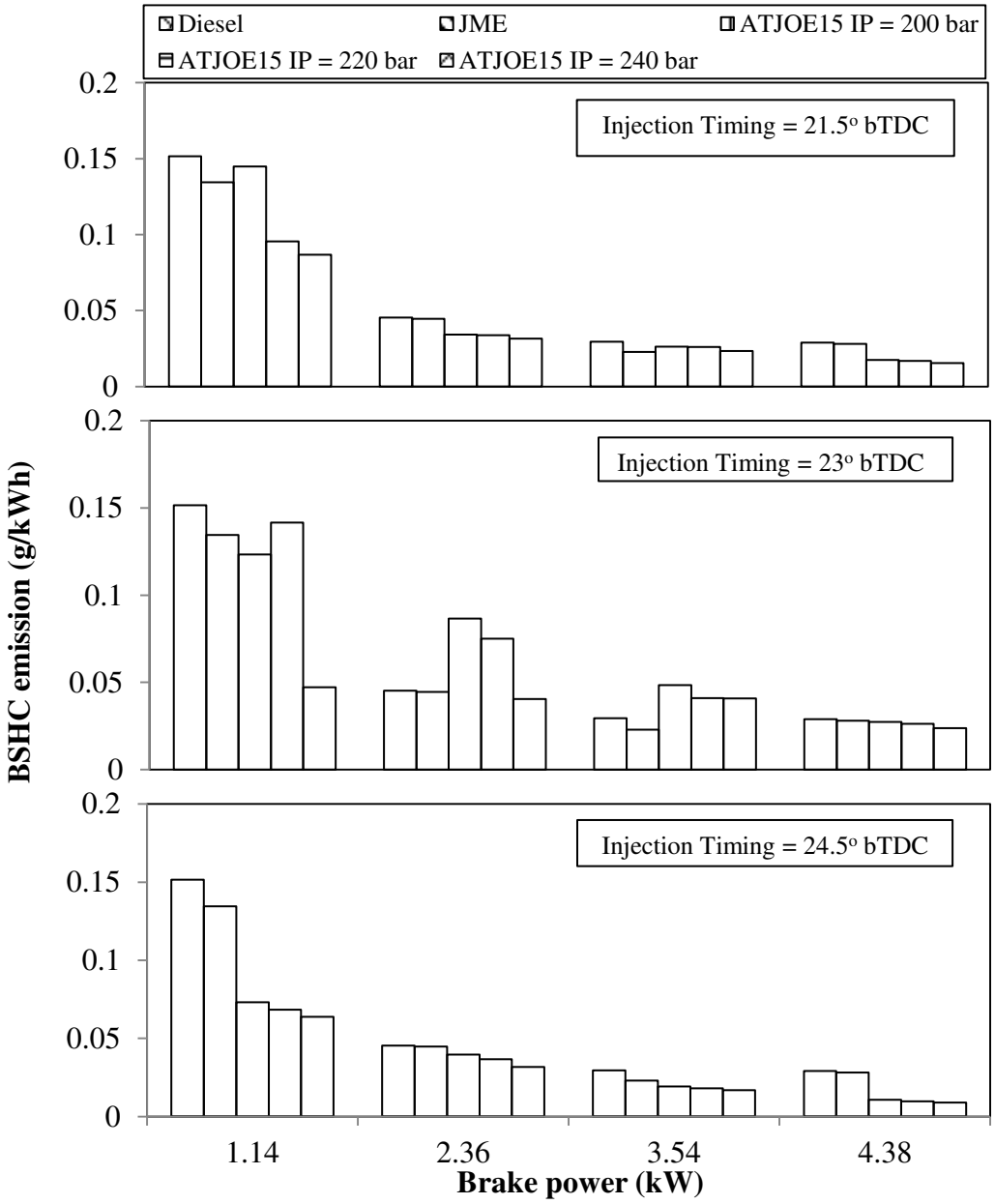

Fig. 5.6.9 Variation of BSHC emission with brake power at different injection timings and nozzle opening pressures

It is apparent from the figure that, with advanced injection timings and higher nozzle opening pressures, the HC emissions are found to be decreased, due to improved fuel-air mixing in the combustion chamber. With the retarded injection timing of 21.5 ^{o}CA, the HC emissions are found to be lesser by an average of 36% and 37%, compared to those of diesel and the JME operations respectively. At the standard injection timing of 23 ^{o}CA, the HC emissions of the ATJOE15 emulsion at different nozzle opening pressures are found to be lower in the range of 6.2% to 17.7% compared to that of diesel at full load. At an advanced injection timing of 24.5 ^{o}CA, the HC emissions of the ATJOE15 emulsion at different nozzle opening pressures are found to be lower between 63.1% and 69.4% compared to that of diesel at full load. At advanced injection timings, the cylinder charge is compressed near the TDC at relatively high temperatures, which diminishes the HC emissions. Similar reasons are also reported by Sayin et al [204] in their study on the performance and emission parameters of DI diesel engine using methanol-blended-diesel fuel.

5.6.4.2 BSCO emissions

Figure 5.6.10 illustrates the variation of brake specific CO emissions with brake power, for the ATJOE15 emulsion at different injection timings and nozzle opening pressures in comparison with the JME and diesel. With the retarded injection timing of 21.5 ^{o}CA, the CO emissions from the ATJOE15 emulsion are higher in the range between 56.2% and 61.2%. The lowest value of CO obtained at this injection timing is about 0.02039 g/kWh, which is higher by about 61.2% compared to that of diesel operation at full load.

At the standard injection timing of 23 ^{o}CA, the CO emissions of ATJOE15 are found to be lower by about 5.9%, 9.1% and 17.7% at 200, 220 and 240 bar nozzle opening pressures respectively, compared to those of diesel operation at full load. The longer spray penetration and larger fuel droplets may be the factors for higher CO emissions in the case of the ATJOE15 emulsion. This reason was supported by Pei Lin Zhou [181], in his research work. It can be observed that the CO emissions are higher at a lower nozzle opening pressure and lower at a high nozzle opening pressure. At the advanced injection timing of 24.5 ^{o}CA, the CO emissions of ATJOE15 are found to be lower by an average of 65% at all nozzle opening pressures, in comparison with diesel operation at full load. The possible reason for this trend could be that, the increased oxidation process between carbon and oxygen molecules happens at higher cylinder temperature.

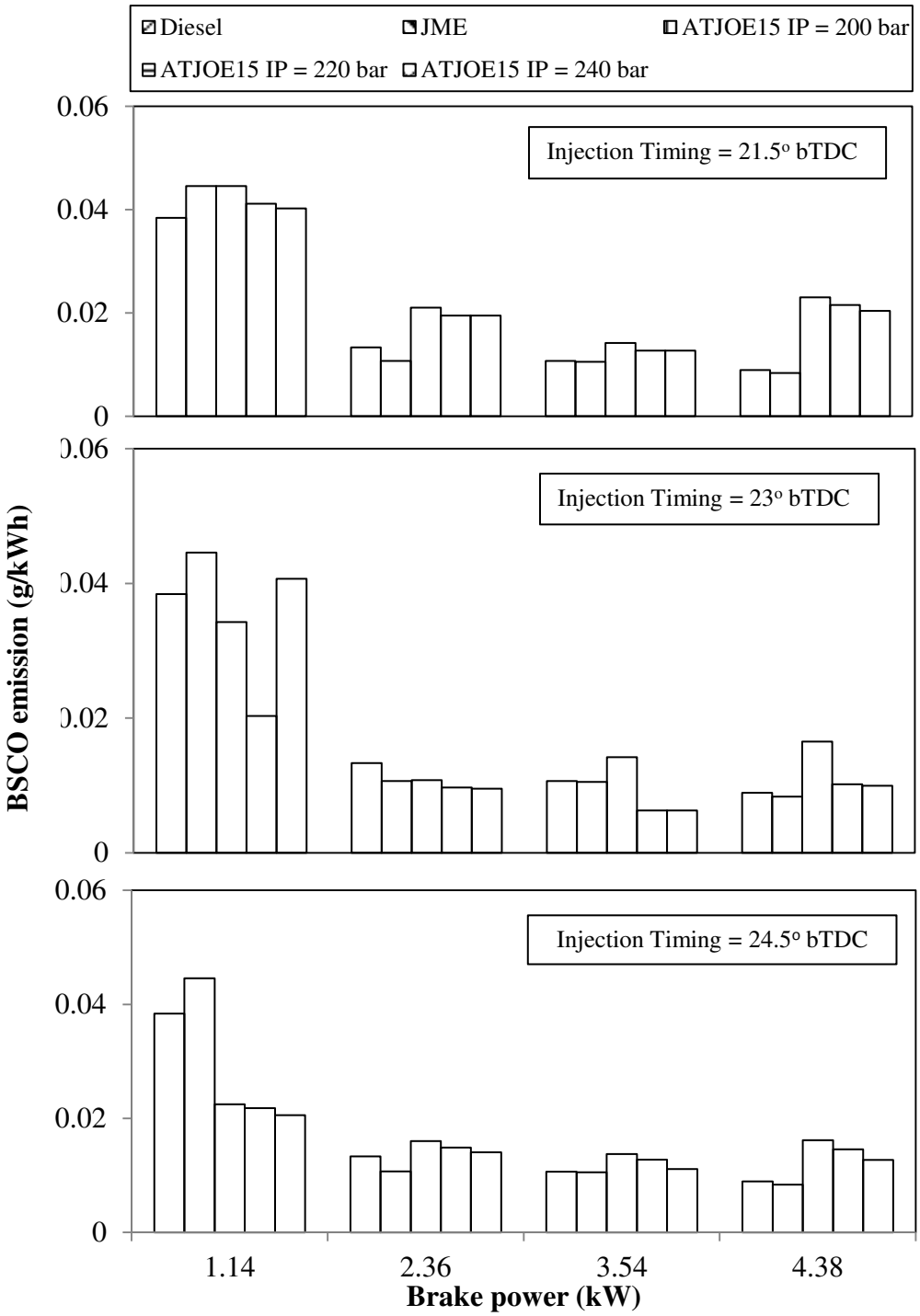

Fig. 5.6.10 Variation of BSCO emission with brake power at different injection timings and nozzle opening pressures

5.6.4.3 BSNO emissions

Figure 5.6.11 depicts the variation of brake specific nitric oxide (BSNO) emissions with respect to the brake power for the ATJOE15 at different injection timings and nozzle opening pressures.

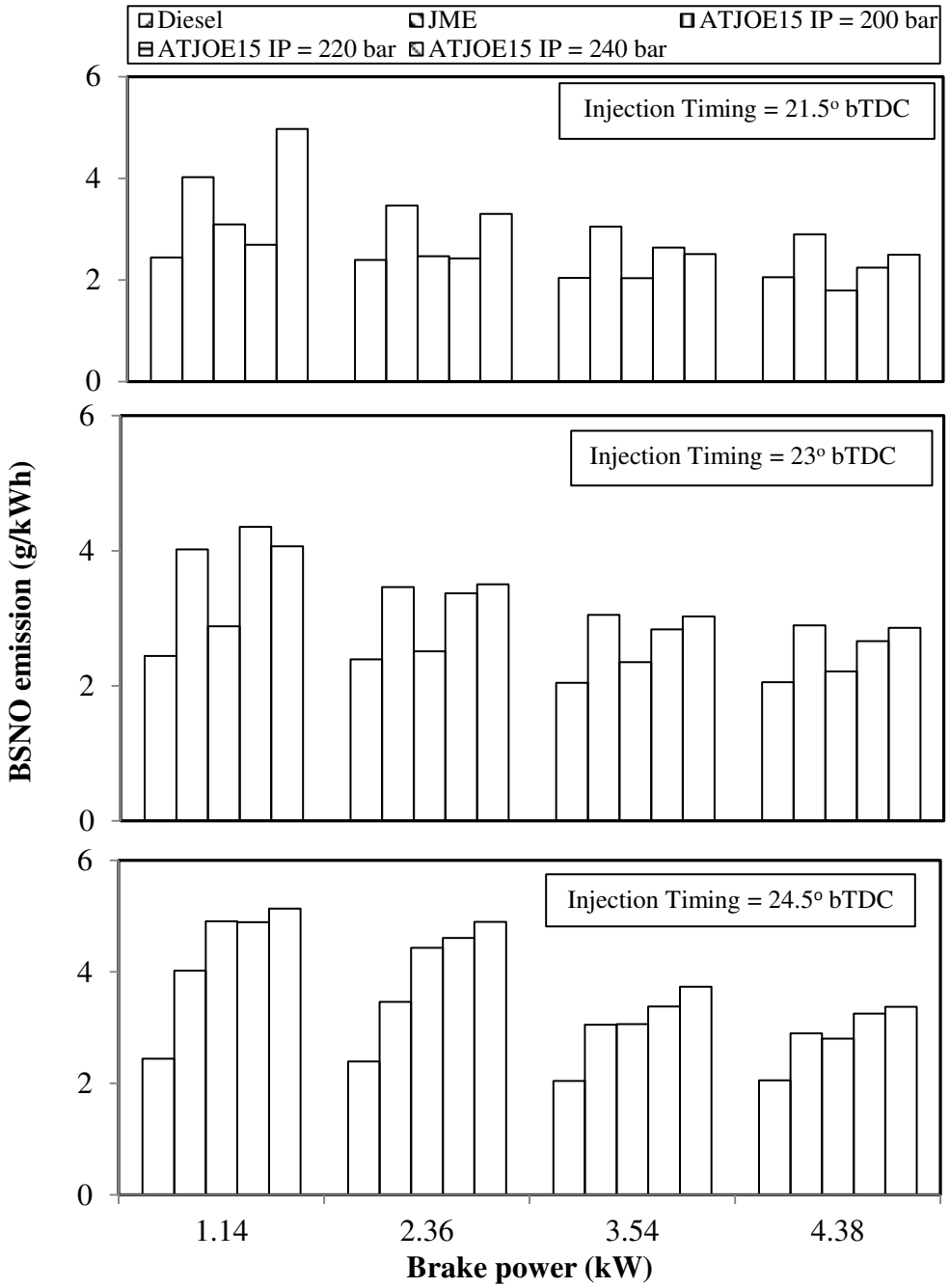

Fig. 5.6.11 Variation of BSNO emission with brake power at different injection timings and nozzle opening pressures

It is apparent from the figure that the BSNO emissions are found to be higher by about 29% and 2% in the JME and ATJOE15 operations, compared to those of diesel at full load, standard injection timing and nozzle opening pressure. Under the same operating condition, a higher nozzle opening pressure leads to further increase in NO emissions by about 29.6% and 39.1% in comparison with diesel at full load. In comparison with the JME, the NO emissions from the ATJOE15 emulsion are found to be lower in the order of 1.3% to 8.1% at an injection timing of 23 ^{o}CA and different nozzle opening pressures. The increase in the nozzle

opening pressure decreases the particle diameter and causes the ATJOE15 emulsion fuel spray to vaporize quickly. So, a higher nozzle opening pressure initially generates faster combustion rates, resulting in higher temperatures. As a consequence, the NO concentrations are observed more at higher nozzle opening pressures. Similar results are reported by Gumus [200], in his work on hazelnut kernel oil of Turkish origin, as an alternative fuel in diesel engines.

With the retarded injection timing of 21.5 ^{o}CA, the NO emissions of the ATJOE15 emulsion are found to be lower by about 12.8%, compared to that of diesel operation at the standard nozzle opening pressure of 200 bar. With the higher nozzle opening pressures of 220 and 240 bar, the NO emissions from the ATJOE15 emulsion are found to be higher by 8.9% and 21.4% respectively in comparison with diesel. In comparison with the JME operation, the NO emissions of the ATJOE15 emulsion are found to be lower in the range between 13.9% and 38.2%. Retarding the injection timing decreases the peak cylinder pressure and peak temperatures. As a consequence, the NO concentration starts to diminish. With the advanced injection timing of 24.5 ^{o}CA, the NO emissions from the ATJOE15 emulsion are found to be higher in the range of 36.4% to 64.3% compared to that of diesel.

5.6.4.4 Smoke opacity

Figure 5.6.12 depicts the variation of smoke opacity with respect to the brake power for the diesel, JME and the ATJOE15 emulsion operations, at different injection timings and nozzle opening pressures. The smoke emissions from JME are found to be lower than those of diesel, as a consequence of the oxygen content in the JME reducing the formation of smoke. In the case of ATJOE15, the smoke opacity is found to be higher by about 8.9% with the standard injection timing and standard nozzle opening pressure of 200 bar. When the nozzle opening pressure is increased to 220 bar and 240 bar, the smoke opacity of the ATJOE15 is found to be reduced by about 3.9% and 26.4% respectively, compared to that of diesel operation. The values of smoke opacity of the ATJOE15 emulsion at nozzle opening pressures of 200 and 220 bar are higher in the range of 28% and 45.2% compared to that of JME operation. With the 240 bar nozzle opening pressure, the smoke opacity of the ATJOE15 emulsion is found to be lower by 1.9% compared to that of JME. With the retarded injection timing of 21.5 ^{o}CA, the smoke opacities of ATJOE15 emulsion at all the nozzle opening pressures is found to be higher in the range between 24.5% and 45.5% compared to

that of diesel operation. With the advanced injection timing of 24.5 ^{o}CA, the smoke opacity of the ATJOE15 emulsion is found to be lower by about 5.3% to 26.7% at all the nozzle opening pressures compared to that of diesel. The smoke opacity decreases with an advancement in the injection timing, due to the existence of a higher combustion temperature which promotes soot oxidation, compared to that of standard injection timing operation, and this is vice versa in case of retarded injection timing.

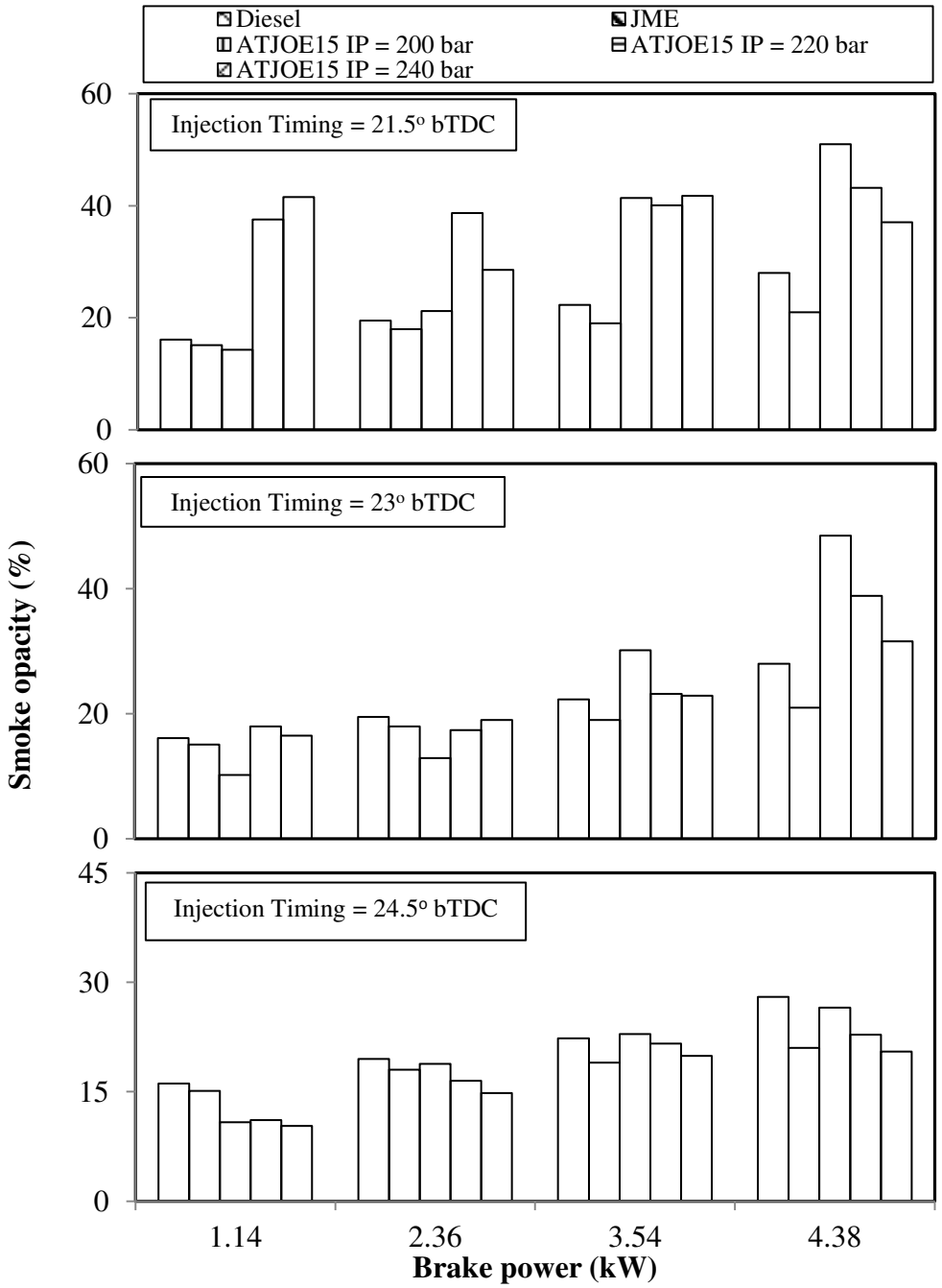

Fig. 5.6.12 Variation of smoke opacity with brake power at different injection timings and nozzle opening pressures

When the nozzle opening pressure is increased, the fuel particle diameter will become smaller. Therefore, the fuel-air mixture will become better throughout the combustion period, and hence, the smoke opacity will be lower. Similar reasons are reported by Sayin and Gumus [201], in their investigation on the impact of the compression ratio and injection parameters on the performance and emissions of a DI diesel engine fueled with biodiesel-blended diesel fuel.

The important findings of the investigation on combined effects of compression ratio, injection timing and nozzle opening pressure, in terms of percentage increase or decrease in different parameters are given in Table 5.3 and best set of parameters for all the tested fuels is given in Table 5.4.

5.6.5 Closure

The summary of the experimental results on the combined effects of injection timing and nozzle opening pressure on the combustion, performance and emission parameters obtained in a single cylinder, diesel engine fueled with the ATJOE15 emulsion, shows that with the retarded injection timing of 21.5 ^{o}CA, the NO emissions are found to be lower by about 12.8%, compared to that of diesel operation at the standard nozzle opening pressure of 200 bar. The brake thermal efficiency of the ATJOE15 emulsion is found to be higher by 4.3% compared to that of diesel in this operating condition. The smoke emissions are noticed to be higher by 23% compared to those of diesel at this condition.

Table 5.3 Percentage increase or decrease in different parameters with respect to diesel at full load

	FULL FACTORIAL DESIGN			Percentage change in the parameter with respect to diesel at full load (%)						
No.	**CR**	**IT**	**IP**	**BTE**	**BSFC**	**EGT**	**UBHC**	**CO**	**NO**	**Smoke**
1	16.5	21.5	200	-5.26	54.15	38.65	>100	>100	-34.97	>100
2	16.5	21.5	220	-1.75	61.98	46.41	>100	>100	-27.31	89.64
3	16.5	21.5	240	-9.06	>100	44.04	>100	>100	**-36.89**	79.64
4	16.5	23	200	-10.17	>100	37.68	>100	>100	-23.05	77.86
5	16.5	23	220	-1.90	44.88	36.53	>100	>100	-31.12	>100
6	16.5	23	240	7.48	47.68	34.59	>100	>100	-1.59	91.43
7	16.5	24.5	200	-2.89	44.09	32.05	>100	>100	4.60	47.14
8	16.5	24.5	220	0.35	48.90	26.03	>100	>100	-0.18	38.21
9	16.5	24.5	240	-2.95	>100	29.10	>100	>100	5.18	39.29
10	17.5	21.5	200	4.40	26.76	36.46	-39.60	>100	-12.87	82.14
11	17.5	21.5	220	6.17	33.91	29.73	94.62	>100	8.98	54.29
12	17.5	21.5	240	14.15	25.02	22.04	63.17	>100	21.41	32.50
13	17.5	23	200	8.24	54.79	16.30	-54.54	84.85	7.82	8.93
14	17.5	23	220	15.21	86.45	14.81	67.13	11.41	29.64	38.93
15	17.5	23	240	20.26	20.71	19.28	79.12	13.98	39.21	84.29
16	17.5	24.5	200	21.33	**17.54**	15.19	**-63.16**	81.21	36.43	-5.36
17	17.5	24.5	220	-12.92	86.45	35.34	>100	>100	24.48	>100
18	17.5	24.5	240	7.06	33.51	29.10	>100	>100	34.49	43.21
19	18.5	21.5	200	1.50	40.08	24.95	52.74	>100	4.07	-4.29
20	18.5	21.5	220	-10.71	59.23	25.41	39.50	72.31	11.43	97.50
21	18.5	21.5	240	0.95	59.07	26.98	86.31	>100	12.00	80.71
22	18.5	23	200	**25.81**	17.85	15.78	-45.00	10.00	4.88	-9.64
23	18.5	23	220	18.79	19.68	13.61	-32.34	5.24	16.89	-31.07
24	18.5	23	240	16.66	22.82	**12.95**	-44.17	11.65	30.75	-4.64
25	18.5	24.5	200	18.28	20.54	13.48	-48.22	**-48.22**	31.86	-11.79
26	18.5	24.5	220	18.12	20.37	18.40	-36.31	11.45	39.48	62.86
27	18.5	24.5	240	19.82	18.66	13.38	-52.24	-44.29	46.17	**-33.57**

Table 5.4 Best set of parameters for different fuel combinations

Sl.No	Parameter	Diesel (Standard conditions)	JME (Standard conditions)	Z2JOE5 (Standard conditions)	ATJOE15 (Standard conditions)	ATJOE15 (Optimum conditions)
Combustion parameters						
1.	Start of ignition (^{o}CA)	356.6	354	354.0	354.5	352.6
2.	Occurrence of maximum pressure (^{o}CA)	372.4	370.4	371.0	371.1	369.5
3.	Ignition delay (^{o}CA)	12.7	10.2	10.1	11.2	11.1
4.	Occurrence of maximum heat release (^{o} CA aTDC)	6.7	8.2	9.4	9.3	7.9
5.	Maximum heat release (J/^{o}CA)	52.02	49.97	51.52	46.4	39.82
6.	Maximum cylinder pressure (bar)	75.70	82.61	82.7	76.49	85.79
7.	90% Mass fraction burned (^{o}CA)	389.9	387.5	386.9	395.7	387
8.	Combustion duration (^{o}CA)	38.4	38	36.9	40.6	37.7
Performance parameters						
9.	Brake thermal efficiency (%)	30.4	30.3	31.7	32.9	36.0
10.	Specific fuel consumption (kg/kWh)	0.269	0.302	0.318	0.3555	0.324
11	Exhaust gas temperature (^{o}C)	270	325	305	301	306
Emission parameters						
12.	BSHC emission (g/kWh)	0.029	0.028	0.018	0.007	0.015
13.	BSCO emission (g/kWh)	0.008	0.008	0.005	0.0165	0.009
14.	BSNO emission (g/kWh)	2.055	2.898	2.489	2.09	2.709
15.	Smoke opacity (%)	28	21	23.1	30.5	24.7

Note: Standard Conditions: Compression Ratio 17.5, Injection Timing 23 ^{o}bTDC, Injection Pressure 200 bar
Optimum Conditions: Compression Ratio 18.5, Injection Timing 24.5 ^{o}bTDC, Injection Pressure 200 bar

5.7 Endurance test on the diesel engine fueled with the ATJOE15 emulsion

5.7.1 General

This chapter discusses the endurance test results obtained from a single cylinder, four stroke, DI diesel engine fueled with the ATJOE15 emulsion. The main objective of the endurance test was to evaluate the wear characteristics of the engine components, and changes in the lubrication oil properties of a test engine fueled with the ATJOE15 emulsion. The photographic views taken before and after the completion of 100 hrs endurance test, and visual inspection of the engine components, wear and carbon deposit results, are discussed in this chapter. The lubricating oil samples collected from the engine were subjected to atomic absorption spectroscopy (AAS) for the measurement of the various wear metal traces present, and the results are discussed in this chapter.

5.7.2 Comparison of carbon deposits on different engine components

5.7.2.1 Cylinder head and piston crown

After running the engine with the ATJOE15 emulsion, black carbon deposits were clearly detected in the combustion chamber, particularly on the engine head and on the piston crown. A comparison of the carbon deposits on the cylinder head and piston crown before and after the endurance test is shown in Figs. 5.7.1 and Fig.5.7.2. About 26 g of carbon deposits were found in the cylinder head and combustion chamber. The formation of deposits is probably due to the properties of WPO in the ATJOE15 emulsion. The ATJOE15 emulsion consists of about unsaturated and saturated fatty acids, which undergoes the chemical reactions at high temperatures inside the combustion chamber. During the chemical reactions, thermal cracking of compounds, particularly at the double bonds, favour combustion through the formation of low molecular weight gases at the fringes of the spray. On the other hand, the polymerisation of the fuel in the liquid core accounts for the contraction at the core of the spray. These polymers can no longer evaporate completely, and will be deposited on the available surfaces. Upon further heating, these deposits form coke-like substances identified as carbon deposits. Similar results are reported by Ziejewski et al. [205], in their investigation on the durability test, with high oleic sunflower and safflower oils in diesel engines.

(a) Before **(b) After**

Fig. 5.7.1 Comparison of cylinder head deposits before and after the endurance test

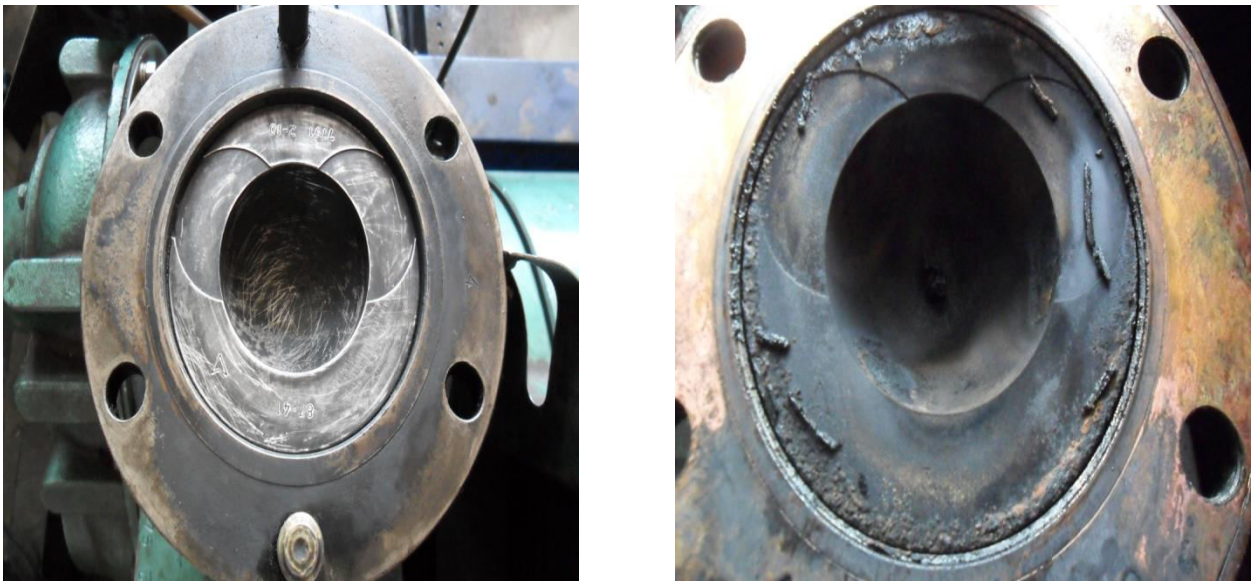

(a) Before **(b) After**

Fig. 5.7.2 Comparison of piston crown deposits before and after the endurance test

5.7.2.3 Fuel injector components

A comparison of the carbon deposits on the injector components, like the needle and nozzle tip, before and after the endurance test, is shown in Figs. 5.7.3 -5.7.5. The deposits were found at the injector nozzle tip and in-between the holes. A spray test was carried out on the nozzle with the

nozzle testing equipment under room conditions. From the visual observation of the spray, a deteriorated quality of the spray or a less misty spray and uneven spray distribution were noticed on the injector.

(a) Before **(b) After**

Fig. 5.7.3 Comparison of fuel injector components before and after the endurance test

(a) Before **(b) After**

Fig. 5.7.4 Comparison of nozzle and needle before and after the endurance test

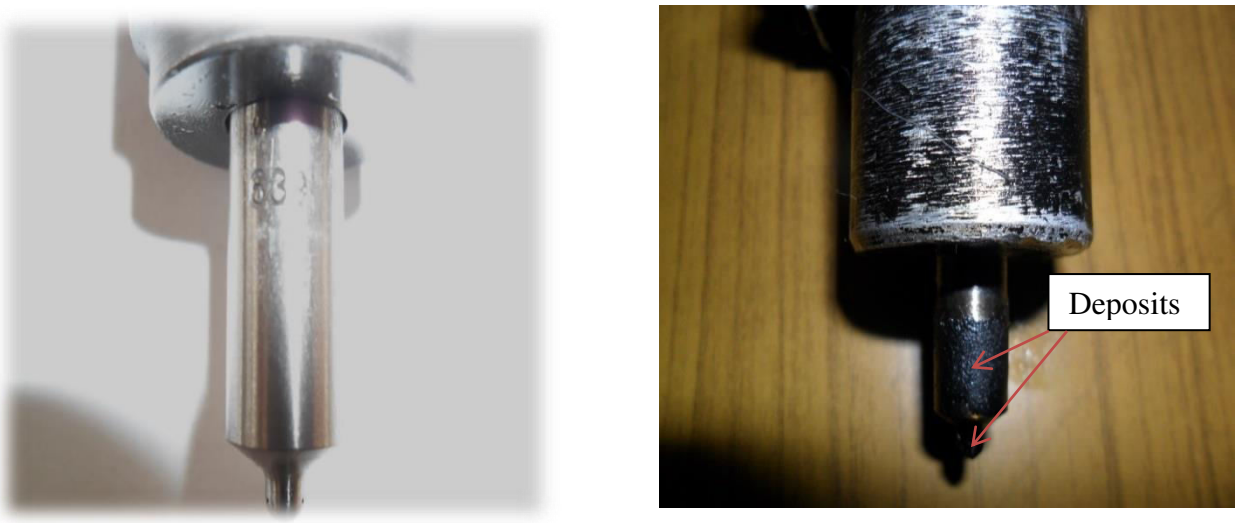

(a) Before **(b) After**

Fig. 5.7.5 Comparison of nozzle tip before and after the endurance test

Usually, a faulty injector tends to produce a distorted spray with a lower atomization of fuel, which in turn, causes less thorough mixing and subsequently unfavourable combustion and engine performance. Similar reasons are reported by Bari et al [206], in their investigation on the durability of the diesel engine fueled with crude palm oil.

5.7.2.6 Fuel injection pump components

The visual inspection of the disassembled fuel injection pump before and after the endurance test, and traces of wear found at the plunger after the endurance test, are shown in Figs. 5.7.6 (a), 5.7.6 (b) and 5.7.7.

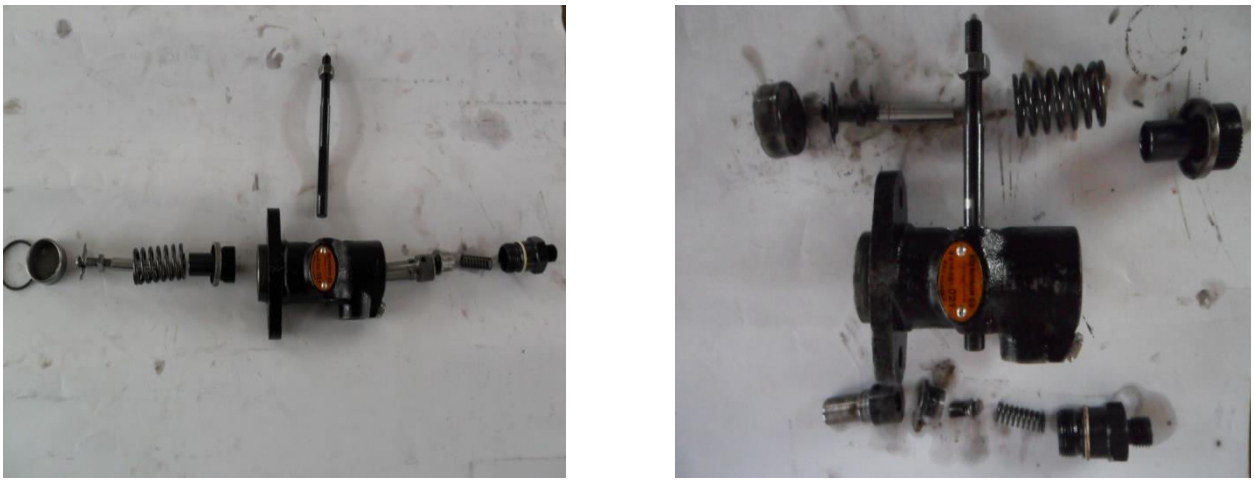

(a) Before **(b) After**

Fig. 5.7.6 (a) & (b) Comparison of fuel injection pump components before and after the endurance test

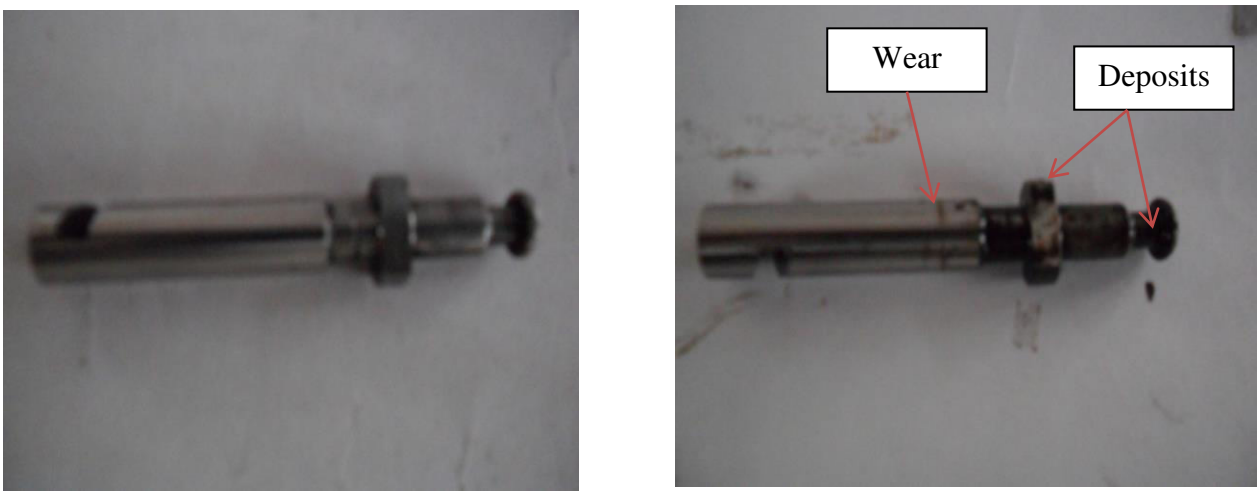

Fig. 5.7.7 Deposits and trace of wear on the plunger after the endurance test

This wear is critical because, under severe conditions, it could affect the sealing between the plunger and the barrel, thereby possibly causing a pressure loss in the injection system, which ultimately affects the injection.

5.7.2.6 Fuel filter

The photographs of the fuel filter before and after the end of the endurance test are shown in Fig.5.7.8.

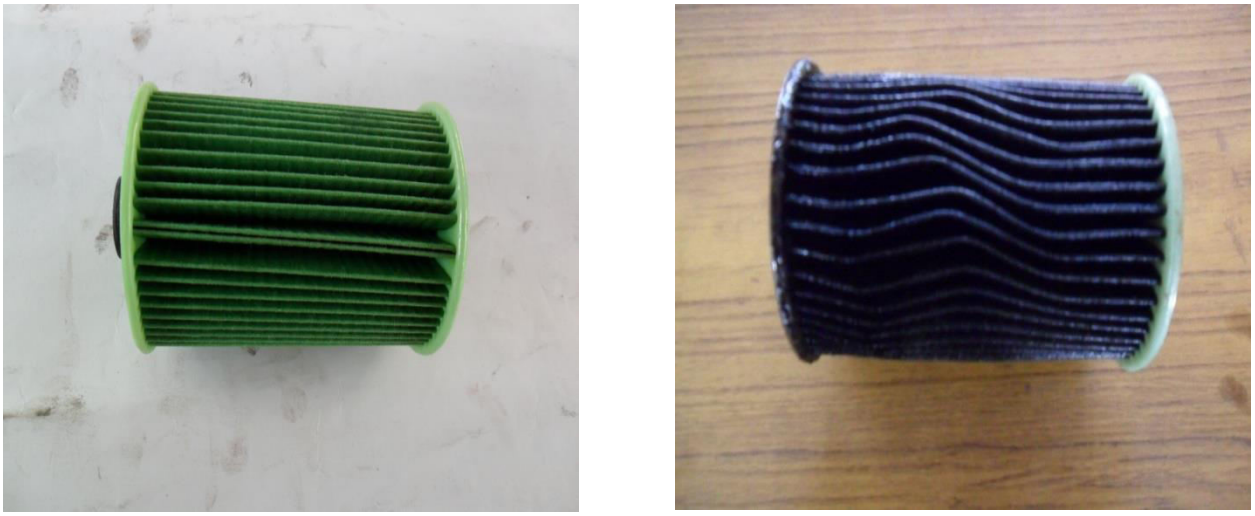

(a) Before **(b) After**

Fig. 5.7.8 Comparison of fuel filter before and after the endurance test

Fig. 5.7.9 Indication of WPO sediments in the ATJOE15 emulsion collected from the fuel filter container after the endurance test

On the visual inspection of fuel filter before and after the endurance test, it is evidenced that the fuel filter is choked after its use for 100 hrs. This may be due to the heavier molecules or sediments present in the WPO. Up to 100 hrs of operation, no problem with the fuel supply system was noticed.

5.7.3 Lubrication oil analysis

5.7.3.1 Determination of the ash content

The lubricating oil samples were kept in the furnace at 450°C for 4 hours and then 600°C for 2 hours to produce ash. The residual ash contains the wear debris of the metal primarily. By weighing the crucible before and after the test, the weight percentage of ash was determined. The calculation procedure of the ash content is as follows:

The weight of the empty crucible No.1 = 20.723 g

The weight of the crucible No.1 (With coke residue of fresh lubrication oil) = 20.781 g

The ash content present in the fresh lubrication oil = 0.058 (wt %)

Similarly, Weight of the empty crucible No.2 = 20.738 g

The weight of the crucible No.2 (With coke residue of used lubrication oil) = 20.825 g

The ash content present in the used lubrication oil = 0.087 (wt %)

More ash content in the lubricating oil after the end of the endurance test is noticed, which may be due to the addition of the metal debris resulting from the wear of the engine components. The viscosity of the lubrication oil after 100 hrs of operation, was found to be increased by about 10% compared to that of reference one.

5.7.3.2 Determination of the metal elements present in the lubrication oil

The engine lubrication oil, used in the test engine fueled with the ATJOE15 emulsion for the endurance test was analyzed by the atomic absorption spectroscopy (AAS). By analyzing a sample of the lubricating oil from the engine after a certain running period, it is possible to collect some information on the operation and condition of the engine. The wear particles generated from the sliding contact of the solid surfaces are suspended in the lubricating oil. In this investigation, the variation in the concentration of the wear metals debris including Fe, Cu, Zn, Al, Cr, Pb and CO in the used lubricating oil with the engine operation time, was obtained using the AAS. The results are presented in part per million (ppm) by weight of the metal to the lubricating oil. A comparison of the metal elements present in the fresh lubricating oil and used lubricating oil, is illustrated in Fig. 5.7.10.

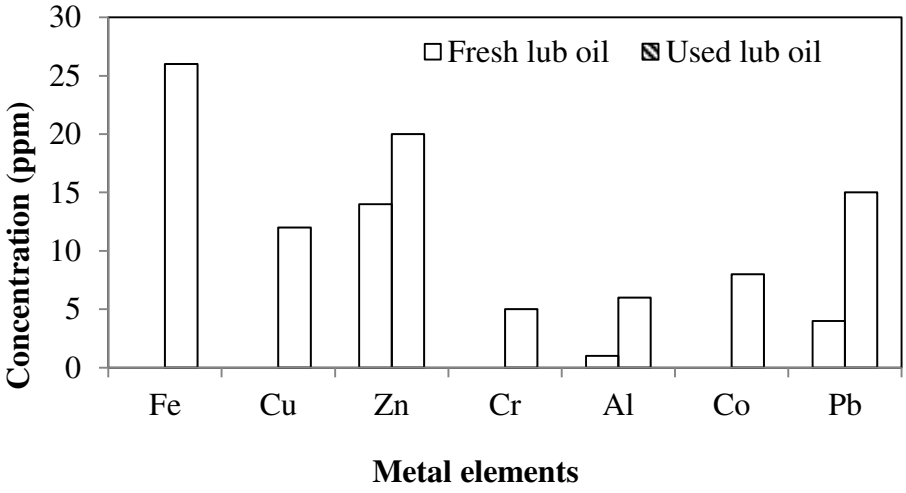

Fig. 5.7.10 Comparison of metal elements present in the fresh lubricating oil and used lubricating oil

In the results obtained, there was a marked increase in Fe concentration in the lubrication oil by about 26 ppm at the end of 100 hours. The iron in the wear debris could be from the cylinder liner, piston, rings, valves, valve guides, gears, shafts, rust and crankshaft. Similar ascending trends of wear metals concentration for Al and Cr were also observed. The aluminum and

chromium in the lubricating oil come from the wear of piston, bearings, cylinder liner, compression rings and crankshaft. With respect to Cu and Pb, the rate of wear is found to be high. The copper and lead in the wear debris may originate from bearings, bushings, paints and grease additives. The Zn elements in the used lubricating oil are found to be higher by 30%, which could be due to the depletion of additives used in bearings and brass components. The Cobalt in the wear debris originates from the wear of bearings. The maximum wear debris present in the used lubricating oil is Fe, but it is far too lower than the condemning level specified for used lubricating oil (50-60 ppm) [207]. Overall, the wear metals did not increase beyond the usual values encountered in the endurance tests.

5.7.4 Comparison of the performance and emission parameters

The percentage change in the performance and emission parameters of the diesel engine fueled with the ATJOE15 emulsion, after the end of the endurance test at full load is presented in Fig. 5.7.11.

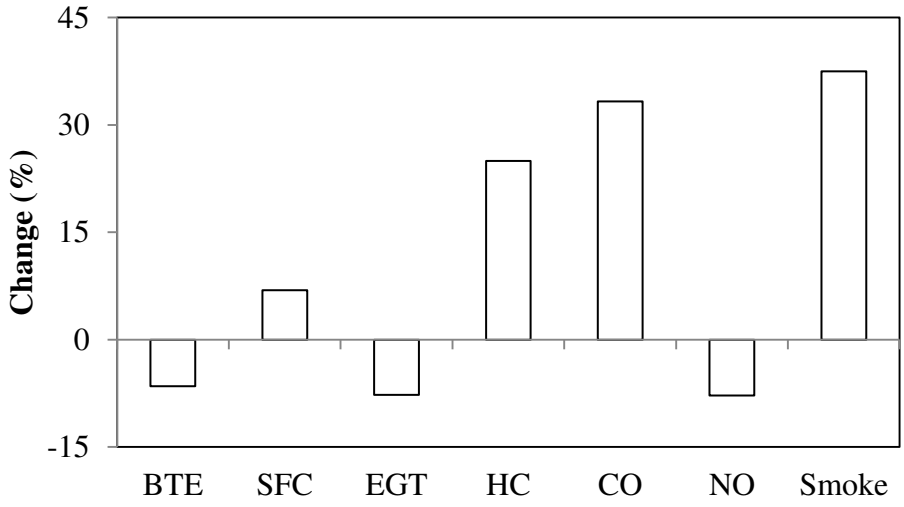

Fig. 5.7.11 Percentage change in the performance and emission parameters of the diesel engine fueled with ATJOE15 emulsion (after endurance test) at full load

It is evidenced from the figure, that the brake thermal efficiency and exhaust gas temperature of the ATJOE15 emulsion is lower by 6.5% and 7.7% respectively, after the end of the endurance test. The specific fuel consumption of the ATJOE15 emulsion is found to be higher by 6.9% after the end of the endurance test. The HC, CO and smoke emissions from the ATJOE15 emulsion after the end of the endurance test are found to be higher by 25%, 33.3% and 37.5% respectively.

The NO emissions are found to be lower by about 7.8%, compared to those of the initial condition (i.e., before the endurance test).

5.7.5 Closure

During the 100 hrs of the endurance test conducted on the diesel engine fueled with the ATJOE15 emulsion, no abnormalities occurred. After the endurance test, on visual inspection of various engine components, carbon deposits were noticed in the cylinder head, combustion chamber and nozzle tip. About 26 g of carbon deposits were found in the cylinder head and combustion chamber. A marginal wear was observed in the plunger of the fuel injection pump. The fuel filter was found to be clogged with the sediments of WPO. From the lubrication oil analysis, an ash content of about 0.087 (wt %) and the existence of various metal debris were noticed. Out of all, Fe was the most abundant wear metal found in the lubrication oil. The viscosity of the lubrication oil after 100 hrs of operation, was found to be increased by about 10% compared to that of reference one. At the end of the endurance test, the engine was able to produce its rated power with a small decrement in the brake thermal efficiency. The specific fuel consumption was found to be higher. The HC, CO and smoke emissions were found to be higher compared to those of the initial condition. The NO emissions alone were found to be lower at the end of the endurance test.

CHAPTER 6

CONCLUSIONS

6.1 General

The combustion, performance and emission characteristics of a single cylinder, four stroke, air cooled, direct injection diesel engine capable of producing 4.4 kW at a constant speed of 1500 rpm, fueled with JME-WPO emulsion with fuel and engine modifications, were analysed, compared with diesel and JME operations of the engine. Also the experimental results were compared with a two zone mathematical model developed. Further, a short term endurance test was also carried out to ensure the technical feasibility of the engine fueled with the JME-WPO emulsion. The conclusions of each technique are given in this section.

6.1.1 Parametric studies on combustion, performance and emissions with the JME-WPO emulsions

- The engine was able to run with a maximum of 15% WPO in the form of emulsions with the JME.
- With 15% WPO in the emulsions, the start of ignition for all the emulsions is found to be earlier than that of diesel at full load.
- The ignition delay of JME-WPO emulsions decreases by about 2.3 ^{o}CA to 2.7 ^{o}CA compared to that of diesel.
- The maximum thermal efficiency is noticed with the Z2JOE15 emulsion compared to all other emulsions tested in this study. The thermal efficiency for Z2JOE15 is found to be higher by 11.3% compared to that of diesel.
- With 15% WPO in the emulsion, the HC emissions are found to be lower from 11.3% to 45.8% compared to that of diesel operation, and 9.6% to 44.8% lower compared to that JME operation are noticed.
- The CO emissions are found to be lower from 43.8% to 68.9%, compared to that of diesel at full load.
- The NO emissions for all the emulsions are found to be lower than that of JME operation, but higher than that of diesel operation. The maximum reduction in the nitric oxide emission by 16.8% is observed with Z2JOE15 emulsion compared to that of JME operation.
- The reduction in smoke for all the emulsions investigated in this study is in the range of 15%, to 27.8%, compared to that of diesel at full load.

- Overall, by considering the combustion, performance and emission parameters, it can be concluded that the Z2JOE15 showed a better performance and lower emissions compared to those of diesel and JME operations.

6.1.2 Experimental studies on combustion, performance and emission characteristics of ATJOE15 emulsion

- The acidity of the Z2JOE15 emulsion was neutralized by acid treatment to avoid the corrosion effect on several engine components.
- The combustion of ATJOE15 emulsion commences earlier than that of diesel at full load. Ignition delay of ATJOE15 is found to be shorter than that of diesel.
- In the performance aspect, the brake thermal efficiency of ATJOE15 emulsion is higher by about 8.2% and 8.5% than those of diesel and JME at full load.
- The BSHC emissions are reduced by about 73% for ATJOE15 emulsion at full load compared to that of diesel. The BSCO emission of ATJOE15 emulsion is found to be higher by about 46% than that of diesel at full load.
- There is about 2% increase in the NO emission is obtained with the ATJOE15 emulsion at full load compared to that of diesel. When fueled with the ATJOE15 the smoke opacity increases by about 8% compared to that of diesel operation.

6.1.3 Analysis of combustion and emission characteristics of a diesel engine fueled with the ATJOE15 emulsion

- The experimental and simulated results show that the peak cylinder pressures of the JME and the ATJOE15 are found to be marginally higher than that of diesel, and about 6.1% lower peak cylinder pressures are obtained with the ATJOE15 emulsion at simulated conditions compared to that of experimental conditions.
- The maximum heat release rates of JME and ATJOE15 are found to be lower than that of diesel fuel, in both the experimental and simulated conditions. Compared to experimental conditions, the maximum heat release rate of the ATJOE15 at simulated conditions is found to be lower by 1.96%.
- Compared to diesel operation, the NO concentration is found to be higher in the case of JME operation, and lower in the case of the ATJOE15 operation at both experimental and simulated conditions. With the simulated conditions, the NO emissions of the ATJOE15 emulsion are found to be higher by 1% compared to that of experimental conditions.

- The soot density is found to be lower for the JME operation and it is higher for the ATJOE15 operation compared to that of diesel. The soot density of the ATJOE15 emulsion at simulated condition is found to be lower by about 4.5% than that of experimental condition.

The presented model can predict the combustion characteristics such as cylinder pressure and heat release which are in good agreement with the experimental results.

6.1.4 Combined effect of compression ratio and injection timing on the performance and emission parameters of diesel engine fueled with the ATJOE15 emulsion

- The peak cylinder pressure is more in the cases of higher compression ratio and advanced injection timing for the ATJOE15 emulsion compared to that of diesel operation. Also the starting of combustion is found to be earlier in such conditions for ATJOE15 emulsion compared to that of diesel.
- The ignition delay of the ATJOE15 emulsion at higher compression ratio is found to be lower compared to that of diesel which results in lower heat release rates at this condition. At lower compression ratio and retarded injection timings this trend is reverse.
- The brake thermal efficiency of the ATJOE15 emulsion at increased compression ratio and advanced injection timings are found to be higher than diesel and JME operations. When the compression ratio is decreased to 16.5, the brake thermal efficiency of ATJOE15 emulsion is found to be lower at all the injection timings.
- The minimum BSFC value of 0.317 kg/kWh is obtained at compression ratio 18.5 and injection timing 23 ^{o}CA bTDC, which is higher by about 17.8% compared to that of diesel.
- At standard compression ratio, the HC emissions of the ATJOE15 emulsion at different injection timings are found to be lower in the range of 39.5% to 65.5% compared to that of diesel at full load.
- The CO emissions of the ATJOE15 emulsion are found to be higher with the lower compression ratio and retarded injection timings. With the advancement in the injection timing, about 48% reduction in the CO emissions are noticed with the ATJOE15 emulsion.
- The NO emissions of the ATJOE15 emulsion are found to be lower with the lower compression ratio and retarded injection timings. With the higher compression ratio of

18.5, the NO emissions from the ATJOE15 emulsion are found to be higher in the range of 4% to 31.8% compared to that of diesel.

- When the injection timing is advanced, the smoke opacity value of the ATJOE15 is found to be lower by about 5.3% compared to that of diesel operation. At reduced compression ratio of 16.5, the smoke opacities of the ATJOE15 emulsion at all the injection timings found to be higher in the range between 32% and 52% compared to that of diesel operation. At higher compression ratio of 18.5, the smoke opacity of the ATJOE15 emulsion at retarded injection timing is found to be lower by about 4.2% and in the advanced injection timing case, the smoke emission values reduced by about 11.7% compared to that of diesel.

6.1.5 Combined effect of compression ratio and nozzle opening pressure on the combustion, performance and emission parameters of diesel engine fueled with the ATJOE15 emulsion

- Among all the tested compression ratios and nozzle opening pressures, the compression ratio of 18.5 and with the nozzle opening pressure of 220 bar, the ATJOE15 operation produced the highest cylinder pressure value of 77.2 bar at 372.1 ^{o}CA, which is earlier by about 0.3 ^{o}CA and later by about 1.6 ^{o}CA than those of diesel and the JME operations respectively.
- The ignition delay of the ATJOE15 emulsion is found to be shorter in the range between 0.3 ^{o}CA and 2.2 ^{o}CA with the compression ratios of 17.5, 18.5 and the higher nozzle opening pressure of 240 bar compared to that of diesel operation. In comparison with the JME operation, the engine fueled with the ATJOE15 emulsion exhibits a longer ignition delay at all operating conditions.
- With a higher compression ratio of 18.5 and nozzle opening pressure of 240 bar, improved performance and lower emissions. The maximum thermal efficiency is noticed at this operating condition.
- A maximum reduction in the HC, CO and smoke emissions by about 52.8%, 55.3% and 36.4% respectively is noticed with ATJOE15 emulsion at the same operating conditions.
- The NO emission at this condition is still found to be higher by about 30.7% compared to that of diesel operation, at full load.
- With the standard compression ratio and standard nozzle opening pressure of 200 bar, the smoke opacity of ATJOE15 is found to be higher by about 8.9%. When the nozzle

opening pressure is increased to 220 bar and 240 bar, the smoke opacity of ATJOE15 is found to be reduced by about 3.9% and 26.4% respectively compared to that of diesel operation.

- When the compression ratio is reduced to 16.5, the NO emissions of the ATJOE15 emulsion are found to be lower by about 23%, 11.6 and 1.6% compared to that of diesel operation at nozzle opening pressures of 200, 220 and 240 bar respectively.
- At reduced compression ratio of 16.5, the smoke opacities of ATJOE15 emulsion at all the nozzle opening pressures found to be higher in the range between 42% and 50.6% compared to that of diesel operation.

6.1.6 Combined effect of injection timing and nozzle opening pressure on the combustion, performance and emission parameters of diesel engine fueled with the ATJOE15 emulsion

- Among all the tested injection timings and nozzle opening pressures, the injection timing of 24.5 ^{o}CA bTDC with the nozzle opening pressure of 200 bar, the ATJOE15 operation produced the highest cylinder pressure value of 79.5 bar at 370.6 ^{o}CA, which is earlier by about 2.2 ^{o}CA and later by about 0.2 ^{o}CA than those of diesel and the JME operations respectively.
- Among all the tested injection timings and nozzle opening pressures, a shorter ignition delay period of 10.36 ^{o}CA is observed for the ATJOE15 operation with the injection timing of 23 ^{o}CA bTDC and nozzle opening pressure of 240 bar.
- For the standard injection timing, with the higher nozzle opening pressures of 220 bar and 240 bar, the brake thermal efficiency of the ATJOE15 emulsion is found to be higher than that of diesel by about 4.6% and 6.1% respectively at full load.
- When the injection timing is retarded to 21.5 ^{o}CA bTDC, the brake thermal efficiency of the ATJOE15 emulsion is found to be higher by an average of 2.5% at nozzle opening pressures at full load.
- With the advanced injection timing of 24.5 ^{o}CA bTDC, the brake thermal efficiency of the ATJOE15 emulsion is found to be higher by an average of 5.5% at all nozzle opening pressures.
- The lowest value of the BSFC obtained for the ATJOE15 emulsion at 24.5 ^{o}CA bTDC is 0.3177 kg/kWh at nozzle opening pressure 240 bar, which is higher by about 17.8% compared to that of diesel operation.

- The HC emissions of the ATJOE15 emulsion are found to be lower with all injection timings and pressures. The CO emissions of the ATJOE15 emulsion are found to be higher with all injection timings and pressures, but it decreases with increase in nozzle opening pressures.
- With the retarded injection timing of 21.5 ^{o}CA, the NO emissions of the ATJOE15 emulsion are found to be lower by about 12.8%, compared to that of diesel operation at standard nozzle opening pressure of 200 bar.
- With the retarded injection timing of 21.5 ^{o}CA, the smoke opacities of ATJOE15 emulsion at all the nozzle opening pressures found to be higher in the range between 24.5% and 45.5% compared to that of diesel operation.

6.1.7 Endurance test on the diesel engine fueled with the ATJOE15 emulsion

- After the end of endurance test, carbon deposits were noticed in the cylinder head, combustion chamber and nozzle tip.
- About 26 g of carbon deposits were found in the cylinder head and combustion chamber.
- A marginal wear was observed in the plunger of the fuel injection pump.
- The fuel filter was found to be clogged with the WPO particles.
- From the lubrication oil analysis, ash content of about 0.087 (wt %) and existence of various metal debris were noticed. Out of all, Fe was the most abundant wear metal found in the lubrication oil.
- The viscosity of the lubrication oil after 100 hrs of operation, was found to be increased by about 10% compared to that of reference one.
- At the end of endurance test, the engine was able to produce its rated power with small decrement in the brake thermal efficiency.
- The specific fuel consumption was found to be higher.
- The HC, CO and smoke emissions from the ATJOE15 emulsion after the end of endurance test are found to be higher by 25%, 33.3% and 37.5% respectively.
- The NO emissions are found to be lower by about7.8% compared to that of initial condition.

6.2 Scope for future work

- The WPO obtained can be upgraded by removal of oxygen content to improve the calorific value of the fuel.
- The water content in the WPO to be removed to avoid corrosion of engine components.
- The chemical stability of the WPO may be increased by esterification process.
- The JME-WPO emulsions can be tested in automotive engines and in gensets.
- Kinetic studies are required for optimization of parameters involved in the production of WPO.

REFERENCES

[1] Website: www.eia.gov/ies. Accessed on 25th November 2010.

[2] M. Gumus, C. Sayin, and M. Canakci. The impact of fuel injection pressure on the exhaust emissions of a direct injection diesel engine fueled with biodiesel–diesel fuel blends. Fuel, vol. 95, 2012, pp. 486–494.

[3] Website: http://en.wikipedia.org/wiki/List_of_countries_by_carbon_dioxide_emissions. Accessed on 5th December 2010.

[4] L.Liang, Y. Zhang, L.Zhang, M.Zhu, S.Liang, and Y. Huang. Study of sugarcane pieces as yeast supports for ethanol production from sugarcane juice and molasses. Journal of Industrial Microbiology & Biotechnology, vol.35, 2008, pp 1605-1613.

[5] M. Balat, and H. Balat. Recent trends in global production and utilization of bio-ethanol fuel. Applied Energy, vol. 86, 2009, pp. 2273–2282.

[6] D.R. Keshwani, and J.J. Cheng. Switchgrass for bioethanol and other value-added applications: A review. Bioresource Technology, vol.100, 2009, pp.1515–1523.

[7] A.Sorensen, P. J.Teller, T. Hilstrøm, and B. K. Ahring. Hydrolysis of Miscanthus for bioethanol production using dilute acid presoaking combined with wet explosion pre-treatment and enzymatic treatment. Bioresource Technology, vol.99, 2008, pp. 6602–6607.

[8] A. Demirbas. Progress and recent trends in biodiesel fuels. Energy Conversion and Management, vol. 50, 2009, pp. 14–34.

[9] A. Faaij. Biomass and biofuels. A background report for the Energy Council of the Netherlands, 2007.

[10] E. Ecklund, R. Bechtold, T. Timbario, and P. McCallum. State-of-the-art report on the use of alcohols in diesel engines. SAE Technical Paper 840118, 1984.

[11] A. Kowalewicz. Emission characteristics of compression ignition engine fuelled with RME/DF and ethanol. Journal of KONES Internal Combustion Engines 2003, vol. 10, pp. 349-357.

[12] S. Chongkhong, C. Tongurai, and P. Chetpattananondh. Continuous esterification for biodiesel production from palm fatty acid distillate using economical process. Renewable Energy, vol. 34, 2009, pp. 1059–1063.

[13] A. Demirbas. Biodiesel: A Realistic Fuel Alternative for Diesel Engines. Springer Publication, 2008, ISBN 978-1-84628-994-1.

[14] G. D. Rai. Non-Renewable energy sources. Khanna publications, New Delhi, 2004.

[15] S.N. Naik, V.V. Goud, P.K. Rout, and A.K. Dalai. Production of first and second generation biofuels: A comprehensive review. Renewable and Sustainable Energy Reviews, vol.14, 2010, pp.578–597.

[16] D.Mohan, C.U. Pittman, and P.H. Steele. Pyrolysis of Wood/Biomass for Bio-oil: A Critical Review. Energy Fuels, vol.20, 2006, pp.848-889.

[17] M.M. Azam, A.Waris, and N.M. Nahar. Prospects and potential of fatty acid methyl esters of some non-traditional seed oils for use as biodiesel in India. Biomass and Bioenergy, vol. 29, 2005, pp.293–302.

[18] P. McCarthy, M.G. Rasul, and S. Moazzem. Analysis and comparison of performance and emissions of an internal combustion engine fuelled with petroleum diesel and different bio-diesels. Fuel, vol. 90, 2011, pp. 2147–2157.

[19] R.K.Pandey, A.Rehman, R.M.Sarviya, and S. Dixit. Development of clean burning fuel for compression ignition engines. Asian Journal of Experimental Science, 2009, vol. 23, pp. 223-234.

[20] S. Jindal, B.P. Nandwana, N.S. Rathore, and V. Vashistha. Experimental investigation of the effect of compression ratio and injection pressure in a direct injection diesel engine running on Jatropha methyl ester. Applied Thermal Engineering, vol. 30, 2010, pp. 442-448.

[21] J.P. Szybist, J. Song, M. Alam, and A.L. Boehman. Biodiesel combustion, emissions and emission control. Fuel Processing Technology, vol. 88, 2007, pp. 679-691.

[22] C.Y. Lin, and H.A. Lin. Diesel engine performance and emission characteristics of biodiesel produced by the peroxidation process. Fuel, vol.85, 2006, pp. 298-305.

[23] A.N. Ozsezen, M.Canakci, and C. Sayin. Effects of biodiesel from used frying palm oil on the performance, injection, and combustion characteristics of an indirect injection diesel engine. Energy & Fuels, vol. 22, 2008, pp.1297–1305.

[24] United States Environmental Protection Agency. A comprehensive analysis of biodiesel impacts on exhaust emissions. Technical Report No. EPA420-P-02-001, 2002, Environmental Protection Agency, Research Triangle Park, North Carolina.

[25] P. Chitra, P. Venkatachalam, and A. Sampathrajan. Optimisation of experimental conditions for biodiesel production from alkali-catalysed transesterification of Jatropha curcas oil. Energy for Sustainable Development, 2005; 9:13–8.

[26] H. Lu, Y. Liu, H. Zhou, Y. Yang, M. Chen, and B. Liang. Production of biodiesel from Jatropha curcas L. oil. Computers and Chemical Engineering, 2009;33:1091–6.

[27] P.K Sahoo, and L.M Das. Process optimization for biodiesel production from Jatropha, Karanja and Polanga oils. Fuel 2009;88:1588–94.

[28] A.K Tiwari, A. Kumar, and H. Raheman. Biodiesel production from jatropha oil (Jatropha curcas) with high free fatty acids: an optimized process. Biomass and Bioenergy 2007; 31:569–75.

[29] S.H Shuit, K.T Lee, A.H Kamaruddin, and S. Yusup. Reactive extraction and in situ esterification of Jatropha curcas L. seeds for the production of biodiesel. Fuel 2009 [Short communication].

[30] S. Tamalampudi, M.R. Talukder, S. Hama, T. Numata, A. Kondo, and H. Fukuda. Enzymatic production of biodiesel from Jatropha oil: a comparative study of immobilized-whole cell and commercial lipases as a biocatalyst. Biochemical Engineering Journal, 2008;39:185–9.

[31] S. Shah, and M.N Gupta. Lipase catalyzed preparation of biodiesel from Jatropha oil in a solvent free system. Process Biochemistry, 2007; 42:409–14.

[32] S. Hawash, N. Kamal, F. Zaher, O. Kenawi, and G. El Diwani. Biodiesel fuel from Jatropha oil via non-catalytic supercritical methanol transesterification. Fuel, 2009;88:579–82.

[33] Z. Ilham, and S. Saka. Two-step supercritical dimethyl carbonate method for biodiesel production from Jatropha curcas oil. Bioresource Technology. 2010;101:2735–40.

[34] C.H Chen, W.H Chen, C.M.J Chang, S.M Lai, and C.H. Tu. Biodiesel production from supercritical carbon dioxide extracted Jatropha oil using subcritical hydrolysis and supercritical methylation. Journal of Supercritical Fluids, 2010;52: 228–34.

[35] D. Kumar, G. Kumar, and C.P. Poonam Singh. Ultrasonic-assisted transesterification of Jatropha curcas oil using solid catalyst, Na/SiO2. Ultrasonics Sonochemistry, 2010:0300, doi:10.1016/j.ultsonch.2010.

[36] Y. Ishii, and R. Takeuchi. Transesterified curcas oil blends for farm diesel engines. Transactions of the ASABE, 1987, vol, 30 (3), pp. 0605-0609.

[37] M. Senthil Kumar, A. Ramesh, and B. Nagalingam. Investigations on the use of Jatropha oil and its methyl ester as a fuel in a compression engine. Journal of Energy Institute, vol. 74, 2001, pp. 24–28.

[38] M. Senthil Kumar, A. Ramesh, and B. Nagalingam. An experimental comparison of methods to use methanol and Jatropha oil in a compression ignition engine. Biomass and Bioenergy, vol.25, 2003, pp. 309-318.

[39] G.A.P. Rao, and P. Ram Mohan. Performance evaluation of DI and IDI engines with Jatropha oil based biodiesel. Institution of Engineers (I) Journal, vol. 86, 2005, pp. 72-76.

[40] P. Mahanta, S.C. Mishra, and Y.S. Kushwah. A comparative study of pongamia pinnata and jatropha curcus oil as diesel substitute. International Energy journal, vol. 7, 2006, pp. 1-8.

[41] N.R. Banapurmath, P.G. Tewari, and R.S. Hosmath. Performance and emission characteristics of a DI compression ignition engine operated on Honge, Jatropha and sesame oil methyl esters. Renewable Energy, vol. 33, 2008, pp. 1982-1988.

[42] G.L. Rao, B.D. Prasad, and S. Sampath. Combustion Analysis of Diesel Engine Fueled with Jatropha Oil Methyl Ester - Diesel Blends. International Journal of Green Energy, vol. 4, 2007, pp.645–658.

[43] T.V. Rao, G.P. Rao, and K.H. Chandra. Experimental Investigation of Pongamia, Jatropha and Neem Methyl Esters as Biodiesel on C.I. Engine. Jordan Journal of Mechanical and Industrial Engineering, vol. 2, 2008, pp. 117 - 122.

[44] S.R. Kalbande and S.D. Vikhe. Jatropha and Karanj Bio-Fuel: An Alternate Fuel. ARPN Journal of Engineering and Applied Sciences, vol. 3, 2008, pp. 7-13.

[45] Y.V. Rao, R.S. Voleti, V.S. Hariharan, and A.V. Raju. Jatropha oil methyl ester and its blends used as an alternative fuel in diesel engine. Thermal Science, vol. 13, 2009, pp. 207-217.

[46] P.K. Sahoo, L.M. Das, M.K. Babu, P. Arora, V.P. Singh, N.R. Kumar, and T.S. Varyani. Comparative evaluation of performance and emission characteristics of jatropha, karanja and polanga based biodiesel as fuel in a tractor engine. Fuel, vol. 88, 2009, pp. 1698-1707.

[47] T.T. Kywe and M.M. Oo. Production of Biodiesel from Jatropha Oil (Jatropha curcas) in Pilot Plant. Proceedings of world academy of science, Engineering and Technology, vol. 38, 2009, pp. 481-487.

[48] S. Jindal, B.P. Nandwana, and N.S. Rathore. Comparative Evaluation of Combustion, Performance, and Emissions of Jatropha Methyl Ester and Karanj Methyl Ester in a Direct Injection Diesel Engine. Energy Fuels, vol.24, 2010, pp. 1565-1572.

[49] M.Senthil Kumar, A. Kastler, and B. Nagalingam. A Comparison of the Different Methods of Using Jatropha Oil as Fuel in a Compression Ignition Engine. Journal of Engineering for Gas Turbines and Power, vol. 132, 2010, pp. 1-10.

[50] R. Ejilah, A.A. Asere, A.B. Adisa, and A. Ejila. The effect of diesel fuel-Jatropha curcas oil methyl ester blend on the performance of a variable speed compression ignition engine. Australian journal of agricultural engineering, vol. 1, 2010, pp. 80-85.

[51] S. Puhan, N. Saravanan, G. Nagarajan, and N. Vedaraman. Effect of biodiesel unsaturated fatty acid on combustion characteristics of a DI compression ignition engine. Biomass and Bioenergy, vol. 34, 2010, pp. 1079–1088.

[52] J. Huang, Y. Wang, J. Qin, and A.P. Roskilly. Comparative study of performance and emissions of a diesel engine using Chinese pistache and jatropha biodiesel. Fuel Processing Technology, vol. 91, 2010, pp. 1761–1767.

[53] T.K. Gogoi, S. Talukdar, and D.C. Baruah. Comparative Analysis of Performance and Combustion of Koroch Seed Oil and Jatropha Methyl Ester blends in a Diesel Engine. World Renewable Energy Congress, Sweden, 2011, pp. 3533-3540.

[54] V.S. Reddy, K.R. Ranjan, V.K. Sharma and S.K. Tyagi. Experimental investigation of a diesel engine fuelled with Jatropha curcas L. seed oil. International Journal of Sustainable Energy, vol. 30,2010, pp. 37-41.

[55] T.Elango and T.Senthil kumar. Combustion and emission characteristics of a diesel engine fuelled with jatropha and diesel oil blends. Thermal Science, vol. 15, 2011, pp. 1205-1214.

[56] R. Prakash, S. Pandey, and S. Chatterji. Performance analysis of CI engine using jatropha oil and their esters. International Journal of Advanced Engineering Technology, vol. 2, 2011, pp. 186-191.

[57] L. Prasad, S. Pradhan, C.S. Madankar, L.M. Das, and S.N. Naik. Comparative study of performance and emissions characteristics of a diesel engine fueled with jatropha and karanja biodiesel. Journal of Scientific & Industrial Research, vol. 70, 2011, pp. 694-698.

[58] B.R. Prasath, P.T. Porai, M.F. Shabir, P. K. Devan, and S. Vigneshwaran. Combustion and Performance Analysis of Single Cylinder DI Diesel Engine Using Jatropha Biodiesel and its Blends. Applied Mechanics and Materials, vol.110–116, 2012, pp.3-7.

[59] D. Vashist and M. Ahmed. A comparative study of castor and jatropha oil source and its methyl ester test on the diesel engine. International Journal of Engineering Science and Technology, vol. 3, 2011, pp. 4765-4773.

[60] D. Kannan, S. Pachamuthu, N. Nabi, J. Einar, and T. Lovas. Theoretical and experimental investigation of diesel engine performance, combustion and emissions analysis fuelled with the blends of ethanol, diesel and jatropha methyl ester. Energy Conversion and Management, vol. 53, 2012, pp. 322-331.

[61] S. Kumar, A. Chaube, and S. K. Jain. Experimental evaluation of C.I. engine performance using diesel blended with Jatropha biodiesel. International Journal of Energy and Environment, vol. 3, 2012, pp. 471-484.

[62] A.Yadav and O. Singh. Investigations on diesel engine performance based on jatropha, karanja and neem biodiesels. Proc. IMechE Part A: Journal of Power and Energy, vol. 226, 2012, pp. 674-681.

[63] A.M. Liaquat, H.H. Masjuki, M.A. Kalam, M. Varman, and M.A. Hazrat. Application of blend fuels in a diesel engine. Energy Procedia, vol. 14, 2012, pp. 1124-1133.

[64] L. Prasad, S. Pradhan, L.M. Das, and S.N. Naik. Experimental assessment of toxic phorbol ester in oil, biodiesel and seed cake of Jatropha curcas and use of biodiesel in diesel engine. Applied Energy, vol. 93, 2012, pp. 245-250.

[65] B.S. Chauhan, N. Kumar, and H. Muk. A study on the performance and emission of a diesel engine fueled with Jatropha biodiesel oil and its blends. Energy, vol. 37, 2012, pp. 616-622.

[66] R. Kumar, A.K. Dixit, G.S. Manes, R. Khurana, and S.K. Singh. Emission and performance characteristics of jatropha ethyl ester blends with diesel fuel in a CI Engine. International Journal of Automobile Engineering Research and Development, vol. 2, 2012, pp. 34-47.

[67] P. Tan, Z. Hu, D. Lou, and Z. Li. Exhaust emissions from a light-duty diesel engine with Jatropha biodiesel fuel. Energy, vol. 39, 2012, pp. 356-362.

[68] G.Shirsath, M.S. Tandale, S.V. Khandal, S. Guluwadi, N.R. Banapurmath, V.S. Yaliwal and P.G. Tewari. Blends of karanja and jatropha biodiesels for diesel engine applications. International Journal of Sustainable Engineering, Vol.5, 2012, pp.252–264.

[69] M. El-kasaby and M.A. Nemit-allah. Experimental investigations of ignition delay period and performance of a diesel engine operated with Jatropha oil biodiesel. Alexandria engineering journal, vol. 52, 2013, pp. 141–149.

[70] V. Pradeep, and R.P. Sharma. Use of hot EGR for NO_x control in a compression ignition engine fuelled with bio-diesel from Jatropha oil. Renewable Energy, vol. 32, 2007, pp. 1136-1154.

[71] D.A. Dhananjaya, C.V. Sudhir and P. Mohanan. Combustion characteristics of diesel engine operating on jatropha oil methyl ester. Thermal Science, vol. 14, 2010, pp. 965-977.

[72] T. Ganapathy, R.P.Gakkhar, and K. Murugesan. An analytical and experimental study of performance on jatropha biodiesel engine. Thermal Science, vol. 13, 2009, pp. 69-82.

[73] A.B. Barboza, N.Yagnesh Sharma and C.V. Sudhir. Cyclic Combustion Studies of a CI Engine Operating on Jatropha B20 Fuel. International Conference on Mechanical and Electrical Technology, 2010, pp. 43-46.

[74] M. Venkatraman, and G. Devaradjane. Effect of compression ratio, injection timing and injection pressure on a diesel engine for better performance fueled with diesel – jatropha methyl ester blend. National Journal on Advances in Building Sciences and Mechanics, vol. 1, 2010, pp. 34-39.

[75] K. Rajan and K.R. Senthil Kumar. Combustion and Emission Characteristics of A Biodiesel Fuelled Diesel Engine with the Effect of Thermal Barrier Coated Internal Jet Piston. Second International Conference on Sustainable Energy and Intelligent System (SEISCON 2011), 2011, pp. 184-189.

[76] T. Ganapathy, R.P. Gakkhar, and K. Murugesan. Influence of injection timing on performance, combustion and emission characteristics of Jatropha biodiesel engine. Applied Energy, vol. 88, 2011, pp. 4376-4386.

[77] S. Jindal. Effect of injection timing on combustion and performance of a direct injection diesel engine running on Jatropha methyl ester. International Journal of Energy and Environment, vol. 2, 2011, pp. 113-122.

[78] M. Gomaa, A.J. Alimin, and K.A. Kamarudin. The effect of EGR rates on NO_x and smoke emissions of an IDI diesel engine fuelled with Jatropha biodiesel blends. International Journal of Energy and Environment, vol. 2, 2011, pp. 477-490.

[79] S. Adinarayana, Y.M.C. Sekhar, B.V.A. Rao, and M. Anil Prakash. Biodiesel as an Alternate Fuel in a Diesel Engine with the Cooled Exhaust Gas Recirculation–A Measure to Reduce Harmful Emissions. International Journal of Applied Research In Mechanical Engineering, Vol.1, pp.10-15.

[80] N. Shrivastava, S.N. Varma, and M. Pandey. A Study on Reduction of Oxides of Nitrogen with Jatropha Oil Based Bio Diesel. International Journal of Renewable Energy Research, vol. 2, 2012, pp. 504-509.

[81] M.V. Nagarhalli, and V.M. Nandedkar. Performance of diesel engine using blends of esters of jatropha and karanja- A novel approach. International Journal of Advanced Engineering Technology, vol.3, 2012, pp.51-54.

[82] C. R. Rajashekhar, T.K. Chandrashekar, C. Umashankar, and R. Harish Kumar. Studies on effects of combustion chamber geometry and injection pressure on biodiesel combustion. Transactions of the Canadian Society for Mechanical Engineering, Vol. 36, 2012, pp.429-438.

[83] K. Venkateswarlu, B. S. R. Murthy, V. V. Subbarao, and K. Vijaya Kumar. Effect of exhaust gas recirculation and ethyl hexyl nitrate additive on biodiesel fuelled diesel engine for the reduction of NOx emissions. Front. Energy, vol. 6, 2012, pp. 304–310.

[84] S. A. Viswanath, V. Dinesh, S. Arivazhagan, and N. Vinayagam. Modeling and analysis of performance, combustion and emission characteristics of jatropha methyl ester blend diesel for CI engine with variable compression ratio. vol. 4, 2012, 3457-3471.

[85] A. Pandhare and A. Padalkar. Investigations on performance and emission characteristics of diesel engine with biodiesel (Jatropha oil) and its blends. Journal of Renewable Energy, vol. 2013, 2013.

[86] P.V. Rao. Experimental Investigations on the Influence of Properties of Jatropha Biodiesel on Performance, Combustion, and Emission Characteristics of a DI-CI Engine. World Academy of Science, Engineering and Technology, vol.75, 2011, pp.855-868.

[87] Y.V.Hanumantha Rao, Ram Sudheer Voleti, A.V.Sitarama Raju and P.Nageswara Reddy. Experimental investigations on jatropha biodiesel and additive in diesel engine. Indian Journal of Science and Technology, vol. 2, 2009, pp. 25-31.

[88] V. Sajith, C. B. Sobhan, and G. P. Peterson. Experimental Investigations on the Effects of Cerium Oxide Nanoparticle Fuel Additives on Biodiesel. Advances in Mechanical Engineering, vol. 2010, Article ID 581407.

[89] J.S. Basha and R.B. Anand. Role of nanoadditive blended biodiesel emulsion fuel on the working characteristics of a diesel engine. Journal of Renewable Sustainable Energy, vol. 3, 2011, pp. 1-17.

[90] U. Vara Prasad, K. M. Murthy and G.A.P. Rao. Effective utilization of B20 blend with oxygenated additives. Thermal Science, vol. 15, 2011, pp. 1175-1184.

[91] K. Varatharajan, M. Cheralathan, and R. Velraj. Mitigation of NOx emissions from a jatropha biodiesel fuelled DI diesel engine using antioxidant additives. Fuel, vol. 90, 2011, pp. 2721–2725.

[92] D. Ganesh, and G. Gowrishankar. Effect of nano-fuel additive on emission reduction in a biodiesel fuelled CI engine. International Conference on Electrical and Control Engineering (ICECE), 2011, pp.3453-3459.

[93] D. Kannan, S. Pachamuthu, N. Nabi, J. Einar, and T. Lovas. Theoretical and experimental investigation of diesel engine performance, combustion and emissions analysis fuelled with the blends of ethanol, diesel and jatropha methyl ester. Energy Conversion and Management, vol. 53, 2012, pp. 322-331.

[94] S. Jain and M.P. Sharma. Engine performance and emission analysis using oxidatively stabilized Jatropha curcas biodiesel. Fuel, vol. 106, 2013, pp. 152-156.

[95] T.K. Gogoi, A.K. Sarma, P.S. Misra, and S.T. Haque. Combustion analysis of jatropha methyl ester and its ethanol and acetone blends in a diesel engine. International Journal of Emerging Technology and Advanced Engineering, vol. 3, 2013, pp. 51-57.

[96] J.A. Bittle, B.M. Knight, and T.J. Jacobs. Interesting behavior of biodiesel ignition delay and combustion duration. Energy Fuels, vol. 24, 2010, pp.4166–4177.

[97] A. Monyem and J. H. Van Gerpen. The effect of biodiesel oxidation on engine performance and emissions. Biomass and Bioenergy, vol. 20, 2001, pp. 317–325.

[98] R.E. Tate, K.C. Watts, C.A.W. Allen, and K.I. Wilkie. The densities of three biodiesel fuels at temperatures up to 300 ^{o}C. Fuel, vol. 85, 2006, pp.1004-9.

[99] C.Y. Choi, R.D. Bower, and R.D. Reitz. Mechanisms of emissions reduction using biodiesel fuels. Final report for the National Biodiesel Board; 1997.

[100] W. Yuan. A. C. Hansen, and Q. Zhang. Combustion optimization of biodiesel for diesel engines with the aid of KIVA-3 code. ASAE Paper No. 026083, 2002.

[101] J. Benajes, S. Molina, C. Gonzalez, and R. Donde. The role of nozzle convergence in diesel combustion. Fuel, vol.87, 2008, pp.1849-1858.

[102] C. Mueller, A. Boehman and G. Martin. An experimental investigation of the origin of increased NOx emissions when fueling a heavy-duty compression-ignition engine with soy biodiesel, SAE Int. J. Fuels and Lubricants. vol. 2, 2009, pp. 789-816.

[103] G.A.Ban-Weiss, J.Y. Chen, B.A.Buchholz, and R.W.Dibble. A numerical investigation into the anomalous slight NO_x increase when burning biodiesel: A new (old) theory. Fuel Processing Technology, vol. 88, 2007, pp. 659-667.

[104] W.Yuan, A. Hansen, M.Tat, J. Van Gerpen, and Z.Tan. Spray, ignition, and combustion modeling of biodiesel fuels for investigating NO_x emissions. Transactions of the ASAE, vol.48, 2005, pp.933-939.

[105] V. Edwin Geo, M. Nadia, M. Tazerout, F. Aloui. Experimental analysis of biofuel as an alternative fuel for diesel engines. Applied Energy, vol. 94, 2012, pp. 224–231.

[106] C.Allen, and K.Watts. Comparative analysis of the atomization characteristics of fifteen biodiesel fuel types. T ASAE, vol.43, 2000, pp. 207-211.

[107] M. Canakci. Combustion characteristics of a turbocharged DI compression ignition engine fueled with petroleum diesel fuels and biodiesel. Bioresource Technology, vol.98, 2007, pp.1167-75.

[108] M.Tat, J. Van Gerpen, and P.Wang. Fuel property effects on injection timing, ignition timing, and oxides of nitrogen emissions from biodiesel-fueled engines. Transactions of the ASAE, vol.50, 2007, pp.1123-8.

[109] Y. Ra, R.Reitz, J, McFarlane, and C. Daw. Effects of fuel physical properties on diesel engine combustion using diesel and biodiesel fuels. SAE Transactions-Journal of Fuels and Lubricants, vol.117, 2008, pp.2101-1379.

[110] S.Garner, R. Sivaramakrishnan, and K. Brezinsky. The high-pressure pyrolysis of saturated and unsaturated C7 hydrocarbons. Proc. Combust. Institute, vol.32, 2009, pp. 464-67.

[111] R. McCormick, M. Graboski, T. Alleman, A. Hening, and K.Tyson. Impact of biodiesel source material and chemical structure on emissions of criteria pollutants from a heavy duty engine. Environmental Science and Technology, vol.35, 2001, pp.1742-7.

[112] M. Lapuerta, O. Armas, and J. Rodriguez-Fernandez. Effect of biodiesel fuels on diesel engine emissions. Progress in Energy and Combustion Science, vol.34, 2008, pp.198-223.

[113] R. McCormick, J.Alvarez, M. Graboski, K.Tyson, and K.Vertin. Fuel additive and blending approaches to reducing NO_x emissions from biodiesel. SAE 2002-01-1658; 2002.

[114] W. Wang, D. Lyons, W.Clark, and N.Gautam. Emissions from nine heavy trucks fueled by diesel and biodiesel blend without engine modification. Environ. Sci. Technology, vol.34, 2000, pp. 933–939.

[115] M. Graboski, and R.McCormick. Combustion of fat and vegetable oil derived fuels in diesel engines. Progress in Energy and Combustion Science, vol. 24, 1998, pp.125-64.

[116] J. Song, V.Zello, and A. Boehman. Comparison of the impact of intake oxygen enrichment and fuel oxygenation on diesel combustion and emissions. Energy Fuel, vol.18, 2004, pp. 1282–90.

[117] J. Mueller, J. Pitz, M. Lyle, L.Pickett, G.Martin, D. Siebers, and C.Westbrook. Effects of oxygenates on soot processes in DI diesel engines: Experiments and numerical simulations. SAE paper No. 2003-01-1791, 2003.

[118] T. Ullman, K. Spreen, and R. Mason. Effects of cetane number, cetane improver, aromatics, and oxygenates on 1994 heavy-duty diesel engine emissions. SAE Transactions: Journal of Fuels and Lubricants, vol.103, 1994, 941020.

[119] J. Bittle, B.Knight, and T.Jacobs. The impact of biodiesel on injection timing and pulse width in a common-rail medium-duty diesel engine. SAE Paper No. 2009-01-2782, 2009.

[120] M. Tat. Investigation of oxides of nitrogen emissions from biodiesel-fueled engines. PhD Dissertation. Iowa State University. Ames, IA; 2003.

[121] N. Usta. An experimental study on performance and exhaust emissions of a diesel engine fuelled with tobacco seed oil methyl ester. Energy Convers. Management, vol. 46, 2005, pp. 2373–86.

[122] D. Deshmukh, A. Madan Mohan, T.N.C. Anand, R.V. Ravikrishna. Spray characterization of straight vegetable oils at high injection pressures. Fuel, vol. 97, 2012, pp. 879–883.

[123] W.Yuan, A. Hansen, M.Tat, J. Gerpen, and Z. Tan. Spray, ignition, and combustion modelling of biodiesel fuels for investigating NO_x emissions. TASAE., 48, pp. 933-39, 2005.

[124] S.N. Anderson and D. Olsen. Survey of straight vegetable oil composition impact on combustion properties. SAE Paper No. 2009-01-0487, 2009.

[125] J. Sun, J.A. Caton, T.J. Jacobs. Oxides of nitrogen emissions from biodiesel-fuelled diesel engines. Progress in Energy and Combustion Science, 36, 2010, pp.677-695.

[126] M. Ahmed, C. Ejim, B. Fleck, and A. Amirfazli. Effect of biodiesel fuel properties and its blends on atomization. SAE Paper No. 2006-01-0893, 2006.

[127] A.K. Hossain, and P.A. Davies. Pyrolysis liquids and gases as alternative fuels in internal combustion engines – A review. Renewable and Sustainable Energy Reviews, vol.21, 2013, pp.165-189.

[128] H.S. Heo, H.J.Park, Y.K.Park, C. Ryu, D.J. Suh, Y.W. Suh, J.H. Yim, S.S.Kim. Bio-oil production from fast pyrolysis of waste furniture sawdust in a fluidized bed. Bioresource Technology, vol.101, 2009, pp.S91–S96.

[129] S. Czernik, D.K. Johnson, S. Black. Stability of wood fast pyrolysis oil, Biomass Energy, vol. 7, 1994, pp. 187-92.

[130] Z.J. Lu, K.Y.Ping. Spray combustion properties of fast pyrolysis bio-oil produced from rice husk. Energy Conversion and. Management, vol. 51, 2010, pp.182-88.

[131] Lu, Z.J., Ming, Y.W., Na, W.N. Bio-oil production from cotton stalk. Energy Conversion and Management. vol. 49, 2008, pp.1724-30.

[132] M.G. Perez, A. Chaala, and C.Roy. Co pyrolysis of sugarcane bagasse with petroleum residue Part II – Product yields and properties. Fuel, vol. 81, 2002, pp. 893-907.

[133] S. Sensoz, I. Demiral, H.F. Gercel. Olive bagasse (Olea europea L.) pyrolysis. Bioresource Technology, vol. 97, 2006, pp. 429-36.

[134] R. Manurung, D.A.Z. Wever, J. Wildschut, R.H.Venderbosch, H. Hidayat, J.E.G.Van Dam, E.J. Leijenhorst, A.A. Broekhuis, and H.J. Heeres. Valorisation of Jatropha curcas L. plant parts: Nut shell conversion to fast pyrolysis oil. Food Bio products Processing, vol. 87, 2009, pp. 187-96.

[135] S.J. Kim, S.H. Jung, and J.S. Kim. Fast pyrolysis of palm kernel shells: Influence of operation parameters on the bio-oil yield and the yield of phenol and phenolic compounds. Bioresource Technology, vol. 101, 2010, pp. 9294-9300.

[136] A.V. Bridgwater, A.J. Toft, and J.G. Brammer. Techno-economic comparison of power production by biomass fast pyrolysis with gasification and combustion. Renewable and Sustainable Energy Reviews, vol. 6, 2002, pp.181-248.

[137] M. Balat, M. Balat, E. Kırtay, and H. Balat. Main routes for the thermo-conversion of biomass into fuels and chemicals. Part 1: Pyrolysis systems. Energy Conversion and Management, vol. 50, 2009, pp. 3147-3157.

[138] G.W. Huber, S. Iborra, and A. Corma. Synthesis of transportation fuels from biomass: chemistry, catalysts, and engineering. Chemical Reviews, vol.106, 2006, pp. 4044-4098.

[139] Z.Qi, C.Jie, W.Tiejun, and X.Ying. Review of biomass pyrolysis oil properties and upgrading research. Energy Conversion and Management, vol.48, 2007, pp. 87-92.

[140] Q. Lu, W.Z. Li, and X.F. Zhu. Overview of fuel properties of biomass fast pyrolysis oils. Energy Conversion and Management, vol.50, 2009, pp.1376-1383.

[141] A. Shihadeh and S. Hochgreb. Impact of biomass pyrolysis oil process conditions on ignition delay in compression ignition engines. Energy & Fuels, vol. 16, 2002, pp. 552-561.

[142] V. Minkova, M. Razvigorova, E. Bjornbom, R. Zanzi, T. Budinova, and N. Petrov. Effect of water vapour and biomass nature on the yield and quality of the pyrolysis products from biomass. Fuel Processing Technology, vol.70, 2001, pp. 53-61.

[143] Y.Solantausta, N.O. Nylund, M.Westerholm, T. Koljonen and A. Oasmaa. Wood-Pyrolysis oil as fuel in a diesel-power plant. Bioresource Technology, vol. 46, 1993, 177-188.

[144] S. Frigo, R. Gentilli, L. Tognotti, S. Zanforlin, and G. Benelli. Feasibility of using wood flash-pyrolysis oil in diesel engines. SAE 982529.1998.

[145] M. Ikura, M. Stanciulescu, Ed. Hogan. Emulsification of biomass derived bio-oil in diesel fuel. Biomass and bioenergy, vol.24, 2003, pp.221-232.

[146] C.Bertoli, J.D. Alessio, N. Del Giacomo, M. Lazzaro, P. Massoli, and V.Moccia. Running light-duty DI diesel engines with wood pyrolysis oil. SAE 2000-01-2975, 2000.

[147] Y.Huang, Xu. Han, S.Shang and Li.Wang. Performance and emissions of a direct injection diesel engine operating on emulsions of corn stalk bio-oil in diesel. Proc IMechE Part D: J Automobile Engineering, vol. 226, 2012, pp.1119–1129.

[148] X .Jiang, and N. Ellis. Upgrading bio-oil through emulsification with biodiesel: thermal stability. Energy and Fuels, vol.24, 2010, pp. 2699–2706.

[149] M.Garcia-Perez, T.T.Adams, J.W. Goodrum, K.C.Das, D.P.Geller. DSC studies to evaluate the impact of bio-oil on cold flow properties and oxidation stability of bio-diesel. Bioresource Technology, vol.101, 2010, pp. 6219–6224.

[150] J.S Basha, and R.B. Anand. An experimental investigation in a diesel engine using carbon nanotubes blended water-diesel emulsion fuel. Proc. IMechE, Part A: J. Power and Energy, vol.225, 2011, pp.279-288.

[151] G.R. Kannan, and R. Anand. Experimental investigation on diesel engine with diestrol-water micro emulsions. Energy, vol.36, 2011, pp.1680-7.

[152] K.S. Chen, Y.C. Lin, L.T. Hsieh, L.F. Lin, and C.C. Wu. Saving energy and reducing pollution by use of emulsified palm-biodiesel blends with bio-solution additive. Energy, vol.35, 2010, pp.2043-8.

[153] A. Alcala, and A.V. Bridgwater. Upgrading fast pyrolysis liquids: Blends of biodiesel and pyrolysis oil. Fuel, vol.109, 2013, pp. 417–426.

[154] M.C. Mayoral, M.T. Izquierdo, J.M. Andreas, B. Rubio. Different approaches to proximate analysis by thermo gravimetric analysis. Thermochem. Acta, vol. 370, 2001, pp. 91–97.

[155] J.B. Heywood. Internal combustion engines fundamentals. McGraw Hill, London, 1989.

[156] R. B. Krieger, G.L. Borman. The computation of apparent heat release in I. C. engines. ASME Paper 66 WA/DGP4, 1966.

[157] S. Murugan, M.C. Ramaswamy and G. Nagarajan. A comparative study on the performance, emission and combustion studies of a DI diesel engine using distilled tyre pyrolysis oil-diesel blends. Fuel, vol. 87, 2008, pp. 2111-2121.

[158] J.R.Clarke, R.J. Tabaczynski. Internal combustion engine with adjustable compression ratio and knock control. US Patent 6135086, 2000-10-24.

[159] R.G.Sykes, Tickford. Methods to reduce the fuel consumption of gasoline engines. Engines Expo 2000 paper.

[160] J.E. Brevick. Variable compression ratio piston. US Patent 5755192, 1998-05-26.

[161] S. Aoyama, H. Fujimoto, K. Moteki. Variable compression ratio mechanism of reciprocating internal combustion engine. European Patent 1170482, 2002-01-09.

[162] J. Beroff. Internal combustion engine with variable capacity and compression ratio. European Patent 1143127, 2001-10-10.

[163] S. Bari, C.W. Yu and T.H. Lim. Effect of fuel injection timing with waste cooking oil as a fuel in a direct injection diesel engine. Proc. IMechE Part D: J. Automobile Engineering, vol.93, 2004, pp. 218.

[164] A.K. Agarwal, D.K. Srivastava, A. Dhar, R.K. Maurya, P.C. Shukla, and A.P. Singh. Effect of fuel injection timing and pressure on combustion, emissions and performance characteristics of a single cylinder diesel engine. Fuel, vol. 111, 2013, pp. 374-383.

[165] H.W. Coleman, and W.G. Steele Jr. Experimentation and uncertainty analysis for engineers. Wiley publications, New York, 1989.

[166] K. Muralidharan, D. Vasudevan, and K.N. Sheeba. Performance, emission and combustion characteristics of biodiesel fuelled variable compression ratio engine. Energy, vol. 36, 2011, pp. 5385-5393.

[167] B. Tesfa, R.Mishra, C. Zhang, F. Gu, and A.D. Ball. Combustion and performance characteristics of CI (compression ignition) engine running with biodiesel. Energy, vol. 51, 2013, pp. 101–115.

[168] D.H.Qi, H.Chen, C.F. Lee, L.M. Geng, and Y.Z. Bian. Experimental studies of a naturally aspirated, DI diesel engine fuelled with ethanol-biodiesel-water micro emulsions. Energy Fuels, vol.24, 2010, pp. 652-663.

[169] M. Senthil Kumar, A. Kerihuel, J. Bellettre, and M. Tazerout. Ethanol animal fat emulsions as a diesel engine fuel – Part 2: Engine test analysis. Fuel, vol.85, 2006, pp.2646-2652.

[170] O. Armas, R. Ballesteros, F.J.Martos, and J.R. Agudelo. Characterization of light duty diesel engine pollutant emissions using water emulsified fuel. Fuel, vol.84, 2005, pp.1011-1018.

[171] D. Agarwal, L. Kumar, and A.K. Agarwal. Performance evaluation of vegetable oil fuelled compression ignition engine. Renewable Energy, vol. 33, 2008, pp.1147-1156.

[172] J. Xue, T.E. Grift, and A.C. Hansen. Effect of biodiesel on engine performances and emissions. Renewable and Sustainable Energy Reviews, vol.15, 2011, pp.1098–1116.

[173] C. Lin, and S. Lin. Effects of emulsification variables on fuel properties of two-and three phase biodiesel emulsions. Fuel, vol.86, 2007, pp.210-217.

[174] M. Karabektas. The effects of turbocharger on the performance and exhaust emissions of a diesel engine fuelled with biodiesel. Renewable Energy, vol.34, 2009, pp. 989-993.

[175] C.Y. Lin, and H.A. Lin. Diesel engine performance and emission characteristics of biodiesel produced by the peroxidation process. Fuel, vol.85, 2006, pp.298–305.

[176] M.N. Nabi, S.M. Najmul Hoque, and M.S. Akhter. Karanja (Pongamia Pinnata) biodiesel production in Bangladesh, characterization of karanja biodiesel and its effect on diesel emissions. Fuel Processing Technology, vol.90, 2009, pp.1080–1086.

[177] R.L. McCormick, and R. Parish. Technical barriers to the use of ethanol in diesel fuel. Milestone report to NREL/MP-540-32674, 2001.

[178] M. A. Gumus. Comprehensive experimental investigation of combustion and heat release characteristics of a biodiesel (hazelnut kernel oil methyl ester) fueled direct injection compression ignition engine. Fuel, vol.89, 2010, pp.2802-2814.

[179] L.N. Rao, R. Gattamaneni, and S. Subramani. Combustion and emission characteristics of diesel engine fuelled with rice bran oil methyl ester and its diesel blends. Thermal science, vol.12, 2008, pp. 139-150.

[180] L. Zhu, C.S. Cheung, W.G. Zhang, and Z. Huang. Combustion, performance and emission characteristics of a DI diesel engine fueled with ethanol–biodiesel blends. Fuel, 90, 2011, pp.1743–1750.

[181] P.L. Zhou. An investigation into the atomisation of emulsified fuels. Ph.D thesis. University of Newcastle upon Tyne, 1992.

[182] M. Nishioka, S. Nakagawa, Y. Ishijawa, and T. Takeno. NO emission characteristics of methane-air double flame. Combustion and Flame, vol. 98, 1994, pp. 127–38.

[183] J.P. Szybist, S.R. Kirby, and A.L. Boehman. NO_x emissions of alternative diesel fuels: A comparative analysis of biodiesel and FT diesel. Energy and Fuels, vol.19, 2005, pp.1484–92.

[184] M.P.Ashok, and C.G. Saravanan. Performance and emission of the emulsified fuel in a DI diesel engine using oxygenated additive diethyl ether with surfactant of Span-80. Energy and Fuels, vol.21, 2007, pp.1878-1882.

[185] W.J.D Annand. Heat transfer in the cylinders of reciprocating internal combustion engines. Proceedings of Institution of Mechanical Engineers, vol.177, 1963, pp.973-990.

[186] J.I. Ghojel. Review of the development and applications of the Wiebe function: a tribute to the contribution of Ivan Wiebe to engine research. International Journal of Engine Research, vol.11, 2010, pp. 297-312.

[187] I.I. Wiebe. Semi-empirical expression for combustion rate in engines. In Proceedings of Conference on Piston engines, USSR, 1956, pp.185-191.

[188] C. Olikara, and G.L. Borman. A computer program for calculating properties of equilibrium combustion products with some applications to I. C. engines. SAE Paper 750468, 1975.

[189] H. Hiroyasu, T. Kadota, and M. Arai. Development and use of a spray combustion modeling to predict diesel engine efficiency and pollutant emissions-Part 1: combustion modeling. Bull. JSME, 26, 1983, pp. 569–575.

[190] H.S. Kent, and R. Curtis. Review of the effects of biodiesel on NOx emissions. Fuel Processing Technology, vol. 96, 2012, pp. 237-249.

[191] J.Ghojel, and D. Honnery. Heat release model for the combustion of diesel oil emulsions in DI diesel engines. Applied Thermal Engineering, vol. 25, 2005, pp.2072-2085.

[192] G.R. Kannan, and R. Anand. Effect of injection pressure and injection timing on DI diesel engine fuelled with biodiesel from waste cooking oil. Biomass bioenergy, vol. 46, 2012, pp.343-352.

[193] V. Arul Mozhi Selvan, R. B. Anand, and M. Udayakumar. Combustion characteristics of diesohol using biodiesel as an additive in a direct injection compression ignition engine under various compression ratios. Energy Fuels, vol. 23, 2009, pp.5413-5422.

[194] Y. Ulusoy, Y. Tekin, M. Cetinkaya, and F. Karaosmano. The engine tests of biodiesel from used frying oils. Energy Sources, vol. 26, 2004, pp.927- 932.

[195] H. Raheman, and S.V. Ghadge. Performance of diesel engine with biodiesel at varying compression ratio and ignition timing. Fuel, vol 87, 2008, pp. 2659-2666.

[196] C. Sayin, M. Gumus, and M. Canakci. Effect of fuel injection timing on the emissions of a direct-injection (DI) diesel engine fueled with canola oil methyl ester-diesel fuel blends. Energy Fuels, vol. 24, 2010, pp. 2675-2682.

[197] C. Sayin, K. Uslu, and M. Canakci. Influence of injection timing on the exhaust emissions of a dual-fuel CI engine. Renewable Energy, vol. 33, 2008, pp.1314-1323.

[198] C. Sayin, M. Gumus, and M. Canakci. Effect of fuel injection pressure on the injection, combustion and performance characteristics of a DI diesel engine fueled with canola

oil methyl esters-diesel fuel blends. Biomass and Bioenergy, vol.46, 2012, pp. 435-446.

[199] G. Zhang, X. Qiao, X. Miao, J. Hong, and J. Zheng. Effects of highly dispersed spray nozzle on fuel injection characteristics and emissions of heavy-duty diesel engine. Fuel, vol.102, 2012, pp.666-673.

[200] M. Gumus. Evaluation of hazelnut kernel oil of Turkish origin as alternative fuel in diesel engines. Renewable Energy, vol.33, 2008, pp.2448-57.

[201] C. Sayin, and M. Gumus. Impact of compression ratio and injection parameters on the performance and emissions of a DI diesel engine fueled with bio-diesel-blended fuel. Applied Thermal Engineering, vol. 31, 2011, pp.3182-3188.

[202] G.R. Kannan, and R. Anand. Experimental evaluation of DI diesel engine operating with diestrol at varying injection pressure and injection timing. Fuel Processing Technology, vol. 92, 2011, pp.2252-2263.

[203] G.R. Kannan, K.R. Balasubramanian, and R. Anand. Artificial neural network approach to study the effect of injection pressure and timing on diesel engine performance fueled with biodiesel. International Journal of Automotive Technology, vol.14, 2013, pp.507-519.

[204] C. Sayin, A.N. Ozsezen, and M.Canakci. The influence of operating parameters on the performance and emissions of a DI diesel engine using methanol-blended-diesel fuel. Fuel, vol. 89, 2010, pp.1407-1414.

[205] M.Ziejewski, H.J. Goettler, H. Hainees and C. Huang. EMA durability tests on high oleic sun flower and safflower oils in diesel engines. SAE paper 961856, 1996.

[206] S.Bari, C.W. Yu and T.H. Lim. Performance deterioration and durability issues while running a diesel engine with crude palm oil. Proc. IMechE, Part D, Journal of Automobile Engineering, vol, 216, 2002, pp.785-792.

[207] Anon. Lube Analyst User's Manual. Gas Tops Ltd. Ottawa, Canada, 1995.

Annexure -1

Cost analysis of ATJOE15 emulsion

I. Generally, the cost for making one litre of ATJOE15 emulsion is described as follows:

(a) Cost of one litre of biodiesel (JME) = INR 80

(b) Cost for producing one litre of WPO = INR 27

(c) Cost of one litre surfactant Span 80 = INR 624

(d) Cost of one litre surfactant Tween 80 = INR 530

II. For making 1litre of ATJOE15, 810 ml of JME, 150 ml of WPO and 40 ml of surfactant (20 ml of Span 80 + 20 ml of Tween 80) has been used.

(a) Cost of 810 ml of JME = 0.810 x 80 = INR 64.8

(b) Cost of 150 ml of WPO = 0.150 x 27 = INR 4.05

(c) Cost of 40 ml surfactant = (0.02 x 624) + (0.02 x 530) = INR 23.08

III. The mechanical stirrer used for emulsification, was connected to a small AC motor, whose capacity was 1/20 HP (37.3W). Hence, the electrical energy consumed for the preparation of each sample was about 0.01865 kWh.

(a) Cost involved in emulsification process = 0.01865 x 3 = INR 0.05595

(b) Amount of KOH used to neutralize 1 litre of ATJOE15 emulsion = 17.6 g

(c) Cost of 500 g of KOH = INR 400

(d) Cost of 17.6 g of KOH = INR 14.08

IV. From the above details, the cost of producing one litre of ATJOE15 will be around INR 106 or 1.69 USD approximately. In larger production, the cost may reduce considerably.

Annexure -2

Technical specifications of the engine

Make	**Kirloskar**
Model	TAF 1
Bore x Stroke, mm	87.5 x 110
Compression ratio	17.5:1
Piston type	Bowl-in-piston
Number of valves	2
Rated power, kW	4.4
Rated speed, rpm	1500
Type of fuel injection	Pump-line-nozzle injection system
Nozzle type	Multi hole
No. of holes	3
Needle lift, mm	0.25
Spray-hole diameter, mm	0.25
Cone angle, deg	110
Start of injection, ^{o}CA bTDC	23
Nozzle opening pressure, bar	200
Inlet valve opening, ^{o}CA bTDC	4.5
Inlet valve closing, ^{o}CA aBDC	35.5
Exhaust valve opening, ^{o}CA bBDC	35.5
Exhaust valve closing, ^{o}CA bBDC	4.5
Method of cooling	Air cooled with radial fan
Connecting rod length, mm	220
Weight, kg	163

Annexure -3

Specification of the pressure transducer

Description	Data
Model	KISTLER, Switzerland
	601 A, air cooled
Range	0-100 bar
Sensitivity	25 mV/bar
Linearity	0.1 <+ % FSO
Acceleration sensitivity	< 0.001 bar / g
Operating temperature range	-196 to 200 ^{o}C
Capacitance	5 PF
Weight	1.7 g
Connector, Teflon insulator	M4 x 0.35

Annexure-4

Specification of the charge amplifier

Description	Data
Make	KISLTER instruments, Switzerland
Measuring ranges	12 stages graded pC 10-50000
	1:2:5 and stepless 1 to 10
Accuracy of two most sensitive ranges	<± 3 %
Accuracy of other range stages	<± 1%
Linearity, of Transducer sensitivity	<±0.5%
Calibration capacitor	1000 ± 0.5 pF
Operating temperature range	-196 to 200 ^{o}C
Calibration input sensitivity	1±0.5 pC/mV
Input voltage, maximum with pulses	+ 12 V
Connector, Teflon insulator	M4 x 0.35

Annexure-5

Technical specification of AVL DiGAS 444 analyzer

Measured quantity	Measuring range	Accuracy
CO	0-10%	< 0.6% vol: ±0.03% vol
		≥ 0.6% vol: ± 5% of initial value
CO_2	0-20%	< 10% vol: ±0.05% vol
		≥ 10% vol: ± 5% of vol
HC	0-20000 ppm vol	< 200 ppm vol: ± 10 ppm vol
		≥ 200 ppm vol: ± 5% of initial value
O_2	0-22% vol	< 2% vol: ±0.01% vol
		≥ 2% vol: ± 5% of vol
NO	0-5000 ppm vol	< 500 ppm vol: ± 50 ppm vol
		≥ 500 ppm vol: ± 10% of initial value
Voltage	11-22 V DC	
Power consumption	≈25W	
Warm up time	≈ 7 min	
Operating temperature	5-45 ^{o}C	
Dimensions (WxDxH)	270x320x85	
Weight	4.5 kg net weight without accessories.	

Annexure-6

Technical specification of AVL 437C Diesel smoke meter

Description	Data
Measuring chamber	0-100% opacity
Accuracy and repeatability	±1 % of full scale
Alarming signal temperature	Lights up when temperature of measuring chamber is below 70 ^{o}C
Linearity check	48.4% - 53.1% or 1.54 m^{-1} - 1.54 m^{-1} of measurement range
Measuring chamber length	430 ± 5 mm
Light source	Halogen lamp, 12V
Sensor	Selenium Photocell
Weight	24 kg

Annexure 7

Calculation of uncertainty for crank angle encoder

X_1 CA	X_2 CA	X_3 CA	X_4 CA	X_5 CA	$\dot{x}$ CA	$(X_1-\dot{x})^2$	$(X_2-\dot{x})^2$	$(X_3-\dot{x})^2$	$(X_4-\dot{x})^2$	$(X_5-\dot{x})^2$	σ	U (Y)	5% Sig.level	% U(Y)
0.574162	0.566037	0.568721	0.567376	0.564264	0.568112	3.66E-05	4.3E-06	3.7E-07	5.42E-07	1.48E-05	0.003762	0.001682	0.003298	0.3298
0.574163	0.566038	0.56872	0.567376	0.564263	0.568112	3.66E-05	4.3E-06	3.7E-07	5.42E-07	1.48E-05	0.003763	0.001682	0.003298	0.3298
0.574163	0.566038	0.568721	0.567376	0.564263	0.568112	3.66E-05	4.3E-06	3.71E-07	5.42E-07	1.48E-05	0.003763	0.001682	0.003298	0.3298
0.574162	0.566038	0.56872	0.567375	0.564264	0.568112	3.66E-05	4.3E-06	3.7E-07	5.43E-07	1.48E-05	0.003762	0.001682	0.003297	0.3297
0.574163	0.566037	0.56872	0.567376	0.564263	0.568112	3.66E-05	4.3E-06	3.7E-07	5.41E-07	1.48E-05	0.003763	0.001682	0.003298	0.3298
0.574163	0.566038	0.568721	0.567376	0.564263	0.568112	3.66E-05	4.3E-06	3.71E-07	5.42E-07	1.48E-05	0.003763	0.001682	0.003298	0.3298
0.574162	0.566038	0.56872	0.567376	0.564264	0.568112	3.66E-05	4.3E-06	3.7E-07	5.42E-07	1.48E-05	0.003762	0.001682	0.003297	0.3297
0.574163	0.566038	0.56872	0.567376	0.564263	0.568112	3.66E-05	4.3E-06	3.7E-07	5.42E-07	1.48E-05	0.003763	0.001682	0.003298	0.3298
0.574163	0.566037	0.568721	0.567376	0.564263	0.568112	3.66E-05	4.31E-06	3.71E-07	5.42E-07	1.48E-05	0.003763	0.001682	0.003298	0.3298
0.574162	0.566038	0.56872	0.567376	0.564264	0.568112	3.66E-05	4.3E-06	3.7E-07	5.42E-07	1.48E-05	0.003762	0.001682	0.003297	0.3297
0.574163	0.566038	0.568721	0.567376	0.564263	0.568112	3.66E-05	4.3E-06	3.71E-07	5.42E-07	1.48E-05	0.003763	0.001682	0.003298	0.3298
0.574163	0.566038	0.56872	0.567376	0.564263	0.568112	3.66E-05	4.3E-06	3.7E-07	5.42E-07	1.48E-05	0.003763	0.001682	0.003298	0.3298
0.574163	0.566037	0.56872	0.567375	0.564264	0.568112	3.66E-05	4.3E-06	3.7E-07	5.43E-07	1.48E-05	0.003762	0.001682	0.003298	0.3298
0.574162	0.566038	0.568721	0.567376	0.564263	0.568112	3.66E-05	4.3E-06	3.71E-07	5.42E-07	1.48E-05	0.003762	0.001682	0.003298	0.3298
0.574163	0.566038	0.56872	0.567376	0.564263	0.568112	3.66E-05	4.3E-06	3.7E-07	5.42E-07	1.48E-05	0.003763	0.001682	0.003298	0.3298
0.574163	0.566038	0.56872	0.567376	0.564263	0.568112	3.66E-05	4.3E-06	3.7E-07	5.42E-07	1.48E-05	0.003763	0.001682	0.003298	0.3298
0.574164	0.566038	0.568724	0.56738	0.564264	0.568114	3.66E-05	4.31E-06	3.72E-07	5.39E-07	1.48E-05	0.003763	0.001682	0.003298	0.3298
0.57416	0.56604	0.56872	0.56737	0.56426	0.56811	3.66E-05	4.28E-06	3.72E-07	5.48E-07	1.48E-05	0.003762	0.0016827	0.003298	0.3298
0.57416	0.56603	0.56872	0.56738	0.56427	0.568112	3.66E-05	4.33E-06	3.7E-07	5.36E-07	1.48E-05	0.003760	0.001681	0.003296	0.3296
											0.003762	0.001682	0.003298	0.3298

Where, X_1, X_2, X_3, X_4 and X_5 are difference in the crank angle (CA) degree values for 20 consecutive readings
Uncertainty with 5% significance level = 1.96 $\sigma/\sqrt{n}$
The calculated uncertainty of crank angle encoder with 5 % significance/confidence level = ± 0.3298 %.

Annexure 8

MATLAB program

```
% Two Zone model: Performance combustion and emission analysis: RUN
clear all
close all
clc
s=0.11;d=0.0875;kkk=0;theta=0;mf=0;mfinjr=0;q=0;pr=2e7;
pphi=0;m11=0;mfj=0;tt=0;tbr=0 ;yty1=0;yty2=0;msn=0;dmsn=0;dnox=0;noxx=0;
mfb=0;
n=1500;                      % Rpm
bp=4.38282;             % brake power in kw
M=48.27;                       % fuel molecular Weight
mfrt=1.615886*(0.028e-3); mfkg=1.615886;          % mass flow rate of fuel in
kg/cycle
dtheta=40;                   % total duration of fuel injection
roa=1.29;                    % density of air in kg/m^3
ro=926.7;                    % density of fuel in kg/m^3
afrs=7.26;                     % stoichiometric air/fuel
afr=14.72876181;                      % afr
mainj=afr*mfrt;            % mass of air present inside cylinder in kg/cycle
LCV=36320;                   % lower calorific value of fuel in kJ/kg
a=12; b=22; g=0; delta=0;
epss=0.210/(a+0.25*b-0.5*g);
er=afrs/afr;     % alpha, beta gamma, delta ,epsilon, equivalence ratio
phi=zeros(1,290);
p=zeros(1,290);
t=zeros(1,290);tu=zeros(1,290); tb=zeros(1,290);
v=zeros(1,290); vu=zeros(1,290);vb=zeros(1,290);
ht=zeros(1,290);
chr=zeros(1,290);Qf=zeros(1,290);x=zeros(1,290);
qq=zeros(1,2);
qg=zeros(1,290);mf=zeros(1,290);mfinjr=zeros(1,290);qh=zeros(1,290);
K=zeros(1,6); c=zeros(1,6); d=zeros(1,3);A=zeros(4,5);
f=zeros(1,4);y=zeros(1,10);
yco2=zeros(1,290); yh2o=zeros(1,290); yn2=zeros(1,290); yo2=zeros(1,290);
yco=zeros(1,290);    yh2=zeros(1,290);    yh=zeros(1,290);    yo=zeros(1,290);
yoh=zeros(1,290); yno=zeros(1,290);
sot=zeros(1,290);noxf=zeros(1,290);N=0.000001;mloss=0;molu=0;molb=0;fp=0;effm
=0;BTE=0;idx=0;idd1=0;ccvv=0;mmf=0;

id=10;       % ignition delay in degree
phis=339+id; % start of combustion
phid=40;     % duration of combustion
aa=6.908;
m=2;         % combustion exponent
Qchr=2200;   % cumm heat release in kJ


phi(1)=-145;
t(1)=360;
p(1)=1.516163e5;
v(1)=0.0000401+0.0003305*(1+4-cos(phi(1)*0.017453)-sqrt(16-
sin(phi(1)*0.017453)*sin(phi(1)*0.017453)));
```

```
 mftot=mfrt/M;          %mass of fuel in kmol
 matot=mainj/29;        %mass of air in kmol

 E(1)=ienergy(t(1))*matot*1000;   %internal energy in J/mol

 for j1=1:122
    phi(j1+1)=phi(j1)+1;
    theta=theta+1;
    v(j1+1)=0.0000401+0.0003305*(1+4-cos(phi(j1+1)*0.017453)-sqrt(16-
sin(phi(j1+1)*0.017453)*sin(phi(j1+1)*0.017453)));
    t(j1+1)=t(j1)*(v(j1)/v(j1+1))^0.4;           % gamma=1.4
    p(j1+1)=(p(j1)*v(j1)*t(j1+1))/(t(j1)*v(j1+1));

    for j2=1:10
        [fe fed dq]=ebalance24(p(j1),p(j1+1),t(j1),t(j1+1),v(j1),v(j1+1));
        t(j1+1)=t(j1+1)-fe/fed;                  %newton raphson method
        ffe(j1)=fe;
        dqqq=dq;
        ddd(j1+1)=dq;
     end
     ht(j1+1)=-dqqq;

 end

          % combustion and expansion
          y(3)=0.1; y(4)=0.1; y(5)=1e-6; y(6)=1e-6;
          vu(123)=v(123);vb(123)=0;tu(123)=t(123);tb(123)=t(123);
 for k11=123:289
    phi(k11+1)=phi(k11)+1;
    pphi=pphi+1;
    v(k11+1)=0.0000401+0.0003305*(1+4-cos(phi(k11+1)*0.017453)-sqrt(16-
sin(phi(k11+1)*0.017453)*sin(phi(k11+1)*0.017453)));
    t(k11+1)=t(k11)*(v(k11)/v(k11+1))^0.4;           % gamma=1.4
    p(k11+1)=(p(k11)*v(k11)*t(k11+1))/(t(k11)*v(k11+1));

    phiii=phi(k11+1)+id+360;

    if phi(k11+1)<(phi(123)+id)
    x(k11+1)=0;
    dmf=0;

    else
 x(k11+1)=1-exp(-((phiii-phis)/phid)^(m+1)); % cumulative mass fraction burn
dmf=mfrt*(x(k11+1)-x(k11));  % mass of fuel to be burn in the time step in kg
mmf=dmf*mfrt*1000/M;
%Qf(k11+1)=(6.908*(m+1)/(phid*0.017453))*(((phiii-phis)/phid)^m)*exp(-
6.908*((phiii-phis)/phid)^(m+1)); % cumm fraction heat release
          %q=Qf*dmf*LCV*1000;   % heat release rate in j/deg
          q=0.446*aa*(m+1)*(Qchr/phid)*(((phiii-phis)/phid)^m)*exp(-
aa*((phiii-phis)/phid)^(m+1));
          ht(k11+1)=q;
          end
     %ccvv=cvmol(t(k11));
     %t(k11+1)=mftot*1000*x(k11)*Qchr/ccvv;t(k11+1)
```

```
     %t(k11+1)=t(123)+t(k11+1);
     %p(k11+1)=p(k11)*(t(k11)/t(k11+1))^3.857;     % cp/cv=1.35

     for kk2=1:10          % energy balance for burning zone
[fe fed dqb dw]=
ebalancec24(p(k11),p(k11+1),tb(k11),t(k11+1),v(k11),v(k11+1),q,mloss,mmf);
        if fed<eps
           t(k11+1)=t(k11);
        else
        t(k11+1)=t(k11+1)-fe(1)/fed(1);        %newton raphson method
        ffe(k11)=fe(1);
        end
        dqqq=dqb;

    end

K(1)=10^(0.432168*log(t(k11+1)/1000)+(-0.112464e5)/t(k11+1)+0.267269e1+(-
0.745744e-4)*t(k11+1)+(0.242484e-8)*(t(k11+1)^2));
K(2)=10^(0.310805*log(t(k11+1)/1000)+(-0.129540e5)/t(k11+1)+0.321779e1+(-
0.738336e-4)*t(k11+1)+(0.344645e-8)*(t(k11+1)^2));
K(3)=10^(-0.141784*log(t(k11+1)/1000)-
0.213308e4/t(k11+1)+0.853461+(0.355015e-4)*t(k11+1)+(-0.310227e-
8)*(t(k11+1)^2));
K(4)=10^(0.0150879*log(t(k11+1)/1000)-
0.470959e4/t(k11+1)+0.646096+(0.272805e-5)*t(k11+1)+(-0.154444e-
8)*(t(k11+1)^2));
K(5)=10^((-0.752364*log(t(k11+1)/1000)+0.124210e5/t(k11+1)-
2.60286+(0.259556e-3)*t(k11+1)+(-0.162687e-7)*(t(k11+1)^2))/100);
K(6)=(10^(((-0.415303e-2)*log(t(k11+1)/1000)+0.148627e5/t(k11+1)-
0.475746e1+(0.124699e-3)*t(k11+1)+(-0.900227e-8)*(t(k11+1)^2))/1e5));

       %K(1)=1;K(2)=1;K(3)=1;K(4)=1;K(5)=4.7;K(6)=12.18;
        c(1)=K(1)/sqrt(p(k11+1)/1e5);
        c(2)=K(2)/sqrt(p(k11+1)/1e5);
        c(3)=K(3);
        c(4)=K(4);
        c(5)=K(5)*sqrt(p(k11+1)/1e5);
        c(6)=K(6)*sqrt(p(k11+1)/1e5);

        d(1)=b/a;
        d(2)=g/a+0.42/(epss*er*a);
        d(3)=delta/a+1.58/(epss*er*a);

                    for fk=1:10
                       yty1=yty1+y(fk);
                    end
     % newton-Raphson method
     for fi=1:10
        D76=0.5*c(1)/sqrt(y(6));
        D103=0.5*c(4)*sqrt(y(4))/sqrt(y(3));
        D84=0.5*c(2)/sqrt(y(4));
        D26=c(5)*sqrt(y(4));
        D94=0.5*c(3)*sqrt(y(6))/sqrt(y(5));
        D24=0.5*c(5)*y(6)/sqrt(y(4));
        D96=0.5*c(3)*sqrt(y(4)/y(6));
        D14=0.5*c(6)*y(5)/sqrt(y(4));
```

```
D104=0.5*c(4)*sqrt(y(3))/sqrt(y(4));
D15=c(6)*sqrt(y(4));

A(1,1)=1+D103;
A(1,2)=D14+D24+1+D84+D104+D94;
A(1,3)=D15+1;
A(1,4)=D26+1+D76+D96;
A(2,1)=0;
A(2,2)=2*D24+D94-d(1)*D14;
A(2,3)=-d(1)*D15-d(1);
A(2,4)=2*D26+2+D76+D96;
A(3,1)=D103;
A(3,2)=2*D14+D24+2+D84+D94+D104-d(2)*D14;
A(3,3)=2*D15+1-d(2)*D15-d(2);
A(3,4)=D26+D96;
A(4,1)=2+D103;
A(4,2)=D104-d(3)*D14;
A(4,3)=-d(3)*D15-d(3);
A(4,4)=0;

  y(7)=c(1)*sqrt(y(6));
  y(8)=c(2)*sqrt(y(4));
  y(9)=c(3)*sqrt(y(4)*y(6));
  y(10)=c(4)*sqrt(y(4)*y(3));
  y(2)=c(5)*sqrt(y(4))*y(6);
  y(1)=c(6)*sqrt(y(4))*y(5);

  f(1)=y(1)+y(2)+y(3)+y(4)+y(5)+y(6)+y(7)+y(8)+y(9)+y(10)-1;
  f(2)=2*y(2)+2*y(6)+y(7)+y(9)-d(1)*y(1)-d(1)*y(5);
  f(3)=2*y(1)+y(2)+2*y(4)+y(5)+y(8)+y(9)+y(10)-d(2)*y(1)-d(2)*y(5);
  f(4)=2*y(3)+y(10)-d(3)*y(1)-d(3)*y(5);

  A(1,5)=-f(1);
  A(2,5)=-f(2);
  A(3,5)=-f(3);
  A(4,5)=-f(4);

   % gauss elimination

  A=rref(A);              % reduced to echelon form
   dy(4)=A(4,5);
   dy(3)=A(3,5);
   dy(2)=A(2,5);
   dy(1)=A(1,5);

y(3)=y(3)+dy(1);
y(4)=y(4)+dy(2);
y(5)=y(5)+dy(3);
y(6)=y(6)+dy(4);
y(7)=c(1)*sqrt(y(6));
y(8)=c(2)*sqrt(y(4));
y(9)=c(3)*sqrt(y(4)*y(6));
y(10)=c(4)*sqrt(y(4)*y(3));
y(2)=c(5)*y(6)*sqrt(y(4));
y(1)=c(6)*y(5)*sqrt(y(4));
```

```
        for fk=1:10
            yty2=yty2+y(fk);
        end

            yco2(k11+1)=y(1);
            yh2o(k11+1)=y(2);
            yn2(k11+1)=y(3);
            yo2(k11+1)=y(4);
            yco(k11+1)=y(5)*0.44;
            yh2(k11+1)=y(6);
            yh(k11+1)=y(7);
            yo(k11+1)=y(8);
            yoh(k11+1)=y(9);
            yno(k11+1)=y(10)*(504e11);

   N=(y(1)+y(5))/(epss*er*a);   % total no of kmol of product per kmol of air

         mloss=(yn2*N*28+yo2*N*32)*1000/29;        % mloss in mol
         matott=matot*1000-mloss;
         vb(k11+1)=N*matot*mftot*8314*tb(k11+1)/p(k11+1);
         vu(k11+1)=v(k11+1)-vb(k11+1);

%t(k11+1)=(N*matot*mftot*tb(k11+1)+matott*tu(k11+1))/(N*matot*mftot+matott);
% mean temp

    end
    ddd(k11+1)=-dqqq;
    p(k11+1)=(p(k11)*v(k11)*t(k11+1))/(t(k11)*v(k11+1));
   %ht(k11+1)=ht(k11+1);

         % soot formation model
         po21=(y(4)/yty1)*p(k11);
         po22=(y(4)/yty2)*p(k11+1);
          ka1= soot(msn,dmf,p(k11),t(k11),po21);    % change mfinjr with dmf
          ka2=ka1+soot(msn,dmf,p(k11+1),t(k11+1),po22);
          dmsn=dmsn+0.5*(ka1+ka2);
         % msn=msn+dmsn;
          sot(k11+1)=dmsn*19.3e8;
         % nox model
                  %yyy=sqrt(1/100*(y(3)));
                  yyy=y(3);
         kaa1=nox(noxx,t(k11),yyy,y(4),y(9),y(10));
         kaa2=0.5*kaa1+nox(noxx,t(k11),yyy,y(4),y(9),y(10));
         kaa3=0.5*kaa2+nox(noxx,t(k11),yyy,y(4),y(9),y(10));
         kaa4=kaa3+nox(noxx,t(k11+1),yyy,y(4),y(9),y(10));
          dnox=dnox+(1/6)*(kaa1+2*kaa2+2*kaa3+kaa4);
         %noxx=noxx+dnox;

          noxf(k11+1)=dnox*(65.37e5);

 end
 chr(1)=ht(1);
 for n11=1:289
     chr(n11+1)=chr(n11)+ht(n11);
```

```
 end
p=p/1e5; ht=ht+1;ddd=-ddd;chr=2.05*chr;

    bmep=75+0.045*n+0.4*(2*n*s/60);   % brake mean eff pressure in kpa
    fp=(5.512e-6)*bmep*n;     % brake mean eff pressure in kw
    effm=bp*100/(bp+fp);      % mechanical efficiency
    BTE=bp*100*3600/(mfkg*LCV);          % brake thermal efficiency


AAA=[phi' p' t' ht' x' noxf' sot'];
xlswrite('2zonSIM.xlsx',AAA,10);

subplot(4,4,1)
plot(phi,p)
xlabel('Crank angle(Degree)')
ylabel('Pressure(bar)')
subplot(4,4,2)
plot(phi,t)
xlabel('Crank angle(Degree)')
ylabel('Temperature(k)')
subplot(4,4,3)
plot(phi,ht)
xlabel('Crank angle(Degree)')
ylabel('Heat Release Rate(J/K)')
subplot(4,4,4)
plot(phi,chr)
xlabel('Crank angle(Degree)')
ylabel('cumm Heat Release Rate(J/K)')
subplot(4,4,5)
plot(phi,yco2)
xlabel('Crank angle(Degree)')
ylabel('co2')
subplot(4,4,6)
plot(phi,yh2o)
xlabel('Crank angle(Degree)')
ylabel('H2O')
subplot(4,4,7)
plot(phi,yn2)
xlabel('Crank angle(Degree)')
ylabel('N2')
subplot(4,4,8)
plot(phi,yo2)
xlabel('Crank angle(Degree)')
ylabel('O2')
subplot(4,4,9)
plot(phi,yco)
xlabel('Crank angle(Degree)')
ylabel('CO')
subplot(4,4,10)
plot(phi,yh2)
xlabel('Crank angle(Degree)')
ylabel('H2')
subplot(4,4,11)
plot(phi,yh)
xlabel('Crank angle(Degree)')
ylabel('H')
```

```
subplot(4,4,12)
plot(phi,yo)
xlabel('Crank angle(Degree)')
ylabel('O')
subplot(4,4,13)
plot(phi,yoh)
xlabel('Crank angle(Degree)')
ylabel('OH')
subplot(4,4,14)
plot(phi,x)
xlabel('Crank angle(Degree)')
ylabel('mfb')
subplot(4,4,15)
plot(phi,noxf)
xlabel('Crank angle(Degree)')
ylabel('NOx')
subplot(4,4,16)
plot(phi,sot)
xlabel('Crank angle(Degree)')
ylabel('soot')

%%%%%%%%%%%%%%%%%%%%%%%%%%%%%%%%%%%%%%%%%%%%%%%%%%%%%%%%%%%%%%%%%%%%%%%%%%%%%%%
function [fe fed dq dw]=ebalancec24(p1,p2,t1,t2,v1,v2,q,mloss,mf)
M=170;
afr=40;
mfrt=1.18;  % in kg/hr
n=1500;
matot=afr*mfrt*2.8e-3/M ;
mat=afr*mfrt;    % total mass of air in kg
s=0.11;d=0.0875;
 E1=iienergy24(t1)*matot*1000;
 E2=iienergy24(t2)*matot*1000;
      dw=0.5*(p1+p2)*(v2-v1);
        tg=0.5*(t1+t2);    ha=ientalpy24(tg);
        mua=3.3*1e-7*(tg^0.7);
        mua=mua/(1+0.027*0.94);
        re=(0.0387*n*s*d)/mua;
        lg=1005*mua/0.7 ;                       % thermal conductivity
        dq=((0.2626/d)*lg*(re^0.6)*(450-tg)+5.67*(1e-8)*(450^4-tg^4))/(6*n);
% annand formula from rajendraprasad paper
          fe=E2-E1+dw-dq-q-mloss*ha-ha*mf;                  %energy balance
          dqd=((0.2626/d)*lg*(re^0.6)*(-1)+5.67*(1e-8)*(-4*tg^3))/(6*n);
          fed=mat*cvmol(t2)*t2;
%%%%%%%%%%%%%%%%%%%%%%%%%%%%%%%%%%%%%%%%%%%%%%%%%%%%%%%%%%%%%%%%%%%%%%%%%%%%%%%
function [fe fed dq dw]=ebalance24(p1,p2,t1,t2,v1,v2)
M=170;
afrs=15;
afr=40;
mfrt=0.5*0.028e-3;        % total mass of fuel kg/cycle
n=1500;
matot=afr*mfrt/29; % total mass of fuel kmol/cycle
mat=afr*mfrt;      % total mass of air in kg
s=0.11;d=0.0875;
 E1=ienergy24(t1)*matot*1000;
 E2=ienergy24(t2)*matot*1000;
      dw=0.5*(p1+p2)*(v2-v1);
```

```
          tg=0.5*(t1+t2);
          mua=3.3*1e-7*(tg^0.7);
          mua=mua/(1+0.027*afr/afrs);
          re=(0.0387*n*s*d)/mua;
          lg=1005*mua/0.7 ;                      % thermal conductivity
          dq=((0.2626/d)*lg*(re^0.6)*(450-tg)+5.67*(1e-8)*(450^4-
tg^4))/(6*n);  % annand formula from rajendraprasad paper
          fe=E2-E1+dw-dq;                 %energy balance
          %dqd=((0.2626/d)*lg*(re^0.6)*(-1)+5.67*(1e-8)*(-4*tg^3))/(6*n);
          fed=matot*1000*cvmol(t2)*t2;

%%%%%%%%%%%%%%%%%%%%%%%%%%%%%%%%%%%%%%%%%%%%%%%%%%%%%%%%%%%%%%%%%%%%%%%%%%%
function [u h]=ienergy24(t)
hn2=8.314*(3.34*t+2.94e-4*t^2+1.95e-9*t^3-6.57e-12*t^4);
ho2=8.314*(3.25*t+6.52e-4*t^2-1.50e-7*t^3+1.54e-11*t^4);
h=0.79*hn2+0.21*ho2;
u=h-8.314*t;        % internal energy in j/mol
%un2=8.314*(3.34*t+2.94e-4*t^2+1.95e-9*t^3-6.57e-12*t^4)-8.314*t;
%uo2=8.314*(3.25*t+6.52e-4*t^2-1.5e-7*t^3+1.54e-11*t^4)-8.314*t;
%u=0.79*un2+0.21*uo2;    %internal energy in j/mol

%%%%%%%%%%%%%%%%%%%%%%%%%%%%%%%%%%%%%%%%%%%%%%%%%%%%%%%%%%%%%%%%%%%%%%%%%%%
function y=soot(msn,dmf,p,t,po2)
n=1500;
dmsf=0.8*dmf^0.8*p^0.5*exp(-3000/(8314*t))*6*n;
dmsc=0.8*msn*(po2/p)*p^2.5*exp(-50000/(8314*t))*6*n;
y=(dmsf-dmsc)/1e12;
```

LIST OF PUBLICATIONS

International Journals

1. R.Prakash, R.K.Singh and S. Murugan, Experimental investigation on diesel engine fueled with bio-oil derived from waste wood-biodiesel emulsions, **Energy, Elsevier publications**, Vol.55, pp. 610-618, 2013.

2. R.Prakash, R.K.Singh and S. Murugan, Experimental investigation on diesel engine fueled by biodiesel and its emulsions with wood pyrolysis oil, **International Journal of Green Energy, Taylor and Francis publications**, Vol.9, No.8, pp.749-765, 2012.

3. R.Prakash, R.K.Singh and S. Murugan, Use of biodiesel and wood pyrolysis oil emulsions as an alternative fuel for direct injection diesel engine, **Waste and Biomass Valorization, Springer publications**, Vol.4, No.3, 475-484, 2013.

4. R.Prakash, R.K.Singh and S. Murugan, Comparison of Performance and Emission Parameters of a Diesel Engine Fueled with Biodiesel and Wood Pyrolysis Oil Emulsions, **International Energy Journal**, Vol.13, pp.123-132, 2012.

5. R.Prakash, R.K.Singh and S. Murugan, Effect of wood pyrolysis oil addition in the Jatropha methyl ester fueled direct injection diesel engine, **International Journal of Oil, Gas and Coal Technology**, **Inderscience publications,** 2013. (Accepted).

6. R.Prakash, R.K.Singh and S. Murugan, Experimental studies on a diesel engine fueled with wood pyrolysis oil diesel emulsions, **International Journal of Chemical Engineering and Applications**, Vol. 2, No. 6, pp. 395-399, 2011.

7. R.Prakash, R.K.Singh and S. Murugan, Biodiesel bio-oil emulsions as alternative fuel for Diesel engine, **International Journal of Emerging Technology and Advanced Engineering,** Volume 3, Special Issue 3: ICERTSD 2013, pp.101-105, 2013.

8. R.Prakash, R.K.Singh and S. Murugan, Experimental studies on combustion, performance and emission characteristics of diesel engine using different biodiesel bio oil emulsions, **Journal of Energy Institute, Elsevier publications**, (Accepted) 2014. DOI : http://dx.doi.org/10.1016/j.joei.2014.04.005.

Conference publications

1. R.Prakash, R.K.Singh and S.Murugan, "Biodiesel bio-oil emulsions as alternative fuel for diesel engine", International Conference on Energy Resources & Technologies for Sustainable Development ICERTSD 2013, February 7-9, 2013.

2. Saroj Ray, R.Prakash and S.Murugan, "Analysis of combustion and emission characteristics of a diesel engine fueled with biodiesel bio-oil emulsions", International conference on Alternate Fuels for I.C. Engines, ICAFICE 2013, MNIT Jaipur during February 6-8, 2013.

3. R.Prakash, R.K.Singh and S.Murugan, Utilization of Biomass Based Fuel in a Naturally Aspirated Diesel Engine, 3rdNirma University International Conference on Engineering (NUiCONE 2012), December 6-8, 2012.

4. Saroj Ray, R.Prakash and S.Murugan, "Theoretical estimation of heat release rates in a CI engine", National Conference on Advances in Automotive Engineering, September 7, 2012, Karpagam college of Engineering, Coimbatore.

5. R.Prakash, R.K.Singh and S.Murugan, Performance and emission studies of a Diesel Engine fueled with wood pyrolysis oil-biodiesel emulsions, SAE world Congress 2012, Detroit, April 24-26, 2012, Paper No.2012-01-1306.

6. R.Prakash, R.K.Singh and S.Murugan, Performance and emission characteristics of biofuel emulsions in diesel engine, accepted for oral presentation in the International conference TIMS-2012, February 5-7, 2012, ITM University, Bhopal.

7. Sunny Madhaw, Gautam Bhardwaj, Prakash Shah, R.Prakash and S.Murugan, "Combustion characteristics of biofuel emulsions in diesel engine", presented in the National Conference on Recent Advances in Chemical and Environmental Engineering, RACEE 2012, January 20-21, 2012 held at NIT, Rourkela.

8. R.Prakash, R.K.Singh and S.Murugan, Performance and emission studies in a diesel engine using bio oil-diesel blends, International Conference on Environment Science and Technology-ICEST 2011, Singapore, February 26-28, 2011.

9. R.Prakash, Gandhi Pullagura, M.V.Saikumar, R.K. Singh and S.Murugan, Prospects of wood pyrolysis oil as alternative fuel, International Conference on Renewable Energy, ICRE 2011, University of Rajasthan, Jaipur, January 17-21, 2011.

10. R.Prakash, Gandhi Pullagura, M.V.Saikumar, R.K. Singh and S.Murugan, Production of bio-oil from pyrolysis process, 16th ISME Conference, IIT Delhi, December 2-4, 2010.

R.PRAKASH

E.mail : prakasu2000@yahoo.com
Mobile : +918895343319, +919176274601

PERSONAL DETAILS

Male/Indian/Married, DOB: 11/06/1978
Father's Name : V. Ramakrishnan
Mother's Name: R. Malliga
Permanent address: Plot No. 257, Baradwaj Nagar, Varadharajapuram
Mudichur, Chennai - 600 048.
Tamil Nadu.
India.

EXPERIENCE

- Working as Assistant Professor in Sri Sairam Engineering College, West Tambaram, Chennai from 28th October 2013 onwards.
- Worked as Junior Research Fellow in a DST sponsored research project at National Institute of Technology, Rourkela from 7th June 2010 to 30th June 2013.
- Worked as Lecturer in Dhanalakshmi College of Engineering, Chennai from 4th July 2007 to 30th April 2010.
- Worked as Lecturer in E.V.P. Engineering College, Chennai from June 2005 to June 2007.
- Worked as Lecturer in P.V. Polytechnic College, Tindivanam from June 1999 to September 2002.

EDUCATION

- Completed M.E. (Internal Combustion Engineering) degree with First Class from College of Engineering, Guindy campus, Anna University in the year 2005.
- Completed B.E. (Mechanical Engineering) degree with First Class from Madras University in the year 1999.

LIST OF PUBLICATIONS

International Journals

1. R.Prakash, R.K.Singh and S. Murugan, Experimental investigation on diesel engine fueled with bio-oil derived from waste wood-biodiesel emulsions, **Energy, Elsevier publications**, Vol.55, pp. 610-618, 2013.

2. R.Prakash, R.K.Singh and S. Murugan, Experimental investigation on diesel engine fueled by biodiesel and its emulsions with wood pyrolysis oil, **International Journal of Green Energy, Taylor and Francis publications**, Vol.9, No.8, pp.749-765, 2012.

3. R.Prakash, R.K.Singh and S. Murugan, Use of biodiesel and wood pyrolysis oil emulsions as an alternative fuel for direct injection diesel engine, **Waste and Biomass Valorization, Springer publications**, Vol.4, No.3, 475-484, 2013.

4. R.Prakash, R.K.Singh and S. Murugan, Comparison of Performance and Emission Parameters of a Diesel Engine Fueled with Biodiesel and Wood Pyrolysis Oil Emulsions, **International Energy Journal**, Vol.13, pp.123-132, 2012.

5. R.Prakash, R.K.Singh and S. Murugan, Effect of wood pyrolysis oil addition in the Jatropha methyl ester fueled direct injection diesel engine, **International Journal of Oil, Gas and Coal Technology**, **Inderscience publications,** 2013. (Accepted).

6. R.Prakash, R.K.Singh and S. Murugan, Experimental studies on a diesel engine fueled with wood pyrolysis oil diesel emulsions, **International Journal of Chemical Engineering and Applications**, Vol. 2, No. 6, pp. 395-399, 2011.

7. R.Prakash, R.K.Singh and S. Murugan, Biodiesel bio-oil emulsions as alternative fuel for Diesel engine, **International Journal of Emerging Technology and Advanced Engineering,** Volume 3, Special Issue 3: ICERTSD 2013, pp.101-105, 2013.

8. R.Prakash, R.K.Singh and S. Murugan, Experimental studies on combustion, performance and emission characteristics of diesel engine using different biodiesel bio oil emulsions, **Journal of Energy Institute, Elsevier publications**, (Accepted) 2014. DOI : http://dx.doi.org/10.1016/j.joei.2014.04.005.

Conference publications

1. R.Prakash, R.K.Singh and S.Murugan, "Biodiesel bio-oil emulsions as alternative fuel for diesel engine", International Conference on Energy Resources & Technologies for Sustainable Development ICERTSD 2013, February 7-9, 2013.

2. Saroj Ray, R.Prakash and S.Murugan, "Analysis of combustion and emission characteristics of a diesel engine fueled with biodiesel bio-oil emulsions", International conference on Alternate Fuels for I.C. Engines, ICAFICE 2013, MNIT Jaipur during February 6-8, 2013.

3. R.Prakash, R.K.Singh and S.Murugan, Utilization of Biomass Based Fuel in a Naturally Aspirated Diesel Engine, 3rdNirma University International Conference on Engineering (NUiCONE 2012), December 6-8, 2012.

4. Saroj Ray, R.Prakash and S.Murugan, "Theoretical estimation of heat release rates in a CI engine", National Conference on Advances in Automotive Engineering, September 7, 2012, Karpagam college of Engineering, Coimbatore.

5. R.Prakash, R.K.Singh and S.Murugan, Performance and emission studies of a Diesel Engine fueled with wood pyrolysis oil-biodiesel emulsions, SAE world Congress 2012, Detroit, April 24-26, 2012, Paper No.2012-01-1306.

6. R.Prakash, R.K.Singh and S.Murugan, Performance and emission characteristics of biofuel emulsions in diesel engine, accepted for oral presentation in the International conference TIMS-2012, February 5-7, 2012, ITM University, Bhopal.

7. Sunny Madhaw, Gautam Bhardwaj, Prakash Shah, R.Prakash and S.Murugan, "Combustion characteristics of biofuel emulsions in diesel engine", presented in the National Conference on Recent Advances in Chemical and Environmental Engineering, RACEE 2012, January 20-21, 2012 held at NIT, Rourkela.

8. R.Prakash, R.K.Singh and S.Murugan, Performance and emission studies in a diesel engine using bio oil-diesel blends, International Conference on Environment Science and Technology-ICEST 2011, Singapore, February 26-28, 2011.

9. R.Prakash, Gandhi Pullagura, M.V.Saikumar, R.K. Singh and S.Murugan, Prospects of wood pyrolysis oil as alternative fuel, International Conference on Renewable Energy, ICRE 2011, University of Rajasthan, Jaipur, January 17-21, 2011.

10. R.Prakash, Gandhi Pullagura, M.V.Saikumar, R.K. Singh and S.Murugan, Production of bio-oil from pyrolysis process, 16th ISME Conference, IIT Delhi, December 2-4, 2010.

R.PRAKASH

E.mail : prakasu2000@yahoo.com
Mobile : +918895343319, +919176274601

PERSONAL DETAILS

Male/Indian/Married, DOB: 11/06/1978
Father's Name : V. Ramakrishnan
Mother's Name: R. Malliga
Permanent address: Plot No. 257, Baradwaj Nagar, Varadharajapuram
Mudichur, Chennai - 600 048.
Tamil Nadu.
India.

EXPERIENCE

- Working as Assistant Professor in Sri Sairam Engineering College, West Tambaram, Chennai from 28th October 2013 onwards.
- Worked as Junior Research Fellow in a DST sponsored research project at National Institute of Technology, Rourkela from 7th June 2010 to 30th June 2013.
- Worked as Lecturer in Dhanalakshmi College of Engineering, Chennai from 4th July 2007 to 30th April 2010.
- Worked as Lecturer in E.V.P. Engineering College, Chennai from June 2005 to June 2007.
- Worked as Lecturer in P.V. Polytechnic College, Tindivanam from June 1999 to September 2002.

EDUCATION

- Completed M.E. (Internal Combustion Engineering) degree with First Class from College of Engineering, Guindy campus, Anna University in the year 2005.
- Completed B.E. (Mechanical Engineering) degree with First Class from Madras University in the year 1999.

REFERENCES

[1] Website: www.eia.gov/ies. Accessed on 25th November 2010.

[2] M. Gumus, C. Sayin, and M. Canakci. The impact of fuel injection pressure on the exhaust emissions of a direct injection diesel engine fueled with biodiesel–diesel fuel blends. Fuel, vol. 95, 2012, pp. 486–494.

[3] Website: http://en.wikipedia.org/wiki/List_of_countries_by_carbon_dioxide_emissions. Accessed on 5th December 2010.

[4] L.Liang, Y. Zhang, L.Zhang, M.Zhu, S.Liang, and Y. Huang. Study of sugarcane pieces as yeast supports for ethanol production from sugarcane juice and molasses. Journal of Industrial Microbiology & Biotechnology, vol.35, 2008, pp 1605-1613.

[5] M. Balat, and H. Balat. Recent trends in global production and utilization of bio-ethanol fuel. Applied Energy, vol. 86, 2009, pp. 2273–2282.

[6] D.R. Keshwani, and J.J. Cheng. Switchgrass for bioethanol and other value-added applications: A review. Bioresource Technology, vol.100, 2009, pp.1515–1523.

[7] A.Sorensen, P. J.Teller, T. Hilstrøm, and B. K. Ahring. Hydrolysis of Miscanthus for bioethanol production using dilute acid presoaking combined with wet explosion pre-treatment and enzymatic treatment. Bioresource Technology, vol.99, 2008, pp. 6602–6607.

[8] A. Demirbas. Progress and recent trends in biodiesel fuels. Energy Conversion and Management, vol. 50, 2009, pp. 14–34.

[9] A. Faaij. Biomass and biofuels. A background report for the Energy Council of the Netherlands, 2007.

[10] E. Ecklund, R. Bechtold, T. Timbario, and P. McCallum. State-of-the-art report on the use of alcohols in diesel engines. SAE Technical Paper 840118, 1984.

[11] A. Kowalewicz. Emission characteristics of compression ignition engine fuelled with RME/DF and ethanol. Journal of KONES Internal Combustion Engines 2003, vol. 10, pp. 349-357.

[12] S. Chongkhong, C. Tongurai, and P. Chetpattananondh. Continuous esterification for biodiesel production from palm fatty acid distillate using economical process. Renewable Energy, vol. 34, 2009, pp. 1059–1063.

[13] A. Demirbas. Biodiesel: A Realistic Fuel Alternative for Diesel Engines. Springer Publication, 2008, ISBN 978-1-84628-994-1.

[14] G. D. Rai. Non-Renewable energy sources. Khanna publications, New Delhi, 2004.

[15] S.N. Naik, V.V. Goud, P.K. Rout, and A.K. Dalai. Production of first and second generation biofuels: A comprehensive review. Renewable and Sustainable Energy Reviews, vol.14, 2010, pp.578–597.

[16] D.Mohan, C.U. Pittman, and P.H. Steele. Pyrolysis of Wood/Biomass for Bio-oil: A Critical Review. Energy Fuels, vol.20, 2006, pp.848-889.

[17] M.M. Azam, A.Waris, and N.M. Nahar. Prospects and potential of fatty acid methyl esters of some non-traditional seed oils for use as biodiesel in India. Biomass and Bioenergy, vol. 29, 2005, pp.293–302.

[18] P. McCarthy, M.G. Rasul, and S. Moazzem. Analysis and comparison of performance and emissions of an internal combustion engine fuelled with petroleum diesel and different bio-diesels. Fuel, vol. 90, 2011, pp. 2147–2157.

[19] R.K.Pandey, A.Rehman, R.M.Sarviya, and S. Dixit. Development of clean burning fuel for compression ignition engines. Asian Journal of Experimental Science, 2009, vol. 23, pp. 223-234.

[20] S. Jindal, B.P. Nandwana, N.S. Rathore, and V. Vashistha. Experimental investigation of the effect of compression ratio and injection pressure in a direct injection diesel engine running on Jatropha methyl ester. Applied Thermal Engineering, vol. 30, 2010, pp. 442-448.

[21] J.P. Szybist, J. Song, M. Alam, and A.L. Boehman. Biodiesel combustion, emissions and emission control. Fuel Processing Technology, vol. 88, 2007, pp. 679-691.

[22] C.Y. Lin, and H.A. Lin. Diesel engine performance and emission characteristics of biodiesel produced by the peroxidation process. Fuel, vol.85, 2006, pp. 298-305.

[23] A.N. Ozsezen, M.Canakci, and C. Sayin. Effects of biodiesel from used frying palm oil on the performance, injection, and combustion characteristics of an indirect injection diesel engine. Energy & Fuels, vol. 22, 2008, pp.1297–1305.

[24] United States Environmental Protection Agency. A comprehensive analysis of biodiesel impacts on exhaust emissions. Technical Report No. EPA420-P-02-001, 2002, Environmental Protection Agency, Research Triangle Park, North Carolina.

[25] P. Chitra, P. Venkatachalam, and A. Sampathrajan. Optimisation of experimental conditions for biodiesel production from alkali-catalysed transesterification of Jatropha curcas oil. Energy for Sustainable Development, 2005; 9:13–8.

[26] H. Lu, Y. Liu, H. Zhou, Y. Yang, M. Chen, and B. Liang. Production of biodiesel from Jatropha curcas L. oil. Computers and Chemical Engineering, 2009;33:1091–6.

[27] P.K Sahoo, and L.M Das. Process optimization for biodiesel production from Jatropha, Karanja and Polanga oils. Fuel 2009;88:1588–94.

[28] A.K Tiwari, A. Kumar, and H. Raheman. Biodiesel production from jatropha oil (Jatropha curcas) with high free fatty acids: an optimized process. Biomass and Bioenergy 2007; 31:569–75.

[29] S.H Shuit, K.T Lee, A.H Kamaruddin, and S. Yusup. Reactive extraction and in situ esterification of Jatropha curcas L. seeds for the production of biodiesel. Fuel 2009 [Short communication].

[30] S. Tamalampudi, M.R. Talukder, S. Hama, T. Numata, A. Kondo, and H. Fukuda. Enzymatic production of biodiesel from Jatropha oil: a comparative study of immobilized-whole cell and commercial lipases as a biocatalyst. Biochemical Engineering Journal, 2008;39:185–9.

[31] S. Shah, and M.N Gupta. Lipase catalyzed preparation of biodiesel from Jatropha oil in a solvent free system. Process Biochemistry, 2007; 42:409–14.

[32] S. Hawash, N. Kamal, F. Zaher, O. Kenawi, and G. El Diwani. Biodiesel fuel from Jatropha oil via non-catalytic supercritical methanol transesterification. Fuel, 2009;88:579–82.

[33] Z. Ilham, and S. Saka. Two-step supercritical dimethyl carbonate method for biodiesel production from Jatropha curcas oil. Bioresource Technology. 2010;101:2735–40.

[34] C.H Chen, W.H Chen, C.M.J Chang, S.M Lai, and C.H. Tu. Biodiesel production from supercritical carbon dioxide extracted Jatropha oil using subcritical hydrolysis and supercritical methylation. Journal of Supercritical Fluids, 2010;52: 228–34.

[35] D. Kumar, G. Kumar, and C.P. Poonam Singh. Ultrasonic-assisted transesterification of Jatropha curcas oil using solid catalyst, Na/SiO2. Ultrasonics Sonochemistry, 2010:0300, doi:10.1016/j.ultsonch.2010.

[36] Y. Ishii, and R. Takeuchi. Transesterified curcas oil blends for farm diesel engines. Transactions of the ASABE, 1987, vol, 30 (3), pp. 0605-0609.

[37] M. Senthil Kumar, A. Ramesh, and B. Nagalingam. Investigations on the use of Jatropha oil and its methyl ester as a fuel in a compression engine. Journal of Energy Institute, vol. 74, 2001, pp. 24–28.

[38] M. Senthil Kumar, A. Ramesh, and B. Nagalingam. An experimental comparison of methods to use methanol and Jatropha oil in a compression ignition engine. Biomass and Bioenergy, vol.25, 2003, pp. 309-318.

[39] G.A.P. Rao, and P. Ram Mohan. Performance evaluation of DI and IDI engines with Jatropha oil based biodiesel. Institution of Engineers (I) Journal, vol. 86, 2005, pp. 72-76.

[40] P. Mahanta, S.C. Mishra, and Y.S. Kushwah. A comparative study of pongamia pinnata and jatropha curcus oil as diesel substitute. International Energy journal, vol. 7, 2006, pp. 1-8.

[41] N.R. Banapurmath, P.G. Tewari, and R.S. Hosmath. Performance and emission characteristics of a DI compression ignition engine operated on Honge, Jatropha and sesame oil methyl esters. Renewable Energy, vol. 33, 2008, pp. 1982-1988.

[42] G.L. Rao, B.D. Prasad, and S. Sampath. Combustion Analysis of Diesel Engine Fueled with Jatropha Oil Methyl Ester - Diesel Blends. International Journal of Green Energy, vol. 4, 2007, pp.645–658.

[43] T.V. Rao, G.P. Rao, and K.H. Chandra. Experimental Investigation of Pongamia, Jatropha and Neem Methyl Esters as Biodiesel on C.I. Engine. Jordan Journal of Mechanical and Industrial Engineering, vol. 2, 2008, pp. 117 - 122.

[44] S.R. Kalbande and S.D. Vikhe. Jatropha and Karanj Bio-Fuel: An Alternate Fuel. ARPN Journal of Engineering and Applied Sciences, vol. 3, 2008, pp. 7-13.

[45] Y.V. Rao, R.S. Voleti, V.S. Hariharan, and A.V. Raju. Jatropha oil methyl ester and its blends used as an alternative fuel in diesel engine. Thermal Science, vol. 13, 2009, pp. 207-217.

[46] P.K. Sahoo, L.M. Das, M.K. Babu, P. Arora, V.P. Singh, N.R. Kumar, and T.S. Varyani. Comparative evaluation of performance and emission characteristics of jatropha, karanja and polanga based biodiesel as fuel in a tractor engine. Fuel, vol. 88, 2009, pp. 1698-1707.

[47] T.T. Kywe and M.M. Oo. Production of Biodiesel from Jatropha Oil (Jatropha curcas) in Pilot Plant. Proceedings of world academy of science, Engineering and Technology, vol. 38, 2009, pp. 481-487.

[48] S. Jindal, B.P. Nandwana, and N.S. Rathore. Comparative Evaluation of Combustion, Performance, and Emissions of Jatropha Methyl Ester and Karanj Methyl Ester in a Direct Injection Diesel Engine. Energy Fuels, vol.24, 2010, pp. 1565-1572.

[49] M.Senthil Kumar, A. Kastler, and B. Nagalingam. A Comparison of the Different Methods of Using Jatropha Oil as Fuel in a Compression Ignition Engine. Journal of Engineering for Gas Turbines and Power, vol. 132, 2010, pp. 1-10.

[50] R. Ejilah, A.A. Asere, A.B. Adisa, and A. Ejila. The effect of diesel fuel-Jatropha curcas oil methyl ester blend on the performance of a variable speed compression ignition engine. Australian journal of agricultural engineering, vol. 1, 2010, pp. 80-85.

[51] S. Puhan, N. Saravanan, G. Nagarajan, and N. Vedaraman. Effect of biodiesel unsaturated fatty acid on combustion characteristics of a DI compression ignition engine. Biomass and Bioenergy, vol. 34, 2010, pp. 1079–1088.

[52] J. Huang, Y. Wang, J. Qin, and A.P. Roskilly. Comparative study of performance and emissions of a diesel engine using Chinese pistache and jatropha biodiesel. Fuel Processing Technology, vol. 91, 2010, pp. 1761–1767.

[53] T.K. Gogoi, S. Talukdar, and D.C. Baruah. Comparative Analysis of Performance and Combustion of Koroch Seed Oil and Jatropha Methyl Ester blends in a Diesel Engine. World Renewable Energy Congress, Sweden, 2011, pp. 3533-3540.

[54] V.S. Reddy, K.R. Ranjan, V.K. Sharma and S.K. Tyagi. Experimental investigation of a diesel engine fuelled with Jatropha curcas L. seed oil. International Journal of Sustainable Energy, vol. 30,2010, pp. 37-41.

[55] T.Elango and T.Senthil kumar. Combustion and emission characteristics of a diesel engine fuelled with jatropha and diesel oil blends. Thermal Science, vol. 15, 2011, pp. 1205-1214.

[56] R. Prakash, S. Pandey, and S. Chatterji. Performance analysis of CI engine using jatropha oil and their esters. International Journal of Advanced Engineering Technology, vol. 2, 2011, pp. 186-191.

[57] L. Prasad, S. Pradhan, C.S. Madankar, L.M. Das, and S.N. Naik. Comparative study of performance and emissions characteristics of a diesel engine fueled with jatropha and karanja biodiesel. Journal of Scientific & Industrial Research, vol. 70, 2011, pp. 694-698.

[58] B.R. Prasath, P.T. Porai, M.F. Shabir, P. K. Devan, and S. Vigneshwaran. Combustion and Performance Analysis of Single Cylinder DI Diesel Engine Using Jatropha Biodiesel and its Blends. Applied Mechanics and Materials, vol.110–116, 2012, pp.3-7.

[59] D. Vashist and M. Ahmed. A comparative study of castor and jatropha oil source and its methyl ester test on the diesel engine. International Journal of Engineering Science and Technology, vol. 3, 2011, pp. 4765-4773.

[60] D. Kannan, S. Pachamuthu, N. Nabi, J. Einar, and T. Lovas. Theoretical and experimental investigation of diesel engine performance, combustion and emissions analysis fuelled with the blends of ethanol, diesel and jatropha methyl ester. Energy Conversion and Management, vol. 53, 2012, pp. 322-331.

[61] S. Kumar, A. Chaube, and S. K. Jain. Experimental evaluation of C.I. engine performance using diesel blended with Jatropha biodiesel. International Journal of Energy and Environment, vol. 3, 2012, pp. 471-484.

[62] A.Yadav and O. Singh. Investigations on diesel engine performance based on jatropha, karanja and neem biodiesels. Proc. IMechE Part A: Journal of Power and Energy, vol. 226, 2012, pp. 674-681.

[63] A.M. Liaquat, H.H. Masjuki, M.A. Kalam, M. Varman, and M.A. Hazrat. Application of blend fuels in a diesel engine. Energy Procedia, vol. 14, 2012, pp. 1124-1133.

[64] L. Prasad, S. Pradhan, L.M. Das, and S.N. Naik. Experimental assessment of toxic phorbol ester in oil, biodiesel and seed cake of Jatropha curcas and use of biodiesel in diesel engine. Applied Energy, vol. 93, 2012, pp. 245-250.

[65] B.S. Chauhan, N. Kumar, and H. Muk. A study on the performance and emission of a diesel engine fueled with Jatropha biodiesel oil and its blends. Energy, vol. 37, 2012, pp. 616-622.

[66] R. Kumar, A.K. Dixit, G.S. Manes, R. Khurana, and S.K. Singh. Emission and performance characteristics of jatropha ethyl ester blends with diesel fuel in a CI Engine. International Journal of Automobile Engineering Research and Development, vol. 2, 2012, pp. 34-47.

[67] P. Tan, Z. Hu, D. Lou, and Z. Li. Exhaust emissions from a light-duty diesel engine with Jatropha biodiesel fuel. Energy, vol. 39, 2012, pp. 356-362.

[68] G.Shirsath, M.S. Tandale, S.V. Khandal, S. Guluwadi, N.R. Banapurmath, V.S. Yaliwal and P.G. Tewari. Blends of karanja and jatropha biodiesels for diesel engine applications. International Journal of Sustainable Engineering, Vol.5, 2012, pp.252–264.

[69] M. El-kasaby and M.A. Nemit-allah. Experimental investigations of ignition delay period and performance of a diesel engine operated with Jatropha oil biodiesel. Alexandria engineering journal, vol. 52, 2013, pp. 141–149.

[70] V. Pradeep, and R.P. Sharma. Use of hot EGR for NO_x control in a compression ignition engine fuelled with bio-diesel from Jatropha oil. Renewable Energy, vol. 32, 2007, pp. 1136-1154.

[71] D.A. Dhananjaya, C.V. Sudhir and P. Mohanan. Combustion characteristics of diesel engine operating on jatropha oil methyl ester. Thermal Science, vol. 14, 2010, pp. 965-977.

[72] T. Ganapathy, R.P.Gakkhar, and K. Murugesan. An analytical and experimental study of performance on jatropha biodiesel engine. Thermal Science, vol. 13, 2009, pp. 69-82.

[73] A.B. Barboza, N.Yagnesh Sharma and C.V. Sudhir. Cyclic Combustion Studies of a CI Engine Operating on Jatropha B20 Fuel. International Conference on Mechanical and Electrical Technology, 2010, pp. 43-46.

[74] M. Venkatraman, and G. Devaradjane. Effect of compression ratio, injection timing and injection pressure on a diesel engine for better performance fueled with diesel – jatropha methyl ester blend. National Journal on Advances in Building Sciences and Mechanics, vol. 1, 2010, pp. 34-39.

[75] K. Rajan and K.R. Senthil Kumar. Combustion and Emission Characteristics of A Biodiesel Fuelled Diesel Engine with the Effect of Thermal Barrier Coated Internal Jet Piston. Second International Conference on Sustainable Energy and Intelligent System (SEISCON 2011), 2011, pp. 184-189.

[76] T. Ganapathy, R.P. Gakkhar, and K. Murugesan. Influence of injection timing on performance, combustion and emission characteristics of Jatropha biodiesel engine. Applied Energy, vol. 88, 2011, pp. 4376-4386.

[77] S. Jindal. Effect of injection timing on combustion and performance of a direct injection diesel engine running on Jatropha methyl ester. International Journal of Energy and Environment, vol. 2, 2011, pp. 113-122.

[78] M. Gomaa, A.J. Alimin, and K.A. Kamarudin. The effect of EGR rates on NO_x and smoke emissions of an IDI diesel engine fuelled with Jatropha biodiesel blends. International Journal of Energy and Environment, vol. 2, 2011, pp. 477-490.

[79] S. Adinarayana, Y.M.C. Sekhar, B.V.A. Rao, and M. Anil Prakash. Biodiesel as an Alternate Fuel in a Diesel Engine with the Cooled Exhaust Gas Recirculation–A Measure to Reduce Harmful Emissions. International Journal of Applied Research In Mechanical Engineering, Vol.1, pp.10-15.

[80] N. Shrivastava, S.N. Varma, and M. Pandey. A Study on Reduction of Oxides of Nitrogen with Jatropha Oil Based Bio Diesel. International Journal of Renewable Energy Research, vol. 2, 2012, pp. 504-509.

[81] M.V. Nagarhalli, and V.M. Nandedkar. Performance of diesel engine using blends of esters of jatropha and karanja- A novel approach. International Journal of Advanced Engineering Technology, vol.3, 2012, pp.51-54.

[82] C. R. Rajashekhar, T.K. Chandrashekar, C. Umashankar, and R. Harish Kumar. Studies on effects of combustion chamber geometry and injection pressure on biodiesel combustion. Transactions of the Canadian Society for Mechanical Engineering, Vol. 36, 2012, pp.429-438.

[83] K. Venkateswarlu, B. S. R. Murthy, V. V. Subbarao, and K. Vijaya Kumar. Effect of exhaust gas recirculation and ethyl hexyl nitrate additive on biodiesel fuelled diesel engine for the reduction of NOx emissions. Front. Energy, vol. 6, 2012, pp. 304–310.

[84] S. A. Viswanath, V. Dinesh, S. Arivazhagan, and N. Vinayagam. Modeling and analysis of performance, combustion and emission characteristics of jatropha methyl ester blend diesel for CI engine with variable compression ratio. vol. 4, 2012, 3457-3471.

[85] A. Pandhare and A. Padalkar. Investigations on performance and emission characteristics of diesel engine with biodiesel (Jatropha oil) and its blends. Journal of Renewable Energy, vol. 2013, 2013.

[86] P.V. Rao. Experimental Investigations on the Influence of Properties of Jatropha Biodiesel on Performance, Combustion, and Emission Characteristics of a DI-CI Engine. World Academy of Science, Engineering and Technology, vol.75, 2011, pp.855-868.

[87] Y.V.Hanumantha Rao, Ram Sudheer Voleti, A.V.Sitarama Raju and P.Nageswara Reddy. Experimental investigations on jatropha biodiesel and additive in diesel engine. Indian Journal of Science and Technology, vol. 2, 2009, pp. 25-31.

[88] V. Sajith, C. B. Sobhan, and G. P. Peterson. Experimental Investigations on the Effects of Cerium Oxide Nanoparticle Fuel Additives on Biodiesel. Advances in Mechanical Engineering, vol. 2010, Article ID 581407.

[89] J.S. Basha and R.B. Anand. Role of nanoadditive blended biodiesel emulsion fuel on the working characteristics of a diesel engine. Journal of Renewable Sustainable Energy, vol. 3, 2011, pp. 1-17.

[90] U. Vara Prasad, K. M. Murthy and G.A.P. Rao. Effective utilization of B20 blend with oxygenated additives. Thermal Science, vol. 15, 2011, pp. 1175-1184.

[91] K. Varatharajan, M. Cheralathan, and R. Velraj. Mitigation of NOx emissions from a jatropha biodiesel fuelled DI diesel engine using antioxidant additives. Fuel, vol. 90, 2011, pp. 2721–2725.

[92] D. Ganesh, and G. Gowrishankar. Effect of nano-fuel additive on emission reduction in a biodiesel fuelled CI engine. International Conference on Electrical and Control Engineering (ICECE), 2011, pp.3453-3459.

[93] D. Kannan, S. Pachamuthu, N. Nabi, J. Einar, and T. Lovas. Theoretical and experimental investigation of diesel engine performance, combustion and emissions analysis fuelled with the blends of ethanol, diesel and jatropha methyl ester. Energy Conversion and Management, vol. 53, 2012, pp. 322-331.

[94] S. Jain and M.P. Sharma. Engine performance and emission analysis using oxidatively stabilized Jatropha curcas biodiesel. Fuel, vol. 106, 2013, pp. 152-156.

[95] T.K. Gogoi, A.K. Sarma, P.S. Misra, and S.T. Haque. Combustion analysis of jatropha methyl ester and its ethanol and acetone blends in a diesel engine. International Journal of Emerging Technology and Advanced Engineering, vol. 3, 2013, pp. 51-57.

[96] J.A. Bittle, B.M. Knight, and T.J. Jacobs. Interesting behavior of biodiesel ignition delay and combustion duration. Energy Fuels, vol. 24, 2010, pp.4166–4177.

[97] A. Monyem and J. H. Van Gerpen. The effect of biodiesel oxidation on engine performance and emissions. Biomass and Bioenergy, vol. 20, 2001, pp. 317–325.

[98] R.E. Tate, K.C. Watts, C.A.W. Allen, and K.I. Wilkie. The densities of three biodiesel fuels at temperatures up to 300 ^{o}C. Fuel, vol. 85, 2006, pp.1004-9.

[99] C.Y. Choi, R.D. Bower, and R.D. Reitz. Mechanisms of emissions reduction using biodiesel fuels. Final report for the National Biodiesel Board; 1997.

[100] W. Yuan. A. C. Hansen, and Q. Zhang. Combustion optimization of biodiesel for diesel engines with the aid of KIVA-3 code. ASAE Paper No. 026083, 2002.

[101] J. Benajes, S. Molina, C. Gonzalez, and R. Donde. The role of nozzle convergence in diesel combustion. Fuel, vol.87, 2008, pp.1849-1858.

[102] C. Mueller, A. Boehman and G. Martin. An experimental investigation of the origin of increased NOx emissions when fueling a heavy-duty compression-ignition engine with soy biodiesel, SAE Int. J. Fuels and Lubricants. vol. 2, 2009, pp. 789-816.

[103] G.A.Ban-Weiss, J.Y. Chen, B.A.Buchholz, and R.W.Dibble. A numerical investigation into the anomalous slight NO_x increase when burning biodiesel: A new (old) theory. Fuel Processing Technology, vol. 88, 2007, pp. 659-667.

[104] W.Yuan, A. Hansen, M.Tat, J. Van Gerpen, and Z.Tan. Spray, ignition, and combustion modeling of biodiesel fuels for investigating NO_x emissions. Transactions of the ASAE, vol.48, 2005, pp.933-939.

[105] V. Edwin Geo, M. Nadia, M. Tazerout, F. Aloui. Experimental analysis of biofuel as an alternative fuel for diesel engines. Applied Energy, vol. 94, 2012, pp. 224–231.

[106] C.Allen, and K.Watts. Comparative analysis of the atomization characteristics of fifteen biodiesel fuel types. T ASAE, vol.43, 2000, pp. 207-211.

[107] M. Canakci. Combustion characteristics of a turbocharged DI compression ignition engine fueled with petroleum diesel fuels and biodiesel. Bioresource Technology, vol.98, 2007, pp.1167-75.

[108] M.Tat, J. Van Gerpen, and P.Wang. Fuel property effects on injection timing, ignition timing, and oxides of nitrogen emissions from biodiesel-fueled engines. Transactions of the ASAE, vol.50, 2007, pp.1123-8.

[109] Y. Ra, R.Reitz, J, McFarlane, and C. Daw. Effects of fuel physical properties on diesel engine combustion using diesel and biodiesel fuels. SAE Transactions-Journal of Fuels and Lubricants, vol.117, 2008, pp.2101-1379.

[110] S.Garner, R. Sivaramakrishnan, and K. Brezinsky. The high-pressure pyrolysis of saturated and unsaturated C7 hydrocarbons. Proc. Combust. Institute, vol.32, 2009, pp. 464-67.

[111] R. McCormick, M. Graboski, T. Alleman, A. Hening, and K.Tyson. Impact of biodiesel source material and chemical structure on emissions of criteria pollutants from a heavy duty engine. Environmental Science and Technology, vol.35, 2001, pp.1742-7.

[112] M. Lapuerta, O. Armas, and J. Rodriguez-Fernandez. Effect of biodiesel fuels on diesel engine emissions. Progress in Energy and Combustion Science, vol.34, 2008, pp.198-223.

[113] R. McCormick, J.Alvarez, M. Graboski, K.Tyson, and K.Vertin. Fuel additive and blending approaches to reducing NO_x emissions from biodiesel. SAE 2002-01-1658; 2002.

[114] W. Wang, D. Lyons, W.Clark, and N.Gautam. Emissions from nine heavy trucks fueled by diesel and biodiesel blend without engine modification. Environ. Sci. Technology, vol.34, 2000, pp. 933–939.

[115] M. Graboski, and R.McCormick. Combustion of fat and vegetable oil derived fuels in diesel engines. Progress in Energy and Combustion Science, vol. 24, 1998, pp.125-64.

[116] J. Song, V.Zello, and A. Boehman. Comparison of the impact of intake oxygen enrichment and fuel oxygenation on diesel combustion and emissions. Energy Fuel, vol.18, 2004, pp. 1282–90.

[117] J. Mueller, J. Pitz, M. Lyle, L.Pickett, G.Martin, D. Siebers, and C.Westbrook. Effects of oxygenates on soot processes in DI diesel engines: Experiments and numerical simulations. SAE paper No. 2003-01-1791, 2003.

[118] T. Ullman, K. Spreen, and R. Mason. Effects of cetane number, cetane improver, aromatics, and oxygenates on 1994 heavy-duty diesel engine emissions. SAE Transactions: Journal of Fuels and Lubricants, vol.103, 1994, 941020.

[119] J. Bittle, B.Knight, and T.Jacobs. The impact of biodiesel on injection timing and pulse width in a common-rail medium-duty diesel engine. SAE Paper No. 2009-01-2782, 2009.

[120] M. Tat. Investigation of oxides of nitrogen emissions from biodiesel-fueled engines. PhD Dissertation. Iowa State University. Ames, IA; 2003.

[121] N. Usta. An experimental study on performance and exhaust emissions of a diesel engine fuelled with tobacco seed oil methyl ester. Energy Convers. Management, vol. 46, 2005, pp. 2373–86.

[122] D. Deshmukh, A. Madan Mohan, T.N.C. Anand, R.V. Ravikrishna. Spray characterization of straight vegetable oils at high injection pressures. Fuel, vol. 97, 2012, pp. 879–883.

[123] W.Yuan, A. Hansen, M.Tat, J. Gerpen, and Z. Tan. Spray, ignition, and combustion modelling of biodiesel fuels for investigating NO_x emissions. TASAE., 48, pp. 933-39, 2005.

[124] S.N. Anderson and D. Olsen. Survey of straight vegetable oil composition impact on combustion properties. SAE Paper No. 2009-01-0487, 2009.

[125] J. Sun, J.A. Caton, T.J. Jacobs. Oxides of nitrogen emissions from biodiesel-fuelled diesel engines. Progress in Energy and Combustion Science, 36, 2010, pp.677-695.

[126] M. Ahmed, C. Ejim, B. Fleck, and A. Amirfazli. Effect of biodiesel fuel properties and its blends on atomization. SAE Paper No. 2006-01-0893, 2006.

[127] A.K. Hossain, and P.A. Davies. Pyrolysis liquids and gases as alternative fuels in internal combustion engines – A review. Renewable and Sustainable Energy Reviews, vol.21, 2013, pp.165-189.

[128] H.S. Heo, H.J.Park, Y.K.Park, C. Ryu, D.J. Suh, Y.W. Suh, J.H. Yim, S.S.Kim. Bio-oil production from fast pyrolysis of waste furniture sawdust in a fluidized bed. Bioresource Technology, vol.101, 2009, pp.S91–S96.

[129] S. Czernik, D.K. Johnson, S. Black. Stability of wood fast pyrolysis oil, Biomass Energy, vol. 7, 1994, pp. 187-92.

[130] Z.J. Lu, K.Y.Ping. Spray combustion properties of fast pyrolysis bio-oil produced from rice husk. Energy Conversion and. Management, vol. 51, 2010, pp.182-88.

[131] Lu, Z.J., Ming, Y.W., Na, W.N. Bio-oil production from cotton stalk. Energy Conversion and Management. vol. 49, 2008, pp.1724-30.

[132] M.G. Perez, A. Chaala, and C.Roy. Co pyrolysis of sugarcane bagasse with petroleum residue Part II – Product yields and properties. Fuel, vol. 81, 2002, pp. 893-907.

[133] S. Sensoz, I. Demiral, H.F. Gercel. Olive bagasse (Olea europea L.) pyrolysis. Bioresource Technology, vol. 97, 2006, pp. 429-36.

[134] R. Manurung, D.A.Z. Wever, J. Wildschut, R.H.Venderbosch, H. Hidayat, J.E.G.Van Dam, E.J. Leijenhorst, A.A. Broekhuis, and H.J. Heeres. Valorisation of Jatropha curcas L. plant parts: Nut shell conversion to fast pyrolysis oil. Food Bio products Processing, vol. 87, 2009, pp. 187-96.

[135] S.J. Kim, S.H. Jung, and J.S. Kim. Fast pyrolysis of palm kernel shells: Influence of operation parameters on the bio-oil yield and the yield of phenol and phenolic compounds. Bioresource Technology, vol. 101, 2010, pp. 9294-9300.

[136] A.V. Bridgwater, A.J. Toft, and J.G. Brammer. Techno-economic comparison of power production by biomass fast pyrolysis with gasification and combustion. Renewable and Sustainable Energy Reviews, vol. 6, 2002, pp.181-248.

[137] M. Balat, M. Balat, E. Kırtay, and H. Balat. Main routes for the thermo-conversion of biomass into fuels and chemicals. Part 1: Pyrolysis systems. Energy Conversion and Management, vol. 50, 2009, pp. 3147-3157.

[138] G.W. Huber, S. Iborra, and A. Corma. Synthesis of transportation fuels from biomass: chemistry, catalysts, and engineering. Chemical Reviews, vol.106, 2006, pp. 4044-4098.

[139] Z.Qi, C.Jie, W.Tiejun, and X.Ying. Review of biomass pyrolysis oil properties and upgrading research. Energy Conversion and Management, vol.48, 2007, pp. 87-92.

[140] Q. Lu, W.Z. Li, and X.F. Zhu. Overview of fuel properties of biomass fast pyrolysis oils. Energy Conversion and Management, vol.50, 2009, pp.1376-1383.

[141] A. Shihadeh and S. Hochgreb. Impact of biomass pyrolysis oil process conditions on ignition delay in compression ignition engines. Energy & Fuels, vol. 16, 2002, pp. 552-561.

[142] V. Minkova, M. Razvigorova, E. Bjornbom, R. Zanzi, T. Budinova, and N. Petrov. Effect of water vapour and biomass nature on the yield and quality of the pyrolysis products from biomass. Fuel Processing Technology, vol.70, 2001, pp. 53-61.

[143] Y.Solantausta, N.O. Nylund, M.Westerholm, T. Koljonen and A. Oasmaa. Wood-Pyrolysis oil as fuel in a diesel-power plant. Bioresource Technology, vol. 46, 1993, 177-188.

[144] S. Frigo, R. Gentilli, L. Tognotti, S. Zanforlin, and G. Benelli. Feasibility of using wood flash-pyrolysis oil in diesel engines. SAE 982529.1998.

[145] M. Ikura, M. Stanciulescu, Ed. Hogan. Emulsification of biomass derived bio-oil in diesel fuel. Biomass and bioenergy, vol.24, 2003, pp.221-232.

[146] C.Bertoli, J.D. Alessio, N. Del Giacomo, M. Lazzaro, P. Massoli, and V.Moccia. Running light-duty DI diesel engines with wood pyrolysis oil. SAE 2000-01-2975, 2000.

[147] Y.Huang, Xu. Han, S.Shang and Li.Wang. Performance and emissions of a direct injection diesel engine operating on emulsions of corn stalk bio-oil in diesel. Proc IMechE Part D: J Automobile Engineering, vol. 226, 2012, pp.1119–1129.

[148] X .Jiang, and N. Ellis. Upgrading bio-oil through emulsification with biodiesel: thermal stability. Energy and Fuels, vol.24, 2010, pp. 2699–2706.

[149] M.Garcia-Perez, T.T.Adams, J.W. Goodrum, K.C.Das, D.P.Geller. DSC studies to evaluate the impact of bio-oil on cold flow properties and oxidation stability of bio-diesel. Bioresource Technology, vol.101, 2010, pp. 6219–6224.

[150] J.S Basha, and R.B. Anand. An experimental investigation in a diesel engine using carbon nanotubes blended water-diesel emulsion fuel. Proc. IMechE, Part A: J. Power and Energy, vol.225, 2011, pp.279-288.

[151] G.R. Kannan, and R. Anand. Experimental investigation on diesel engine with diestrol-water micro emulsions. Energy, vol.36, 2011, pp.1680-7.

[152] K.S. Chen, Y.C. Lin, L.T. Hsieh, L.F. Lin, and C.C. Wu. Saving energy and reducing pollution by use of emulsified palm-biodiesel blends with bio-solution additive. Energy, vol.35, 2010, pp.2043-8.

[153] A. Alcala, and A.V. Bridgwater. Upgrading fast pyrolysis liquids: Blends of biodiesel and pyrolysis oil. Fuel, vol.109, 2013, pp. 417–426.

[154] M.C. Mayoral, M.T. Izquierdo, J.M. Andreas, B. Rubio. Different approaches to proximate analysis by thermo gravimetric analysis. Thermochem. Acta, vol. 370, 2001, pp. 91–97.

[155] J.B. Heywood. Internal combustion engines fundamentals. McGraw Hill, London, 1989.

[156] R. B. Krieger, G.L. Borman. The computation of apparent heat release in I. C. engines. ASME Paper 66 WA/DGP4, 1966.

[157] S. Murugan, M.C. Ramaswamy and G. Nagarajan. A comparative study on the performance, emission and combustion studies of a DI diesel engine using distilled tyre pyrolysis oil-diesel blends. Fuel, vol. 87, 2008, pp. 2111-2121.

[158] J.R.Clarke, R.J. Tabaczynski. Internal combustion engine with adjustable compression ratio and knock control. US Patent 6135086, 2000-10-24.

[159] R.G.Sykes, Tickford. Methods to reduce the fuel consumption of gasoline engines. Engines Expo 2000 paper.

[160] J.E. Brevick. Variable compression ratio piston. US Patent 5755192, 1998-05-26.

[161] S. Aoyama, H. Fujimoto, K. Moteki. Variable compression ratio mechanism of reciprocating internal combustion engine. European Patent 1170482, 2002-01-09.

[162] J. Beroff. Internal combustion engine with variable capacity and compression ratio. European Patent 1143127, 2001-10-10.

[163] S. Bari, C.W. Yu and T.H. Lim. Effect of fuel injection timing with waste cooking oil as a fuel in a direct injection diesel engine. Proc. IMechE Part D: J. Automobile Engineering, vol.93, 2004, pp. 218.

[164] A.K. Agarwal, D.K. Srivastava, A. Dhar, R.K. Maurya, P.C. Shukla, and A.P. Singh. Effect of fuel injection timing and pressure on combustion, emissions and performance characteristics of a single cylinder diesel engine. Fuel, vol. 111, 2013, pp. 374-383.

[165] H.W. Coleman, and W.G. Steele Jr. Experimentation and uncertainty analysis for engineers. Wiley publications, New York, 1989.

[166] K. Muralidharan, D. Vasudevan, and K.N. Sheeba. Performance, emission and combustion characteristics of biodiesel fuelled variable compression ratio engine. Energy, vol. 36, 2011, pp. 5385-5393.

[167] B. Tesfa, R.Mishra, C. Zhang, F. Gu, and A.D. Ball. Combustion and performance characteristics of CI (compression ignition) engine running with biodiesel. Energy, vol. 51, 2013, pp. 101–115.

[168] D.H.Qi, H.Chen, C.F. Lee, L.M. Geng, and Y.Z. Bian. Experimental studies of a naturally aspirated, DI diesel engine fuelled with ethanol-biodiesel-water micro emulsions. Energy Fuels, vol.24, 2010, pp. 652-663.

[169] M. Senthil Kumar, A. Kerihuel, J. Bellettre, and M. Tazerout. Ethanol animal fat emulsions as a diesel engine fuel – Part 2: Engine test analysis. Fuel, vol.85, 2006, pp.2646-2652.

[170] O. Armas, R. Ballesteros, F.J.Martos, and J.R. Agudelo. Characterization of light duty diesel engine pollutant emissions using water emulsified fuel. Fuel, vol.84, 2005, pp.1011-1018.

[171] D. Agarwal, L. Kumar, and A.K. Agarwal. Performance evaluation of vegetable oil fuelled compression ignition engine. Renewable Energy, vol. 33, 2008, pp.1147-1156.

[172] J. Xue, T.E. Grift, and A.C. Hansen. Effect of biodiesel on engine performances and emissions. Renewable and Sustainable Energy Reviews, vol.15, 2011, pp.1098–1116.

[173] C. Lin, and S. Lin. Effects of emulsification variables on fuel properties of two-and three phase biodiesel emulsions. Fuel, vol.86, 2007, pp.210-217.

[174] M. Karabektas. The effects of turbocharger on the performance and exhaust emissions of a diesel engine fuelled with biodiesel. Renewable Energy, vol.34, 2009, pp. 989-993.

[175] C.Y. Lin, and H.A. Lin. Diesel engine performance and emission characteristics of biodiesel produced by the peroxidation process. Fuel, vol.85, 2006, pp.298–305.

[176] M.N. Nabi, S.M. Najmul Hoque, and M.S. Akhter. Karanja (Pongamia Pinnata) biodiesel production in Bangladesh, characterization of karanja biodiesel and its effect on diesel emissions. Fuel Processing Technology, vol.90, 2009, pp.1080–1086.

[177] R.L. McCormick, and R. Parish. Technical barriers to the use of ethanol in diesel fuel. Milestone report to NREL/MP-540-32674, 2001.

[178] M. A. Gumus. Comprehensive experimental investigation of combustion and heat release characteristics of a biodiesel (hazelnut kernel oil methyl ester) fueled direct injection compression ignition engine. Fuel, vol.89, 2010, pp.2802-2814.

[179] L.N. Rao, R. Gattamaneni, and S. Subramani. Combustion and emission characteristics of diesel engine fuelled with rice bran oil methyl ester and its diesel blends. Thermal science, vol.12, 2008, pp. 139-150.

[180] L. Zhu, C.S. Cheung, W.G. Zhang, and Z. Huang. Combustion, performance and emission characteristics of a DI diesel engine fueled with ethanol–biodiesel blends. Fuel, 90, 2011, pp.1743–1750.

[181] P.L. Zhou. An investigation into the atomisation of emulsified fuels. Ph.D thesis. University of Newcastle upon Tyne, 1992.

[182] M. Nishioka, S. Nakagawa, Y. Ishijawa, and T. Takeno. NO emission characteristics of methane-air double flame. Combustion and Flame, vol. 98, 1994, pp. 127–38.

[183] J.P. Szybist, S.R. Kirby, and A.L. Boehman. NO_x emissions of alternative diesel fuels: A comparative analysis of biodiesel and FT diesel. Energy and Fuels, vol.19, 2005, pp.1484–92.

[184] M.P.Ashok, and C.G. Saravanan. Performance and emission of the emulsified fuel in a DI diesel engine using oxygenated additive diethyl ether with surfactant of Span-80. Energy and Fuels, vol.21, 2007, pp.1878-1882.

[185] W.J.D Annand. Heat transfer in the cylinders of reciprocating internal combustion engines. Proceedings of Institution of Mechanical Engineers, vol.177, 1963, pp.973-990.

[186] J.I. Ghojel. Review of the development and applications of the Wiebe function: a tribute to the contribution of Ivan Wiebe to engine research. International Journal of Engine Research, vol.11, 2010, pp. 297-312.

[187] I.I. Wiebe. Semi-empirical expression for combustion rate in engines. In Proceedings of Conference on Piston engines, USSR, 1956, pp.185-191.

[188] C. Olikara, and G.L. Borman. A computer program for calculating properties of equilibrium combustion products with some applications to I. C. engines. SAE Paper 750468, 1975.

[189] H. Hiroyasu, T. Kadota, and M. Arai. Development and use of a spray combustion modeling to predict diesel engine efficiency and pollutant emissions-Part 1: combustion modeling. Bull. JSME, 26, 1983, pp. 569–575.

[190] H.S. Kent, and R. Curtis. Review of the effects of biodiesel on NOx emissions. Fuel Processing Technology, vol. 96, 2012, pp. 237-249.

[191] J.Ghojel, and D. Honnery. Heat release model for the combustion of diesel oil emulsions in DI diesel engines. Applied Thermal Engineering, vol. 25, 2005, pp.2072-2085.

[192] G.R. Kannan, and R. Anand. Effect of injection pressure and injection timing on DI diesel engine fuelled with biodiesel from waste cooking oil. Biomass bioenergy, vol. 46, 2012, pp.343-352.

[193] V. Arul Mozhi Selvan, R. B. Anand, and M. Udayakumar. Combustion characteristics of diesohol using biodiesel as an additive in a direct injection compression ignition engine under various compression ratios. Energy Fuels, vol. 23, 2009, pp.5413-5422.

[194] Y. Ulusoy, Y. Tekin, M. Cetinkaya, and F. Karaosmano. The engine tests of biodiesel from used frying oils. Energy Sources, vol. 26, 2004, pp.927- 932.

[195] H. Raheman, and S.V. Ghadge. Performance of diesel engine with biodiesel at varying compression ratio and ignition timing. Fuel, vol 87, 2008, pp. 2659-2666.

[196] C. Sayin, M. Gumus, and M. Canakci. Effect of fuel injection timing on the emissions of a direct-injection (DI) diesel engine fueled with canola oil methyl ester-diesel fuel blends. Energy Fuels, vol. 24, 2010, pp. 2675-2682.

[197] C. Sayin, K. Uslu, and M. Canakci. Influence of injection timing on the exhaust emissions of a dual-fuel CI engine. Renewable Energy, vol. 33, 2008, pp.1314-1323.

[198] C. Sayin, M. Gumus, and M. Canakci. Effect of fuel injection pressure on the injection, combustion and performance characteristics of a DI diesel engine fueled with canola

oil methyl esters-diesel fuel blends. Biomass and Bioenergy, vol.46, 2012, pp. 435-446.

[199] G. Zhang, X. Qiao, X. Miao, J. Hong, and J. Zheng. Effects of highly dispersed spray nozzle on fuel injection characteristics and emissions of heavy-duty diesel engine. Fuel, vol.102, 2012, pp.666-673.

[200] M. Gumus. Evaluation of hazelnut kernel oil of Turkish origin as alternative fuel in diesel engines. Renewable Energy, vol.33, 2008, pp.2448-57.

[201] C. Sayin, and M. Gumus. Impact of compression ratio and injection parameters on the performance and emissions of a DI diesel engine fueled with bio-diesel-blended fuel. Applied Thermal Engineering, vol. 31, 2011, pp.3182-3188.

[202] G.R. Kannan, and R. Anand. Experimental evaluation of DI diesel engine operating with diestrol at varying injection pressure and injection timing. Fuel Processing Technology, vol. 92, 2011, pp.2252-2263.

[203] G.R. Kannan, K.R. Balasubramanian, and R. Anand. Artificial neural network approach to study the effect of injection pressure and timing on diesel engine performance fueled with biodiesel. International Journal of Automotive Technology, vol.14, 2013, pp.507-519.

[204] C. Sayin, A.N. Ozsezen, and M.Canakci. The influence of operating parameters on the performance and emissions of a DI diesel engine using methanol-blended-diesel fuel. Fuel, vol. 89, 2010, pp.1407-1414.

[205] M.Ziejewski, H.J. Goettler, H. Hainees and C. Huang. EMA durability tests on high oleic sun flower and safflower oils in diesel engines. SAE paper 961856, 1996.

[206] S.Bari, C.W. Yu and T.H. Lim. Performance deterioration and durability issues while running a diesel engine with crude palm oil. Proc. IMechE, Part D, Journal of Automobile Engineering, vol, 216, 2002, pp.785-792.

[207] Anon. Lube Analyst User's Manual. Gas Tops Ltd. Ottawa, Canada, 1995.

Experimental Studies on a DI Diesel Engine Fueled with Jatropha Methyl Ester-Wood Pyrolysis Oil Emulsions

A Thesis

Submitted by

R.PRAKASH

(Roll No: 510ME607)

In Partial Fulfillment of

the Requirement for the Degree

of

DOCTOR OF PHILOSOPHY

Department of Mechanical Engineering
National Institute of Technology,
Rourkela –769 008
India

September 2013